## § 1. Preface and introductions

This work began in 1995 under the co-supervision of now Emiritus Professor David John Bell and Emiritus Professor Graham Arthur Davies. The main theme of it is the percolation on porous media and Voronoi tessellation. The objectives are to study the characteristics and nature of Voronoi tessellation and percolation, and then look at their application on porous media, which includes such things as membranes.

As a brief background to this project, the dissertation for my master degree in Control and Information Technology, dated September 1995, was on the percolation on a two-dimensional Voronoi tessellation. From 1996 to 1998 I had been doing a PhD in Japan on topics related to Control System. Parts of my work there are recorded in the few *technical reports* that I wrote during that time and presented to my supervisor, now Emeritus Professor Katsuhisa Furuta. In September 2000 I came back to UMIST to do a PhD in Translation but a few months later changed my mind to resume this research on Tessellation with Graham Davies.

Throughout my research I kept hand written notes which I called *work books*. All results exist in two places, either in the thesis or in the form of the TEX documents which I call *work notes*. Materials sometimes move from the work notes to the thesis. Apart from simulation results, these work notes also contains ideas for future works. All these worknotes were written during 2001. Their importance is that they represent the essential momentum or the underlying potential at work behind every percolative process. But most of the breakthroughs in this project came during 2002. I solved numerically a problem on the two-dimensional continuum percolation of squares on the plane. My algorithm can also give solutions for the continuum percolations of $n$-polygons, for $n \geq 3$ and $n \in I^+$.

The idea of writing these worknotes came from a book I had read about the work notes written by Michael Ventriswhile he was deciphering the Mycenean Linear B script. I wrote no worknotes during 2002. During the first half of 2003, however, I resumed my writing again and this time produced not worknotes but books which I published under the trademark name of ≻Kittix.

I started to use Latex in 1994 to write a design exercise report for Dr. Martin Zarrop of the Control System Centre at UMIST. Back then, most people I know liked the program better than its progenitor TEX, which most thought was difficult. I used Latex for writing my master degree dissertation in 1995, and continued using while in Japan and until early 2001 when I first turned to TEX then held fast to it. In the past when I still used LaTEX I could hardly adjust, but has to accept the existing formats. One awkward example is seen in my technical report number 6 where one reference (Fitzgerald *et al*, 1971) appears everywhere as "[FCKK71]", which looks very awkward.

Topics are divided into Voronoi structure and geometry, percolation, and membrane science. Voronoi tessellation has been used to model the array of the somata and cone cells in retina of mammals. (Ammermuller et al 1993; Ahnelt et al, 2000; Zhan et al, 2000) Curcio et al (1992) found anisotropy in cone spacing. For readers who are interested in the theoretical works on stochastic geometry may look at Møller (1989).

None of the papers and articles in § C has appeared in print elsewhere. It may be true that nothing worthwhile is ever without trouble. This project has had its share of problems. But 'What happened is history!', as Graham once said to me, or 'It is over!' as I to students in a lab I demonstrated with whom at times I had sympathised regarding problems beyond their power which affected them, and to whom I had passed down all the essentials of a programmer, there is no point keep on complaining about the past. Being a subset of the Superset I shall not judge. Being a me then the Me in Christ in God, how could I judge other subsets myself being merely another subset. It is not for a part to judge a fellow part, but let the Whole be the only One who judges, and let that alone suffice! Having done my tasks I am now only a writer who believes in the one Creator from whom all things come and to whom the same return. As Percolation may compass percolations my works is in Science in Him.

I completed a two-dimensional percolation program and used it to compute the critical probability of a Voronoi graph in time for my M.Sc. dissertation. I used the C program developed by Nicholas Jackson and maintained by Riaz Jafferali to generate the Voronoi network, and wrote my own program on Matlab to find the percolation probability. Before I went to Tokyo in September of the same year, we agreed that I would carry on doing some more work along the same line while I was in Japan. Graham suggested that I looked at the viscous fingering, a phenomenon which occurs

when a low viscosity fluid penetrates a high viscosity one in the form of thin branches, which is of great importance in the replacement of oil in a reservoir by water.

I telneted across half the globe from Tokyo to log on to the workstations at the Chemical Engineering Department in Manchester, but instead of writing another program to do viscous fingering I only managed to find the percolation probability of the road network in Bangkok using the program I from my M.Sc. I also carried further the work I had previously done with Martin Zarrop on object location using self-tuning control; and had an idea that if we could construct a network of people with an internal flow of money, we would be able to explain economic crises such as hyperinflation by using the percolation theory. On the topic of percolation and Voronoi tessellation I presented one paper at a conference in St. Louis (1996); on object location at two conferences, one in Atagawa (1996) and another one in Singapore (1997); and on economic modelling one at a conference in Tokyo (1997).

The original objectives of the present project are the following. Firstly, to study the statistics of the three-dimensional Voronoi tessellation, namely the number of vertices, coordination probabilities of nodes, number of faces, volumes, area of each face, number of sides and edges of faces, and perimeter. Next, to 'formulate a simulation of Voronoi tessellation,' that is to say, polygons in two dimensions and polyhedra in three dimensions; then analyse the lattices for the number of cells, sides, and edges. In two dimensions find the fractional expected area per cell, and expected number of vertices and edges. In three dimensions find the expected number of vertices, edges, faces, the fractional expected volume per cell, area of faces and fractional area per cell. Then section the Voronoi tessellation in two dimensions using a straight line and repeat the same thing in three dimensions using a random plane. In two-dimensional section of three-dimensional lattices using orthogonal planes, find the number of cells, edges, and the area. And then compress the lattice in one plane, with compression ratios $0 \leq c \leq 0.8$, and find the volume and surface area of cells for $c = 0$, 0.4, and 0.6; plot a section structure for $(\text{x–y})_{c_z=0}$, $0 < z < 1.0$, $c_y = 0$, 0.4, 0.6; $(\text{x–z})_{c_y=0}$, $0 < y < 1.0$, $c_z = 0$, 0.4, 0.6; compare the number of vertices, edges, and the area with those obtained from the case when $c_z = 0$, $c_y = 0$, and $z = 1$. Study transformations of Voronoi structures, for example the effect on the statistics when Voronoi graphs have a thickness. For each of the expected values mentioned above, find the first, second, and third moments. And finally, from the observation I have made that a three-dimensional tessellation have a bias towards an even number of vertices, find an explanation. To conclude the study of Voronoi tessellation, find affine transformations on two- and three-dimensional lattices and use the AVS program to print out sections of 3-d lattices †. Then for affine transformations, for example stretching, write algorithms to reposition the structure. For 2-d lattices, find the critical percolation probability (CPP), compare these with previous data and carry on to find the CPP on higher dimension lattices. To look at the application to the technical problems of membranes, foams, plant cells, *etc*, and if possible to compare my results with models to describe other physical and natural phenomena. Relevant to the application in foams is perhaps the population balance equations. Care should be taken to ensure that any application mentioned is described in details how it can fit in with real problems. Of no less importance is to study methods of adjusting structures to fit the applications. These methods include modifications to Poisson point processes and, again, affine transformations of the cellular structure.

Filters used in aluminium smeltering must withstand a temperature higher than 700°Csince aluminium alloy melts at 650–680°C. These filters are used in order to separate the oxide froth which otherwise would form pits when the aluminium is casted. The process of manufacturing filters often introduces asymmetry elements to their structure, for instance there may be elongation in one dimension because of gravity, or in cases where material is drawn out to make the filter the structure may become distorted from the shear force of drawing. The texture of bread is anisotropic because the internal pressure from gas produced by the yeast press es the dough against its own surface tension. The elongated cells inside bamboos appear in various sizes, which explain why bamboos are at the same time strong and flexible. Certainly one sees the Voronoi tessellation wherever one looks. I feel that I have learnt so much from Graham.

The following summarises our original outline of the project. The objective is to study a *foam like* porous medium. Describe the statistics of structures in three-dimensional space, state the reason why we need the statistics and the roles they play in application. For the Voronoi tessellation, created from the Delaunay triangulation of Poisson points, give algorithms which generate the structure from

---

† This has been done using Matlab instead.

one- up to $n$-space ‡, and give examples of these [structures found in nature]. Give the analyses of the static geometrical data, namely the length scale $l < L$ in one dimension; the area $a < A$, $n_1$, $n_2$, $L$ in two dimensions; and the volume $v < V$, $n_1$, $n_2$, $n_3$ in three dimensions, where $n_{d+1}$ is the number of the $d$-dimensional entities, $L = V^{\frac{1}{3}}$, $A = V^{\frac{2}{3}}$, and $V = \sum_i v_i$. Include the translation that I have made of the seminal papers by Voronoi and Dirichlet, a section on the transformations made on the structures, possible future developments of the project, and the applications.

Over the course of doing the project its title has changed from the original *Voronoi tessellation and porous media*, to *Division of space by Voronoi graphs, application to the models of porous membranes*, then to *A twentieth-century definition of the ancient theme, Voronoi network and percolation in porous media*, and to *On suspension blockages of filtering membranes as continuum percolation under van der Waals influences in centroidal Voronoi networks*, and finally into the present name.

I have observed that a Voronoi cell in three dimensions always have vertices and edges in an integral multiple of two and three respectively. I found the reason for this and have given one proof for the first observation, and two for the second one (§ 3.7).

Related to the present study is the stress-strain analysis in the bonds of a Voronoi structure in three dimensions as well as the study of randomly placed rods. Also interesting is the problem of percolation of randomly placed squares, which he thought would be useful in the growth process of synthetic zeolites. The zeolite problem mentioned above I have found to be identical to the so-called *continuum percolation* of squares. I have developed an algorithm to solve this not only for squares but also for the general case of n-gons. The program uses some of the ideas behind the basic movements in the Ayudhàyạ sword fighting. The algorithm has been intuitively arrived at from my own experience of several years holding a square, hind shield in one hand while in another brandishing a Thai sword for a troupe when our sword school demonstrated for that matter. It was only afterwards that I found the rigorous proofs for all its parts. However, I have not carried the work further to three dimensions because, for one thing, I personally do not believe the crystal growing to be random. Crystals grown within the same solution should have some kind of quantum coordination which allows them to align themselves with one another when they meet. The random appearance seems to be only their various habits.

The nature of discoveries and progresses in science is according to Bacon (Francis Bacon, 1620) *a birth of Time rather than a birth of Wit.* This is the same idea of percolation and the description he gave is the very picture of the theory. According to him major scientific progresses come in revolutions which are sparsely distributed in both time and regions. There have only been three periods of major progress out of the *five and twenty centuries over which the memory and learning of men extends*, namely the Greeks, the Romans and the nations of Western Europe. These are narrow limits of time, the periods in between of which are unfavourable to development. A discovery or an invention, then, comes as a chance accident in the scale of an individual, and as a certainty when looking from a distance.

When the time is right and all the hidden momentum built up, theories will come on by itself as a rule. This does not negate the excellence of an individual, but in a society where there are enough multitude of individuals the show will always go on, with or without a particular genius. This idea can very well explain cases of multiple discoveries. According to Kekulé in his *Benzolfest* speech in 1890, when he ascribed his conception of the cyclic nature of Benzene in dreams, *certain ideas at certain times are in the air* and *if one man does not enunciate them, other will do so soon afterwards.*

To see the relationship of this with percolation it is possible to look at two different things in turn, first at the discoveries and then at the discoverers. With a unit being that of a *discovery* the connection to percolation is that big discoveries come as connections of other smaller and less obvious ones. A theory often has more than one perspective, and which one of them comes to the fore first depends much on which combination happens to percolate through first. The discoveries of Schrödinger and Heisenberg in Quantum Physics can bear witness to this both in the *combination* and the *multiple discoveries* parts of this argument.

Let us turn our attention now to the scientist and look at the one who does the discovering instead. The theory of percolation tells us that at the point of discovery he is by no mean the sole integral ingredient. If he does not do it, then someone else will certainly do. In order to see this, I did four simulations for the cell, bond, vertice, and edge percolations on a two-dimensional Voronoi network and then another four with the same respective blockage of each case but considering the

‡ In one variation, $n \leq 5$.

inverse phase instead. The number of units considered for the four cases are $n_c = 200$, $n_b = 416$, $n_v = 298$, and $n_e = 426$. With the order of simulations as described above, at just one step before percolation occurs there are respectively 10.6, 13.4, 11.5, 1.1, 11.24, 10.0, 19.4, and 7.9 percents among the remaining units which will readily trigger the onset of percolation. In other words, these are atoms which are able to link up existing clusters and form a percolating cluster.

The formation of mobs is an interesting phenomenon comparable with phase change in physics. What happens is that an agglomerate of individuals becomes one and a single creature, the underlying mechanism of which still baffles any effort towards understanding it. Likely enough it has got something to do with psychology and the mind. But to me at least, the phenomenon is percolative. Having gained some acceptance from my previous writings (Tiyapan, 1995–1996, KNT3(iv), KNT4(i) and [kbukt]; respectively §'s E.5, E.6 and E.7 of Tiyapan, 2003, KNT8(iii)) I gave my new work which briefly discusses the mechanism underlying the formation of mobs to an editor of the Sakkayaphab journal whom I know. At that time a political turmoil unequal in its degree and extent has been going on for five years. Whether by fate or by design there has been a successful but tragic use of mob in Bangkok. The word *mob* has joined the list of those synonym to *distrust*, namely *communist* or, in western community now for that matter, *Islam* and *evil*. Whether because of this or something else, the article (Tiyapan, 1996, KNT4(vii); or § E.15 of Tiyapan, KNT8(iii)) simply and mysteriously got lost; no one would admit having seen it, and the translation of another subsequent article of mine (1996, KNT4(viii); or § E.16 of Tiyapan, KNT8(iii)) has not been without a noticeable negligence. Thus to me distrust is also percolative. The list of things one finds over-distrusted without reasonable explanation goes on indefinitely, homosexuality, communism, *etc.* The same seems to be the case with bad habits. My father used to teach me using the following poem,

> Bad habit gathers by unseen degree
> like brook makes river, river runs to sea.

Looking back, it could have been the title of that article, *on pragmatists and idealists*, which has somehow convinced the editors into believing that it was political which to me is nonsensical. I only meant literary, even if at times philosophical. I include it here because it contains a curve showing a critical emotional transition.

The formation of the United States, the European Union, or the Commonwealth comes from the trust which acts to join countries together like glue boxes in TEX. Like all binding forces, trust is mutual and spreads in the same way as a growing cluster does. The cluster grows bigger as one or more members are added, and it becomes stronger as the level of the mutual trust increases. In a similar way, distrust is also mutual and also spreads. If I distrust you and you distrust me, I will make sure that I remain as far away from you as possible while you will certainly avoid me by all means in return.

Only these two are possible, so there are only two phases to consider, that of trust and distrust. The relationship where one trusts while the other distrusts would not be stable, since the former will soon learn to join the latter. Trust forms clusters of one phase, distrust another. The size of these clusters vary in a way similar to those in percolation of geometrical networks. The strength of the glue is analogous to the probability either of becoming or remaining a member of a cluster.

The rise of dictators, the proliferation of weapons of mass destruction, *etc*, these things I believe are the products of changes of something hidden within the underlying structure. Unless we find out what is happing in the background, these things will unavoidably occur. I believe that this unseen thing behind the scene is governed by some phenomena similar to that of percolation. I think that the key towards understanding many unexplainable phenomena is to investigate, in the light of the percolation theory, the working of agglomeration of countries or states like those of the United States and the European Union.

The believe that scientific discoveries are a birth of time, rather than of wit (*cf* Larsen, 1993), is the same as the idea of percolation. We know because we remember. And all the various discoveries of our time together with the knowledge we possess of the past bring us closer to another discovery. Scientific discoveries, then, is the collective product of humanity rather than property of a single person (*cf* Merton, 1965).

And because all species are also the product of percolation in time, our knowledge and consciousness, too, are the product of the universe. One may say that it is a personification when we refer to a collective noun, for instance a mob, as an individual. But the truth is that, under the percolation theory, it is in fact a separate individual without any need for the use of a simile. The renormalisation group theory tells us that there exists a structure in a bigger scale that behaves like the individual components that comprise it. It seems, therefore, that for humans these collective

beings of ours are still primitive compared with each of us as an individual. This is the reason why, whenever we come together, we alway make wars. In our case, then, we seem to be conscientiously percolated only individually not collectively. In the case of bees, on the other hand, it is the other way round. This is why a colony of bees does things which make far better sense than a bee does. But one can not say that even a *colony* of bees has consciousness, because there seems to be no morals in what it does. I do not know whether there are other beings in the universe both the collective and individual beings of whom have percolated conscientiously. But I believe they exist, in which case they should be more intelligent than us, though this is by no means necessarily the case.

## § 1.1 Mathematics

A map, denoted by $f : \mathrm{X} \mapsto \mathrm{Y}$, is an assignment of an image $y$ in the target Y to a preimage $x$ in the source X, where $f$ is called a function and $f(x) = y$. A composition of $f : \mathrm{X} \mapsto \mathrm{Y}$ and $g : \mathrm{Y} \mapsto \mathrm{Z}$ is the map $h : \mathrm{X} \mapsto \mathrm{Z}$ such that $h(x) = g(f(x))$ for every $x$ in X. There are three types of function, each one having at least three names. Table 1.1 lists these three types together with the sources of their various names. The prefix *epi-* in Greek means *on* and *isos-* means *equal*.

| *Anglo-Saxon* | | *Greek* | | *Latin* | |
|---|---|---|---|---|---|
| an to an | one to one | monomorphos | monomorphism | injectus | injective |
| on to | onto | epimorphos | epimorphism | superjectus | surjective |
| an to an and on to | 1–1 and onto | isomorphos | isomorphism | bijectus | bijective |

**Table 1.1** *Three types of function and the source of their names.*

A concrete category is a set of function that is closed under composition and contains the identity map for every source and target. The maps in $C$ are the morphisms of a category $\mathcal{C}$, and both its sources and targets are objects. The topological category $\mathcal{T}$ is a category of topological spaces and continuous maps.

Furthermore, a functor is a map of categories which preserves composition and takes identities to identities. A covariant functor has $F(f \circ g) = F(f) \circ F(g)$, whereas a contravariant functor has $F(f \circ g) = F(g) \circ F(f)$. Homology is a covariant functor from $\mathcal{T}$ to the category of abelian groups and homomorphisms, while cohomology is a contravariant functor from $\mathcal{T}$ to the category of rings and ring homomorphisms.

A relation is an equivalent relation, denoted by $\sim$, if and only if three axioms, namely that of reflexivity, symmetry and transitivity are satisfied. A set of all $x$ in $A$ such that $x \sim a \in A$ is the equivalence class of $a$. A partition of $A$ is formed by the set of equivalence classes of equivalence relations, and is a family of disjoint subsets of $A$ covering $A$. Then $A$ is the union of the equivalence classes, and each equivalence class has an empty intersection with any other. That is, every $a$ in $A$ is also in an equivalence class $E(a)$, and $E(a) \cap E(b) \neq \emptyset$ implies that $E(a) = E(b)$. Conversely, every partition of $A$ gives an equivalence relation on $A$, and $a$ is equivalent to $b$ if and only if $a$ and $b$ are in the same subset of the partition.

With the discovery of the equation $f_0 - f_1 + f_2$ by Euler in 1752 a new era of mathematic began, and that is the era of topology. The Euler's equation in its equivalent forms are written as $\sum_{i=0}^{d}(-1)^i f_i(P) = 1$ or $\sum_{i=-1}^{d}(-1)^i f_i(P) = 0$ (*cf* Grünbaum, 1967).

Partitions of numbers in the theory of numbers (*cf* Hardy and Wright, 1979) has a similar idea to what we shall do in § 6.11 for finding the Voronoi sections and their grids. Moreover, the random nature of these two problems, that is percolation and the number theory, as well as their omnipotence seem to point out that there could be some closer relationship between the two than mathematicians and physicists believe at present.

Also there is another similarity between these two fields, that is both are easy to state but very difficult to solve.

Sphere packing studies the density of packings of hard spheres. Here the kissing number problem studies the number of spheres that can be arranged such that all of them touch one central sphere of the same size. In other words it is the maximum number of neighbours that a sphere can have. It is also called the ligancy or Newton-, contact or coordination numbers.

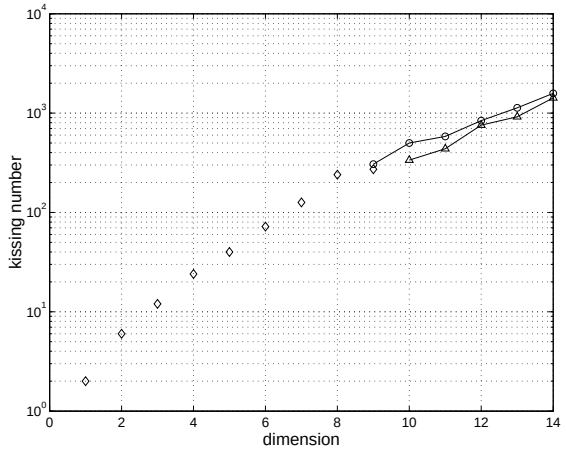


For $n$ dimensions the lower bound for the kissing number is $\eta = \zeta(n)/2^{n-1}$, where

$$\zeta(n) = \frac{1}{\Gamma(n)} \int_0^\infty \frac{x^{n-1}}{e^x - 1} \mathrm{d}x$$

is the Riemann zeta function. In Figure 1.1 the a diamond symbol represents an exact value for a lattice, a triangle the lower bound for a lattice, while a circle the lower bound for a nonlattice. The lines linking these symbols are for the ease of look only.

**Figure 1.1** Kissing number versus dimension.

On the other hand, the covering problem is a problem that tries to find the least dense way to cover a space in $n$ dimensions with overlapping spheres of the same size while the quantising problem studies how to place points in such a way that minimise the average second moment of their Voronoi cell, which finds application in the conversion from analogue to digital (Conway, 1988). In two dimensions the hexagonal lattice solves the packing, kissing, covering and quantising problems. But the packing problem of hard spheres is still unsolved. Everybody knows that the solution is approximately 0.7405 or exactly $\pi/3\sqrt{2}$ but no one has been able to prove it.

For any lattice the fundamental polytope, *i.e.* a polytope consisting of points $\sum_i^n \theta_i \nu_i$ where $0 \leq \theta_i < 1$, is its fundamental region. The proportion of space occupied by the spheres is the volume of one sphere divided by the volume of fundamental region, while the latter quantity is equal to $(\det \Lambda)^{1/2} = \det M$. Here $M = [\nu_{i,j}]$, $1 \leq \nu_{ij} \leq m$, is the generator matrix for lattice $\Lambda$ and each $\nu_i$ is a basis vector having $\nu_{ij}$ coordinates.

## § 1.2 Geometry

If the equation of a plane be $ax + by + cz + d = 0$, then $(a, b, c)^T$ is a vector normal to it and the parametric equations of this line is $x = at + p$, $y = bt + q$ and $z = ct + r$, $t \in R$, and $(p, q, r)$ is a point on the line.

The simplest geometrical figure is a circle while the simplest of all polygons is a triangle. The degree of freedom of triangles increases from the equilateral to the isosceles and the right triangles to the scalene triangles. While spending the summer of 1990 in a traineeship through AIESEC the author was introduced to a geometrical puzzle which, as he later knew, is called the *flexatube*. It could have come from ancient China. This puzzle is made up of sixteen right isosceles triangles tiled into four squares, each comprising of four triangles, which are in turn joined together to form a loop. It can be easily made up using some hard papers, a pair of scissors and cello tape. There are in total twenty hinges, four of which are as long as the hypothenuse while the other sixteen have their length equal to the shorter side of the triangle. By turning these rigid triangles upon their hinges the inside surface of the strip can become the outside and vice versa. Tiyapan found one solution and later on the same year learnt about another. It has not yet been proved whether these two are the only possible solutions. Geometry plays not a small part in our everyday's life, for instance the symbol for the men's toilets in Budapest is an equilateral triangle, while that for women's toilets is a circle. Thus the geometrical information, having passed through the eyes, goes directly to the brain and we understand with no words being needed.

The median of a triangle is the line joining its vertex with the mid point of the opposite side. All the medians of a triangle intersect one another at its centroid. The lines connecting all mid points of a triangle divide it into four equal triangles. Let the length of the median from the corner $A$ to its opposite side $a$ of a triangle be $m_a$, then $m_a = (2b^2 + 2c^2 - a^2)^{1/2}/2$, and similarly for $m_b$ and $m_c$. We have the relations $\mathrm{A}(\triangle m_a m_b m_c) = 3\mathrm{A}(\triangle abc)/4$, where $\mathrm{A}(\triangle\cdot)$ is the area of a triangle, and $m_a^2 + m_b^2 + m_c^2 = 3(a^2 + b^2 + c^2)/4$.

One end of a median is at a vertex, the other one at the mid point of a side. The lines which bound the first ones is the triangle itself, those which join the second ones create the medial triangle. A bisector of a medial triangle divides the perimeter of the original triangle into two equal parts.

The incentre of the medial triangle, the Spieke point, is the c.g. of the wire-framed triangle $\triangle ABC$. The incentre, the geocentre and the Spieke point, all lie on a single straight line. The geocentre on the Euler line is one third away from the circumcentre to the orthocentre, that point where the altitudes of the triangle intersect.

In general dimension we talk about spheres. A sphere in $d$ dimensions has its volume, $V$, proportional to $r^d$ and its surface, $A$, to $r^{d-1}$, so that $V \propto A^{d/(d-1)}$.

The area of sphere in three dimensions is $A = 4\pi r^2$ and the volume $V = \frac{4}{3}\pi r^3$. When $V = 1$, $r = -(-3/\pi)^{1/3}/2^{2/3}$, $(3/\pi)^{1/3}/2^{2/3}$, or $(-1)^{2/3}(3/\pi)^{1/3}/2^{2/3}$ which are numerically $-0.310175 - 0.537239\imath$, $0.62035$, $-0.310175$, $-0.310175 + 0.537239\imath$ in that order. Therefore $\alpha = A|_{V=1} = 6^{2/3}\sqrt[3]{\pi} = 4.83598$

When $V = 8$, $r = (6/\pi)^{1/3}$ and therefore $A = 46^{2/3}\pi^{1/3} = 19.3439$. In order to find $\alpha$, the surface area per unit volume, one divide the area by $V^{2/3}$, in other words $\alpha = V^{1/3} \cdot A/V = A/V^{2/3}$.

The same is true for other polyhedra. For example in a tetrahedron where $x$ is the length of the side, the vertices can be $(0,0,0)$, $(x,0,0)$, $\left(\frac{x}{2}, \frac{\sqrt{3}}{2}x, 0\right)$, $\left(\frac{x}{2}, \frac{\sqrt{3}}{6}x, \frac{1}{2}\sqrt{\frac{93}{35}}x\right)$. When $V = 1$, one can obtain $x$ by solving the equation

$$1 = \frac{1}{6}\,\mathrm{abs}\begin{pmatrix}\begin{vmatrix} 0 & 0 & 0 & 1 \\ x & 0 & 0 & 1 \\ \frac{x}{2} & \frac{\sqrt{3}}{2}x & 0 & 1 \\ \frac{x}{2} & \frac{\sqrt{3}}{6}x & \frac{1}{2}\sqrt{\frac{93}{35}}x & 1 \end{vmatrix}\end{pmatrix}.$$

This gives $x = 2\left(\frac{35}{31}\right)^{\frac{1}{6}} = 2.0409$ as the only real positive answer. When $x$ is doubled, $V$ increases from 1 to 8, which means that one would be dividing $A$ by $V^{\frac{2}{3}}$ to obtain $\alpha$.

The perimeter of a triangle is $s = 3d_e$ and the area $A = (\sqrt{3}/4)l^2$. When $A = 1$, $d_e = \pm 2/3^{1/4} = \pm 1.51967$. Therefore $s = 4.55901$.

Vertices shared by two cells make up a common face between them. Two way have been tried for finding the edges. The first one was by looking at all neighbouring cells of every cell in turn three at a time. The edges are then made up of those vertices that are common among these three cells. Only those edges which have exactly two vertices are considered. They are called *good edges* as contrasted with edges on the boundary. This is a much longer way than the second one, which is to consider vertices common to any two faces of a cell. Similar to the first case, such vertices forms a good edge if and only if there are only two of them. The two methods above give exactly the same list of edges, so they confirm each other. It has been tested that all edges having more than two vertices are boundary ones, that is they have at least one vertex outside the boundary of the unit cube considered.

By drawing some of the cells as a solid using *fill* command it has been tested that the result from `convhull` covers the entire cell surface. This confirms the step where areas are calculated.

The hexagon or honeycomb is perhaps the pattern which is most frequently found in nature. Even though the world we live in is three-dimensional, cells normally divide and spread in two dimensions in the form of layers. Moreover, they are packed in these layers in patterns which most often resemble the honeycomb (*cf* Williams and Bjerknes, 1972).

An octagon is an eight-sided polygon. It is the shape of the cross section of every chimney in the mills built in Manchester during its industrial era of the nineteenth century, as well as that of the terrets in the Main Building of UMIST. Perhaps one of the reasons for its popularity is that it looks strong while having the style of a good taste. May be the reason why it looks strong is that it possesses eight axes of symmetry, on top of another symmetry around the origin.

There are nine regular polyhedra. Among these are five regular convex solids known to the ancient Greek called Platonic polyhedra. They are tetrahedron, cube, dodecahedron, octahedron, and icosahedron. They have regular congruent faces and regular polyhedral angle vertices. Their face angles and their dihedral angles at every vertex are equal. The other four regular polyhedra have only been discovered much later and are not convex. They are called the Kepler-Poinsot polyhedra and are nonconvex. The small stellated dodecahedron and the great stellated dodecahedron were found by Kepler (1571–1630). The great icosahedron and the great dodecahedron were found by Poinsot (1777–1859). The small stellated dodecahedron and the great dodecahedron do not satisfy Euler's equation. The process of creating it by extending nonadjacent faces until they meet is called *stellating*. There are also polyhedra called quasi-regular.

The semi-regular polyhedra are called the Archimedean polyhedra. Here all faces are regular polygons but not all are of the same kind. Every vertex is congruent to all others. They comprise of an infinite group of prisms, an infinite group of antiprisms or prismoid, and another thirteen polyhedra. Each prism or prismoid is made up of two regular polygons on parallel planes where the vertices are aligned in the former case or shifted half way to the next neighbouring vertices in the latter case. Each vertex in prisms is joined to a corresponding vertex of the opposite polygon, while in prismoid it is joined to two corresponding vertices. All faces of an Archimedean solid are regular and all its polyhedral angle vertices congruent.

On the other hand the Archimedean duals have the property that all their faces are congruent to one another and all their polyhedral angles regular. These solids are important in crystallography. They are vertically regular and include an infinite group of dipyramids, an infinite group of trapezohedra, and additionally thirteen other polyhedra.

The surface area per unit volume $\alpha$ of a solid can be computed from the actual volume $V$ and the actual surface area $A$ as $\alpha = V^{1/3}A/V = AV^{-2/3}$. Another way of finding the perimeter per unit area of an $n$-gon follows the steps listed in Algorithm 1.1. Here $\theta$ is the angle made by the lines from the centre of gravity of an $n$-gon to its two consecutive vertices, $\alpha$ half the angle between two edges, $h$ the distance from the c.g. to each edge, that is the height of one of the $n$ identical triangles all of which have a vertex at the c.g., $a$ the area of each of such triangles, $A(d)$ the area of the $n$-gon in terms of the edge length, $s$ the perimeter and $d$ the edge length $d_e$. Algorithm 1.1, however, may be reduced to two steps, namely solving for $(nd^2/4)\tan[(n-2)\pi/(2n)]$ and then $s = nd$. Of course, if $n$ increases towards infinity then $s$ approaches $2\sqrt{\pi} \approx 3.5449$.

**Algorithm 1.1** *Perimeter per unit area of regular polygons.*

$\theta \leftarrow 2\pi/n$;
$\alpha \leftarrow (\pi - 2\pi/n)/2$;
$h \leftarrow (d/2)\tan\alpha$;
$a \leftarrow (1/2)dh$;
$A(d) \leftarrow na$;
**solve** $A(d) = 1$ **for** $d$
$s \leftarrow nd$; □

| *Polygon* | $n_e$ | $A$ | $s$ *(numerical)* |
|---|---|---|---|
| Triangle | 3 | $(\sqrt{3}/4)d^2$ | 4.55901 |
| Square | 4 | $d^2$ | 4 |
| Pentagon | 5 | $5(1+\sqrt{5})d^2/\left[4(10-2\sqrt{5})^{1/2}\right]$ | 3.8119 |
| Hexagon | 6 | $3\sqrt{3}d^2/2$ | 3.7224 |
| Heptagon | 7 | $(7/4)d^2\tan(5\pi/14)$ | 3.6721 |
| Octagon | 8 | $2d^2\tan(3\pi/8)$ | 3.6407 |
| Nonagon | 9 | $(9/4)d^2\tan(7\pi/18)$ | 3.6198 |
| Decagon | 10 | $5\left[(5+\sqrt{5})/2\right]^{1/2}d^2/(-1+\sqrt{5})$ | 0.3605 |
| Undecagon | 11 | $(11/4)d^2\tan(9\pi/22)$ | 3.5944 |
| Dodecagon | 12 | $3(2+\sqrt{3})d^2$ | 3.5863 |

**Table 1.2** *Perimeter per unit area of n-gons.*

In a similar fashion the surface area and volume of regular solids can be found, but first we need to know more about these solids. Table 1.3 lists some of the important properties of regular solids. Here cyc$(\cdot)$ is the cyclical permutations and $\tau = (1+\sqrt{5})/2$, *i.e.* the golden ratio. Regular polyhedra can also be represented by Schlafi's symbol as $\{p, q\}$ where $p$ and $q$ are respectively the face- and vertex figures.

| *solid* | *aka* | $n_v$ | $n_e$ | $n_f$ | $x_v$ | $d_e$ | $r_v$ | $r_e$ | $r_f$ | *dual* |
|---|---|---|---|---|---|---|---|---|---|---|
| tetrahedron | 3\|2 3 | 4 | 6 | 4 | $(\pm1,\pm1,\pm1)$ even or odd -1's | $2\sqrt{2}$ | $\sqrt{3}$ | 1 | $1/\sqrt{3}$ | itself |
| cube | 3\|2 4 | 8 | 12 | 6 | $(\pm1,\pm1,\pm1)$ | 2 | $\sqrt{3}$ | $\sqrt{2}$ | 1 | octahedron |
| octahedron | 4\|2 3 | 6 | 12 | 8 | cyc$(\pm1,0,0)$ | $\sqrt{2}$ | 1 | $1/\sqrt{2}$ | $1/\sqrt{3}$ | cube |
| dodecahedron | 3\|2 5 | 20 | 30 | 12 | cyc$(0,\pm\tau,\pm1/\tau)$, $(\pm1,\pm1,\pm1)$ | $2/\tau$ | $\sqrt{3}$ | $\tau$ | $\tau[(\tau+2)/5]^{1/2}$ | icosahedron |
| icosahedron | 5\|2 3 | 12 | 30 | 20 | cyc$(\pm1,0,\pm\tau)$ | $2\tau$ | $\sqrt{2+\tau}$ | 1 | $(6+5\tau)^{1/2}/3$ | dodecahedron |

**Table 1.3** *Some important properties of regular solids.*

The ratio between the edge length and distance to face, the surface area, the volume and the ratio between surface area and volume of some solids are shown in Table 1.4.

| *solid* | $d_e/r_f$ | $A$ | $V$ | $\alpha$ |
|---|---|---|---|---|
| Tetrahedron $(3^3)$ | $2\sqrt{6}$ | $24\sqrt{3}r^2$ | $8\sqrt{3}r^3$ | 7.2056 |
| Cube, $(4^3)$ | 2 | $24r^2$ | $8d^3$ | 6 |
| Octahedron, $(3^4)$ | $\sqrt{6}$ | $12\sqrt{3}r^2$ | $4\sqrt{3}r^3$ | 5.7191 |
| Dodecahedron,$(5^3)$ | $\frac{4\sqrt{10}}{(3+\sqrt{5})(5+\sqrt{5})}$ | $300\frac{2}{5-\sqrt{5}}^{\frac{1}{2}}\frac{(1+\sqrt{5})r^2}{25+11\sqrt{5}}$ | $100\left(\frac{2}{5-\sqrt{5}}\right)^{\frac{1}{2}}\frac{(1+\sqrt{5})r^3}{25+11\sqrt{5}}$ | 5.3116 |
| Icosahedron, $(3^5)$ | $3(1+\sqrt{5})\left[6+\frac{5}{2}(1+\sqrt{5})\right]^{\frac{1}{2}}$ | $180\sqrt{3}\frac{(3+\sqrt{5})r^2}{17+5\sqrt{5}}$ | $60\sqrt{3}\frac{(3+\sqrt{5})r^3}{17+5\sqrt{5}}$ | 8.0484 |
| Sphere | $\infty$ | $4\pi r^2$ | $(4/3)\pi r^3$ | 4.8360 |

**Table 1.4** *Surface area per volume of regular solids.*

Algorithm 1.2 finds the values given in Table 1.4. Here $p$ is the face figure, $n = n_f$ the number of faces, $r = r_f$ the distance from the centre of the polyhedron to each face, $d = d_e$ the edge length, $s = A/V$ and $\tau = \left[1+\sqrt{5}\right]^{1/2}/2$ the golden mean. Furthermore, $a$ and $v$ are respectively the area of each face and the volume of the pyramid whose base is the face and the apex of which is the centre of the polyhedron.

**Algorithm 1.2** *Area per volume of regular polyhedra.*

$\theta \leftarrow 2\pi$;
$\alpha \leftarrow (\pi - 2\pi/p)/2$;
$h \leftarrow d\tan\alpha/2$;
$a \leftarrow pdh/2$;
$v \leftarrow ar/3$;
$A(r) \leftarrow na$;
$V(r) \leftarrow nv$;
**solve** $V = 1$ for $r$;
$s(r) \leftarrow A(r)/V(r)$; □

Since Algorithm 1.2 will be used to proof Theorem 1.1, we shall give it a formal proof.

**Proof.** Each face of a regular polyhedron is a regular polygon by definition. The lines connecting the centre and c.g. of a face with all its vertices divide $2\pi$ radian into $p$ equal portions, where $p$ is the face figure. Each portion then represents the angle in radian made by two consecutive vertices of the face as seen from its centre. Let this angle be $\theta$, then it follows that $\theta = 2\pi/p$. From the symmetry around the c.g., all these angles together with the sides of the face form $p$ identical isosceles triangles whose two equal triangles are at the vertices of the face. Moreover, this angle, $\alpha$, is half the internal angle of a face vertex. Then, because we know that all the internal angles of a regular polygon sum up to $2\pi(n-1)/n$ radian, it follows that $\alpha = (\pi - 2\pi/p)/2$. The area of each face is therefore $a = p(d_e h/2)$, where $h = (d_e/2)\tan\alpha$ is the distance from the centre of the face to its edges. The volume of the pyramid which have the face as its base and the c.g. of the polyhedron as its apex is thus $v = ar_f/3$, and the polyhedral surface area and volume are respectively $A = n_f a$ and $n_f v$. Comparing the above with Algorithm 1.2 completes the proof. □

From the results in Table 1.4 we can see that the sphere has the ratio $\alpha$ less than every regular polyhedron; in fact one could conjecture that it has the smallest $s$ of all solids. Icosahedron, on the other hand, is a regular polyhedron which has maximised $\alpha$. So now we know, for instance, that a virus wants to maximise its surface area.

The ratio $\alpha$ here is not simply obtained by dividing the surface area by the volume of a solid, as Algorithm 1.4 also tells. We take the volume of a solid to be the unity first, then proceed to find its correspondent surface area. As an example to show that these two values are not the same, consider an icosahedron whose $d_e = 2\sqrt{2}$ and $r_f = 1/\sqrt{3}$. From the values of $d_e$ and $r_f$ the surface area and volume are respectively 362.765 and 37.8252, which result in $A/V$ being 9.5906 which is not the same as our $\alpha$.

The numerical ratios given in both Tables 1.4 and 1.4 are rounded approximates, to make them easier to read. The exact values can easily be obtained by following the steps of calculation in Algorithms 1.2 and 1.2.

After having worked with Algorithm 1.4 it turns out that $\alpha$ depends on $r_f$. A little investigation confirms this, and Theorem 1.1 arises as a result. A platonic solid is a regular solid and vice versa.

**Theorem 1.1.** *Let $\alpha$ be the surface area of a Platonic solid and $r_f$ the distance from its centre to each face. Then $\alpha r_f = 3$.*

**Proof.** There are five and only five such solids, therefore we find $\alpha$ of every one of them. Assuming that Algorithm 1.2 together with the resulting $A$'s and $V$'s shown in Table 1.4 are correct. Then

simply divide each $A(r)$ by the corresponding $V(r)$ for the regular solids from the table to get $\alpha = A(r)/V(r) = 3/r$. □

Collorary 1.1[1] follows immediately from Theorem 1.1 and the definition of $\alpha$, but such interesting consequence as it is deserves being called a collorary.

**Corollary 1.1[1].** *In a regular polyhedron,* $Ar_f = 3V$.

The duality among regular polyhedra is shown in Table 1.4. In particular, the tetrahedron is dual to itself, the octahedron and the cube are dual to each other and likewise the dodecahedron and the icosahedron. The icosahedron is a popular shape among viruses. As regarding duality, it is worth noting that all pyramid are self-dual.

Deltahedra are polyhedra which have all faces equilateral triangles. They have $2n$ faces, $3n$ edges and $n + 2$ vertices. There are eight deltahedra, namely regular tetrahedron (4 faces), triangular dipyramid (6), regular octahedron (8), pentagonal dipyramid (10), snub disphenoid (12), triaugmented triangular prism (14), gyroelongated square dipyramid (16) and icosahedron (20).

A cube is sometimes called a hexahedron because it has six faces. But there are other polyhedra which also have six faces, for instance the triangular dipyramid (5 vertices, 9 edges), the pentagonal pyramid and the tetragonal antiwedge (6, 10), the hemiobelisk and hemicube (7, 11) and the pentagonal wedge (8, 12).

| *polyhedron* | $n_v$ | $n_e$ | $n_f$ |
|---|---|---|---|
| antiprism | $2n$ | $4n$ | $2n+2$ |
| antiwedge | $2n-2$ | $4n-6$ | $2n-2$ |
| cupola | $3n$ | $5n$ | $2n+2$ |
| cupola pyramid | $3n+1$ | $7n$ | $4n+1$ |
| cupolarotunda (ortho-, gyro-) | $5n$ | $10n$ | $5n+2$ |
| deltohedron | $2n+2$ | $4n$ | $2n$ |
| dipyramid | $n+2$ | $3n$ | $2n$ |
| hemiprism | $2n-1$ | $3n-1$ | $n+2$ |
| ortho(,gyro-)bicupola | $4n$ | $8n$ | $4n+2$ |
| ortho(,gyro-)birotunda | $6n$ | $12n$ | $6n+2$ |
| prism | $2n$ | $3n$ | $n+2$ |
| pyramid | $n+1$ | $2n$ | $n+1$ |
| rotunda | $4n$ | $7n$ | $3n+2$ |
| rotundapyramid | $4n+1$ | $9n$ | $5n+1$ |
| wedge | $2n-2$ | $3n-3$ | $n+1$ |

**Table 1.5** *The number of vertices, edges and faces of some polyhedra*

The nearest neighbour and minimum spanning tree have been applied to the problem of taxonomy in botany. Clayton (1972), working on the characters of plants to manually classify them (*eg* Clayton, 1970) with the use of only the binary dendrogram and trial and error, adopted a numerical method which finds the minimum spanning tree in a multi-dimensional character space. Since taxonomy can be considered as a kind of dictionary, it is possible to apply a similar approach to machine translation and the compilation of dictionaries.

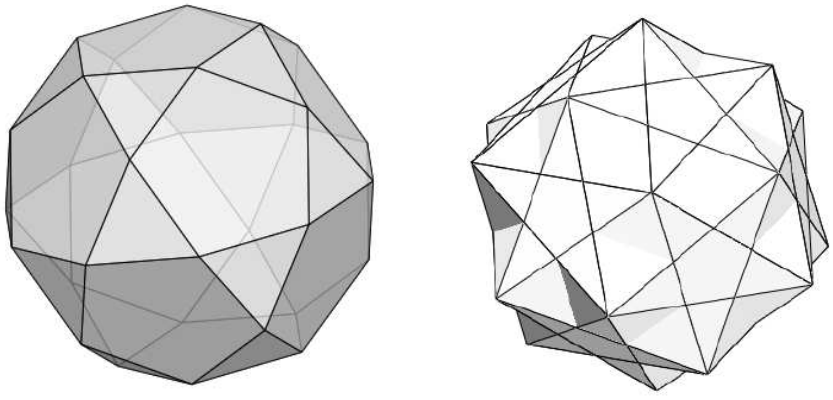

(a) (b)

**Figure 1.2** (a) *Icosidodecahedron, rhombic triacontahedron,* 2|3 5. (b) *Small ditriagonal icosidodecahedron, small triambic icosahedron,* 3|5/2 3

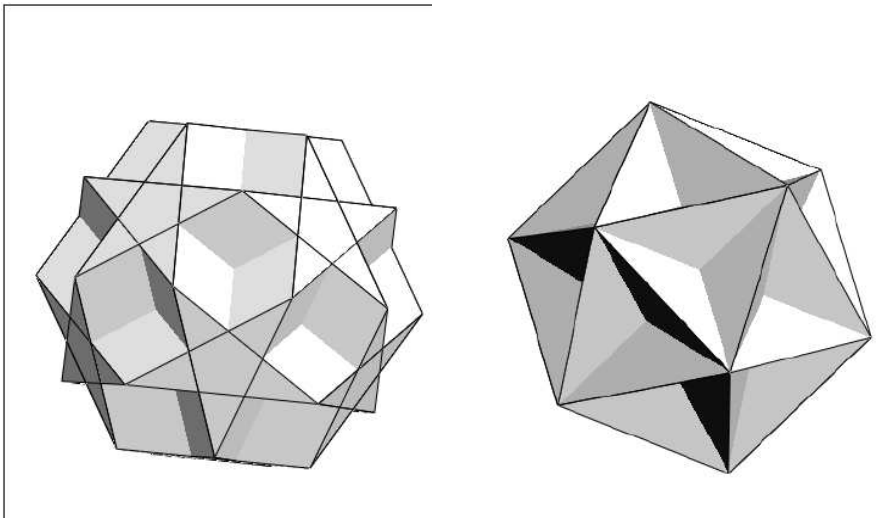

(a) (b)

**Figure 1.3** (a) *Great dodecadodecahedron, medial rhombic triacontrahedron,* 2|5/2 5. (b) *Great dodecahedron, small stellated dodecahedron,* 5/2|2 5

The polyhedra from Figure 1.4 to 1.6 are semi-regular.

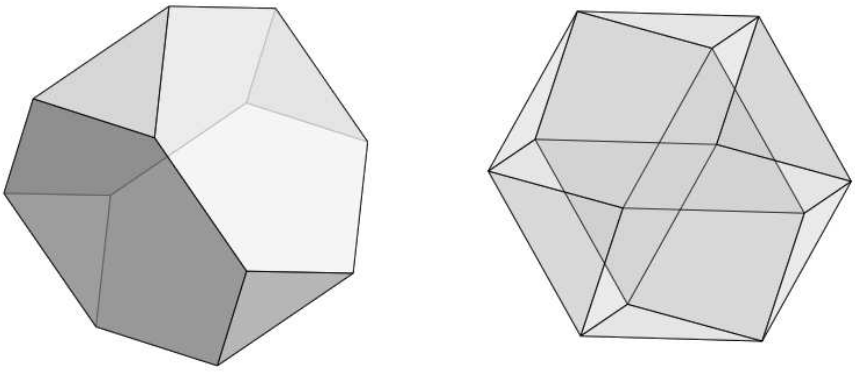

(a) (b)

**Figure 1.4** (a) *Truncated tetrahedron, triakistetrahedron,* 2 3|3. (b) *Octahemioctahedron, octahemioctacron,* 3/2 3|3

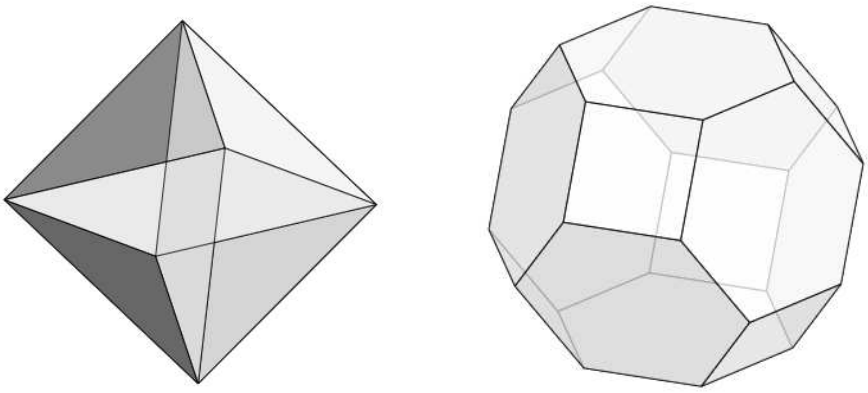

(a) (b)

**Figure 1.5** (a) *Tetrahemihexahedron, tetrahemihexacron,* 3/2 3|2. (b) *Truncated octahedron, tetrakishexahedron,* 2 4|3

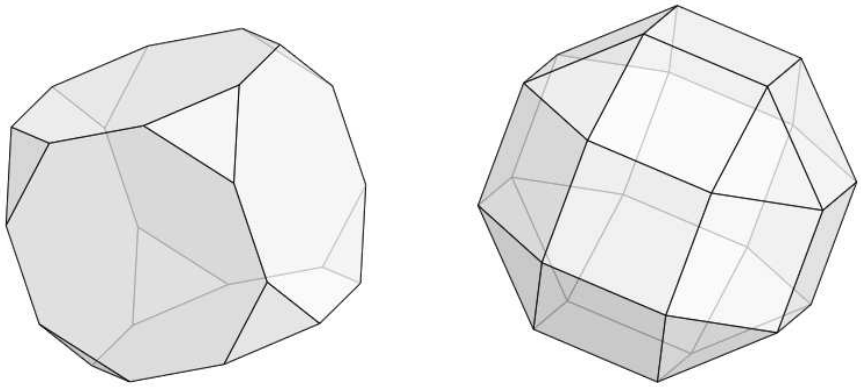

(a) (b)

**Figure 1.6** (a) *Truncated cube, triakisoctrahedron,* 2 3|4. (b) *Rhombicuboctahedron, deltoidal icositetrahedron,* 3 4|2

Polyhedra in Figure 1.7 are snub polyhedra.

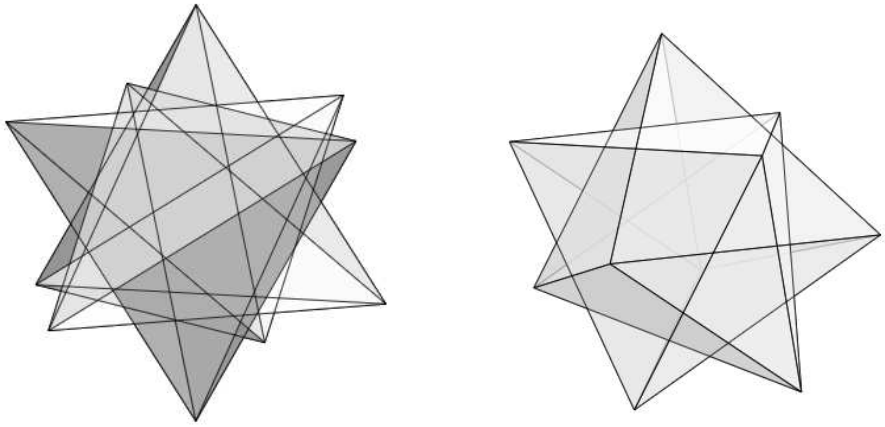

(a) (b)

**Figure 1.7** (a) *Pentagrammic crossed antiprism, pentagrammic concave deltohedron,* |2 2 5/3. (b) *Pentagrammic antiprism, pentagrammic deltohedron,* |2 2 5/2

The surface of Fullerene is made up of pentagons six-sided figures. Its shape represents that of the geodesic domes developed by Buckminster Fuller, and hence the name *Fullerene*. The latter may either be hexagons or figures all the six sides in each one of which form two sets of three sides having an equal length. The simplest Fullerene, the carbon-60 molecule, has the same shape as that of a football and a handball. With some thought the reason for this is not difficult to see. With its thirty-two faces it closely resemble the sphere. Also the two different shapes of all its components are symmetrically distributed and therefore enable colouring with only two different colours, namely one for each of the two shapes. To see how this helps, suppose one made a football in the shape of a bloated dodecahedron. Then it would be impossible to colour it using more than one colour at the same time of giving it a symmetrical appearance when viewed from more than a few directions. With the fullerene shape and the colouring scheme mentioned, however, the football looks symmetrical when viewed from 54 different directions symmetrically distributed around it. These directions corresponds to those when one looks at it in the direction perpendicular to the centre of each of its faces and when in the direction through the middle of each of the 22 edges lying between two hexagonal faces.

Making polyhedron models is an educating experience. Contrary to the general believe that you need to make an accurate drawing for the required parts (Wenninger, 1971), this needs not be so. Examples of this are the origami models of polyhedra where complex polyhedron structures are

made from interlocking pieces each of which is made by folding a piece of paper of a rectangular or square shape.

A set of elements with the sum and the product of any two elements defined is a commutative ring if under these two operations it satisfies the following postulates: closure, uniqueness, commutative, associative, and distributive laws, identity (zero and unity), and additive inverse. An integral domain is an ordered domain if its positive elements satisfy the laws of addition, multiplication, and trichotomy. A subset of an ordered domain is well-ordered if every nonempty subset of it contains a smallest member. $a|b$ means that $.b$ is divisible by $a$. The Euclidean algorithm or division algorithm states that $a = bq + r, 0 \leq r < b$. Two integers are relatively prime if their only common divisors are $\pm 1$. $a \equiv b (\mathrm{mod}\, m)$ if and only if $m|(a - b)$. The commutative ring $Z_2$ is the properties of multiplication and addition of even (0) and odd (1) numbers.

| $+$ | *0* | *1* |
|---|---|---|
| *0* | 0 | 1 |
| *1* | 1 | 0 |

| $\cdot$ | *0* | *1* |
|---|---|---|
| *0* | 0 | 0 |
| *1* | 0 | 1 |

The following is $Z_5$.

| $+$ | *0* | *1* | *2* | *3* | *4* |
|---|---|---|---|---|---|
| *0* | 0 | 1 | 2 | 3 | 4 |
| *1* | 1 | 2 | 3 | 4 | 0 |
| *2* | 2 | 3 | 4 | 0 | 1 |
| *3* | 3 | 4 | 0 | 1 | 2 |
| *4* | 4 | 0 | 1 | 2 | 3 |

| $\cdot$ | *0* | *1* | *2* | *3* | *4* |
|---|---|---|---|---|---|
| *0* | 0 | 0 | 0 | 0 | 0 |
| *1* | 0 | 1 | 2 | 3 | 4 |
| *2* | 0 | 2 | 4 | 1 | 3 |
| *3* | 0 | 3 | 1 | 4 | 2 |
| *4* | 0 | 4 | 3 | 2 | 1 |

There is a close link between geometry and algebra. Geometrical surfaces can be described as algebraical equations. For example, for circles and polygons the equations are binary quadratic, while for spheres and polyhedra they are ternary quadratic. Even one-sided surfaces can be described algebraically. The equation of Klein bottle, when deformed into a sphere with two circles removed and replaced by two cross-caps, is a quartic equation

$$a^2(x^2 + y^2)(b^2 - x^2 - y^2) = z^2(a^2x^2 + b^2y^2),$$

while the Steiner surface is also a quartic one

$$y^2z^2 + z^2x^2 + x^2y^2 + xyz = 0.$$

Two surfaces is homomorphic to each other if it is possible to continuously transform one into the other. All convex polyhedra are homomorphic to a sphere. The Steiner surface is homomorphic to the heptahedron, which is an Archimedean polyhedron with diametral plane.

In the plane, a second-degree equation gives either two straight lines, a circle, an ellipse, a parabola, or a hyperbola. In space, it can give two planes, cylinders and cones (circular, elleptic, parabolic, or hyperbolic), aphere, spheroid, ellipsoid, two hyperboloids, and (elliptic or hyperbolic) paraboloid.

*Partition*, *tessellation* and *division of space* are the same thing. In the context of set theory, a partition of set $X$ is a family of sets $A_1$, $A_2$, ..., $A_k$ which are subsets of $X$, such that $A_i \neq \emptyset$; $A_i \cap A_j = \emptyset$; $\bigcup_i A_i = X$, where $i$, $j = 1, 2, \ldots, k$ and $i \neq j$. (*cf* Berge, 1958) A further condition that makes any tessellation a Voronoi one is that, for all $i$ there exists a unique point $a_i$ within $A_i$ such that every point in $A_i$ is closer to $a_i$ than to any other $a_j$, $j \neq i$.

Voronoi tessellation in three dimensions can be constructed by imagining each region as a spherical cell growing outwards to meet neighbouring cells and continue growing to fill the gaps. The centre of each sphere is a unique nucleus point of the region such that it is closest to any point belonging to that region than any nuclei points. If the rate of growth is the same from every cell, the resulting partitions will be planes which can be described by ternary quadratic equations. However, if this rate differs from one cell to another, the partitions will be curved surfaces and the result is a non-Voronoi tessellation. It is possible to impose a constraint of minimum distance between neighbouring nuclei. Such cases can be looked at as spheres of an equal nonzero radius expanding away from nucleus centre points. If the radii differ from one sphere to another, or if some nonspherical solids are used instead of spheres, the tessellation obtained will be non-Voronoi.

Consider the case where all spheres are of equal size. If these spheres already touch their neighbours before the expanding starts, the case is that of packed spheres expanded to form a Voronoi tessellation. There are two types of close-packing: cubic (face-centred) and hexagonal. In both cases each sphere has twelve neighbours. Both cases have the same density, which is $\frac{\pi}{3\sqrt{2}}$. The Voronoi regions produced from the cubic case are rhombic dodecahedra and the faces are rhombuses.

In the case of hexagonal close-packing, the corresponding regions are trapezo-rhombic dodecahedra and the faces are either rhombics or trapezia. Where the spheres meet with their three neighbours in the layer above and their three neighbours in the layer below, the faces are rhombics. Where they meet with the six neighbours on the same layer they are trapezia.

For geometrical calculation, an example of a definitive book is that written by Salmon (1912).

The gamma function,

$$\Gamma(z) = \int_0^\infty e^{-t} t^{z-1} \mathrm{d}t, \quad \mathrm{Re}(z) > 0, \qquad (\mathbf{1})_\mathrm{i}$$

got its name from Legendre and is known as the Euler gamma function or simply the second Euler function. The formula $\Gamma(z+1) = z\Gamma(z) = z!$ recursively calculates the gamma function from, for instance, $\Gamma(1/5) \approx 4.5908$, $\Gamma(1/4) \approx 3.6256$, $\Gamma(1/3) \approx 2.6789$, $\Gamma(2/5) \approx 2.2182$, $\Gamma(1/2) = \sqrt{\pi} \approx 1.7725$, $\Gamma(3/5) \approx 1.4892$, $\Gamma(2/3) \approx 1.3541$, $\Gamma(3/4) \approx 1.2254$, and $\Gamma(4/5) \approx 1.1642$. The Stirling's formula was found by de Moivre which approximates the gamma function. The gamma function expansions is

$$\Gamma(x+1) = \lim_{k\to\infty} \frac{k^x 1 \cdot 2 \cdot 3 \cdots k}{(x+1)(x+2)\cdots(x+k)}, \qquad (\mathbf{2})_\mathrm{i}$$

and the gamma function of negative numbers can be obtained from

$$\Gamma(-z) = \frac{-\pi}{z\Gamma(z)\sin \pi z}. \qquad (\mathbf{3})_\mathrm{i}$$

The incomplete gamma function is

$$\Gamma(z,x) = \int_0^x e^{-t} t^{z-1} \mathrm{d}t = \int_x^\infty e^{-t} t^{z-1} \mathrm{d}t, \qquad (\mathbf{4})_\mathrm{i}$$

and the normalised or regularised incomplete gamma function is $\Gamma(z,x)/\Gamma(z)$

Archimedean solids are dual to Catalan solids. The fullerene $C_{60}$ is the truncated icosahedron, an Archimedean solid. Table 1.6 shows some statistics of the Archimedean solids.

| *Archimedean solid* | $n_v$ | $n_e$ | $n_f$ | *dual, Catalan solid* |
|---|---|---|---|---|
| truncated tetrahedron | 12 | 18 | 8 | triakis tetrahedron |
| cuboctahedron | 12 | 24 | 14 | rhombic dodecahedron |
| truncated cube | 24 | 36 | 14 | triakis octahedron |
| truncated octahedron | 24 | 36 | 14 | tetrakis cube |
| rhombicuboctahedron | 24 | 48 | 26 | deltoidal icositetrahedron |
| snub cube | 24 | 60 | 38 | pentagonal icositetrahedron |
| icosidodecahedron | 30 | 60 | 32 | rhombic triacontahedron |
| great rhombicuboctahedron | 48 | 72 | 26 | disdyakis dodecahedron |
| truncated icosahedron | 60 | 90 | 32 | pentakis dodecahedron |
| truncated dodecahedron | 60 | 90 | 32 | triakis icosahedron |
| rhombicosidodecahedron | 60 | 120 | 62 | deltoidal hexacontahedron |
| snub dodecahedron | 60 | 150 | 92 | pentagonal hexacontahedron |
| great rhombicosidodecahedron | 120 | 180 | 62 | disdyakis triacontahedron |

**Table 1.6** *Archimedean solids*

The analogue of polyhedra in four dimensions is sometimes called polychora, with the 4-d equivalent of the Euler-Descartes formula being $n_v - n_e + n_f - n_c = 0$ where $n_c$ is the number of its 3-d facets called cells. For dimensions higher than four the analogies are polytopes. An $n$-dimensional polytope is bound by hyperfaces of polytopes of $(n-1)$ dimension which join at hyperedges of $(n-2)$ dimensions.

The Euler characteristic $\chi$ is 1 for a point, invariant in a topological homeomorphism and additive for disjoint sets. For Euclidean space in $n$ dimensions, $\chi = (-1)^n$ as that of ordinary open polytopes. The $\chi$ of all ordinary closed polytopes is the $\chi$ of a closed $n$-dimensional ball, and $\chi = 1$ for any $n$ dimensions. If the hypercell itself, *i.e.* the interior of the polytope, is not counted then the right hand side of the formula becomes 2 when $n$ is odd and 0 otherwise, for example $n_v - n_e + n_f - n_c + n_t - n_p + n_h = 2$ in 7 dimensions, where $t$, $p$ and $h$ are respectively the tetrafaces (sometimes called hyperpoints), pentafaces (hyperedges) and hexafaces (hyperfaces).

As a revision of the sixth form mathematics, selections are *combination* if the order is irrelevant, and are *permutation* otherwise. The formula is for the former ${}^nC_k = n!/[n!(n-k)!]$, and ${}^nP_k = n!/(n-k)!$ for the latter.

Definitions which are useful when describing the time- and storage complexities of an algorithm are $O(f(n)) = \{g(n) : \exists c, n_0 \in R^+, g(n) \leq cf(n) \forall n \geq n_0\}$, $\Omega(f(n)) = \{g(n) : \exists c, n_0 \in R^+, cf(n) \leq g(n) \forall n \geq n_0\}$, $\theta(f(n)) = \{g(n) : \exists c_1, c_2, n_0 \in R^+, c_1 f(n) \leq g(n) \leq c_2 f(n) \forall n \geq n_0\}$ and $o(f(n)) = \{g(n) : \forall c \in R^+ \exists n_0 \in R^+, g(n) \leq cf(n) \forall n \geq n_0\}$, the most commonly used for the purpose being the $O(\cdot)$.

A geometry, in Klein's view, is a set $S$ and a subgroup $G$ of the group $B_{ij}(S)$ of all bijections from $S$ to itself. The elements of $S$ are points, and $G$ acts on $S$ by mapping points to points. Two subsets of $S$ are equivalent if there is an element of $G$ which takes one set into the other. In general, $S$ has an extra structure which $B_{ij}(S)$ preserves. A map $f : \mathrm{R}^m \mapsto \mathrm{R}^n$ is linear if it maps a linear combination of vectors to the same linear combination of the images. A matrix $(a_{ij})$, $1 \leq i \leq m$ and $1 \leq j \leq n$, transforms each basis element $b_i$ to a combination of the basis elements $b_j$. The map is a bijection if $f^{-1}$ exists or equivalently if the determinant of its matrix is non-zero. The general linear group, $GL(n, \mathrm{R})$, is the set of all invertible linear transformations from the vector space $\mathrm{R}^n$ to itself. The special linear group $SL(n, \mathrm{R})$, a subgroup of $GL(n, \mathrm{R})$, is the set of all invertible transformations with determinant 1. The orthogonal group, $O(n)$, the set of all orthogonal transformations $T$. The special orthogonal group $SO(n)$, a subgroup of $O(n)$, is the set of all orthogonal transformations whose matrix has determinant 1.

The group $l(\mathrm{R}^n)$ of all isometries of $\mathrm{R}^n$ consists of composites $T_a \circ L$, where $T_a : x \mapsto x + a$ is a translation and $L$ an orthogonal map. The set of all translations forms a normal subgroup of $l(\mathrm{R}^n)$ which is isomorphic to the group $\mathrm{R}^n$ under addition.

A summetry group of the subset $X$ of $S = \mathrm{R}^2$ is the subgroup of $l(\mathrm{R}^2)$ whose all elements map to themselves. Rotation by $\pi/n$ generates a subgroup which is isomorphic to $C_n$, the cyclic group of order $n$. The dihedral group $D_n$, whose order is $2n$, is the group of symmetries of a regular $n$-gon. For $n \geq 3$, $D_n$ is a non-abelian group.

The affine group, $A(\mathrm{R}^n)$, is the group of all affine transformations or affinities of $\mathrm{R}^n$, that is to say, the transformation of the form $T_a \circ L$ where $T_a$ is a translation and $L \in GL(n, \mathrm{R})$. Affine transformations preserve no distance, angle, area or volume. But they preserve collinearity, parallelism and ratios. A similarity transformation or similitude, $T_a \circ \lambda L$ with $L \in O(n)$ and $\lambda > 0$, is an affine map which preserves angles.

Affine theorems are theorems which can be proved by only those concepts which are preserved by affine transformations. In other words, they are theorems which can be proved by vector methods without using norms, dot- or vector products. Examples of such theorems are the coincidence of the medians of a triangle, Ceva's theorem and Menelaus's theorem.

The homogeneous coordinates of a point $x$ on the affine line are $(\alpha, \beta)$, where $x = \alpha/bta$. Here a line $OA$ through the origin and a point $A$ on the line $y = 1$ is described by a vector $(\alpha, \beta)$ in it. The point at infinity has homogeneous coordinates $(1, 0)$. The projective line is denoted by $RP^1$.

The projective group, $PGL(n, F) = GL(n, F)/\{\lambda I | \lambda \in F - \{0\}\}$ where $F$ is any field, is the set of all projective transformations or projectivities. The standard reference points on $RP^1$ are $\infty$, 0 and 1. There is a unique projective transformation which takes any three distinct points to any other three distinct points. Let $a$, $b$, $c$ and $d$ be points in $RP^1$, and $\theta$ the map which takes $a$, $b$ and $c$ respectively to $\infty$, 0 and 1. Then the cross-ratio is $\theta(d) = (a, b; c, d) = (d-b)/(d-a) \cdot (c-a)/(c-b)$. This cross-ratio is preserved by projective transformations.

The general form of an algebraic surface is $f(x, y, z) = 0$l, where $f(x, y, z)$ is a polynomial in $x$, $y$ and $z$. A surface of order one is a plane, of order two a quadratic surface, for example ellipsoids and hyperboloids, and of order three a cubic surface.

## § 1.3 Physics

Percolation has been introduced and developed in the 1950s. (Hammersley et. al., 1954; Broadbent et. al., 1957) A typical physical problem which gives rise to problems in percolation is that of finding the probability that the centre of a sufficiently large porous stone gets wet when immersed in water. The internal structure of such a stone can be viewed as comprised of pores and solids. Water can seep through clusters of pores but is blocked when solids are encountered. Therefore the water can only reach the centre of the stone if there exists an open path, in other words a single cluster of pores, which leads it there. When the size of the rock is sufficiently large, this cluster is called an infinite cluster.

If on the other hand we consider the solids instead of the voids, we can reason that since the stone is rigid there have to exist at least one infinite cluster of solids. Then, because there must be rocks of various degrees of porosity which allow water to pass through, there must be a range

of porosity which at one end is a nonpermeable stone where there exists an infinite cluster of solids but not an infinite cluster of pores, while at the other end it is the other way round, that is there exists an infinite cluster of pores but not one of solids. In other words, the latter case is the case where the rock has disintegrated into pieces. If one considers the pores and the solids as being two phases opposite to each other, then one can reason that the total volume of the two stays the same, whereas the ratio between them could vary.

The study of blockages in porous media can be translated into the study of percolation on the media when pores randomly turn into solids. In other words, it is the study of the formation of an infinite cluster of one phase within the infinite mass of the other. More often the latter infinite mass is taken for granted as always exists and remains the same. The domain of consideration is thus reduced to only the original pore spaces. Then, the study becomes that of inversion between two phases, namely the infinite cluster of free pores and the finite clusters of free pores. While the existence of an infinite cluster or finite clusters of blockages is of no consequences when one is only interested in the percolation point, it is considerably important when one wants to contemplate on the behaviours on either side of that critical point. It is important also when one studies changes in the rate of flow through the media.

One example is the study of traffic networks. Traffic congestion can be described as three degrees of flowability: free-flowing, congested, and stand-still. In a free-flowing traffic there are infinite clusters of roads and finite clusters of blocked roads. In a congested traffic there are both infinite clusters of roads and infinite clusters of blocked roads. In a stand-still traffic there are no infinite clusters of roads, while there are infinite clusters of blocked roads.

Applications of the percolation theory includes the study of forest fires and epidemics, the study of defects in semiconductors, the study of the effective resistance of a disordered mixture of two materials, the study of the Curie point of spontaneous magnetisation in ferromagnets and the Ising model, and the study of the rigidity of networks.

Phenomena which contain phase transitions are normally related to percolation theory. Examples of physical phase transition includes the boiling point and the point of evaporation, the transition of materials into superconductivity state, the triggering of a chain reaction in nuclear fission, and the triggering of nuclear fusion of hydrogen burning in a new-born star. Apart from these, there are philosophical phase transitions which include the nature of understanding, the nature of scientific discoveries and technological progress, the making of mobs, revolutions and wars, enlightenment, and, of course, love. Nature is essentially made up of numerous local linear or gradual relationships bound together in a larger scale by abrupt transitions.

The word *percolation* is derived from the word *percolator*, a coffee making machine. The connotation is therefore that of fluid flowing through a porous medium. In dynamic and everyday applications the emphasis is usually on the fluid part, and one studies the point of transition when the flow becomes blocked. There is another side of the same system where one studies the structure of underlying network. In that case the emphasis is on the solid part, and one is interested to find the point where particles percolate to form a solid structure.

Thus the study of percolation falls broadly into two branches, the continuum percolation and the network percolation. The former finds applications in crystallisation where one would like to know the number density of crystals that will make, for example, a synthetic zeolite membrane; in etching of metallic surface where one would like to find the estimates of the shapes and sizes of the etch pits which overlap and form clusters according to etching time and concentration of the acid; or in telecommunication networks where one would like to determine the number of mobile phone cells which percolates a city. The latter finds applications in filtration where one would like to discard filters just before they become blocked or in traffic networks where one could compare the robustness to standstill between two traffic network configurations.

Phase transition occurs in various areas. Wherever it is seen, it has the same characteristic of an intensely exponential change in a short period within a long stretch of a much more gradual one. The rate of change at the point of transition is generally astronomical. The sudden switch from one phase to another found in the study of percolation is a phase transition. The assumption of the existence and occurrence of infinite clusters as an explanation for these transitions can be justified by considering the promptness and the scale of theoretical transitions in a cosmological setting, namely the turning on of the general relativity at Planck time $10^{-43}$ seconds after the bigbang, the Grand Unified phase transition at $10^{-35}$ seconds and the start of nucleosynthesis at 1 second (cf. Croswell, 1995).

Temperature of the universe according to the Big Bang theory. The temperature of the universe decreases exponentially and its trend against time has to be plotted on a log-log scale to be comprehensible for otherwise it would lie almost on top of the coordinate axes. Such a plot as shown in Figure 1.8, produced from the data taken from Vaas (2002), roughly approximates a straight line with a negative slope. The percolation at the big bang could possibly be a phase change between matter and antimatter.

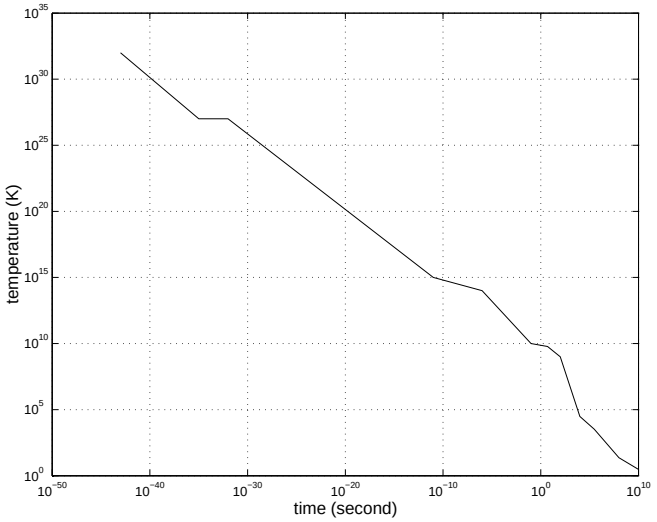


**Figure 1.8** Temperature of the universe.

There is an idea in cosmology which could easily be as old as the oldest known religion, that describes the universe as alternating in cycles of destruction and creation. One current theory holding that idea tries to explain the big bang as the collision between two universes in five dimensional space-time. I believe that the universe undergoes phase changes periodically and percolates at the point the same one of which is differently called the big bang, the big crunch, or the big bounce depending how one looks at it. What we see now is only one side of the coin. We can not calculate pass the singularity at the big bang using our present theories because it is another phase complementary to us. That is why that creative singularity baffles us. I believe a theory must exist which can explain both or, if there are more than two, all phases as well as the transition point. And when we finally discover it we will understand the cosmic history and, hopefully, percolation.

In an asymmetric membrane the top dense layer determines the transport rate while the porous sublayer acts as a support. Because the permeation rate is inversely proportional to the thickness of the transport barrier, asymmetric membranes show a much higher permeation rate than homogeneous symmetric membranes of the same thickness.

Soap is solution of a sodium salt of a fatty acid, for example sodium stearate ($C_{17}H_{35}COO^{-}Na^{+}$). The films of soap bubbles are made up of a monomolecular layer of amphipathic ions, which have a hydrophilic and a hydrophobic parts. The former forms a hydrophilic polar carboxyl head, which in the case of sodium stearate is the $COO^{-}$. The latter forms a tail of hydrocarbon chain, in this case $C_{17}H_{35}$.

| | **Laboratorical scale** | | **Industrial scale** | |
|---|---|---|---|---|
| *Process* | *Origin* | *Application* | *Origin* | *Application* |
| *microfiltration* | Germany, 1920 | bacteria filter | | |
| *ultrafiltration* | Germany, 1930 | laboratory use | America, 1960 | concentration of macromolecules |
| *hemodialysis* | Netherland, 1950 | artificial kidney | | |
| *electrodialysis* | | | America, 1955 | desalination |
| *hyperfiltration* | | | America, 1960 | sea water desalination |
| *gas separation* | 1860 | gas treatment | America, 1979 | hydrogen recovery |
| *membrane distil -lation* | | | Germany, 1981 | concentration of aqueous solutions |
| *pervaporation* | | | Germany and Netherlands, 1982 | dehydration of organic solvents |

**Table 1.7** *Origin of membrane processes.*

J K Mitchell observed gas separation in 1831. In 1860 Thomas Graham made a systematic study of it (*cf* Ismail *et al*, 2002).

There are three categories of synthetic membranes: porous, nonporous, and carrier. Micro- and ultrafiltration use porous membranes while nonporous membranes are used for dialysis, vapour permeation, gas separation and pervaporation. All membranes are required to be mechanically, thermally, and chemically stable. The means of separation, however, varies. For porous membranes

it is the pore dimension, for nonporous membranes the difference in diffusivity or solubility, and for carrier membranes the properties of carrier molecules.

| *Methods* | *pore size ($\mu m$)* | *porosity* |
|---|---|---|
| *coating* | | |
| *phase inversion* | | |
| *sintering* | 0.1–10 | 10–20% |
| *stretching* | 0.1–3 | 90% max |
| *leaching* | 0.005 min | |
| *etching* | 0.02–10 | 10% max |

**Table 1.8** *Methods of preparation of membranes.*

In cosmology, the structure of the Abell Clusters shows a nonrandom distribution which suggests the existence of a second-order grouping, the clusters of clusters of galaxies (Abell, 1958). Apart from the Milky Way and the Andromeda galaxies (M31 or NGC224) there are at least 44 other galaxies in our Local Cluster. The Local Cluster is on the edge of the Local Supercluster which is flattened in shape and the approximate centre of which is at the Virgo Cluster. The Local Supercluster is separated by a nonspherical void of low galaxy density from the Pisces-Perseus supercluster. The latter lies nearly perpendicular to our line of sight, has the shape of a linear filament, and spans over 90° across the sky. The study of superclusters of galaxies often requires the use of superclusters of computers.

Abell (1958) plotted the distribution of the clusters in what he called, the 'Aitoff equal area projection'. By this he probably means the Hammer, aka Hammer-Aitoff, projection because that is what is normally used for astronomical maps in galactic coordinates as well as for maps of the whole world. Inspired by the Aitoff projection, it was created by H. H. Ernst von Hammer as a modification of the Lambert Azimuthal Equal Area projection. The Hammer projection is equal area while the Aitoff projection is not. Both are similar to each other in that both are modified azimuthal projections where the central meridian is a straight line half the length of the equator, the only point free from distortion is the centre point, and there is a moderate distortion throughout. From investigations I conclude that it is a normal practice in Astronomy and Cosmology to call the Hammer projection as the Aitoff projection.

Powles and Quirke (1984) analyse the numerical trajectory of a molecule in liquid circles by using an empirical fractal parameter called the Richardson coefficient, $\alpha$. In their simulation they used the Lennard-Jones (12,6) intermolecular potential together with a reduced density and pressure. For the length of molecular trajectories in an argonlike liquid they found $\alpha = 0.65$, in comparison with a similar analysis done on a randomised Koch curve of order 6 which gives $\alpha = 0.25$ and the exact $\alpha = 0.2618\ldots$ for $K_\infty$, the Koch curve of an infinite order. The length of a fractal curve is $L(\epsilon) \propto \epsilon^{-\alpha}$, where $\epsilon$ is the step distance or scale. The graph between $\log(L(\epsilon)/\sigma)$ and $-\log(\epsilon/2)$ is a straight line with a positive slope represented by the equation $\log(L(\epsilon)/\sigma) = -\alpha \log(\epsilon/\sigma) + K$ where $K = \log k - (1+\alpha)\log 2$, $k$ being a constant. The Leonard-Jones (n,6) potential is the Van der Waals potential between two atoms which is described in the form $V(r) = C_n/r^n - C^6/r^6$ where $C_n$ and $C_6$ are constants, and $r$ is the distance between the centres of the two atoms. Similarly, the Leonard-Jones (12,6) potential is $V(r) = 4\epsilon\left((\sigma/r)^{12} - (\sigma/r)^6\right)$. It is sometimes written as $V(r) = \epsilon\left((R/r)^{12} - 2(R/r)^6\right)$, where $R = R_i + R_j$, $\epsilon = \sqrt{\epsilon_i \epsilon_j}$, $R_i$ and $\epsilon_i$ being the radius and respactively the interaction energy of each atom. In other words, in the last formula $\epsilon$ is the geometrical mean of the interaction energy of each atom while $R$ is the atomic cross-section which is a property of a pair of atoms.

## § 1.4 Cosmological structure

The Lorentz transformation was first written down by Voigt in 1887 as $x' = x - vt$, $y' = y/g$, $z' = z/g$, and $t' = t - vx/c^2$, then by Larmor in 1898, and finally by Lorentz in 1899. Poincaré stated in 1898 on the measure of time that there is no absolute equality of two time intervals. He named the Lorentz transformation after Lorentz and showed that together with the rotations they form a group. Working on the transformations, Einstein announced the special relativity in 1905 as a theory merited by its simplicity and beauty rather than being an explanation of experimental results. For the special relativity and the Lorentz transformations Minkowski founded a four dimensional non-Euclidean space to represent space-time which Einstein adopted used as a basis for his general relativity which appeared in 1915.

Whether the universe is homogeneous or isotropic depends on the scale in which one consider. If the scale is large enough then they can be considered both so but not otherwise. Similarly, an infinite Voronoi network originated from Poisson generators may be considered as being both isotropic and homogeneous because all the irregularities averages out.

Cosmology is related to the study of membranes and filters. Molecules of liquids in a membrane experience forces due to induced dipoles and fixed dipoles. The induced dipoles results in the Lennard–Jones potential whereas the fixed dipoles give rise to a permanent dipole moment between fluid molecules or between molecules of very fine particles.

Inter molecular interactions are approximated by considering the charged parts of the molecule as point charges. The force between charged parts of each molecule and those of its neighbours can be estimated by the Coulomb potential, $V = q_1 q_2/(4\pi\varepsilon_0 r)$, and the Coulomb force between each pair of molecules is $F = q_1 q_2/(4\pi\varepsilon_0 r^2)$.

Analogous to the $1/r$, Coulomb potential in electrostatics is the $1/r$ potential in Swarzshield's expansion for the ten metric or gravitational potential of Einstein for the effect of an elementary concentration of mass in a space-time continuum that is asymptotically flat, that is

$$\mathrm{d}s^2 = \sum_{\alpha\beta} g_{\alpha\beta}\mathrm{d}x^\alpha \mathrm{d}x^\beta = \left(1 - \frac{2Gm}{(c^2 r)}\right)\mathrm{d}r^2 + r^2[\mathrm{d}\theta^2 + \sin^2\theta \mathrm{d}\psi^2] - \left(1 - \frac{2Gm}{(c^2 r)}\right)\mathrm{d}T^2. \qquad (\mathbf{5})_{\mathrm{i}}$$

However, this is not as applicable as the Coulomb potential since the equations in the gravitation theory are nonlinear and therefore the superposition principle does not apply.

The Big Bang can be nothing but a change of phase of the universe. What the other phase may be we can not know, because there is a singularity which divides us from the Yonder Side. But one thing is indisputable, that is if we want to understand the universe, or in plainer words to make any sense out of it, we need to understand the singularity. And since we have to include the percolation theory in our final calculations, we might as well make it the beginning of our quest for a grand unified theory. Whether it is the percolation theory that we already know or another one not yet found is of no consequence. A percolation theory will still be a percolation theory no matter what form it may take, or indeed whatever name you may call it by. Our percolation theory is no percolation theory in a sense that it leaves out half of the picture, that is to say, the singularity that it still does not know how to explain. A true percolation theory is a theory which can includes singularities in its calculation while leaving out nothing that we know already. Give it some other name if you like, but *that* is the real percolation theory.

We now know many things in details, for example how stellar equations must account for mechanical, energy and thermal equilibria and that nuclear reactions imply conservation of charge, nuclear number and lepton number (*cf* Cooper *et al*, 1985). But at the Big Bang every one of these is supposed to break down. Because of this, our picture of the universe will always be incomplete until we can come to terms with that singularity which is our theoretical creator, the Big Bang.

## § 1.5 Filtration

Filtrationis the operation of separating a heterogeneous mixture of a fluid and particles of solids by means of a filtering medium which lets the fluid pass through but not the particles. The name filtration comes from the art of wine making. There are two processes involved, namely the flow of the fluid through the cake and the medium, and the filtration where particles are deposited on or in the medium. The objective is to understand how the rate of flow depends on the properties of both the suspension and the medium, and on the operational conditions.

Both the cake and the medium are porous. As is the case with the cosmological structure (*cf* § ℵ), a filtering medium can be considered as being homogeneous on the large scale, whereas on the small scale it nearly never is (*cf* Heertjes, 1964). In other words, on the scale of the particles and the pores everything concerned is inhomogeneous to a high degree, that is to say, the slurry, the flow, and the cake. The micro-inhomogeneity in the cake can lead to a macro-inhomogeneity. Furthermore, the interaction among the particles, cake, medium and fluid makes the study of filtration ideal ground for numerical studies.

Heertjes (1964) describes the flow through a filter by the Fanning equation, $v = \mathrm{d}V/\mathrm{d}t = (1/\eta\gamma)\mathrm{d}(\Delta P)^\delta/\mathrm{d}R$, where $\eta$ is viscosity and $R$ the resistance. For viscous flow $\gamma = \delta = 1$, whereas for turbulent flow $\gamma = 0.11$ and $\delta = 0.55$. Both the cake ($c$) and the medium ($m$) have the say, so $R_c + R_m = R$, $\Delta P_c + \Delta P_m = P$, and $\Delta P_c/R_c = \Delta P_m/R_m$. The specific resistance of the cake is $r = \mathrm{d}R_c/\mathrm{d}w$, and therefore $R_c = \int_0^w r\mathrm{d}w = w(r)w$, where $w(\cdot)$ represents the mean value in contrast with $w$ which is the weight of particles in the cake per unit surface of filter. From slurry ($s$) the

filtrate passes through the slurry-cake ($sc$-) and the cake-medium ($cm$) interfaces. A volume $V_{sc} = (1 + c/\rho_s)$ of slurry is needed to produce $V_{sc}$. Here $c$ is the concentration- and $\rho_s$ the density of particles. Assuming the amount of particles contained in the filter to be negligible, then $w = cV_{sc}$. Then from $V_c = V_m$, $V_{sc} = V_m + V_R$, $V_R = w \cdot \bar{\epsilon}/[\rho_s(1 - \bar{\epsilon})]$ and $\epsilon_s = \rho_s/(\rho_s + c)$ we have

$$w = \frac{cV_m}{1 - \frac{(1-\epsilon_s)}{\epsilon_s}\frac{\bar{\epsilon}}{(1-\bar{\epsilon})}} \qquad (6)_{\mathrm{i}}$$

The filtration coefficient $\lambda$ in $-\mathrm{d}c/\mathrm{d}l = \lambda c$ is not a constant but change with time because of particles adsorbed by the bed. If one assumes that particles are bound to the wall by London-van der Waals force only, then $\lambda = K(\epsilon_0 - \sigma)$ where $\sigma$ is the specific deposit of solids in filter bed described as volume of solid per unit filter volume, $\epsilon_0$ the initial porosity of the bed and $K$ a function of London-van der Waals constant, $d$, $\epsilon$, $\eta$ and $W$. The equation of continuity is $W_0(\mathrm{d}c/\mathrm{d}l) = \mathrm{d}(\sigma)/\mathrm{d}\theta$. Cake is stabilised by the flow force and consolidates when it has reached a critical thickness and the velocity dropped below a critical value. The cake pressure is highest at the interface with the filter, so it is here that it starts to consolidate. Vibration is normally used to loosen it.

In the Diffusion Limited Aggregation model (*cf* Houi and Lenormand, 1986) particles $a_i$ are placed on the lattice while particles $b_i$ move towards them from a distance. These travelling particles stick to the first thing they meet, thus forming clusters, but they disappear whenever they stray too far away from the clusters. The density $\rho \sim nd^2/(hl) = na/(\tilde{x}l)$, $\tilde{x} = x/a$, approaches a fractal power law $\rho \sim \tilde{x}^{D-2}$ with the fractal dimension $D$ such that the deposit is homogeneous when $D = 2$ and heterogeneous when $D < 2$; $l$ is the length of the filter, $x$ the thickness of the deposit and $d$ the particle diameter. They consider two models, one to study the effects of random motion while the other that of ballistic trajectory. In the first model particles move in a square network, jumping from one site to one of its nearest neighbours with a probability $q$ towards the filter and $p$ in the other three directions. The diffusive- and the ballistic probabilities are respectively $4p$ and $1 - 4p$. The ratio between convective and diffusive displacement, a Péclet number, is defined as $P_e = (1 - 4p)/4p$. For the ballistic motion $P_e \to \infty$ while for the Brownian motion $P_e = 0$. In their second model particles move through space and $P_e = |u|/|r|$, where $u$ is a constant displacement vector in the flow direction while $r$ is in random direction. Particle A sticks to B when $\alpha < \beta$ or rolls on it if $\beta < \alpha < \gamma$. In this latter situation, A will stick to B if it is prevented from reaching the angle $\gamma$ comparative to A, but if at last $\alpha > \gamma$ A and B will separate.

The hydro dynamic forces act to transport particles through the medium. When the solid parts come close together, there is a viscous resistance which increases with the inverse of the separation between them. The van der Waals force acts at a close range, is always attractive and is theoretically infinite when particles touch a solid. Brownian motion affects particles smaller than $1\mu$m and results in a heterogeneous deposit, whereas the ballistic trajectory occurred in sedimentation or filtration of big particles yield a deposit that is homogeneous.

Prefilters used to protect fibre bed coalescers from the damage caused by suspended solid can become a bottle neck from being ladened with the solids itself. Chan (1990) was interested in such problem as the processing of hydrocarbon liquids on offshore platforms. In this process the four phase system, that of hydrocarbon gas, condensate, glycol and solids, is treated. The gas is separated and distillated to fractionate off butane and propane for uses in petrochemical manufacture. The other fluids contain hydrocarbon condensate and glycol which is added to prevent gas hydrates, a solid phase, from forming. But ethylene glycol has to be separated before it enters the purification system, for otherwise it would foul heat exchangers and the trays of distillation column. This can be conveniently done using a fibre bed coalescer. But solids suspended in one of the constituents, gas condensate glycol, will deposit and block these beds unless removed first by using a prefilter, which would then in turn become blocked and causes the bottle neck to the whole process.

Dead end filtration is simpler to simulate on the computer, but crossflow filtration is used more often in industry. Hydrophobic polymers in general have the advantage of good chemical and thermal stability, but hydrophilic polymers are becoming more and more attractive as membrane materials because they tend to have less adsorption. Adsorbed layer means more resistance to flow and a decline in flux. Moreover, these layers are difficult to remove by normal cleaning methods. Cellulose and its derivatives are among the best known hydrophilic polymers used as membrane materials. Examples of these are cellulose acetate, cellulose triacetate, cellulose tripropionate, cellulose nitrate, cellulose acetate-butyrate and ethyl cellulose. They are used in micro-, ultra- and hyperfiltration as well as in dyalysis and gas separation. Cellulose is hydrophilic but not soluble in water. It has a regular chain structure and is quite crystalline. Cellulose nitrate and cellulose acetate are used in

micro- and ultrafiltration. Cellulose esters have excellent membrane properties except with regard to their sensitivity to biological-, chemical- and thermal degradations. They are made by air-casting or dry phase inversion. In phase inversion, a polymer is transformed from a liquid- to a solid state. Solidification is often started by liquid demixing, the transition of one liquid into two liquids. Phase inversion techniques include evaporation and precipitation the widely used for membrane of which is immersion precipitation (*cf* Schumacher, 1996). The top layer of an asymmetric membrane is dense and therefore responsible for most of the filtration. The sublayer is porous and provides the support to the top layer. Macrovoids are often found in the sublayer which lead to weak spots in the membrane and must be avoided, especially in high pressure applications which use dead end filtration. Tetrahydrofunate and acetone give membranes with a dense top layer as the result of delayed demixing. Dimethylsulfoxid and Dimethylformiade give membranes with a more porous structure from instantaneous demixing. Analogous to this is how pumice is very porous from the instantaneous solidification when it forms.

During the separation the flux through the membranes declines or decreases with time from adsorption, concentration polarisation, fouling, gel layer formation and pore pluggings. This is especially severe in micro- and ultrafiltration, with the decline in the flux often exceeding ninety per cent.

Darcy's law gives the volumetric flux of a pure liquid through a membrane, $J = \Delta P/(\eta R)$ where $R$ is the overall resistance of the membrane which includes the resistances from adsorbed particles, cake, concentration polarisation, gel, pore blocking and membrane. Adsorption decreases the pore radius according to the Hagen-Poiseuille equation, $\Delta r/r = 1 - (J/J_m)^{1/4}$. At steady state the convective transport balances the permeate flow past the membrane and the diffusive back flow which results from the accumulation of solute at the membrane surface, $Jc + D\partial c/\partial x = Jc_p$ where $D$ is the diffusion coefficient. Then from the boundary conditions $c = c_m$ at $x = 0$ and $c = c_b$ at $x = 1$, $(c_m - c_p)/(c_b - c_p) = \exp(J\delta/D)$. In other words, $c_m/c_b = \exp(J/k)/[R_n + (1 - R_n)\exp(J/k)]$ where the mass transfer coefficient $k = D/\delta$ and the intrinsic retention $R_n = 1 - c_p/c_m$. When the solute is completely retained by the membrane, $R_n = 1$ and $c_p = 0$, and therefore $c_m/c_b = \exp(J/k)$.

Across the filtering medium there is a driving force, in other words the pressure drop. There are four driving forces, centrifugal, gravity, pressure and vacuum. Filters in use in practice are either surface- or depth filters. In the former the solids are deposited on the surface in the form of a cake, thus the name *cake filtration*, while in the latter they are deposited inside the medium, thus *deep bed filtration.*

In filtration, Darcy's law is often written $Q = A\Delta p/(\mu R)$, where $R = L/K$ is the medium resistance, $L$ the thickness- and $K$ the permeability of the bed. If there is a cake, $R = R + R_c$ where $R_c$, the cake resistance, is $R_c = \alpha w$, $\alpha$ being the specific cake resistance in $\mathrm{mkg}^{-1}$ and $w$ is the mass of cake deposited per unit area. Cakes are normally compressible, so $\alpha$ changes with $\Delta p_c$ and is approximated as $\alpha_a$, where $1/\alpha_a = (1/\Delta p_c)\int_0^{\Delta p_c} \mathrm{d}(\Delta p_c)/\alpha$. There is an experimental empirical relation $\alpha = \alpha_0/(\Delta p_c)^n$, where $n$ is the compressibility index, and $\alpha_a = (1 - n)\alpha_0(\Delta p_c)^n$.

The mass of cake deposited is $wA = cV$, where $c$ is the concentration of solids in the suspension. For incompressible cake, $Q = \Delta pA/[\alpha\mu c(V/A) + \mu R]$ or equivalently $\mathrm{d}t/\mathrm{d}V = \alpha\mu cV/(A^2\Delta p) + \mu R/(A\Delta p)$. If $\Delta p$ is constant, $t = a_1V^2/(2A^2\Delta p) + b_1V/(A\Delta p)$, where $a_1 = \alpha\mu c$ and $b_1 = \mu R$. The experimental determination of $\alpha$ and $R$ works with this equation in the form $t/V = aV + b$, where $a = a_1/(2A^2\Delta p)$ and $b = b_1/(A\Delta p)$; or rather in a more detailed form $(t - t_s)/(V - Vs) = \alpha\mu c(V + V_s)/(2A^2\Delta p) + \mu R/(A\Delta p)$, where $t_s$ is the starting time at the beginning of the truly constant pressure period.

In constant rate filtration, $Q$ is kept constant,

$$Q = \frac{\Delta p(t)A}{\frac{\alpha\mu cV(t)}{A+\mu R}}.$$

In other words, $\Delta p = \alpha\mu cQ^2t/A^2 + \mu RQ/A$, or $\Delta p = a_1v^2t + b_1v$, where $v = Q/A$ is the approach velocity of the filtrate.

In many cases, operation demands constant rate followed by constant pressure, in which case $\Delta p = a_1v^2t + b_1v$ for $t < t_s$ and $\Delta p = \Delta p_s$ a constant for $t \geq t_s$. This amounts to $V = Q_1t$ for $V \leq V_s$ and $(t - t_s)/(V - V_s) = a(V + V_s) + b$ for $V > V_s$.

If a centrifugal pump is used, it is the case of variable pressure and variable rate. Here the equation is $V = A(\Delta pA/Q - \mu R)/(\alpha\mu c)$, and the filtration time necessary is $t = \int_0^V \mathrm{d}V/Q$.

For compressible cakes, $\Delta p = \Delta p_c + \Delta p_m$, where $\Delta p_m = \mu RQ/A$ and $\Delta p_c = \alpha_a\mu cVQ/A^2$.

And $\Delta p_c = (1-n)\alpha_0 \Delta p_c^n \mu c V Q / A^2$, that is to say,

$$\frac{\mu c V Q}{A^2} = \frac{(\Delta p_c)^{1-n}}{(1-n)\alpha_0}.$$

Then, for the constant rate filtration, $(\Delta p_c)^{1-n} = \alpha_0(1-n)\mu c Q^2 t / A^2$. And for the variable pressure and variable rate operation,

$$V = \frac{A^2}{((1-n)\alpha_0 \mu c)} \cdot \frac{(\Delta p - \Delta p_m)^{1-n}}{Q}, \qquad (7)_{\mathrm{i}}$$

where $\Delta p_c$, $\Delta p_m$, $V$, $Q$ and $t$ are all variable.

The relationship between the specific cake resistance, porosity and specific surface is the Kozeny-Carman equation, $\alpha = K_0 S_0^2 (1-\varepsilon)/(\rho_s \varepsilon^3)$, where $K_0$ is the Kozeny constant which is approximately 5 for the lower porosity ranges, $S_0$ is the specific surface of the particles making up the bed, that is the ratio between the surface area and the volume of solids, $\rho_s$ the solid density and $\varepsilon$ the porosity, that is the ratio between the volume of voids and the volume of cake.

Fluid within porous media is essentially stagnant and the flow is laminar. Perhaps second only to the Hubble's constant in Cosmology in the matter of elusiveness is the $k$-factor which accounts for the tortuosity in porous filters, which, according to Kozeny and Carman, is $k = k_0(L_e/L)^2$, where $k_0$ is the shape factor, $L_e/L$ the tortuosity factor, $L_e$ being the interstitial length followed by the streamline and $L$ is the thickness of the bed. There are many other formulae (*cf* Piekaar and Clarenburg, 1967), for instance $k = k_0/\rho$ suggested by Sullivan where $\rho = \overline{(\sin^2 \phi)}$ is the orientation factor.

Transport mechanism in filters is due to diffusion, gravity and hydrodynamic force. The efficiency is minimum at about the particle size of 1 $\mu$m. Filter normally runs about 24 hours between washes, with a rate between 5 and 15 $\mathrm{m \cdot h^{-1}}$. Wash rates are approximately 0.5 $\mathrm{m \cdot min^{-1}}$. (*cf* Ives, 1977).

## § 1.6 Statistics

Poisson distribution, defined by $p(x,\lambda) = \left[\lambda^x e^{-\lambda}/x!\right] \mathrm{I}_{[0,\infty)}$, is the binomial distribution, $p(x,n,p) = {}^n\mathrm{C}_x \theta^x (1-\theta)^{n-x} \mathrm{I}_{[0,n]}$, when $n$ goes to infinity, $\theta$ goes to zero, while $n\theta = \lambda$. Here $\theta$ is the probability of success of each trial. It is used when counting the number of occurences of a random event. Analogously Poisson point process, which has $p(x = n(v)) = \left[\lambda |v| e^{-\lambda |v|} x/x!\right] \mathrm{I}_{[0,\infty)}$, is the binomial point process, $p(x = n(v)) = {}^n\mathrm{C}_x \theta^x (1-\theta)^{n-x} \mathrm{I}_{[0,n]}$, when the volume $V$ goes to infinity, while $n/|V| = \lambda$. Here $\theta = |v|/|V|$ is the probability of points within $V$ being placed in $v \subset V \subset R^d$, and $\lambda$ the density or intensity of points. Therefore the density of point of a Poisson point process is constant by definition. A point process is a procedure which generates points on a domain within a space of $d$ dimensions.

The Poisson point process thus derived has the properties that $0 < p_{n(v)=0} < 1$ for $0 < |v| < \infty$, $\lim_{|v|\to 0} p(n(v) \geq 1) = 0$, $n(v_i)$ mutually independent and $n(\bigcup_n v_i) = \sum_n n(v_i)$ when $A_i$ are disjoint, and $\lim_{|v|\to 0} [p(n(v) \geq 1)/p(n(v) = 1)] = 1$.

The weighted mean of a group of data is $\mathbf{x} = \sum_i f_i x_i / n$ and the weighted variance is $\sigma^2 = \sum_i f_i (x_i - \mathbf{x})^2 / n$, where $f_i$ is the occurrence frequency of $x_i$ and $\sum_i f_i = n$. Likewise the $r^{\mathrm{th}}$-moment around the average is $m_r = \sum_i f_i (x - \mathbf{x})^r / n$, while the $r^{\mathrm{th}}$-moment around the origin is $m'_r = \sum_i f_i x^r / n$ (*cf* Spiegel, 1975). Some relations among these various moments are $m_1 = 0$, $m_2 = m'_2 - {m'_1}^2$, $m_3 = m'_3 - 3m'_1 m'_2 + 2{m'_1}^2$, and $m_4 = m'_4 - 4m'_1 m'_3 + 6{m'_1}^2 m'_2 - 3{m'_1}^4$.

The variance when normalised by $n-1$ gives the best unbiased estimated variance if the sample has a normal distribution. On the other hand the variance which is normalised by $n$ is identical with the second moment of the sample about its mean.

The log-normal distribution is closely related to the normal distribution. If $\ln x$ has a normal distribution with $\mu$ and $\sigma^2$, then $x$ has a log-normal distribution with $\mu$ and $\sigma^2$. In other words, a log-normal distribution curve will appear as a normal curve when plotted with a log scale in the $x$ axis. Its probability distribution function is

$$f(x|\mu,\sigma) = \frac{1}{x\sigma\sqrt{2\pi}} e^{-\frac{(\ln x - \mu)^2}{(2\sigma^2)}}. \qquad (8)_{\mathrm{i}}$$

It is positive definite, and therefore attractive in some areas of application where this is required, for example the amount of rain fall or particle size distribution. Both the log-normal and the normal distributions require only two parameters to describe, that is its mean and variance.

The most common drop size distribution in agitated heterogeneous liquid-liquid systems are the normal and the log-normal distributions (Giles *et al*, 1971). A straight line is obtained when the diameter of drops, $d$,with normal size distribution is plotted against cumulative percentage frequency, or in the case where they have log-normal size distribution, when $\log d$ is plotted against cumulative percentage frequency.

Monte Carlo methods (*cf* Hammersley and Morton, 1954) use random numbers. They have found applications in a wide variety of fields, ranging from numerical analysis to recreation. Random numbers sometime come from nature, for instance the generator which creates random numbers from a resistance noise suggested by A. M. Turing, in which case they are truly random in nature. In 1927 L. H. C. Tippett compiled a table of random numbers, and in 1955 RAND Corporation (*cf* Knuth, 1998). For the premium bonds lottery ERNIE is used in the UK since $2^{nd}$ June 1957 to generate a 9-digit sequence of random numbers by exploiting the random frequency instability in a free-running oscillator. ERNIE was upgraded in 1973 and the present version, introduced in 1988, is Mark 3.

Normal distribution is a family of curves which have two parameters, namely the mean $\mu$ and the standard deviation $\sigma$. The standard normal distribution, $\Phi(x)$, has $\mu = 0$ and $\sigma = 1$. It is related to the error function by the relation $\mathrm{erf}(x) = 2\Phi(x\sqrt{2}) - 1$. The central limit theoram states that, as the sample size increases to infinity, the sum of independent samples from some distribution of finite mean and variance converges to the normal distribution.

## § 1.7 Poisson process

The Poisson process is the probability model with one parameter, which represents all processes in which points occur randomly in time. The gamma experiment is to run the process to find the time $t_k$ of the $k^{\text{th}}$ arrival, whereas the Poisson experiment is to run it to find the number of arrivals $n_t$ in the interval $(0, t]$, $t \geq 0$. These two experiments give rise to two sets of random variables dual to one another, and $n_t \geq k$ if and only if $t_k \leq t$. The regeneration property says that the process after any time $t$ is independent of the process before $t$ and is probabilistically the same as the original process. The interarrival time is $x_1 = t_1$, $x_k = t_k - t_{k-1}$ for $k = 2, 3, \cdots$.

In a Poisson process the number of changes in each of the non-overlapping intervals is independent from that in the others. Let $\nu$ be the number of one change, $h = 1/n$ a sufficiently small interval and $n$ the number of trials. Then the probability of exactly one change in $h$ is $p = \nu h = \nu/n$. The probability of two or more changes in $h$ is zero. The number of $k$ changes occurring in $n$ trials is the continuous limit of the discrete binomial distribution

$$p(k) = \frac{n!}{k!(n-k)!}\left(\frac{\nu}{n}\right)^k \left(1 - \frac{\nu}{n}\right)^{n-k} \qquad (\mathbf{9})_{\mathrm{i}}$$

## § 1.8 Phase transition

In the Ising model each spin has two possible states, that is up and down, and the hamiltonian is $H = J_0 \sum_{<i,j>} \sigma_i \sigma_j$ where the summation is over the nearest neighbours. Since it has been exactly solved, the Ising model provides a good model for the understanding of phase transition. This model can represent the transition from ferro- to paramagnetic at the critical temperature where the correlation length becomes infinite. Characteristic to the Ising model is the peak in the specific heat at the critical temperature.

The two-dimensional $xy$ model is a model of spins confined to a plane, the hamiltonian of which is $H = J_0 \sum_{<i,j>} \cos(\theta_i - \theta_j)$. This model can represent the superconducting and the superfluid films. For this model there is no phase transition showing long-range ordering. One example is the two-dimensional Coulomb gas model where the vortex-antivortex pairs, which are bound to each other at low temperature, increases in number as the temperature increases and become separated at the KT temperature that marks the phase transition.

It had been generally believed that no phase transition can exist for the $xy$ model when Kosterlitz *et al* (1973) showed that there is another kind of phase transition, arisen from the topological excitation of vortex-antivortex pairs instead of from the long-range ordering found in a spontaneous magnetisation. They consider the two-dimensional model of gas with charges $\pm q$ where the interaction potential is

$$U(|\mathbf{r}_i - \mathbf{r}_j|) = -2q_i q_j \ln \left| \frac{(\mathbf{r}_i - \mathbf{r}_j)}{\mathbf{r}_0} \right| + 2\mu \qquad (\mathbf{10})_{\mathrm{i}}$$

when $r > r_0$, and 0 when $r < r_0$. The problem is reduced to that of solving an equation of the form $(\mathrm{d}y/\mathrm{d}x) = -e^{-xy}$. The application mentioned there is in the $xy$ model of magnetism, the solid-liquid transition, and the neutral superfluid, but not in a superconductor and a Heisenberg ferromagnet.

The frustrated $xy$ model, the hamiltonian of which is $H = J_0 \sum_{<i,j>} \cos(\theta_i - \theta_j - A_{ij})$, occurs when a magnetic field is applied perpendicular to the two-dimensional plane of the $xy$ model. The frustration parameter, $f = \Phi/Phi_0$, is a measure of the average external magnetic flux. When $f = 1/2$ the model is called the fully frustrated $xy$ model. The local chirallity, $m(r_i) = \frac{1}{2\pi}\sum(\theta_i - \theta_j - A_{ij})$, which describes the property of the ground state, where it can either be $+\frac{1}{2}$ or $-\frac{1}{2}$. The network configuration at $\mathrm{T} < \mathrm{T}_c$ is that of a draught board, and has $\mathrm{Z}_2$ symmetry. This regularity is broken by the formation of domain walls in an Ising phase transition at $\mathrm{T}_c$.

Renormalisation group method has shown that there exist larger structures that behave like a smaller one. This means that the same structure can recur infinitely many times in infinitely many different scales, and that is the same idea that makes fractal geometry. This is why the study of cluster structure and the use of fractal dimension to characterise clusters becomes important (*cf* Stauffer and Aharony, 1985).

Percolation in Physics means Statistical Mechanics. Much of the contemporary vocabularies in the former has come from the lexicons of the latter from Ising Models to Renormalisation group and then to finite size scaling (*cf* Pathria, 1996).

## § 1.9 Random processes

A synonym to *random* is *stochastic* (*cf* Miles, 1972). Any algorithm which employs a random element is called Monte Carlo. Random processes can have various types of distribution. The beta distribution has a probability density function $f_{X_{\alpha,\beta}}(x) = x^{\alpha-1}(1-x)^{\beta-1}/B(\alpha,\beta)$, $0 \le x \le 1$, where $\alpha > 0$ and $\beta > 0$ are shape parameters, and $B(\alpha,\beta)$ is the beta function. There are three types of shape; the bridge shape has $\alpha > 1$ and $\beta > 1$, the J-shape $\alpha \le 1$ and $\beta \ge 1$, or $\alpha \ge 1$ and $\beta \le 1$, and the U-shape $\alpha < 1$ and $\beta < 1$.

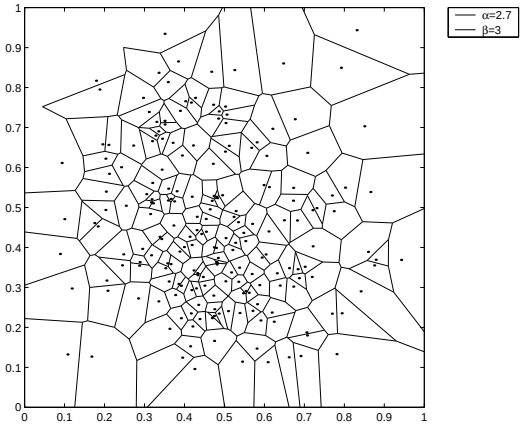


The 200 generators used in Figure 1.9 are randomly chosen with beta distribution with the shape parameters $\alpha = 2.7$ and $\beta = 3$, that is bridge shape. Both $x$ and $y$ in Figure 1.10 have J-shaped distribution with the shape parameters $\alpha = 2$ and $\beta = 0.8$. The density is unbounded at $x = 1$ and at $y = 1$ because $\beta < 0$ for both. The shape parameters in Figure 1.11 are $\alpha = 0.5$ and $\beta = 0.3$, that is U shape. The density is unbounded at $x = 0$, 1 and at $y = 0$, 1 because $\alpha$ is also less than zero.

**Figure 1.9** Voronoi graph with bridge-shaped beta distribution..

The random variable of the F-distribution is $F_{n_1,n_2} = n_2 X/(n_1(1-X))$, where $X$ is a beta variate with $\alpha = n_1/2$ and $\beta = n_2/2$.

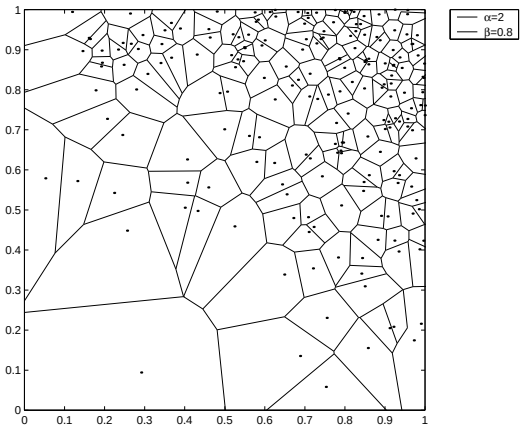


The probability density function of some of the distributions of random numbers found in practice are shown in Table 1.9. For the negative binomial distribution, $p$ is a probability of success and is constant and $r$ the number of successes required before stopping. With $rq/p$ as the mean, $q = 1 - p$, and the variance $rq/p^2$,it is used to model consecutive trials. For the noncentral$f$ distribution, $S_{n_1,\mu_1}$ and $S_{n_2,\mu_2}$ are chi-squared random variables which are independent and noncentral, $S_{n,\mu} = \chi^2_{n-1} + (Z_n - \mu^{1/2})^2$.

**Figure 1.10** Voronoi graph with J-shaped beta distribution..

It has the mean $\nu_2(\delta+\nu_1)/\nu(\nu_2-2)$, where $\nu > 2$, and the variance

$$2\left(\frac{\nu_2}{\nu_1}\right)^2\left[\frac{(\delta+\nu_1)^2+(2\delta+\nu_1)(\nu_2-2)}{(\nu_2-2)^2(\nu_2-4)}\right],$$

where $\nu_2 > 4$. This means that it is the general case of the $f$-distribution, which is the case where $\delta = 0$. The parameters $\nu_1$ and $\nu_2$ are degrees of freedom.

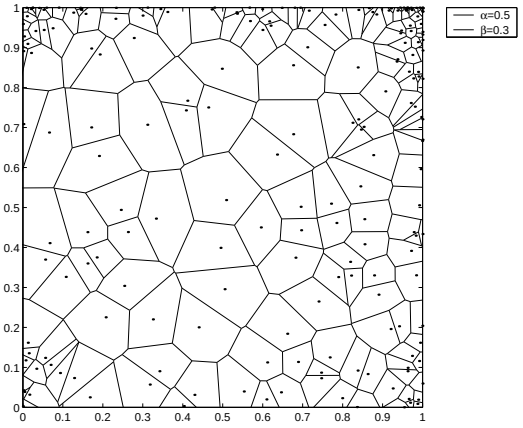


**Figure 1.11** Voronoi graph with U-shaped Beta distribution..

The noncentral $t$ distribution has $F(x|a,b)$ as the incomplete beta function with parameters $a$ and $b$, and $\nu$ the degrees of freedom. It is the generalisation of the student's $t$-distribution. It's mean is

$$\delta\left(\frac{\nu}{2}\right)^{\frac{1}{2}}\frac{\Gamma\left(\frac{(\nu-1)}{2}\right)}{\Gamma\left(\frac{\nu}{2}\right)}, \qquad (\mathbf{11})_{\mathrm{i}}$$

where $\nu > 1$, and it's variance $\nu/(\nu-2)(1+\delta^2) - \nu/2\delta^2\left[\Gamma((\nu-1)/2)/\Gamma(\nu/2)\right]^2$. The noncentrality parameter for all noncentral distributions, *viz.* the noncentral $f$-, $t$- and chi-square distributions is represented by $\delta$.

The mean of the normal distribution is $\mu$ and the variance $\sigma^2$. The standard normal distribution has $\mu = 0$ and $\sigma = 1$. The probability mass function of the Poisson distribution is sometimes written $y = f(x|\lambda) = \lambda^x/x!e^{-\lambda}\mathrm{I}_{0,1,\ldots}(x)$. It has a value when $x$ is a nonnegative integer. Otherwise the density function is zero.

The Rayleigh distribution has a parameter $b$. Its mean is $b\sqrt{x/2}$ and its variance $(4-x)b^2/2$. The uniform distribution has the mean $(a+b)/2$ and the variance $(b-a)^2/12$. For the standard uniform distribution $a = 0$ and $b = 1$. The discrete uniform has the mean $(N+1)/2$ and the variance $(N^2-1)/12$.

The Weibull distribution is sometimes written $y = f(x|a,b) = abx^{b-1}e^{-ax^b}\mathrm{I}_{0,\infty}(x)$. The Weibull distribution with a single parameter has $a = 1$. The three-parameter Weibull distribution has a p.d.f. $f_X(x) = c(x-a)^{c-1}e^{-((x-a)/b)^c}b^{-c}$ when $x \geq a$, otherwise $f_X(x) = 0$.. The mean is $a^{-(1/b)\Gamma(1+b^{-1})}$ and the variance is $a^{-2/b}\left[\Gamma(1+2b^{-1}) - \Gamma^2(1+b^{-1})\right]$.

| | |
|---|---|
| Beta | $f_{X_{\alpha,\beta}}(x) = x^{\alpha-1}(1-x)^{\beta-1}/B(\alpha,\beta),\ 0 \leq x \leq 1$ |
| Binomial | $f_{X_{n,p}}(x) = {}^n\mathrm{C}_x p^x q^{n-x},\ x = 0,1,\ldots,n,\ 0 \leq p \leq 1$ and $q = 1-p$ |
| Chi-square | $f_{\chi^2_n}(x) = e^{-x/2}x^{(n/2)-1}/2^{n/2}\Gamma(n/2),\ 0 \leq x \leq 1$ |
| Exponential | $y = f_{x\|\mu} = e^{-x/\mu}/\mu$ |
| F | $f_{F_{n_1,n_2}}(x) = n_1^{n_1/2}n_2^{n_2/2}x^{(n_1/2)-1}/B(n_1/2,n_2/2)(n_2+n_1x)^{(n_1+n_2)/2}$ |
| Lognormal | $y = f_{x\|\mu,\sigma} = e^{-(\ln(x)-\mu)^2/2\sigma^2}/x\sigma\sqrt{2x}$ |
| Negative Binomial | $y = f_{x\|r,p} = {}^{r+x-1}\mathrm{C}_x p^r q^x \mathrm{I}_{0,1,\ldots}(x)$, |
| Noncentral $f$ | $F_{n_1,n_2} = \sqrt{S_{n_1,\mu_1}/n_1}/\sqrt{S_{n_2,\mu_2}/n_2}$ |
| Noncentral $t$ | $\mathrm{P}(-t < x < t\|(\nu,\delta)) = \sum_{j=0}^{\infty}\left[(\delta^2/2)^j e^{\delta^2/2}/j!\right]\mathrm{I}\left(x^2/(\nu+x^2)\|1/2+j,\nu/2\right)$ |
| Noncentral Chi-square | $F(x\|\nu,\delta) = \sum_{j=0}^{\infty}\left[(\delta/2)^j e^{\delta/2}/j!\right]\mathrm{P}(\chi^2_{\nu+2j} \leq x)$ |
| Normal | $y = f(x\|\mu,\sigma) = e^{-(x-\mu)^2/2\sigma^2}/(\sigma\sqrt{2\pi}),\ \mu > 0$ |
| Poisson | $f_X(x) = \mu^x e^{-\mu}/x!,\ x \geq 0$ |
| Rayleigh | $y = f(x\|b) = (x/b^2)e^{(-x^2/2b^2)}$ |
| T | $y = f(x\|\nu) = \Gamma((\nu+1)/2)/\Gamma(\nu/2)\cdot 1/\sqrt{\nu x}\cdot 1/(1+x^2/\nu)^{\nu+1/2}$ |
| Uniform | $y = f(x\|a,b) = (1/(b-a))\mathrm{I}_{[a,b]}(x),\ b > a$ |
| Discrete Uniform | $y = f(x\|N) = (1/N)\mathrm{I}(1,\ldots,N)(x)$ |
| Weibull | $f_X(x) = ax^{a-1}e^{-(x/b)^a}/b^a,\ x \geq 0$ and $a,b > 0$ |

**Table 1.9** *Probability density functions.*

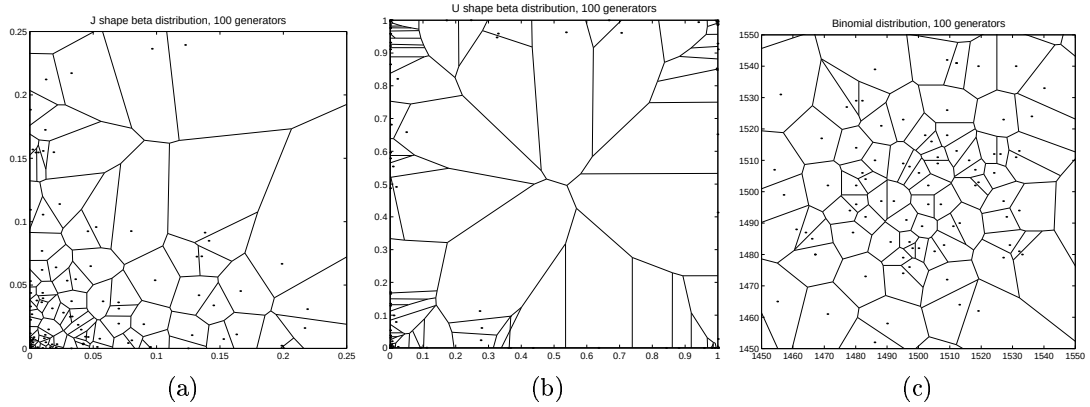
J shape beta distribution, 100 generators
U shape beta distribution, 100 generators
Binomial distribution, 100 generators

(a) (b) (c)

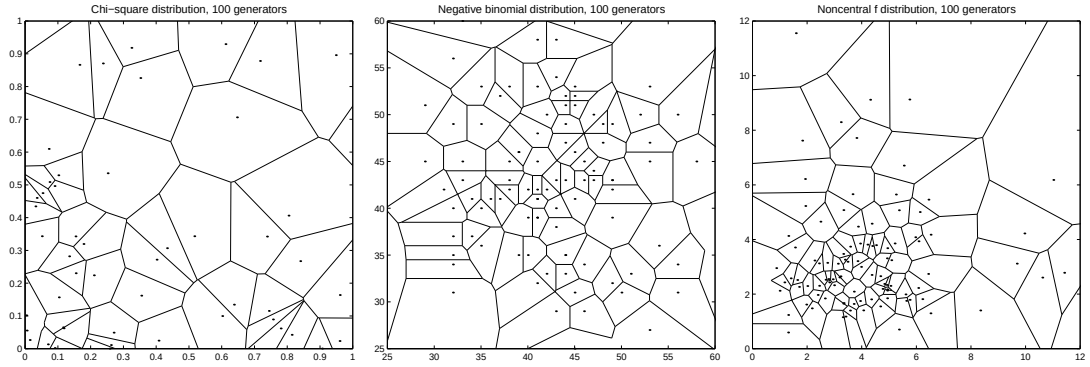
Chi−square distribution, 100 generators
Negative binomial distribution, 100 generators
Noncentral f distribution, 100 generators

(d) (e) (f)

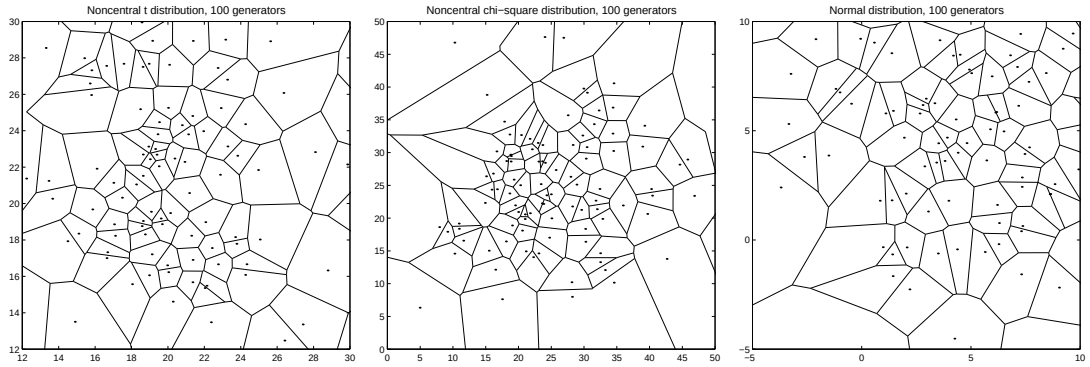
Noncentral t distribution, 100 generators
Noncentral chi−square distribution, 100 generators
Normal distribution, 100 generators

(g) (h) (i)

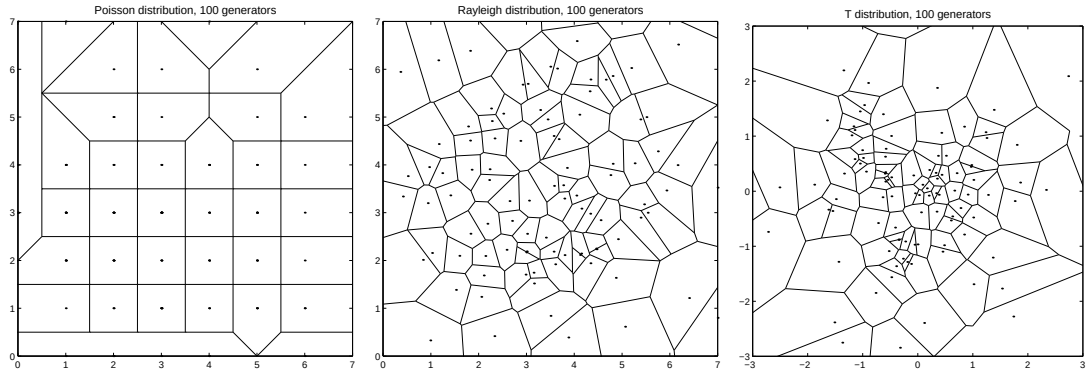


(j) (k) (l)

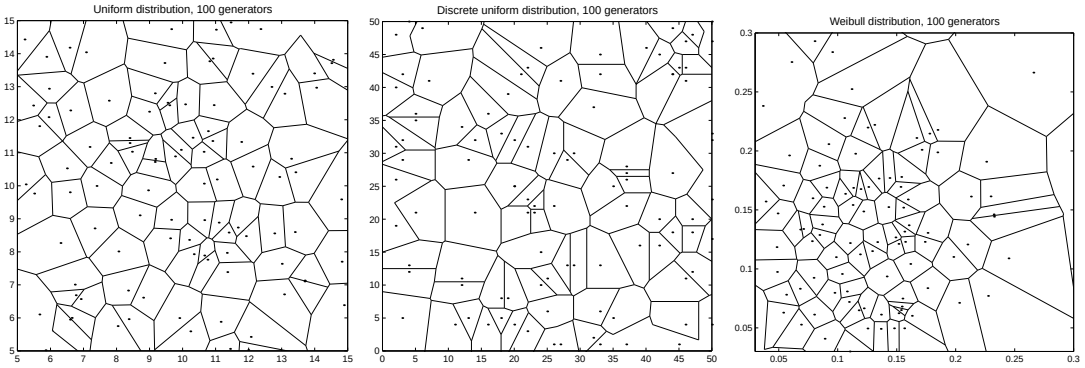
Uniform distribution, 100 generators
Discrete uniform distribution, 100 generators
Weibull distribution, 100 generators

(m) (n) (o)

**Figure 1.12** *Voronoi graphs of various random p.d.f.'s, whose distributions are* (a) *J-shaped Beta,* $\alpha = 0.5$ *and* $\beta = 10$, *in both* $x$ *and* $y$, (b) *U-shaped Beta,* $\alpha = 0.1$ *and* $\beta = 0.2$, (c) *Binomial,* $n = 3{,}000$ *and* $p = 0.5$, (d) *Chi-squared,* $n = 1$, (e) *negative binomial,* $p = 0.7$ *and* $r = 100$, (f) *noncentral* $f$, $\nu_1 = 7$ *and* $\nu_1 = 12$, $\delta = 20$, (g) *noncentral* $t$, $\nu = 10$ *and* $\delta = 20$, (h) *noncentral chi-square,* $\nu = 7$ *and* $\delta = 20$, (i) *normal,* $\mu = 5$ *and* $\sigma = 4$, (j) *Poisson, 100 generators* $(x, y)$, $\lambda = 3$, (k) *Rayleigh,* $b = 3$, (l) $t$,$\nu = 7$, (m) *uniform,* $a = 15$ *and* $b = 5$, (n) *discrete uniform, from 100 points,* $N = 50$ *and* (o) *Weibull,* $a = 50$ *and* $b = 2$.

There are five methods for generation of Poisson processes, two of which are the time-scale transformation and the thinning algorithm. The first one changes a heterogeneous process $T_{(i)}$ in $[0, t_0]$ into a homogeneous process $\tau_{(i)}$ by a new time scale $\tau = \in t_0^T \lambda(u)du$, where $\lambda$ is the rate function. We have $\tau_{(i)} = \Delta(T_{(i)})$ and $T_{(i)} = \Delta^{-1}(\tau_{(i)})$, for $\tau_{(i)} \leq \Delta(t_0)$. If $\lambda(t) = e^{\alpha+\beta t}$, then $\Delta(T) = e^{\alpha}(e^{\beta T} - 1)/\beta$ and $T_{(i)} = (1/\beta)\ln(\beta\tau/e^{\alpha} + 1)$. The second one follows Algorithm 1.3 with the input $\lambda^*, \lambda(\cdot), t_0$.

**Algorithm 1.3** *Thinning algorithm.*

$T \leftarrow 0$;
**while** $T \geq t_0$ **do**
  **generate** $U$, $V \sim U(0,1)$;
  **while** $V > \lambda(T)/\lambda^*$ **do**
    $T \leftarrow T - \ln U/\lambda^*$;
  **endwhile**
**endwhile**

□

Figure 1.13 shows that the result from the point process in two dimensions involving two random variables, *i.e.* $r(\theta) = r\angle\theta$, is not homogeneous even though it may be on average isotropic with respect to the centre for a very large network. In Figure 1.14 where the domain is also circular but each point is simply a 2-d Poisson point process, the average distance is constant for a large system. Figure 1.15 is also 2-d Poisson point process, but the space here is square. In all of the figures, *i.e.* Figure 1.13–1.15, (a) and (b) start from 200-, whereas (c) and (d) from 1,000 point generators. Boundary effects are reduced by excluding those vertices and edges along the border.

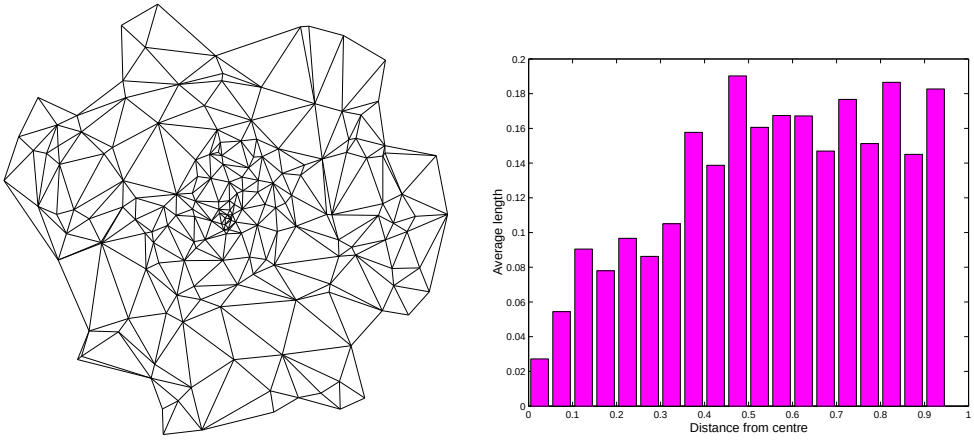

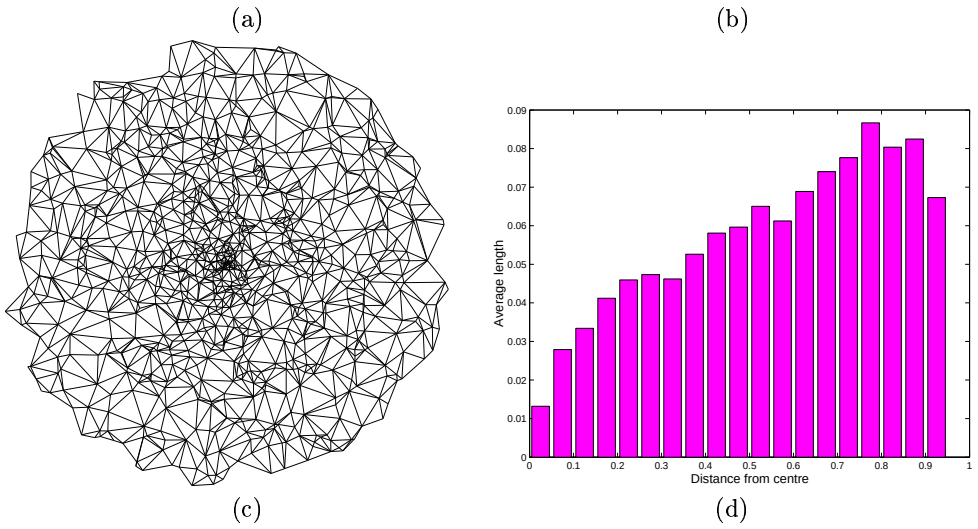


**Figure 1.13** *Point process $r\angle\theta$, where both $r$ and $\theta$ are independent random generators; (a) the Delaunay triangulation, 182 vertices shown, (b) average distance between neighbours vs distance from centre of the network, (c) another similar network, 947 vertices shown in total, (d) average edge length of the Delaunay triangulation.*

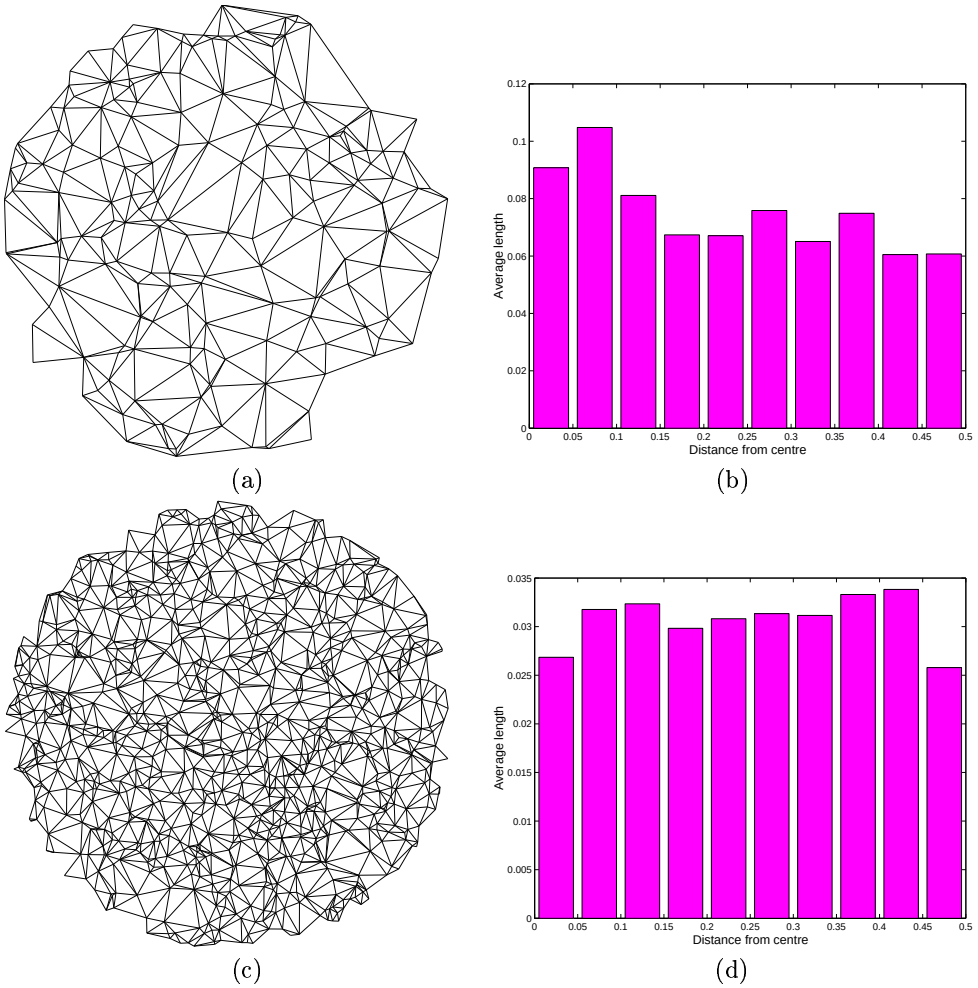


**Figure 1.14** *Point process $x, y$, where $x$ and $y$ are independent random generators in a circular domain; (a) the Delaunay triangulation with 184 vertices, (b) average edge length vs distance from centre of the network, (c) another similar network, 909 vertices shown in total, (d) average edge length of the Delaunay triangulation.*

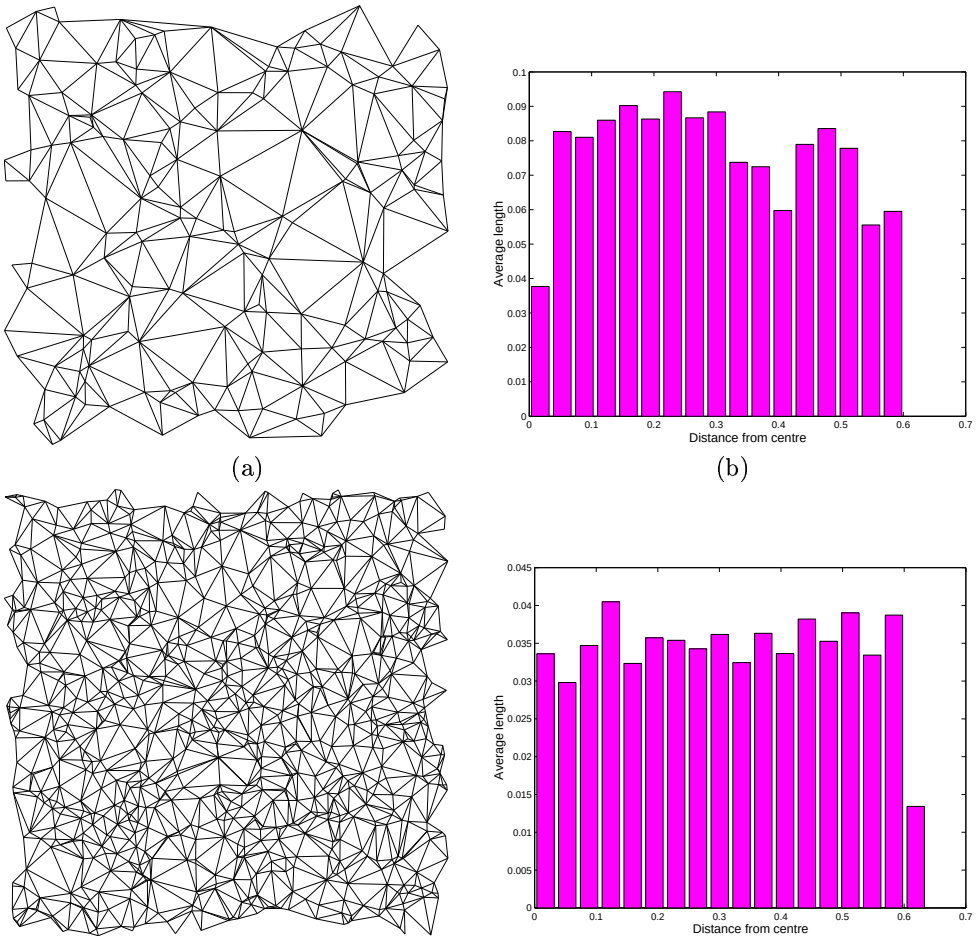


**Figure 1.15** *Point process $x, y$, where $x$ and $y$ are independent random generators within a square domain; (a) the Delaunay triangulation with 168 vertices, (b) average edge length vs distance from centre of the network, (c) another similar network, 816 vertices shown in total, (d) average edge length of the Delaunay triangulation vs the distance from centre.*

The codes used in carrying out these investigations are listed in § A.25. Figure 1.15 effectively tells us that the random point process $r\angle\theta$ gives particle distribution shaped like a bell with density decreasing away from the centre. One might almost say that this is similar to what a spiral galaxy looks like. There is still much room to explore what particle distribution the different topologies of random process give rise to, for example, 'What would the distribution in 2-d be of points that are generated from random points on a line swept in circle at a constant speed?' The algorithm is as simple as Algorithm 1.4, but the room for imagination and the scope of exploration are unlimited. There are only two variables, that is the nuclei positions $x$ and the triangulation edges $e$.

**Algorithm 1.4** *Triangulation edge length distribution.*

$x \leftarrow$ random process**;**
$e \leftarrow$ **find** triangulation of $x$**;**
$(x, e) \leftarrow (x - \partial x, e - \partial e)$**;**
**compare** $|e|$**;**

□

## § 1.10 Structures in nature

Prusinkiewicz and Lindenmayer (1990) model the structures in plants after having briefly discussed about the difference between the Chomsky grammars and the L-system, both of which being a mean for doing string rewriting, but the latter is based on the Turtle geometry which makes it convenient for the geometric rewriting of fractals. The states of a turtle consists of its position coordinates and the direction in which it is facing. Meinhardt (1995) models the patterns on sea shells by using mathematical based on the partial differential equations governing the system of activator, inhibitor,

and substrate. Starting from a homogeneous initial condition, small deviations therein undergo a positive feedback and therefore increase. Activator catalyses both the production of itself and that of its inhibitor. The latter acts as a negative feedback which limits and makes the reaction local.

Random tissue in three dimensions has four edges, six faces and four cells meeting at each vertex. It is thus surrounded by four cell nuclei, as well as by six bonds forming a tetrahedral cage. The four edges meeting at a vertex resemble a caltrop, and similarly the lines from it to the four nuclei. If a vertex had more than four edges it would have been structurally unstable, because then it can be split into two normal vertices by an infinitesimal deformation. Continuous random networks, for example models of covalent glasses like vitreous silica, are excluded from this restricted class since theirs may be more than three non-planar faces to an edge even if they still have four edges to a vertex (Revier, 1982).

Unlike crystallography, the ideal random structure is by no means unique because it is the solution of a statistical problem. There are, however, certain geometrical and topological invariances, the most famous of which is possibly the Euler's theorem. In two dimensions this theorem states that $f - e + v = \chi$, where $\chi$ is an Euler-Poincaré characteristic and integer of order one, $\chi$ being for instance 1 and 2 respectively for plane and sphere; in three dimensions it is $f - e + v = 2$. The valence relations, $\sum nf_n = 2e = 3v$, hold for 2-d and 3-d alike.

Stumbling upon some observations, Theorem's 3.3 and 3.4 resulted. These two theorems help explain together with Algorithm 3.2 on page 86, the valence relations. Theorem 1.2 is also another product obtainable from applying both the Euler's theorem and the valence relations (*cf* Prause, 2000).

**Theorem 1.2.** *The average number of edges per polygon in a large pattern is six.:*

**Proof.** From Euler's theorem, $f - e + v = 1$, and the valence relations, $\sum_n f_n = 2e = 3v$, it follows by applying the latter to the former that $f - \sum nf/2 + \sum nf/3 = 1$. Since $\bar{n}$ is the average number of edges per face, it follows that $f - \bar{n}f/2 + \bar{n}f/3 = 1$. Then $f(1 - n/6) = 1$, and consequently $1 - 1/f = n/6$. As the network becomes large, $f$ becomes infinite and as a result $\bar{n} = 6$. □

It is interesting to note that Theorem 1.2 posts no restrictions on whether the network is random or regular. The only assumption made is that three and only three edges meet at each vertex. One is almost tempted to say that, as the size of a network becomes infinite, nature somehow follows this theorem and make sure that each of the polygons has six edges on average.

When I translated the three papers by Voronoi (Tiyapan, 2001) I used the term *vertex* to mean a vertex of a specific polygon or polyhedron. For any vertex, I used the term *vertice*, and for more than one vertex vertices. It turns out that I am not the only one who concerns himself with the word. Moore and Angell (1993), for instance, use *apex* for a single corner, *vertex* to mean any point in a tessellation in two or three dimensions where its apices meet.

Rivulets flowing inside a pack bed have been studied by several authors (*cf* Porter, 1968). They are said to flow independently of each other, with no mixing among one another. Diffusion theory has been used to treat a random walk process.

The van der Waals force in combination with double layer repulsion play an important part in the study of filter and particle movements in porous media. Both are electrical forces and can be used to explain the particle capturing mechanism.

Percolation is related to chemical engineering contexts (*cf* Mohanty *et al*, 1982). But the necessary background in stochastic processes for the purpose of simulation has already been described earlier, for example the modelling of colmatage, the retaining of particles suspended in a fluid flowing through a porous medium (Litwiniszyn, 1963 and 1967). In general, however, few authors in all engineering fields relate their works directly to the percolation theory. The majority of studies in this area are based on dynamics and fluid dynamics theories (*cf* Mulder and Gimbel, 1990; Kock and Judd, 1965).

The reason for the lack of percolation material in engineering literature may be because the percolation process generally works behind the scene and only shows itself as critical phenomena. Most engineering studies are concerned with things under some operational condition, within the range of which percolation seems to be absent. By contrast, in Physics where extreme conditions are considered, there is an enormous and increasing amount of publications which are directly under the topic of percolation. But this by no means means that within a pacific range there is no place for percolation. In fact it is precisely this lack of mentioning in the literature that induces one to this kind of research. Because our idea of criticality is by tradition closely linked to the idea of time, percolation seems to be present only when there are instantaneous changes. But if in a steep s-curve

we only rotate the axis clockwise by $\pi/2$ radian, such that to make the time axis vertical instead of horizontal, then we will see that in place of one critical point in the middle of the graph connecting two different levels, there are now two critical phenomena on both sides, one on each side, and in the middle a flat region where time hardly changes. Looking at it this way percolation seems to be a symmetry between time and space. In physical systems spaces percolates, but in the dual world where criticality is continuity it is the time instead which percolates.

Having said that, without rotating the time-space axes backwards and forwards too often one should still find ways to investigate what a pacified percolation does. In this regard, the study of economics seems to be an ideal place to start, if simply because one knows there exists such thing as hyperinflation but one never wants to study that when it happens. This automatically forces the researcher to find ways of doing researches which would not ruin his pocket or put his life in jeopardy. Another ground with a good prospect is in traffic congestion, even though its worst effect is not yet devastating, apart from what it sometimes does to the economy.

With these digressions in mind, if we now turn our thought at this point to our chemical engineering studies, we will not fail to see how ideal filtration fits the no-ruins requirement. For here we have a process which percolates routinely, often needs to be backflushed, but where the effect it produce is probably that of giving engineers a headache and, at its worst, putting a decent company out of business. But even with this advantage, I still believe that the study of filtration should not concentrate only on the fouling of filters, but should try to understand both the percolated and nonpercolated situations, preferably the latter for the lack of it in literature, and to connect what happens in a working filter to what happens, or does not happen, in a fouled one.

The revolutionising discovery made by F. August Kekulé (Kekulé, 1865, cited in Wotiz, 1993) that benzene has cyclic nature gave rise to the structural theory of organic chemistry.

## § 1.11 Computational geometry

The altitude lines of a triangle are concurrent. The bisectors of the angles of a triangle are concurrent. Ceva's theorem says that, all the three lines in a triangle which contain a vertex and a point on its opposite side are concurrent if and only if no two among them are parallel and the product of the three ratios of division of the sides made in one direction around the circumference of the triangle is one. In Gergonne's theorem, the three lines of a triangle which are made by the vertices and the points of tangency of the incircle on the side opposite to them are concurrent. The intersection between the three lines tangent to the circumcircle of a triangle and the sidelines opposite to them are collinear.

A point is an extreme point of a plane convex set $s$ unless it lies in a triangle which has vertices in $s$ but is no vertex of the triangle. A ray from inside a bounded convex figure intersects the boundary of the latter at exactly one point. Consecutive vertices of a convex polygon exist in sorted angular order about any interior point. A subfacet of a simple polytope is shared by two and only two facets. Two facets share a subfacet if and only if the latter is determined by $d-1$ vertices in their set; these two facets and the subfacet are called adjacent. A line segment defined by two points is an edge of the convex hull if and only if all other points of the set lie on, or to one side of it.

The diameter of a convex figure is the largest distance between parallel lines of support. The diameter of its convex hull determines the diameter of a set. Every vertex of the Voronoi graph is the intersection of three of its edges. Every nearest neighbour of a Voronoi polygon defines an edge.

VT and the triangulation of its nuclei are dual to each other. A Voronoi graph on $n$ points has at most $2n-5$ vertices and $3n-6$ edges. The convex hull of a Voronoi graph on $n$ can be found in linear time.

Modern programming philosophy puts much emphasise on modularity of a program and on information hiding of modules. Though undoubtedly information hiding can be good for the finished products, during the course of development it sometimes works against yourself when you try to pinpoint an error in order to debug. Some modularisations are more about hierarchies than simplicity. Whenever this is the case, it is necessary to unconventionally seek a simpler path.

The explicit equation in 2-d is $y = mx + c$ or $ax + by + c = 0$. Imposing the constraint $a^2 + b^2 = 1$, that is multiplying all the terms by $(a^2 + b^2)^{-1/2}$, puts the equation into the canonical or normalised form. This makes $a = \cos\alpha$, $b\cos\beta$ and $c = -r$, where $a$ and $b$ are directional cosines, *i.e.* the cosines of the angles that the normal line makes with the $x$ and $y$ axes respectively. Examples of possible conventions are to have a normal line point towards outside of the region, to have the line direction always to the right of the normal vector, or to keep $c$ positive always.

A parametric form of line equation in 2-d is by introducing a third variable $t$ and write the equations as $x = x_0 + ft$ and $y = y_0 + gt$, where $(x_0, y_0)$ is the point on the line corresponding to $t = 0$. A line through a point $p$ which makes angles $\alpha$ and $\beta$ with the $x$ and the $y$ axes respectively has the parametric equations $x = x_p + t\cos\alpha$ and $y = y_p t\cos\beta$. One convention is to vary $t$ from 0 to 1 over a line segment, another is to normalise it by multiplying its coefficient by $(f^2 + g^2)^{-1/2}$.

An implicit line equation $ax + by + c = 0$ can be turned into a parametric form as $x = -ac/(a^2 + b^2)^{1/2} + bt$ and $y = -bc/(a^2 + b^2)^{1/2} - at$. And a parametric line described by $x = x_0 + ft$ and $y = y_0 + gt$ is converted into the implicit form as $-gx + fy + (x_0 g - y_0 f) = 0$

The implicit plane equation in three dimensions is $ax + by + cz + d = 0$. The parameters can be found by using Cramer's rule, $a = \det(1, y_i, z_i)$, $b = \det(x_i, 1, z_i)$, $c = \det(x_i, y_i, 1)$ and $d = \det(x_i, y_i, z_i)$, which gives $a = y_1 z_{32} + y_2 z_{13} + y_3 z_{21}$, $b = z_1 x_{32} + z_2 x_{13} + z_3 x_{21}$, $c = x_1 y_{32} + x_2 y_{13} + x_3 y_{21}$ and $d = x_1(y_2 z_3 - y_3 z_2) + x_2(y_3 z_1 - y_1 z_3) + x_3(y_1 z_2 - y_2 z_1)$.

A normalised form has a constraint $a^2 + b^2 + c^2 = 1$. This amounts to multiplying its implicit equation by $(a^2 + b^2 + c^2)^{-1/2}$ to get $\alpha x + \beta y + \gamma z + \delta = 0$. Here $\alpha$, $\beta$ and $\gamma$ are cosines of the angles which the normal to the plane makes with the coordinate axes. The distance between two parallel normalised planes is $\delta_2 - \delta_1$. A normalised implicit plane equation can be used to represent a planar half-space by multiplying every tems by $-1$ and then assign a convention that the vector formed by the direction cosines always points towards the outside or the inside of the region.

The distance from a point to a plane, if the plane is $ax + by + cz + d = 0$ and the point is $(x_p, y_p, z_p)$, is $r = \left[(ax_p + by_p + cz_p + d)^2/(a^2 + b^2 + c^2)\right]^{1/2}$. The intersection of two planes, from the planes $a_1 x + b_1 y + c_1 z + d_1 = 0$ and $a_2 x + b_2 y + c_2 z + d_2 = 0$, is $x = x_0 + ft$, $y = y_0 + gt$ and $z = z_0 + ht$ where $f = \det(b_i, c_i)$, $g = \det(c_i, a_i)$ and $h = \det(a_i, b_i)$, $i = 1$ and 2.

The intersection of three planes is found by Algorithm 1.5, Here the minor matrices $a^{ij}$ is $\delta^{ab}_{23}$, $\delta^{ac}_{23}$, or $\delta^{bc}_{23}$ as the case may be.

**Algorithm 1.5** *Intersection among three planes.*

$\Delta \leftarrow \sum_{(a,b,c)}(-1)^{i+j} a_{ij} a^{ij}$;
**if** $|\Delta| < \epsilon$ **then**
  at least two of the planes are parallel;
**else**
  $x \leftarrow (b_1\delta^{dc}_{23} - d_1\delta^{bc}_{23} - c_1\delta^{db}_{23})/\Delta$;
  $y \leftarrow (d_1\delta^{ac}_{23} - a_1\delta^{dc}_{23} - c_1\delta^{ad}_{23})/\Delta$;
  $z \leftarrow (b_1\delta^{ad}_{23} + a_1\delta^{db}_{23} - d_1\delta^{ab}_{23})/\Delta$;
**endif** □

The intersection between a line and the plane $ax + by + cz + d = 0$ is $(x_1 + x_{12}a, y_1 + y_{12}a, z_1 + z_{12}a)$, where $a = -(ax_1 + by_1 + cz_1 + d)/(ax_{12} + by_{12} + cz_{12})$, $x_{12} = x_2 - x_1$ and similarly for $y_{12}$ and $z_{12}$.

The area of a circle is $\pi r^2$ and that of its segment is $\theta r^2/2$. A segment is its pie cut reaching its centre while a sector is a plane slice through the sphere. The area of a sector is this area subtracted by that of a triangle, or $r^2(\theta - \sin\theta)/2$. The centre of gravity or the centroid lies on the bisector of the central angle with the distance of $4r\sin(\theta/2)/3\theta$ for a sector and $4r\sin^3(\theta/2)/3(\theta - \sin\theta)$ for a segment.

The volume of a pyramid is $Ah/3$, where $A$ is the area of base and $h$ is the height of the pyramid. The volume of a sphere is $4\pi r^3/3$, and the distance from its centroid to the sphere centre is $(3r/4)\left[\sin^4(\theta/2)/(2 - 3\cos(\theta/2) + \cos^3(\theta/2))\right]$ That of a sector of a sphere is $(\pi r^3/3)(2 - 3\cos(\theta/2) + \cos^3(\theta/2))$ The volume of a tetrahedron is $V = (1/6)\det(x_{12}, x_{13}, x_{14}; y_{12}, y_{13}, y_{14}; z_{12}, z_{13}, z_{14})$, where $x_{ij} = x_j - x_i$,or $V = (1/6)\det(x_i, y_i, z_i, 1)$. The former is limited to the case of three dimensions, and is in fact $V = (1/6)(a \times b) \cdot c$, where $a$, $b$ and $c$ are respectively the lines from O to A, B and C in a tetrahedron OABC.

Generalising the latter to higher dimensions, we have the volume of a $d$-dimensional simplex $V = (1/d!)\det(x_{ij}, 1)$, where $x_{ij}$ is now $(x_j)_i$, $1 \le i \le (d + 1)$ and $1 \le j \le d$. Here the information found in existing literature seems to be wrong, some lists the multiplying factor as $1/d$, some simply uses $1/6$ throughout all $(d \ge 3)!$ § 3.13 mentions in more detail how I arrived at the value used here.

Some of of the algorithms found in literature are the following. The algorithm to find whether a point is inside a polygon, Algorithm 1.6. The arbitrary line $l$ here, which is taken for simplicity to be horizontal, passes through $z$.

**Algorithm 1.6** *Point inside a polygon.*

$r \leftarrow 0$;
**for** $i = 1$ to $n$ **do**
  **if** edge $i$ and $l$ not parallel **then**
    **if** $i$ intersects $l$ to the left of $z$ at any point except its lower extreme **then**
      $r \leftarrow r + 1$;
    **endif**
  **endif**
  **if** $r$ odd **then**
    $z$ is internal to $p$;
  **else**
    $z$ is external;
  **endif**
**endfor** □

To find the inclusion in a convex polygon, $q \in p$ being a known fixed point within the polygon, find the wedge in which $z$ lies by doing a binary search and test whether $\angle(zqp_{i+1})$ is a right turn- while $\angle(zqp_i)$ a left turn angle. If $\angle(p_ip_{i+1}z)$ is a left turn angle, then $z$ is inside $p$.

The Euclidean minimum spanning tree may be obtained by Algorithm 1.7.

**Algorithm 1.7** *Euclidean minimum spanning tree.*

$f \leftarrow 0$;
**for** $i$ from 1 to $n$ **do**
  $s(p_i) \leftarrow 0$;
  $f \leftarrow p_i$;
**endfor**
**while** $f$ contains more than one number **do**
  $t \leftarrow f$;
  **if** (s(t)=j) **then**
    clean up;
    $j \leftarrow j + 1$;
  **endif**
$(u, v) \leftarrow$ shortest unselected edge incident on $t$, $u \in t$;
$t' \leftarrow$ tree in $f$ containing $v$;
$t'' \leftarrow$ **merge** $(t, t')$];
**delete** $(t')$ from $f$;
$s(t'') \leftarrow \min(s(t), s(t')) + 1$;
$f \leftarrow t''$
**endwhile** □

To rotate $v = (v_1, v_2)^{\mathrm{T}}$ to $v' = (v_1', v_2')^{\mathrm{T}}$, use $v^{\mathrm{T}} = Av$ where $A = [\cos\theta, -\sin\theta; \sin\theta, \cos\theta]$ is the transformation matrix and $\theta$ is the anti-clockwise angle of the rotation.

To rotate a general line in three dimensions by $\theta$ around an arbitrary axis, the transformation matrix becomes $A = T^{-1}RT$, where

$$R(\theta) = R_x^{-1}(\alpha)R_y^{-1}(\beta)R_z(\theta)R_y(\beta)R_x(\alpha)T = R_x(-\alpha)R_y(-\beta)R_z(\theta)R_y(\beta)R_x(\alpha).$$

The translation $T$ translates one point of the line to the origin and $R_x$ rotates around the $x$-axis by $\alpha$ which puts $u$ on to the $xz$ axis, $R_y$ around $y$-axis by $\beta$ and puts $u'$ on to the $z$ axis, and $R_z$ around $z$-axis. Since the vector $v$ is $(x_{12}, y_{12}, z_{12})$, we have the $a$, $b$, $c$ and the unit vector $u = (a, b, c)/|v| = (x_{12}, y_{12}, z_{12})/|v|$. Then it follows that $\cos\alpha = c/d$, $\sin\alpha = b/d$, $\cos\beta = d$ and $\sin\beta = -a$. All of these can perhaps be summarised as a linear procedure in Algorithm 1.8.

**Algorithm 1.8** *Rotation in three dimensions*

$v \leftarrow (x_{12}, y_{12}, z_{12})$;
$m \leftarrow |v|$; $a \leftarrow x_{12}/m$;
$b \leftarrow y_{12}/m$;
$c \leftarrow z_{12}/m$;
$d \leftarrow (b^2 + c^2)^{1/2}$;
$r_{xx} \leftarrow c/d$;
$r_{xy} \leftarrow b/d$;
$r_{yx} \leftarrow d$;

$r_{yy} \leftarrow -a$;
$T \leftarrow [\mathrm{I}(3), -(x_1, y_1, z_1)^{\mathrm{T}}; 0(3)^{\mathrm{T}}, 1]$;
$R_x \leftarrow [1, 0(3)^{\mathrm{T}}; 0, r_{xx}, -r_{xy}, 0; 0, r_{xy}, r_{xx}, 0; 0(3)^{\mathrm{T}}, 1]$;
$R_y \leftarrow [r_{yx}, 0, -r_{yy}, 0; 0, 1, 0, 0; -r_{yy}, 0, r_{yx}, 0; 0(3)^{\mathrm{T}}, 1]$;
$R_z \leftarrow [[\cos\theta, -\sin\theta; \sin\theta, \cos\theta], 0(2,2); 0(2,2), \mathrm{I}(2)]$;
$R \leftarrow T^{-1} R_y^{-1} R_z R_y R_x$; $v' = Rv$. □

Also in three dimensions, the rotation around the $x$-axis is

$$R_x = [\{r_{11} = 1, m_{23} = [\cos\theta, -\sin\theta; \sin\theta, \cos\theta]\}],$$

around $y$-axis is

$$R_y = [\{r_{22} = 1, m_{13} = [\cos\theta, \sin\theta; -\sin\theta, \cos\theta]\}]$$

and around $z$-axis is

$$R_z = [\{r_{33} = 1, m_{12} = [\cos\theta, -\sin\theta; \sin\theta, \cos\theta]\}].$$

The minor containing parts of the $i^{\mathrm{th}}$ and $j^{\mathrm{th}}$ rows and columns is $m_{ij}$.

The right hand coordinate system is where a 90° rotation around the $x$-, $y$- and $z$-axis bring respectively the $y$- to $z$-, $z$- to $x$- and $x$- to $y$-axis. Scaling and translating a vector $v$ in three dimensions amounts to calculating $[v'; w] = A[v; w]$, where $A$ is respectively $[\mathrm{I}(3)s, 0(3); 0(3)^{\mathrm{T}}, 1]$ and $[\mathrm{I}(3), \Delta v; 0(3)^{\mathrm{T}}, 1]$, $\Delta v = (\Delta x, \Delta y, \Delta z)^{\mathrm{T}}$.

A quaternion can be described as a pair $(s, v)$ of a scalar $s$ and a vector $v = (a, b, c)$. The rotation by $\theta$ around an axis in the direction of a unit vector $u$ is then the quaternion $(\cos\theta/2, u\sin\theta/2)$. Let $q = (s, v)$. Then $q^{-1} = (s, -v)$. The multiplication of quaternions is $q_1 q_2 = (s_1, v_1) \cdot (s_2, v_2) = (s_1 s_2 - v_1 \cdot v_2, s_1 v_2 + s_2 v_1 + v_1 \times v_2)$, where the cross product is described in minors as $v_1 \times v_2 = [\delta^{yz}; -\delta^{xz}; \delta^{xy}]$.

Let $q$ represent a rotation. Then a vector $p$ is rotated to $p'$ by $P' = qPq^{-1}$, where $P$ and $P'$ are respectively $(0, p)$ and $(0, p')$. In simplified words, this means $p' = s^2 p + (p \cdot v)v + 2s(v \times p) + v \times (v \times p)$. Then we have the transformation matrix for the general rotation around $u$ in three dimensions,

$$R_u(\theta) = \begin{bmatrix} (1 - 2b^2 - 2c^2) & (2ab - 2sc) & (2ac + 2sb) \\ (2ab + 2sc) & (1 - 2a^2 - 2c^2) & (2bc - 2sa) \\ (2ac - 2sb) & (2bc + 2sa) & (1 - 2a^2 - 2b^2) \end{bmatrix}$$

where $s = \cos\theta/2$ and $v = (a, b, c) = u\sin\theta/2$. Furthermore, if $q_1$ is a rotation by $\theta_1$ around $v_1$ and likewise $q_2$ by $\theta_2$ around $v_2$, then $q_3 = q_2 q_1$ is a rotation by $\theta_3 = 2\cos^{-1} s_3$ around $v_3$ such that $\sin\theta_3 \geq 0$.

Quaternion is an extension of complex number to higher dimensions where there are three imaginary parts instead of one. It is defined as $q = s + ia + jb + kc$, where $a$, $b$, $c$ and $s$ are real numbers, $i^2 = j^2 = k^2 = -1$ and $ij = -ji = k$.

Let a plane be described by $(v - p) \cdot n = 0$, where $p$ is a point on-, and $n$ a perpendicular to the plane. This means that, for all points $v$ lying in the plane $(p, n)$, $(v - p) \cdot n = 0$. If the plane $(p, n)$ is transformed into $(Ap, m)$, then $Av$ lies in $(Ap, m)$ and consequently $A^{\mathrm{T}} m = n$ or $m = (A^{\mathrm{T}})^{-1} n$.

A vector normal to the surface remains normal if it is transformed by $(A^{\mathrm{T}})^{-1}$. When a transformation matrix $A$ has the property $A = (A^{\mathrm{T}})^{-1}$, for example rotation, all surface normals remain normal. But in general this equality does not hold, so we have for instance the non-uniform scaling where these normals cease to be normal.

To test for the intersection between a ray and a triangle using Plücker's coordinates is described in Algorithm 1.9.

**Algorithm 1.9** *Ray and triangle intersection.*

**find** Plücker's coordinates for vertices and the ray;
**test** ray against each of the edges;
**if** ray hits an edge, passes all of them clockwisely or all of them counter-clockwisely **then**
  ray intersects the triangle;
**else**
  ray and triangle intersect not;
**endif** □

If these vertices are $v_1$, $v_2$ and $v_3$, and the ray is $r = r_{12} = r_2 - r_1$, where $r_1$ and $r_2$ are any two points on the ray, then Plücker's coordinates for the vector $v_{12}$ are $(u, v) = (v_2 - v_1, v_2 \times v_1)$, and similarly for $v_{23}$, $v_{31}$ and $r_{12}$. For the test between the ray and each edge, find $c = u_r \cdot v_i + v_r \cdot u_i$.

Then the ray $r$ counter-clockwisely passes the edge $i$, hits it or clockwisely passes it respectively as $c < 0$, $c = 0$ or $c > 0$.

A 3-d line can be represented by the six numbers that come with coordinates of two distinct points, or by the eight numbers that come with the coordinates of two distinct planes. Plücker's coordinates, however, provides a mean which suits geometrical computation better than both of these. It redefines the coordinates as $u = p - q$ and $v = p \times q$, where $p$ and $q$ are two points on a line, neither quantity of which depends on $p$ or $q$.

Let a tetrahedron has its vertices at $a_i$, $i = 1$ to 4. Then the centre of its circumsphere is at $a_1 + \delta$ and its corresponding radius $r = |\delta|$, where

$$\delta = \left[|a_{12}|^2(a_{13} \times a_{14}) + |a_{13}|^2(a_{14} \times a_{12}) + |a_{14}|^2(a_{12} \times a_{13})\right] /2|a_{12}^{\mathrm{T}}; a_{13}^{\mathrm{T}}; a_{14}^{\mathrm{T}}|.$$

A triangle $\triangle p_1p_2p_3$, where $p_i = (x_i, y_i)$ and $i = 1$ to 3, has an area $A = |x, y, 1(3)|$, which is positive if and only if $\triangle p_1p_2p_3$ forms a counter clockwise cycle or $\angle p_1p_2p_3$ is left-turned. Or equivalently the area is $A = \det(x_{12}, x_{13}; y_{12}, y_{13})$, which is positive if the points are in anti-clockwise order of the indices and negative otherwise. Or the area is $A = [s(s - d_1)(s - d_2)(s - d_3)]^{1/2}$, where the the semi perimetre $s$ is $s = \sum_i d_i/2$, where $d_i$, $i = 1$ to 3, are the lengths of the three sides of the triangle.

For a convex polygon, the area can be found by adding together the $n$ triangles formed by any two adjacent vertices and one fixed point within the polygon. Here $n$ is the number of vertices it contains. Or it can be found by adding the $(n - 2)$ triangles formed by one fixed vertex and any two adjacent vertices of those remaining. Another way of finding the area is $A = (1/2)\sum_{i=0}^{n-1}(x_iy_{i+1} - y_ix_{i+1})$, where $(x_i, y_i)$ are vertices. Rearranging to make it faster and more accurate, $A = (1/2)\sum_{i=0}^{n-1}((x_i + x_{i+1})(y_{i+1} - y_i))$. If the dimension of the polygon is higher than two, $A = (1/2)\left|N \cdot \sum_{i=0}^{n-1}(v_i \times v_{i+1})\right|$, where $N$ is a unit vector normal to the plane. The area of a polygon can also be computed, without loosing generality, by subtracting the area under its lower edges by that of its upper edges.

A vector normal to a plane is simply $n = v_{12} \times v_{13}$.

The ordering of vertices on a face of a polygon is done for the purpose of drawing it or for finding vertice pairs which form edges. This can be done in two ways. One is to get inside the polygon and look at all the vertices around comparing their angles relative to one another. Another one is to look at the polygon from a distance and compare their angles as before, as well as their distance from the viewing point. The angle is $\theta = \arccos[(v_1 \cdot v_2)/(|v_1||v_2|)]$, where $v_1$ and $v_2$ are vectors to vertices from the distant point, and $\theta$ the angle between them.

To find the convex hull in three dimensions, one may use Algorithm 1.10.

**Algorithm 1.10** *Convex hull in three dimensions.*

**sort** $s$ by $x_1$ such that $x_i(p_i) < x_i(p_j)$ if and only if $i < j$;
**if** $|s \leq k|$ **then**
  **construct** $c(s)$;
**else**
  $s_1 \leftarrow \{p_1, \ldots, p_{\lfloor n/2 \rfloor}\}$;
  $s_2 \leftarrow \{p_{\lfloor n/2 \rfloor}, \ldots, p_n\}$;
  $p_1 \leftarrow c(s_1)$;
  $p_2 \leftarrow c(s_2)$;
  $p \leftarrow$ **merge** $p_1$ and $p_2$;
**endif** □

Here $c(s)$ is the convex hull of $s$. Two convex hulls are merged with each other by first constructing a cylindrical triangulation T which supports $p_1$ and $p_2$ along two circuits $e_1$ and $e_2$ respectively, then remove from both $p_1$ and $p_2$ the portions which have been obscured by T.

The following Jarvis's march algorithm, Algorithm 1.11, finds a convex hull in two dimensions.

**Algorithm 1.11** *Convex hull in two dimensions*

$p_1 \leftarrow$ the lowest point in $s$;
$q_1 \leftarrow$ the highest point in $s$;
**while** next point $\neq q_1$ **do**
  **find** $p_i \in s$, $i = 2, 3, \ldots$, with an increasing order of the polar angles
    with respect to $p_1$;
**endwhile**

**while** next point $\neq p_1$ **do**
  **find** $q_i \in s$, $i = 2, 3, \ldots$, with an increasing order of the polar angles
    with respect to $q_1$ and the negative $x$ axis;
**endwhile** □

The polar angle is an angle with respect to the positive $x$-axis. The lowest and the highest points are on the convex hull.

Algorithm 1.12 is the quick hull algorithm.

**Algorithm 1.12** *Quick hull algorithm.*

$l \leftarrow (x_0, y_0)$;
$r \leftarrow (x_0, y_0 + \epsilon)$;
**if** $s = \{l, r\}$ **then**
  **return** $(l, r)$;
**else**
  **find** $k \in s$ that gives $\max A_{\triangle klr}$ or ($\max A_{\triangle klr}$ and $\max \angle klr$);
  $s^1 \leftarrow p \in s$, such that $p$ is on the left of $\overrightarrow{lh}$;
  $s^2 \leftarrow q \in s$, such that $q$ is on the left of $\overrightarrow{hr}$;
  $\{h\} \leftarrow (s^1; l, h)$;
  $\{h\} \leftarrow (s^2; h, r) - h$;
**endif** □

The convex hull is $\{h\}$. The points $l$ and $r$ are with respectively the smallest and the largest abscissa. In other words they are the left-most and the right-most points. And $k$ is the furthest point with respect to $l$ and $r$.

Let $p = \{p_1, p_2, \ldots, p_n\}$ be a set of $n$ generators in $\nu$-dimensional space, the coordinates of which are $(x_{ij})$, $i = 1$ to $d$ and $j = 1$ to $n$. Then the Delaunay tessellation in $d$ dimensions which spans $p$ is generated by,

**for** $j = 1$ to $n$ **do**
  $\{q\} \leftarrow q_j = (x_{ij}, \sum_j x_{ij}^2)$;
**endfor**
$h \leftarrow c(q)$;
**project** all the lower $n$-faces of $c(q)$ parallel to the $d^{\text{th}}$ axis on to the original $n$-d space;
□

Okabe *et al* (1992) give a good review of algorithms for generating VT's. Given the set of generator points $\{p_i\}$, $i = 1$ to $n$, a brute force albeit simple method generates for all $i$ and $j$ from 1 to $n$ the $(n-1)$ half planes $h(p_i, p_j)$, $1 \leq j \leq n$, $i \neq j$, and then proceeds to construct all $\mathcal{V}(p_i)$ of the VT from their common intersections.

On the other hand, the following Algorithm 1.13 is the quaternary incremental method whose inputs comprise the $(n-3)$ generators $p_i$, $i = 4$ to $n$, where all the $p_i$ are in $s = \{(x, y) | 0 \leq x, y \leq 1\}$, and three additional generators $p_1 = (0.5, 0.5(1 + 3\sqrt{2}))$, $p_3 = (0.25(2 - 3\sqrt{6}), 0.25(2 - 3\sqrt{2}))$ and $p_3 = (0.25(2 + 3\sqrt{6}), 0.25(2 - 3\sqrt{2}))$.

**Algorithm 1.13** *Quaternary incremental method.*

$k \leftarrow \min(k_i)$ such that $k_i \in \mathrm{I}^+$ and $n < 4^{k_i}$;
$s_{ij} \leftarrow (i - 1, i/2^k, j - 1, j/2^k)$;
**construct** a quaternary tree;
**scan** leave buckets from left to right, top to bottom, **put** generators in buckets;
$\{p_i\}$ **do** quaternary reordering on the generators;
$\mathcal{V} \leftarrow$ **construct** Voronoi for $p_1$, $p_2$ and $p_3$;
**for** $i =$ **4 to** $n$ **do**
  repeat $\leftarrow 1$;
  **while** repeat **do**
    **find** $p_\alpha$ such that $\mathrm{d}(p_\alpha, p_\ell) = \min_j \mathrm{d}(p_j, p_\ell)$;
    **if** $\mathrm{d}(p_m, p_\ell) < \mathrm{d}(p_\alpha, p_\ell)$ **then**
      repeat $\leftarrow \neg$**repeat**;
    **elseif** $p_m \leftarrow p_\alpha$ **do** nothing;
    **else**
      repeat $\leftarrow \neg$**repeat**;
    **endif**

**endwhile**
$\{w_{i1}, w_{i2}\} \leftarrow$ the intersections between the perpendicular
bisector of $p_i p_l$ and $\Omega(\mathcal{V}(p_i))$, $1 \leq i \leq \ell - 1$;
$\Omega \leftarrow$ **construct** the boundary of $\mathcal{V}(p_i)$ formed by these $\overline{w_{i1} w_{i2}}$;
$\{\mathcal{V}_\ell\} \leftarrow (\{\mathcal{V}_{\ell-1}\} \bigcup \Omega) - \{\mathcal{V} | \mathcal{V} \in \{\mathcal{V}_{\ell-1}\}, \mathcal{V}$ is within $\Omega\}$;
**endfor**
$\{\mathcal{V}\} \leftarrow \{\mathcal{V}_n\}$;

The construction of $s_{ij}$ is such that $s_{ij} = (i-1, i/2^k] \times (j-1, j/2^k]$, where $i, j \in \mathrm{I}^+$, $i$ and $j$ are 1, 2, ... up to $2^k$. The nearest neighbour search finds from $\ell$ generators, $p_1, \ldots, p_\ell$, and $\{\mathcal{V}_{\ell-1}\}$, the generator point $p_m$ such that $\mathrm{d}(p_m, p_\ell) < \mathrm{d}(p_m, p_i)$ for all $i = 1$ to $\ell$, $i \neq m$ and $i \neq \ell$; $p_j$ are all generators adjacent to $\mathcal{V}(p_i)$. The boundary growing procedure gives the sequence of boundaries $\{\Omega\}$. The additional generators mentioned in the procedure is graphically shown in Figure 1.16.

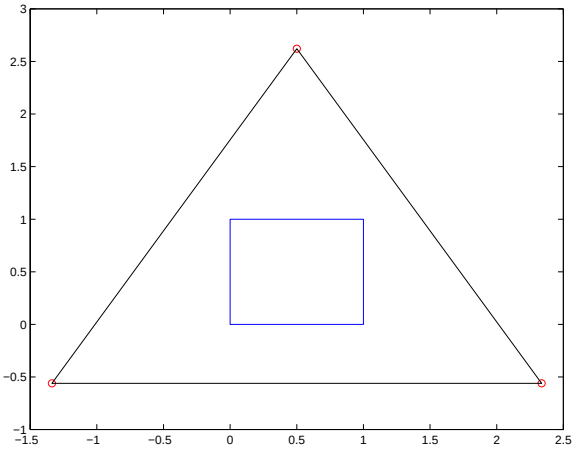


**Figure 1.16** Additional generators for the incremental method.

If we draw a horizontal line through each point in two dimensions, or a horizontal plane each point in three dimensions, we divide the space into slabs the line segments within which do not intersect one another. In three dimensions, and for a polygonal model of porous media, we can for instance divide the model into such slabs, then find the effective cross sectional area of each slab, and then determine where the bottle neck to the flow occurs within the media. Whether this would produce the correct determination of the pressure of flow across the material is another matter because flows through porous media may be governed by the combination of the various tortuous paths through the pores, the interrelationship of which can be complicated.

These slabs provide another method in finding the area, or in three dimensions the volume, of each cell of the tessellation. Here the cell is divided into slabs, and then the area or volume of each section calculated.

In three dimensions, rotation around the $x$-axis is done by $\begin{bmatrix} 1 & 0 & 0 \\ 0 & \cos\theta & -\sin\theta \\ 0 & \sin\theta & \cos\theta \end{bmatrix}$, around $y$-axis by $\begin{bmatrix} \cos\theta & 0 & \sin\theta \\ 0 & 1 & 0 \\ -\sin\theta & 0 & \cos\theta \end{bmatrix}$ and around $z$-axis by $\begin{bmatrix} \cos\theta & -\sin\theta & 0 \\ \sin\theta & \cos\theta & 0 \\ 0 & 0 & 1 \end{bmatrix}$.

## § 1.12 Geometric algorithms

The program `findfarea.m` in § A.26 finds the area and plane parameters of a face from a matrix containing the list of the coordinates of the ordered vertices. Its synopsis is `(a,p)=findfarea(v)`, where `a` is the face area, `p` the list of the plane parameters and `v` the coordinate matrix.

Real problems are algebraical or analytical whereas computer simulations are arithmetical and numerical (*cf* Knuth, 1997). In between these two lie computer programs. Therefore the latter are mapping from the analytical to the arithmetical world. There are different ways to solve a problem analytically, and there are different ways numerically. Therefore numerical study by simulation is an endless pursuit. Several programs listed in § A do the same job, but each one does it differently.

Hamiltonian's are essentially a function that maps $N$ bodies pairwisely to account for all pairs of their mutual interactions. They occur in most fields where there are particles interacting with each other. In quantum mechanics, for example, the time independent Schrödinger equation for a system of $N$ particles interacting via the Coulomb interaction is $H\Psi = E\Psi$, where the Hamiltonian is

$$H = \sum_{i=1}^{N} \left( -\frac{\hbar}{2m_i} \nabla_i^2 \right) + \frac{1}{2} \sum_{i=1}^{N} \sum_{j \neq i}^{N} \frac{z_i z_j}{4\pi\epsilon_0 |r_i - r_j|}, \qquad (12)_{\mathrm{i}}$$

where $\Psi$ is the $N$-body wavefunction, $z$ the charges of the individual particles and $E$ the energy of either the ground or an excited state of the system. Similarly from Rushbrooke and Morgan (1961), using their notations, the Hamiltonian of the Ising problem is

$$\mathcal{H} = -2J \sum_{\langle i,j \rangle} s_3^{(i)} s_3^{(j)} - g\beta H \sum_{(i)} s_3^{(i)}, \qquad (\mathbf{13})_{\mathrm{i}}$$

where $\beta$ is the Bohr magneton, $g$ the gyromagnetic ratio and $J$ the magnitude of the exchange interaction.

When simulating such systems, the number of pairwise summation terms can be reduced by half because they represents a symmetric matrix. The total number of terms is thus reduced from $N(N-1)$ to $N(N-1)/2$ (*cf* Wray *et al*, 1983). Because $i \neq j$, all the diagonal components of the matrix are excluded, which makes the number of pairs $n^2 - n = n(n-1)$. In a program, this is equivalent to two $if$ statements, one embedded within the other in the form $i(j(\cdot))$, where the index $i$ runs from 1 to $(n-1)$ and $j$ from $(i+1)$ to $n$; this has been discovered from experience, as can be seen by comparing the present work with the earlier one (Tiyapan, 1995, KNT3(iii)).

## § 1.13 TEXnicalities

LaTEX is a macro which runs on TEX. It gives one convenience but not without a tradeoff in understanding. Also one may not have much freedom in writing macros on LaTEX. Tiyapan used TEX for his Work Notes dated $12^{th}$ February 2001 .

LaTEX(Lamport, 1985) is written by Leslie Lamport. Newer versions of it has come up at a regular interval. Unlike most other macros which run on TEX, her source code is free for none but herself. Moreover, having used TEX to do what it wants, LaTEX thereby castrates her progenitor in such a way that it is impossible for her users to define new macros efficiently by using the `\def` command. With `\def` disabled, the lion has lost its fangs and users become as docile and dependent as a lobotomised patient. There can be no doubt that with the TEX users having such idea as this, sooner or later LaTEX will have to change in these respects. But this is the way things are at present.

One of the first macros written is the code to change the date format. The algorithm first sets $x = date$, then it assigns the ordinate endings *st, nd, rd* or *th* depending on the value of *ordinate*, which is calculated from

if $x > 30$ then $ordinate = 1$ else
  if $x > 20$ then $ordinate = x - 20$ else
    $ordinate = date$
  endif
endif

The macros which are either newly written or adapted from elsewhere, mainly from the *manmac* macroby Knuth, are listed in § 1.13. Apart from these, this thesis uses the *plain* and the *manmac* macros. Another set of macros developed here is that which deals with languages. The definition of language here is quite wide. It contains many languages among which are those which are used here, for example the languages for Chemistry, Chinese, Czech, German, French, grammatical jargons, Japanese, Lanna, Latin, latin grammar, Mathematics, Pali, Physics, Russian, Sanskrit, and Thai (Daiy), *etc.* Only parts of this set of macros are useful for the writing of this thesis, not least so those which are used for writing the dedication page.

In the original account of his, Tiyapan (2003, KNT8(iii)) wrote,

> When I first started using TEX instead of LaTEX, I only used the macro `plain.tex`. Then in my first book typeset with TEX (Tiyapan, 2001, KNT8(ii)), I used in addition to the plain TEX `manmac.tex` and `epsf.tex`. Now to my amazement, I have discovered many other excellent macros, for instance `rotate.tex`, and found that I could understand how they work when I read them. This is one of the benefits that comes with talking in TEX instead of, for instance, LaTEX. I also know now the difference between the primitive TEX and plain TEX, and that the latter is only one of the infinitely many possible implementations of TEX. However, since all TEX gurus I know use plain TEX as a basis, there is no reason why I should be too proud to follow the practice. Having said that, my next plan is to improvise on the primitive TEX without any direct reference to the plain TEX macro.

The citation program BibTEX was intended to be used with LaTEX. Karl Berry and Oren Patashnik have written `btxmac.tex` which makes BibTEX usable from plain TEX. But for the present

purpose I merely use my own macros, which are much simpler, and do not need BibTEX. Ultimately such database program as BibTEX would have been extremely useful. But I wish to develop something similar to it on my own.

There are still some unsolved problems in the TEX macros, for example the page references which are embedded within groups are sometimes slightly wrong, that is they may appear to be one more or one less than their actual position. Since publishing macros play but a minor part here compared with mathematics and physics, this problem has been systematically minimised and then tolerated. The solution and explanation of it will be dealt with and published elsewhere.

When lines of text appear beside a picture there are macros which make the latter always stay next to the outer rim of the page. These work satisfactorily well, and those cases in the results which appear to say otherwise are in fact the result of some other more primitive macros earlier written.

## § 2. Division of space

A stochastic system which is stochastically invariant under arbitrary translation, that is under the transformation $x \to a + x$, is homogeneous. Homogeneity lets us use the ergodic theory, namely $\dot{F}_{Z,q}(z) \to \dot{F}_Z(z)$ with probability one as $q$ approaches infinity for all $z$ in $Z$, in other words the empiric- implies the ergodic distribution function of the characteristic $Z$ for the cell $C$ in $Q(q)$. Empirical moments, $\dot{E}_q(z) = \int z \mathrm{d}\dot{F}_{Z,q}$, almost surely converge to the corresponding ergodic moments, $E(z) = \int z \mathrm{d}F_Z(z)$. The study of random division of space aims at defining classes of parameter dependent random divisions and determining their important ergodic distribution. The most important ergodic distribution is the volume (Miles, 1972). But $E(V)$ itself is not particularly informative because it only shows the scale of the model. The best representative of the nature of a random division is then the *coefficient of variation*, $\mathrm{cv}(V)$, which is the ratio of the standard deviation to the mean. The mean 1-projection or mean caliper diameter, $M_1$, of a domain is the mean length of its orthogonal projection onto an isotropic random line, whereas the mean 2-projection is the mean area of its orthogonal projection onto the same. For a polyhedron, $M_1(4\pi)^{-1} \sum d_e^i(\pi - \theta_i)$ where $\theta_i$ is the dihedral angles in radians. The $i$-facets of a polyhedron, $i = 0, 1, 2$, are its vertices, edges and faces respectively. The seven values of the basic integral geometric polyhedral quantities are $V$, $A$, $M_1$, $d_e$, $n_c^f$, $n_c^e$ and $n_c^v$. If a polyhedron is simple, *i.e.* each vertex is in three and only three faces, then $3n_c^v = 2n_c^e$ and from Euler's formula, $n_c^v - n_c^e + n_c^f = 2$, then it follows that the value of any one of $n_c^v$, $n_c^e$ and $n_c^f$ determines the value of the other two. The mean value of $n_c^f$ give a good idea of the overall interface structure, and so is only next in importance to the $\mathrm{cv}(V)$. The homogeneous Poisson $s$-flats in $\mathrm{R}^d$, $\mathcal{P}(s, d)$, underlies most forms of random divisions of space (*cf* Miles, 1972), in particular $\mathcal{P}(0, d)$ where $d = 2$ or 3. Under this notation the standard Poisson process is $\mathcal{P}(0, 1)$. The basic properties of $\mathcal{P}(0, 3)$ are that

$$\mathrm{P}(\text{there are } n \text{ particles in } X \subset V) = e^{-\rho V}(\rho V)^n / n! \qquad (\mathbf{14})_{\mathrm{ii}}$$

where $n = 0, 1, \cdots$, that is the probability is a Poisson $(\rho V)$ distribution, and that the numbers of particles in disjoint domains are mutually independent. Miles (1972) gives descriptions of various kinds of random tessellation, for example the box tessellation and particularly the generalised Johnson-Mehl model, described here as Algorithm ℵ, which includes both the standard Johnson-Mehl and the Voronoi tessellation in three dimensions as special cases.

**Algorithm 2.1** *Generalised Johnson-Mehl model, Miles (1972)*

**for** each time step **do**
  **while** more nuclei to be born **do**
    **borns** a nucleus;
    **if** the new nucleus would occupied a site already occupied **then**
      **remove** the nucleus;
    **endif**
  **endwhile**
  **for** all growing nuclei **do**
    **for** all its rays still growing **do**
      nucleus **radiates** with speed $v$;
    **endfor**
  **endfor**
  **for** all those nuclei which has just grown **do**
    **for** all its rays just grown **do**
      **if** it has met with a ray of another nucleus **then**
        **label** both rays as grown;
      **endif**
    **endfor**
    **if** all its rays are grown **then**
      **label** the nucleus as fully grown;
    **endif**
  **endfor**
**endfor** □

Similar to the Minkowski space, the stochastic nucleus birth process is in (3+1)-dimensional space, $(x, y, z; t)$-space where $t \geq 0$ which can be denoted by $\mathrm{R}^4_+$. This process is homogeneous in $(x, y, z)$ but not necessarily so in $t$ because in the actual development process it is always inhomogeneous with respect to time. Then this birth process is a Poisson point process in $\mathrm{R}^4_+$, which is inhomogeneous in $t$ and with the intensity $\alpha(t)$. For the standard Johnson-Mehl, $\alpha(t) = \alpha$ is a constant, whereas for the Voronoi $\mathcal{V}(3,3)$, $\alpha(t) = \rho\delta(t)$, where $\delta(\cdot)$ is the Dirac $\delta$ function. This model is thus a general one which can be fitted to a wide range of data by choosing some appropriate $\alpha(\cdot)$.

Each $i$-facet of the Voronoi tessellation $\mathcal{V}$, created from $\mathcal{P}(0,3)$, is an $i$-facet of $4-i$ members of $\mathcal{V}$, with each point on the $i$-facet being equidistant from the corresponding $4-i$ nuclei where $i = 0, 1, 2$. The exact values of the moments of the 3-d Voronoi tessellation in the notation used by Miles (1972) are: for first order moments, $\mathrm{E}(V) = \rho^{-1}$, $\mathrm{E}(S) = (256\pi/3)^{1/3}\Gamma(5/3)\rho^{-2/3} = 5.821\rho^{-2/3}$, $\mathrm{E}(M_1) = 4^{2/3}\pi^{5/3}\Gamma(1/3)\rho^{-1/3}/(3^{5/3}5) = 1.458\rho^{-1/3}$, $\mathrm{E}(L_1) = 12\,\mathrm{E}(M_1) = 17.50\rho^{-1/3}$, $\mathrm{E}(N_2) = (48\pi^2/35) + 2 = 15.54$, $\mathrm{E}(N_2^*) = 8$, $\mathrm{E}(N_1) = 144\pi^2/35 = 40.61$ and $\mathrm{E}(N_0) = 96\pi^2/35 = 27.07$; for a second moment, $\mathrm{E}(V^2) = 1.180\rho^{-2}$; for the aggregate of edges, $\mathrm{E}(L) = \mathrm{E}(L_1)/\,\mathrm{E}(N_1) = 0.4309\rho^{-1/3}$; for the aggregate of faces, $\mathrm{E}(A) = \mathrm{E}(S)/\,\mathrm{E}(N_2) = 0.3746\rho^{-2/3}$, $\mathrm{E}(B) = 2\,\mathrm{E}(L_1)/\,\mathrm{E}(N_2) = 2.252\rho^{-1/3}$ and $\mathrm{E}(N) = 3\,\mathrm{E}(N_0)/\,\mathrm{E}(N_2) = 5.228$; for the plane section, $\mathrm{E}_2(A) = 1/\rho\,\mathrm{E}(M_1) = 0.6859\rho^{-2/3}$, $\mathrm{E}_2(B) = (6/\pi)^{1/3}5\Gamma(2/3)\rho^{-1/3} = 3.136\rho^{-1/3}$, $\mathrm{E}(N) = 6$ and $\mathrm{E}(A^2) = 0.698\rho^{-4/3}$; and for the line section, $\mathrm{E}_1(L) = 4/\rho\,\mathrm{E}(S) = 0.6872\rho^{-1/3}$, $\mathrm{E}_1(L^2) = 0.682\rho^{-4/3}$, $\mathrm{E}_1(L^3) = 0.668\rho^{-1}$ and $\mathrm{E}_1(L^4) = 0.774\rho^{-4/3}$. In our terminology, $\rho$, $S$ and $L_1$ are respectively $\rho_c$, $A$ and $d_e$, $N_0$, $N_1$, $N_2$ and $B$ respectively $n_c^v$, $n_c^e$, $n_c^f$ and $s$. The Delaunay tessellation, on the other hand, is better understood since we know that

$$\mathrm{E}(V^k) = \frac{35\pi^{1/2}(k+2)!(2k+4)!}{256\Gamma\left(\frac{1}{2}k+2\right)\Gamma\left(\frac{1}{2}(3k+9)\right)(8\pi\rho)^k}. \qquad (\mathbf{15})_{\mathrm{ii}}$$

Shape is the most fundamental geometrical property. Shape and size are all the geometrical information that remain when location and rotational effects are filtered out from an object (Dryden and Mardia, 2002), and between these two you can take the size away so that only shape remains for further analysis. When we talk about particle sizes in simulation, it is usually the case that we have already assumed some kind of particle shape. This is because the definition of size is only meaningful if you have some idea about the shape. Shape analysis works with landmarks, which are also known as anchor-, control-, design-, key-, model-, profile-, or sampling points, facets, markers, nodes, sites, fiducial markers, *etc.* Dryden and Mardia (*ibid.*) work with three types of landmarks, *viz.* anatomical-, mathematical- and pseudo landmarks. Their work could become very interesting if combined with another problem of object location (*cf* Tiyapan, 1996, KNT4(v) and KNT4(vi)). A landmark can be unlabelled or labelled with a name or number. A particular member of the shape set which is used as a representative of all other members is the icon of that set. For the shape analysis in two dimensions the thin-plate spline is a convenient tool which is bijective and is analogous to the monotone cubic spline.

## § 2.1 Stereographic projection

*Stereographic projection* (*cf* Phillips, 1949) is used to represent a three-dimensional figure in two dimensions. It is useful in the study of symmetry of crystals. The stereographic projection of a cube is shown in Figure 2.1.

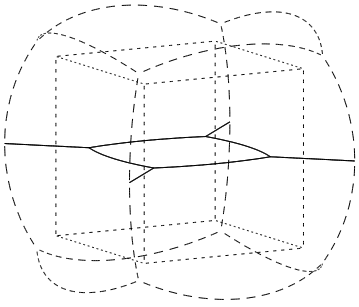

Figure 2.1 *Stereographic projection* of a cube. A stereographic projection is drawn by first projecting each vertex on to the surface of a sphere encircling the polyhedron along the line coming from the origin of the sphere. The projected point on the sphere surface is then projected on to the plane $z = 0$ (ie. $(x, y, 0)$) along the line which originates from it and goes towards the nadir point relative to the half-sphere surrounding it that rests on the $z = 0$ plane.

With this kind of projection, points that are symmetrical to each other with respect to the plane $z = 0$ are projected on to the same point on that plane. Therefore it is a normal practice to

distinguish points of the two hemispheres by drawing those in one of them as dots, while drawing the rest as circles. Continuous lines going from one hemisphere to another will become discontinuous on the projected plane. In Figure 2.1, the top and the bottom squares of the cube is projected on top of each other, while the four edges parallel to the $z$-axis go to the circumference of the great circle of the projected plane first, then retrace their ways back to their vertices.

Figure 2.1 shows that, in effect, what the stereographical projection does is to bloat a polyhedron out into a spherical balloon, and then project the image obtained on the balloon on to the horizontal plane. What the second projection does is to look at the hemisphere above it with a 90° wide-angled lens from the nadir position. In order to compare the shape of the original polyhedron with the top-view of the balloon as well as the stereographical image, Figure 2.2 draws our cube rotated one radian around the vector $(0.3, 0.4, 0.866)$. Such rotation can be done by using the transformation matrix

$$M = \begin{bmatrix} 1-2(y^2+z^2) & 2(xy-wz) & 2(xz+wy) \\ 2(xy+wz) & 1-2(x^2+z^2) & 2(yz-wx) \\ 2(xz-wy) & 2(yz+wx) & 1-2(x^2+y^2) \end{bmatrix},$$

where $[(x,y,z),w] = q$, a quaternion, $(x,y,z) = u\sin\alpha$ and $w = \cos\alpha$. Here $u = (a,b,c)$ is the direction cosine vector of the axis of rotation and $\theta = 2\alpha$ is the angle of rotation.

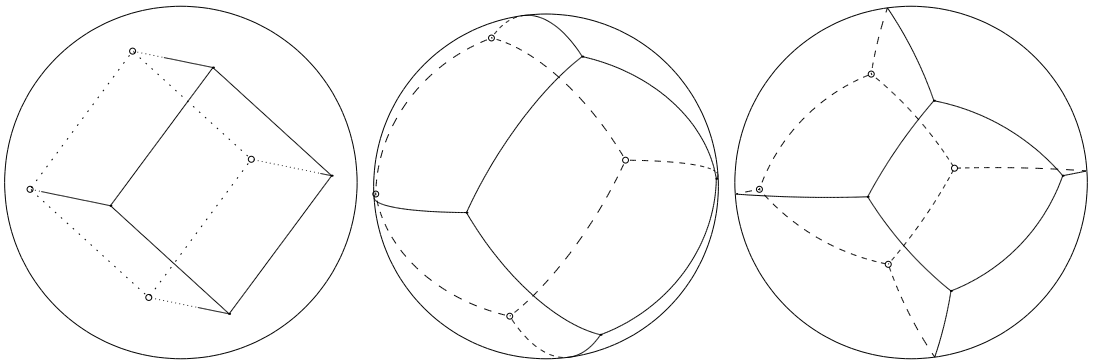

(a) (b) (c)

**Figure 2.2** *Rotated cube, (a) top-view, (b) top-view of its bloated sphere and (c) the stereographic projection. While (c) shows the same amount of symmetry information as the other two, it incorporates more information regarding the z-coordinate than the others, (b) being the least informative in this respect.*

The information regarding symmetries of the polyhedron is preserved by the projection. In practice, when it is applicable and possible, the sphere is positioned such that its centre coincides with the centre of symmetry of the polyhedron, the plane $z = 0$ on one of the symmetry planes, and the planes $y = 0$ and $x = 0$ on two others. Thus Figure the projection of 2.2 clearly shows the symmetry around the centre as well as the reflection symmetries with respect to the planes $z = 0$, $y = 0$, $x = 0$, $x = y$ and $x = -y$. Figure 2.2, on the other hand, only shows the symmetry around the centre.

The stereographic projection is an example of a homeomorphism, that is to say, a mapping of one figure onto another that is both continuous and one to one.

A stereographic net is called the Wulff net. It comprises a family of great circles at 2° intervals and a family of small circles. The great circles are equivalent to the meridians of longitude while the small circles the parallel latitudes (*cf* Cox *et al*, 1974).

The stereogram which is made up of two 2-d pictures, one for each eye, can also be used for visualising a crystal structure in three dimensions. It works by tricking or brain to see the virtual 3-d image from the input prepared for both eyes. Unlike the stereoscope which requires a viewing device, an autostereogram requires none and only a little practice. During the 1990's there has been a boom in businesses related to a certain type of stereogram referred to as SIRDS, Single Image Random Dot Stereogram, which was only a new name for the autostereogram. The boom of this business had the origin in Japan and was fueled by consumers in the east-asian countries, including Thailand. In this kind of autostereogram there are no two separate images. The two images appear as dot patterns embedded within a random pattern of dots in the background. This makes one see the 3-d images arising out of the blue amidst a seemingly chaotic random mixing of dots. SIRDS sometimes appears as another variant called Single Image Stereogram, SIS, which uses patterns in

place of dots.

Stereograms and Autostereograms have no depth of field. This gives it a peculiar sharpness because all points from the highest to the deepest appear in focus at once, whereas in viewing the real world our eyes focus on one distance at a time. The reason behind the surge in the popularity of SIRDS's mentioned must be that they help relax the eyes. Because there is no special gadgets required, one needs to look at the image wide-eyed, that is to say, with one eye focusing parallel to the other, and this is very relaxing to the muscles of the eyes. By contrast, cross-eyed viewing can induce headache and eyestrain. One procedure for drawing a stereogram from a crystal or crystal model is shown in Algorithm 2.2.

**Algorithm 2.2** *A procedure for drawing stereograms from crystal models.*

**make** drawings of the crystal;

**label** all the different faces;

**select** prominent zones;

**for** every zone **do**

  **measure** all the interfacial angles;

**endfor**

**plot** the prominent zone in the primitive circle;

**mark** the centre of the stereogram;

**locate** $a$ arbitrarily;

**mark** the remaining face poles;

□

The interfacial angles are measured using a contact goniometre. The sum of the interfacial angles in a complete zone is 360°. Face poles are marks obtained from intersections of small circles with with primitive circles.

The programs on stereographic projection are collectively called `stp.m` and listed in § A.32. Some of the pictures drawn during its developmental stages are given in Figure 2.3 (a) and (b) while those for future developments in Figure 2.3 (c) and (d).

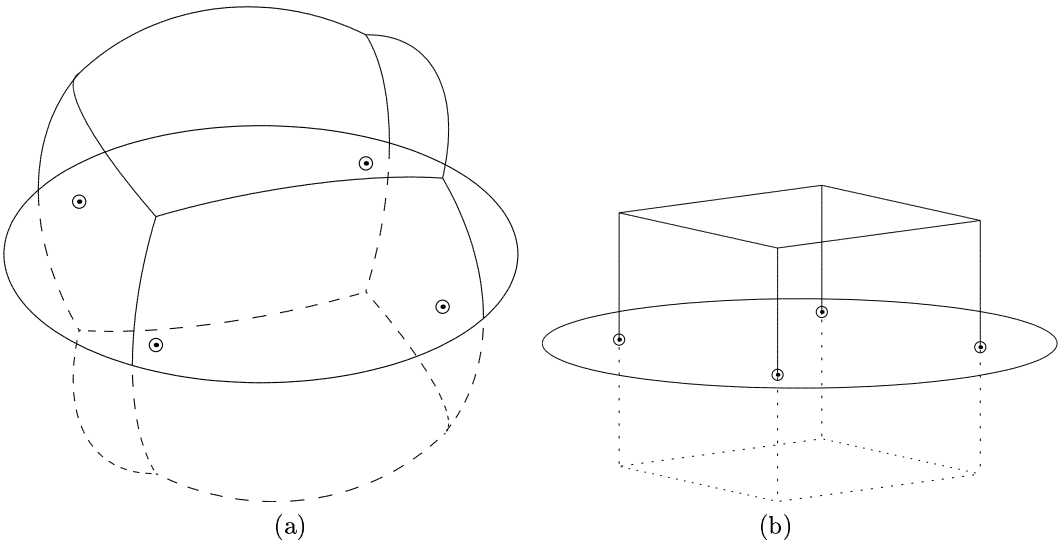

(a) (b)

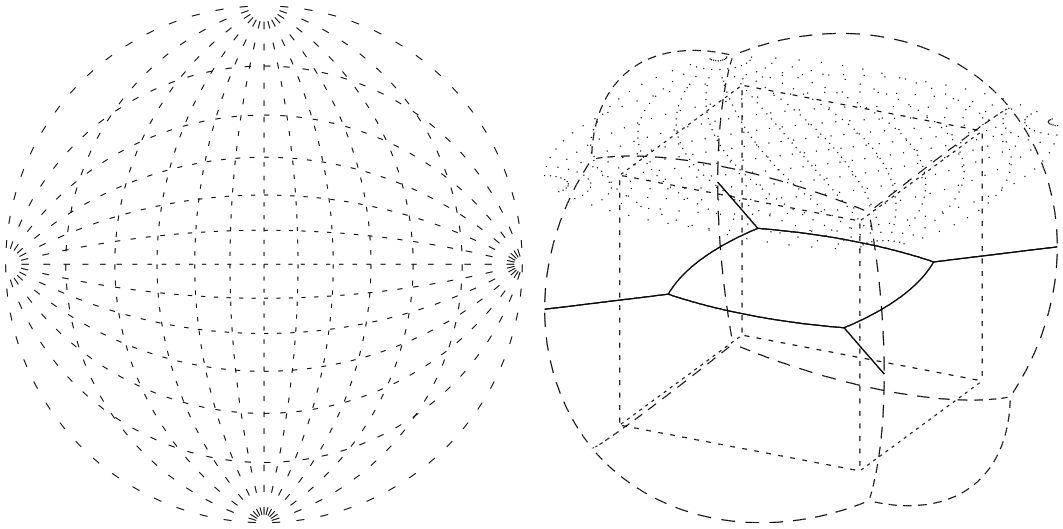

(c) (d)

**Figure 2.3** *Developmental stages of programs for the stereographic projection;* (a) *and* (b) *for the cube,* (c) *and* (d) *the great circles.*

The parameters of any two faces of a crystal are always rationally related to each other. One way of uniquely presenting the relationship between angles of the faces and those of the crystallographic axes is by using the Miller indices. These idices are obtained by first finding intersections between a face and $a$-, $b$ and $c$ axes. Then divide by the $b$-axis intersection to get parameters of the face, and then divide these by the respective values of the parametral plane chosen. What is obtained after this stage are the ratio of the parameters to those of the parametral plane, the reciprocal of which gives the Miller indices.

## § 2.2 Covering lattices

A covering lattice of any two-dimensional lattice is the lattice obtained by joining midpoints of consecutive edges together. The code in § A.7 finds covering lattices up to the eighth one and computes the total area of the cells for each case.

The square lattice is the only regular covering lattice, that is it is both the dual and the covering lattices of itself. But all polygonal tilings and tessellations can have a covering lattice, or in fact an infinite orders of covering lattices. Coverings of some lattices can be seen in § 3 (*cf* Tiyapan, 2001, KNT8(ii)).

Coverings can be generalised to a general dimension $d$. In two dimensions they are lines, *i.e.* having two vertices, straight lines each of which join two lines across a corner. For three-dimensional polyhedral tessellations they are planes with three vertices, triangles each of which join three planes across a corner, in other words a coign. Then in four dimensions they may be polyhedra with four vertices, tetrahedra each of which joins four 4-d polytopes across a four-edged corner in four dimensions, and so on. In $d$ dimensions, then, perhaps they are polytopes with $d$ vertices, three-cornered $(d-1)$-polytopes each of which joins $d$ $d$-dimensional polytopes across a $d$-edged corner in $d$-dimensions.

One interesting property of covering lattices is that they leave the voids intact while reducing only their size. Thus the structure and complexity of the original tessellation remain unchanged. This can be useful when we want to exclude some of the volume. In filtering membrane studies, for instance, this is ideal since all the voids still remain in the same position.

The process of covering is similar to that of shrinkage in cell in that there is a retreat away from corners. This could be because corners are hard to maintain. Surface tension is high there, and like a nook, recess, or remote, unstrategic parts of a country the cost of maintaining and governing is high. In the case of a country, conflict in such parts is analogous to the high surface tension in corners of cells.

When an empire or a metropolitan city declines, the process is similar. Such far corners are the first parts to fall into chaos. Law, order and security shrink away from them. The Roman Empire is an excellent example of this. In its heyday it reached out to every corner of Europe, however far. When it came to the decline, it literally *pulled itself together*, though it never could pull itself

together again after that. It drew away first from those far corners, England for instance, and then towards its nucleus and died.

Manchester is another interesting example. After the industrial revolution, and under the governance of the Conservative party, the city declined. And as it did, all the different nuclei became prominent, if only because the distance between them became more so. Thus Bolton, Altrincham and Stockport, for example, shrunk towards their nuclei, leaving behind dangerous districts where mugging, murder and crime are rampant like the Moss Side decades ago until shortly after the IRA bombing of the city centre. When an urban area fades away it does not do so suddenly but like the plant cell subject to a dewatering process or a polygonal tessellation to a covering one.

Random fluctuation can create areas of irregularity within a homogeneous and isotropic universe. These irregularities become nuclei, and from duality of the structure fine partitions start to develop around them which become Voronoi facets. Gradually but steadily the gas shrinks to form the galaxies of our present universe.

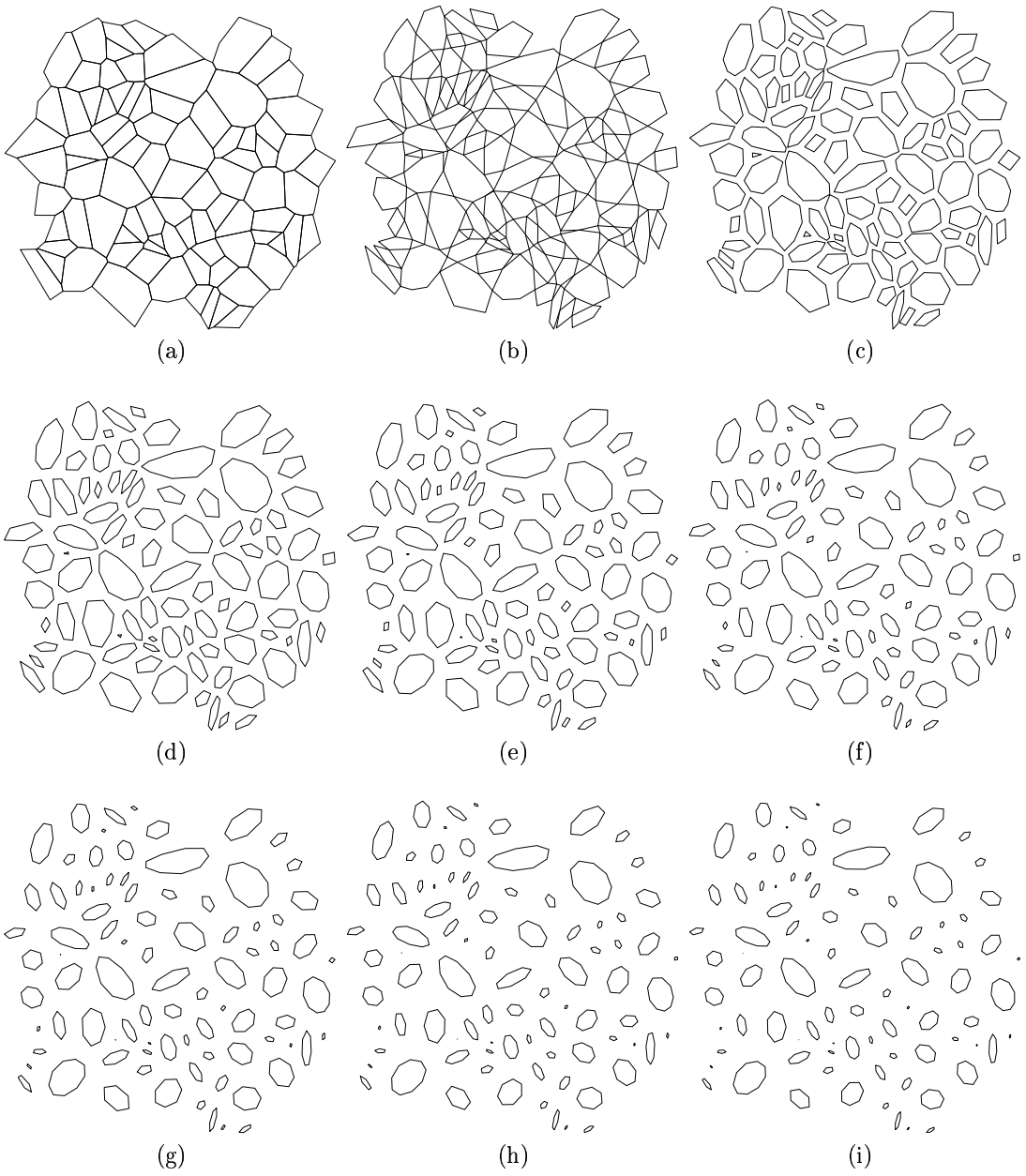


**Figure 2.4** *Covering lattices, stone pavements, or galaxies in the forming?* (a) $\mathcal{V}$, (b) $\mathrm{C}^1(\mathcal{V})$, (c) $\mathrm{C}^2(\mathcal{V})$, (d) $\mathrm{C}^3(\mathcal{V})$, (e) $\mathrm{C}^4(\mathcal{V})$, (f) $\mathrm{C}^5(\mathcal{V})$, (g) $\mathrm{C}^6(\mathcal{V})$, (h) $\mathrm{C}^7(\mathcal{V})$, (i) $\mathrm{C}^8(\mathcal{V})$.

Figure 2.5 (a) to (i), which are the results of the covering operator applied to a Voronoi graph eight times in succession, represent this situation. Figure 2.5 shows the area of multiply covered cells $C^n(\mathcal{V})$, $n = 0$ to 8, where $C^0(\mathcal{V})$ is the Voronoi graph $\mathcal{V}$. Circles are the per cent total area, and the curve is $y = 10^{-0.8x+2}$. The code `gxy.m` to find the covering contours above is given in § A.8. The area of the cells decreases from the covering operator, not linearly but with deceleration as Figure 2.5 shows.

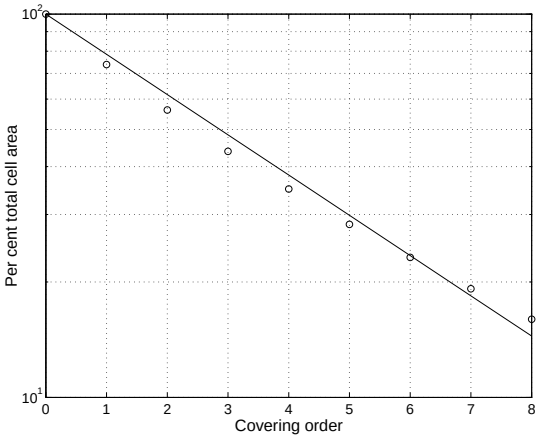


**Figure 2.5** The area of multiply covered cells.

On taking a closer look at Figure 2.5, one can interestingly notice that even though all pores shrink from the application of the covering operator, some does so much quicker than others. In particular, round pores shrink but slower. The more corners a pore has the less acute are the angles, which makes it the more stable and thus able to maintain its original size.

Geometrically, one can see that the most unfortunate of all polygons is the triangle. The area of a triangles of any shape reduces by 75 per cent upon being covered. The circle is the most fortunate in this matter since it has no corners and therefore it is impossible for these to be cut. This is in accordance with our argument that corners are unstable region.

## § 2.3 Viscous fingers

Viscous fingering is a happening which occurs when a low viscosity fluid with high pressure penetrates the border of a higher viscosity fluid in a form of thin branching fingers resembling a flash of lightnings in shape. An experimental account as well as descriptive pictures and diagrams are given by Nittmann et al (1985). However, a reference made to one previous work (Hele-Shaw, 1898) was inaccurate in at least three ways, one of which is in the initials of its author, while the rest in the actual contents. The first one can easily be verified with a little research, is that the initials of the author of the paper is H. S., not J. S. S. as given his full name being Henry Selby Hele-Shaw (1854–1941). For the remaining two, firstly the paper by Hele-Shaw is about fluid flow pass free boundary of solid, *not* viscous fingering instability. Secondly, Hele-Shaw was in fact an engineer who has been a professor at University college in Liverpool for 17 years, whose interest was in layer parallel motion (laminar) and sinuous (turbulent) flows pass various bodies of uniform cross section as well as in flows through channels of varying cross section. Born at Billericay, Essex, and a holder of Whitworth scholarships while a student at University college, Bristol, he was elected to the Royal Society in 1899 because of his experiments done on streamline flow. He has successfully introduced the use of air bubbles in experiments to help portray the stream lines of the flow; his cited work mentions neither the physics of nor the application to petroleum science as the context would have us believe. However, his other and subsequent work (Hele-Shaw, 1899) does mention briefly about the importance of viscosity in nature and the difficulty of modelling the motion of viscous fluids mathematically, but nowhere in either one of these two papers did he consider the interaction between fluids of different viscosity.

The simulation for the viscous fingering problem may be related to that for the propagation through rivulets or channels that we study here in § 6.11. It may also be related to the front tracking simulation of dendritic growth. Front tracking has been to solve various problems numerically, for example shocks, flame-, chemical reaction and solidification fronts. In this method a dynamical problem in $n$ dimensions is transformed into a set of partial differential or integro-differential equations which are then solved numerically at a finite set of points on the front or interface (Srolovitz, 1990).

Dendritic growths, on the other hand, are characterised by their rich patterns and share one property that is similar to percolation, which is that it is very difficult, if not impossible, to completely describe the mathematics of their dynamic evolution.

As in other microstructural simulations, the underlying structure where these fingerings occur can be simplified by the mean-field method, which replaces the microstructure by a typical grain, or by making a simple geometrical model to represent it, for example a Voronoi tessellation. The

computer simulation can be done using Monte Carlo methods, which describes the energy of the structure in terms of the location of defects and is based on a kinetic rate, or by numerically integrating the equations of motion that describe the evolution of the defects.

## § 2.4 Crystals, quasicrystals, and polycrystals

### Crystals, quasicrystals, and polycrystals

The shape of individual grains in polycrystal and the inter granular surface can be found by stereoscopic microradiography, but using random plane section is more convenient in practice (Aboav and Langdon, 1969). The grains of polycrystals are not arranged at random but in a characteristic way which can be expressed in simple terms and seems to be scale-free (Aboav, 1970). The average number of sides of neighbours of a grain is $n_n^e = 5+8/n_e$ where $n_e$ is the number of sides of the grain. Aboav (1970) studies grains of polycrystalline magnesium oxide and finds $n_e = 5.85$. He also finds that most of the time $n_n^e > n_e$ which seems like a contradiction but is because the probability that a point lies in a grain of a particular shape depends on the size and abundance of such grains. He also finds the average number of $n$-sided grain $n_c^{n-e} \propto (n-2)$. Grains of a polycrystal are different from cells of a soap foam in that they possess a stable grain diameter, which only depends on the temperature.

This stable diameter of grain, $d_e$, is the average grain diameter at which the growth ceases, and is $d_e^{1/2} = c(T - T_0)$ (Aboav, 1971). For cadmium $T_0 = -53°\mathrm{C}$, $0°\mathrm{C} < T < 170°\mathrm{C}$. The distribution of grain size is $z = z_m \exp\left\{-\alpha^2\left[(x/x_m)^{1/2} - 1\right]^2\right\}$ where $z$ is the number of grain sections in a plane section, $\alpha$ a constant, $x$ the diameter of grain section and $x_m$ the value of $x$ at $z_m$.

There are similar patterns of grains in a polycrystalline ceramic, magnesium oxide, cadmium, *etc.* The moments of distribution above $n = 6$ is $\mu_m = \sum_n (n-6)^N f_n$ where $f_n$ is the fraction of cells with $n$ sides. The second moment $\mu_2 > 0$ unless all cells have six sides, and we have a purely topological relation $\sum_n n_n^e n_e f_n = \mu_2 + 36$. If $n_n^e \propto 1/n_e$, then $n_n^e = (6 - a + b\mu^2/6) + (6a + (1-b)\mu_2)/n$. If $a = 1$ and $b = 0$, this equation is reduced to $n_n^e = 5 + (6 + \mu_2)/n$ and furthermore if $\mu_2 = 0$, $n_n^e = 5 + 8n_e$. In a polycrystal the distribution of $n_e$ does not usually vary as the grains grow. Typically $\mu_2 = 2.4$. Soap foams resemble a polycrystal (Aboav, 1980), and $n_n^e = A + B/n_e$, $n_n^e = (6-a) + (6a + \mu_2)/n$, $a = 1.2$.

The growth process of both crystals and quasicrystals are nonlocal in nature, but that of polycrystals is of a multigrain growth. Crystals with a very large unit cell exists. Quasicrystals cannot grow in the same manner as playing a jig-saw puzzle (Penrose, 1989) because no matter how many steps one looks ahead there will come a point where there is a gap that none of the available basic building blocks can fit in. A *legal* tiling contains no gaps or overlaps; if it can be extended to cover the whole plane it is also a *correct* tiling. A *mistake* occurs when a tile added to a correct tiling renders it a legal but incorrect one. By using the basic units to build larger units having the same structure as these basic units and then recursively repeat the process, one can in the end reach a correct tiling. But this is also a nonlocal process since one still requires the ability to look ahead in order to make sure that the units are always structurally the same.

The fact that zeolites are crystalline seems to rule out the randomness assumption that one may otherwise use to model their growths as random continuum percolation. One needs to resort to the methods and tools used by the geologists if one wants to study zeolites, synthetic as well as natural ones.

*Krýstallos* is the Greek word for ice. Crystallography is nowaday the science of the crystalline state which, apart from the crystals themselves, includes such seemingly unlikely materials as plastics, rubber, silk, wool, liquids and gases (*cf* Phillips, 1949). There are four kinds of symmetry axes in crystal models, corresponding to $n = 2$ to 6 in the formula for the angles $\frac{360°}{n}$ by the rotation of which a crystal will repeat itself. These axes are respectively called *diad*, *triad*, *tetrad*, and *hexad*.

| *Crystals* | *centres of symmetry* | *planes of symmetry* | *diad* | *triad* | *tetrad* | *hexad* |
|---|---|---|---|---|---|---|
| *Cube* | 1 | 9 | 6 | 4 | 3 | |
| *Rhombohedron* | 1 | 3 | 3 | 1 | | |

**Table 2.1** *Symmetries of crystals*

The symmetries of the seven crystal systems, the Triclinic contains no axes of symmetry, Monoclinic one diad axis, Orthorhombic three diad axes, Tetragonal one tetrad ais, Cubic four triad axes, Trigonal one triad axis, and Hexagonal one hexad axis. A *monoclinic* crystal has all three axes unequal and one oblique intersection while an *anorthic*, aka *triclinic*, crystal has all three axes

unequal and intersecting at oblique angles. The relative development of crystals in different forms give rise to the *habit* of crystal. Thus if one gradually truncates the coigns of a cube one will come to an octahedron, and vice versa. All the continuous transformations between the cube and the octahedron are called *cubo-octahedron*. Crystal models of different habits readily yield on inspection the same symmetry group, but real crystals often look irregular and determination of the symmetry is based on the law of consistency of angle and uses goniometers.

The number of faces in crystals are usually even numbers. Take for example the 33 non isometric crystal forms (Klein and Hurlbut, 1993). Here only three have their faces in odd number, *viz.* pedion which has only one face, and trigonal prism and trigonal pyramid which have three faces each. For the rest, those which have two faces are pinacoid, dome and sphenoid; four faces rhombic prism, tetragonal prism, rhombic pyramid, tetragonal pyramid, rhombic disphenoid and tetragonal disphenoid; six faces ditrigonal prism, hexagonal prism, ditrigonal pyramid, hexagonal pyramid, trigonal dipyramid, trigonal trapezohedron and rhombohedron; eight faces ditetragonal prism, ditetragonal pyramid, rhombic dipyramid, tetragonal dipyramid, tetragonal trapezohedron and tetragonal scalenohedron; twelve faces dihexagonal prism, dihexagonal pyramid, ditrigonal dipyramid, hexagonal dipyramid, hexagonal trapezohedron and hexagonal scalenohedron; sixteen faces ditetragonal dipyramid; and twenty-four faces dihexagonal dipyramid. Among these, there is none which has its faces in a number of 5, 7, 9–11, 13–15, 23, or 25 and above. In Figure 2.6 the distribution curve for even numbers of faces is a scaled Chi-square distribution $y = K \cdot (x/3)^{(\nu-2)/2} \exp(-(x/3)/2)/(2^{\nu/2}\Gamma(\nu/2))$, where the degree of freedom $\nu$ is four and $K = 35$, while the curve for odd numbers of faces is the contour of a scaled Poisson distribution $y = K \cdot \lambda^{2x} \exp(-\lambda)/(2x)!$, where $K = 12$, $\lambda = 5$, and $2x$ is any positive integer or zero.

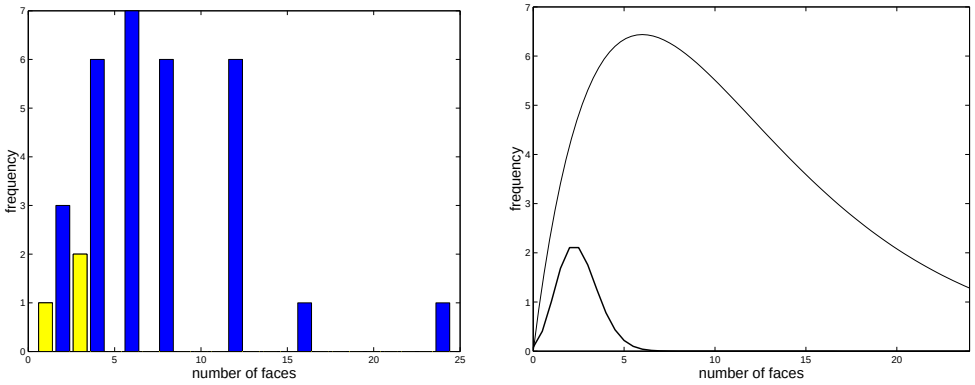


(a) (b)

**Figure 2.6** *(a) number of faces of the thirty-three non isometric crystal forms; (b) approximation curves, the heavy line encompasses* $y = 12\exp(-5) \cdot 5^{2x}/(2x!)$ *while the lighter line* $y = (35/12)x\exp(-x/6)$.

Miller indices define the shape of crystals in terms of their faces by numbering their axial intercepts. These indices are $h = a/X$, $k = b/Y$ and $l = c/Z$ where $X$, $Y$ and $Z$ are respectively the $x$-, $y$- and $z$-intercepts. First, decide the three crystallographic axes. Then choose as the standard or parametral plane a plane that inclines against all these three axes. The shape of crystal, which according to the proportion of each crystal face is called the crystal habit, is governed by the slowest growing face and is affected by the presence of the additive solvent or impurities. Stereoisomerism is the difference in the spatial arrangements of the same atoms and functional groups in a molecule. Enantiomers occur in pairs. They are also known as optical isomers and are mirror images of each other. Polymorphs are substances which can crystallise into different forms the chemical formulae of which are similar to one another. For example, carbon can occur as graphite, diamond, or fullerenes. Isomorphous crystals always appear in one form. In pharmaceutical industries it is important to know the different properties of enantiomorphs of a drug, and to be able to grow each of them separately from the other. Crystalline materials have a tendency to cake or bind together during storage. The dimension of the particles is characterised in one of the following ways: as spheres where $V = \pi d^3/6$ and $A = \pi d^2$; as cubes, $A = 6L^2$, $V = L^3$ and $d = \sqrt{3}L$; as the maximum characteristic chord length of an irregularly shaped particle; as an equivalent diameter or characteristic length. The shape factor for the surface is $f_s = A/L^2$ while for the volume it is $f_v = V/L^3$. Their values are subjected to an inequality constraint, namely $f_s \geq \pi$ and $f_v \geq \pi/6$ where the equality is for the case of a sphere. The ratio $r_f = f_s/f_v$ called the specific surface shape factor, whereas the surface

area ratio between that of the sphere and that of the particle of equal volume is called the sphericity, $\Psi$. The specific surface is $\alpha = A/V$ and onsequently $r_f = \alpha L$. The specific surface of particles is the surface area of particles per volume of particles, $\alpha_p = r_f/\bar{d}_s$, while the specific surface of bed is the surface area of particles per total volume of bed, $\alpha_b = (1-\varepsilon)\alpha_p$. The particle size distribution is usually described by the cumulative mass fraction which is the fraction of mass of each particle size, the differential mass fraction $x = \mathrm{d}m/\mathrm{d}d$ or $\int_0^\infty x\mathrm{d}d = 1$, or the size increments. The number of particles in mass fraction $x_i$ is $n_i = x_i/(\rho_s f_v d_i^3)$, where $x_i$ is the ratio of the mass in sizes in the $i^{\text{th}}$ interval to the total mass of all particles, and $n_i$ is the product between the number, the volume, and the density of particles. The weight- or volume mean size is

$$\bar{d}_w = \frac{\sum_i x_i d_i}{\sum_i x_i} = \sum_i x_i d_i = \frac{\sum_i n_i d_i^4}{\sum_i n_i d_i^3}, \qquad (16)_{\text{ii}}$$

where $\sum_i x_i = 1$. The mean weight- or volume size, $d_{\bar{w}}$, is the size of each particle of a mono-disperse powder such that $f_v d_{\bar{w}}^3 \sum_i n_i = f_v \sum_i (n_i d_i^3)$, which gives

$$d_{\bar{w}} = \left(\frac{\sum_i (n_i d_i^3)}{\sum_i n_i}\right)^{1/3} = \left(\frac{1}{\sum_i (x_i/d_i^3)}\right)^{1/3}. \qquad (17)_{\text{ii}}$$

The surface mean size† is

$$\bar{d}_s = \frac{\sum_i V_i}{\sum_i S_i} = \frac{\sum_i d_i S_i}{\sum_i S_i} = \frac{\sum_i n_i d_i^3}{\sum_i n_i d_i^2} = \frac{\sum_i x_i}{\sum_i (x_i/d_i)} = \frac{1}{\sum_i (x_i/d_i)}. \qquad (18)_{\text{ii}}$$

The mean surface size is the uniform size of mono-disperse particles which makes the surface area of the particles equal to the surface area of actual the powder. In other words, $\sum_i n_i f_s d_s r^2 = \sum_i n_i f_s d_i^2$, which gives $d_s r = [\sum_i n_i d_i^2 / \sum_i n_i]^{1/2} = [\sum_i (x_i/d_i) / \sum_i (x_i/d_i^3)]$. The specific surface is the surface area of a powder per unit mass or volume, $\alpha = f_s \bar{d}_s^2/\rho_s f_v \bar{d}_s^3 = r_f/\rho_s \bar{d}_s$. The coefficient of variation (cv) describes the spread of the distribution about the mean, cv $= \sigma/d$ where $d$ is the mean size and $\sigma$ standard deviation. The void fraction or voidage, $0 < \varepsilon < 1$, is the ratio of the particulate void volume to the total bed volume which comprises of the volume of voids and solids. Sieve test is used to find the distributions of particles. The mesh number of a sieve is the number of apertures per unit length of sieve, $N = 1/(L+W)$ where $L$ is the aperture size and $W$ the wire width. Crystal defects include point defects, edge- and screw dislocations.

The electrical double layer is $V_d = B' r \exp(-kh)$ where $B'$ is related to the surface charge. The interaction energy from electric field of two charged particles has two minima, $L_1 < L_2$ where $L_1$ is the primary minimum which occurs at $d_1 < d_2$.

At $L_1$ the coagulation is rapid whereas at $L_2$ it is slow. Added polymers may stabilise a colloidal system when the charged adsorbed polymer layers repel each other, or they may destabilise it by making the particles more susceptible to salts or by forming polymer bridges which flocculate the particles.

The superficial velocity, $u$, is the flowrate per cross-sectional area of bed, $u = Q/A$, and is known as the *velocity flux* or the volumetric flowrate per unit cross-sectional area. The interstitial velocity, $v$, is the true linear velocity of the fluid. It is the flowrate per unit cross-sectional area of voids, *viz.* $v = Q/(\varepsilon A) = u/\varepsilon$. An ideal particle moves in a fluid with the velocity $v$ as a function of $\mu$, $\rho$, $\rho_s$ and $d$. The momentum equation in one dimension for such particle is $\rho_s(\partial/\partial t + v\partial v/\partial z) = B + F - \partial p/\mathrm{d}z$, where $B$ is all the body forces and $F$ all the surface forces acting on the solid phase that is not included in the pressure gradient $-\partial p/\partial z$. The drag force per unit area on a single lone particle is $F/A = c_\infty \rho v^2/2$ where $F$ is force, $A$ the projected area, and $c_\infty$ the single particle drag coefficient at infinite dilution. For sphere, $F = c_\infty \pi d^2 \rho v^2/8$. The force balance equation is $W - B - F = M$ or $mg - m'g - F = m\mathrm{d}v/\mathrm{d}t$ where $m$ and $m'$ are the mass of particle and fluid displaced, and thus the second term represents the buoyancy. Balancing the accelerative and the resistive forces leads to $(\pi/6)d^3(\rho_s - \rho)g = c_\infty \pi d^2 \rho v_t^2/8$, where $v_t$ is the terminal velocity, *i.e.* when $\mathrm{d}v/\mathrm{d}t = 0$, which gives $v_t = [4d(\rho_s - \rho)g/3\rho c_\infty]^{1/2}$. The Reynolds number of the particle is $\mathrm{Re} = \rho v d/\mu$. When $\mathrm{Re} < 0.2$ the flow is laminar and Stokes' law applies and the force balance equation becomes $(\pi/6)d^3(\rho_s - \rho)g = 3\pi\mu d v_t = F$, which gives $v_t = d^2 g(\rho_s - \rho)/18\mu$, $c_\infty = 24/\mathrm{Re}$ and the Stokes diameter $d_s t = [18\mu v_t/g(\rho_s - \rho)]^{1/2}$.

The mass flux is defined as the multiplicative product of concentration and velocity. In laminar flow, Darcy's law applies, that is $u = \mathrm{d}V/A\mathrm{d}t = K_1 \Delta P/H$, where $K_1$ is the bed permeability,

† aka volume mean or Sauter mean.

a measure of the total drag force. The inverse linear relationship between the viscosity and permeability is $u = B\Delta P/\mu H$, where $B = K_1\mu$ is the permeability coefficient in $m^2$. Let the pore diameter be $d_1$, its length $H_1$ and velocity $v$. Assume that the fluid in pore velocity is $v = u/\varepsilon$, the hydraulic pore diameter is $\delta$ is related to $d_1 = v_b\varepsilon/v_b s_b = \varepsilon/s_b$, and the pore length $H_1$ depends on the bed depth $H$. For laminar flow through a pipe with viscous drag the Hagen-Poisseuille equation applies, that is $v = d_1^2\Delta P/(32\mu H_1)$. For the capillary model, $v = u/\varepsilon = \varepsilon^2\Delta P/(K_2 s_b^2\mu H)$. The bed specific surface area, $s_b$, and the particle specific surface area, $s_p$, are related to each other by $s_b = s_p(1-\varepsilon)$, and thus $u = v\varepsilon = \varepsilon^3\Delta P/(K_2 s_p^2(1-\varepsilon)^2\mu H)$, the Carmen-Kozeny equation, from where $B = \varepsilon^3/(K_2 s_p^2(1-\varepsilon)^2)$, where the Kozeny constant $K_2$ lies between 3.5 and 5.5 and is normally taken to be 5. In compressible beds voidage is a function of $P$ or $\Delta P$ and the Carman-Kozeny equation for $dx$ is $-dp/dx = K_2\mu(1-\varepsilon)^2 s_p^2 u/\varepsilon^3$. For turbulent flow $\Delta P/\Delta H = K'(1-\varepsilon)\rho u^2/(\varepsilon^3 d)$, while a linear sum of the laminar and turbulent flow is $\Delta P/\Delta H = K^3(1-\varepsilon)^2\mu u/(\varepsilon^3 d^2) + K_4(1-\varepsilon)\rho u^2/(\varepsilon^3 d)$ where $K_3 = 150$ and $K_4 = 1.75$ (Jones, 2002). Across a filter cake the modified Darcy equation is $u = dV/Adt = \Delta p_c/(r\mu H)$ where $V$ is the volume of filtrate which passed through the cake. If the specific cake volume, *i.e.* the volume of cake per unit volume of filtrate, is $v_c$, then the total volume of cake is $Vv_c = HA$ where $H$ is the thickness or height of the cake. Then $dV/dt = A^2\Delta p_c/(r\mu v_c V)$. This, together with the Carman-Kozeny equation for packed beds $u = \varepsilon^3\Delta p_c/[5(1-\varepsilon)^2 s_p^2\mu H]$, gives the specific cake resistance $r = 5(1-\varepsilon)^2 s_p^2/\varepsilon^3$ There are two modes of filtration, the constant rate- and the constant pressure modes. In the former $dV/dt$ is constant and, from $V/t = A^2\Delta p_c/(r\mu v_c V)$ which is also constant, it follows that $\Delta p_c/V$ is also constant. In the latter $\Delta p_c$ is constant and equals to $\Delta p_{\max}$. It follows that $V^2 = 2A^2\Delta p_c t/(r\mu v_c) = k_1 t$ and $t/V = r\mu v_c V/(2A^2\Delta p_c) = k_2 V$ When the effect of the filter medium is considered $\Delta p$ will comprise of two components, from the cloth and from the cake. The first one includes also the particles held in the filter. The resistance is $R = r(H+L)$ where $L$ is the equivalent cake thickness of the filter. The filtration equation becomes $dV/Adt = \Delta p/[r\mu(H+L)]$, in other words $dV/dt = A^2\Delta p/[r\mu v_c(V + LA/v_c)]$ For the constant rate filtration $V_1^2 + (LA/v_c)V_1 = (A^2\Delta p/r\mu v_c)t_1$, while for the constant pressure filtration $(t-t_1)/(V-V_1) = [r\mu v_c/(2A^2\Delta p)](V-V_1) + r\mu v_c V_1/(A^2\Delta p) + r\mu L/(A\Delta p)$. Agglomeration of crystals can be on either an individual or collective basis. The first one is sometimes called primary agglomeration examples of which are parallel, dendritic and twin growths. The second one is also known as secondary agglomeration and is essentially those cases where crystals within the solution come together to form clusters. Secondary agglomeration can be perikinetic, from Brownian motion of small particles, or orthokinetic, from velocity gradients in the fluid. Crystals flocculate or coagulate loosely together, then they aggregate by starting to join one another, and then they agglomerate strongly together to become a single poly-crystalline particle. There are four main classes of forces, namely colloidal, stochastic, direct- and indirect systematic forces. Surface adsorbs certain ionic species which in turn attract opposite ions, thus forming electrical double layers which repel each other There are three types of particle interaction, that is van de Waals, electrostatic and steric. These depend on shape and size of the particle, surface charge, solution's pH and ionic strength, temperature and the separation distance between the particles. The van der Waals forces are between molecules having closed shells and do not obey inverse square laws. Three of these are attractive, namely the orientation effect between permanent dipoles, the induction effect between a permanent- and a temporary dipoles, and the dispersion effect or London force between temporary dipoles and induced dipoles. The potential equations is $V_v = -A_{12}f(h)$ where $A_{12}$ is the Hamaker constant of the material.

## § 2.5 Random lines and percolation

Miles (1964) studies the line system, $p = x\cos\theta + y\sin\theta$, where $-\infty < p < \infty$ and $0 \le \theta < \pi$. Chan (1990) studied numerical properties of such structure of random lines using the same generator and then used it to model the structure of non-woven media. This amounts to the study by simulation of filters the internal structure of which is fibre mat, for example polypropylene. The algorithm he developed deals with mechanical blocking and back-flushing of the fibres. Wilcock's study (1994), on the other hand, deals with woven materials. With them she tried to demistify the myth and mysteries surrounding the rule of thumb techniques in designing wire mesh demisters. Her algorithms first weave the mesh and then apply Monte Carlo to it for the simulation.

The steel and carbon fibres in cement pastes contributes respectively to hole- and electron conductions (Wen and Chung, 2000). This is a problem of percolation of interconnected random lines. On the other hand, we can also study the resistance instead of conductance, which is what Pennetta *et al* (2000) does for a random network of resistors. Interest in researches on random

resistor or conductor networks is strong (for example, Pennetta *et al*, 2001). Cheng *et al*(2001) look at NiMH (nickel metal hydride) batteries' electrodes. In their presentation they wrap all the ends of those fibres that stick out from the prototile. This gives the periodicity which they use in their simulation. The NiMH has high porosity, no less than 97 per cent, and it contains two or more phases.

Some recent developments related to polypropylene are those done by Mironi-Harpaz and Narkis (2001), Narkis *et al* (2000), and Zhang *et al* (2001). Those who study the conductivity and resistivity of materials are, for example, Benoit *et al* (2001), Broderix *et al* (2001), Flandin *et al* (2001), Hindermann-Bischoff and Ehrburger-Dolle (2001), Huang *et al* (2001), Hunt (2001), Jevtic *et al* (2001), Nielson (2000), Petrovsky and Rak (2001), and Stenull *et al* (2001). An example of the application to dentistry is that which is reported by Sharp *et al* (2000). Rong *et al* (2001) look at tensile curves and study the resistance to thermal deformation in nanocomposites.

## § 2.6 Convex hull

The set of extreme points $E$ in some superset $S$ is the smallest subset of $S$ such that the convex hulls of both $E$ and $S$ are identical. Extreme points never lie in a triangle.

The Graham's scan algorithm (*cf* Preparata and Shamos, 1985) positions itself in the midst of the points and then scans around in one direction. It determines three points in turn, and rejects a mid point among the three if the angle made there is reflexive, *i.e.* $\alpha$ such that $\alpha \geq \pi$ in the anti-clockwise direction. In other words, an angle is a right turn if it is reflexive; it is a left turn otherwise. The algorithm is shown in Algorithm 2.3. Here $\{h\}$ is a stack which contains the points on convex hull

**Algorithm 2.3** *Graham's scan.*

$i \leftarrow 1$;
$j \leftarrow 2$;
$k \leftarrow 3$;
**while** there exist unprocessed points **do**
  **if** $\angle p_i p_j p_k \geq \pi$ **then**
    $j \leftarrow i$;
    $i \leftarrow i - 1$;
  **else**
    $i \leftarrow j$;
    $j \leftarrow k$;
    $k \leftarrow k + 1$;
  **endif**
**endwhile** □

The algorithm starts from a known extreme point. It can also start from two points which are known to be extreme, in which case the space is divide into an upper- and a lower hulls. Similarly to the Graham's scan, Jarvis's march finds one extreme point after another as it wraps a line around the convex hull. The Quickhull algorithm in two dimensions is described in Algorithm 2.4.

**Figure 2.4** *Quickhull in two dimensions.*

$l \leftarrow$ the point with the smallest abscissa;
$r \leftarrow$ the point with the largest abscissa;
$\{s\} \leftarrow$ all points above $\overline{lr}$;
$\{s\} \leftarrow$ all points below $\overline{lr}$;
**while** there remains an unprocessed $s_i$ in $\{s\}$ **do**
  $h \leftarrow$ point in $s_i$ which maximises the area of $\triangle hlr$;
  **reject** points bound by $\triangle hlr$;
  $\{s\} \leftarrow$ all points outwards from $\overline{lh}$;
  $\{s\} \leftarrow$ all points outwards from $\overline{rh}$;
**endfor** □

The divide-and-conquer algorithms divides a problem into subproblems, finds the convex hull for each one of them and then merges these together by finding the convex hull of convex hulls. Algorithm 2.5 finds the convex hull of two convex hulls.

**Algorithm 2.5** *Convex hull of convex hulls*

$p \leftarrow$ one point in $h_1$;

**if** $p$ is also in $h_2$ **then**
  $h \leftarrow$ **scan** around from $p$, and **merge** $h_1$ and $h_2$;
**else**
  $(u, v) \leftarrow$ points on $h_2$ such that $\angle upv$ is maximised;
  $c \leftarrow$ the chain from $u$ to $v$ which is furthest away from $p$;
  $h \leftarrow$ **merge** $c$ and $h_1$;
**endif** □

There are also dynamic algorithms for finding the convex hulls. In this case the input is online and one can not look ahead at the input. This kind of algorithms may be useful for online applications, for example the traffic control in real time. Two things can happen in such dynamic algorithms; points are inserted or points are deleted.

The gift-wrapping methods, which are similar to the Jarvis's march, can be extended to the general $d$ dimensions. Here a point is beneath a facet if it is on the same side of it as the hull, otherwise it is beyond it. Also, with respect to a point $p$, if $p$ is beneath all facets that contain $v$ then $v$ is concave; if $p$ is beyond the same then $v$ is reflex; otherwise $v$ is supporting.

## § 2.7 From convex hull to the Voronoi tessellation

The earlier studies of the Voronoi structure used the program `qhull` to create the structures. Programs were developed on Matlab to manipulate the data and find the statistics. These programs were tested on small structures first. Contrary to what the literature says, these very small networks turned out to have all the statistics in close agreement with those much larger ones. This confirms an earlier report (Tiyapan, 1995, KNT3(iii)) that the average values of the statistics stays the same over a wide range of network sizes. So a Voronoi is a Voronoi, as one could have said, almost like an Englishman.

Voronoi tessellation is the solution of a proximity problem, namely the division of the space into $n$ partitions around $n$ particles, such that all points within the $i^{\text{th}}$ partition is closest to the $i^{\text{th}}$ particle than any other particle. There are a host of proximity problems which, in the end, are related to one another and to the Voronoi problem. Some example of these are the problems concerning the nearest neighbour, the closest pair and the Euclidean minimum spanning tree. The minimum spanning tree always contains the shortest edge of the graph.

Given a convex hull containing $n$ points, one can join all the points together by straight line segments such that the whole region inside the convex hull is tessellated by the triangles formed by them. This problem is related to the nearest neighbour problem, since among all straight lines connecting to each point there is one which joins it to its nearest neighbour. Moreover, the problem is related to a problem of spatial proximity the solution of which is the Voronoi tessellation. The solutions of these two problems are dual to each other. The triangular tessellation is called the Delaunay triangulation.

Descartes was the first person to draw a picture of a Voronoi tessellation (Descartes, 1644). In his essay, he imagine vorticities surrounding heavenly bodies. The path of an object through space, he says, passes along edges and vertices of what is now known as the Voronoi tessellation. The idea he introduced was original but the discourse philosophical, which is perhaps why his name was never associated with the tessellation which could easily have borne his name instead of that of Voronoi. Even though we regard Philosophy very highly as the mother of all sciences, as is probably the reason why we call our highest formal education 'Doctor of Philosophy' or Ph.D., but from our experience we could see that philosophy in our dictum generally means only one thing, that is mathematics. Therefore the tessellation is named after Voronoi because he was the first person to have written a *substantial* amount of mathematics on it. In short, Descartes has provided the idea and philosophy, Dirichlet the geometrical description and Voronoi the mathematics. Voronoi could easily have claimed having written the most amount of mathematics on the tessellation which now bears his name, than any other person to date. To see the contest between Voronoi and Dirichlet, for instance, compare their seminal papers (Dirichlet, 1850; Voronoi, 1908, 1909) (*cf* Tiyapan, 2001, KNT8(i)). Ironically it was Descartes' philosophy that all knowledges must be based on mathematics, so he should not have minded.

The pictures of all Voronoi cells in a group of 71 cells are given in Figure 2.7. These are all the inner cells of a larger group of 200, the rest of which are cells on the boundary.

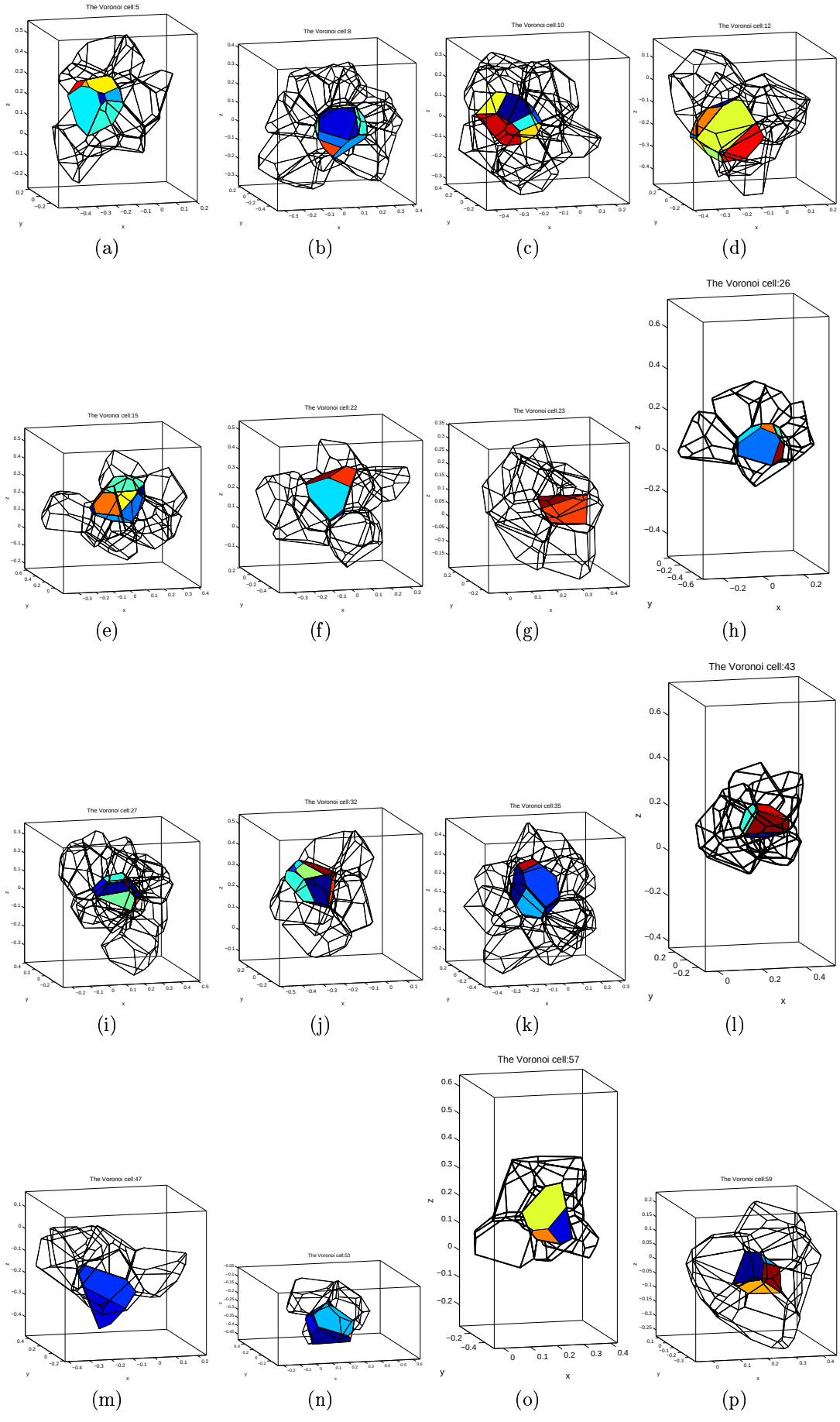
The Voronoi cell:5
The Voronoi cell:8
The Voronoi cell:10
The Voronoi cell:12
(a)
(b)
(c)
(d)
The Voronoi cell:15
The Voronoi cell:22
The Voronoi cell:23
The Voronoi cell:26
(e)
(f)
(g)
(h)
The Voronoi cell:27
The Voronoi cell:32
The Voronoi cell:35
The Voronoi cell:43
(i)
(j)
(k)
(l)
The Voronoi cell:47
The Voronoi cell:53
The Voronoi cell:57
The Voronoi cell:59
(m)
(n)
(o)
(p)

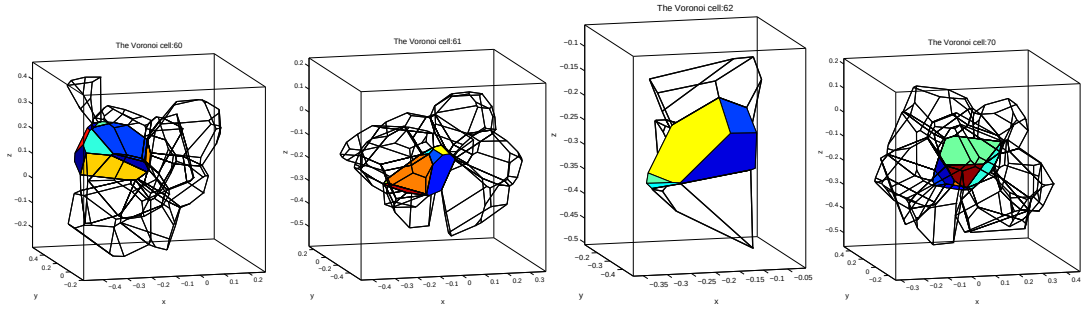


(q) (r) (s) (t)

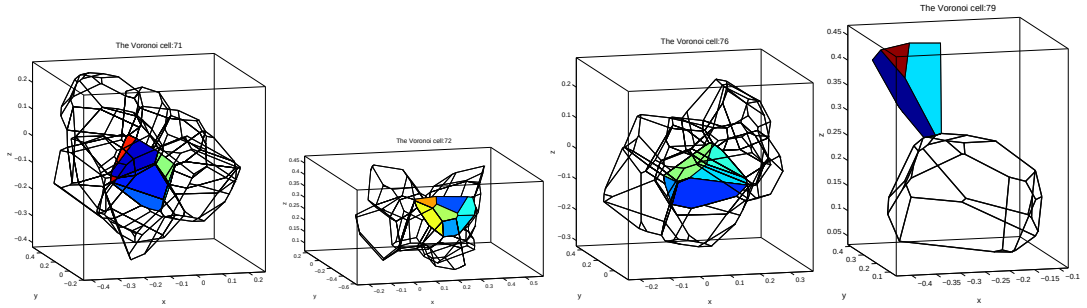


(u) (v) (w) (x)

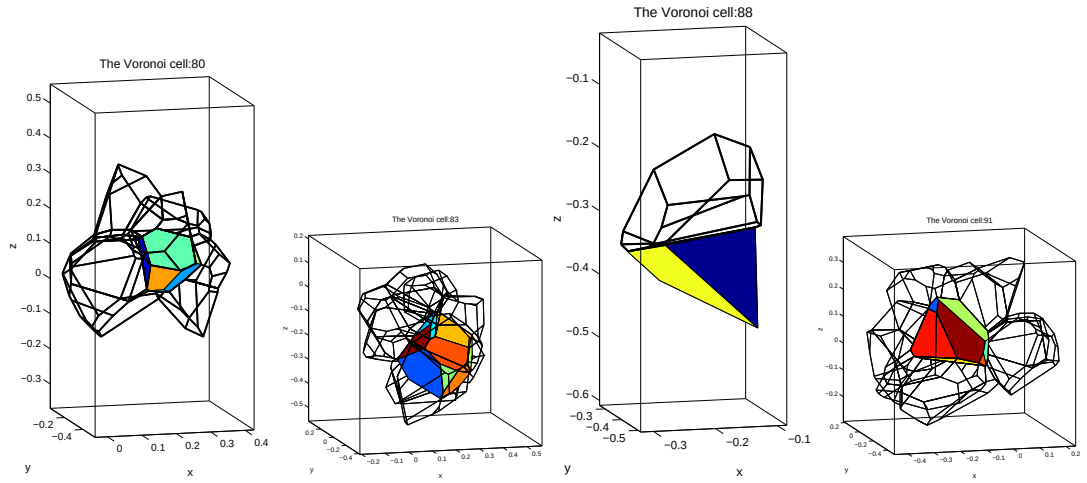


(y) (z) (A) (B)

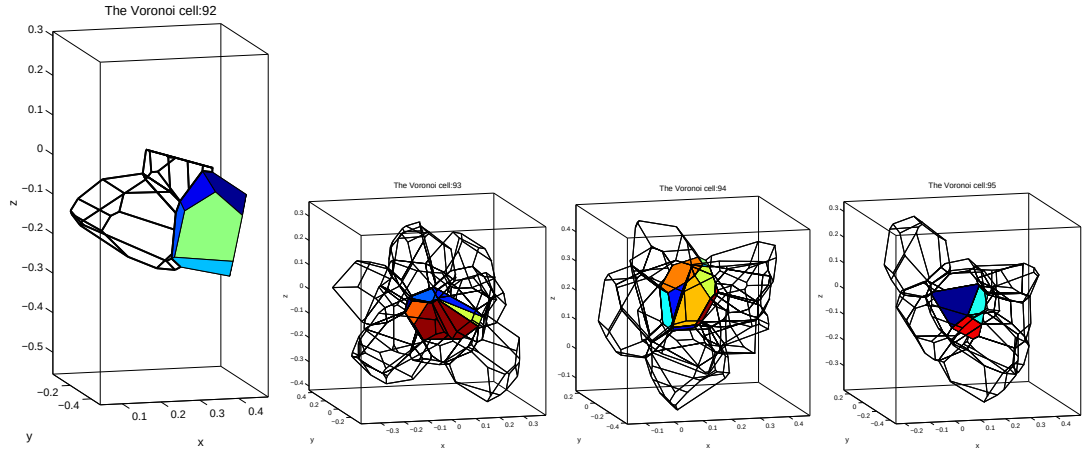


(C) (D) (E) (F)

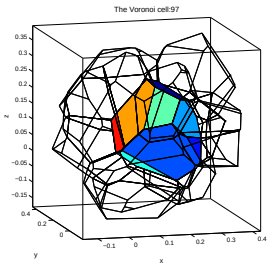


(G)

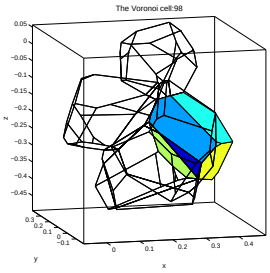


(H)

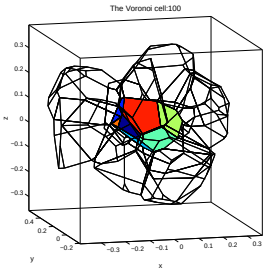


(I)

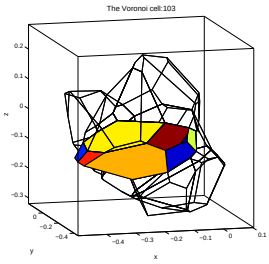


(J)

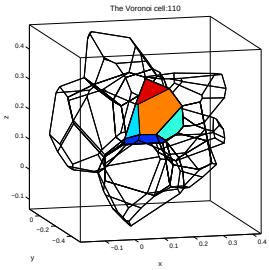


(K)

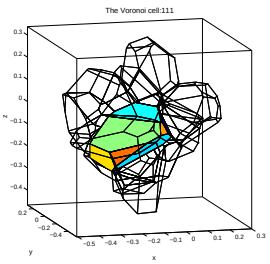


(L)

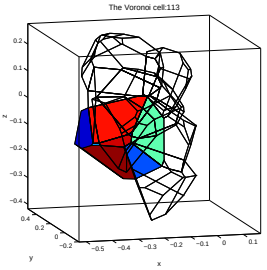


(M)

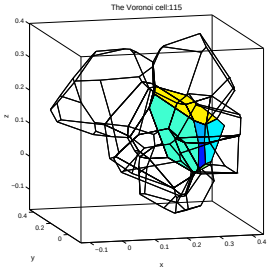


(N)

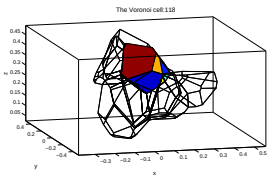


(O)

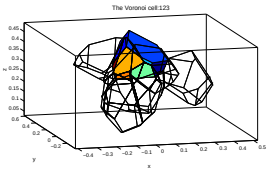


(P)

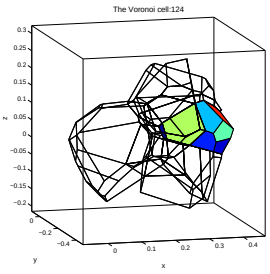


(Q)

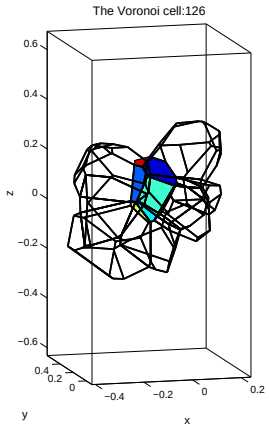


(R)

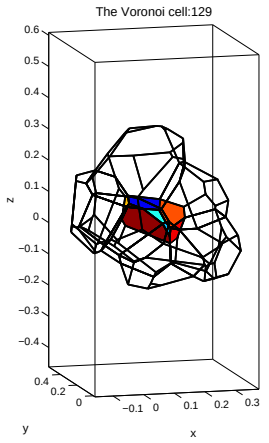


(S)

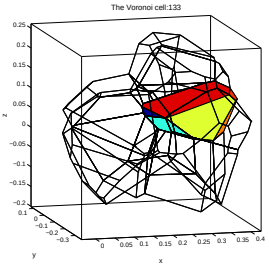


(T)

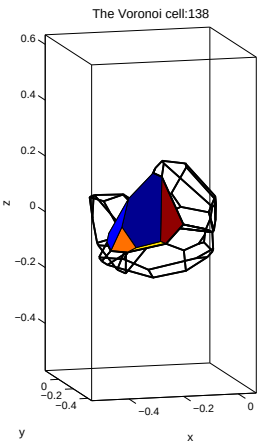


(U)

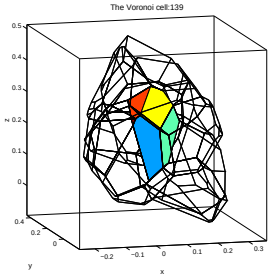


(V)

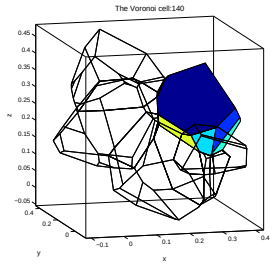


(W)

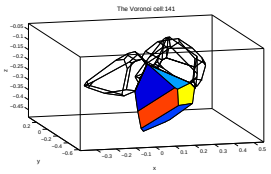


(X)

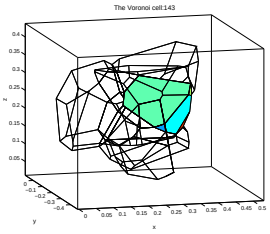


(Y)

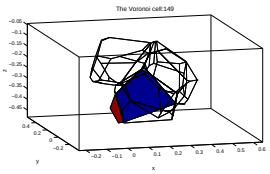


(Z)

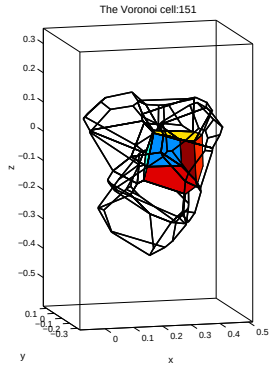


(aa)

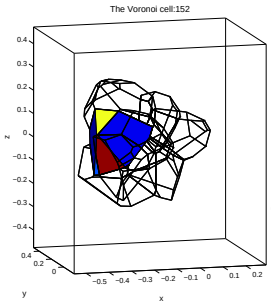


(ab)

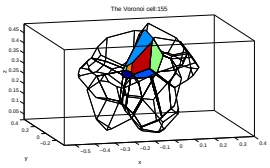


(ac)

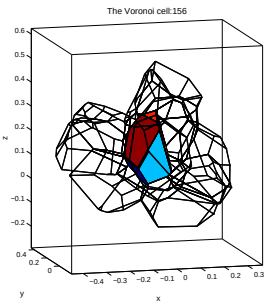


(ad)

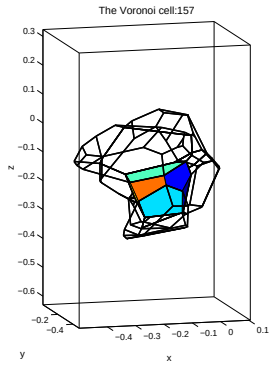


(ae)

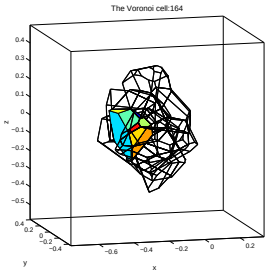


(af)

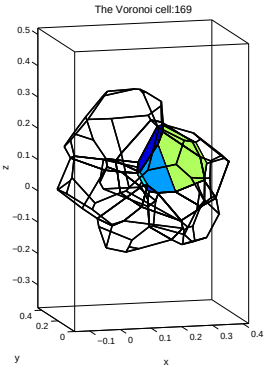


(ag)

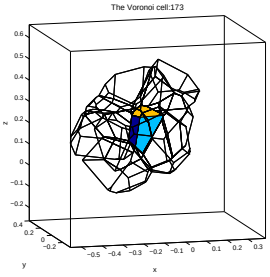


(ah)

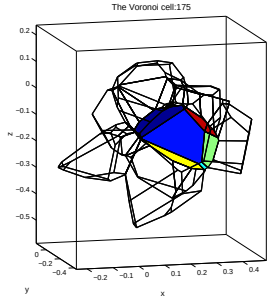


(ai)

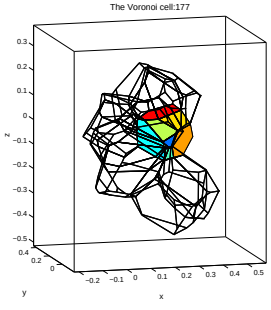


(aj)

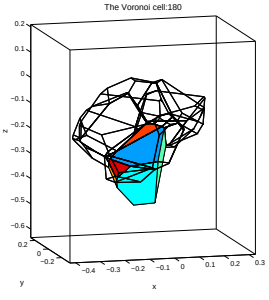


(ak)

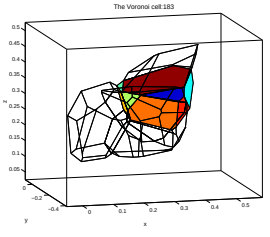


(al)

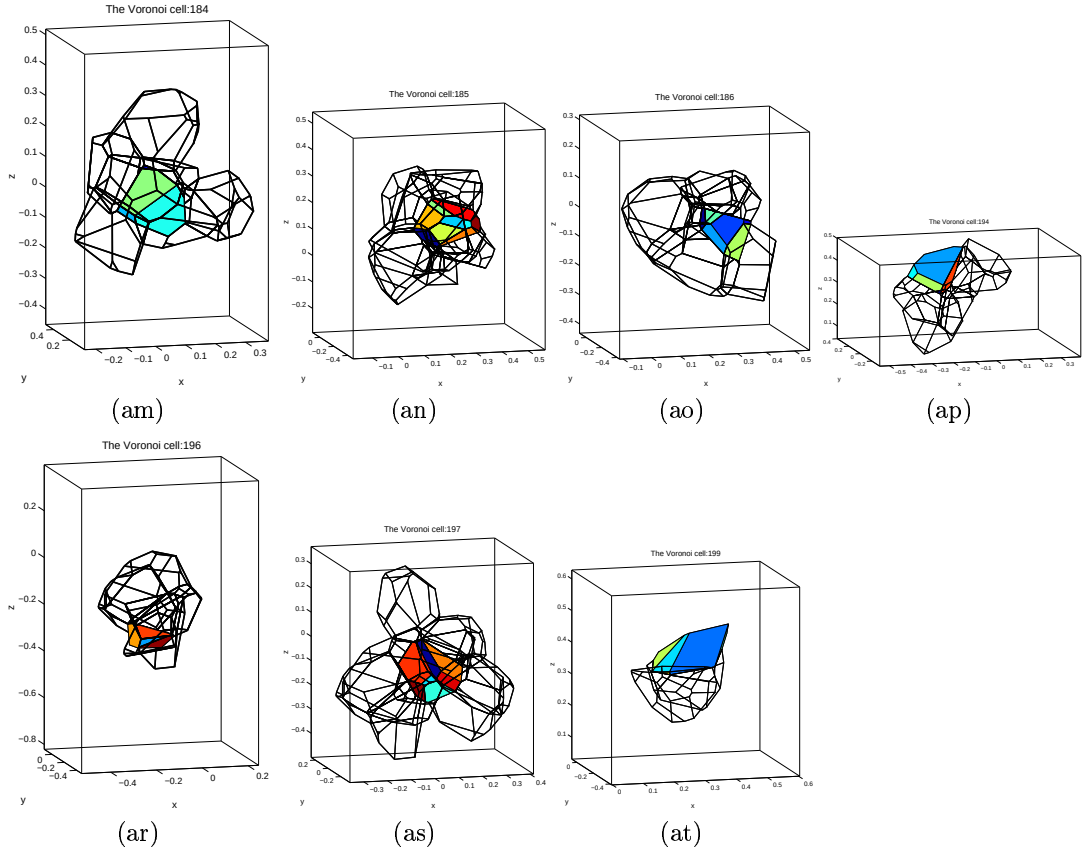


**Figure 2.7** *The 71 Voronoi cells in an aggregation.*

The statistics of these 71 cells are the following. There are originally 200 cells, but these statistics represent 71 inner cells among these. The rest, 129 cells, are on the boundary and are not considered. The abbreviation 'mn' stands for the mean-, while 'cb' the cube normal.

*Number of faces per inbound cell*
Mean: 14.2113
Variance: 11.0262
Minimum: 6
Maximum: 23
Second moment: 10.8709
Third moment: 14.0161
Kurtosis: 3.109624
Geometric mean: 13.8246
Harmonic mean: 13.4227
Median: 13
Mean absolute deviation: 2.7169

*Number of vertices per inbound cell*
Mean: 24.4225
Variance: 44.1046
Minimum: 8
Maximum: 42
Second moment: 43.4834
Third moment: 112.1287
Kurtosis: 3.109624
Geometric mean: 23.5039
Harmonic mean: 22.5058
Median: 22
Mean absolute deviation: 5.4338

*Area of surface of inner cell*
Mean: 0.1599
Variance: 0.0024
Minimum: 0.0628
Maximum: 0.2660
Second moment: 0.0023
Third moment: $7 \times 10^{-6}$
Kurtosis: 2.3015
Geometric mean: 0.1520
Harmonic mean: 0.1435
Median: 0.1602
Mean absolute deviation: 0.0398

*Area of surface of inner cell (mn)*
Mean: 1.000000
Variance: 0.0926
Minimum: 0.3928
Maximum: 1.6634
Second moment: 0.0913
Third moment: 0.0017
Kurtosis: 2.3015
Geometric mean: 0.9505
Harmonic mean: 0.8972
Median: 1.0018
Mean absolute deviation: 0.2489

*Area of surface of inner cell (cb)*
Mean: 0.3031

Variance: 0.0085
Minimum: 0.1191
Maximum: 0.5042
Second moment: 0.0084
Third moment: $4.8 \times 10^{-5}$
Kurtosis: 2.3015
Geometric mean: 0.2882
Harmonic mean: 0.2720
Median: 0.3037
Mean absolute deviation: 0.0754

*Volume of inbound cell*
Mean: 0.0261
Variance: 0.0018
Minimum: $5.5944 \times 10^{-3}$
Maximum: 0.3315
Second moment: 0.0017
Third moment: 0.0004
Kurtosis: 42.2383
Geometric mean: 0.0183
Harmonic mean: 0.0153
Median: 0.0167
Mean absolute deviation: 0.0177

*Volume of inbound cell (mn)*
Mean: 1.0000
Variance: 2.5764
Minimum: 0.2146
Maximum: 12.7188
Second moment: 2.5402
Third moment: 24.1689
Kurtosis: 42.2383
Geometric mean: 0.7012
Harmonic mean: 0.5879
Median: 0.6408
Mean absolute deviation: 0.6795

*Volume of inbound cell (cb)*
Mean: 1.0000
Variance: 2.5764
Minimum: 0.2146
Maximum: 12.719
Second moment: 2.5402
Third moment: 24.1689
Kurtosis: 42.2383
Geometric mean: 0.7012
Harmonic mean: 0.5879
Median: 0.6408
Mean absolute deviation: 0.6795

*Number of vertices per inbound face*
Mean: 5.1114
Variance: 2.1650
Minimum: 3
Maximum: 10
Second moment: 2.1619
Third moment: 1.8902
Kurtosis: 3.0234
Geometric mean: 4.9065
Harmonic mean: 4.7086
Median: 5
Mean absolute deviation: 1.1655

*Perimeter of inner face*
Mean: 0.3899
Variance: 0.0434
Minimum: 0.0017
Maximum: 1.0067
Second moment: 0.0433
Third moment: $9.88 \times 10^{-4}$
Kurtosis: 2.3090
Geometric mean: 0.3071
Harmonic mean: 0.1497
Median: 0.3940
Mean absolute deviation: 0.1720

*Perimeter of inner face (mn)*
Mean: 1.0000
Variance: 0.2854
Minimum: 0.0043
Maximum: 2.5819
Second moment: 0.2850
Third moment: 0.0167
Kurtosis: 2.3090
Geometric mean: 0.7877
Harmonic mean: 0.3839
Median: 1.010419
Mean absolute deviation: 0.4410

*Perimeter of inner face (cb)*
Mean: 0.3288
Variance: 0.0308
Minimum: 0.0014
Maximum: 0.8488
Second moment: 0.0308
Third moment: 0.0006
Kurtosis: 2.3090
Geometric mean: 0.2590
Harmonic mean: 0.1262
Median: 0.3322
Mean absolute deviation: 0.1450

*Area of faces of inner cell*
Mean: 0.0110
Variance: 0.0001
Minimum: $4.0594 \times 10^{-8}$
Maximum: $7.2892 \times 10^{-2}$
Second moment: $1.22 \times 10^{-4}$
Third moment: $2 \times 10^{-6}$
Kurtosis: 5.2926
Geometric mean: 0.0045
Harmonic mean: $2.2 \times 10^{-5}$
Median: 0.0074
Mean absolute deviation: 0.0087

*Area of faces of inner cell (mn)*
Mean: 1.0000
Variance: 1.0085
Minimum: $3.6840 \times 10^{-6}$
Maximum: 6.6151
Second moment: 1.0071
Third moment: 1.4244
Kurtosis: 5.2926

Geometric mean: 0.4086
Harmonic mean: 0.0020
Median: 0.6715
Mean absolute deviation: 0.7933

*Area of faces of inner cell (cb)*
Mean: 0.1253
Variance: 0.0158
Minimum: $4.6179 \times 10^{-7}$
Maximum: 0.8292
Second moment: 0.0158
Third moment: 0.0028
Kurtosis: 5.2926
Geometric mean: 0.0512
Harmonic mean: 0.0003
Median: 0.0842
Mean absolute deviation: 0.0994

## § 2.8 Tilings and patterns

All two dimensional lattices are tilings. The *kagome* latticedeserves some mention here since it is a first-order covering lattice of the honeycomb lattice, which in turn is dual to the triangular lattice. Some physicists conjecture that the name originates from a name of a person. Apart from a few exceptions from the reason that the word is written in the wrong script, those scientists who are japanese should know that the word from their own language which means, according to the dictionary by Nelson (1962), *basket interstices* or *woven bamboo pattern*. A better translation is simply *basket pattern* (*cf* Tiyapan, 2001, KNT8(i)), *kago* (*rad*: *take* and *tatsu*) meaning *basket* and *me* a radical word for *eye* which also means *pattern*.

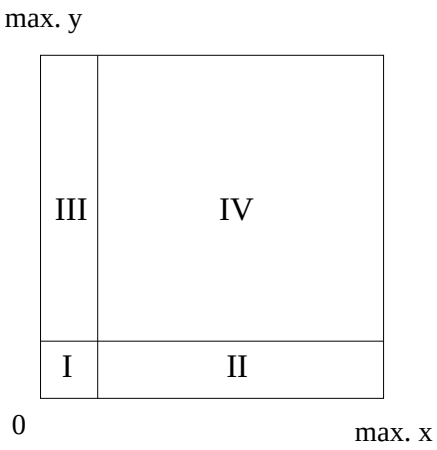


Those who do not know follow the established practice and write it as *kagomé* (*cf*, for example, Tiyapan, 1995, KNT3(iii)) with the *l'accent aigue* (acute accent) as if it were a french word. For the case of two dimensions, Algorithm 2.6 gives the algorithm for producing patterns in general. It is used for producing the 2-homohedral tilings in § 4.9 and is the basis of the program in § A.6. In this algorithm pseudo-prototiles are produced which fill the space. We shall call these our unit tiles. There are four types of these unit tiles corresponding to the four sections or groups as shown in Figure 2.8. The first group contains only one tile, *i.e.* the one at the origin, the second one contains those unit tiles to be put at the bottom row, the third one yet those to be put at the left-most column. The rest and majority of tiles belong to the fourth group.

**Figure 2.8** Four groups of tiles.

Vertices in each unit tile are divided into five groups, namely one for the boundary in each direction, *i.e.* north, east, west and south, and the fifth those in the midst of the unit tile. This is essentially in order to avoid creating a vertex twice, which would have resulted in duplicates. Those unit tiles in the fourth group take their left-most vertices from the unit tile to their left and their bottom-most vertices from the unit tile immediately below it. Unit tiles in the third group create their own left-most vertices but still take from the unit tile below them their bottom-most ones. On the other hand, unit tiles in the second group create their bottom-most vertices while taking their left-most ones from their neighbour who lives on their left. Lastly the only unit tile of the first group creates all its vertices, which include the bottom-most and left-most ones.

There are three types of edges, namely internal-, left and bottom edges, the latter two of which link respectively to vertices in their left and bottom neighbours. And then, there are four types of cells, namely middle, south, west and south-west cells, the latter three of which contains the other half of its edges in their neighbour in the corresponding direction. Each unit tile is divided into grids by lines parallel to $x$ and $y$ axes. All vertices lie on some intersection of these grids.

**Algorithm 2.6** *Tilings in two dimensions.*

**for** every unit tile **do**

**decide** its type;
**assign** all vertices according to its type;
**connect** bonds according to the connection rules;
**define** cells by their vertices;
**endfor** □

When faced with an unfamiliar tiling, we first decide upon their pseudo-prototile, that is their unit tile. Then list the coordinates of their vertices. And then list the bonds, that is the numbers of the two vertices that define each of them. We also have to divide the bonds into groups as mentioned, and include this information in our input.

The program keeps the two lists of coordinates, one for each axis. Coordinates of vertices are then referred to in grid numbers instead of the actual lengths concerned. This helps reading and using the program and procedure simpler. It marks the division between delight and despair. Also, the group information can then be represented in the program as a mapping of border vertices from a previous unit to the present one.

A cross-border bond normally has one end on the border. However there are those neither ends of which are on the border. These bonds make up a separate group of their own, or rather they make up two groups corresponding to the two groups, II and III.

This program when tried on a few well known regular lattices gives satisfactory results. Because these lattices are small, their coordination numbers $x$ differ from the true values. But since this must be because of the jagged borders of the networks created the discrepancy is systematic and so there is nothing to worry about. Also there is nothing one can do about it unless one makes changes to the program. The problem lessens but never goes away when the size of the network becomes larger. As the four sides that make up the border are in total $4d/d^2$, *i.e.* $4/d$ parts of the area, increasing the network size by one hundred times, *i.e.* $d = 10$, probably would reduce the error by 60 per cent.

It is possible to improve the program as regarding to this problem, and this is the plan for the future work. At present, this shortcoming will have some effect on the values of the six percolation probabilities obtained from each system simulated.

For the first test, the program was run on a square lattice. The six representative networks produced, which subsequently become the ground for the corresponding six values of percolation thresholds, have their statistics as follows:

$n_C = 100$, $x_C = 6.8400$, $n_B = 342$, $x_B = 12.4211$, $n_c = 100$, $x_c = 3.6000$, $n_b = 180$, $x_b = 5.3778$, $n_v = 121$, $x_v = 3.3058$, $n_e = 200$ and $x_e = 5.4100$.

Then from $2 \times 5$ runs, *i.e.* two runs for each of the five permuted list of blockages, the values of percolation thresholds are

$p_C = 0.3920 \pm 0.0627$, $p_B = 0.2459 \pm 0.0373$, $p_c = 0.5610 \pm 0.1272$, $p_b = 0.4806 \pm 0.0750$, $p_v = 0.5942 \pm 0.0802$ and $p_e = 0.5040 \pm 0.0740$.

To explain the results, the capital $C$ and $B$ in the subscript mean respectively cells and bonds when neighbours mean that they share at least one vertex. When in lower case letters $c$ and $b$ mean respectively cells and bonds when neighbourhood means sharing at least one edge. Neither the vertices nor the edges, respectively $v$ and $e$, is ambiguous since the former has zero dimension while the latter has only one. In this case, as it is in general, $p_C$ and $p_B$ are nothing that one normally talks about, while $p_c$ and $p_b$ should be the same as $p_v$ and $p_e$ in that order. Because all connections end at the boundary, it is to be expected that the values of all $x$'s are lower than their exact values for an infinite network. The results above show that, for this case at least, $x_c$ falls short of its exact value by 10 per cent, while similarly $x_b$ by 10.37, $x_v$ by 17.35 and $x_e$ by 9.83 per cent. Because $c$ and $b$ naturally form one pair while $v$ and $e$ another, it is interesting to note that $x_c$ should fare better than $x_v$ while on the other hand $x_e$ is more accurate than $x_b$. For the probability values, $p_c$ is off the mark by (*cf* § 4) $-5.36$ per cent and $p_b$ by $-3.9$ per cent, while $p_v$ does so by 2.5 per cent and $p_e$ by a mere 0.8 per cent. The first one of these pairs seems to be on the lower side while the second one, on the other hand, is on the higher end and more accurate than the first. This first test gives a result in accordance with our expectation that for vertices and edges the results should be more accurate than those from cells and bonds since the first two come from the input, while the last two are secondary values derived up from them by the program. Figure 2.9 shows the networks simulated for this test.

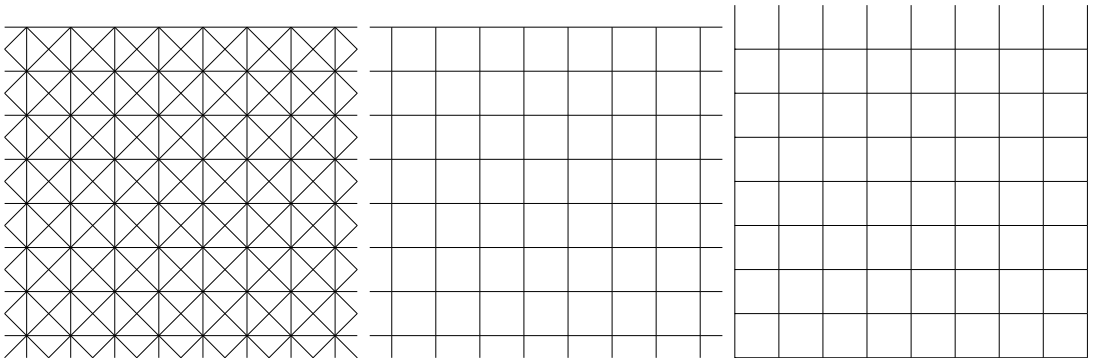


**Figure 2.9** *Percolation of networks related to the square lattice. Networks comprising of* (a) *Cells and Bonds,* (b) *cells and bonds, and* (c) *vertices and edges.*

The next test is on the honeycomb lattice. Here the results obtained from the simulation is $n_C = n_c$ 202, $x_C = x_c$ 5.4554, $n_B = n_b$ 551, $x_B = x_b$ 9.2777, $n_v = 479$, $x_v = 2.8058$, $n_e = 672$ and $x_e = 3.8244$. For the probabilities of percolation $p_C = p_c$ $0.4889 \pm 0.0704$, $p_B = p_b$ $0.3342 \pm 0.0385$, $p_v = 0.6833 \pm 0.0369$ and $p_e = 0.6382 \pm 0.0410$. These results are obtained from $2 \times 10$ simulations in the case of statistics on cells and bonds, whereas in the case of vertices and edges they are obtained from $2 \times 5$ runs. Their pictures are shown in Figure 2.10.

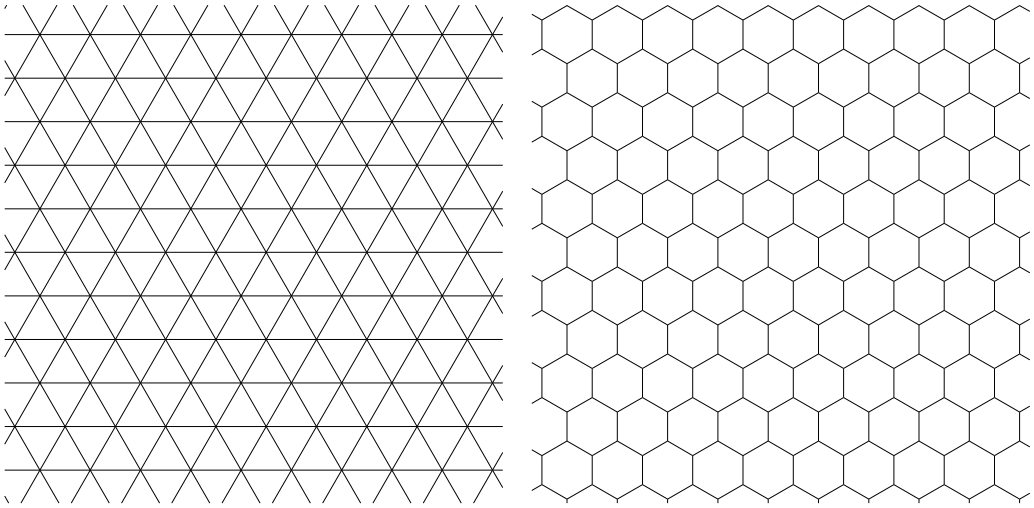


**Figure 2.10** *Percolation of networks related to the honeycomb lattice. Networks are made up of* (a) *Cells and Bonds, or cells and bonds,* (b) *vertices and edges.*

For the honeycomb lattice, the errors are for $p_c$ $-2.22$, for $p_b$ $-3.77$, for $p_v$ $-1.85$ and for $p_e$ $-2.22$ per cent. The errors for the network statistics are for $x_c = -9.08$, $x_b = -7.22$, $x_v = -6.47$ and $x_e = -4.39$ per cent.

The Kagome lattice is the next test. Here the statistics obtained for the networks are

$n_C = 230$, $x_C = 6.4087$, $n_B = 737$, $x_B = 13.1452$, $n_c = 230$, $x_c = 3.2783$, $n_b = 377$, $x_b = 5.2944$, $n_v = 316$, $x_v = 3.7342$, $n_e = 590$ and $x_e = 5.7017$.

The percolation probabilities are

$p_C = 0.4222 \pm 0.0734$, $p_B = 0.2463 \pm 0.0482$, $p_c = 0.6548 \pm 0.0787$, $p_b = 0.5332 \pm 0.0532$, $p_v = 0.6760 \pm 0.0288$ and $p_e = 0.5309 \pm 0.0651$.

Here comparison with literature is already limited as published data begins to be rare. We can compare with exact values and say that $x_v$ obtained contains an error of $-6.65$ per cent, $p_v$ of 3.68 per cent and $p_e$ of 1.70 per cent. Figure 2.11 shows the networks created and simulated.

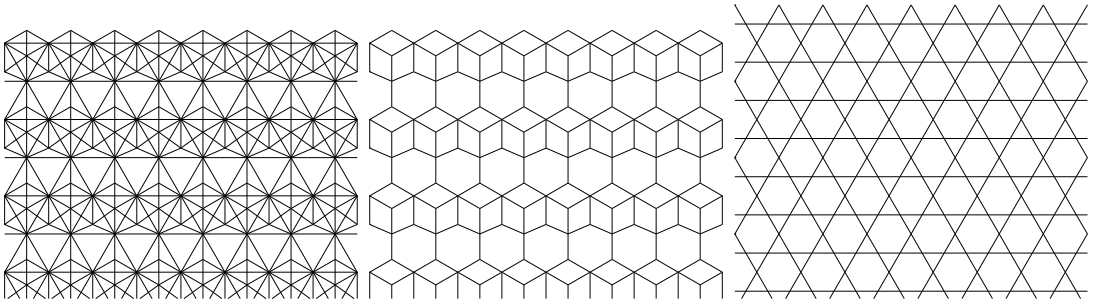

(a) (b) (c)

**Figure 2.11** *Percolation of networks related to the basket pattern, kagome lattice. The networks of* (a) *Cells and Bonds,* (b) *cells and bonds, and* (c) *vertices and edges.*

From these tests we can see that, even for a rather small size, our programs for creating the network and finding percolation show approximately five per cent error.

## § 3. Voronoi tessellation

In a puzzle of Figure 3.1 there are five rooms with doors in the position as shown. The problem is whether one can walk through every door only once and the answer according to the graph theory is *no*, because there are more than two rooms which has an odd number of doors. The proof of Theorem 3.1 was from Gomsan Bajàraṛvàṇijỳa around 1989. From this, when one plays a puzzle like that of Figure 3.1 one always starts off from a room with an odd number of doors and ends in another such room.

This is the same thing as saying that one starts and ends outside rooms with an even number of doors. Therefore the number of the latter is of no consequence, but that of the former is crucial for the existence of a solution and must never be any number other than two. Puzzle of five rooms with doors. In Figure 3.1 there are three rooms with five doors, two with four, and one with nine. There are here four rooms with an odd number of doors. Starting off from one of these four one can only end up in one of the other three, which leaves the remaining two rooms unaccounted for. In other words at least two doors will necessarily remain unvisited.

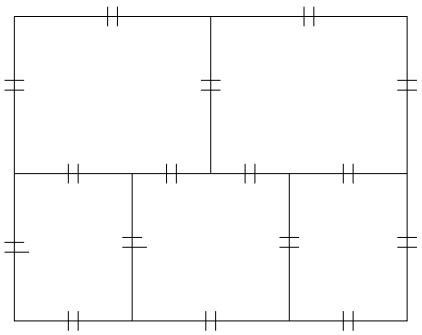

**Figure 3.1** Rooms with doors puzzle.

**Theorem 3.1.** *A travel along a network can only starts and ends at nodes which have an odd coordination number.*

**Proof.** Looking at Figure 3.2, if one starts from inside a room with an odd number of doors one always ends up outside it. On the other hand one always ends up inside a room with an even number of doors if one starts of from it. In the second picture such a room is all the area outside the circle. □The following Corollaries 3.1[1], 3.1[2] and 3.1[3] assume nondegeneracy of the Voronoi network. Such a path as mentioned in these corollaries is also called *self-avoiding.*

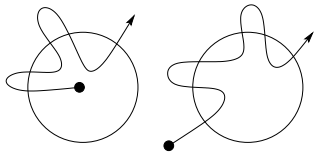

**Figure 3.2** Departure and arrival rooms.

**Corollary 3.1[1].** *There can be no path which traverses all edges of a Voronoi graph only once.*

**Proof.** This follows from Theorem 3.1 because a two dimensional Voronoi network has a coordination number three. □

**Corollary 3.1[2].** *On a three dimensional Voronoi structure there always exists a path that runs through every edge once and only once.*

**Proof.** This also readily follows from Theorem 3.1 since a three dimensional Voronoi network has a coordination number of four. □

**Corollary 3.1[3].** *Take any Voronoi cell of the three dimensional network, it is impossible to walk through all its edges without repeating some of them.*

**Proof.** Again from Theorem 3.1 and because the surface of a Voronoi polyhedron is a two dimensional network of polygons which has the coordination number three. □

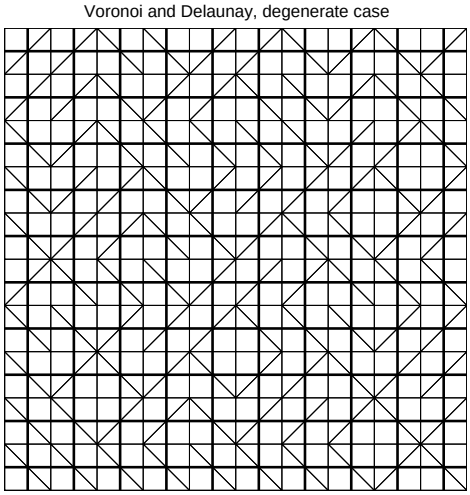


Jerauld *et al* (1984) compared the Voronoi, with the triangular networks and found that the bond percolation probability of the former is 4.3% or 0.015 less than that of the latter, small site clusters more, and small bond clusters less likely. When a square lattice was fed to *voronoi* and *delaunay* in Matlab, by the program `degen.m` in § A.15, there were error messages saying that points were collinear and possibly triangulation is incorrect. This case, Figure 3.3, is degenerative.

**Figure 3.3** Voronoi from degenerative data.

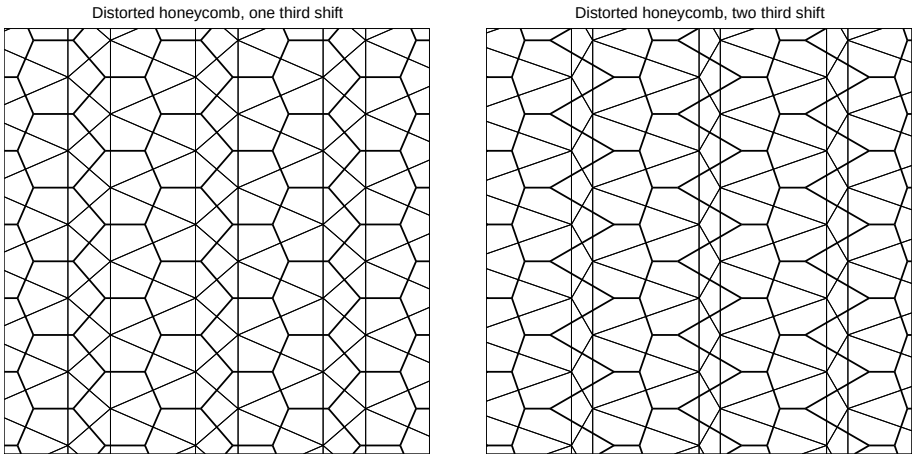


**Figure 3.4** *The honeycomb or hexagonal lattice whose alternate y-plane has been shifted (a) one-third, and (b) two-third respectively. Triangulation is shown with thinner lines. The program used is* `honey.m`

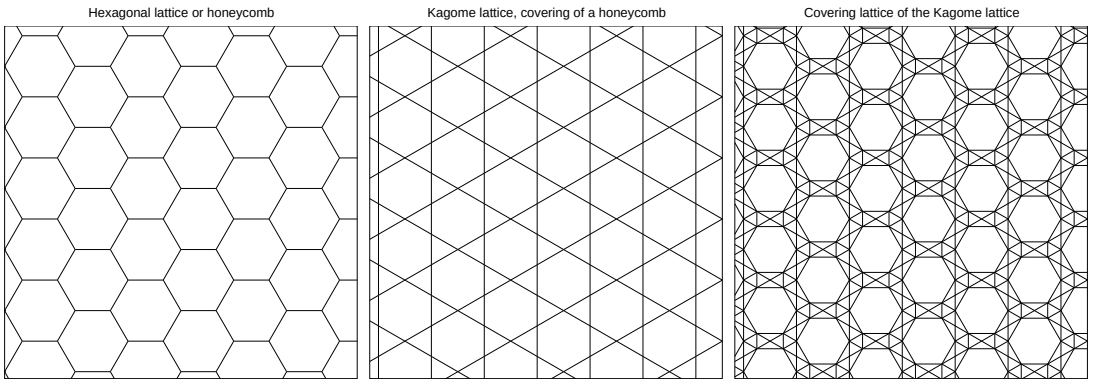


**Figure 3.5** (a) *The hexagonal lattice,* (b) *its covering lattice (Kagome), and* (c) *the covering lattice of its covering lattice (i.e. covering of Kagome).* (`cover.m`, `covers.m`, *and* `coverss.m`)

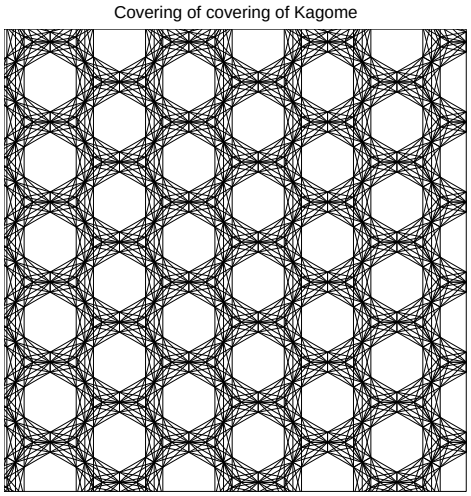


If we indicate by $C_v^n(x)$ the $n^{\text{th}}$-order covering lattice of a lattice $x$, then the first picture is Hexagonal, the second one Kagome or $C_v^1$(Hexagonal) and the third one $C_v^2$(Hexagonal) or in other words $C_v^1$(Kagome). Figure 3.6 is the next iteration, a $C_v^3$(Hexagonal) or $C_v^2$(Kagome). Now let us look at the Voronoi graph and its covering lattices. Pictures in Figure 3.7 are drawn by first creating and cropping a Voronoi graph with the help of the program `crop.m`, then use the recursive procedure described above to find up to the third covering lattice.

**Figure 3.6** The next covering lattice.

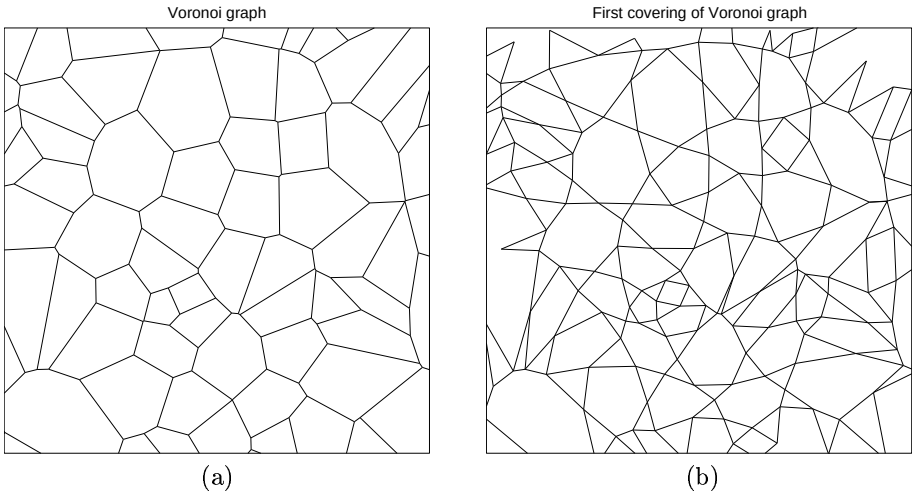

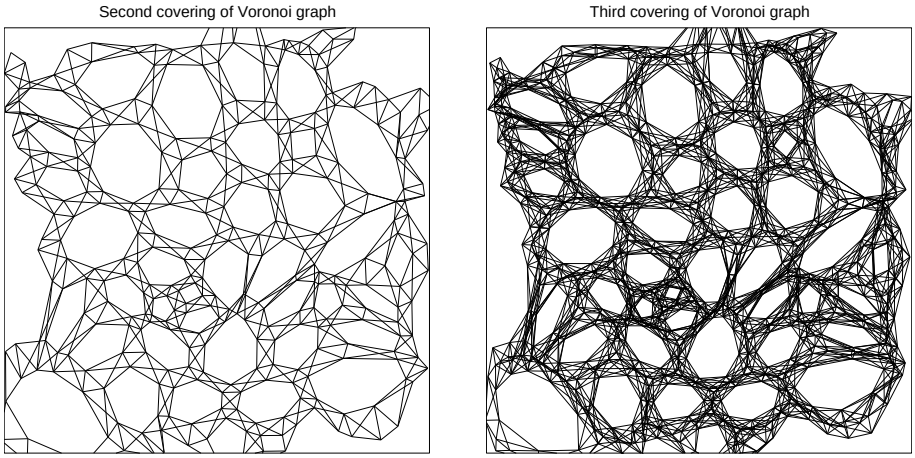


(c) (d)

**Figure 3.7** (a) *Voronoi graph (V.g.),* (b) $C_v^1$(**V.g.**), (c) $C_v^2$(**V.g.**), (d) $C_v^3$(**V.g.**).

Notice that the covering lattices retain the skeleton structure of the original Voronoi graph. Those of higher orders represent closer the structures of nature where walls have thickness.

## § 3.1 Quadratic equations

Quadratic equations are equations of binary quadratic forms. Around 400 BC Barbilonia had algorithmic equivalences of quadratic equations which are based on the method of completing the square and where all answers are unsigned, *i.e.* positive, lengths. Because there was no notion for zero, Diophantus considered three types of quadratic equations $ax^2 + bx = c$, $ax^2 = bx + c$, and $ax^2 + c = bx$. Euclid, *circa* 300 BC, used geometric equivalences or quadratic equations whose roots are also lengths. Brahmagupta allowed negative quantities, which he called debts, and used abbreviations for the unknown. Al-Khwarizmi classified quadratics into six types, namely squares equals roots, squares equals numbers, roots equal numbers, squares and roots equal number, squares and numbers equal roots, and roots and numbers equal squares. In his book *Liber embadorum*, published in 1145, Abraham bar Hiyya Ha-Nasi (aka Savasorda) gives the complete solution of quadratic equations. Luca Pacioli published *Summa de arithmetica, geometrica, proportioni et proportionalita* (or Summa) in 1494. He also applied quadratic methods to quartics of the form $x^4 = a + bx^2$. Scipione del Ferro solved the cubic equations of the form $x^3 + mx = n$.

## § 3.2 Quadratic forms

The theory of quadratic forms and the theory of matrix are inseparable though the history of these two subjects are somewhat fragmentary. A bilinear form in the sets $x_i$ and $y_i$, $i = 1 \ldots n$, is $\sum_{i,j} x_i y_j$, or $\mathbf{x}^{\mathrm{T}}\mathbf{A}\mathbf{y}$. If $x_i = y_i$ for all $i$, then the form is quadratic in $x_i$. In other words, a quadratic form is a general expression which contains second order terms.

A quadratic form in the variables $x_i$ is the homogeneous quadratic polynomial $\sum_{i,j=1}^{n} a_{ij} x_i x_j$, where $a_{ij}$ are arbitrary scalars. The set of all quadratic forms in $x_i$ with coefficients in a field $\mathcal{F}$ is a vector space over $\mathcal{F}$. A bilinear form in the variables $x_i$ and $y_i$ is the homogeneous polynomial $\sum_{j=1}^{m} \sum_{i=1}^{n} a_{ij} x_i y_j$, where $a_{ij}$ are arbitrary scalars. The set of all bilinear forms with coefficients in a field $\mathcal{F}$ is a vector space over $\mathcal{F}$ (*cf* Hohn, 1958). A quadratic form can also be represented in a matrix form as $X^{\mathrm{T}}AX$. Distinct $n \times n$ matrices $A_1$ and $A_2$ have the same quadratic polynomial if all corresponding $a_{ij} + a_{ji}$ are equal. Given the quadratic form, it is not possible to identify the corresponding matrix $A$ by inspection. This ambiguity is eliminated by replacing each pair of the coefficients $a_{ij}$ and $a_{ji}$ by their mean $(a_{ij} + a_{ji})/2$, which amounts to replacing $A$ by $(A + A^{\mathrm{T}})/2$ which is symmetric. If $x_i$ are independent variables, the rank and the determinant of $A$ are respectively the rank and the discriminant of the form. Two quadratic forms $X^{\mathrm{T}}A_1X$ and $\widetilde{X}^{\mathrm{T}}A_2\widetilde{X}$ are equivalent if and only if there is a nonsingular transformation $X = B\widetilde{X}$ such that $X^{\mathrm{T}}A_1X = \widetilde{X}^{\mathrm{T}}B^{\mathrm{T}}A_1B\widetilde{X} = \widetilde{X}^{\mathrm{T}}A_2\widetilde{X}$, that is if and only if for a suitable nonsingular matrix $B$, $A_2 = B^{\mathrm{T}}A_1B$. Then $A_1$ and $A_2$ have the same rank and are said to be congruent to each other.

Lattice can be represented by quadratic forms and vice versa, therefore the classification of quadratic forms is also the classification of lattices.

## § 3.3 Voronoi algorithms

Green and Sibson (1978) gives the algorithm that produces Voronoi graphs, as summarised in Algorithm 3.1. They call a Voronoi tessellation 'Dirichlet tessellation'. The points outside the window are ignored, and points on the periphery has tile bounded in part by sequences of effective constraints instead of by inter-tile edges. Contiguous tiles have a boundary sequences in common. A degenerate vertex, that is a vertex where four or more tiles meet, causes an incorrect record of diagonal contiguity. From the Euler-Poincaré formula, $f - e + v = 2$, where in the plane the infinite region is counted as a face, gives rise to the total number of contiguities to be recorded $4\times$ `effective constraints` $+6\times$ `accepted points` $-6$. A square lattice has all its vertices degenerate.

**Algorithm 3.1** *Voronoi 2-d algorithm, Green and Sibson (1978)*

**define** window as a set of linear inequality constraints $ax + by + c < 0$;
**do**
  **add** a new point $n$ randomly within the window;
  **do**
    **find** the line $b_i$ joining $n$ and its nearest neighbour $p_i$;
    **find** $l_i$ the perpendicular bisector of $b_i$;
    **find** the intersection between $l_i$ and the edge $e_i$ of its nearest tile,
      going clockwise with respect to $n$;
    **add** $l_1$ to the object- and contiguity lists;
  **until** $2\pi$ radian around $n$ traversed
**until** no more new points added **enddo** □

Moore and Angell developed a algorithm which can cope with degenerate cases. Because their program could find them, they are no longer considered degenerate and they fittingly called these *vertices of* $(> 3)$*-hedral valency.*

## § 3.4 Voronoi statistics in literature

Van de Weygaert (1994) studies linear section of three dimensional Voronoi network where the mean length is

$$\langle\lambda\rangle = L = \frac{d\Gamma(d-1/2)\Gamma((d+1)/2)^2}{(d-1)!\rho_c^{1/d}2\Gamma(d/2+1)^{2-(1/d)}\Gamma(2-1/d)}. \qquad (19)_{\text{iii}}$$

For two dimensions $\langle\lambda\rangle = \pi/(4\sqrt{\rho})$, while for three dimensions $\langle\lambda\rangle = [81/(32\pi\rho)]^{1/3}/\Gamma(2/3)$. Consequently for two dimensions $\langle\lambda\rangle = 0.7854\rho^{-1/2}$ while for three dimensions $\langle\lambda\rangle = 0.6872\rho^{-1/3}$, $\langle\lambda^2\rangle = 0.632\rho^{-2/3}$, $0.668\rho^{-1}$ and $\langle\lambda^4\rangle = 0.774\rho^{-4/3}$. For 3-d Poisson-Voronoi tessellation the exact values for the moments are shown in Table 3.1.

| | | | | |
|---|---|---|---|---|
| $\rho_v$ | $\frac{24}{35}\pi^2\rho_c$ | $6.763\rho_c$ | number density of vertices | $J_0$ |
| $\rho_e$ | $\frac{48}{35}\pi^2\rho_c$ | $13.535\rho_c$ | number density of edges | $J_1$ |
| $\rho_f$ | $\left(\frac{24}{35}\pi^2+1\right)\rho_c$ | $7.768\rho_c$ | number density of faces | $J_2$ |
| $\rho_c$ | $\rho_c$ | $\rho_c$ | number density of cells | $J_3$ |
| $n_c^v$ | $\frac{96}{35}\pi^2$ | 27.07 | number of vertices per cell | $\mathrm{E}(N_0)$ |
| $n_c^e$ | $\frac{144}{35}\pi^2$ | 40.61 | number of edges per cell | $\mathrm{E}(N_1)$ |
| $n_c^f$ | $\frac{48}{35}\pi^2+2$ | 15.54 | number of faces per cell | $\mathrm{E}(N_2)$ |
| $n_f^v$ or $n_f^e$ | $\frac{144\pi^2}{24\pi^2+35}$ | 5.228 | number of vertices or edges per face | $E_2(N_0)$ or $E_2(N_1)$ |
| $V_c$ | $\frac{1}{\rho_c}$ | $\frac{1}{\rho_c}$ | volume of cell | $\mathrm{E}(V)$ |
| | $\frac{1.180}{\rho_c^2}$ | $\frac{1.180}{\rho_c^2}$ | | $\mathrm{E}(V^2)$ |
| $A_c$ | $\left[\frac{256\pi}{3\rho_c^2}\right]^{1/3}\Gamma\left(\frac{5}{3}\right)$ | $5.821\rho_c^{-2/3}$ | surface area of cell | $\mathrm{E}(A_c)$ |
| $s_c$ | $\frac{(4\pi)^{5/3}\Gamma(1/3)}{5(9\rho_c)^{1/3}}$ | $17.496\rho_c^{-1/3}$ | perimeter of cell | $\mathrm{E}(s_c)$ |
| $A_f$ | $\frac{35(2^{8/3})\pi^{1/3}\Gamma(2/3)}{(9\rho_c)^{2/3}(24\pi^2+35)}$ | $0.3747\rho_c^{-2/3}$ | area of face | $\mathrm{E}(A_w)$ |
| $s_f$ | $\frac{7(2^{10/3})\pi^{5/3}\Gamma(1/3)}{(9\rho_c)^{1/3}(24\pi^2+35)}$ | $2.252\rho_c^{-1/3}$ | perimeter of face | $\mathrm{E}(s_w)$ |
| $d_e$ | $\frac{7\Gamma(1/3)}{9(36\pi\rho_c)^{1/3}}$ | $0.4309\rho_c^{-1/3}$ | length of edge | $\mathrm{E}(L)$ |

**Table 3.1** *Moments of 3-d Poisson-Voronoi tessellation, cf van de Weygaert (1994).*

The moments of 2-d section of 3-d Voronoi tessellation are shown in Table 3.2.

| | | | | |
|---|---|---|---|---|
| $\rho_v$ | $\frac{2\Gamma\left(\frac{1}{3}\right)\left(\frac{16\pi^5\rho^2}{9}\right)^{1/3}}{15}$ | $2.9159\rho_c^{2/3}$ | number density of vertices | $J_0$ |
| $\rho_e$ | $\frac{3}{2}\rho_v$ | $4.3739\rho_c^{2/3}$ | number density of edges | $J_1$ |
| $\rho_c$ | $\frac{1}{2}\rho_v$ | $1.4530\rho^{2/3}$ | number density of cells | $J_2$ |
| $n_c^v$ or $n_c^e$ | 6 | 6 | number of vertices or edges per cell | E($N_0$) or E($N_1$) |
| $A_c$ | $\frac{15}{\Gamma\left(\frac{1}{3}\right)\left(\frac{16\pi^5\rho_c^2}{9}\right)^{1/3}}$ | $0.6859\rho^{-2/3}$ | | E($A$) |
| | | $0.698\rho_c^{-4/3}$ | | E($A^2$) |
| $s_c$ | $\frac{30\Gamma\left(\frac{2}{3}\right)}{(36\pi\rho_c)^{1/3}\Gamma\left(\frac{1}{3}\right)}$ | $3.1356\rho_c^{-1/3}$ | perimeter of cell | E($S$) |
| $d_e$ | $\frac{5\Gamma\left(\frac{2}{3}\right)}{(36\pi\rho_c)^{1/3}\Gamma\left(\frac{1}{3}\right)}$ | $0.5226\rho_c^{-1/3}$ | length of edge | E($L$) |

**Table 3.2** *Moments of 2-d section of 3-d Voronoi, cf van de Weygaert (1994).*

The form factor of a cell, $f_c = 36\pi V_c^2/A_c^3$, is a dimensionless parameter which partially describes the shape of the cell. The form factor of a face is $f_f = 4\pi A_f/s_f^2$, which is the unity when the face is a circle. Regularly shaped cells have their shape approaching that of the sphere where $f_f = 1$. Statistics of 3-d VT which van de Weygaert (1994) gives include those listed here in Table 3.3.

| | $\mu(\cdot)$ | $\sigma(\cdot)$ | $\gamma_1(\cdot)$ | $\gamma_2(\cdot)$ | |
|---|---|---|---|---|---|
| $\rho_v$ | $6.747 \pm 0.014$ | | | | $J_0$ |
| $\rho_e$ | $13.493 \pm 0.028$ | | | | $J_1$ |
| $\rho_f$ | $7.747 \pm 0.014$ | | | | $J_2$ |
| $\rho_c$ | $1.000 \pm 0.000$ | | | | $\rho$ |
| $n_c^v$ | $26.986 \pm 0.055$ | $6.61 \pm 0.18$ | $0.346 \pm 0.029$ | $-0.029 \pm 0.030$ | $N_0$ |
| $n_c^e$ | $40.479 \pm 0.083$ | $9.92 \pm 0.27$ | $0.346 \pm 0.029$ | $-0.029 \pm 0.030$ | $N_1$ |
| $n_c^f$ | $15.493 \pm 0.028$ | $3.305 \pm 0.091$ | $0.346 \pm 0.029$ | $-0.029 \pm 0.030$ | $N_2$ |
| $V_c$ | $1.000 \pm 0.000$ | $0.418 \pm 0.009$ | $0.73 \pm 0.11$ | $0.70 \pm 0.39$ | $V_{cell}$ |
| $A_c$ | $5.801 \pm 0.018$ | $1.461 \pm 0.043$ | $0.28 \pm 0.11$ | $-0.01 \pm 0.17$ | $A_{cell}$ |
| $s_c$ | $17.443 \pm 0.054$ | $3.655 \pm 0.094$ | $0.305 \pm 0.035$ | $0.00 \pm 0.13$ | $S_{cell}$ |
| $f_c$ | $0.540 \pm 0.006$ | $0.082 \pm 0.003$ | $-0.565 \pm 0.032$ | $0.36 \pm 0.11$ | $F_{cell}$ |
| $n_f^v$ | $5.2255 \pm 0.0014$ | $1.564 \pm 0.016$ | $0.582 \pm 0.016$ | $0.058 \pm 0.024$ | $N_0^w$ |
| $A_f$ | $0.3744 \pm 0.0015$ | $0.3722 \pm 0.0037$ | $1.266 \pm 0.047$ | $1.40 \pm 0.19$ | $A_{wall}$ |
| $s_f$ | $2.2518 \pm 0.0092$ | $1.2009 \pm 0.0050$ | $0.089 \pm 0.022$ | $-0.796 \pm 0.029$ | $S_{wall}$ |
| $f_f$ | $0.6389 \pm 0.0005$ | $0.1635 \pm 0.0011$ | $-0.855 \pm 0.035$ | $0.40 \pm 0.13$ | $F_{wall}$ |
| $d_{cf}$ | $0.6402 \pm 0.0017$ | $0.2092 \pm 0.0051$ | $-0.024 \pm 0.022$ | $-0.333 \pm 0.074$ | $D_{nw}$ |
| $V_{cf}$ | $0.0645 \pm 0.0001$ | $0.0579 \pm 0.0009$ | $1.177 \pm 0.097$ | $1.52 \pm 0.47$ | $V_{nw}$ |
| $d_e$ | $0.4309 \pm 0.0018$ | $0.3216 \pm 0.0023$ | $0.829 \pm 0.020$ | $0.209 \pm 0.044$ | $L$ |
| $\alpha_{ee}$ | $111°\text{C}107 \pm 0.018$ | $35°\text{C}310 \pm 0.078$ | $-0.499 \pm 0.012$ | $-0.276 \pm 0.039$ | $\alpha_{ee}$ |
| $\alpha_{ff}$ | $120°\text{C}0 \pm 0.0$ | $23°\text{C}53 \pm 0.30$ | $-0.296 \pm 0.014$ | $-0.255 \pm 0.038$ | $\alpha_{ww}$ |

**Table 3.3** *Statistics of 3-d VT, van de Weygaert (1994).*

His statistics on the planar section of the 3-d Voronoi tessellation is shown here as Table 3.4.

| | $\mu(\cdot)$ | $\sigma(\cdot)$ | $\gamma_1(\cdot)$ | $\gamma_2(\cdot)$ |
|---|---|---|---|---|
| $\rho_s^c$ | 1.4530 | 0.0592 | 0.2871 | -1.0099 |
| $\rho_s^v$ | 2.9060 | 0.1134 | 0.2871 | -1.0099 |
| $\rho_s^e$ | 4.3590 | 0.1776 | 0.2871 | -1.0099 |
| $n_s^v$ | 6.0000 | 1.6895 | 0.3311 | -0.1142 |
| $A_s^c$ | 0.6882 | 0.4741 | 0.4573 | -0.3902 |
| $s_s^c$ | 3.1418 | 1.2212 | -0.5819 | -0.2879 |
| $f_s^c$ | 0.7050 | 0.1433 | -1.3425 | 2.0875 |
| $d_s^e$ | 0.5221 | 0.3631 | 0.6223 | -0.2321 |
| $\alpha_s^{ee}$ | 120°C0000 | 31°C6039 | -0.6351 | 0.1321 |
| $\alpha_s^{ff}$ | 63°C1812 | 18°C5232 | -0.6351 | -0.3520 |

**Table 3.4** *Statistics of the planar section of the 3-d Voronoi tessellation, van de Weygaert (1994).*

Then Table 3.5 lists the statistics he gave for the line section of 3-d VT.

| | $\mu(\cdot)$ | $\sigma(\cdot)$ | $\gamma_1(\cdot)$ | $\gamma_2(\cdot)$ |
|---|---|---|---|---|
| $\lambda$ | 0.6703 | 0.3942 | 0.2600 | -0.6923 |
| $\sigma(\lambda)$ | 0.6123 | 0.1159 | 0.0643 | 0.0204 |
| $\alpha_l^{fl}$ | 44°C69 | 19°C5325 | 0.0067 | -0.8080 |
| $\alpha_l^{ff}$ | 75°C4123 | 30°C9389 | -0.0185 | -0.5829 |

**Table 3.5** *Statistics for the line section of the 3-d Voronoi tessellation, van de Weygaert (1994).*

Tables 3.5, 3.5 and 3.5 are all on VT's which are created from $\mathcal{P}(0,3)$. Apart from these, van de Weygaert (*ibid.*) also gives results based on VT's with anticorrelated- and correlated nuclei the statistics of which are not listed here.

Another interesting statistics is the correlation between the number of sides of a grain $n_e$, and the expected number of sides of its neighbouring grains $n_n^e$. Aboav (1970), in his investigation of polycrystalline MgO, empirically found it to be $n_n^e = 5+8/n_e$ and Weaire (1974) found a theoretical value of $n_n^e = 5+6/n_e$.

Later Aboav (1983) published another finding in which he studied a thin film of arsenic-selenium glass, $As_2Se_3$. This time with the initial assumption that $n_n^e = 6 - a + (6a+\mu_2)/n$ and $\mu_2 = \sum_n (n-6)^2 f_n = \langle (n-6)^2 \rangle$ he empirically finds $n_n^2 = 4.79 + 8.98/n$.

## § 3.5 Voronoi statistics

In two dimensions the statistical descriptions are as follows.

The curve in Figure 3.8 is

$$y = 0.62/n^{0.13}.$$

First the edge lengths are normalised by the edge length of the equivalent or characteristic square . A *equivalent square* is defined as the square figure whose area is equal to the area of the polygon in question, here a Voronoi polygon. Then find the average of the edge lenghts in each cell.

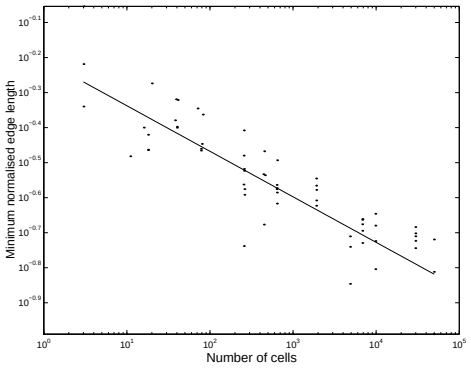


**Figure 3.8** The minimum of the average normalised edge length.

In Figure 3.9 the curve is

$$y = \left| (n/15)^{1/2} \right| + 0.7 \ .$$

Of these cell-averaged normalised edge length obtained from simulations on various sizes of networks the minimum values are plotted in Figure 3.8, the maximum in Figure 3.9, and the expected value in Figure 3.10. Note that the last quantity is the average over the whole structure of all the averages obtained one from each cell.

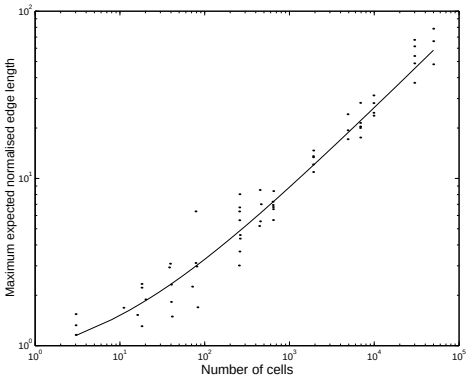


**Figure 3.9** The maximum of the average normalised edge length.

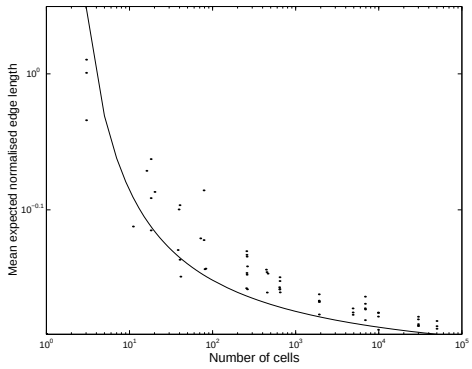


In Figure 3.10 the curve is

$$y = 10^{0.2/\log x} - 0.4$$

To summarise, as the networks gets larger its minimum, maximum, and mean of the edge lenghts when compared with the characteristic length approach constant values. The characteristic length is defined as $l = [\sum_{i=1}^{n} A_i/n]^{1/2}$, where $A_i$ is the area of the $i^{\text{th}}$ polygon and $n$ is the number of cells.

**Figure 3.10** The mean of the average normalised edge length.

That the three values mentioned become constant may not seem obvious by the look of Figures 3.8 to 3.10 because the scale used there is a logarithmo-logarithmic scale, not a Euclidean one. These figures emphasise the smaller ranges of size. Figure 3.11 below on the other hand is plotted using a normal scale which enables one to see the asymptotic effect more clearly. Here the figures (a), (b), and (c) are respectively Figure 3.8, 3.9, and 3.10. Let the term *representative* stands for 'of the cell-average normalised', and *length* means 'edge length' in this context.

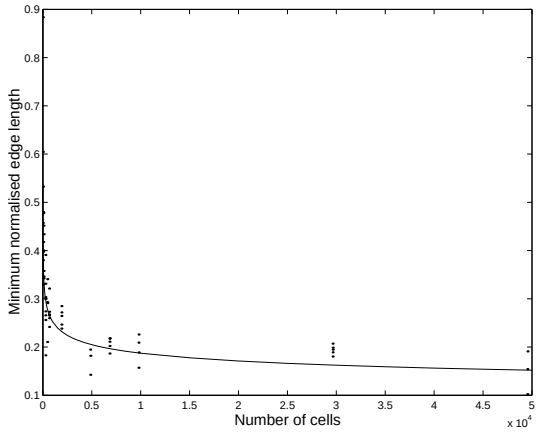


(a)

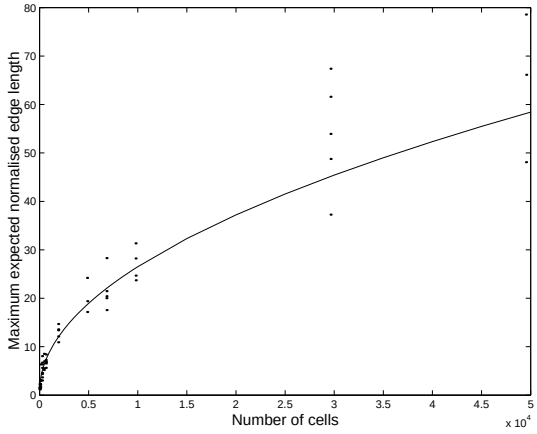


(b)

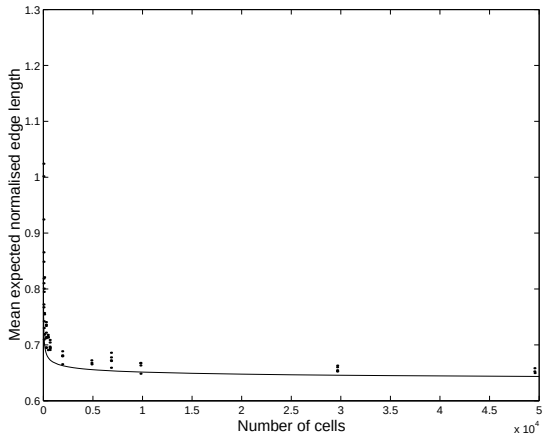


Then the *minimum representative length* approaches 0.15 from Figure 3.11 (a), the *maximum representative length* is ever increasing, seemingly by a power law of approximately 0.5, while *mean representative length* approaches the value of 0.65. Properties of the Voronoi tessellation can be divided into individual and collective properties. With this in mind the term *length* above represents a property, *representative* means individual, and *minimum*, *maximum* and *mean* show the collective attributes.

**Figure 3.11** Mean, maximum, and mean of the cell-average normalised edge length..

This $\sigma^2(\mathcal{N}_v^c(E(l_e)))$ increases very slowly with the increasing sizes of the networks. The curve shown has the equation

$$y = \left| \left[ \frac{x}{8 \times 10^4} \right]^{1/3} \right| + 0.05 \ .$$

The number of vertices per cell increases dramatically as one goes up the dimension ladder. The program in § A.10 contains the essential part of the code which produces Figure 3.13.

**Figure 3.12** The variance of the expected values of the normalised length of edges of a cell.

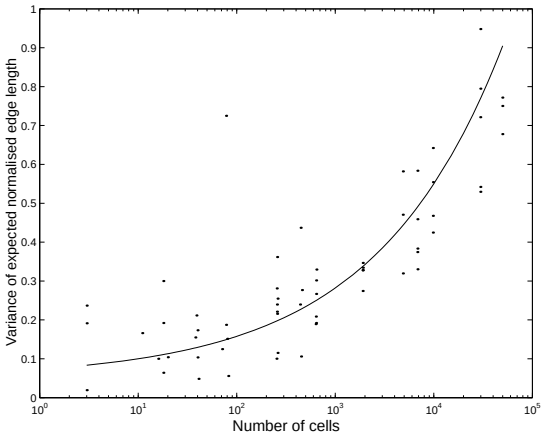


The straight line shown is $0.093(4+e)^n$. Notice the trend towards a greater rate of increase at dimensions higher than the maximum six shown. Only Voronoi cells which lies within the original domain and the vertices of these are considered. The same program also gives Figure 3.14. The expanse and the hypervolume of the Voronoi tessellation increases at an enormous rate, which results in the number of cells totally bounded within the original domain decreasing rapidly in Figure 3.14 as the dimension goes up.

**Figure 3.13** Number of vertices per cell.

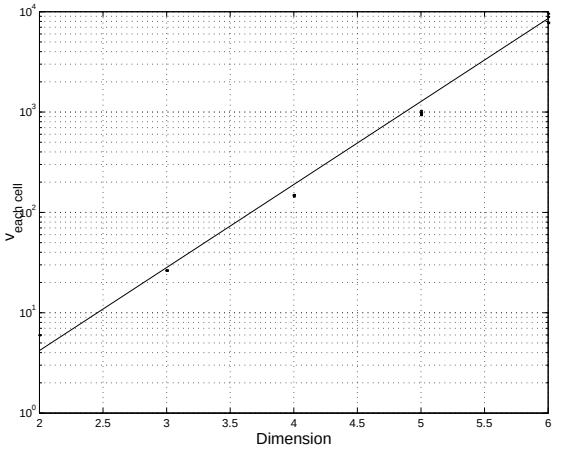


The effect at close to the zero ratio is emphasised by using the log scale for the $y$-axis. Also with the logarithmic scale the polynomial estimation curves that give negative values of the ratio is automatically excluded. One can fit the polynomial $p(x) = p_1x^n + p_2x^{n-1} + \ldots + p_nx + p_{n+1}$ to the data with a least square algorithm. If $\mathbf{x}$ is the vector containing the data, then the the $(n+1)$ coefficients of the estimated polynomial can be found from $\hat{\mathbf{x}} = (\mathbf{x} - \mathrm{E}(\mathbf{x}))/\sigma(\mathbf{x})$.

**Figure 3.14** Ratio of cells in the original domain.

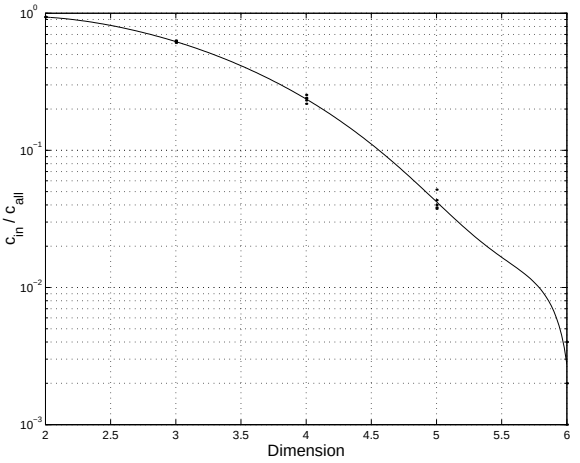


For data containing independent normal errors with a constant variance, the error bounds contain at least half of the predictions. The curve shown in Figure 3.14 is $p(x) = -0.048x^4 + 0.064x^3 - 0.203x^2 - 0.459x + 0.263$, the average value $\mathrm{E}(\mathbf{x})$ is 3.917, and the standard deviation $\sigma(\mathbf{x})$ is 1.412. The structure of the polynomial fit can be described using the Cholesky factor of the Vandermonde matrix

$$R = \begin{bmatrix} -12.19 & -1.56 & -6.08 & -0.47 & -3.17 \\ 0 & 8.46 & -0.45 & 4.47 & -0.44 \\ 0 & 0 & 1.21 & 0.33 & 2.93 \\ 0 & 0 & 0 & -1.63 & 0.30 \\ 0 & 0 & 0 & 0 & 2.25 \end{bmatrix},$$

the degree of freedom which is 19, and the norm of the residuals which is 0.034 in this case.

## § 3.6 Voronoi section

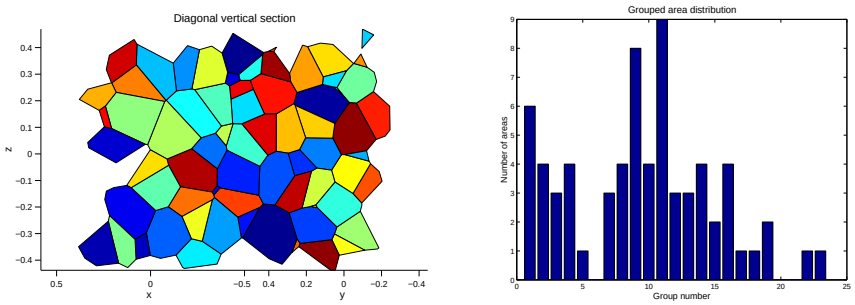


(a) (b)

**Figure 3.15** *(a) Section by the plane $x - y + \epsilon z = \epsilon, \epsilon = 10^{-4}$. (b) Grouped distribution of area, the number of groups is approximately one-third the number of regions.*

| | $\mathcal{V}_c$ | $\aleph_c$ | $A_c^{fr}$ | $V_c^{fr}$ | $n_c^e$ | $E(n_{f,c}^e)$ | $\sigma(n_{f,c}^e)$ |
|---|---|---|---|---|---|---|---|
| min | 8 | 6 | $2.2191 \times 10^{-4}$ | $9.9722 \times 10^{-5}$ | 12 | 4 | 0.6030 |
| max | 46 | 25 | $4.7015 \times 10^{-3}$ | 0.14364 | 69 | 5.52 | 2.5690 |
| $\mu$ | 26.338 | 15.169 | $1.8975 \times 10^{-3}$ | $1.8975 \times 10^{-3}$ | 39.507 | 5.1712 | 1.5586 |
| $\sigma^2$ | 40.608 | 10.152 | $5.2144 \times 10^{-7}$ | $4.2313 \times 10^{-5}$ | 91.368 | 0.035983 | 0.1186 |
| $\sigma$ | 6.3725 | 3.1862 | $7.2210 \times 10^{-4}$ | $6.5048 \times 10^{-3}$ | 9.5587 | 0.18969 | 0.3444 |
| $\mu_g$ | 25.543 | 14.829 | $1.7572 \times 10^{-3}$ | $1.1575 \times 10^{-3}$ | 38.315 | 5.1676 | 1.5169 |
| $\mu_h$ | 24.703 | 14.478 | $1.6026 \times 10^{-3}$ | $8.5548 \times 10^{-4}$ | 37.054 | 5.1638 | 1.4700 |
| med | 26 | 15 | $1.8125 \times 10^{-3}$ | $1.1660 \times 10^{-3}$ | 39 | 5.2 | 1.5706 |
| mad | 5.0068 | 2.5034 | $5.6975 \times 10^{-4}$ | $1.4250 \times 10^{-3}$ | 7.5103 | 0.14465 | 0.2715 |
| $\mathcal{M}^2$ | 40.531 | 10.133 | $5.2045 \times 10^{-7}$ | $4.2233 \times 10^{-5}$ | 91.195 | 0.035915 | 0.1184 |
| $\mathcal{M}^3$ | 72 | 9 | $2.5644 \times 10^{-10}$ | $5.4435 \times 10^{-6}$ | 243 | $-8.3404 \times 10^{-3}$ | -0.0060 |
| $\mathcal{M}^4$ | 5088.9 | 318.06 | $1.0467 \times 10^{-12}$ | $7.6653 \times 10^{-7}$ | 25763 | $7.9566 \times 10^{-3}$ | 0.041906 |
| $\mathcal{K}$ | 3.0978 | 3.0978 | 3.8644 | 429.77 | 3.0978 | 6.1689 | 2.9916 |

**Table 3.6** *Simulation uses rbox (1000 random points, seed 234985) and qhull (option v and o); $d = 3$, $n^c = 527$, $n^v = 6357$, CPU time 6,466.99 sec for the counting of statistics, 270.56 sec for finding area of the faces, 4.47 sec for calculating cell volume and 2.8 sec for finding the number of edges.*

## § 3.7 Number of vertices and edges

It has been observed from the simulations that in three dimensions cells always have vertices in even numbers and edges odd ones. This can be explained by the following theorems.

**Theorem 3.2.** *(cf Miles, 1972) In a simple three dimensional Voronoi tessellation, $3n_c^v = 2n_c^e$.*

**Proof.** Pick any Voronoi cell of the tessellation. Suppose that it has $n^v$ vertices. Add up the number of edges connected to all vertices. Because every cell is a simple polyhedron, there are exactly three edges connected to each vertex. The number of edges thus counted is therefore $3n^v$. But each of the edges is connected to two vertices, so we have counted every one of them twice. Therefore,

$$2n^e = 3n^v.$$

This is the case for any cell, hence the theorem is proved. □

This theorem gives rise the following two theorems.

**Theorem 3.3.** *The number of vertices of any cell within a simple three dimensional Voronoi tessellation is an even positive integer.*

**Proof.** Observe that the term $2n_c^e$ in the theorem above is divisible by 2. This term is equal to $3n_c^v$, therefore the latter is also divisible by 2. Since 2 can not divide into 3, the only term left, $n_c^v$, must be divisible by 2 and hence even number. □

**Theorem 3.4.** *The number of edges of any cell within a simple three dimensional Voronoi tessellation is a positive integer divisible by three.*

**Proof.** With the same line of reasoning as above, observe that $3n_c^v$ is divisible by 3. Therefore $2n_c^e$, and hence $n_c^e$, is also divisible by 3. □

Another proof for both the above theorems is the following.

**Proof.** For an equality to hold, both sides must have the same factors. By supposing an unknown common factor $i$ and by cross-multiplying the coefficients on both sides, one obtains $2\cdot(3\cdot i) = 3\cdot(2\cdot i)$, where $i$ is a positive integer. Therefore $n_c^e = 3i$ and $n_c^v = 2i$. In other words, $n_c^e$ is divisible by three and $n_c^v$ is even. □

The theorems above assume that every cells are simple. This can not be the case in real situation where edges have dimensions and rather represent tubes than one-dimensional lines. Such case is similar to the so-called *degenerative* case in a computational model of Voronoi tessellation where there exist vertices the number of edges connected to each of which exceeds four. Even in the degenerative case, one would perhaps still expect a tendency for $n_c^v$ to be an even number and for $n_c^e$ to be divisible by three to hold.

In nature there are things which have a tendency towards even numbers. The following graph shows the the abundance in cosmic materials from the compilation by Cameron (1973). The year of publication of this paper is often misquoted as 1970, due to misprints in a footnote on the first page of the paper. Even the legendary Fred Hoyle had consistently made this mistake and never corrected it all through the whold of his career, that is to say, in two of his books and at least one of his papers, spanning the period of approximately forty years in total (*cf* Hoyle, 1977). Out of a sample of 278 of those papers which cite this work, this misprint resulted in 80% of the total number of errors in the year cited, which in turn amounts to 1.8% of the number of samples.

*The abundances of the chemical elements* in the universe. They are assumed to be the same as those found in the primitive solar nebula, which had been deduced from data on abundances found in chondritic meteorites and those found in the Sun. All abundances are relative to that of Si which is taken to be $10^6$. Missing bars appear where the atomic numbers are unstable. Except for the atomic number 1 of Hydrogen, which is the most universal element, all other elements with even atomic numbers are locally more abundant than those with near-by odd atomic numbers.

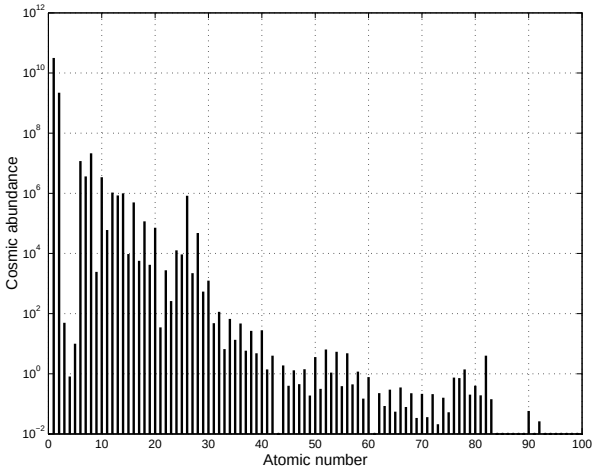


**Figure 3.16** Abundance of elements.

Of interest are also the electrical resistivity and conductivity of solid matters.The conductivity $\sigma$ is by definition the reciprocal of the resistivity $\rho$. Some of the solids, particularly boron, carbon, silicon, sulphur, germanium, selenium and tellurium, have a distinctively higher resistivity than the majority. Interestingly all of these, with only one exception of boron whose atomic number is five, are of an even atomic number, which respectively from carbon are 6, 14, 16, 32, 34, and 52. This can be seen in Figure 3.17 the data of which are taken from Podesta (2002).

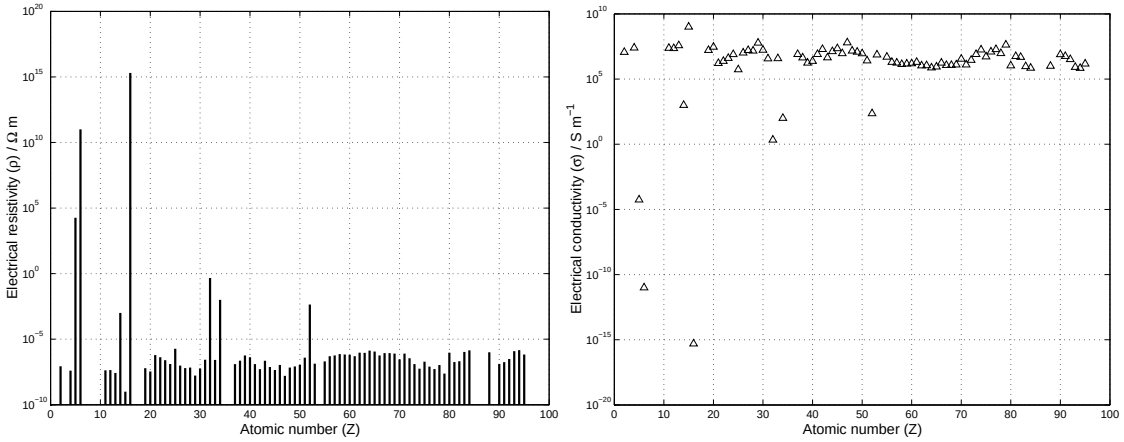


(a) (b)

**Figure 3.17** *The electrical resistivity, (a), and conductivity, (b), of elements which are solid at the room temperature.*

| | $n_c^e$ | $\mathcal{N}_v^c(E(l_c^e))$ | $\mathcal{N}_v^c(\wp_c)$ | $\mathcal{N}_v^c(A_c)$ |
|---|---|---|---|---|
| min | 3 | 0.20716 | 0.2749 | 0.058428 |
| max | 11 | 8.1072 | 10.134 | 22.307 |
| $\mu$ | 5.8973 | 0.70626 | 1.0089 | 1 |
| $\sigma^2$ | 1.8955 | 0.18607 | 0.2942 | 1.4379 |
| $\sigma$ | 1.3768 | 0.43136 | 0.54241 | 1.1991 |
| $\mu_g$ | 5.742 | 0.66036 | 0.94795 | 0.79225 |
| $\mu_h$ | 5.5904 | 0.62941 | 0.89999 | 0.61799 |
| med | 6 | 0.65709 | 0.96614 | 0.84267 |
| mad | 1.0736 | 0.17995 | 0.24357 | 0.49216 |
| $\mathcal{M}^2$ | 1.8912 | 0.18565 | 0.29355 | 1.4347 |
| $\mathcal{M}^3$ | 1.6194 | 0.96371 | 1.7931 | 22.703 |
| $\mathcal{M}^4$ | 12.438 | 6.8376 | 15.785 | 468.03 |
| $\mathcal{K}$ | 3.4775 | 198.38 | 183.18 | 227.39 |

**Table 3.7** *Neighbour statistics. Here for the normalisation purpose,* $l^e_{\text{basis}} = 0.046662, \wp_{\text{basis}} = 0.18665, A_{\text{basis}} = 0.0021773$. *Simulation uses* `voronoin` *command in Matlab;* $d = 2$, $n^c = 448$, $n^v = 946$, *CPU time 1.19 seconds.*

Next simulation was done with $d = 2$, $n^c = 3$ to 49551.

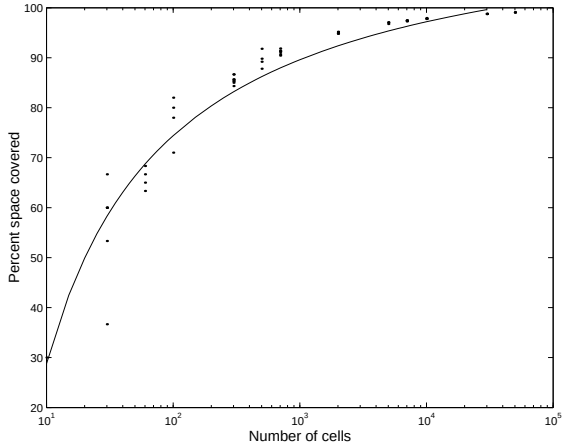


Figure 3.18 shows the percentage of space covered by a Voronoi structure. The number of cells is the total number of cells generated. The percent space covered is the volume of the structure after boundary cells, that is cells which extrude the unit volume boundary, have been excluded. The equation of the reference curve is

$$y = -210/\log x + 120.$$

**Figure 3.18** Space covered by Voronoi.

The reference line in Figure 3.19 is the linear equation

$$y = 2x + 10.$$

In other words the relationship between $n_c$ and $n_v$ is linear, which is to be expected in any random tessellation and is a necessity in any regular tessellation. The larger the network the more linear this relationship becomes. Bound ary cells have been excluded.

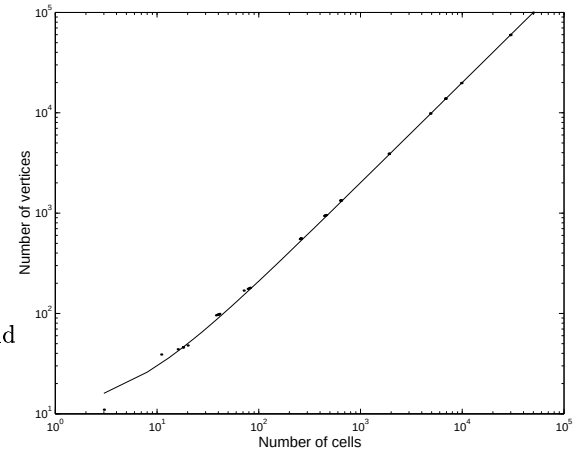


**Figure 3.19** Number of vertices versus number of cells.

The curve in Figure 3.20 is the result of curve fitting by cubic spline interpolation which fits a different cubic polynomial between each pair of data points.

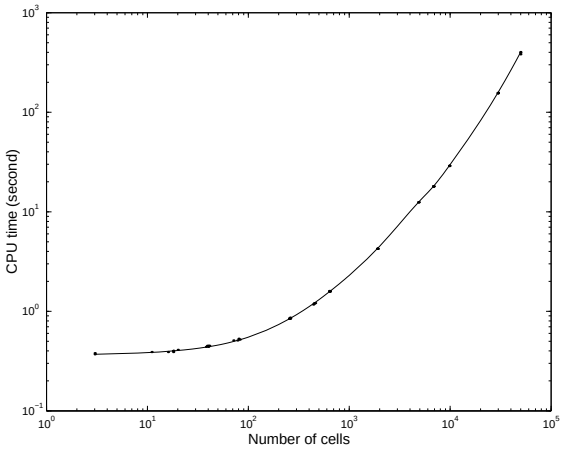


**Figure 3.20** The CPU time in seconds.

The characteristic length is the length of the side of the cubic structure having the same number of cells and the same total volume as the Voronoi structure. The characteristic lengths in Figure 3.21 are shown as dots. The reference line is

$$y = 0.7/x^{0.45}.$$

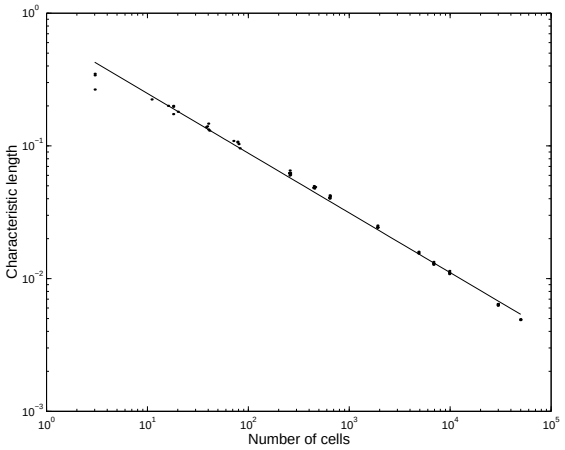


**Figure 3.21** Characteristic length versus the number of cells.

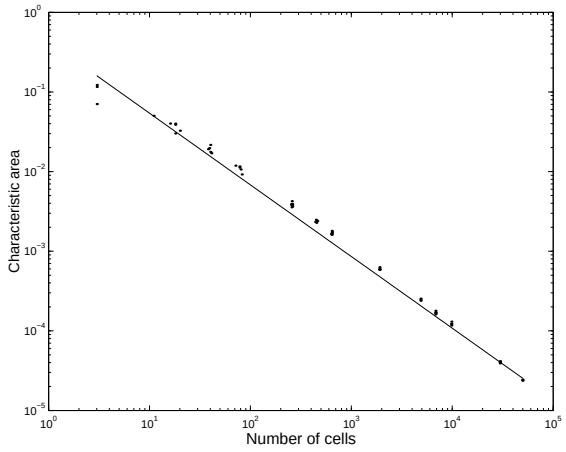


The characteristic area is the area of each square in the assembly the total volume and the number of cells of which are the same as those of the Voronoi graph. The reference curve shown in Figure 3.22 is

$$y = 0.43/x^{0.9}.$$

Both Figure 3.21 and Figure 3.22 are hyperbolic.

**Figure 3.22** Characteristic area versus the number of cells.

| | $n_c^v$ | $n_f^v$ | $\mathcal{N}_v^c(\mathcal{P}_c^f)$ | $\mathcal{N}_v^c(A_f)$ | $\mathcal{N}_v^c(A_c)$ | $\mathcal{N}_v^c(V_c)$ | $n_c^f$ |
|---|---|---|---|---|---|---|---|
| min | 8 | 3 | 0.001414 | $4.6179 \times 10^{-7}$ | 0.11908 | 0.21464 | 6 |
| max | 42 | 10 | 0.84885 | 0.82919 | 0.50425 | 12.719 | 23 |
| $\mu$ | 24.423 | 5.1114 | 0.32876 | 0.12535 | 0.30315 | 1.0000 | 14.211 |
| $\sigma^2$ | 44.105 | 2.1650 | 0.030844 | 0.015846 | 0.008511 | 2.5764 | 11.026 |
| $\mu_g$ | 23.504 | 4.9065 | 0.25897 | 0.051216 | 0.28815 | 0.70118 | 13.825 |
| $\mu_h$ | 22.506 | 4.7086 | 0.12620 | $2.50 \times 10^{-4}$ | 0.27198 | 0.58794 | 13.423 |
| med | 22 | 5 | 0.33219 | 0.084165 | 0.30368 | 0.64077 | 13 |
| mad | 5.4338 | 1.1655 | 0.14499 | 0.099433 | 0.075445 | 0.67950 | 2.7169 |
| $\mathcal{M}^2$ | 43.483 | 2.1619 | 0.030800 | 0.015823 | 0.008391 | 2.5401 | 10.871 |
| $\mathcal{M}^3$ | 112.13 | 1.8902 | $5.92 \times 10^{-4}$ | 0.002805 | $4.8 \times 10^{-5}$ | 24.169 | 14.016 |
| $\mathcal{K}$ | 3.1096 | 3.0234 | 2.3090 | 5.2926 | 2.3015 | 42.238 | 3.1096 |

**Table 3.8** *From* `rbox` *(200 random points, seed 34565473) and* `qhull` *(option v and o);* $d = 3$, $n^c = 71$.

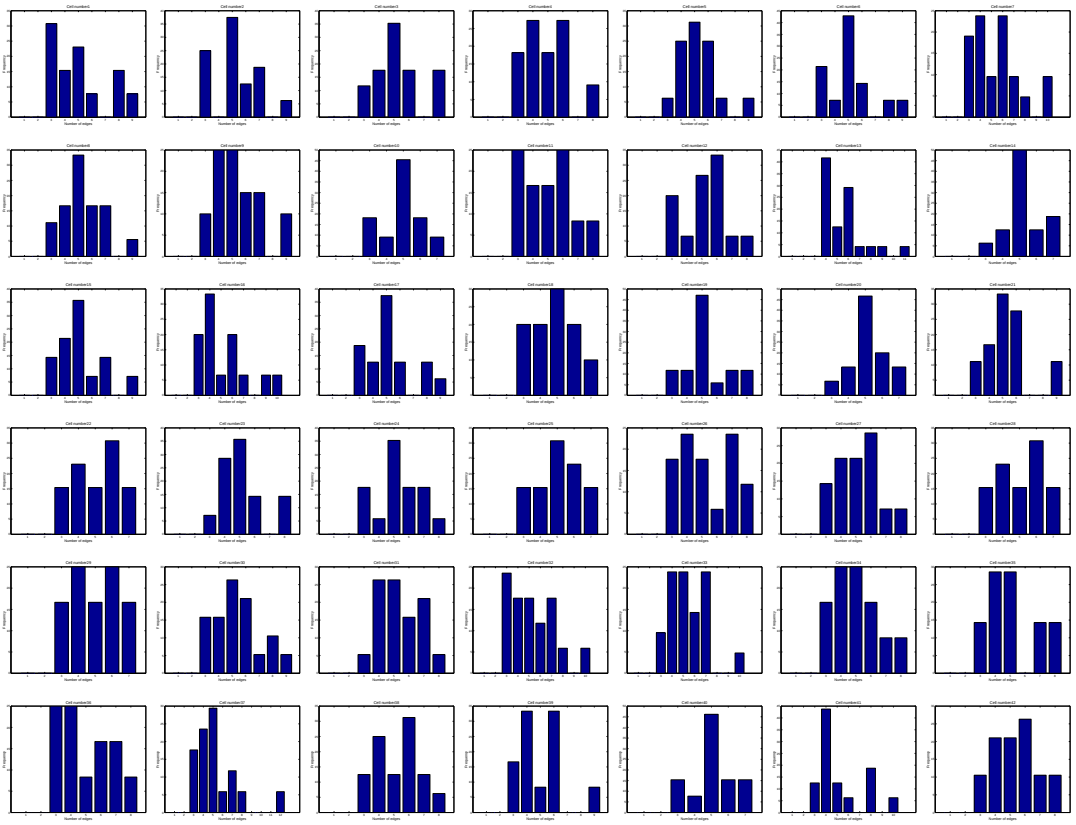

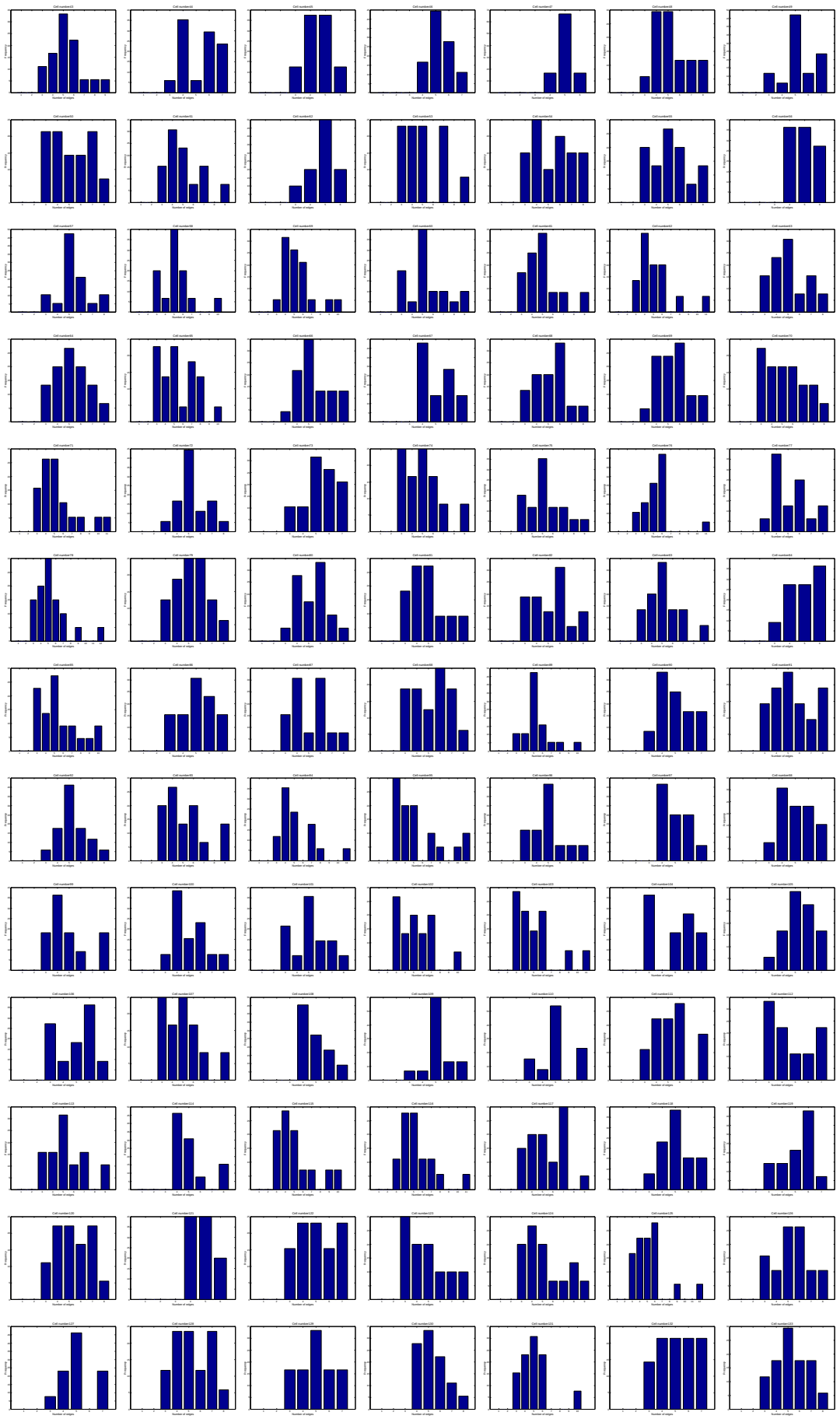

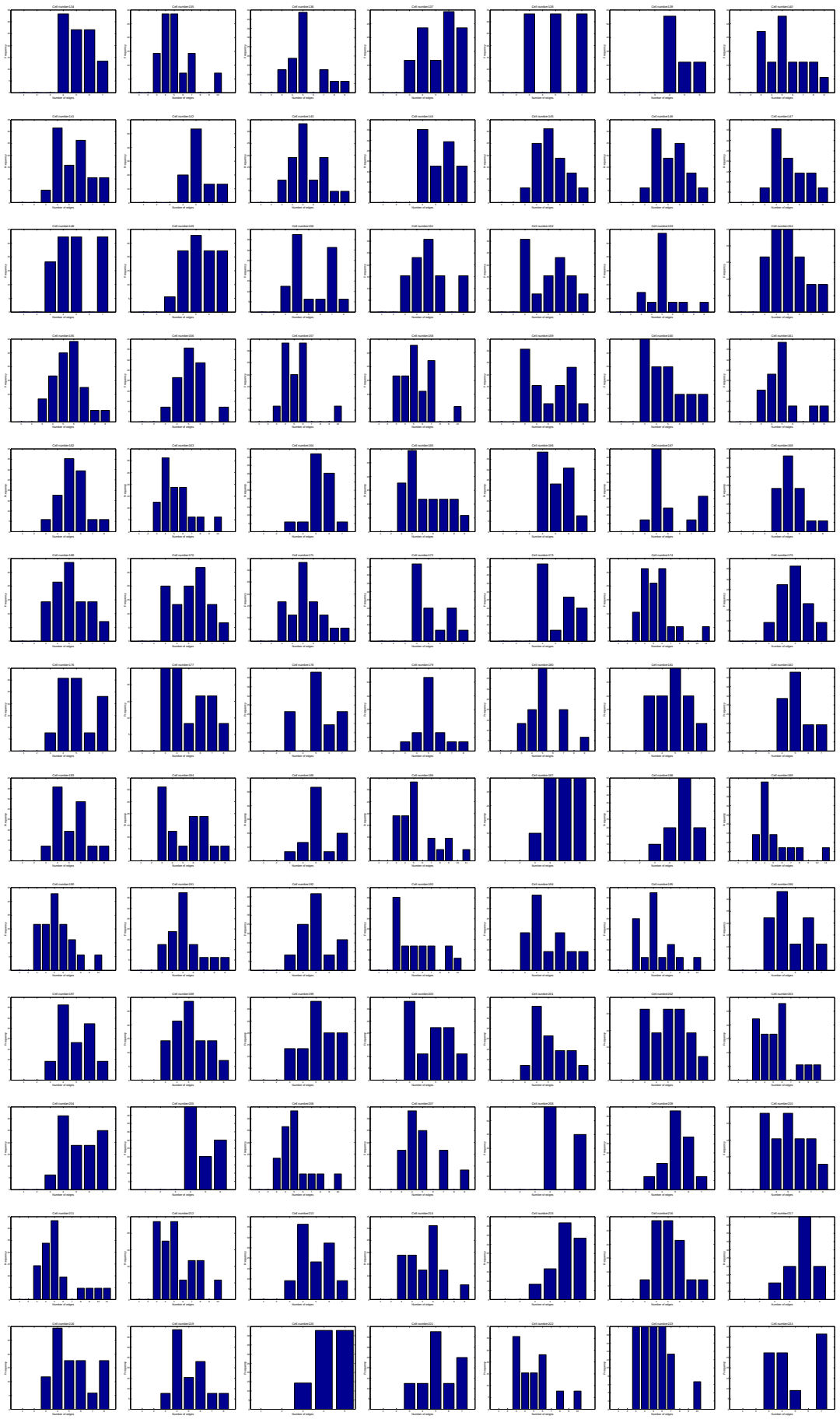

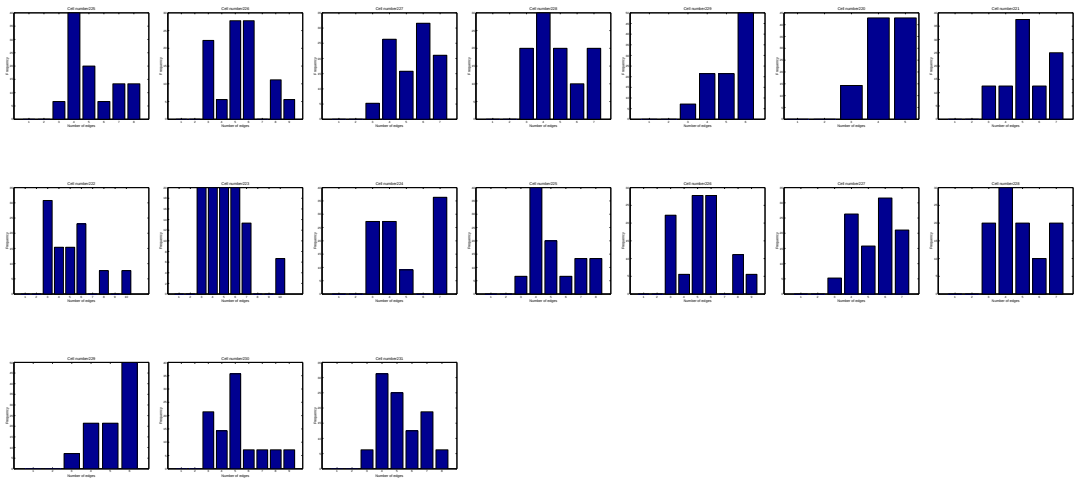

**Figure 3.23** *Distribution of the number of edges per face. Each picture is an individual cell. The distribution shows the relative abundance or the number of faces (the vertical axes) having the number of edges as shown by the horizontal axes. The horizontal axis scales are positive integers starting from zero at the origin. Simulation uses* `rbox` *(500 random points, seed 893280) and qhull (option v and o); $d = 3$, $n^c = 231$, $n^v = 3{,}107$, CPU time 81.1 sec for finding face area, 2.22 sec for cell volume, 49.59 sec for counting edges and 0.03 sec for finding the number of edges and faces.*

The minimum number of edges for each face is three. This number is the same as the number of vertices of that face. From these figures most of the cells have at least one face with three edges. There are only 19 cells (8.23 per cent) which does not have any three-edged face, and all of them have some four-edged faces. Therefore there is no cell with five as the minimum number of edges per face. The maximum number of edges per face is less clear-cut. There are twelve cells (5.19 per cent) with 11 as the maximum number of edges per face and two (0.87 per cent) with 12.

| | $n_c^v$ | $\aleph_c$ | $A_c^{fr}$ | $V_c^{fr}$ | $\alpha$ | $n_c^e$ | $E(n_{f,c}^e)$ | $\sigma(n_{f,c}^e)$ |
|---|---|---|---|---|---|---|---|---|
| min | 10 | 7 | $1.0989 \times 10^{-3}$ | $2.5790 \times 10^{-4}$ | 0.0406 | 15 | 4.2857 | 0.6030 |
| max | 44 | 24 | $1.0956 \times 10^{-2}$ | 0.24840 | 4.2505 | 66 | 5.5000 | 2.7028 |
| $\mu$ | 25.974 | 14.987 | $4.3290 \times 10^{-3}$ | $4.3290 \times 10^{-3}$ | 1.2515 | 38.961 | 5.1601 | 1.5450 |
| $\sigma^2$ | 40.852 | 10.213 | $3.3308 \times 10^{-6}$ | $2.9419 \times 10^{-4}$ | 0.3802 | 91.916 | 0.0372 | 0.1243 |
| $\sigma$ | 6.3915 | 3.1958 | $1.8250 \times 10^{-3}$ | $1.7152 \times 10^{-2}$ | 0.6166 | 9.5873 | 0.1928 | 0.3526 |
| $\mu_g$ | 25.166 | 14.642 | $3.9633 \times 10^{-3}$ | $1.8465 \times 10^{-3}$ | 1.0816 | 37.749 | 5.1564 | 1.5030 |
| $\mu_h$ | 24.323 | 14.288 | $3.6026 \times 10^{-3}$ | $1.2471 \times 10^{-3}$ | 0.8241 | 36.484 | 5.1526 | 1.4580 |
| med | 26 | 15 | $4.1467 \times 10^{-3}$ | $1.5715 \times 10^{-3}$ | 1.1915 | 39 | 5.2000 | 1.5315 |
| mad | 5.1532 | 2.5766 | $1.4064 \times 10^{-3}$ | $4.5864 \times 10^{-3}$ | 0.4720 | 7.7298 | 0.1505 | 0.2794 |
| $\mathcal{M}^2$ | 40.675 | 10.169 | $3.3163 \times 10^{-6}$ | $2.9291 \times 10^{-4}$ | 0.3785 | 91.518 | 0.0370 | 0.1238 |
| $\mathcal{M}^3$ | 59.377 | 7.4222 | $5.7258 \times 10^{-9}$ | $6.3817 \times 10^{-5}$ | 0.2143 | $2.0040 \times 10^{2}$ | -0.0071 | 0.0058 |
| $\mathcal{M}^4$ | $4.5398 \times 10^{3}$ | $2.8374 \times 10^{2}$ | $4.6684 \times 10^{-11}$ | $1.5395 \times 10^{-5}$ | 0.7390 | $2.2983 \times 10^{4}$ | 0.0063 | 0.0463 |
| $\mathcal{K}$ | 2.7440 | 2.7440 | 4.2448 | $1.7943 \times 10^{2}$ | 5.1578 | 2.7440 | 4.5730 | 3.0230 |

**Figure 3.24** *Statistics of a 231 cells Voronoi structure.*

Because the Voronoi tessellation being studied is simple, $\aleph_c^v = \aleph_c^f = n_c^f$. In other words, any two cells having at least one vertex in common are neighbours to each other, and the number of neighbours around any cell in an infinite network is equal to the number of its faces.

Figure 3.25 shows the distributions of the number of faces and edges per cell.

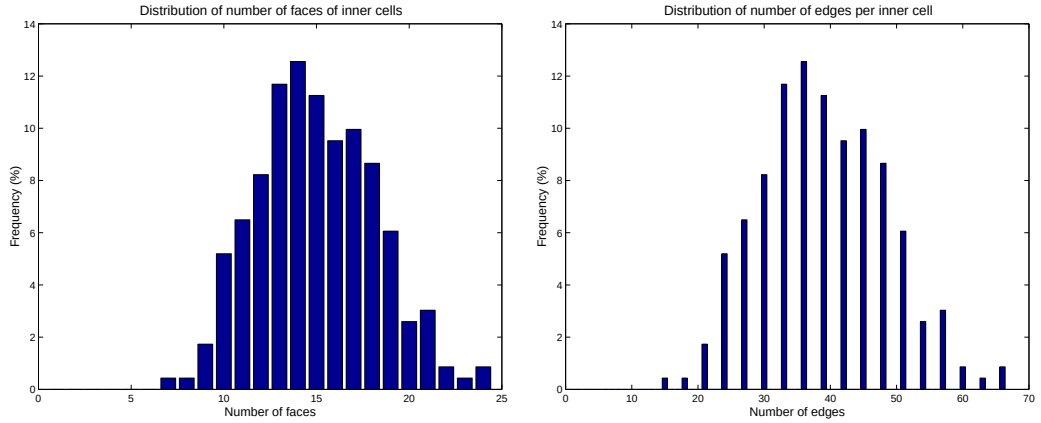


**Figure 3.25** *The distributions of the number of* (a) *faces, and* (b) *edges, per cell.*

The results from 527 Voronoi cells are shown next. Table 3.9 is from a 3-d Voronoi structure generated from 1,000 cells. The creation codes started with a random seed of 234985. They spent 6,466.99 seconds for the counting of statistics, 270.56 for finding area of the faces, 4.47 for calculating cell volume and additional 2.8 seconds to find statistics for the number of edges. There are 6,357 vertices generated, plus another added distant vertice. Boundary cells were discarded, which leaves us with 527 inner cells which are taken into account.

| | $v_{c_{in}}$ | $\aleph_{v,c_{in}}$ | $A_{fr,c_{in}}$ | $V_{fr,c_{in}}$ | $n_{f,c_{in}}$ | $n_{e,c_{in}}$ | |
|---|---|---|---|---|---|---|---|
| Min | 8 | 6 | $2.2191 \times 10^{-4}$ | $9.9722 \times 10^{-5}$ | 6 | 12 | |
| Max | 46 | 25 | $4.7015 \times 10^{-3}$ | 0.14364 | 25 | 69 | |
| $\mu$ | 26.338 | 15.169 | $1.8975 \times 10^{-3}$ | $1.8975 \times 10^{-3}$ | 15.169 | 39.507 | |
| $\sigma$[2] | 40.608 | 10.152 | $5.2144 \times 10^{-7}$ | $4.2313 \times 10^{-5}$ | 10.152 | 91.368 | |
| $\sigma$ | 6.3725 | 3.1862 | $7.2210 \times 10^{-4}$ | $6.5048 \times 10^{-3}$ | 3.1862 | 9.5587 | |
| $\mu_g$ | 25.543 | 14.829 | $1.7572 \times 10^{-3}$ | $1.1575 \times 10^{-3}$ | 14.829 | 38.315 | |
| $\mu_h$ | 24.703 | 14.478 | $1.6026 \times 10^{-3}$ | $8.5548 \times 10^{-4}$ | 14.478 | 37.054 | |
| Med | 26 | 15 | $1.8125 \times 10^{-3}$ | $1.1660 \times 10^{-3}$ | 15 | 39 | |
| $\delta_\mu$ | 5.0068 | 2.5034 | $5.6975 \times 10^{-4}$ | $1.4250 \times 10^{-3}$ | 2.5034 | 7.5103 | |
| $M$[2] | 40.531 | 10.133 | $5.2045 \times 10^{-7}$ | $4.2233 \times 10^{-5}$ | 10.133 | 91.195 | |
| $M$[3] | 72 | 9 | $2.5644 \times 10^{-10}$ | $5.4435 \times 10^{-6}$ | 9 | 243 | |
| $M$[4] | 5088.9 | 318.06 | | $1.0467 \times 10^{-12}$ | $7.6653 \times 10^{-7}$ | 318.06 | 25763 |
| $\kappa$ | 3.0978 | 3.0978 | 3.8644 | 429.77 | 3.0978 | 3.0978 | |

**Table 3.9** *Statistics from 527 Voronoi cells.*

The mean value of the mean numbers of edges per face obtained was 5.1712. This can be called $\mathrm{E}(\mathrm{E}(n_{e,f}))$, the expected value over all cells of the mean number of edges in a face averaged over all its faces. The variance was 0.035983, minimum value 4, maximum 5.52, standard deviation 0.18969, geometric mean 5.1676, harmonic mean 5.1638, median 5.2, mean absolute deviation 0.14465, $2^{nd}$ moment 0.035915, $3^{rd}$ moment -0.0083404, and kurtosis 6.1689. The mean and standard deviation of all faces are given in Appendix 9.6. The standard deviation of $\mathrm{E}(n_{e,f})$ averaged over all faces of bounded cells is 1.5586. The rest are $\sigma^2 = 0.1186$, $\sigma = 0.3444$, minimum 0.6030, maximum 2.5690, $\mu_g = 1.5169$, $\mu_h = 1.4700$, median 1.5706, $\delta_\mu = 0.2715$, $M^2 = 0.1184$, $M^3 = -0.0060$, and $\kappa = 2.9916$.

Figure 3.26 shows the ratios between the number of vertices and the number of cells in Voronoi networks of various dimensions. The line shown in Figure 3.26 is

$$y = 0.2410e^n,$$

where $n$ is the dimension of the network and is the horizontal axis; the coefficient of the exponential term is obtained by averaging over the averages in each dimension, each of which in turn comes from five batch runs.

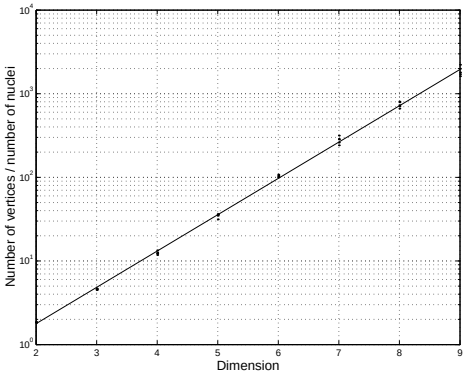


**Figure 3.26** $v_n/c_n$ in Voronoi networks of various dimensions.

Figure 3.27 shows the CPU time in creating the Voronoi networks for Figure 3.26. The line shown in Figure 3.27, found manually by trial and error, has the equation

$$y = 4.61 \times 10^{-6}(2 + e)^n.$$

In comparison, substituting the average cpu time for each dimension for $y$ in the equation $y = Ae^n$ to obtain $A$ and then find the average again over all dimensions results in $\overline{A} = 1.612 \times 10^{-4}$. The program which produces both Figure 3.27 and ℵ is given in § A.9.

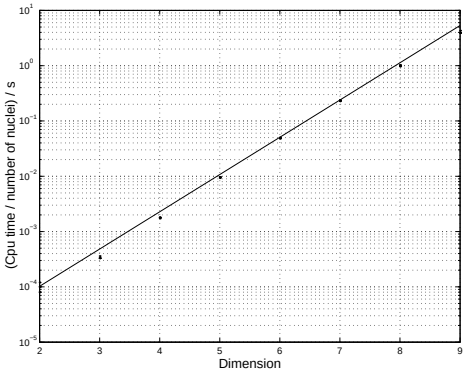


**Figure 3.27** CPU time in creating the Voronoi networks.

The number of vertices of higher dimensions is investigated briefly in the following Table 3.10 and Figure 3.28 the simulation of which was carried out by the program in § A.18.

| **Dimension** | 4 | 5 | 6 | 8 | 9 | 10 |
|---|---|---|---|---|---|---|
| $N_c$ | 300 | 300 | 300 | 30 | 30 | 30 |
| $N_v$ | 6,577 | 27,150 | 118,534 | 5,465 | 10,467 | 17,442 |
| $n_c$ | 132 | 104 | 14 | 2 | 3 | 0 |
| $\min(n_c^v)$ | 26 | 244.00 | 1,020.0 | 952.002 | 2,353.0 | 4,287.0 |
| $\max(n_c^v)$ | 255 | 1,142.0 | 5,852.0 | 2,638.0 | 5,534.0 | 9,528.0 |
| $\bar{n}_c^v$ | 109.90 | 543.51 | 2,766.5 | 1,640.2 | 3,489.7 | 6,396.0 |
| $(\sigma^2_{n_v})_c$ | 1,155.9 | 22,974 | $6.0898 \times 10^5$ | $1.7964 \times 10^5$ | $7.0328 \times 10^5$ | $2.3635 \times 10^6$ |
| $\sigma_c^{n_v}$ | 33.999 | 151.57 | 780.37 | 423.84 | 838.62 | $1.5374 \times 10^3$ |
| $\mu_g(n_c^v)$ | 104.41 | 523.06 | 2,666.1 | 1,589.9 | 3,398.4 | 6,225.6 |
| $\mu_h(n_c^v)$ | 98.389 | 502.94 | 2,571.4 | 1,542.3 | 3,313.9 | 6,065.2 |
| $\mathrm{med}(n_c^v)$ | 107.50 | 527.00 | 2,651.0 | 1,568.5 | 3,272.5 | 5,816.5 |
| $\mathrm{mad}(n_c^v)$ | 27.366 | 119.39 | 588.19 | 331.96 | 687.47 | 1,296.6 |
| $m^2(n_c^v)$ | 1,152.1 | 22,897 | $6.0695 \times 10^5$ | $1.7365 \times 10^5$ | $6.7984 \times 10^5$ | $2.2847 \times 10^6$ |
| $m^3(n_c^v)$ | 15,555 | $2.2871 \times 10^6$ | $5.1556 \times 10^8$ | $4.7965 \times 10^7$ | $3.9108 \times 10^8$ | $1.8988 \times 10^9$ |
| $m^4(n_c^v)$ | $4.5760 \times 10^6$ | $1.8905 \times 10^9$ | $1.7964 \times 10^{12}$ | $8.5043 \times 10^{10}$ | $1.1967 \times 10^{12}$ | $1.1638 \times 10^{13}$ |
| $\kappa(n_c^v)$ | 3.4476 | 3.6059 | 4.8764 | 2.8202 | 2.5892 | 2.2296 |

**Table 3.10** *Statistics of the number of vertices in 4, 5, 6, 8, 9, and 10 dimensions.*

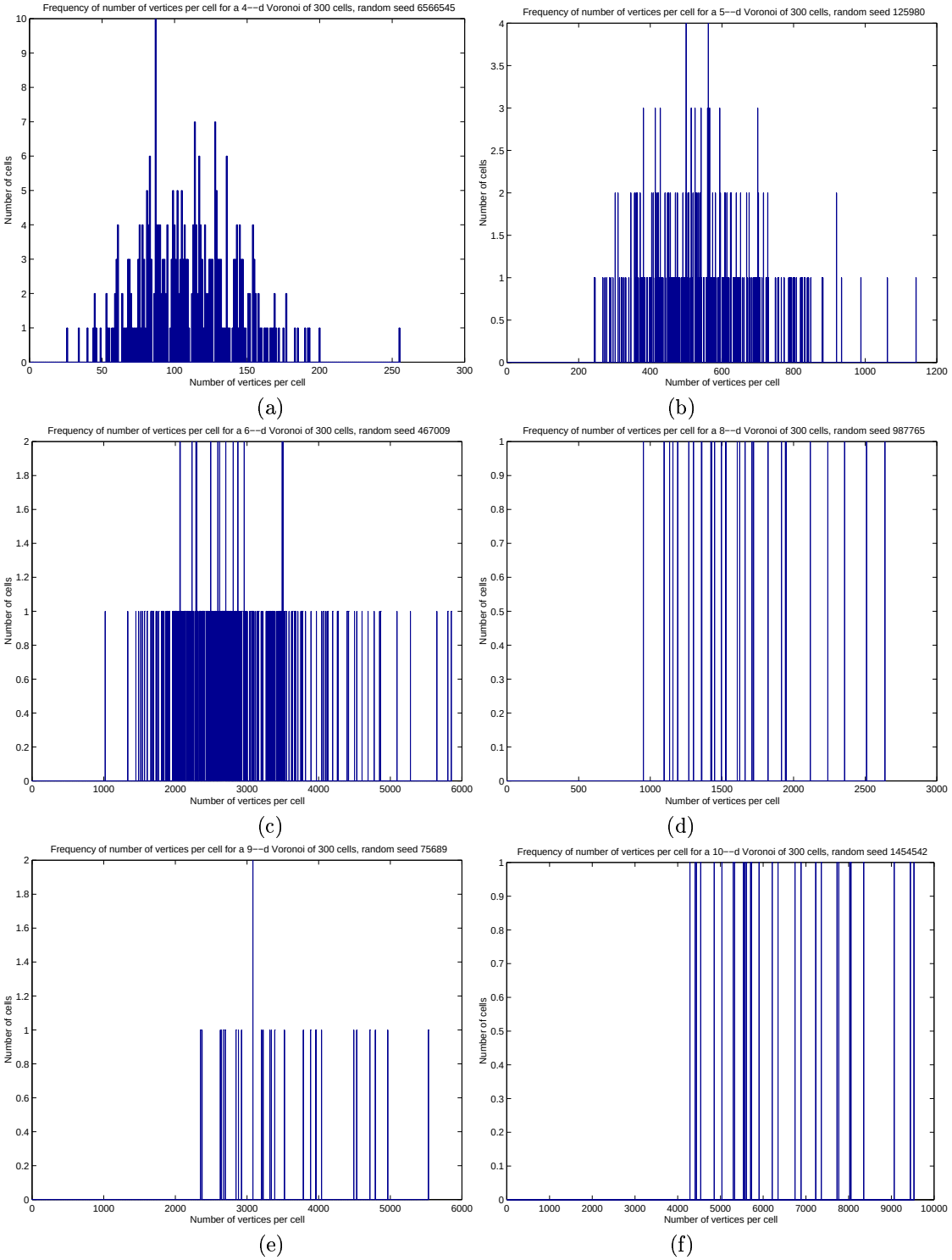
Frequency of number of vertices per cell for a 4−−d Voronoi of 300 cells, random seed 6566545
Number of cells
Number of vertices per cell
(a)
Frequency of number of vertices per cell for a 5−−d Voronoi of 300 cells, random seed 125980
Number of cells
Number of vertices per cell
(b)
Frequency of number of vertices per cell for a 6−−d Voronoi of 300 cells, random seed 467009
Number of cells
Number of vertices per cell
(c)
Frequency of number of vertices per cell for a 8−−d Voronoi of 300 cells, random seed 987765
Number of cells
Number of vertices per cell
(d)
Frequency of number of vertices per cell for a 9−−d Voronoi of 300 cells, random seed 75689
Number of cells
Number of vertices per cell
(e)
Frequency of number of vertices per cell for a 10−−d Voronoi of 300 cells, random seed 1454542
Number of cells
Number of vertices per cell
(f)

**Figure 3.28** *Distribution of vertices in* (a) *4,* (b) *5,* (c) *6, and* (d) *8,* (e) *9,* (f) *10 dimensions.*

To obtain the number of vertices per cell, $n_c^v$, of a six-dimensional Voronoi structure of 1,000 cells a batch program was used, for instance the one listed in § A.19. The Matlab macro that this program refers to opens and reads from a file the number of vertices and then finds the statistical values, *viz.* $\min(n_c^v) = 1{,}198$; $\max(n_c^v) = 9{,}923$; $\bar{n}_c^v = 4{,}201.1$; $(\sigma^2_{n_v})_c = 1.4069 \times 10^6$; $\sigma_c^{n_v} = 1186.1$; $(\bar{n}_g)_c^v = 4035.4$; $(\bar{n}_h)_c^v = 3866.8$; $\mathrm{med}(n_c^v) = 4122.5$; $\mathrm{mad}(n_c^v) = 931.81$; $m^2(n_c^v) = 1.4055 \times 10^6$; $m^3(n_c^v) = 1.0462 \times 10^9$; $m^4(n_c^v) = 7.7148 \times 10^{12}$; and $\kappa(n_c^v) = 3.9053$.

The following figure shows the frequency of the number of vertices. Interested readers may find the data in § 9.6 which give rise to Figure 3.29 interesting. These results are not the most useful ones because of the presence of border cells.

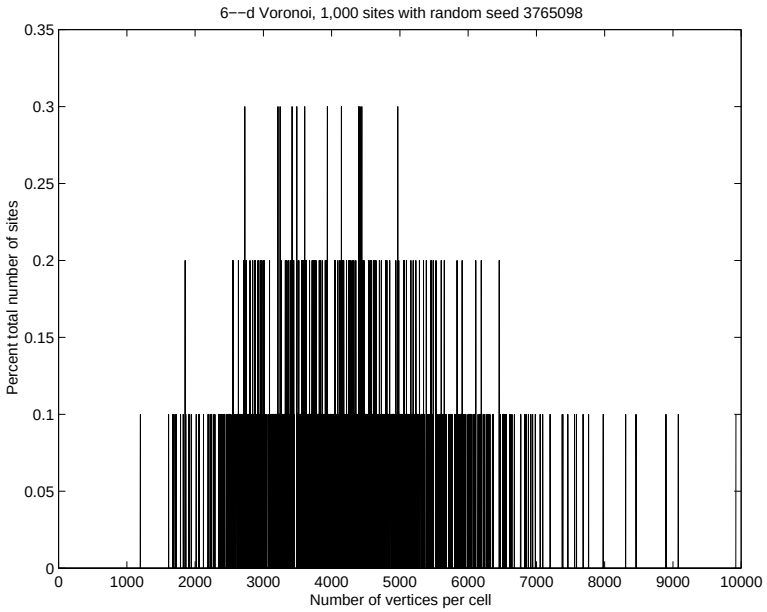


**Figure 3.29** *Distribution of vertices in a 6-d Voronoi structure*

**AVS**

The first picture I created on AVS was a Trigonal Dipyramidal. The program was the following .inp file.

```
5 2 0 0 0
1 0 0 1.2910
2 2 0 1.2910
3 1 1.7321 1.2910
4 1 0.5774 0
5 1 0.5774 2.5820
1 1 tet 1 2 3 4
2 1 tet 1 2 3 5
1 2
```

The connection of modules was ReadUCD to ExternalEdges to UViewer3D.

The following simulation was done on a 3–d systems with a joggled-input option in `qhull`. The number of vertices, however, also takes into account those belonging to the boundary cells. The minimum $n_{v,c}$ was 6, maximum $n_{v,c}$ 52, $\bar{n}_{v,c}$ 25.269, $2^{nd}$–Moment 49.363, $3^{rd}$–Moment 228.87, $4^{th}$–Moment 8,704.9, $\sigma^2_{n_{v,c}}$ 49.412, $\sigma_{n_{v,c}}$ 7.0294, $\mu_{g,n_{v,c}}$ 24.317, $\mu_{h,n_{v,c}}$ 23.365, $\widetilde{n}_{v,c}$ 24, $\delta_\mu(n_{v,c})$ 5.5428, $\kappa(n_{v,c})$ 3.5725 .

Following figure is a distribution graph.

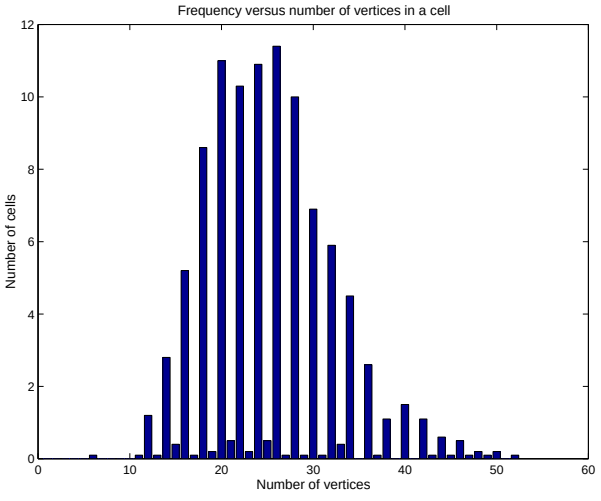


In Figure 3.30 boundary cells have not been excluded. So there are still some cells which have an odd number of vertices. But even these are few and far between, and only because of them that the lacks of odd vertice-numbered cells has been noticed. Had there been nothing there it is difficult to see how this uniform characteristic, or invariance, of the Voronoi tessellation could have come to light.

**Figure 3.30** Number of cells having a particular number of vertices.

Theorem's 3.4 and 3.4 above are observations which are not only useful but essential when you try to understand the valence relations. Assuming that the Euler's theorem is true, then these two theorems give rise to Algorithm 3.2 which I have devised for counting all the components in these relations. Here $n_e$ and $n_v$ are all the edges, and respectively vertices, of the original structure originally counted, $n_b^e$ all the additional edges, going to infinity, which are drawn to complete the valences of some of the boundary vertices, $c_n$ cells with $n$ edges and $f_n$ the frequency occurences of $c_n$.

**Algorithm 3.2** *Valence relations for planes in two dimensions.*

**draw** an addition bond for all boundary vertices which have valence 2;
$e \leftarrow \lfloor \mathbf{n_e} + \mathbf{n_b^e}/3 \rfloor$;
**draw** an additional $(n_e + n_b^e - e)$ on boundary vertices;
**if** $\lfloor n_v/2 \rfloor \bmod 2 \neq 0$ **then**
  **draw** an additional vertex at infinity;
  $v \leftarrow n_v + 1$;
**else**
  $v \leftarrow n_v$;
**endif**
$f \leftarrow 1 + e - v$;
**label** all the $f_n$ bound faces;
**if** $(n_f + n_b^f) = f$ **then**
  **label** all the $f_b^n$ unbound faces;
**else**
  **label** $(f - n_f)$ unbound faces;
  **label** all the remaining $(n_f + n_b^f - f)$ unbound faces together as a single face;
**endif**

□

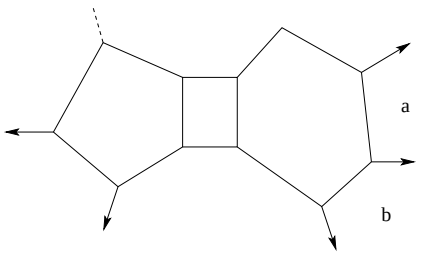


In Algorithm 3.2 the vertex at infinity mentioned does not necessarily have to be literally at the infinity. Although Algorithm 3.2 is for planes in two dimensions, it should be possible to extend it to other topolgical objects and to higher dimensions by simply changing the Euler's equation to the appropriate one. When labelling $f$, if $(n_f + n_b^f) \neq f$, we know that $(n_f + n_b^f) > f$ with probability one.
Paradoxically this relation holds only for infinite networks, but its derivation, as well as its verification, can only be done on a tessellation of finite size. Counting the components of the valence relation one sees in a graph involves both the Euler's theorem and Theorem's 3.4 and 3.4.

**Figure 3.31** Counting the valences.

## § 3.8 Faces in different dimensions

Considering only those cells bound within the unit box, vertices and all, the following, namely Tables 3.11, 3.12 and 3.13, are the results from five simulations in two, three and four dimensions respectively, using the program listed in § A.16.

| | *Random seed* | | | | |
|---|---|---|---|---|---|
| | 829247 | 134315 | 67453 | 432243 | 231215 |
| $N_v$ | 187 | 187 | 186 | 189 | 183 |
| $n_v$ | 170 | 167 | 168 | 163 | 170 |
| $n_c$ | 72 | 69 | 70 | 65 | 72 |
| $n_c^v$ | 169 | 165 | 166 | 159 | 170 |
| $\mu_c^v$ | 5.875 | 5.8116 | 5.8429 | 5.9077 | 5.8194 |
| $(\sigma_v^2)_c$ | 2.0264 | 1.8022 | 1.6706 | 1.7726 | 1.5022 |
| $m^2(n_c^v)$ | 1.9983 | 1.7761 | 1.6467 | 1.7453 | 1.4813 |
| $m^3(n_c^v)$ | 1.1263 | 1.6917 | 0.96591 | 0.57642 | 0.96103 |
| $n_{1f}$ | 241 | 235 | 237 | 227 | 241 |
| $n_c^{1f}$ | 240 | 233 | 235 | 223 | 241 |
| $t_{CPU}$(second) | 20.36 | 20.39 | 20.09 | 20.6 | 19.76 |

**Table 3.11** *Faces of Voronoi in two dimensions.* $N_c = 100$.

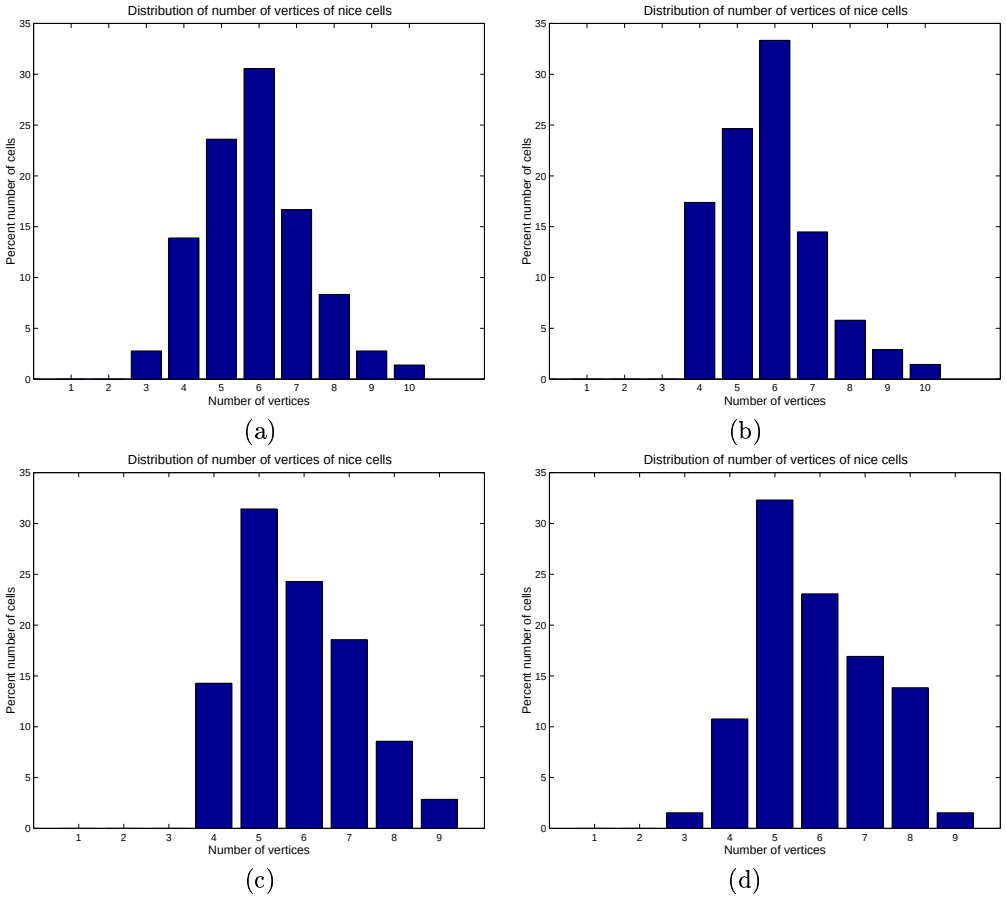


Figure 3.32 shows the distribution of $v_c$ in each simulation on 2-d Voronoi. The size of the network is very small, which explains why the shape of the distribution varies greatly from one simulation to another. This is also the reason why all the bars in the graph have only limited number of possible heights.

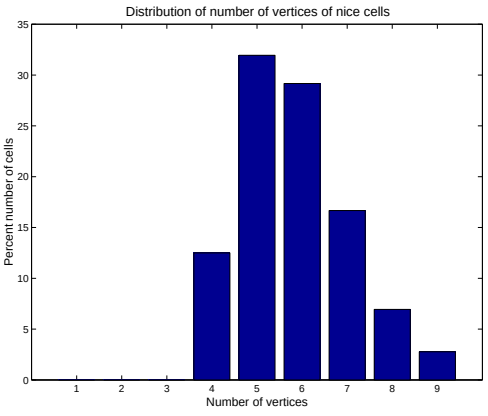


**Figure 3.32** Distribution of $v_c$ in two dimensions.

| | *Random seed* | | | | |
|---|---|---|---|---|---|
| | 42398198 | 83250 | 34959 | 743690 | 1321 |
| $N_v$ | 204 | 221 | 224 | 225 | 214 |
| $n_v$ | 148 | 147 | 143 | 155 | 146 |
| $n_c$ | 7 | 5 | 7 | 8 | 7 |
| $n_c^v$ | 99 | 79 | 85 | 109 | 97 |
| $\mu_c^v$ | 21.714 | 23.6 | 20.286 | 21 | 21.714 |
| $(\sigma_v^2)_c$ | 4.5714 | 14.8 | 31.238 | 34.286 | 21.905 |
| $m^2(n_c^v)$ | 3.9184 | 11.84 | 26.776 | 30 | 18.776 |
| $m^3(n_c^v)$ | -4.6181 | -16.128 | -42.402 | 171 | 69.831 |
| $n_{2f}$ | 114 | 110 | 111 | 123 | 113 |
| $\mu_{2f}^v$ | 4.9211 | 4.7727 | 4.7928 | 4.8293 | 4.7788 |
| $(\sigma_v^2)_{2f}$ | 1.2592 | 1.6268 | 1.5476 | 2.0772 | 1.656 |
| $m^2(n_{2f}^v)$ | 1.2482 | 1.612 | 1.5336 | 2.0603 | 1.6413 |
| $m^3(n_{2f}^v)$ | 0.16453 | 0.99264 | 1.1334 | 1.7676 | 1.1444 |
| $n_c^{2f}$ | 76 | 60 | 69 | 88 | 75 |
| $(\mu_{2f}^v)_c$ | 5.0526 | 5.05 | 4.9855 | 4.9545 | 5.0533 |
| $(\sigma_v^2)_c^{2f}$ | 1.1439 | 1.811 | 1.3674 | 2.0209 | 1.7268 |
| $m^2((n_{2f}^v)_c)$ | 1.1288 | 1.7808 | 1.3476 | 1.9979 | 1.7038 |
| $m^3((n_{2f}^v)_c)$ | 0.19004 | 0.28275 | 1.5224 | 1.4544 | 0.98057 |
| $n_c^{1f}$ | 167 | 133 | 146 | 187 | 163 |
| $t_{CPU}$(second) | 24.28 | 25.67 | 28.49 | 34.23 | 26.46 |

**Table 3.12** *Various faces of Voronoi in three dimensions.* $N_c = 50$.

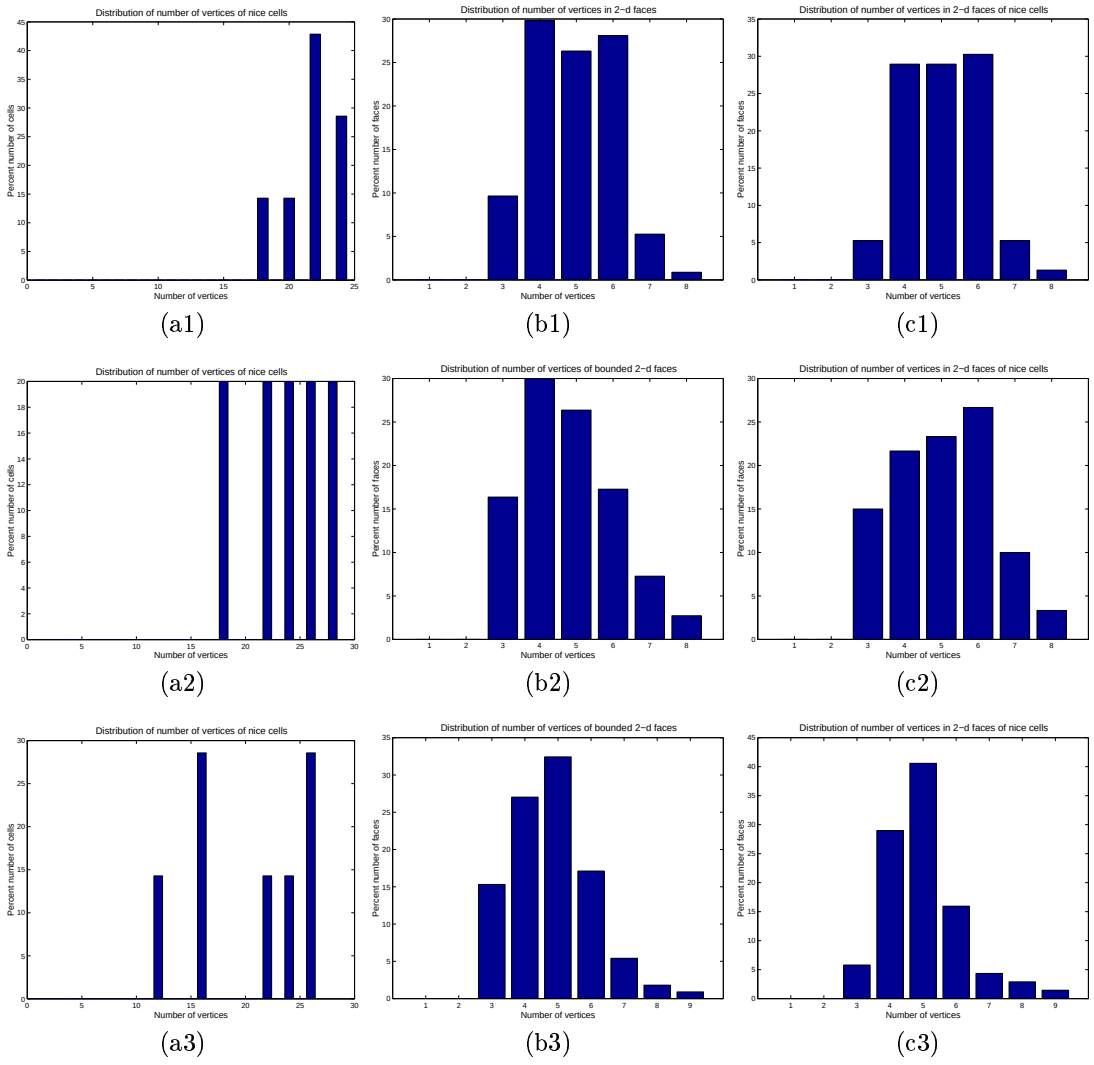

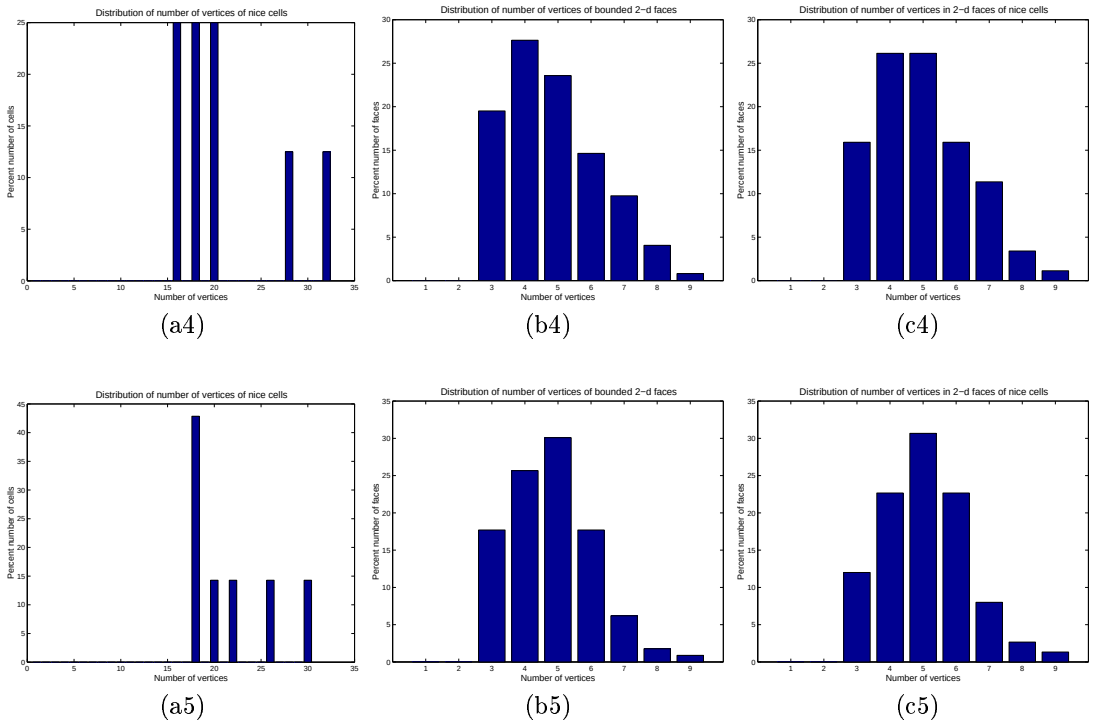
Distribution of number of vertices of nice cells
Percent number of cells
Number of vertices
(a4)
Distribution of number of vertices of bounded 2−d faces
Percent number of faces
Number of vertices
(b4)
Distribution of number of vertices in 2−d faces of nice cells
Percent number of faces
Number of vertices
(c4)
Distribution of number of vertices of nice cells
Percent number of cells
Number of vertices
(a5)
Distribution of number of vertices of bounded 2−d faces
Percent number of faces
Number of vertices
(b5)
Distribution of number of vertices in 2−d faces of nice cells
Percent number of faces
Number of vertices
(c5)

**Figure 3.33** *Distribution of* (ai) $v_c$, (bi) $v_{2\mathrm{f}}$, *and* (ci) $v_c^{2\mathrm{f}}$ *of the* $i^{\mathrm{th}}$ *simulation on 3-d Voronoi.*

| | *Random seed* | | | | |
|---|---|---|---|---|---|
| | 24098 | 802723 | 1453 | 732849 | 20480 |
| $\mathrm{N}_v$ | 1684 | 1719 | 1674 | 1586 | 1600 |
| $n_v$ | 938 | 921 | 860 | 889 | 904 |
| $n_c$ | 5 | 1 | 1 | 1 | 2 |
| $n_c^v$ | 442 | 172 | 149 | 117 | 200 |
| $\mu_c^v$ | 114 | 172 | 149 | 117 | 110 |
| $(\sigma_v^2)_c$ | 174.5 | 0 | 0 | 0 | 72 |
| $m^2(n_c^v)$ | 139.6 | 0 | 0 | 0 | 36 |
| $m^3(n_c^v)$ | -547.2 | 0 | 0 | 0 | 0 |
| $n_{3\mathrm{f}}$ | 83 | 102 | 84 | 83 | 95 |
| $\mu_{3\mathrm{f}}^v$ | 8.8675 | 8.3137 | 8.5952 | 8.9398 | 8.7789 |
| $(\sigma_v^2)_{3\mathrm{f}}$ | 18.848 | 18.198 | 19.449 | 17.496 | 19.77 |
| $m^2(n_{3\mathrm{f}}^v)$ | 18.621 | 18.019 | 19.217 | 17.286 | 19.562 |
| $m^3(n_{3\mathrm{f}}^v)$ | 75.225 | 102.38 | 95.854 | 62.919 | 118.61 |
| $n_c^{3\mathrm{f}}$ | 32 | 8 | 10 | 7 | 19 |
| $(\mu_{3\mathrm{f}}^v)_c$ | 8.8675 | 9.25 | 10.8 | 11.143 | 9.8947 |
| $(\sigma_v^2)_c^{3\mathrm{f}}$ | 18.848 | 13.643 | 21.511 | 14.476 | 28.655 |
| $m^2((n_{3\mathrm{f}}^v)_c)$ | 18.621 | 11.938 | 19.36 | 12.408 | 27.147 |
| $m^3((n_{3\mathrm{f}}^v)_c)$ | 75.225 | 18.281 | 66.624 | 8.5364 | 195.1 |
| $n_c^{2\mathrm{f}}$ | 11 | 0 | 5 | 2 | 7 |
| $n_c^{1\mathrm{f}}$ | 2 | 0 | 0 | 0 | 1 |
| $\mathrm{t}_{\mathrm{CPU}}$(second) | 315.07 | 358.94 | 324.56 | 281.85 | 283.82 |

**Table 3.13** *Faces of Voronoi in four dimensions.* $\mathrm{N}_c = 100$.

The number of vertices in each 2-d face is a constant equals to three while that of a 1-d face is two. In the first run the number of vertices in each of the cells is 95, 108, 117, 120 and 130; in the last run, this number is 104 and 116.

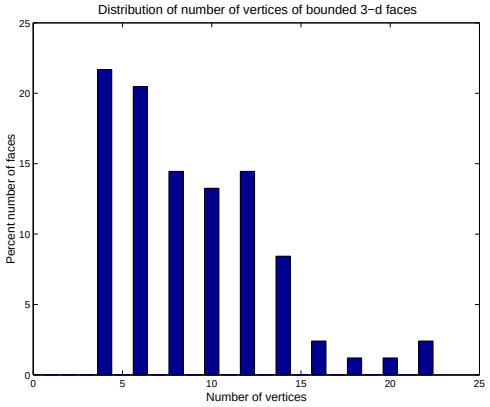


(a1)

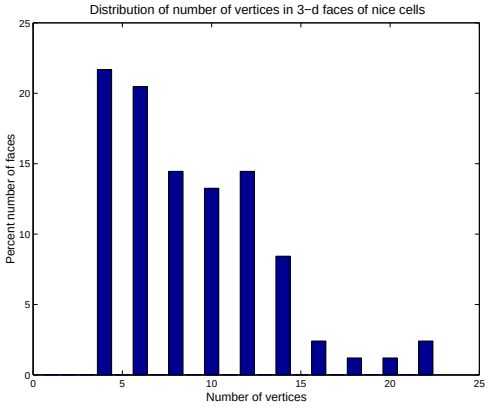


(b1)

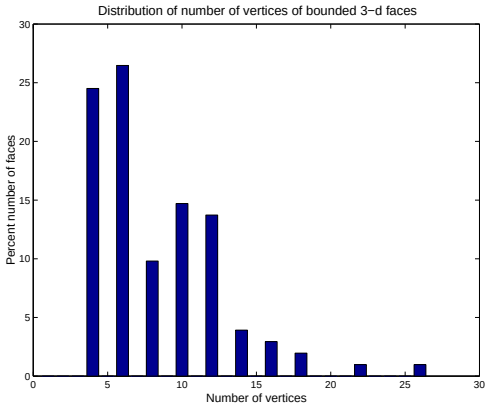


(a2)

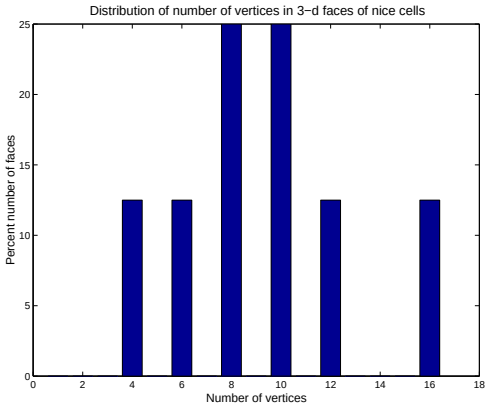


(b2)

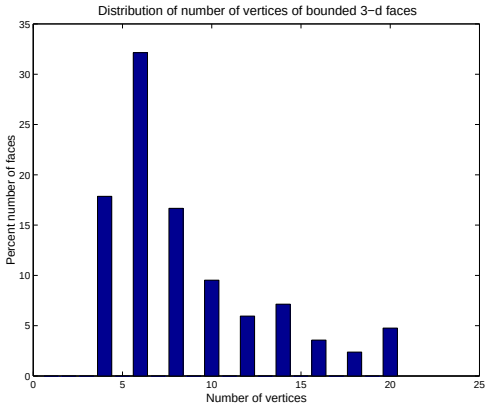


(a3)

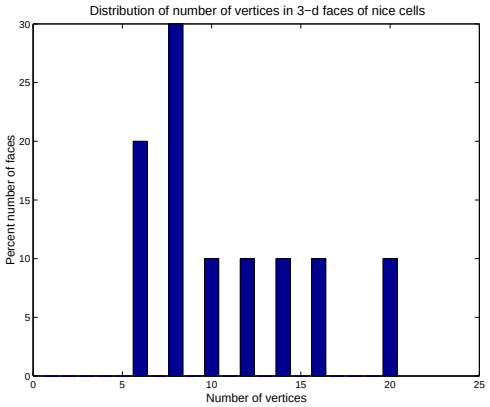


(b3)

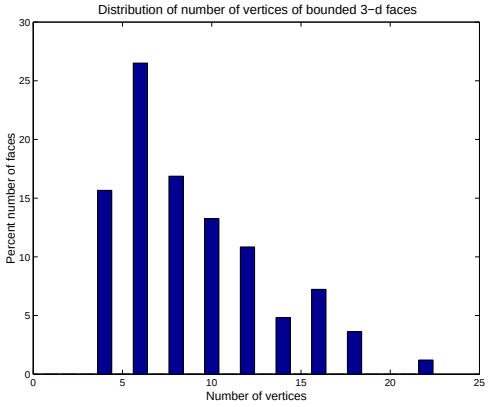


(a4)

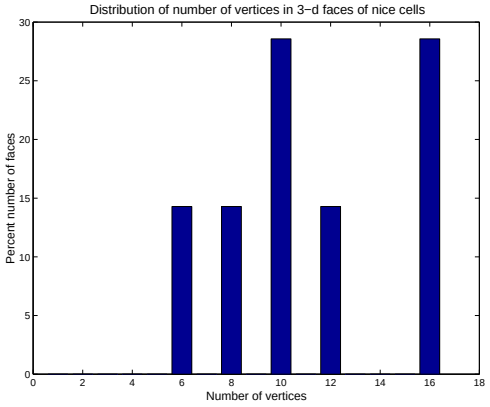


(b4)

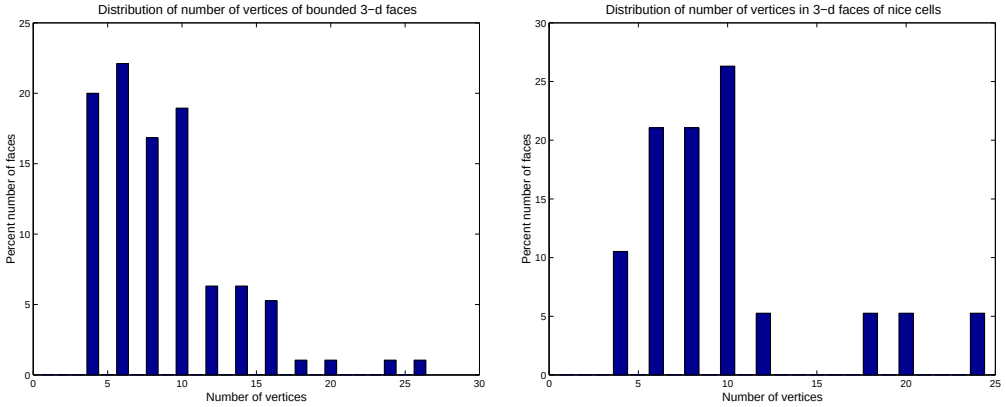
Distribution of number of vertices of bounded 3−d faces
Percent number of faces
Number of vertices
Distribution of number of vertices in 3−d faces of nice cells
Percent number of faces
Number of vertices

(a5) (b5)

**Figure 3.34** *Distribution of* (ai) $v_{3\mathrm{f}}$ *and* (bi) $v_c^{3\mathrm{f}}$ *of the* $i^{\mathrm{th}}$ *simulation on 4-d Voronoi.*

Table 3.14 contains the results obtained from a 4-d Voronoi network of 300 original nuclei. The numbers of vertices of the sixteen cells are 97, 99, 112, 141, 145, 160, 170, 171, 176, 176, 184, 186, 188, 192, 216 and 235.

| *Random seed* | 91876 | | | | |
|---|---|---|---|---|---|
| $\mathrm{N}_v$ | 6776 | $m^3(n_c^v)$ | $-1.7507 \times 10^4$ | $(\mu_{3\mathrm{f}}^v)_c$ | 9.9875 |
| $n_v$ | 3848 | $n_{3\mathrm{f}}$ | 444 | $(\sigma_v^2)_c^{3\mathrm{f}}$ | 31.1697 |
| $n_c$ | 16 | $\mu_{3\mathrm{f}}^v$ | 9.1486 | $m^2((n_{3\mathrm{f}}^v)_c)$ | 30.9748 |
| $n_c^v$ | 1687 | $(\sigma_v^2)_{3\mathrm{f}}$ | 24.0411 | $m^3((n_{3\mathrm{f}}^v)_c)$ | 203.3116 |
| $\mu_c^v$ | 165.5000 | $m^2(n_{3\mathrm{f}}^v)$ | 23.9869 | $n_c^{2\mathrm{f}}$ | 60 |
| $(\sigma_v^2)_c$ | $1.5100 \times 10^3$ | $m^3(n_{3\mathrm{f}}^v)$ | 170.4755 | $n_c^{1\mathrm{f}}$ | 3 |
| $m^2(n_c^v)$ | $1.4156 \times 10^3$ | $n_c^{3\mathrm{f}}$ | 160 | $\mathrm{t_{CPU}}$(second) | $1.6013 \times 10^4$ |

**Table 3.14** *Face statistics of 300 nuclei Voronoi in four dimensions.*

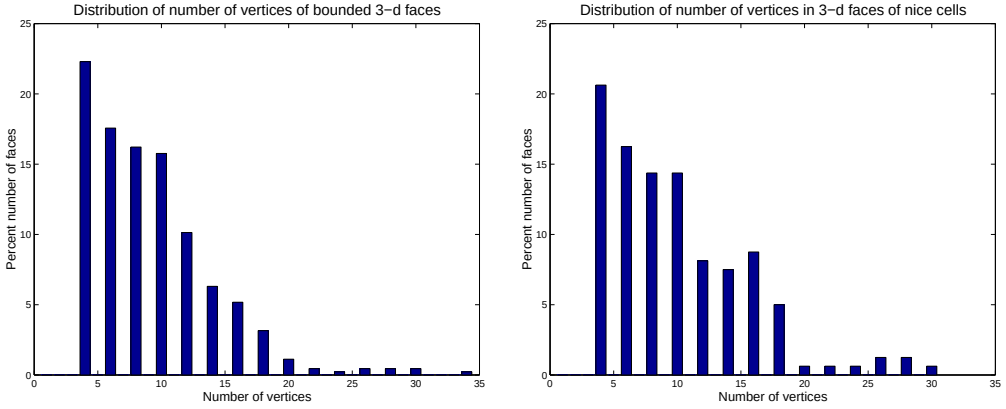
Distribution of number of vertices of bounded 3−d faces
Percent number of faces
Number of vertices
Distribution of number of vertices in 3−d faces of nice cells
Percent number of faces
Number of vertices

(a) (b)

**Figure 3.35** *Distribution of* (a) $v_{3\mathrm{f}}$ *and* (bi) $v_c^{3\mathrm{f}}$ *of 4-d Voronoi, 300 nuclei.*

Table 3.15 is obtained from Voronoi in five dimensions.

| *Random seed* | 39378 | | | $\mathrm{N}_v$ | 16212 |
|---|---|---|---|---|---|
| $n_v$ | 6449 | $n_{4\mathrm{f}}$ | 175 | $(\sigma_v^2)_c^{4\mathrm{f}}$ | 352.2909 |
| $n_c$ | 1 | $\mu_{4\mathrm{f}}^v$ | 15.9200 | $m^2((n_{4\mathrm{f}}^v)_c)$ | 320.2645 |
| $n_c^v$ | 864 | $(\sigma_v^2)_{4\mathrm{f}}$ | 163.7752 | $m^3((n_{4\mathrm{f}}^v)_c)$ | 351.8362 |
| $\mu_c^v$ | 864 | $m^2(n_{4\mathrm{f}}^v)$ | 162.8393 | $n_c^{3\mathrm{f}}$ | 1 |
| $(\sigma_v^2)_c$ | 0 | $m^3(n_{4\mathrm{f}}^v)$ | $4.8764 \times 10^3$ | $(\mu_{3\mathrm{f}}^v)_c$ | 4 |
| $m^2(n_c^v)$ | 0 | $n_c^{4\mathrm{f}}$ | 11 | $n_c^{2\mathrm{f}}$ | 1 |
| $m^3(n_c^v)$ | 0 | $(\mu_{4\mathrm{f}}^v)_c$ | 29.0909 | $\mathrm{t_{CPU}}$(second) | $1.8908 \times 10^4$ |

**Table 3.15** *Face statistics of 200 nuclei Voronoi in five dimensions.*

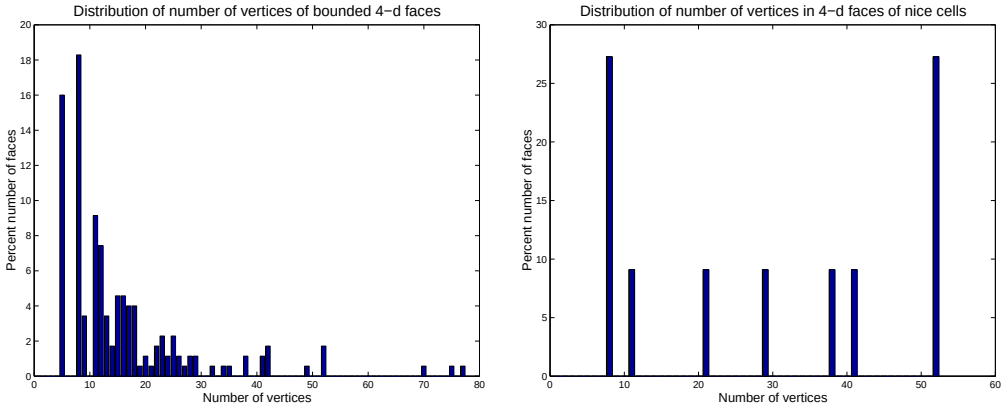
Distribution of number of vertices of bounded 4−d faces
Percent number of faces
Number of vertices
Distribution of number of vertices in 4−d faces of nice cells
Percent number of faces
Number of vertices

(a) (b)

**Figure 3.36** *Distribution of* (a) $v_{4\mathrm{f}}$ *and* (bi) $v_c^{4\mathrm{f}}$ *of 5-d Voronoi, 200 nuclei.*

## § 3.9 Beam intersection study

For this study of sectioning by a line the Voronoi in two dimensions, first generate on Matlab 500 points within a square box from $-0.25$ to 1.25 in both axes. The beam is simply a straight line $y = mx + c$ where $m$ is the slope and $c$ a constant. The term *pencil beam* is used in Astronomy to describe the probing into the depth of the universe with a window of very narrow width. The data collected thus therefore in effect represent data along a Euclidean straight line at various distances. It is largely a very limited technique, but there are no other choices in Astronomy as regard the vast space that separates us from anywhere.

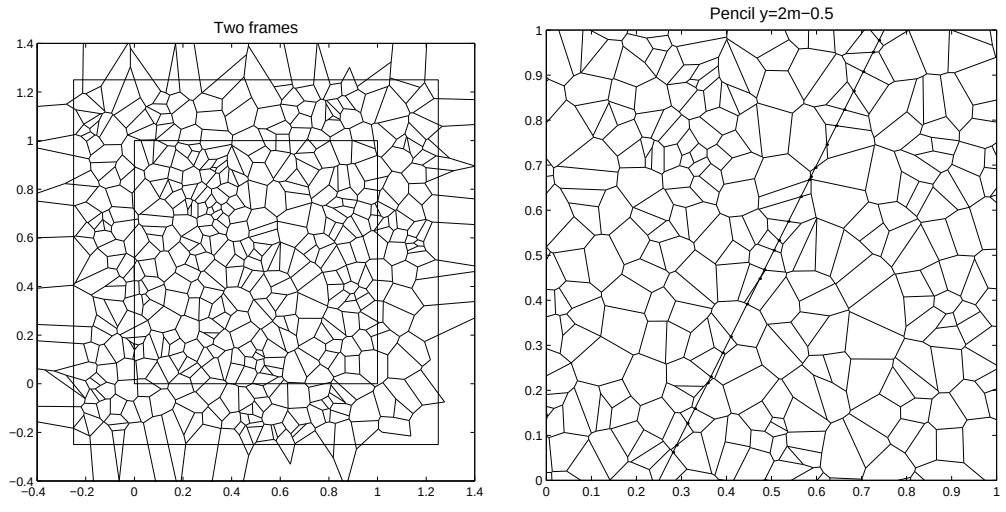


(a) (b)

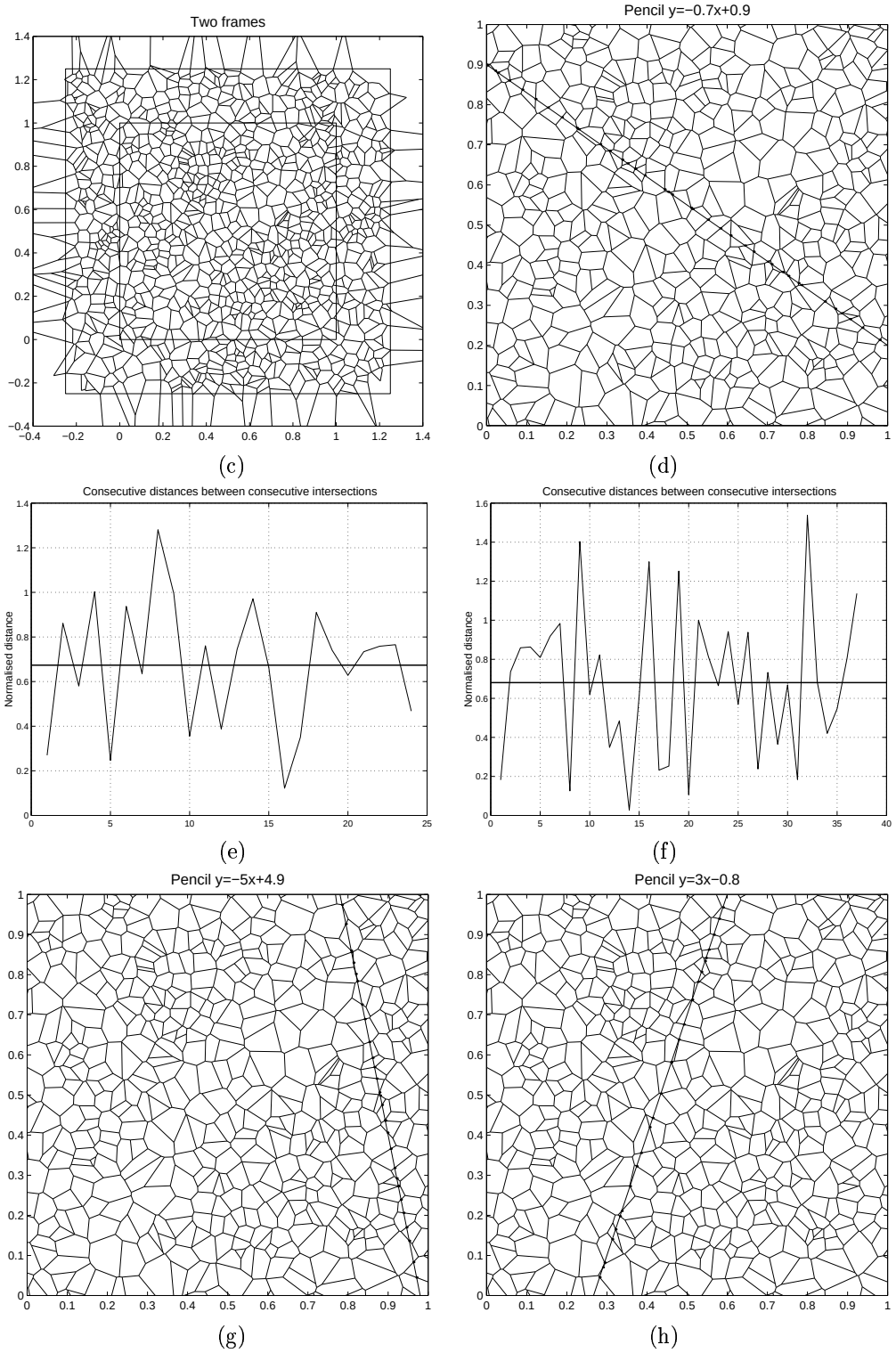


**Figure 3.37** *Intersection by a line.* (a) *is intersected by* (b) $y = 2x - 0.5$*;* (c) *is intersected by* (d) $y = -0.7x + 0.9$*;* (e) *and* (f) *are corresponding distances of respectively* (b) *and* (d)*;* (c) *is intersected by* (g) $y = -5x + 4.9$ *and* (h) $y = 3x - 0.8$.

A natural basis for the normalisation is the expected distance. Another possible basis is $(1/\sqrt{239}) = 0.064685$. I call *mean normalisation* the normalisation using the first-, and *homogeneity normalisation* the second basis. Graphs of the closest pair distances look the same for both types of normalisation.

| *Simulation* | 1 | 2 | 3 | 4 |
|---|---|---|---|---|
| $N_c$ | 500 | 1,000 | | |
| $N_e$ | 1,463 | 2,955 | | |
| $n_c$ | 239 | 463 | | |
| $n_e$ | 789 | 1,455 | | |
| Line equation | $y = 2x - 0.5$ | $y = -0.7x + 0.9$ | $y = -5x + 4.9$ | $y = 3x - 0.8$ |
| $\bar{d}$ | $4.6867 \times 10^{-2}$ | $3.163 \times 10^{-2}$ | $3.2448 \times 10^{-2}$ | $3.7843 \times 10^{-2}$ |
| $\sigma_d^2$ | $3.9422 \times 10^{-4}$ | $3.1174 \times 10^{-4}$ | $2.9005 \times 10^{-4}$ | $4.9535 \times 10^{-4}$ |
| Normalisation | | | | |
| by mean | $1 \pm 0.4237$<br>$0.1713$<br>$-8.1332 \times 10^{-3}$ | $1 \pm 0.5582$<br>$0.3032$<br>$3.5783 \times 10^{-2}$ | $1 \pm 0.5249$<br>$0.2656$<br>$-3.7762 \times 10^{-3}$ | $1 \pm 0.5881$<br>$0.3321$<br>$2.2989 \times 10^{-2}$ |
| by homogeneity | $0.7245 \pm 0.3070$<br>$8.9936 \times 10^{-2}$<br>$-3.0936 \times 10^{-3}$ | $0.68059 \pm 0.3799$<br>$0.1404$<br>$1.128 \times 10^{-2}$ | $0.6982 \pm 0.3665$<br>$0.1295$<br>$-1.2853 \times 10^{-3}$ | $0.81428 \pm 0.4789$<br>$0.2202$<br>$1.2412 \times 10^{-2}$ |

The program used is listed in § A.17. The space position vector of the intersection between the two vectors $AB$ and $CD$ is $P = A + r(B - A)$, where $AB = B - A$ and $CD = D - C$ are vectors or directed lines and $A, B, C, D$ are space vectors, $r = \begin{vmatrix} CD' \\ CA' \end{vmatrix} \Big/ \begin{vmatrix} AB' \\ CD' \end{vmatrix}$ and $s = \begin{vmatrix} AB' \\ CA' \end{vmatrix} \Big/ \begin{vmatrix} AB' \\ CD' \end{vmatrix}$ Here $AB = A + r(B - A)$, and $CD = C + s(D - C), 0 \leq r, s \leq 1$ are directed lines. $P$ exists if $0 \leq r \leq 1$ and $0 \leq s \leq 1$.

If the denominator $\begin{vmatrix} AB' \\ CD' \end{vmatrix}$ is zero, then the two lines are parallel. Also, if the nominator of $r$ is zero, that is $\begin{vmatrix} CD' \\ CA' \end{vmatrix} = 0$, then both lines are collinear.

Consider the line section of Rayleigh distributed Voronoi where both the coordinates $x$ and $y$ are random numbers with Rayleigh distribution. The probability density function of the Rayleigh distribution is $y = f(x/b) = (x/b^2)\exp(-x^2/2b^2)$. The mean of this distribution is $b\sqrt{\pi/2}$ and the variance is $((4 - \pi)/2)b^2$. With $b = 1, 2, \ldots, 1000$ choose the random numbers from the Rayleigh distribution, then scale and use them as the coordinates.

In Figure 3.38 the structure in (a) is intersected by (b) $y = 3x - 0.8$, (c) $y = x$, (d) $y = 2x$, (e) $y = 0.2x$, (f) $y = -x + 1$, (g) $y = -x + 0.3$.

The following codes generate and scale the points of Rayleigh distribution.

```
X=raylrnd([1:NumCell])';Y=raylrnd([1:NumCell])';Max=0.8*max([X;Y]);X=X/Max;Y=Y/Max;
```

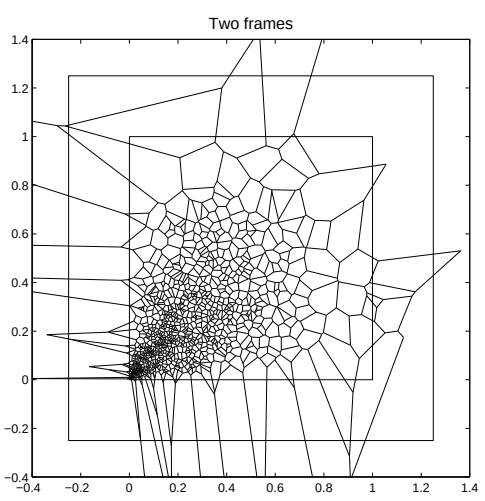


(a)

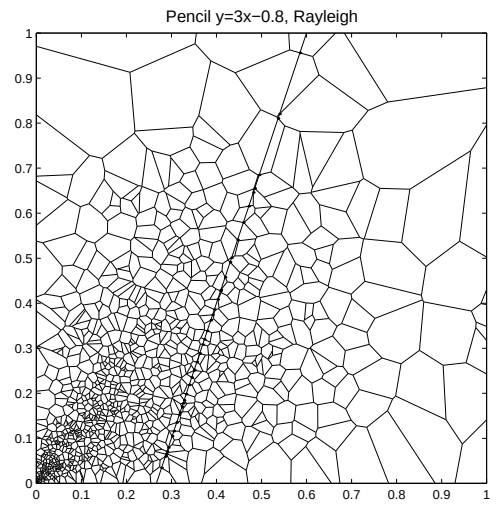


(b)

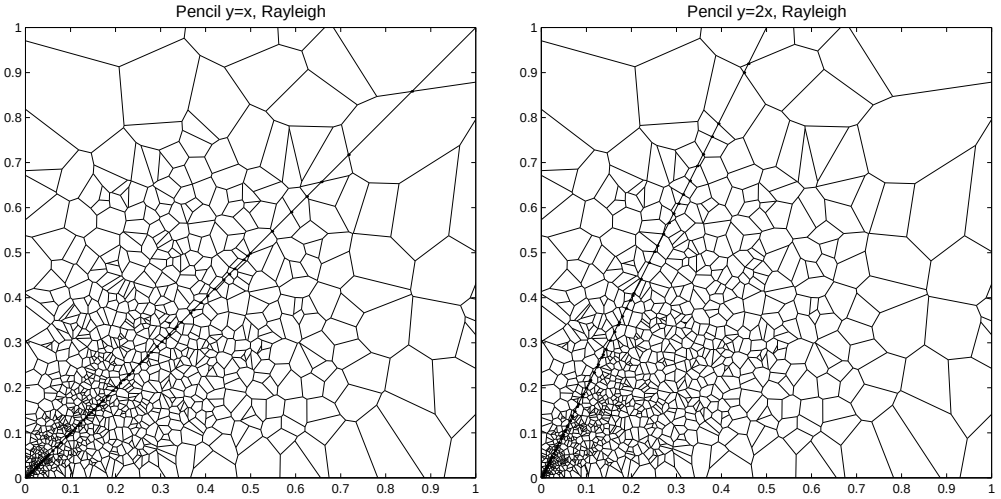


(c) (d)

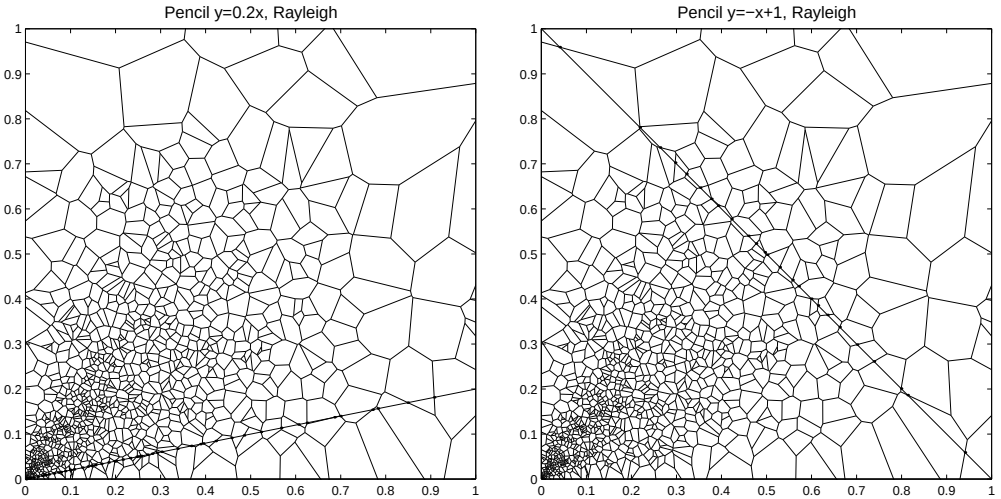


(e) (f)

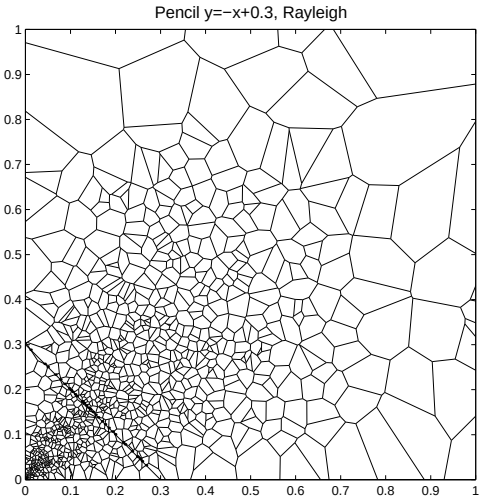


(g)

The values of $Cx$ and $Dx$ will need to be adjusted manually from the pencil beam equation. It is the value of $x$ at both points of intersection between the beam and the $[0, 1]$ square box. A random Voronoi network can either be both homogeneous and isotropic or, nonhomogeneous and nonisotropic depending on whether the probability distribution function is a constant.

**Figure 3.38** Line intersection in a Voronoi with Rayleigh distribution.

| *Simulation* | 1 | 2 | 3 | 4 | 5 | |
|---|---|---|---|---|---|---|
| $N_c$ | 1,000 | | | | | |
| $N_e$ | 2,975 | | | | | |
| $n_c$ | 988 | | | | | |
| $n_e$ | 2,912 | | | | | |
| Line eq. | $y = 3x - 0.8$ | $y = x$ | $y = 2x$ | $y = 0.2x$ | $y = -x + 1$ | $y = -x + 0.3$ |
| $\bar{d}$ | $2.3621 \times 10^{-2}$ | $1.4253 \times 10^{-2}$ | $1.3853 \times 10^{-2}$ | $1.7434 \times 10^{-2}$ | $4.4401 \times 10^{-2}$ | $1.027 \times 10^{-2}$ |
| $\sigma_d^2$ | $8.1582 \times 10^{-4}$ | $6.2922 \times 10^{-4}$ | $2.9647 \times 10^{-4}$ | $3.0991 \times 10^{-4}$ | $1.1584 \times 10^{-3}$ | $3.5365 \times 10^{-5}$ |
| Normalised | | | | | | |
| by mean | 1±1.2092<br>1.4256<br>5.5516 | 1±1.7599<br>3.0609<br>28.351 | 1±1.2429<br>1.5239<br>7.6499 | 1±1.0098<br>1.0004<br>1.6643 | 1±0.7665<br>0.56204<br>1.2114 | 1±0.5791<br>0.3245<br>0.1755 |
| by homog. | 0.7425±0.8978<br>0.7859<br>2.2721 | 0.4480±0.7885<br>0.6144<br>2.5493 | 0.4354±0.5412<br>0.2890<br>0.6316 | 0.548±0.5533<br>0.3004<br>0.2739 | 1.3956±1.0698<br>1.0947<br>3.293 | 0.3228±0.1869<br>$3.3813 \times 10^{-2}$<br>$5.9021 \times 10^{-3}$ |

**Table 3.17** *Line intersection statistics of Rayleigh distributed Voronoi.*

## § 3.10 Voronoi of a Voronoi

A Voronoi of a Voronoi is still a Voronoi, provided that by 'Voronoi' one means Voronoi Tessellation. But what are the effects of applying the Voronoi tessellating operator on a set of points? And what are the effects of applying this operator twice?

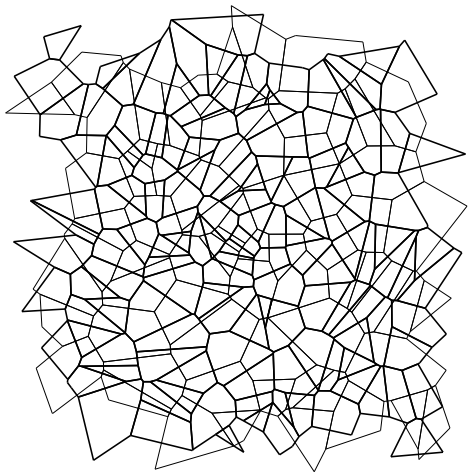

It is an interesting question to consider whether Voronoi tessellation as an operator alters, for instance, the nature of the distribution of the original set of points. Figure 3.39 shows the first Voronoi operator applied to the original points and then the second Voronoi operator applied to the vertices obtained. Here the Voronoi operator is applied twice in succession. In Figure the Voronoi operator is twiced in succession, *i.e.* $\mathcal{V}^2(\cdot)$, starting from a set of 100 points.

**Figure 3.39** Two Voronoi operators applied in succession.

Let $\mathcal{V}^n(\cdot)$ be the $n^{\text{th}}$-order Voronoi operator. Figure 3.39 shows as an example $\mathcal{V}^2(x)$ where $x$ is the original generator points. In Figure 3.40 this operator is applied six times in succession. The Voronoi operator is a mapping which maps a set of points into a set of Voronoi vertices having the former points as the Voronoi nuclei. The program used for Figures 3.39 to 3.41 is listed in § A.20.:

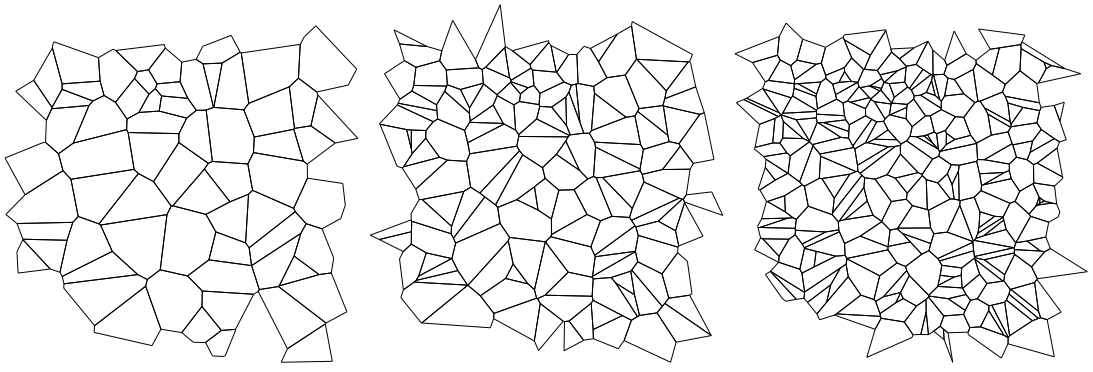

(a) (b) (c)

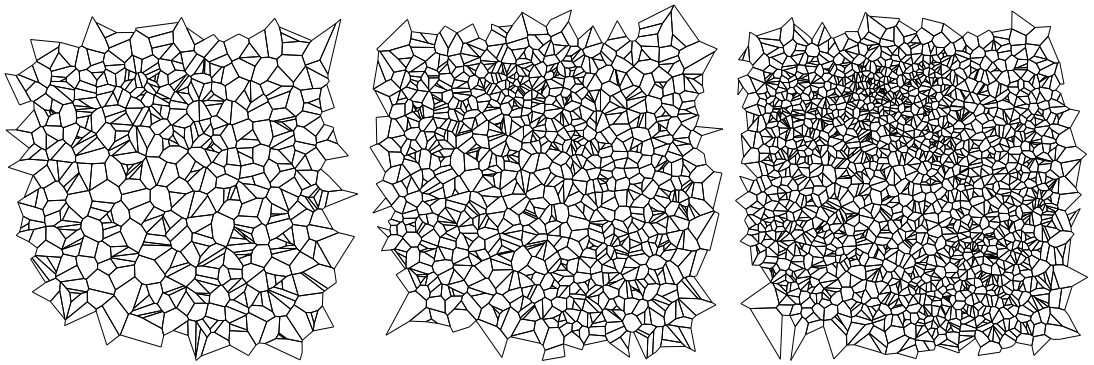

(d) (e) (f)

**Figure 3.40** *The Voronoi operations,* (a) $\mathcal{V}(x)$, (b) $\mathcal{V}^2(x)$, (c) $\mathcal{V}^3(x)$, (d) $\mathcal{V}^4(x)$, (e) $\mathcal{V}^5(x)$, (f) $\mathcal{V}^6(x)$, *where* $x$ *is the original set of 100 points.*

Figure 3.41 shows the effect produced by the Voronoi operators of various degrees on the number of cells, $n_c$, and vertices, $n_v$ of the network.

Figure 3.41 recursively apply the Voronoi operators of various orders. The number of cells and vertices when recursively applying the Voronoi operators of various orders on the set of point $x$ is shown in Figure 3.41, that is to say, $\mathcal{V}(x)$, $\mathcal{V}^2(x)$, $\cdots$, $\mathcal{V}^6(x)$. From Figure 3.41, the increase of $n_c$ and $n_v$ with the order $n$ of $\mathcal{V}^n(\cdot)$ is exponential. And from Figure 3.41 (a) to (f), apart from the unevenness affected at the boundary, the grephs shows the degree of lumpiness in the original distribution retained by the Voronoi operator. This is analogous to the increase in the entropy in physical processes.

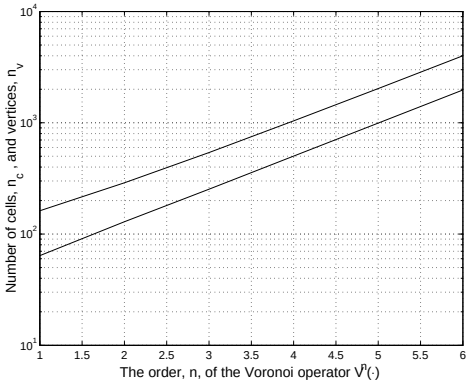


**Figure 3.41** The number of cells and vertices when recursively applying the Voronoi operator.

## § 3.11 Transformations of a Voronoi

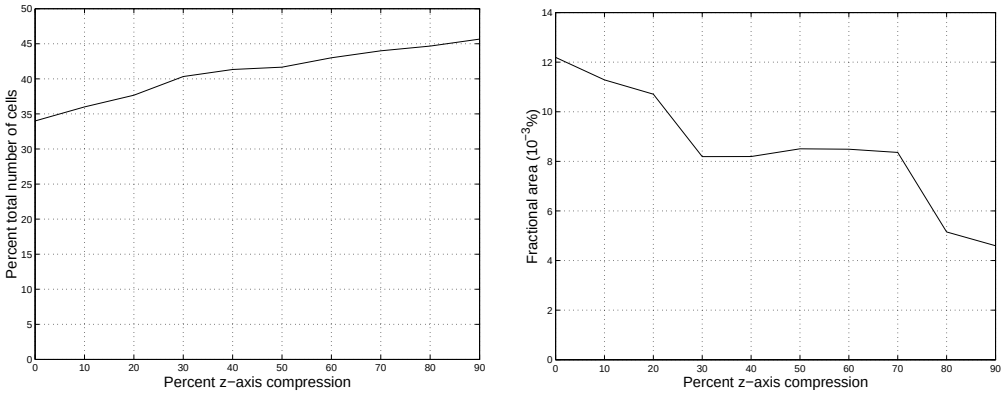


(a) (b)

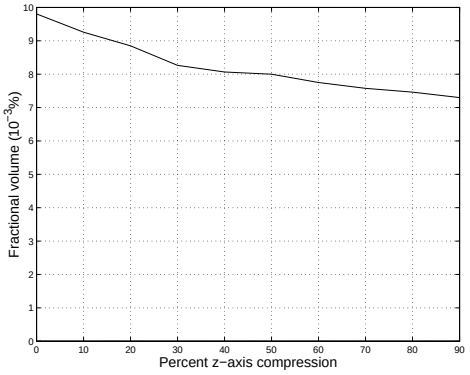


The simplest of transformations is compression where the coordinates of each vertex in multiplied by a factor less than one. Figure 3.42 shows, within a fixed box, the effect the compression along the $z$-axis has on the number of cells, surface area and volume of cells within the box. It shows the effects of a $z$-axis compression on (a) the number of cells in the box, (b) the surface area of a cell and (c) the volume of a cell.

(c)

**Figure 3.42** The effects of axis compression.

## § 3.12 Compressed Voronoi

The following study looks at compression of the Voronoi tessellation in three dimensions. With the compression simultaneously in the $x$- and $y$ axes, the mean and standard deviation of cell's surface area are shown as contours in Figure 3.43. The numerical values are shown in Figure's 3.18 and 3.19. Here $x_i$ and $y_i$ are respectively transformed to $r_x x_i$ and $r_y y_i$. All the values here are normalised by their corresponding values in the case without compression. In this case, the network was created from 100 generators within one unit cube, only 21 inner cells are considered, the mean and the standard deviation of the cell surface area are respectively 0.2330 and 0.0544.

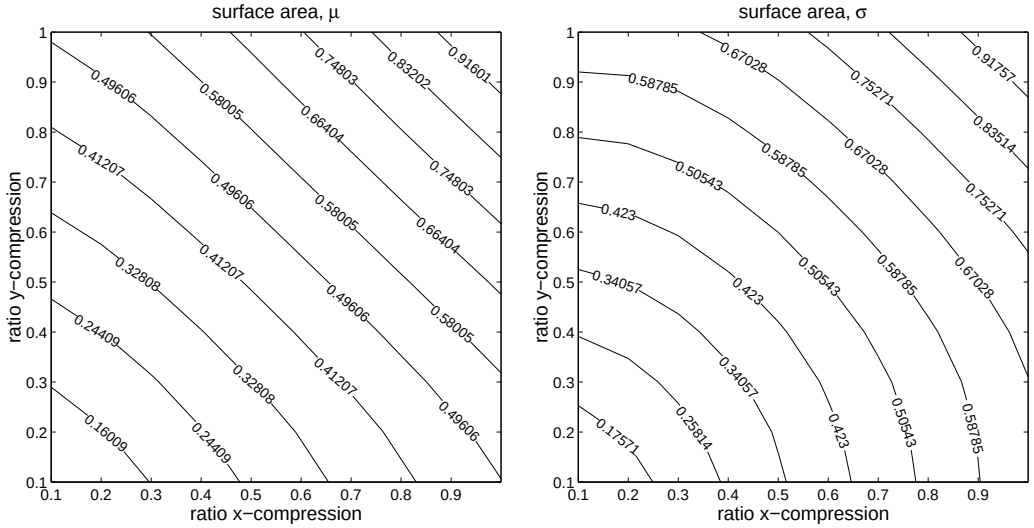


(a) (b)

**Figure 3.43** (a) *Mean, and* (b) *standard deviation of surface area of cells under compression, normalised against the corresponding values of the uncompressed case. In other words,* (a) $\mu(a_{ij})/\mu(a_{11})$, *and* (b) $\sigma(a_{ij})/\sigma(a_{11})$.

$\boxed{\mu(a_{ij})}$

| | | $r_x$ | | | | | | | | | |
|---|---|---|---|---|---|---|---|---|---|---|---|
| | | *1.0* | *0.9* | *0.8* | *0.7* | *0.6* | *0.5* | *0.4* | *0.3* | *0.2* | *0.1* |
| $r_y$ | *1.0* | 1.0000 | 0.9337 | 0.8688 | 0.8058 | 0.7450 | 0.6870 | 0.6326 | 0.5828 | 0.5396 | 0.5060 |
| | *0.9* | 0.9318 | 0.8683 | 0.8061 | 0.7457 | 0.6873 | 0.6315 | 0.5790 | 0.5310 | 0.4892 | 0.4566 |
| | *0.8* | 0.8650 | 0.8042 | 0.7447 | 0.6866 | 0.6305 | 0.5768 | 0.5261 | 0.4797 | 0.4391 | 0.4073 |
| | *0.7* | 0.8001 | 0.7419 | 0.6847 | 0.6290 | 0.5749 | 0.5230 | 0.4740 | 0.4289 | 0.3893 | 0.3581 |
| | *0.6* | 0.7375 | 0.6816 | 0.6267 | 0.5730 | 0.5208 | 0.4706 | 0.4230 | 0.3789 | 0.3400 | 0.3092 |
| | *0.5* | 0.6777 | 0.6240 | 0.5711 | 0.5193 | 0.4687 | 0.4199 | 0.3734 | 0.3300 | 0.2914 | 0.2605 |
| | *0.4* | 0.6217 | 0.5699 | 0.5188 | 0.4685 | 0.4193 | 0.3715 | 0.3257 | 0.2826 | 0.2439 | 0.2123 |
| | *0.3* | 0.5707 | 0.5205 | 0.4708 | 0.4217 | 0.3735 | 0.3264 | 0.2808 | 0.2375 | 0.1979 | 0.1648 |
| | *0.2* | 0.5269 | 0.4779 | 0.4293 | 0.3810 | 0.3333 | 0.2863 | 0.2404 | 0.1962 | 0.1547 | 0.1188 |
| | *0.1* | 0.4939 | 0.4457 | 0.3976 | 0.3497 | 0.3020 | 0.2546 | 0.2078 | 0.1617 | 0.1171 | 0.0761 |

**Table 3.18** *Mean of the cell surface area of compressed Voronoi*

| $\sigma(a_{ij})$ | | $r_x$ | | | | | | | | | |
|---|---|---|---|---|---|---|---|---|---|---|---|
| | | *1.0* | *0.9* | *0.8* | *0.7* | *0.6* | *0.5* | *0.4* | *0.3* | *0.2* | *0.1* |
| $r_y$ | *1.0* | 1.0000 | 0.9381 | 0.8789 | 0.8231 | 0.7715 | 0.7255 | 0.6868 | 0.6577 | 0.6407 | 0.6382 |
| | *0.9* | 0.9360 | 0.8761 | 0.8186 | 0.7641 | 0.7135 | 0.6678 | 0.6288 | 0.5986 | 0.5799 | 0.5751 |
| | *0.8* | 0.8756 | 0.8173 | 0.7611 | 0.7075 | 0.6573 | 0.6116 | 0.5720 | 0.5403 | 0.5195 | 0.5122 |
| | *0.7* | 0.8199 | 0.7626 | 0.7071 | 0.6539 | 0.6037 | 0.5574 | 0.5165 | 0.4830 | 0.4596 | 0.4495 |
| | *0.6* | 0.7699 | 0.7130 | 0.6576 | 0.6041 | 0.5532 | 0.5058 | 0.4631 | 0.4271 | 0.4005 | 0.3870 |
| | *0.5* | 0.7269 | 0.6696 | 0.6136 | 0.5592 | 0.5069 | 0.4576 | 0.4123 | 0.3731 | 0.3426 | 0.3249 |
| | *0.4* | 0.6924 | 0.6340 | 0.5766 | 0.5205 | 0.4661 | 0.4141 | 0.3654 | 0.3219 | 0.2864 | 0.2634 |
| | *0.3* | 0.6676 | 0.6076 | 0.5482 | 0.4897 | 0.4324 | 0.3769 | 0.3240 | 0.2751 | 0.2331 | 0.2030 |
| | *0.2* | 0.6536 | 0.5914 | 0.5296 | 0.4682 | 0.4076 | 0.3481 | 0.2902 | 0.2350 | 0.1848 | 0.1451 |
| | *0.1* | 0.6495 | 0.5853 | 0.5212 | 0.4573 | 0.3936 | 0.3302 | 0.2675 | 0.2059 | 0.1466 | 0.0933 |

**Table 3.19** *Standard deviation of the cell surface area of compressed Voronoi*

Mistakes reveal some interesting characteristics worth investigating further, namely those shown in Figure 3.44.

Let $a_{ij}$ be the surface area of cells when subjected to compressions $i$ and $j$ respectively along the $x$- and $y$ axes, that is to say, $r_x = i$ and $r_y = j$. And let $a_{ij}(k)$ be that surface area of the $k^{\text{th}}$ cell among those undergoing these compressions $ij$. Then Figure 3.44 (b) and (c) are possible when we pick one cell as the basis for our normalisation, while Figure 3.44 (a) is when we normalise each compressed case by its own mean.

For cell volume of the same network the results are shown in Figure 3.45. The mean value and the standard deviation of cell volumes are respectively 0.0075 and 0.0032.

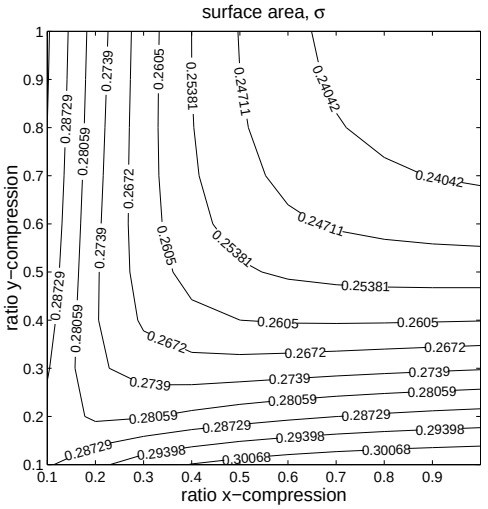


(a)

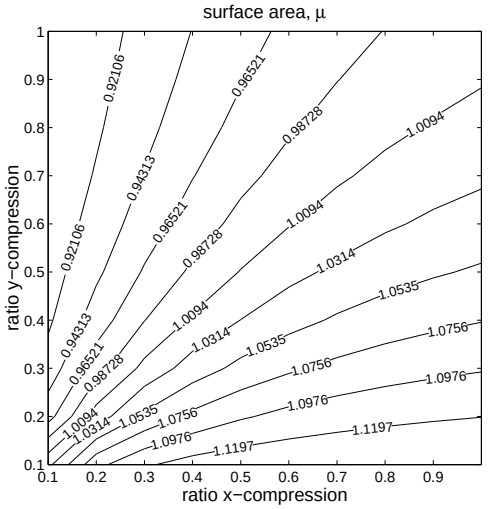


(b)

In Figure 3.44 ome hidden characteristics are revealed from out choice of the normalisation basis; respectively for (a), (b) and (c) the following,

$$\sigma\left(\frac{a_{ij}}{\mu(a_{ij})}\right), \quad \frac{\mu(a_{ij}/a_{ij}(1))}{\mu(a_{11}/a_{11}(1))}, \quad \frac{\sigma(a_{ij}/a_{ij}(1))}{\sigma(a_{11}/a_{11}(1))}.$$

(c)

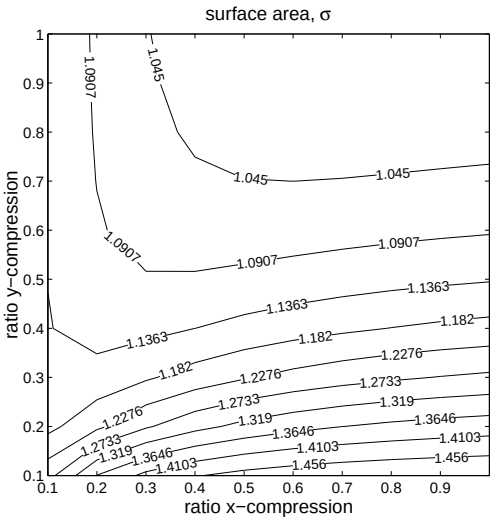


**Figure 3.44** Some hidden characteristics revealed.

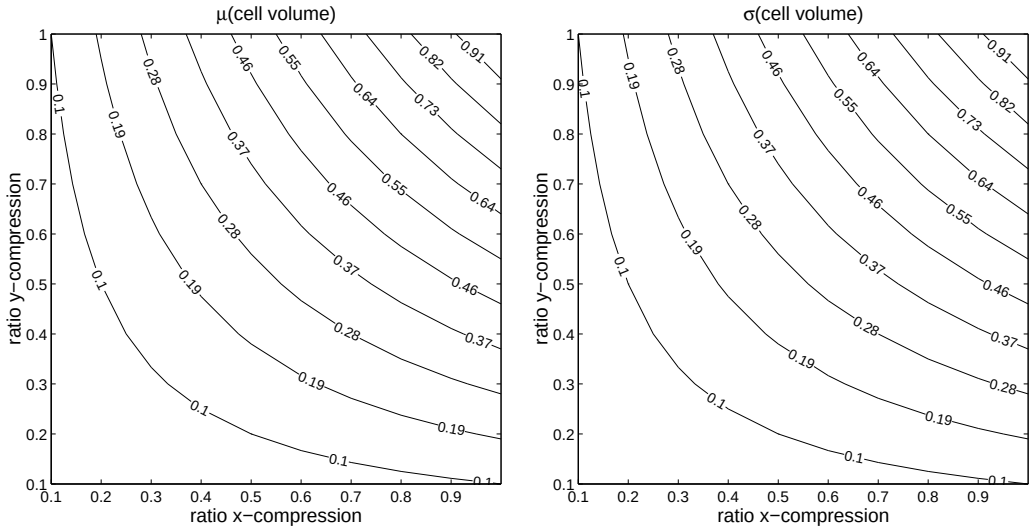


**Figure 3.45** *Volume of compressed Voronoi cells;* (a) $\mu(V_{ij}))and$(b) $\sigma(V_{ij})$.

Table 3.20 gives the numerical values of the mean, while Table 3.21 those of the standard deviation plotted in Figure 3.45.

$\boxed{\mu(V_{ij})}$

| | | $r_x$ | | | | | | | | | |
|---|---|---|---|---|---|---|---|---|---|---|---|
| | | *1.0* | *0.9* | *0.8* | *0.7* | *0.6* | *0.5* | *0.4* | *0.3* | *0.2* | *0.1* |
| | *1.0* | 1.0000 | 0.9000 | 0.8000 | 0.7000 | 0.6000 | 0.5000 | 0.4000 | 0.3000 | 0.2000 | 0.1000 |
| | *0.9* | 0.9000 | 0.8100 | 0.7200 | 0.6300 | 0.5400 | 0.4500 | 0.3600 | 0.2700 | 0.1800 | 0.0900 |
| | *0.8* | 0.8000 | 0.7200 | 0.6400 | 0.5600 | 0.4800 | 0.4000 | 0.3200 | 0.2400 | 0.1600 | 0.0800 |
| | *0.7* | 0.7000 | 0.6300 | 0.5600 | 0.4900 | 0.4200 | 0.3500 | 0.2800 | 0.2100 | 0.1400 | 0.0700 |
| | *0.6* | 0.6000 | 0.5400 | 0.4800 | 0.4200 | 0.3600 | 0.3000 | 0.2400 | 0.1800 | 0.1200 | 0.0600 |
| $r_y$ | *0.5* | 0.5000 | 0.4500 | 0.4000 | 0.3500 | 0.3000 | 0.2500 | 0.2000 | 0.1500 | 0.1000 | 0.0500 |
| | *0.4* | 0.4000 | 0.3600 | 0.3200 | 0.2800 | 0.2400 | 0.2000 | 0.1600 | 0.1200 | 0.0800 | 0.0400 |
| | *0.3* | 0.3000 | 0.2700 | 0.2400 | 0.2100 | 0.1800 | 0.1500 | 0.1200 | 0.0900 | 0.0600 | 0.0300 |
| | *0.2* | 0.2000 | 0.1800 | 0.1600 | 0.1400 | 0.1200 | 0.1000 | 0.0800 | 0.0600 | 0.0400 | 0.0200 |
| | *0.1* | 0.1000 | 0.0900 | 0.0800 | 0.0700 | 0.0600 | 0.0500 | 0.0400 | 0.0300 | 0.0200 | 0.0100 |

**Table 3.20** *Numerical values of the mean and standard deviation of compressed cell volume.*

$\boxed{\sigma(V_{ij})}$

| | | $r_x$ | | | | | | | | | |
|---|---|---|---|---|---|---|---|---|---|---|---|
| | | *1.0* | *0.9* | *0.8* | *0.7* | *0.6* | *0.5* | *0.4* | *0.3* | *0.2* | *0.1* |
| | *1.0* | 1.0000 | 0.9000 | 0.8000 | 0.7000 | 0.6000 | 0.5000 | 0.4000 | 0.3000 | 0.2000 | 0.1000 |
| | *0.9* | 0.9000 | 0.8100 | 0.7200 | 0.6300 | 0.5400 | 0.4500 | 0.3600 | 0.2700 | 0.1800 | 0.0900 |
| | *0.8* | 0.8000 | 0.7200 | 0.6400 | 0.5600 | 0.4800 | 0.4000 | 0.3200 | 0.2400 | 0.1600 | 0.0800 |
| | *0.7* | 0.7000 | 0.6300 | 0.5600 | 0.4900 | 0.4200 | 0.3500 | 0.2800 | 0.2100 | 0.1400 | 0.0700 |
| | *0.6* | 0.6000 | 0.5400 | 0.4800 | 0.4200 | 0.3600 | 0.3000 | 0.2400 | 0.1800 | 0.1200 | 0.0600 |
| $r_y$ | *0.5* | 0.5000 | 0.4500 | 0.4000 | 0.3500 | 0.3000 | 0.2500 | 0.2000 | 0.1500 | 0.1000 | 0.0500 |
| | *0.4* | 0.4000 | 0.3600 | 0.3200 | 0.2800 | 0.2400 | 0.2000 | 0.1600 | 0.1200 | 0.0800 | 0.0400 |
| | *0.3* | 0.3000 | 0.2700 | 0.2400 | 0.2100 | 0.1800 | 0.1500 | 0.1200 | 0.0900 | 0.0600 | 0.0300 |
| | *0.2* | 0.2000 | 0.1800 | 0.1600 | 0.1400 | 0.1200 | 0.1000 | 0.0800 | 0.0600 | 0.0400 | 0.0200 |
| | *0.1* | 0.1000 | 0.0900 | 0.0800 | 0.0700 | 0.0600 | 0.0500 | 0.0400 | 0.0300 | 0.0200 | 0.0100 |

**Table 3.21** *Numerical values of the mean and standard deviation of compressed cell volume.*

Perimeters prove to be the most difficult to find. Figure 3.46 (a) and (b) show the mean and standard deviation of the cell perimeter while Table 3.22 lists the $\mu(s_c)$ matrix that makes up one of these graphs. The values before normalisation are $\mu(s_{ij}) = 3.0158$ and $\sigma(s_{ij}) = 0.4291$.

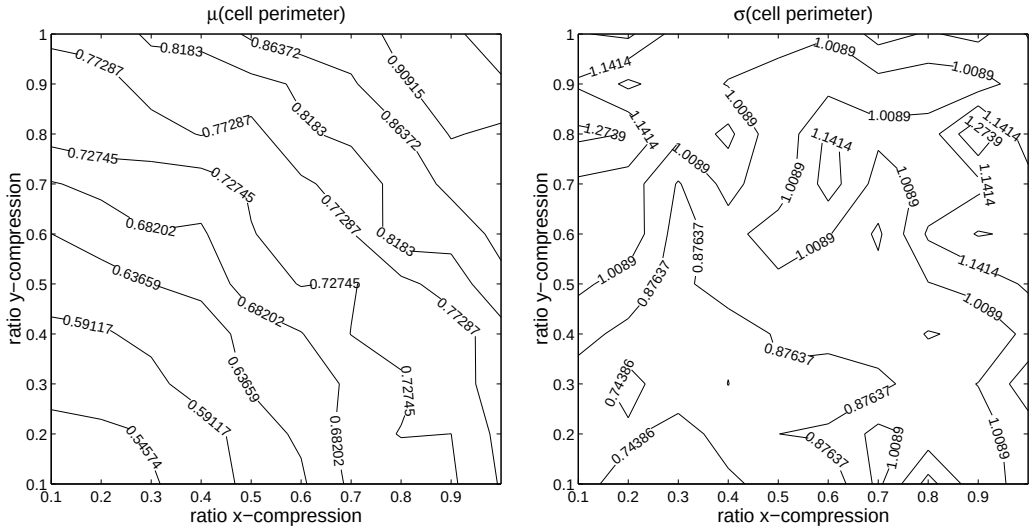


**Figure 3.46** *Cell perimeter;* (a) *the normalised mean, i.e.* $\mu(s_{ij})/\mu(s_{11})$*, and* (b) *the standard deviation,* $\sigma(s_{ij})/\sigma(s_{11})$*.*

| $\boxed{\mu(s_{ij})}$ | | $r_x$ | | | | | | | | | |
|---|---|---|---|---|---|---|---|---|---|---|---|
| | | *1.0* | *0.9* | *0.8* | *0.7* | *0.6* | *0.5* | *0.4* | *0.3* | *0.2* | *0.1* |
| $r_y$ | *1.0* | 1.0000 | 0.9376 | 0.9227 | 0.8878 | 0.8918 | 0.8717 | 0.8324 | 0.8271 | 0.7906 | 0.7835 |
| | *0.9* | 0.9437 | 0.9333 | 0.9039 | 0.8577 | 0.8241 | 0.8046 | 0.7922 | 0.7906 | 0.7556 | 0.7472 |
| | *0.8* | 0.8996 | 0.9127 | 0.8580 | 0.8266 | 0.8131 | 0.7558 | 0.7752 | 0.7560 | 0.7580 | 0.7441 |
| | *0.7* | 0.8840 | 0.8766 | 0.8334 | 0.7928 | 0.7644 | 0.7313 | 0.7054 | 0.7042 | 0.6937 | 0.6788 |
| | *0.6* | 0.8780 | 0.8339 | 0.8473 | 0.7684 | 0.7392 | 0.7261 | 0.6757 | 0.6806 | 0.6575 | 0.6363 |
| | *0.5* | 0.8509 | 0.7948 | 0.7592 | 0.7228 | 0.7301 | 0.7017 | 0.6550 | 0.6364 | 0.6166 | 0.6036 |
| | *0.4* | 0.8019 | 0.7457 | 0.7649 | 0.7284 | 0.6798 | 0.6613 | 0.6011 | 0.6036 | 0.5858 | 0.5847 |
| | *0.3* | 0.7852 | 0.7609 | 0.7129 | 0.6883 | 0.6618 | 0.6408 | 0.6161 | 0.5767 | 0.5755 | 0.5662 |
| | *0.2* | 0.7860 | 0.7273 | 0.7305 | 0.7008 | 0.6431 | 0.6189 | 0.5638 | 0.5476 | 0.5334 | 0.5264 |
| | *0.1* | 0.7771 | 0.7198 | 0.6895 | 0.6911 | 0.6296 | 0.6090 | 0.5538 | 0.5440 | 0.5124 | 0.5003 |

**Table 3.22** *Numerical means of the cell perimeter of compressed Voronoi.*

Figure 3.47 shows the plot of the change in the perimeter of faces when the Voronoi structure is compressed. The normalised mean and standard deviation are shown in the form of contours. The values before normalisation are $\mu(\mu(z_{ij})) = 0.3766$ and $\sigma(\mu(z_{ij})) = 0.0532$.

Both the surface and the perimeter are embedded in three dimensions, the former as 2-d facets while the latter as 1-d facets. But, comparing Figure 3.46 (a) with Figure 3.46 (a), the trend of changes in the mean is smoother for surfaces than for perimeters. The difference between the threnD of the standard deviation is even more pronounced, as can be readily seen by comparing Figure 3.46 (b) with Figure 3.46 (b). This may imply the reduction in the correlation between different statistical properties as the structural differences increase, as surface is directly related to the convex hull of the volume while perimeter is a convex hull embedded in another convex hull. Also, this means that convex hull as a mapping or function is not smooth, or it could mean that it is a smooth function only up to the order one, that is to say, when we apply it only once not twice or more.

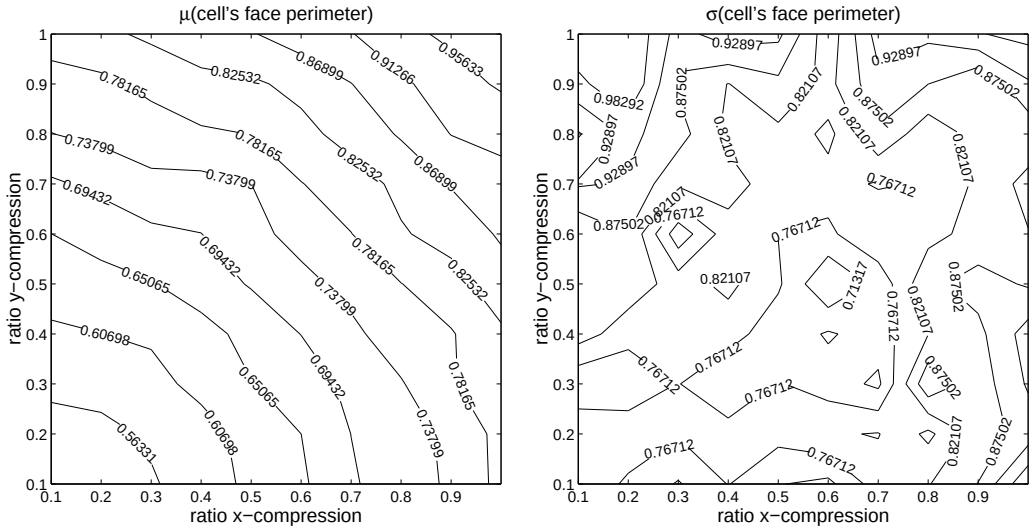


(a) (b)

**Figure 3.47** *Face perimeter;* (a) *its normalised mean, i.e.* $\mu(\mu(z_{ij}))/\mu(\mu(z_{11}))$, *and* (b) *the standard deviation,* $\sigma(\mu(s_{ij}))/\sigma(\mu(s_{11}))$.

$\boxed{\mu(\mu(z_{ij}))}$

| | | $r_x$ | | | | | | | | | |
|---|---|---|---|---|---|---|---|---|---|---|---|
| | | *1.0* | *0.9* | *0.8* | *0.7* | *0.6* | *0.5* | *0.4* | *0.3* | *0.2* | *0.1* |
| | *1.0* | 1.0000 | 0.9640 | 0.9460 | 0.9103 | 0.8907 | 0.8659 | 0.8523 | 0.8339 | 0.8155 | 0.8056 |
| | *0.9* | 0.9620 | 0.9384 | 0.9040 | 0.8681 | 0.8371 | 0.8186 | 0.8124 | 0.7927 | 0.7717 | 0.7606 |
| | *0.8* | 0.9262 | 0.9137 | 0.8738 | 0.8409 | 0.8129 | 0.7823 | 0.7755 | 0.7608 | 0.7489 | 0.7372 |
| | *0.7* | 0.8956 | 0.8722 | 0.8355 | 0.8058 | 0.7801 | 0.7378 | 0.7246 | 0.7276 | 0.7053 | 0.6874 |
| | *0.6* | 0.8745 | 0.8404 | 0.8214 | 0.7807 | 0.7527 | 0.7252 | 0.6936 | 0.6849 | 0.6661 | 0.6504 |
| $r_y$ | *0.5* | 0.8485 | 0.8093 | 0.7808 | 0.7514 | 0.7255 | 0.6977 | 0.6734 | 0.6479 | 0.6368 | 0.6283 |
| | *0.4* | 0.8186 | 0.7780 | 0.7614 | 0.7284 | 0.6951 | 0.6659 | 0.6335 | 0.6139 | 0.6065 | 0.5987 |
| | *0.3* | 0.8125 | 0.7771 | 0.7347 | 0.7075 | 0.6670 | 0.6490 | 0.6210 | 0.5916 | 0.5772 | 0.5731 |
| | *0.2* | 0.7958 | 0.7459 | 0.7225 | 0.6946 | 0.6506 | 0.6254 | 0.5870 | 0.5685 | 0.5528 | 0.5466 |
| | *0.1* | 0.7938 | 0.7451 | 0.7154 | 0.6897 | 0.6433 | 0.6181 | 0.5815 | 0.5594 | 0.5350 | 0.5196 |

**Table 3.23** *Numerical mean values of the face perimeter in a compressed Voronoi.*

$\boxed{\sigma(\mu(z_{ij}))}$

| | | $r_x$ | | | | | | | | | |
|---|---|---|---|---|---|---|---|---|---|---|---|
| | | *1.0* | *0.9* | *0.8* | *0.7* | *0.6* | *0.5* | *0.4* | *0.3* | *0.2* | *0.1* |
| | *1.0* | 1.0000 | 0.9795 | 0.9413 | 0.9524 | 0.7858 | 0.9426 | 0.9614 | 0.9060 | 1.0364 | 1.0311 |
| | *0.9* | 0.9221 | 0.8227 | 0.8754 | 0.9145 | 0.8047 | 0.8613 | 0.8197 | 0.8653 | 1.0369 | 0.9671 |
| | *0.8* | 0.8363 | 0.8407 | 0.7857 | 0.8670 | 0.7517 | 0.8090 | 0.8055 | 0.8980 | 0.9424 | 0.8702 |
| | *0.7* | 0.8939 | 0.8322 | 0.7718 | 0.7612 | 0.7903 | 0.7904 | 0.8453 | 0.8296 | 0.9233 | 0.9350 |
| | *0.6* | 0.8724 | 0.8413 | 0.8031 | 0.8155 | 0.7560 | 0.7662 | 0.7972 | 0.6784 | 0.8740 | 0.8279 |
| $r_y$ | *0.5* | 0.8689 | 0.8957 | 0.8640 | 0.7293 | 0.6592 | 0.7756 | 0.8340 | 0.7986 | 0.8512 | 0.8750 |
| | *0.4* | 0.9538 | 0.8608 | 0.8199 | 0.7414 | 0.7733 | 0.7324 | 0.7916 | 0.7954 | 0.7916 | 0.8463 |
| | *0.3* | 0.9359 | 0.8457 | 0.9174 | 0.7016 | 0.7422 | 0.7711 | 0.7139 | 0.7697 | 0.7137 | 0.7206 |
| | *0.2* | 0.8985 | 0.8447 | 0.7545 | 0.8238 | 0.8155 | 0.7855 | 0.7918 | 0.7724 | 0.8133 | 0.8138 |
| | *0.1* | 1.0322 | 0.8763 | 0.8181 | 0.7953 | 0.6991 | 0.7159 | 0.7692 | 0.7085 | 0.7546 | 0.8212 |

**Table 3.24** *Numerical standard deviations of the face perimeter in Voronoi network under various degrees of compression.*

The simulation above is then repeated again for a second time, where now $\mu(s_{11}) = 2.1206$, $\sigma(s_{11}) = 0.8154$, $\mu(\mu(z_{11})) = 0.3840$ and $\sigma(\mu(z_{11})) = 0.0518$. Figure 3.48 shows the results for both the cell perimeter $s$ and the face perimeter $z$. Also, compare these pictures with Table 3.25.

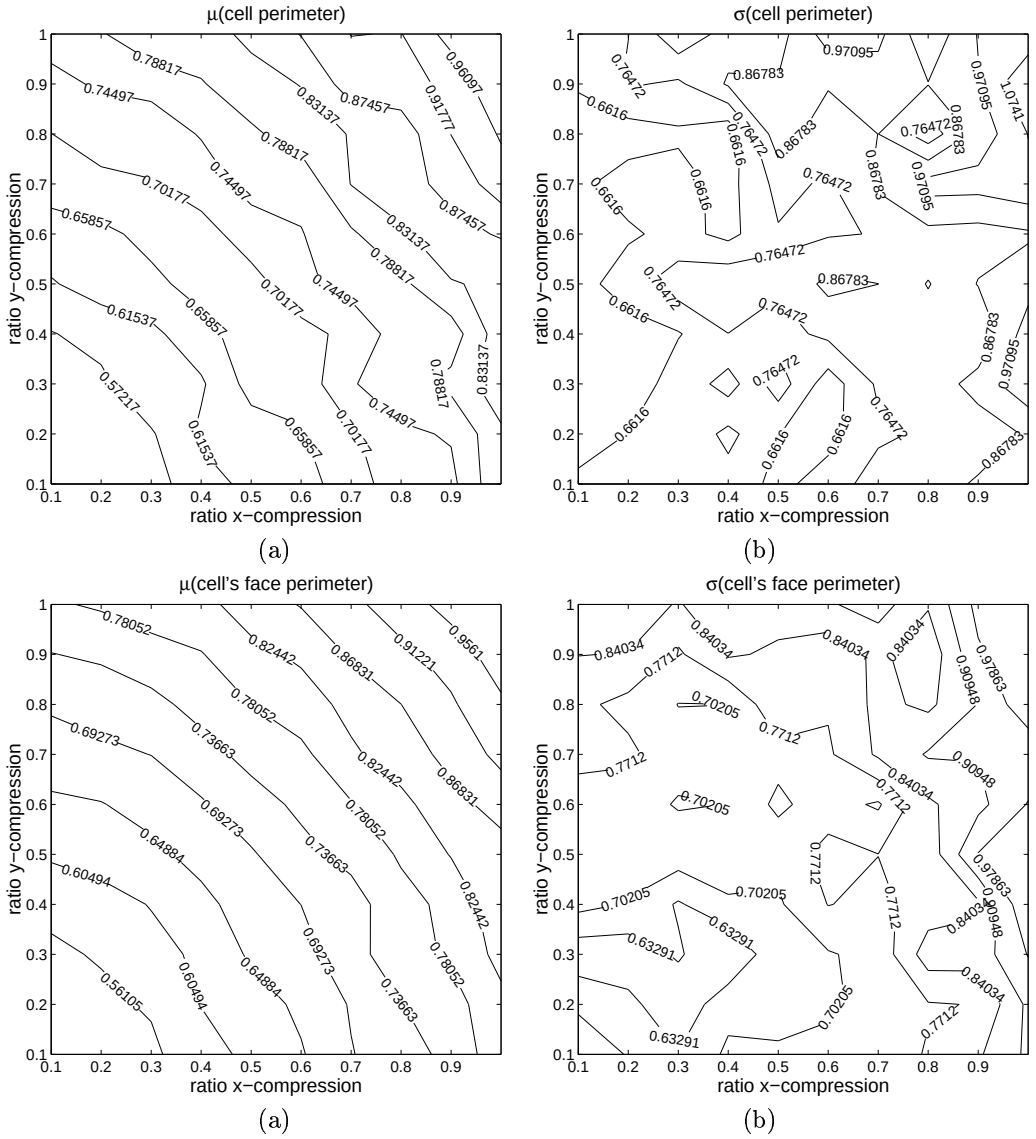


**Figure 3.48** *The cell perimeter and the face perimeter;* (a) $\mu(s_{ij})/\mu(s_{11})$, (b) $\sigma(s_{ij})/\sigma(s_{11})$, (c) $\mu(\mu(z_{ij}))/\mu(\mu(z_{11}))$ *and* (d) $\sigma(\mu(z_{ij}))/\sigma(\mu(z_{11}))$

$\boxed{\mu(s_{ij})}$

| | | $r_x$ | | | | | | | | | |
|---|---|---|---|---|---|---|---|---|---|---|---|
| | | *1.0* | *0.9* | *0.8* | *0.7* | *0.6* | *0.5* | *0.4* | *0.3* | *0.2* | *0.1* |
| | *1.0* | 1.0000 | 0.9781 | 0.9164 | 0.9188 | 0.8766 | 0.8417 | 0.8126 | 0.8282 | 0.7834 | 0.7633 |
| | *0.9* | 1.0042 | 0.9292 | 0.9004 | 0.8959 | 0.8330 | 0.8144 | 0.7851 | 0.7555 | 0.7511 | 0.7323 |
| | *0.8* | 0.9654 | 0.9185 | 0.8512 | 0.8339 | 0.8090 | 0.7808 | 0.7475 | 0.7256 | 0.7120 | 0.7015 |
| | *0.7* | 0.9422 | 0.8868 | 0.8596 | 0.8327 | 0.7596 | 0.7573 | 0.7262 | 0.6988 | 0.6964 | 0.6763 |
| | *0.6* | 0.8780 | 0.8621 | 0.8241 | 0.7817 | 0.7425 | 0.7278 | 0.6810 | 0.6723 | 0.6474 | 0.6397 |
| $r_y$ | *0.5* | 0.8411 | 0.8281 | 0.7785 | 0.7604 | 0.7350 | 0.6821 | 0.6752 | 0.6475 | 0.6352 | 0.6116 |
| | *0.4* | 0.8568 | 0.7661 | 0.7653 | 0.7156 | 0.6856 | 0.6833 | 0.6423 | 0.6052 | 0.5874 | 0.5698 |
| | *0.3* | 0.8605 | 0.7999 | 0.7731 | 0.7409 | 0.6744 | 0.6747 | 0.6093 | 0.6080 | 0.5627 | 0.5641 |
| | *0.2* | 0.8234 | 0.7491 | 0.7368 | 0.6950 | 0.6551 | 0.6370 | 0.6231 | 0.5672 | 0.5677 | 0.5361 |
| | *0.1* | 0.8255 | 0.7332 | 0.7161 | 0.6898 | 0.6345 | 0.6265 | 0.5977 | 0.5548 | 0.5552 | 0.5290 |

(a)

$\boxed{\sigma(s_{ij})}$

| $r_y$ \ $r_x$ | *1.0* | *0.9* | *0.8* | *0.7* | *0.6* | *0.5* | *0.4* | *0.3* | *0.2* | *0.1* |
|---|---|---|---|---|---|---|---|---|---|---|
| *1.0* | 1.0000 | 0.9773 | 0.7894 | 0.9984 | 1.0195 | 0.8271 | 0.8252 | 0.9487 | 0.7626 | 0.7128 |
| *0.9* | 1.1772 | 0.9638 | 0.8714 | 0.9202 | 0.8793 | 0.8753 | 0.8798 | 0.7462 | 0.7780 | 0.6670 |
| *0.8* | 1.0766 | 0.9053 | 0.7051 | 0.8686 | 0.7943 | 0.9349 | 0.5831 | 0.6456 | 0.6093 | 0.6356 |
| *0.7* | 1.0506 | 1.0094 | 1.0137 | 0.8884 | 0.7487 | 0.7961 | 0.6260 | 0.7008 | 0.7110 | 0.6383 |
| *0.6* | 0.8534 | 0.8277 | 0.8383 | 0.7692 | 0.7554 | 0.7554 | 0.6306 | 0.6991 | 0.6439 | 0.5835 |
| *0.5* | 0.9281 | 0.8727 | 0.7584 | 0.8685 | 0.8945 | 0.7790 | 0.8540 | 0.8201 | 0.7273 | 0.6109 |
| *0.4* | 1.0266 | 0.7761 | 0.8214 | 0.7686 | 0.7893 | 0.7270 | 0.7635 | 0.6527 | 0.6022 | 0.5956 |
| *0.3* | 1.0474 | 0.9116 | 0.7985 | 0.7823 | 0.6053 | 0.8193 | 0.6155 | 0.7399 | 0.5585 | 0.5668 |
| *0.2* | 0.8807 | 0.8048 | 0.7829 | 0.7438 | 0.6276 | 0.6633 | 0.7936 | 0.6742 | 0.6638 | 0.6000 |
| *0.1* | 0.8996 | 0.8820 | 0.8161 | 0.8172 | 0.7064 | 0.6345 | 0.7206 | 0.6647 | 0.7240 | 0.6899 |

(b)

$\boxed{\mu(\mu(z_{ij}))}$

| $r_y$ \ $r_x$ | *1.0* | *0.9* | *0.8* | *0.7* | *0.6* | *0.5* | *0.4* | *0.3* | *0.2* | *0.1* |
|---|---|---|---|---|---|---|---|---|---|---|
| *1.0* | 1.0000 | 0.9740 | 0.9327 | 0.9028 | 0.8710 | 0.8447 | 0.8119 | 0.8070 | 0.7864 | 0.7749 |
| *0.9* | 0.9817 | 0.9287 | 0.9023 | 0.8735 | 0.8320 | 0.8126 | 0.7782 | 0.7608 | 0.7442 | 0.7353 |
| *0.8* | 0.9482 | 0.9068 | 0.8681 | 0.8373 | 0.8039 | 0.7809 | 0.7508 | 0.7248 | 0.7079 | 0.7004 |
| *0.7* | 0.9246 | 0.8814 | 0.8465 | 0.8174 | 0.7699 | 0.7500 | 0.7208 | 0.6933 | 0.6843 | 0.6670 |
| *0.6* | 0.8846 | 0.8544 | 0.8126 | 0.7773 | 0.7453 | 0.7189 | 0.6878 | 0.6667 | 0.6467 | 0.6424 |
| *0.5* | 0.8510 | 0.8268 | 0.7861 | 0.7496 | 0.7240 | 0.6879 | 0.6644 | 0.6370 | 0.6243 | 0.6118 |
| *0.4* | 0.8542 | 0.7924 | 0.7657 | 0.7184 | 0.6930 | 0.6720 | 0.6354 | 0.6071 | 0.5865 | 0.5697 |
| *0.3* | 0.8378 | 0.7876 | 0.7612 | 0.7213 | 0.6755 | 0.6554 | 0.6135 | 0.5900 | 0.5643 | 0.5549 |
| *0.2* | 0.8126 | 0.7632 | 0.7354 | 0.6962 | 0.6575 | 0.6289 | 0.6062 | 0.5653 | 0.5530 | 0.5329 |
| *0.1* | 0.8088 | 0.7494 | 0.7170 | 0.6906 | 0.6449 | 0.6155 | 0.5873 | 0.5531 | 0.5413 | 0.5172 |

(c)

$\boxed{\sigma(\mu(z_{ij}))}$

| $r_y$ \ $r_x$ | *1.0* | *0.9* | *0.8* | *0.7* | *0.6* | *0.5* | *0.4* | *0.3* | *0.2* | *0.1* |
|---|---|---|---|---|---|---|---|---|---|---|
| *1.0* | 1.0000 | 0.9998 | 0.8469 | 0.9409 | 0.9015 | 0.8691 | 0.9077 | 0.8331 | 0.8906 | 0.8925 |
| *0.9* | 1.0290 | 0.9684 | 0.7922 | 0.8566 | 0.7914 | 0.8284 | 0.8495 | 0.7599 | 0.8379 | 0.8420 |
| *0.8* | 1.0285 | 0.9118 | 0.8258 | 0.8582 | 0.7783 | 0.8267 | 0.7019 | 0.7007 | 0.7504 | 0.7876 |
| *0.7* | 0.9241 | 0.9131 | 0.9166 | 0.8512 | 0.7612 | 0.7458 | 0.7123 | 0.7265 | 0.7861 | 0.7844 |
| *0.6* | 0.9830 | 0.8897 | 0.8278 | 0.6931 | 0.7288 | 0.7882 | 0.7028 | 0.6968 | 0.7300 | 0.7506 |
| *0.5* | 0.9891 | 0.9817 | 0.7976 | 0.7720 | 0.8001 | 0.7218 | 0.7600 | 0.7386 | 0.7329 | 0.7131 |
| *0.4* | 1.0478 | 0.8275 | 0.8022 | 0.7546 | 0.7731 | 0.6930 | 0.6875 | 0.6249 | 0.6975 | 0.7238 |
| *0.3* | 0.9820 | 0.8738 | 0.8755 | 0.7251 | 0.6961 | 0.6874 | 0.5638 | 0.6426 | 0.5881 | 0.5863 |
| *0.2* | 0.9251 | 0.7740 | 0.7667 | 0.7174 | 0.6943 | 0.6578 | 0.6800 | 0.5811 | 0.6519 | 0.6929 |
| *0.1* | 0.9230 | 0.8312 | 0.7762 | 0.7384 | 0.7160 | 0.7186 | 0.7152 | 0.6357 | 0.6987 | 0.7378 |

(d)

**Table 3.25** *Numerical values of cell and face perimeters.* (a) $\mu(s_{ij})/\mu(s_{11})$, (b) $\sigma(s_{ij})/\sigma(s_{11})$, (c) $\mu(\mu(z_{ij}))/\mu(\mu(z_{11}))$ *and* (d) $\sigma(\mu(s_{ij}))/\sigma(\mu(s_{11}))$.

Codes for finding volume, surface area, cell- and face perimeters can be found in § A.28. There only some of the printing commands have been left out.

The procedure in general follows Algorithm 3.3. The volume is the summation of all tetrahedral volumes obtained from the triangulation. The surface area is summed over all triangular faces of a convex hull. Plane parameters are then calculated for all of these faces, *viz.* $a = |1, y_i, z_i|$, $b = |x_i, 1, z_i|$, $c = |x_i, y_i, 1|$ and $d = |x_i, y_i, z_i|$, in order to group them together into polyhedral faces.

**Algorithm 3.3** *Volume, area and perimeter algorithms.*

$(v, v_c) \leftarrow$ Voronoi tessellation;
**exclude** boundary vertices;
**exclude** boundary cells;
**for** every cell **do**
  **find** its Delaunay triangulation;
  $V \leftarrow \sum |x_i, y_i, z_i, 1|/6$;
  **find** its convex hull;
  $A \leftarrow \sum (s(s-a)(s-b)(s-c))^{1/2}$;

**for** all facets of the convex hull **do**
  $(a, b, c, d) \leftarrow$ plane parameters;
  **group** hull facets into polyhedral faces;
  **for** all hull facets in every face **do**
    $\{v_f\} \leftarrow$ vertices of all coplanar facets;
    **find** convex hull of $v_f$;
    $\beta \leftarrow$ sum area of these hull segments;
    **count** number of occurrences of their edges;
    $\{e_f\} \leftarrow$ edges counted only once;
    $\{e_c\} \leftarrow e_f$;
    $z \leftarrow \sum(\sum(\Delta x_i)^2)^{1/2}$;
  **endfor**
**endfor**
$s \leftarrow (\sum z_i)/2$;
**endfor** □

The program `varea.m` was written long before `vareac.m`. It is listed after the latter in § A.28, although most of the variable names have been changed. The old names were long, for example `CubeNormalVolumePerInnerCell` which is now changed into `cbnafn`. The original program has not been published (Tiyapan, 2001, KNT8(i)).

Some of the past results are shown in Figure 3.49.

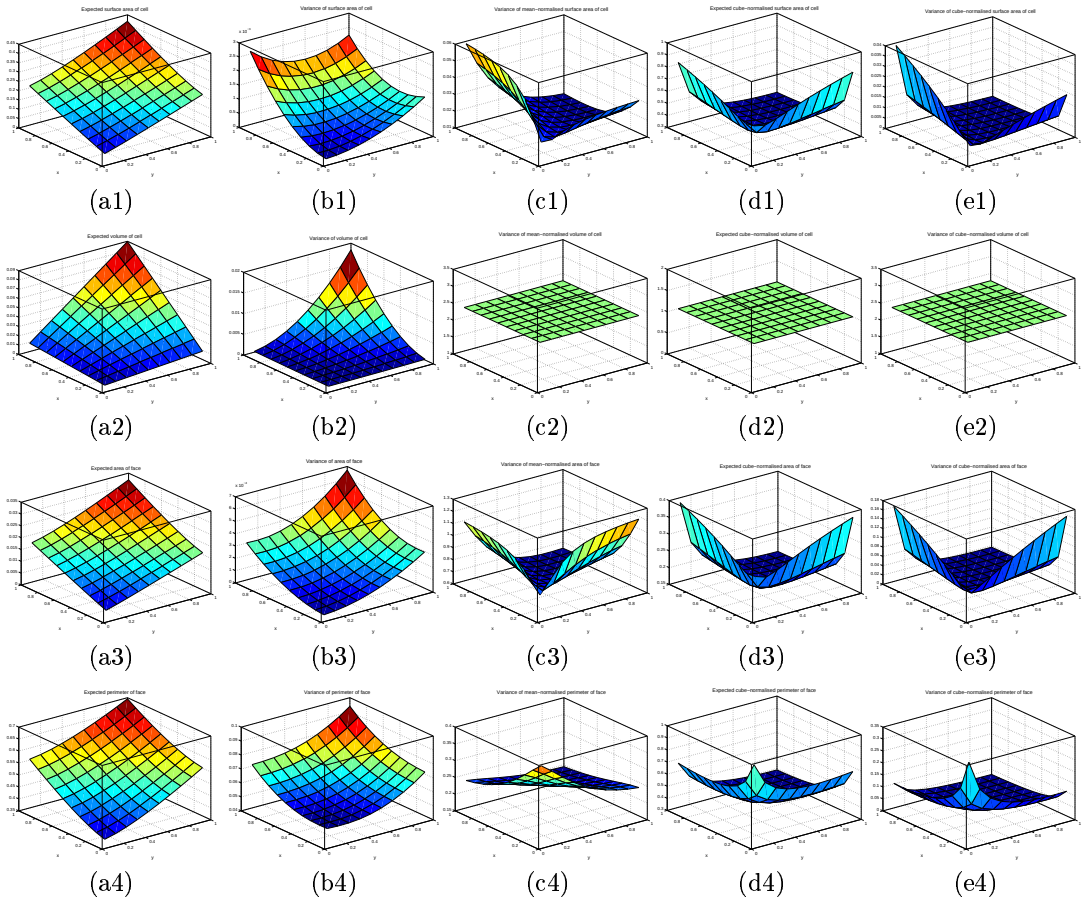


**Figure 3.49** *Past results of area, volume and perimeter.* (a), (b), (c), (d) *and* (e) *are respectively expected value, variance, variance of mean-normalised values, expected cube-normalised value and variance of the cube-normalised values, whereas* (1) *are values for surface area,* (2) *the volume of cell,* (3) *the area of face and* (4) *the perimeter of face.*

In addition, there is Table 3.26 lists the numerical statistics of the area and perimeter of face. Both this table and Figure 3.49 are from an unpublished work (Tiyapan, 2001, KNT8(i), *ibid.*).

| $\beta_{ij}$ | | | | | $r_x$ | | | | | |
|---|---|---|---|---|---|---|---|---|---|---|
| | *1.0* | *0.9* | *0.8* | *0.7* | *0.6* | *0.5* | *0.4* | *0.3* | *0.2* | *0.1* |
| *1.0* | 0.0322 | 0.0300 | 0.0278 | 0.0257 | 0.0237 | 0.0218 | 0.0200 | 0.0183 | 0.0169 | 0.0158 |
| *0.9* | 0.0301 | 0.0280 | 0.0259 | 0.0239 | 0.0219 | 0.0201 | 0.0183 | 0.0167 | 0.0153 | 0.0142 |
| *0.8* | 0.0280 | 0.0260 | 0.0240 | 0.0221 | 0.0202 | 0.0184 | 0.0167 | 0.0151 | 0.0138 | 0.0127 |
| *0.7* | 0.0261 | 0.0241 | 0.0222 | 0.0203 | 0.0185 | 0.0168 | 0.0151 | 0.0136 | 0.0122 | 0.0112 |
| *0.6* | 0.0242 | 0.0223 | 0.0204 | 0.0186 | 0.0169 | 0.0152 | 0.0136 | 0.0121 | 0.0107 | 0.0097 |
| $r_y$ *0.5* | 0.0224 | 0.0205 | 0.0188 | 0.0170 | 0.0153 | 0.0136 | 0.0120 | 0.0106 | 0.0092 | 0.0082 |
| *0.4* | 0.0206 | 0.0189 | 0.0172 | 0.0155 | 0.0138 | 0.0122 | 0.0106 | 0.0091 | 0.0078 | 0.0067 |
| *0.3* | 0.0191 | 0.0174 | 0.0157 | 0.0140 | 0.0124 | 0.0108 | 0.0092 | 0.0077 | 0.0064 | 0.0052 |
| *0.2* | 0.0177 | 0.0161 | 0.0144 | 0.0128 | 0.0112 | 0.0096 | 0.0080 | 0.0065 | 0.0051 | 0.0038 |
| *0.1* | 0.0166 | 0.0150 | 0.0134 | 0.0118 | 0.0102 | 0.0086 | 0.0070 | 0.0054 | 0.0039 | 0.0025 |

(a)

| $\sigma(\mu(z_{ij}))$ | | | | | $r_x$ | | | | | |
|---|---|---|---|---|---|---|---|---|---|---|
| | *1.0* | *0.9* | *0.8* | *0.7* | *0.6* | *0.5* | *0.4* | *0.3* | *0.2* | *0.1* |
| *1.0* | 0.6952 | 0.6728 | 0.6514 | 0.6313 | 0.6126 | 0.5956 | 0.5806 | 0.5679 | 0.5581 | 0.5516 |
| *0.9* | 0.6733 | 0.6504 | 0.6285 | 0.6079 | 0.5886 | 0.5711 | 0.5555 | 0.5423 | 0.5320 | 0.5251 |
| *0.8* | 0.6526 | 0.6291 | 0.6067 | 0.5855 | 0.5657 | 0.5475 | 0.5313 | 0.5175 | 0.5067 | 0.4995 |
| *0.7* | 0.6330 | 0.6090 | 0.5861 | 0.5643 | 0.5438 | 0.5251 | 0.5082 | 0.4938 | 0.4824 | 0.4747 |
| $\delta(y]$ *0.6* | 0.6147 | 0.5903 | 0.5668 | 0.5444 | 0.5234 | 0.5039 | 0.4865 | 0.4714 | 0.4593 | 0.4511 |
| *0.5* | 0.5981 | 0.5731 | 0.5491 | 0.5261 | 0.5045 | 0.4844 | 0.4662 | 0.4504 | 0.4377 | 0.4289 |
| *0.4* | 0.5832 | 0.5578 | 0.5332 | 0.5097 | 0.4875 | 0.4667 | 0.4478 | 0.4313 | 0.4178 | 0.4084 |
| *0.3* | 0.5706 | 0.5447 | 0.5196 | 0.4956 | 0.4727 | 0.4514 | 0.4318 | 0.4145 | 0.4002 | 0.3900 |
| *0.2* | 0.5605 | 0.5342 | 0.5087 | 0.4842 | 0.4608 | 0.4389 | 0.4186 | 0.4006 | 0.3856 | 0.3746 |
| *0.1* | 0.5537 | 0.5270 | 0.5012 | 0.4763 | 0.4525 | 0.4301 | 0.4094 | 0.3908 | 0.3750 | 0.3633 |

(a)

**Table 3.26** (a) *The area of face and* (b) *the perimeter of face.*

These much earlier results show in addition the face area statistics. Another set of codes to do the same job has been developed in the style presently used. It used to be `qhull` then, but now `voronoin` on Matlab is used instead. This is the reason why there are many programs listed in the appendix, from page 213 to page 304. It is a good practice to use more than one program for doing the same job, in order to cross check between the programs. As a program develops, the style and approach of the programs he writes also change. This is why it is difficult to leave out any certain piece of codes. What you see here are in fact merely snapshots that have survived from the continually changing virtual working ground.

The results for the face area of a VT under compressions are made up of $\mu(\mu(\beta_{ij}))$, $\sigma(\mu(\beta_{ij}))$, $\mu(\sigma(\beta_{ij}))$ and $\sigma(\sigma(\beta_{ij}))$. These are normalised respectively by $\mu(\mu(\beta_{11})) = 0.0065$, $\sigma(\mu(\beta_{11})) = 0.0018$, $\mu(\sigma(\beta_{11})) = 0.0065$ and $\sigma(\sigma(\beta_{11})) = 0.0029$, where $\beta_{ij}$ is the face area under a compression such that $r_x = i$ and $r_y = j$. These resusts are shown together as Figure 3.50.

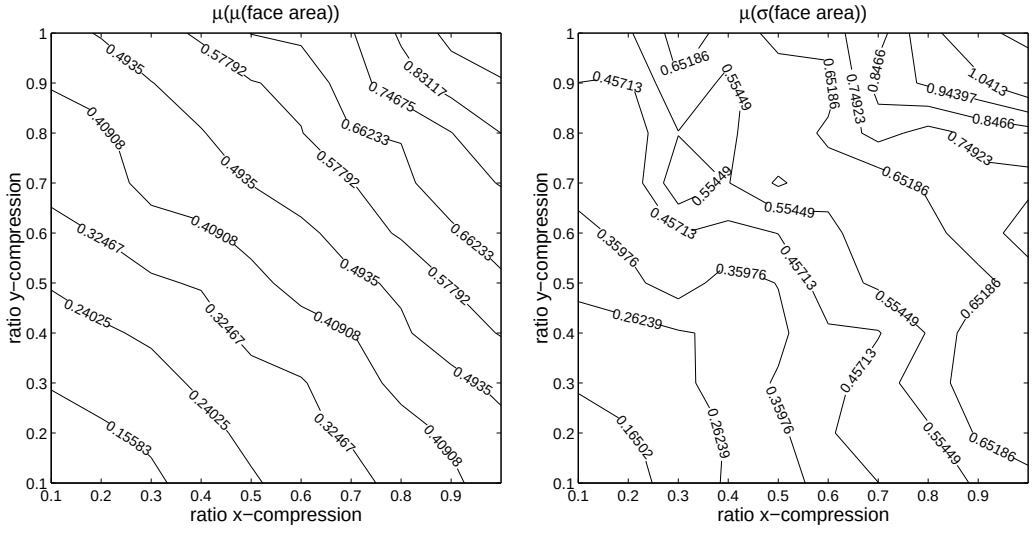


(a) (b)

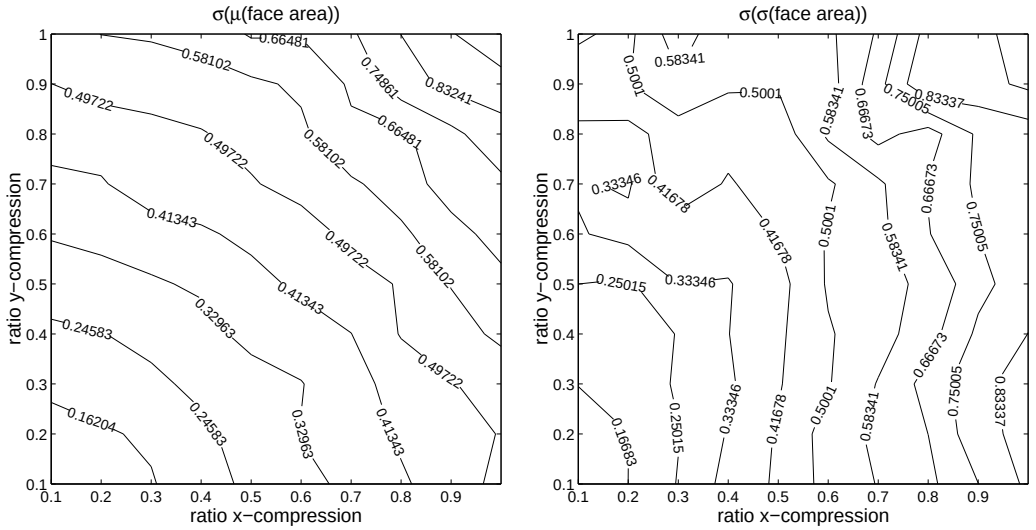


**Figure 3.50** *Statistics of face areas under compression;* (a) *the normalised mean of mean* $\mu(\mu(\beta_{ij}))/\mu(\mu(\beta_{11}))$, (b) *standard deviation of mean* $\sigma(\mu(\beta_{ij}))/\sigma(\mu(\beta_{11}))$, (c) *mean of standard deviation* $\mu(\sigma(\beta_{ij}))/\mu(\sigma(\beta_{11}))$ *and* (d) $\sigma(\sigma(\beta_{ij}))/\sigma(\sigma(\beta_{11}))$ *standard deviation of standard deviation.*

Table 3.27 has the normalised numerical values used for plotting these contours.

| $\beta_{ij}$ | $r_x$ | | | | | | | | | |
|---|---|---|---|---|---|---|---|---|---|---|
| | *1.0* | *0.9* | *0.8* | *0.7* | *0.6* | *0.5* | *0.4* | *0.3* | *0.2* | *0.1* |
| *1.0* | 1.0000 | 0.9427 | 0.8435 | 0.7402 | 0.6837 | 0.6645 | 0.5893 | 0.5488 | 0.5002 | 0.4608 |
| *0.9* | 0.9052 | 0.8674 | 0.7970 | 0.7112 | 0.5991 | 0.5730 | 0.5306 | 0.4914 | 0.4389 | 0.4155 |
| *0.8* | 0.8316 | 0.7443 | 0.6698 | 0.6590 | 0.5745 | 0.5346 | 0.4893 | 0.4592 | 0.3924 | 0.3679 |
| *0.7* | 0.7487 | 0.7311 | 0.6343 | 0.5752 | 0.5438 | 0.4958 | 0.4651 | 0.4474 | 0.3593 | 0.3512 |
| *0.6* | 0.7221 | 0.6408 | 0.5886 | 0.5331 | 0.4699 | 0.4371 | 0.3904 | 0.3614 | 0.3302 | 0.2965 |
| *0.5* | 0.6392 | 0.5815 | 0.5073 | 0.4759 | 0.4408 | 0.3837 | 0.3311 | 0.3157 | 0.2762 | 0.2468 |
| *0.4* | 0.5825 | 0.5418 | 0.4803 | 0.4062 | 0.3724 | 0.3489 | 0.2880 | 0.2522 | 0.2293 | 0.2007 |
| *0.3* | 0.5183 | 0.4655 | 0.4324 | 0.3713 | 0.3183 | 0.2948 | 0.2527 | 0.2132 | 0.1886 | 0.1624 |
| *0.2* | 0.4633 | 0.4208 | 0.3781 | 0.3317 | 0.3141 | 0.2619 | 0.2139 | 0.1702 | 0.1422 | 0.1151 |
| *0.1* | 0.4478 | 0.3951 | 0.3437 | 0.3059 | 0.2757 | 0.2296 | 0.1870 | 0.1410 | 0.1030 | 0.0714 |

(a)

| $\beta_{ij}$ | $r_x$ | | | | | | | | | |
|---|---|---|---|---|---|---|---|---|---|---|
| | *1.0* | *0.9* | *0.8* | *0.7* | *0.6* | *0.5* | *0.4* | *0.3* | *0.2* | *0.1* |
| *1.0* | 1.0000 | 1.0757 | 1.0285 | 0.8041 | 0.7212 | 0.6669 | 0.6257 | 0.6937 | 0.5409 | 0.5482 |
| *0.9* | 1.1387 | 1.0314 | 0.9593 | 0.8929 | 0.5949 | 0.6301 | 0.5234 | 0.6477 | 0.4421 | 0.4561 |
| *0.8* | 0.8035 | 0.7713 | 0.7159 | 0.7835 | 0.6792 | 0.5606 | 0.5531 | 0.5506 | 0.3955 | 0.4186 |
| *0.7* | 0.7238 | 0.7318 | 0.6668 | 0.5928 | 0.5840 | 0.6665 | 0.5509 | 0.6229 | 0.3910 | 0.3941 |
| *0.6* | 0.7988 | 0.6993 | 0.6248 | 0.6091 | 0.5329 | 0.4589 | 0.4261 | 0.4609 | 0.3835 | 0.3318 |
| *0.5* | 0.6963 | 0.6241 | 0.5705 | 0.5704 | 0.5172 | 0.3629 | 0.3178 | 0.4090 | 0.3335 | 0.2881 |
| *0.4* | 0.6974 | 0.7181 | 0.5614 | 0.4507 | 0.4437 | 0.3370 | 0.2802 | 0.2536 | 0.2256 | 0.2190 |
| *0.3* | 0.7246 | 0.6884 | 0.6228 | 0.5051 | 0.4242 | 0.3712 | 0.3013 | 0.2415 | 0.2232 | 0.1792 |
| *0.2* | 0.6779 | 0.6656 | 0.5349 | 0.4740 | 0.4543 | 0.3349 | 0.2668 | 0.2204 | 0.1519 | 0.1118 |
| *0.1* | 0.6377 | 0.5708 | 0.4823 | 0.4569 | 0.3863 | 0.3285 | 0.2744 | 0.1997 | 0.1332 | 0.0677 |

(a)

| $\beta_{ij}$ | $r_x$ | | | | | | | | | |
|---|---|---|---|---|---|---|---|---|---|---|
| | *1.0* | *0.9* | *0.8* | *0.7* | *0.6* | *0.5* | *0.4* | *0.3* | *0.2* | *0.1* |
| *1.0* | 1.0000 | 0.9084 | 0.8333 | 0.7368 | 0.6714 | 0.6736 | 0.6061 | 0.5907 | 0.5819 | 0.5499 |
| *0.9* | 0.8728 | 0.8531 | 0.7962 | 0.6763 | 0.5947 | 0.5654 | 0.5499 | 0.5301 | 0.5263 | 0.4965 |
| *0.8* | 0.8034 | 0.7278 | 0.6479 | 0.6501 | 0.5653 | 0.5264 | 0.4911 | 0.4755 | 0.4539 | 0.4318 |
| *0.7* | 0.7317 | 0.7075 | 0.6189 | 0.5687 | 0.5301 | 0.4897 | 0.4648 | 0.4613 | 0.4055 | 0.4026 |
| *0.6* | 0.6995 | 0.6318 | 0.5663 | 0.5195 | 0.4533 | 0.4326 | 0.4019 | 0.3749 | 0.3567 | 0.3367 |
| *0.5* | 0.6402 | 0.5842 | 0.5038 | 0.4658 | 0.4286 | 0.3875 | 0.3421 | 0.3191 | 0.2929 | 0.2841 |
| *0.4* | 0.5954 | 0.5522 | 0.5028 | 0.4123 | 0.3740 | 0.3565 | 0.2989 | 0.2651 | 0.2437 | 0.2298 |
| *0.3* | 0.5370 | 0.4913 | 0.4437 | 0.3856 | 0.3260 | 0.2916 | 0.2620 | 0.2316 | 0.2010 | 0.1837 |
| *0.2* | 0.5022 | 0.4578 | 0.4273 | 0.3598 | 0.3321 | 0.2795 | 0.2300 | 0.1747 | 0.1520 | 0.1252 |
| *0.1* | 0.5170 | 0.4616 | 0.4006 | 0.3424 | 0.3132 | 0.2611 | 0.2164 | 0.1553 | 0.1106 | 0.0782 |

(a)

| $\beta_{ij}$ | $r_x$ | | | | | | | | | |
|---|---|---|---|---|---|---|---|---|---|---|
| | *1.0* | *0.9* | *0.8* | *0.7* | *0.6* | *0.5* | *0.4* | *0.3* | *0.2* | *0.1* |
| *1.0* | 1.0000 | 0.8684 | 0.8660 | 0.6771 | 0.5656 | 0.5652 | 0.5111 | 0.6327 | 0.4786 | 0.5118 |
| *0.9* | 0.9335 | 0.8894 | 0.9131 | 0.7232 | 0.5467 | 0.5089 | 0.5093 | 0.5697 | 0.4969 | 0.4564 |
| *0.8* | 0.7918 | 0.7649 | 0.6294 | 0.6942 | 0.5991 | 0.4490 | 0.4575 | 0.4608 | 0.3869 | 0.4027 |
| *0.7* | 0.7996 | 0.7652 | 0.6721 | 0.5689 | 0.4886 | 0.4718 | 0.4056 | 0.4858 | 0.3228 | 0.3420 |
| *0.6* | 0.8140 | 0.7501 | 0.6625 | 0.5617 | 0.5076 | 0.4206 | 0.3724 | 0.3551 | 0.3605 | 0.3261 |
| *0.5* | 0.7978 | 0.7256 | 0.5948 | 0.5663 | 0.5091 | 0.3878 | 0.3282 | 0.3337 | 0.2370 | 0.2504 |
| *0.4* | 0.8344 | 0.7665 | 0.6332 | 0.5491 | 0.4925 | 0.4023 | 0.3317 | 0.2549 | 0.1905 | 0.2046 |
| *0.3* | 0.8675 | 0.8142 | 0.6973 | 0.5885 | 0.4942 | 0.4097 | 0.3201 | 0.2617 | 0.1907 | 0.1702 |
| *0.2* | 0.8592 | 0.8078 | 0.6670 | 0.6029 | 0.5355 | 0.4258 | 0.3402 | 0.2465 | 0.1663 | 0.1066 |
| *0.1* | 0.8505 | 0.7491 | 0.6472 | 0.5872 | 0.5286 | 0.4294 | 0.3623 | 0.2548 | 0.1670 | 0.0835 |

**Table 3.27** *The numerical values of face area.*

## § 3.13 Voronoi tessellation in higher dimensions

In § 3.13 it is mentioned that the volume of a tetrahedron is $|x_i, y_i, z_i, 1|/6$, for which the absolute value must be taken before adding two or more together. This is what to be found in the existing literature. But I think that this definition is flawed because, for one thing, it does not work for the case of two dimensions. Imagine what happens if we let a unit cube to always have a unit volume. It works as shown in the following. What I discovered here could well be new.

**Assumption 3.4.** *A unit cube has a unit volume in all dimensions $d$, $d \geq 2$.*

But, apart from the fact that it does not work for the case of two dimensions, the volume equation above still appeals to our commonsense, because it looks symmetrical, so we assume further.

**Assumption 3.4.** *The equation for volume of a $d$-simplex is $V = \text{abs}(|x_{ij}, 1|)/k$, where $x_{ij}$, $1 \leq j \leq d$, is the $j$:th coordinate of the $i^{\text{th}}$ point, $1 \leq i \leq d+1$, and 1 is a unit vector of $(d+1)$ dimensions.*

Under Assumption's 3.4 and 3.4, and by trial and error, a conclusion is found that the volume of a general $d$-simplex must be such that the $k$ Assumption 3.4 is $d!$. Therefore we arrive at Definition 3.1. I actually tried $d(d-1)$ and $2^d - 2$ before looking at $d!$ and realised that this is the solution for $k$.

**Definition 3.4.** *The volume of a $d$-simplex is* $\text{abs}(|x_{ij}, 1|)/d!$, *where $x_{ij}$ is the $j^{\text{th}}$ coordinate of the $i^{\text{th}}$ vertex of the simplex.*

We can only test the appropriateness of our definition, *i.e.* Definition 3.4, against the cases of two and three dimensions, since four dimensions and above are unfamiliar grounds. But for cubes or hypercubes of two dimensions and above, the fit looks encouraging, as can be seen in Table 3.28.

| | | $d$ | | | | | | | | |
|---|---|---|---|---|---|---|---|---|---|---|
| | | *2* | *3* | *4* | *5* | *6* | *7* | *8* | *9* | *10* |
| | *1* | 1 | 1 | 1 | 1 | 1 | 1 | (1) | (1) | (1) |
| $\ell$ | *2* | 4 | 8 | 16 | 32 | 64 | 128 | ($2^8 = 256$) | ($2^9 = 512$) | ($2^{10} = 1{,}024$) |
| | *3* | 9 | 27 | 81 | 243 | 729 | 2,187 | ($3^8 = 6{,}561$) | ($3^9 = 19{,}683$) | ($3^{10} = 59{,}049$) |

**Table 3.28** *Volume of $d$-hypercubes whose dimension is $\ell$. Values in brackets are implied not calculated.*

The above is, to put it in other words, our attempt at defining the equation for the volume of $d$-simplices and the test of this equation against squares, cubes and $d$-hypercubes. The equation of Definition 3.4 is also rather appealing for the reason that it allows us to calculate the volume of the cube as $V = \text{abs}(|x_{ij}, 1|)/d! = \ell^d = \prod(\Delta x_i)$, where $\ell$ is the length of the side of the hypercube and the product is over all coordinates $x_i$.

Table 3.28 justifies our intuitive equation regarding the volume of hypercubes which says that such volume is $V = \ell^d$.

The program used in doing the simulations is shown in § A.29. There is also the code for testing the formula, which automates the generation of vertices of hypercubes before calculating their volume.

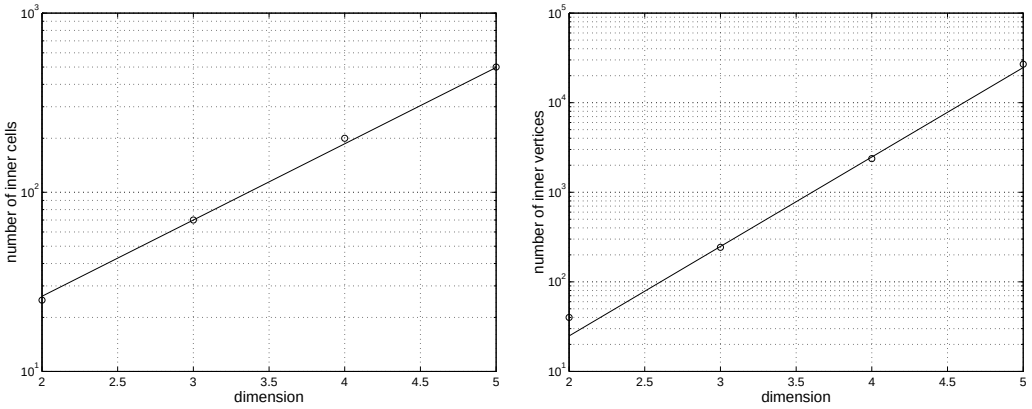


(a) (b)

**Figure 3.51** *Number of generators required for ten inner cells. The dotted line in* (a) *has the equation* $y = 3.7\exp(0.98x)$ *while for* (b) $y = 0.25\exp(2.3x)$.

The general procedure is to generate the Voronoi cells, exclude boundary vertices, and then boundary cells (compare Algorithm 3.3, page 104). This means that producing ten usable cells, that is to say, cells in the inner reach, requires for each dimension approximately the number of generators plotted in Figure 3.51 (a). Figure 3.51 (b) is the corresponding number of vertices.

For a Voronoi cell in $d$ dimensions we may draw a box around them such that the walls of the box are all parallel to the coordinate planes. For the plane, a Voronoi graph consumes some 60 per cent such binding rectangle. For higher dimensions, this ratio goes down from 0.6 to 0.33, 0.15 and 0.6 respectively for 3, 4 and 5 dimensions. The trend for the standard deviations is also similar to this. Both the mean and the standard deviation decrease with dimension, but their curves seemed difficult to define if we try to plot it on a semilog graph. The curve turns out to be parabola, as shown in Figure 3.52.

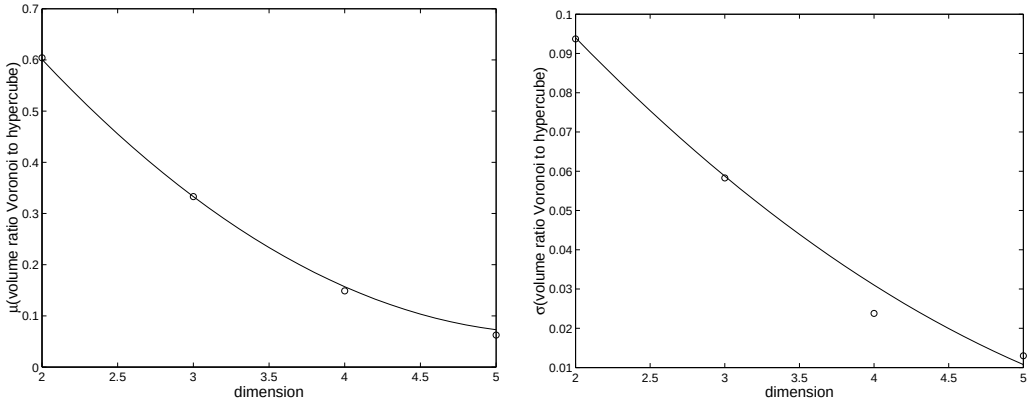


(a) (b)

**Figure 3.52** *Mean and standard deviation of the ratio Voronoi per defining cube. Both graphs fit well with the parabolic equation* $y = ax^2 + bx + c$; (a) *has* $a = 0.046$, $b = -0.498$ *and* $c = 1.413$, *while* (b) *has* $a = 0.00375$, $b = -.054$ *and* $c = 0.187$.

Additional results on a 6-dimensional VT generated from 1,200 generators are $\mu(V_p/V_h) = 0.0252$ and $\sigma(V_p/V_h) = 8.5 \times 10^{-4}$. The results are shown in Table 3.29.

| $n_g$ | $c_{in}$ | $d$ | $\mu(V_p/V_h)$ | $\sigma(V_p/V_h)$ | $V_{in}$ |
|---|---|---|---|---|---|
| 25 | 10 | 2 | 0.6041 | 0.0937 | 33 |
| 30 | 16 | 2 | 0.6034 | 0.0769 | 44 |
| 70 | 13 | 3 | 0.3331 | 0.0583 | 241 |
| 200 | 11 | 4 | 0.1488 | 0.0238 | 2,374 |
| 500 | 9 | 5 | 0.0638 | 0.0098 | |
| 500 | 11 | 5 | 0.0625 | 0.0130 | 26,893 |
| 1,200 | 4 | 6 | 0.0252 | $8.5 \times 10^{-4}$ | 306,710 |

**Table 3.29** *Voronoi volume in higher dimensions; $V_p$ is the Volume of the polytope, $V_h$ that of the hypercube and $n_g$ number of the generators.*

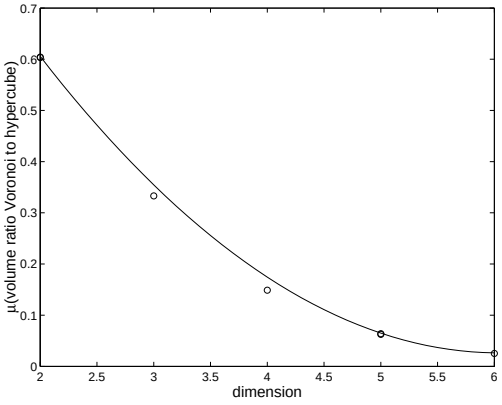


The accompanying curve plotted in Figure 3.53 is a parabola $y = 0.0354x^2 - 0.428x + 1.32$. On the other hand, neither the mean value nor the standard deviation of the volume ratio can possibly follow a parabolic curve, for the obvious reason that both decrease monotonically towards zero.

**Figure 3.53** The ratio $V_p/V_h$, dimension from 1 to 6.

## § 4. Percolation

The 1970's and the 1980's saw a proliferation of variations on the theme of percolation. Every year there seemed to be a new percolation problem or two. For a *Bethe lattice* Chalupa *et al* (1979) reported a *bootstrap percolation* where those randomly occupied sites with less than $m$ occupied neighbours are recursively emptied one by one until a stable configuration is reached. The problem they are interested in is that where the impurity concentration, dilution and crystal-field interaction compete in magnetic materials compete against the exchange interaction, resulting in the magnetic moments and consequently the magnetic order being destroyed.

Wilkinson and Willemsen (1983) introduced *invasion percolation*. Working with Schlumberger they were interested in the real problem in the oil industry where water displaces oil via capillary action. Their approach was that of a constant flow rate, not one of a constant pressure as usual. Here water displaces oil in the smallest available pores. But when water completely surrounds any region of oil, no further advance into that region will be possible, oil being incompressible. Such regions are called *trappings* and cause a problem generally known by the name of *residual oil*, an economic bane for oil industry.

In the above example the hydrophobic versus hydrophilic propertyplays an important role in the replacement of oil in pores with water. And water is prevented from penetrating trapped oil regions by much the same principle as that which prevents the water in the contents of a sandwich from crossing the spread layer of butter to wet the hydrophilic bread. For this latter case the pores in question are those within the bread texture, and the soaking of the bread is best prevented provided that the trapped regions of butter or margarine percolates in two dimensions to form a single layer or film which entirely covers the sectioning surface of the bread. Moreover, there is a similarity also in the internal structure of both the rock and the bread. The density of pores in bread is not homogeneous as a result of the tension on the surface of the dough caused by internal air pressure originated from the yeasts inside, as well as because of the heat applied to it when inside the oven, which dehydrolises the surface and makes it dry and hardened. The same inhomogeneity can be found inside the rocks which form the oil reservoirs where the regions of oil are surrounded by rocks which are less porous and have less permeability.

For Adler and Aharony (1988) a random walker, aka ant, treads on clusters. The ant enlarges a cluster by stepping on to an empty site next to it which meets certain conditions. They called this problem *diffusion percolation*. An example of a condition met is where the empty site has two or more occupied neighbours on a square lattice.

Most percolation in studies happens by randomly toggling the phases of sites or bonds in regular lattices. Kerstein (1983) considered randomly located spheres, take the complementary region of their union, and then perform percolation on the former. He showed that such percolation problem is equivalent to a percolation on a Voronoi lattice whose sites are the sphere centres.

In the same way as an infinite loop in computer science means that one can not come to the termination of a program going along the time dimension, an infinite cluster in percolation means that one can not come to the end of a cluster shifting along either one of the dimensions. The former case is along the one dimension of time and is only possible because of the time flows in one direction. Therefore half the line spanned is considered as being infinite. In one nondirectional dimension, except for the trivial case where one can consider the entire space as being one single cluster, no infinite cluster is possible. In simulation, when a cluster spans the whole of the space considered along any dimension we say that it is infinite since as one moves a cross section along that dimension, it always contains a section of the cluster.

The bond percolation program of two-dimensional Voronoi network by Tiyapan (1995, KNT3(iii), p. 78) takes $\mathrm{O}(n^2)$ time provided we assume that the contribution made by the number of clusters together with the that by each cluster comparison amount to a linear time complexity term. In order to justify this assumption, consider first the number of clusters. The maximum number of clusters possible depends on the size of the system, in other words it must vary as $n_1^k$, where $0 < k_1 < 1$. This maximum value should be approximately 0.5 because of symmetry between occupancy and void clusters. Next consider the time involved in comparing two clusters. On Matlab this is a sparse vector comparison which is likely to involves some linked lists, and similarly should take time as a function of $n_2^k$, $0 < k_2 < 1$. Because on average the size of clusters is always small before Pc, $k_2$ will be less than 0.5. Therefore $n_1^k \cdot n_2^k < n$ and it is safe to assume $\mathrm{O}(n)$ time from both of them combined. *q.e.d.*. A C translation (Tiyapan 1995, *ibid.*, p. 80) of this program, though not as bad

as it may seem because constant coefficients are small, gives $O(n^5)$ time in comparison.

In the field of geology Miller *et al* (2000) studies the analogy between the dilatant slip in earthquakes and the hydrofraction occurred in melting and dehydration, the percolation of the latter in the permeability network internal to the fault being the cause of the former. According to them, the existence of toggle switches in the permeability rules out the assumption that the permeability throughout the whole system is homogeneous. Instead, the system reorganises itself into sytems of different scales of interaction according to the degree and nature of its inhomogeneity. At the critical state the scale of interaction is equal to the scale of the model.

The percolation probabilities given by Stauffer and Aharony (1994) are, the first number being for sites and the second for bonds, for the honey comb lattice 0.6962, 0.65271; square 0.592746, 0.50000; triangular 0.50000, 0.34729; diamond 0.43, 0.388; simple cubic 0.3116, 0.2488; body-centred cubic 0.246, 0.1803; face-centred cubic 0.198, 0.119; 4-d hypercubic 0.197, 0.1601; 5-d hypercubic 0.141, 0.1182; 6-d hypercubic 0.107, 0.0942; 7-d hypercubic 0.089, 0.0787.

De Gennes *et al* (1959) investigated disordered binary solid solution AB where active atoms A are randomly replace the nodes of the periodic matrix B. There exists a critical concentration A in B below which all clusters are finite, and above which both finite and non-finite, *i.e.* infinite, clusters exist. Such solid solution in networks can represent the spin waves in alloys with one ferromagnetic component or the impurity bands in semiconductors. They cited seminal work on percolation by Broadbent *et al* (1957), but no mention was made about the Ising model.

In a way, percolation is similar to diffusion. In diffusion the particles considered move about randomly, whereas in percolation they can only crop up randomly at predetermined locations on a network which is fixed. We could imagine, for instance, cars running along the roads within a traffic network as diffusing through them. Then the percolation could occur on a larger scale, that is the scale of a road. The cars move along, that means they diffuse; but the roads remain fixed, and so their phases could percolate. In other words, in diffusion the particles move while in percolation, whether there are moving particles or not, it is the phases that percolate. Since historically percolation began as the study of diffusion of particles in a network of tubes in which the phases are naturally defined as the tubes being blocked or unblocked, these definitions have become most frequently used in other areas of application, for example in filtering membranes and traffic networks.

But this is not necessarily the case. Instead of dealing with a fixed network, one may consider a model of percolation in a continuum, for example by randomly patching an area until all the patches connect with one another somehow and percolate. The patch could be of any shape, as well as polygonal and circular. We can consider the percolation in a certain area as having occurred when there appears a cluster of patches which traverses any two opposite sides. One application of this is in the study of occurrences of epidemics. Hoyle and Wickramasinghe (1979), having given a convincing argument in favour of viruses and various forms of diseases being carried to Earth from space by comets, talk about patchiness of pathogenic clouds. According to them, simultaneous attacks across vast region rules out person-to-person theory. Moreover, influenza epidemics are generally characterised by sudden onsets and equally sudden ends. These epidemics and plagues may be thought of as the percolation of these patches in a sufficiently large, predefined area. The bacteria and viruses coming from space adding to gene give the possibility of jump patterns in evolution (*cf* Smith and Szathmáry, 1995). The cells deliberately refuse to block viruses because they could prove to be useful in the long run, generally not by individuals but by the species. Historical examples are the disease described by Thucydides between 431 and 404 BC, five epidemics of 'English Sweats' between 1485 and 1552, and more than ten influenza pandemic from 1700 to 1900. Example of diseases which are caused by bacteria and viruses are bubonic plague, chicken pox (varicella), cholera, common cold, Legionnaires' disease, leprosy, measles, mumps, poliomyelitis, small pox, tuberculosis, and trachoma. Examples of major evolutionary transitions are those going from RNA to DNA, from prokaryotes to eukaryotes, and from asexual cloning to sexual propagation. Another example is the transition from primate to human both of whom differ from each other neurologically in the ability to use language and the power to conceptualise. One description of the Great Plague in London (Dickens, 1851). There was a rumour that a few people died in the winter of 1664. In May 1665 the disease burst out in St. Giles's which raged through July and September in every part of England; approximately 10,000 people died in London alone. But then the equinox winds virtually blew the disease away, and the Plague quickly disappeared. The existence of interstellar organic matters is supported by strong evidences with more and more complex substances constantly found (*cf* Hoyle and Wickramasinghe, 1978).

Gas turns into liquid by the growth of larger and larger clusters. But unlike percolation in

networks, clusters in condensation process are not well defined. Crystalisation is also characterised by the growth of one phase within another. But here the orientations are an inherent part of the clusters themselves, and there is a long range coordination among clusters. One important thing in percolation is for the system size to be infinite. Random discs overlapping one another in a continuum helps correct counts of bacteria cultures (*cf* Essam, 1980). Let $p_c$ be the critical probability and $P(p)$ the percolation probability. Then as $p$ approaches $p_c$ from above, $P(p) \approx (p - p_c)^{\beta}$ where $0.4 < \beta < 0.5$ is the critical exponent. If $p$ approaches $p_c$ from below, $S(p) \approx (p_c - p)^{-\gamma}$ and $\xi(p) \approx (p_c - p)^{-\nu}$ where $S(p)$ is the conditional average $\langle s|F\rangle$, $s$ the number of particles in a cluster, and $F$ the event that the origin $O$ is occupied and belongs to a finite cluster. In other words, $S(p)$ is the mean size of cluster at the origin given that $F$ occurs. This last event occurs with probability $p_F = p(1 - P(p))$ and $p_F = p$ for $p < p_c$. Furthermore, $S(p) = p_F^{-1} \sum_r C(r,p)$ and $\xi^2(p) = [p_F S(p)]^{-1} \sum_r r^2 C(r,p)$ where the pair-connectedness function is $C(r,p) = \langle \eta(r)|F\rangle p_F$, and $\eta(r)$ is the indicator defined to be one if $r$ is connected to $O$ and zero otherwise. When $F$ occurs, $s = \sum_r \eta(r)$. There are two different definitions of the critical probability, $p_c = \sup\{p|P(p) = 0\}$ and $\pi_c = \sup\{p|P(p) = 0 \text{ and } S(p) < \infty\}$, sometimes denoted by $p_H$ and $p_T$ for Hammersley and Temperley respectively. By definition, $\pi_c \leq p_c$. When $p$ approaches $p_c$ from above, $\gamma'$ and $\nu'$ are similarly defined respectively by $S(p) \approx (p - p_c)^{\gamma'}$ and $\xi(p) \approx (p - p_c)^{\nu'}$ It is generally assumed as $\gamma' = \gamma$ and $\nu' = \nu$. No proofs for these assumptions exist, even though they are consistent with the series expansions. Estimates of $\gamma$ and $\nu$ are $1.6 < \gamma < 1.7$ and $0.8 < \nu < 0.9$. In a dilute ferromagnet a cluster containing $s$ spins each of which has a unit magnetic moment has a probability $p = \exp(\frac{1}{2}sh)/\left[\exp(-\frac{1}{2}sh) + \exp(\frac{1}{2}sh)\right]$ of being parallel to the magnetic field $H > 0$. Here $h = 2H/k_BT$ where $k_BT$ is the thermal energy. For an infinite cluster, $p = 1$. The zero-field magnetic moment is $\mu_0(p) \propto P(p)$. The zero-field magnetic moment is $\mu_0(p) \propto P(p) \sim (p - p_c)^{\beta}$. The field dependent magnetic moment at $p_c$ is $\langle (1 - \exp(-sh))/(1 + \exp(-sh))\rangle_F$ and $\frac{1}{2}(1 - G(p_c,h)) \leq \mu_c(h) \leq 1 - G(p_c,h)$ where $G(p,h) = \langle \exp(-sh)\rangle_F$. Therefore the critical probability $\delta$ is defined by $\mu_c(h) \sim 1 - G(p_c,h)h^{1/\delta}$. The correlation function between $\sigma$ on site $i$ and $j$ is defined by $\Gamma_{ij} = \langle \sigma_i\sigma_j\rangle_T - \langle \sigma_i\rangle_T\langle \sigma_j\rangle_T$ where $\langle\cdot\rangle_T$ is an average over spin states. Then $\Gamma_{ij} = 1$ when $i$ and $j$ belong to the same cluster and zero otherwise. The fluctuation formula is $k_BT\langle\chi\rangle = \sum_j \langle \Gamma_{ij}\rangle$ where $\langle \Gamma_{ij}\rangle = C(r_j - r_i, p)$, the mean susceptibility is $\langle\chi\rangle = p_F S(p)/k_BT \sim (p_c - p)^{-\gamma}$ and the mean free energy is $\langle F\rangle = (k_BT \ln 2)K(p)$ where $K(p)$ is the mean number of clusters and $K(p) \sim (p_c - p)^{2-\alpha}$, where the index assigned to the third derivative divergence is $1 + \alpha$, $\alpha \approx -0.5$.

The growth mechanism of clusters in percolation is all so found in biology. Williams and Bjerknes (1972) simulate a tumour in the basal layer of an epithelium. The basal cells become less sensitive to Charlone which controls cellular division, and thus they divide $\kappa$ times faster than the normal cells where $\kappa > 1$ is the carcinogenic advantage. Abnormal cells interior to the basal layer divide, push, and then replace the neighbouring cells leaving the overall configuration unchanged except at the border where the abnormal cells exert a thrust of $\kappa - 1$ on their normal neighbours, that is $\frac{dN}{dt} = (\kappa - 1)n$ where $n$ and $N$ are respectively the numbers of peripheral and total abnormal cells. They found that dimensionality of fractal is involved and the dimension 1.1, instead of 1, must be assigned to the periphery, which means that $n$ is proportional to $N^{0.55}$ not $N^{0.5}$. They found that abnormal cells push out faster in this order: the triangular, square, and hexagonal lattice. We may explain this, by looking at the coordination numbers of these three lattices, that the higher coordination number the lattice sites have, the slower the cluster expands. Added coordination means a higher degree-of-freedom the newly divided cells have to move about while still remaining local.

Percolation is a field full of far more open questions than discovered answers. This is one of the reasons it is more suitable to research than university examinations (*cf* Stauffer and Aharony, 1998). The fascination not so well hidden within the field is reflected in the number of research monographs written on this field that is close to percolating, which makes it impossible to give a full list of references. Percolation deals with the clusters formed by randomly occupying the each site of a very large lattice with probability $p$ independent of its neighbours. Most of the studies to date concentrate on the critical phenomena, which exist in a very narrow range in each problem, and the scaling theory which tries to describe them. The contiguity criteria are easier to define in applications in physics and physical sciences, because here problems can be described by, or easily simplified into some definite geometry, whereas in other applications this may not be the case. For example, in economic modelling the nature of the geometry or even the number of dimensions of such structure is still not well understood (*cf* Tiyapan, 1997, KNT5(vii) and KNT5(viii)), let alone the problem of contiguousness. Traffic network (*cf* Tiyapan, 1997, KNT5(i) and KNT5(ix)) is another example. Here

the flow is along channels within tubes, *i.e.* roads, both of which could be directed, which make the network a pool of tangled threads not only difficult to imagine but also to define such things as congestion and contiguousness. Even in geographical problems like that of forest fire, the spread of fire may be defined in at least three ways, namely by next-nearest neighbour, neighbour or double neighbour respectively in cases of a common corner, a common side or two neighbours. Reservoirs occur when the petroleum, formed in sedimentary rocks, migrates into permeable sedimentary rocks like sandstone. Around 70% of North Sea oil fields also date from the Jurassic period. These include Beatrice, Brent, Cormorant, Murchison and Tartan. Oil companies want to exploit reservoirs where $p > p_c$. Moreover, they want to tap into the largest cluster in these reservoirs. For this purpose bore hole samplings are carried out which collected within $L \times L$ frames and then the number of points, $m(L)$, belonging to the same cluster counted. It turns out that $m(L)$ is proportional to $L^{1.9}$. In general $m \propto L^d$ where $d$ is either integral, in which case it is the Euclidean dimension, or nonintegral, in which case it is the fractal dimension introduced by Benoit Mandelbrot. There exists a correlation length $\xi$ such that $m(L) \propto L^{1.9}$ for $L < \xi$, and $m(L) \propto L^2$ for $L > \xi$. This correlation length is a measure of the largest hole of the largest cluster and decreases as $p$ is increased above $p_c$.

One way of finding the percolation threshold is by using the *ant in a labyrinth* algorithm shown here as Algorithm 4.1.

**Algorithm 4.1** *Ant in a labyrinth. At $p_c$, $k = 1/3$, whereas $k = 0$ for a constant distance, and $k = 1/2$ for normal diffusion.*

**for** various $p$ **do**
  **repeat** a large amount of times
    **occupy** the sites with probability $p$;
    $sum \leftarrow 0$;
    **for** a large number of simulations $n$ **do**
      **for** various $t$ up to a large number **do**
        $sumr \leftarrow 0$;
        **for** $i = 1$ to $t$
          ant randomly occupies an occupied site;
          identify neighbours;
          move into an occupied neighbour randomly chosen;
          $r \leftarrow$ distance traveled;
          $sumr \leftarrow sumr + r$;
        **endfor**
        $sumrsq \leftarrow sumr^2$;
      **endfor**
    **endfor**
    $sum \leftarrow sum + sumrsq$;
    $R \leftarrow sum^{1/2}$;
    **plot** $R$ against $t$ in double logarithmic scales;
  **endrepeat**
  $k \leftarrow$ the slope of the straight line just plotted;
endfor
$p_c \leftarrow$ the $p$ such that $k = 1/3$;) □

Also, the number of steps the ant takes, $t$, for the linear size of a region it visited, $R$, is fractal, that is $t \propto R^{1/k}$. They give several percolation probabilities for selected lattices, which are shown in Table 4.1, as well as the exact values of $p_c$'s, which are for the square bond percolation $1/2$, triangular site $1/2$, triangular bond $2\sin(\pi/18)$, and honeycomb bond $1 - 2\sin(\pi/18)$. For the honeycomb site percolation, $p_c < 1/\sqrt{2}$. Site percolation on hypercubic lattices of high dimensions have $p_c = 1/(2d - 1)$.

| *lattice* | *site* | *bond* |
|---|---|---|
| honeycomb | 0.6962 | 0.65271 |
| square | 0.592746 | 0.50000 |
| triangular | 0.500000 | 0.34729 |
| diamond | 0.43 | 0.388 |
| simple cubic | 0.3116 | 0.2488 |
| body-centred cubic | 0.246 | 0.1803 |
| face-centred cubic | 0.198 | 0.119 |
| 4-d hypercubic | 0.197 | 0.1601 |
| 5-d hypercubic | 0.141 | 0.1182 |
| 6-d hypercubic | 0.107 | 0.0942 |
| 7-d hypercubic | 0.089 | 0.0787 |

**Table 4.1** *Percolation thresholds from Stauffer and Aharony (1998)*

There is no percolation in one dimension because in such case the percolating cluster must necessarily contain the whole space. But there are some applications where the critical blockage is important, for example the blockage of drainage grilles by pea shingle is one-dimensional. Here the critical amount of blockage depends on the critical rate of flow which in turn depends on the amount of water and the rate of accumulation of water to be drained. The maintenance of gullies and grilles is done by cleaning, flushing and grit bucket emptying (*cf* Harrison and Trotman, 2002).

For the Bethe lattice $p_v = p_e = 1/(z-1)$. In general, $p_e \leq p_v$. For a network of $d$ dimensions, $zp_e \approx d/(d-1)$. In his review, Sahimi (1994) gave some of the current know $p_c$'s which are listed in Table 4.2 here.

| | $d$ | $z$ | $p_e$ | $zp_e$ | $p_v$ |
|---|---|---|---|---|---|
| honeycomb | 2 | 3 | $1-\sin(\pi/18)$ | 1.96 | 0.6962 |
| square | 2 | 4 | 1/2 | 2 | 0.5927 |
| kagome | 2 | 4 | 0.522 | 2.088 | 0.652 |
| triangular | 2 | 6 | $2\sin(\pi/18)$ | 2.084 | 1/2 |
| diamond | 3 | 4 | 0.3886 | 1.55 | 0.4299 |
| simple cubic | 3 | 6 | 0.2488 | 1.49 | 0.3116 |
| body-centred cubic | 3 | 8 | 0.1795 | 1.44 | 0.2464 |
| face-centred cubic | 3 | 12 | 0.198 | 1.43 | 0.119 |

**Table 4.2** *Percolation probabilities, cf Sahimi (1994).*

The accessible fraction, $f_\alpha$, is the fraction of occupied bonds that belong to the infinite cluster. The backbone fraction, $f_\beta$, is the fraction of those accessible bonds which belong to a transport path, *i.e.* a path with all dead ends excluded. The correlation length, $\lambda$, is the length scale over which the random network is macroscopically homogeneous. In a Monte Carlo simulation it is necessary that the size $L$ of the network is sufficiently larger than this correlation length in order to obtain a $p_c$ which is independent of $L$. The expected cluster size $m$ is $\mathrm{E}(m) = \sum_m m^2 n_m / (\sum_m m n_m)$, where $n_m(p)$ is the expected number of clusters of size $m$ per lattice site and $mn_m$ the probability that a site belongs to an $m$-cluster. The fraction of the network which can accommodate flow has various names associated to each application, for example the effective electrical conductivity $g_e$, the effective diffusivity $D_e$ and the hydrodynamic permeability $k$. The effective elastic moduli, $G$, are the elastic moduli of the network a fraction $p$ of bonds of which are elastic elements, while the rest are rigid or stiff. The fraction of isolated occupied sites is $f_i(p) = p - f_\alpha(p)$. The universal scaling laws state that $p_c(p) \sim (p-p_c)^{b_p}$, $f_\alpha(p) \sim (p-p_c)^{b_p}$, $f_\beta(p) \sim (p-p_c)^{b_\beta}$, $\lambda(p) \sim |p-p_c|^{-\nu_p}$, $k(p) \sim |p-p_c|^{-\gamma_p}$, $g_e(p) \sim (p-p_c)^{\mu}$ and $G(p) \sim (p-p_c)^{f}$, where $b_\beta$, $b_p$, $\nu_p$ and $\gamma_p$ are topological exponents, completely universal, depend only on the dimensionality but not the microscopic details of the system. The effective diffusivity $D_e(p) \sim (p-p_c)^{\mu - b_p}$ because $g_e \sim n_e D_e$ and $n_e \sim f_\alpha(p)$. Near $p_c$, $k(p) \sim (p-p_c)^e$. For network percolations $e = \mu$, but for the continuum percolation this may not be the case.

As $p \to p_c^-$, perfectly conductive clusters become larger and $g_e$ increases. Then $g_e(p) \sim (p_c - p)^{-s}$ near $p_c$ and diverges at $p_c$. In two dimensions, $\mu = m$. If $p$ edges are totally rigid while the rest are elastic, then $G$ diverges as $p \to p_c^-$ such that $G \sim (p_c - p)^{-\zeta}$ For large $m$ near $p_c$, $n_m \sim m^{-\tau_p} f\left[(p-p_c)m^{\sigma_p}\right]$, where $\tau_p$ and $\sigma_p$ are universal and $f(0) \neq 0$. Some relations among the geometrical exponents are $\tau_p = 2 + b_p\sigma_p$ and $\nu_p d = b_p + 1/\sigma_p = 2b_p + \gamma_p$. Sahimi (*ibid.*) listed some values of the current critical exponents and fractal dimensions which we list again here as Table 4.3.

| | $d=2$ | $d=3$ | Bethe lattices |
|---|---|---|---|
| $b_p$ | 5/26 | 0.41 | 1 |
| $b_\beta$ | 0.48 | 1.05 | 2 |
| $\nu_p$ | 4/3 | 0.88 | 1/2 |
| $\gamma_p$ | 43/18 | 1.82 | 1 |
| $\sigma_p$ | 36/91 | 0.45 | 1/2 |
| $\tau_p$ | 187/91 | 2.18 | 5/2 |
| $D_c$ | 91/48 | 2.52 | 4 |
| $D_\beta$ | 1.64 | 1.8 | 2 |
| $D_{\min}$ | 1.13 | 1.34 | 2 |
| $\mu$ | 1.3 | 2.0 | 3 |
| $m$ | 1.3 | 0.73 | 0 |

**Table 4.3** *Critical exponents and fractal dimensions, cf Sahimi (1994).*

The system is macroscopically homogeneous when $L \gg \lambda$ but not when $L \ll \lambda$ where the cluster spanning the sample is self-similar and fractal at all length scales up to $\lambda$. Its mass is $M \sim \lambda^{D_c}$, where $D_c = d - b_p/\nu_p$ is the fractal dimension of the cluster. For $L \gg \lambda$, $D_c = d$. Similarly the backbone is also a fractal object when $L \ll \lambda$, and it has the fractal dimension $D_\beta = d - b_\beta/\nu_p$. When $L < \lambda$ one should replace $\lambda$ by $L$, at $\lambda$ diverges at $p = p_c$ and the red bonds have $M_r \sim L^{D_r}$, $D_r = 1/\nu_p$, when $L \ll \lambda$. The minimal or chemical path between two points of a percolation cluster is the shortest path between the two points, and $L_{\min} \sim L^{D_{\min}}$ for $L \ll \lambda$.

Finite-size scaling is the effect of finite size on the critical properties. As $p \to p_c$, $\lambda \to L$, and the variations of a property $P_L$ becomes $P_L \sim L^{-x} f(u)$, where $u = L^{1/\nu_p}(p - p_c) \sim (L/\lambda)^{1/\nu_p}$ and $f(0) \neq 0$. When $p \to p_c$ and $L \to \infty$, $P_\infty \sim (p - p_c)^\delta$ and $x = \delta/\nu_p$. There is also a shift in the percolation threshold, and $p_c - p_c(L) \sim L^{-1/\nu_p}$ where the percolation probability is $p_c$ for the infinite system while its effective value for a finite system is $p_c(L)$. Correction should be made whenever the system simulated is small, that is $P_L \sim L^{-x}[a_1 + a_2 g_1(L) + a_2 g_2(L)]$, where $g_1$ and $g_2$ are the correction terms to the scaling. For transport properties, for example conductivity, diffusivity and elastic moduli, $g_1 = (\ln L)^{-1}$ and $g_2 = L^{-1}$ are often good enough.

Sahimi (1994) mentions a random distribution of inclusions, such as circles, spheres, or ellipses, in an otherwise uniform system or continua; a percolation on random polyhedra such as the VT; and also a random distribution of random conducting sticks of with given aspect ratio, or plates a given extent, which is important in modelling fracture networks in rocks. In the study of percolation in continua, one considers a continuous, random function $h(r)$, defined for all points $r$'s in the entire space, such that $\langle h(r) \rangle = 0$. All regions of space where $h(r) < R$ are in a phase which is different from the rest, the volume of which goes from zero to infinite as $R$ changes from negative- to positive infinite. As $R$ becomes larger, so do the islands, and the phase grows and percolates at the critical $R_c$. For continua percolation, the critical occupied volume fraction is defined as $\phi_c = p_c f$, where $f$ is the filling factor of a lattice when all its sites are occupied by an impermeable sphere in such a manner that those which are nearest neighbours touch each other. This volume fraction seems to be an invariant, approximately 0.45 for two- and 0.15–0.17 for three dimensions. If the spheres are permeable, then $\phi_c = 1 - \exp(-B_c/8)$ where $B_c = z p_b$ is the number of bonds per sites at $p_c$, and in continua percolation $B_c \to p_c z$ as $z \to \infty$. If $\phi_c$ is an invariant of continuous systems, then $R_c$ is given by $\phi_c = \int_{-\infty}^{R_c} h(r) \mathrm{d}V$, where $V$ is the volume of the system.

## § 4.1 S-curves and the percolative phenomena

Before any abrupt change occurs there must be a graduation process leading up to it. In processes where the time constant is long, the characteristic s-shape is obvious, take for example a learning curve. But even where time constants are short, it is doubtful whether such thing as a strictly abrupt change exists. At the very point of transition, undoubtedly there may be a singularity, for instance at the Big Bang. But even the Big Bang can not exist alone by itself. To preserve the symmetry of nature, there must be another process at the other end leading up to it. It is only because such process must necessarily be on the other side from us and we can not see it from here. That side may belong to the antimatter or the anti-universe, but I believe whenever there is a singularity there must be a symmetry.

An earlier work by Tiyapan (2003, KNT8(iii)) can be used as an example. The per cent extraction curves which I drew then (Tiyapan, 1991, KNT1(i)) all show the change to be abrupt, starting off from zero time immediately with a positive gradient. This can not happen in the real world, so

there must have been a foot of the characteristic s-curve at the beginning. It must have been that the sampling time used is too long, and anyhow the nature of the reaction may make it impossible to observe the development in detail with accuracy.

The predicted value of the heat capacity of monoatom solids according to the Debye theory, from de Podesta (1996), is shown in Figure 4.1. According to Debye, $C_V = (1944p/\Theta_D^3)T^3$ $\mathrm{JK}^{-1}\mathrm{mol}^{-1}$ (*cf* de Podesta, 1996). The curve in Figure 4.1 shows the characteristic s-shape which should have appeared in Tiyapan (2003, KNT8(iii)).

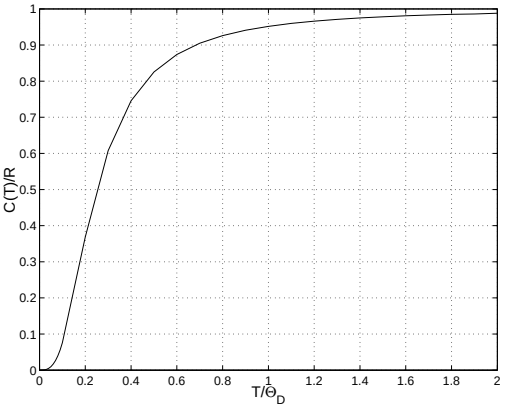


**Figure 4.1** predicted value of the heat capacity of monoatomic solids according to Debye.

The foot of a positive s-curve has a positive, nonzero second derivative. This corresponds with the positive cooperativity of the product curve in studies of enzyme assay and kinetics. In enzyme assay, the product versus time graph shows a positive cooperativity characteristic when the Hill constant $h > 1$ in the equation $y_s = [s]^h/(K + [s]^h)$, where $y_s$ is the fractional saturation of the enzyme with substrate while $s$ the concentration of the substrate (Eisenthal and Danson, 2002). Cooperativity reflects the equilibrium binding of substrate or other ligand. The binding of a substrate molecule to an enzyme either facilitates, when the cooperativity is positive, or hinders, when the same is negative, the binding among molecules of the same substrate.

## § 4.2 Voronoi percolation in two dimensions

The percolation of Voronoi tessellation in two dimensions can be achieved by the following algorithm.

**Algorithm 4.2** *Network percolation in 2-d.*

**generate** random points;
**generate** Voronoi tessellation and Delaunay triangulation;
**find** vertices within the square box bounded by *lower* and *upper bounds*;
**find** neighbours of all cells, bonds, vertices, and edges;
**for** *unit = cell, bond, vertice* and *edge* **do**
  **find** *number of units*;
  **permute** *list of units*;
  **clear** *cluster list 1, cluster list 2, set of resultant clusters*;
  *cluster percolated* ← false;
  **for** $i = 1$ **to** *number of units* **do**
    *existing cluster joined* = false;
    **for** $j = 1$ **to** *number of clusters in cluster list 1* **do**
      **if** *the* $j^{th}$ *cluster* contains *the* $i^{th}$ *unit in permuted list* **do**
        **merge** *the* $i^{th}$ *unit* **into** *the* $j^{th}$ *cluster* ;
        *existing cluster joined* ← true;
      **end**
      **if** *existing cluster joined* is true
        **move** *the* $j^{th}$ *cluster of cluster list 1* **to** *cluster list 2* ;
        **for** $k = 1$ **to** *number of clusters in cluster list 1* **do**
          **if** *the* $k^{th}$ *cluster in cluster list 1* touches *the cluster in cluster list 2* **do**
            **merge** the former **into** the latter;
          **else**
            **append** the former **to** *cluster list 2*;
          **end**
        **end**
        **test** percolation of the cluster just updated;
        **move** *cluster list 2* **to** *cluster list 1*;

```
            clear cluster list 2;
            break;
          end
        end
        if existing cluster joined is false
          create a new cluster of size one and append it to cluster list 1;
        end
        append cluster list 1 to set of resultant clusters ;
      end
    end
```

The Pc probabilities are found to be ${}^{Vn\ 2d}_{4(\mathbf{1}),14(\mathbf{2})}p_c = 0.5110 \pm 0.0856$, ${}^{Vn\ 2d}_{17(\mathbf{2})}p_b = 0.3095 \pm 0.0523$, ${}^{Vn\ 2d}_{16(\mathbf{2})}p_v = 0.7231 \pm 0.0616$ and ${}^{Vn\ 2d}_{16(\mathbf{2})}p_e = 0.6801 \pm 0.0468$.

And the coordination numbers are $.2436\ {}^{Vn\ 2d}_{2(\mathbf{1}),7(\mathbf{2})}x_c = 5.2320$ , $.2979\ {}^{Vn\ 2d}_{8(\mathbf{2})}x_b = 9.5022$ , $.0259\ {}^{Vn\ 2d}_{8(\mathbf{2})}x_v = 2.8617$ and $.0382\ {}^{Vn\ 2d}_{8(\mathbf{2})}x_e = 3.8064$ .

The percolation theory in two dimensions has benefited much from discoveries regarding the Ising model in Physics. The Ising model is to date probably the most successful model in percolation theory. This is not only because it can describe in details the phenomena of ferromagnetism and antiferromagnetism, but also because it does so by replacing a noncrystalline solid in the atomic scale with a perfect lattice.

When a bar of iron is placed in a external magnetic field at a constant temperature, the field will induce some magnetisation in the bar. If the external field is slowly turned off, there are two scenarios possible. If $T < T_c$ the bar retains some of its internal magnetisation, but if $T > T_c$ the magnetisation completely disappears. The transition temperature $T_c$ is known as the Curie point.

The Ising model represents the iron bar by lattices, for instance a square lattice. Then it defines two power series, namely the low- and the high temperature series. The low temperature series comes from a bivariate generating function which is generated from the number of colourings for which there are $p$ black sites and $q$ black-white edges. In other words if we let $A(p,q)$ be the said number of colourings, then our bivariate generating function becomes $a(x,y) = \sum_{p,q} A(p,q)x^p y^q$ and the power series is obtained from $\alpha(x,y)\lim_{N\to\infty}(1/N)\ln(a(x,x))$.

On the other hand, the high temperature series of the Ising model changes its form with the dimension. In one dimension it degenerates, while in two dimensions it is isomorphic to the low temperature case and comes from a bivariate generating function that is generated from the number of even polygonal drawings whose area is $p$ and which has $q$ edges. In three dimensions it comes from a univariate function that in turn is generated by the number of even polygonal drawings which have $q$ edges. An even polygonal drawing on a lattice is a union of its subgraphs that uses each edge of the latter at most once and each site an even number of times. It is also known as an Eulerian subgraph and is indeed a union of simple, closed and edge-disjoint polygons which need not be connected.

In three dimensions if we let $B(q)$ be the number of even polygonal drawings mentioned, then our univariate generating function becomes $b(z) = \sum_q B(q)z^q$ and the power series can then be obtained from $\beta(z) = \lim_{N\to\infty}(1/N)\ln(b(z))$.

Two main problems remain unsolved regarding the Ising model, namely that of finding closed-form expressions, of $\alpha(x,y)$ for two dimensions and of $\beta(z)$ for three.

## § 4.3 Voronoi percolation in three dimensions

In three dimensions the procedure of finding $p_c$ is similar to that used in the 2-d case. Algorithm 4.3 written was used in doing the simulation. Developed for running on Matlab, it does every thing in matrix form. As a consequence, there are various types of data all of which are matrices. These data structures can be summarised into the following.

A *list* is a one-dimensional matrix whose dimension is the number of its members. An *index* is a matrix whose members are either one or zero. These index matrices in two dimensions are like a map or an array. They are normally one or two dimensions, and map the relationship between the members of one set and another. A *set* is an $m \times n$ matrix every one of the members $a_{ij}$ of which is a matrix. A *pair matrix* is a square diagonal index matrix that maps among members within the same set. It contains the information about relationships like neighbourhood, group membership, connection, *etc.* A pair matrix or an index can also contain information other than the existence or membership flags, for example the edge length in the case of a vertices pair edge matrix. In a bond or an edge the mid point represents its position.

The program can be divided into three parts, creating and arranging the Voronoi data, finding the neighbourhood matrix and the percolation simulation for $p_c$. Putting the vertices of a face in order amounts to juggling from one end of each stick, *i.e.* edge, to another. Edges are traced in one direction only until all the edges are successfully linked head to tail. Two lists receive the result from the tracing, vertices which match go to one of them while those which do not is put in the other and recycled.

**Algorithm 4.3** *Managing the Voronoi data in three dimensions.*

$x \leftarrow$ **create** random points;
$(v_a, c_a) \leftarrow$ **create** Voronoi tessellation;
$t \leftarrow$ **create** Delaunay tessellation;
**find** $v_n$ such that for all $v_a$, $0 < v_a < 1$;
**find** $c_n$ such that all vertices of $c_a$ are in $v_n$;
$c \leftarrow c_n$;
**for** all **do**
  $m_b \leftarrow$ **find** mid bond coordinates;
  $b_l \leftarrow$ **find** bond length;
**endfor**
**for** all pairs of cells **do**
  $f_a \leftarrow$ **find** shared vertices when either of the two cells is in $c_n$;
**endfor**
**for** all $v_n$, $v \leftarrow v_a$;
**for** all $c_n$, $f \leftarrow f_a$;
**for** all $f$'s **do**
  **if** it has three vertices **then**
    all the three possible pair combinations are neighbours;
  **else**
    $(a, b, c) \leftarrow$ **find** the face equation from three vertices;
    $\theta_i \leftarrow ka$ where $k = 1/(a^2 + b^2 + c^2)$ and $i = 1$, 2 and 3;
    max $\leftarrow 0$;
    **for** $j = 1$ to 3 **do**
      **if** $\theta <$ max **then**
        $j_m \leftarrow j$;
        max $\leftarrow \theta(j_m)$;
      **endif**
    **endfor**
    **if** $j_m = 1$ **then**
      $p \leftarrow y$; $q \leftarrow z$;
    **elseif** $j_m = 2$ **then**
      $p \leftarrow x$; $q \leftarrow z$;
    **else**
      $p \leftarrow x$; $q \leftarrow y$;
    **endif**
    $d \leftarrow$ **find** delaunay triangulation from $p$ and $q$;
    **for** all edges of all triangles of $d$ **do**
      **record** the number of times they occur;
    **endfor**
    neighbours $\leftarrow$ vertices of edges which occur only once;
    **for** all $f$'s **do**
      **order** all their vertices;
    **end**
  **endif**
**endfor** □

The terms *vertices* and *edges* refer to the Voronoi tessellation only. The vertices and edges of the Delaunay tessellation are cells and bonds of the VT. The program `perco3d.m` can find $p_c$ for all of these. For each one of them we must find the neighbourhood matrix as well as lists of the upper- and the lower boundaries. The order of blockages is completely decided in advance by finding a

permuted list of numbered items. The program finds the history of clusters for the whole range of $p$, *i.e.* from 0 to 1.

To obtain the matrix of cell neighbours, first crop out between 5 and 10 per cent the boundary in all directions. Then the neighbour matrix is found from the DT matrix.

The bond neighbour matrix is simply the rearrangement of the cell neighbour matrix obtained. We have already found the vertices neighbour matrix earlier while searching for vertices shared between cells. This is rearranged for the use in the percolation program, and then again for the edge neighbour matrix.

Next is Algorithm 4.4 which carries out the percolation simulation. The cluster information is swapped alternately between three variables, $A$, $B$ and $tmp$, to facilitate the flow; $A(i)$ is the $i^{\text{th}}$ cluster in $A$. All variables are assumed to be cleared at the start of the algorithm. At the end of each run the value of $p_c$ is computed, and the list $p$ is reversed and reused for a second time if it was the first run.

**Algorithm 4.4** *Voronoi percolation in three dimensions.*

**for** each permuted item $p(i)$ in the list **do**
  **joined** $\leftarrow 0$;
  **for** each cluster $A(j)$ in $A$ **do**
    **if** A(j) contains p(i) **then**
      $A(j) \leftarrow A(j) \cap p(i)$;
      $B(1) \leftarrow A(j)$;
      $tmp \leftarrow A$;
      $A \leftarrow tmp - A(j)$;
      **for** all $A(k)$ in $A$ **do**
        **if** $A(k) \wedge B(1)$ **then**
          $B(1) \leftarrow A(k) \cap B(1)$;
        **else**
          $B(++n_B) \leftarrow A(k)$;
        **endif**
      **endfor**
      *percolated ?*;
      $A \leftarrow B$;
      **break;**
    **endif**
  **endfor**
  **if** joined **then**
    $A(++n_A) \leftarrow p(i)$;
  **endif**
**endfor** □

The resulted Pc probabilities from simulation are ${}^{Vn\ 3d}_{12(\mathbf{2})}p_c = 0.2340 \pm 0.0448$, ${}^{Vn\ 3d}_{2(\mathbf{2}),10(\mathbf{3})}p_b = 0.1178 \pm 0.0271$, ${}^{Vn\ 3d}_{2(\mathbf{2}),10(\mathbf{3})}p_v = 0.2941 \pm 0.0831$ and ${}^{Vn\ 3d}_{12(\mathbf{3})}p_e = 0.4311 \pm 0.0324$.

And the coordination numbers are $.3329\ {}^{Vn\ 3d}_{6(\mathbf{2})}x_c = 11.1231$, $.5996\ {}^{Vn\ 3d}_{1(\mathbf{2}),5(\mathbf{3})}x_b = 23.0548$, $.0245\ {}^{Vn\ 3d}_{1(\mathbf{2}),5(\mathbf{3})}x_v = 3.6926$ and $.0432\ {}^{Vn\ 3d}_{6(\mathbf{3})}x_e = 5.5002$.

Four different types of percolation have been performed, namely cell, bond, vertice and edge percolation. Vertices are inherently zero dimension, edges and bonds one dimension and cells, which in reality have three dimensions, is considered for this purpose as having none. When considering vertice- and cell percolation, the position of the vertices and nuclei determines whether they could connect somewhere to somewhere else. When the object the percolation of which we consider has a nonzero dimension and the dimension of the network is small, that is to say, in the same order as that of itself, $p_c$ obtained will depend on the network dimension. In other words, there will be an influence from the size of the objects on, and distort, the space in which the percolation occurs.

Additional results on a larger network are, the Pc probabilities from simulation are ${}^{Vn\ 3d}_{20(\mathbf{2})}p_c = 0.2039 \pm 0.0410$, ${}^{Vn\ 3d}_{20(\mathbf{3})}p_b = 0.0963 \pm 0.0114$, ${}^{Vn\ 3d}_{20(\mathbf{3})}p_v = 0.1659 \pm 0.0571$ and ${}^{Vn\ 3d}_{28(\mathbf{3})}p_e = 0.4172 \pm 0.0242$, and the coordination numbers are ${}^{Vn\ 3d}_{1(\mathbf{3})}x_c = 12.4177$, ${}^{Vn\ 3d}_{,1(\mathbf{3})}x_b = 25.7077$, ${}^{Vn\ 3d}_{1(\mathbf{3})}x_v = 3.8126$ and ${}^{Vn\ 3d}_{1(\mathbf{3})}x_e = 5.7050$. In this case the network was originally built from 1,000 Poisson point generators, and for the simulation we have $n_c = 723$, $n_b = 4{,}489$, $n_v = 4{,}855$ and $n_e = 9{,}255$.

## § 4.4 Percolation of 2-dimensional Voronoi sections

The program in § A.4 does a 2-d section of the 3-d VT. Algorithm 4.5 describes how it works. It assumes that the Voronoi tessellation already exists. Here $d_m$ means a denominator while $n_r$ a numerator, $V$ and $C$ means vertices and cells of the 3-d Voronoi tessellation while $v$ and $c$ those of the 2-d section. In particular, $c \in C$

**Algorithm 4.5** *Plane section of Voronoi in three dimensions*

$(\Delta x, \Delta y, \Delta z)_i \leftarrow (x_2 - x_1, y_2 - y_1, z_2 - z_1)_i$ for all edges $i$;
**for** all edges $i$ **do**
  $d_m \leftarrow a\Delta x + b\Delta y + c\Delta z$;
  **if** $d_m$ nonzero **then**
    $n_r \leftarrow ax_1 + by_1 + cz_1$;
    $t \leftarrow -n_r/d_m$;
    **if** $0 \le t \le 1$ **then**
      $(x, y, z) \leftarrow (x_1 + \Delta x, y_1 + \Delta y, z_1 + \Delta z)_i$;
      $\{v_s\} \leftarrow (x, y, z)$;
    **endif**
  **else**
    $a \leftarrow a + \epsilon$;
    $d_m \leftarrow a\Delta x + b\Delta y + c\Delta z$;
    $n_r \leftarrow ax_1 + by_1 + cz_1$;
    $t \leftarrow -n_r/d_m$;
    **if** $0 \le t \le 1$ **then**
      $(x, y, z) \leftarrow (x_1 + \Delta x, y_1 + \Delta y, z_1 + \Delta z)_i$;
      $\{v_s\} \leftarrow (x, y, z)$;
    **endif**
    **if** $n_r = 0$ **then**
      $\{v_s\} \leftarrow (x_1, y_1, z_1)$;
      $\{v_s\} \leftarrow (x_2, y_2, z_2)$;
    **endif**
  **endif**
**endfor**
**for** all $c_s$ **do**
  **find** the Delaunay triangulation;
  **count** $n_e$ of all the triangles, add the numbers into a single list;
**endfor** □

The intersection of a plane $ax + by + cz + d = 0$ by the line which is defined by $x = x_1 + \Delta x t$, $y = y_1 + \Delta y t$ and $z = z_1 + \Delta z t$, where $\Delta x$, $\Delta y$ and $\Delta z$ are respectively $(x_2 - x_1)$, $(y_2 - y_1)$ and $(z_2 - z_1)$, is determined by $t = -(ax_1 + by_1 + cz_1 + d)/(ai\Delta x + b\Delta y + c\Delta z)$. If the denominator is zero the line is parallel to the plane, and if the nominator is also zero contained therein.

The results from the percolation simulation on the section $\mathcal{V}_3^2$ are ${}^{Vn\ (2,3)s}_{18(\mathbf{1}),4(\mathbf{2})}p_c = 0.5494 \pm 0.1223$, ${}^{Vn\ (2,3)s}_{10(\mathbf{1}),10(\mathbf{2})}p_b = 0.3515 \pm 0.0764$, ${}^{Vn\ (2,3)s}_{8(\mathbf{1}),12(\mathbf{2})}p_v = 0.7557 \pm 0.0757$, ${}^{Vn\ (2,3)s}_{20(\mathbf{2})}p_e = 0.6210 \pm 0.0665$.

The coordination numbers are $.2212\ {}^{Vn\ (2,3)s}_{8(\mathbf{1}),1(\mathbf{2})}x_c = 4.6894$, $.6021\ {}^{Vn\ (2,3)s}_{5(\mathbf{1}),4(\mathbf{2})}x_b = 8.8100$, $.0387\ {}^{Vn\ (2,3)s}_{4(\mathbf{1}),5(\mathbf{2})}x_v = 2.7495$, $.1118\ {}^{Vn\ (2,3)s}_{9(\mathbf{2})}x_e = 3.6691$.

When sectioned by the plane $(a, b, c, d) = (0.01,\ 0.5,\ 0.5,\ -0.5)$, our VT gives a picture as shown in Figure 4.2. Here the points shown are merely the average of the coordinates of all vertices in each cell. From ten simulations of these 118 cells, 300 bonds, 288 vertices and 405 edges having respectively the coordinate numbers of 5.0847, 9.7933, 2.8125 and 3.7333, we obtain $p_c = 0.5220 \pm 0.0966$, $p_b = 0.3107 \pm 0.0391$, $p_v = 0.7014 \pm 0.0573$ and $p_e = 0.6259 \pm 0.0603$.

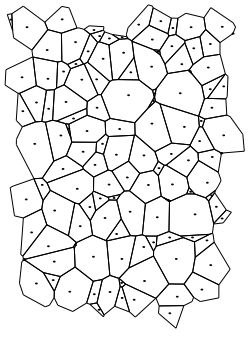

**Figure 4.2** Section by the plane (0.01, 0.5, 0.5, -0.5).

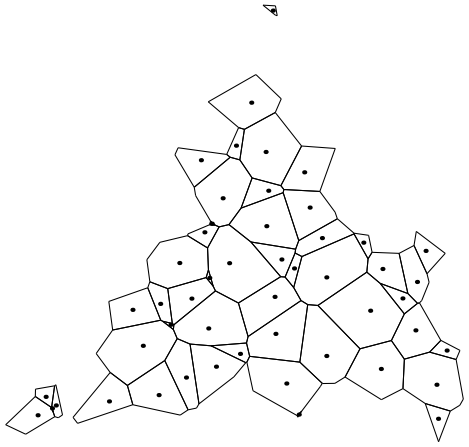

When sectioned by the plane $(a, b, c, d) = (0.5, -0.5, 0.5, 0.01)$, our VT gives a picture as shown in Figure 4.3. Here the points shown are merely the average of the coordinates of all vertices in each cell. From fourteen simulations of these 50 cells, 104 bonds, 140 vertices and 187 edges having respectively the coordinate numbers of 4.1600, 8.2500, 2.6714 and 3.5080, we obtain $p_c = 0.6914 \pm 0.1424$, $p_b = 0.4533 \pm 0.1108$, $p_v = 0.7760 \pm 0.0821$ and $p_e = 0.6929 \pm 0.0897$.

**Figure 4.3** Section by the plane (0.5, −0.5, 0.5, 0.01).

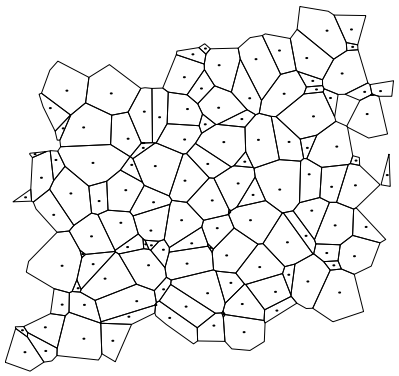

When sectioned by the plane $(a, b, c, d) = (-0.7, -0.3, 1, 0.01)$, our VT gives a picture as shown in Figure 4.4. Here the points shown are merely the average of the coordinates of all vertices in each cell. From twenty simulations of these 121 cells, 305 bonds, 291 vertices and 411 edges having respectively the coordinate numbers of 5.0413, 9.4426, 2.8247 and 3.7518, we obtain $p_c = 0.5413 \pm 0.1107$, $p_b = 0.3584 \pm 0.0494$, $p_v = 0.7077 \pm 0.0572$ and $p_e = 0.6749 \pm 0.0470$.

**Figure 4.4** Section by the plane (−0.7, −0.3, 1, 0.01).

For the purpose of doing these simulations, the code for finding percolation has been rewritten into a function. To my surprise and delight, the same function works for both the 3–d VT and its 2–d section. In choosing a sectioning plane it is better if we choose the parameter $d$ small, as the plane will then pass close to the origin. Also, choosing $a+b+c \approx 0$ seems to make a more wholesome section than otherwise. The codes for sectioning work well for oblique planes but do not like planes which are parallel to an axis. This shortcoming can be avoided if we make our plane only nearly parallel, when we want it to be parallel to an axis. Then to be able to view in a head on fashion such planes which have been plotted in three dimensions, we can look from the position $(a, b, c)$, which is in effect the vector normal to the plane. The function mentioned above is listed as `perc.m` and is in § A.26.

## § 4.5 Network percolation

In the study of networks an important parameter is the coordination number, which is the number of neighbours of an element which in the graph theory is usually the vertex. Each vertex or site of a graph is connected to each of its neighbouring vertices by a bond, so the coordination number of a graph is the number of bonds connected to a vertex.

Clusters and their various characteristics play an important role in the study of percolation of networks. With a material science application in mind, Levy *et al* (1982) numerically represent the shape of a cluster by the *shape parameter* $S$, defined as $S = b/N$ or more generally $S = (1/2)\sum_{i=1}^{z} i\nu_i / \sum_{i=1}^{z} \nu_i$ where $b$ or $i$ is the number of bonds and $N$ or $\nu_i$ the number of elements in a cluster having $b$ or $i$ bonds respectively.

## § 4.6 Percolation statistics in literature

Rushbrooke and Morgan (1961) studied the Heisenberg and Ising ferromagnetics and found that the critical concentration $p_c$ is the same for both Heisenberg and Ising problems. Moreover, this value is irrelevant to the magnitude of the spin $s$. By studying point-clusters and link-diagrams, they found approximations to the exact values of the percolation probabilities for, the face-centred cubic lattice $p_c = 0.18$, the body-centred cubic lattice $p_c = 0.22$, tthe simple cubic lattice $p_c = 0.28$, and the

plane square $p_c = 0.48$. Only vertices of their point-clusters, not link-diagrams, need to have a bond between them in order to be neighbours.

Frisch *et al* (1961) give the site critical probabilities for various types of lattices in two- and three dimensions. In the terminology used here, these are $p_c$ of vertices of the networks considered. Their results are shown in Table 4.4.

| **lattice** | *dimension* | $z$ | $p_c$ *(N=1,000)* | $p_c$ *(N=2,000)* |
|---|---|---|---|---|
| triangular | 2 | 6 | $0.487 \pm 0.021$ | $0.493 \pm 0.018$ |
| square | 2 | 4 | $0.575 \pm 0.017$ | $0.581 \pm 0.015$ |
| hexagonal | 2 | 3 | $0.683 \pm 0.020$ | $0.688 \pm 0.017$ |
| h.c.p. | 3 | 12 | $0.204 \pm 0.008$ | – |
| f.c.c. | 3 | 12 | $0.199 \pm 0.008$ | – |
| simple cubic | 3 | 6 | $0.325 \pm 0.023$ | – |
| tetrahedral | 3 | 4 | $0.434 \pm 0.013$ | $0.436 \pm 0.012$ |
| ice (quartz) | 3 | 4 | $0.432 \pm 0.013$ | $0.433 \pm 0.011$ |

**Table 4.4** *Critical probabilities from Frisch et al (1961).*

From their investigations they also realise that the critical probabilities of two homohedral tilings may not be the same. For instance, a plane lattice with $z = 3$ may have the vertex- and edge percolation probabilities different from those of the hexagonal lattice, even though the coordination number is the same for both.

Both Monte Carlo technique and series expansion method are means by which one can numerically study percolation problems. Dean (1963) used Monte Carlo method because, according to him, it provides more precise information. In a network of $N$ sites $pN$ of which are occupied, the probability of site occupation at the next time step becomes $q = p + 1/N$. The critical probabilities he found are shown in Table 4.5.

| | *lattice size* | | | |
|---|---|---|---|---|
| | $12 \times 12$ | $24 \times 24$ | $48 \times 48$ | |
| *lattice type* | $p_c \pm$ s.d. | $p_c \pm$ s.d. | $p_c \pm$ s.d. | $p_c \pm$ s.d., (lattice size) |
| square (s) | $0.507 \pm 0.090$ | $0.582 \pm 0.032$ | $0.580 \pm 0.018$ | 0.569, $(78 \times 78)$ |
| triangular (s) | $0.435 \pm 0.029$ | $0.494 \pm 0.037$ | $0.486 \pm 0.017$ | 0.486, $(84 \times 84)$ |
| square ($1^{st}$ and $2^{nd}$) (s) | $0.322 \pm 0.047$ | $0.381 \pm 0.029$ | $0.387 \pm 0.014$ | 0.401, $(90 \times 90)$ |
| honeycomb (s) | $0.641 \pm 0.061$ | $0.675 \pm 0.027$ | $0.688 \pm 0.015$ | 0.679, $(\frac{3}{4} \times 84 \times 84)$ |
| kagome (s) | $0.609 \pm 0.047$ | $0.643 \pm 0.028$ | $0.635 \pm 0.020$ | 0.655, $(72 \times 72)$ |
| four-eight (s) | $0.679 \pm 0.039$ | $0.718 \pm 0.023$ | $0.732 \pm 0.015$ | 0.739, $(84 \times 84)$ |
| square (b) | $0.468 \pm 0.049$ | $0.469 \pm 0.028$ | $0.492 \pm 0.011$ | 0.498, $(\frac{3}{4} \times 96 \times 96)$ |
| triangular (b) | $0.279 \pm 0.038$ | $0.324 \pm 0.046$ | $0.329 \pm 0.021$ | 0.349 |
| kagome (b) | $0.419 \pm 0.058$ | $0.432 \pm 0.045$ | $0.449 \pm 0.032$ | 0.435, $(84 \times 84)$ |
| four-eight (b) | $0.615 \pm 0.050$ | $0.649 \pm 0.028$ | $0.675 \pm 0.027$ | 0.661, $(\frac{3}{4} \times 78 \times 78)$ |

**Table 4.5** *Critical probabilities and the standard deviation (s.d.), $p_c \pm$ s.d., for sites (s) and bonds (b), from Dean (1963).*

The effect of shape of arrays found by him is such that for array sizes of $6 \times 96$, $12 \times 48$, and $24 \times 24$ the percolation probabilities are respectively $0.707 \pm 0.043$, $0.594 \pm 0.039$, and $0.568 \pm 0.032$. The *modified second moment* of the cluster size distribution for a lattice has been defined as $\mu_2^* = \sum \sigma_i^2 / (\sum \sigma_i)^2$, where $\sigma_i$ is the size of the $i^{th}$-cluster. And the percolation probability for the finite lattice has been defined to be the value of $p$ at which $\Delta\mu_2^*/\Delta p$ is maximum, $\Delta$ being an increment of one step.

Tiyapan (1995, KNT3(iii)) finds from 27 simulations on 2-d Voronoi networks of between 70 and 500 cells the percolation probability of cells $p_c = 0.507$, and from 75 simulations on 2-d Voronoi networks of between 100 and 8,600 bonds $p_c$ =0.658. For honey comb lattices between 100 and 3,000 bonds he finds the bond percolation probability $p_c = 0.640$, for Kagome lattices between 300 and 3,000 bonds $p_c = 0.517$, for square lattices between 200 and 2,000 bonds $p_c = 0.467$, and for triangular lattices between 300 and 3,000 bonds $p_c = 0.341$. These results from simulations are usually less than the exact values by a few per cent.

Mecke and Seyfried (2002) find pseudocritical threshold for different types of lattices and then extrapolate these by using finite-size scaling laws to obtain the critical probability for the infinite network. They use the Hoshen-Kopelman method to find the largest cluster of the system and then determine the percolation in fifteen steps by increasing or decreasing $p$ by $\frac{\Delta p}{2}$ depending on whether the system percolates or not. Here $\Delta p = p_2 - p_1$, $p_2 > p_1$, such that the system only percolates

at $p_2$ not $p_1$. In two dimensions the network percolates when two opposite sides connect with each other whereas in three dimensions the same is true when four opposite sides connect together. The pseudocritical percolation threshold is $p_c(L)$, where $L$ is the network size. The finite-size scaling theorem is $p_c(L) = p_c(\infty) + aL^b$. In two dimensions they find $p_c$ =0.59278(4), while in three dimensions $p_c = 0.31162(8)$.

In its early days the percolation theory concerned itself much with self-avoiding walks. The connective constant or the walk limit is defined as a measure of the connectivity of the lattice as $\ln \mu = \lim_{n\to\infty}(1/n)\ln c_n$, or sometimes as $\kappa = \ln \mu$. Shante and Kirkpatrick (1971) gives results from both the Monte Carlo and series method as shown in Table 4.6.

| | $z$ | $\mu$ | *Monte Carlo* | | *series method* | |
|---|---|---|---|---|---|---|
| | | | $p_e$ | $p_v$ | $p_e$ | $p_v$ |
| honeycomb | 3 | 1.8484 | 0.640 | 0.688, 0.679 | 0.6527 | 0.700 |
| kagome | 4 | | 0.435 | 0.655 | | 0.6527 |
| square | 4 | 2.6390 | 0.493, 0.489 | 0.581, 0.569 | 0.5000 | 0.590 |
| triangular | 6 | 4.1515 | 0.341, 0.349 | 0.493, 0.486 | 0.3473 | 0.5000 |
| diamond | 4 | 2.878 | 0.390 | 0.436 | 0.388 | 0.425 |
| s.c. | 6 | 4.6826 | 0.254 | 0.325 | 0.247 | 0.307 |
| b.c.c. | 8 | 6.5288 | | | 0.178 | 0.243 |
| f.c.c. | 12 | 10.0350 | 0.125 | 0.199 | 0.119 | 0.195 |
| h.c.p. | 12 | | 0.124 | 0.204 | | |

**Table 4.6** *Critical probabilities and connective constants, Shante and Kirkpatrick (1971), where s.c. means simple cubic, b.c.c. body centred cubic, f.c.c. face centred cubic and h.c.p. hexagonal close packing.For critical probabilities, all the values given in four decimal places are exact where as those given in three decimal places are numerical.*

## § 4.7 Percolation of $n$-gons in continuum

Consider the continuum percolation of regular polygons in two dimensions. Polygons are placed on the plane randomly with regards to both their position and orientation. From their position one can find the Delaunay triangulation. Using the bonds of the triangulation obtained as reference axes, one for each pair of polygons, one then finds the orientation of any two neighbouring polygons with reference with the axis connecting them.

Unlike in the case of Voronoi percolation where the size of each cell depends on the density of the generating points, in continuum percolation the size of the polygons has been decided in advance. The expanse of the region of interest is then determined relative to this size. The area being simulated can then be imagined as lying within an infinite plane where the number density of polygons is homogeneous.

The area of the n-gon is $A = n \cdot 2 \cdot (1/2)yz$. But $y = R\sin\theta$ and $z = R\cos\theta$, where $R$ is the radius of the circumscribing circle. Therefore we have $R = A/(n\sin\theta\cos\theta)$. The radius of the inscribed circle is $r = z$.

A list is made of every angle that the rays perpendicular to the sides of the polygons make with the $x$-axis in the counterclockwise direction. Then the key procedure of the algorithm is to find for each pair the ray which lies closest to the reference line joining the two polygons. The angles that these two rays make with the reference axis determines whether or not the two polygons intersect.

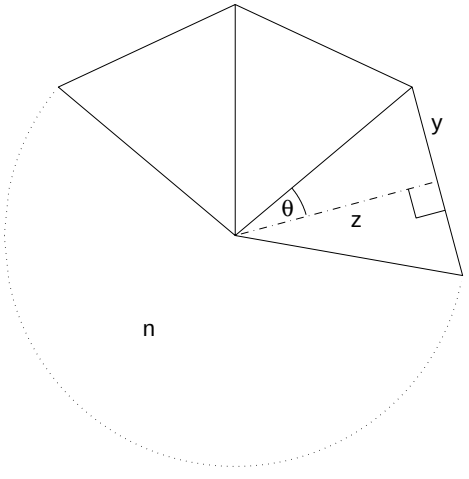


Figure 4.5

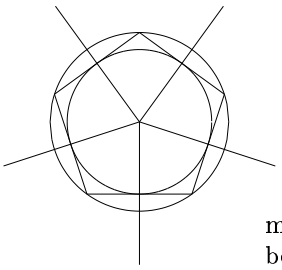

Figure 4.6

The inscribed circle and the circumscribing circle both play a role in deciding whether two polygons form a cluster. Let the radius of the former be represented by $r$ and the radius of the latter $R$. If any two polygons are less than $2r$ apart, then they must overlap. They just touch if they are exactly $2r$ apart. And if the distance between them is more than $2R$, then they can never touch each other. When the distance lies between $2r$ and $2R$ there is a probability that they will touch. Whether this is the case or not depends on the orientation of the two polygons.

Among all the rays similar to those shown in Figure 4.7 one can find the one closest to the line between the centres of the two polygons, ie $\theta_1$ and $\theta_2$ of Figure 4.8 are a pair of minimum angles for $c_1$ and $c_2$. Let the centres of these polygons be $c_1$ and $c_2$, and the line joining them $\overline{c_1c_2}$. Two such lines obtained from the two polygons can fall into on of the two cases; they can either be on the same side of $\overline{c_1c_2}$, or they are on the opposite side of each other as shown in Figure 4.8 (a) and (b) respectively. In either case, the following theorem is true.

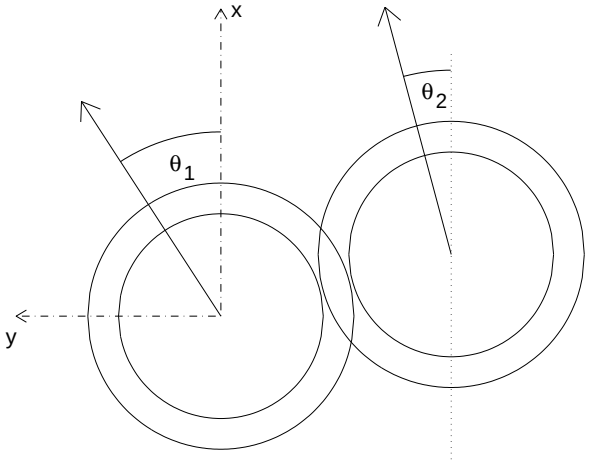


Figure 4.7

**Theorem 4.1.** *The line segments $\overline{a_1a_2}$ and $\overline{b_1b_2}$ always intersect $\overline{c_1c_2}$.*

**Proof.** Without losing generality, consider only the case of $\overline{a_1a_2}$. Suppose the above statement is false and $\overline{a_1a_2}$ did not intersect $\overline{c_1c_2}$. Then, because $\overline{a_1a_2}$ is a part of the circumference of a polygon, there would always be another ray $d_k$ originating from $c_1$ which has $\overline{a_ia_j}$ connected to it, such that $\overline{a_ia_j}$ intersects $\overline{c_1c_2}$, $i, j$ and $k$ being positive intergers. But the two triangles $\triangle c_1a_1a_2$ and $\triangle c_1a_ia_j$ are identical. Therefore the angle $\theta_k$ between $\overline{a_ia_j}$ and $\overline{c_1c_2}$ would be smaller than $\theta_1$ and we replace $d_1$ with $d_k$ because the latter is closer to $\overline{c_1c_2}$. □

Furthermore, between $\theta_1$ and $\theta_2$ the one which is greater would belong to an *aggressive* cell, while the other one is in a *passive* state. Suppose that $\theta_1 > \theta_2$, then $c_1$ would be the one which does the touching first. Theorem 4.2 states this in a more formal manner.

**Theorem 4.2.** *If the distance between any two identical regular polygons allows them a certain probability $p$ of overlap, such that $0 \leq p \leq 1$, then the polygon whose ray is furthest from the line connecting their centres will be the one which causes the two to intersect.*

**Proof.** Let $c_1$ and $c_2$ be the two identical polygons in question. As mentioned earlier, there are two cases to be considered, which are represented by Figure 4.8 (a) and (b). Because the distance between them is more than the diameter of the inscribed circle, when $\theta_1 = \theta_2 = 0$ the two polygons do not touch each other. The two polygons being identical, it is suffice to consider only one of them. But because there is an overlap area between the two as shown in Figure 4.7 where there is a probability of colliding to occur, and as the distance from a centre $c_1$ increases as one goes from a midpoint $d_1$ of an edge to the next vertex $d_2$ closest to $\overline{c_1c_2}$, the greater $\theta_1$ is, the further away from $c_1$ is the point of intersection between $\overline{d_1b_2}$ and $\overline{c_1c_2}$, the more that polygon overlaps into the collision hazard zone mentioned above, and therefore the more contribution to the probability of the collision. □

**Alternative proof.** As shown in Figure 4.8 (c), with $\theta_1 > \theta_2$ it is the corner $a_2$ which collides with the flat of the side $b_1b_2$ and penetrates into the second polygon.

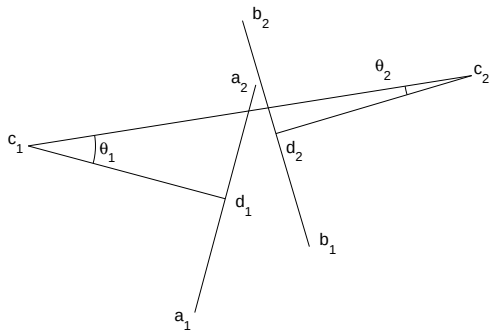


(a)

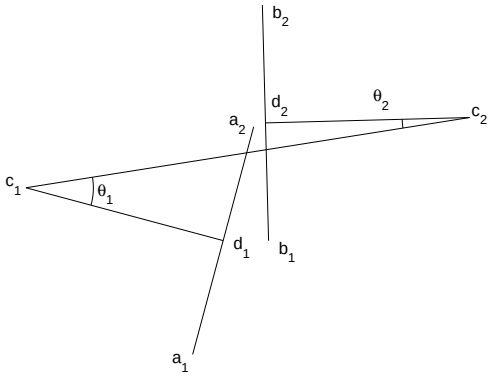


(b)

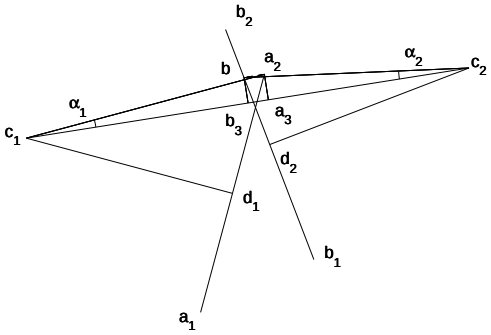


(c)

Imagine the polygons revolving around until they collide. At the point of collision if their vertices touch, then $\theta_1 = \theta_2$ and it is a special case where both contribute equally to the touch. The case of Figure 4.8 (b) where the two angles lie on the opposite side of each other follows a similar line of reasoning. □In Figure 4.8 The distance between $c_1$ and $c_2$ is less than the diameter of the circumscribing circle but more than the diameter of the inscribed circle.

**Figure 4.8** When two $n$-gons practise the Ayudhya sword together.

Figure 4.8 looks as though two $n$-gons were practising with each other the Ayudhya *ḍaḅ* (sword).

If $\theta_1 > \theta_2$, then $d\left(\overline{c_1 a_3}\right) > d\left(\overline{c_2 b_3}\right)$. Furthermore, a touch or penetration implies that $d\left(\overline{c_1 a_3}\right) + d\left(\overline{c_2 b}\right) = d\left(\overline{c_1 c_2}\right)$. If $d\left(\overline{c_1 a_3}\right) + d\left(\overline{c_2 b}\right) < d\left(\overline{c_1 c_2}\right)$ then the two polygons do not touch each other. The case when they merely touch at vertices is the case where $d\left(\overline{c_2 b}\right) = d\left(\overline{c_2 b_3}\right)$. On the other hand, the condition $d\left(\overline{c_1 a_3}\right) + d\left(\overline{c_2 b_3}\right) \geq d\left(\overline{c_1 c_2}\right)$ does not say anything much because $a_2$ may just pass under $b_2$ without touching the side in Figure 4.8 (a), or it may be the case where the two opposing sides lean towards the same direction as in Figure 4.8 (b). Therefore, we now have the following theorem which is later used in Algorithm 4.6 for finding overlaps.

**Theorem 4.3.** *Any two polygons $p_1$ and $p_2$ touch each other if and only if $d\left(\overline{c_1 a_3}\right) + d\left(\overline{c_2 b}\right) = d\left(\overline{c_1 c_2}\right)$.*

**Proof.** See explanation above together with Figure 4.8. □

**Algorithm 4.6** *Find continuum percolation of regular polygons on a plane.*

**place** polygons randomly;
**find** radii of their inscribed circles and the circumscribing circles;
**find** coordinates of the vertices;
**find** Delaunay triangulation;
**for** $i = 1$ **to** *number of triangles* **do**
  **for** $j = 1$ **to** 3 **do**
    **find** *distance between the $j^{th}$-pair vertices of the $i^{th}$ triangle;*
    **if** this *distance* $\leq 2r$ **then** polygons overlap **do**
      **record** cells overlap;
    **elseif** *distance* $\leq 2R$ **then** polygons could overlap **do**
      **record** cells to find whether overlap;
    **endif**
  **endfor**
  **find** *angle* of each of the two polygons when viewed from the other
**endfor**

**for** *every side of every polygon* **do**
  **find** *angles of the normal ray counterclockwise from the positive x-axis;*
**endfor**
**for** *every cell which could still overlap* **do**
  **find** *normal rays closest to the lines going towards its neighbours;*
**endfor**
**complete** the overlap check for all remaining cells;
**check** percolation; □

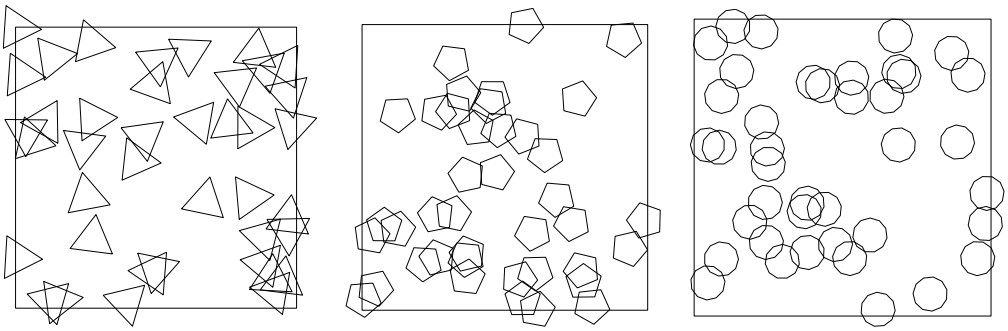

(a) (b) (c)

Figure 4.9 **(a)** Randomly placed *triangles.* Here the program tells us that the largest cluster has seven triangles, and the next largest one has six. There are 8 isolated triangles, 5 clusters of two, and three clusters of three. According to the program, the two clusters of sizes six and two on the upper right corner do not quite touch. **(b)** The largest cluster in this case has got nine *pentagons.* **(c)** These 11-*gons* are also too sparsely placed to percolate. The largest cluster in this case has got 8 members. The number of all 11-gons is 40, the same as in the two previous cases, and six of which are isolated. There are one cluster of four, four clusters of three, and five clusters of two.

The program in § A.5 uses the theorems above to find whether an aggregate of polygons percolate or not. Here each polygon has a unit area. The area of an $n$-gon is $nr^2\cos(\theta/2)\sin(\theta/2)$, where $r$ is the radius of its circumscribed circle. By setting this area to one we can find $r$, which, together with the decided orientation of each polygon gives the coordinates of its vertices. The program is explained in Algorithm 4.6.

A percolation threshold normally means the critical percentage by number. But in the case of percolation in a continuum where there is no fixed amount of lattice sites to refer to, the per cent area covered may be a better candidate for $p_c$. Finding this area can become quite computationally intensive it is a problem of finding the union among sets which, for the case of three sets is $A \cup B \cup C = A+B+C-AB-AC+ABC$, for four sets $A \cup B \cup C \cup D = A+B+C+D-AB-AC-AD-BC-BD-CD+ABC+ABD+ACD+BCD-ABCD$, *etc.* For the general case where there are $n$ sets intersecting one another, then, $\bigcup_n A_i = \sum_n Ai - \sum_{(n,2)} A_{ij} + \sum_{(n,3)} A_{ijk} - \cdots + \sum_n A_{i^{(n-1)}} + (-1)^{(n+1)} A_{i^{(n)}} = \sum_k^n (-1)^{(k+1)} A_{i^{(n)}}$, where $A_{ijk\ldots}$ means $A_i \cap A_j \cap A_k \cap \cdots$, the subscripts $(n,k)$ is the combination ${}^n\mathrm{C}_k = n!/\left[k!(n-k)!\right]$ and $i^{(n)} = ijk\cdots$ up to the $n^{\text{th}}$ term.

## § 4.8 Polygon percolation threshold

Because, unlike lattices however random, the continuum has neither underlying sites nor vertices and therefore has no definite number of these. To describe the percolation threshold in such situation we need to define the some new parameter other than our usual $p_c$, which not only depends on the number of polygons but also their area relative to that of the domain which they are in. We define the threshold area ratio as Definition 4.1. This definition disregards the intersection of the polygons, and therefore can only be used to compare networks which have the same type of distribution.

**Definition 4.3.** *For an aggregate of n-gons all the centres of which are Poisson points within a space of area A, the threshold area ratio is* $\alpha_n = \sum_n |a_i|/A$, *where* $a_i$ *is the area of each n-gon. If all n-gons have an equal area, then* $\alpha_n = na/A$.:

The program in § A.5 is transformed into a function which is then reused several times in the course of operation of another program, listed in § A.33, which finds $\alpha_n$. Both the program,

`ppgt.m`, and the function, `cmpc.m`, are here listed concatenated together whereas in practice they must separately exist.

The program first proceeds to find whether percolation occurs for aggregates containing increasing numbers of pentagons in step of 16. This step size is in fact $2^k$ for some integral $k$, and can be chosen to be optimum for a certain size of the network. At the end of these steps we find whether our aggregate percolate. If it does, then we know that somewhere within the last increasing step exists the point where percolation sets in. The precise location of this point can then be found by doing binary searching. There are altogether $k$ steps of these searches, at the end of each one of which there is again a test for percolation. If this test for the last and $k^{\text{th}}$ step is successful, then the last picture represents the aggregate which starts to percolate, otherwise one needs to know how many consecutive percolation tests have failed up to that point. With the knowledge of that number, one can count backward and reach the picture in question. The program `ppgt.m` fails to do this last job, but it has been added, together with the generalisation to $2^k$ steps, to make `ppgk.m`.

Figure 4.10 is the sample run on an aggregate of pentagons. Each of the pentagons is one unit area, and the space containing them, or rather the space which contains all their centres, is $10 \times 10$ in size.

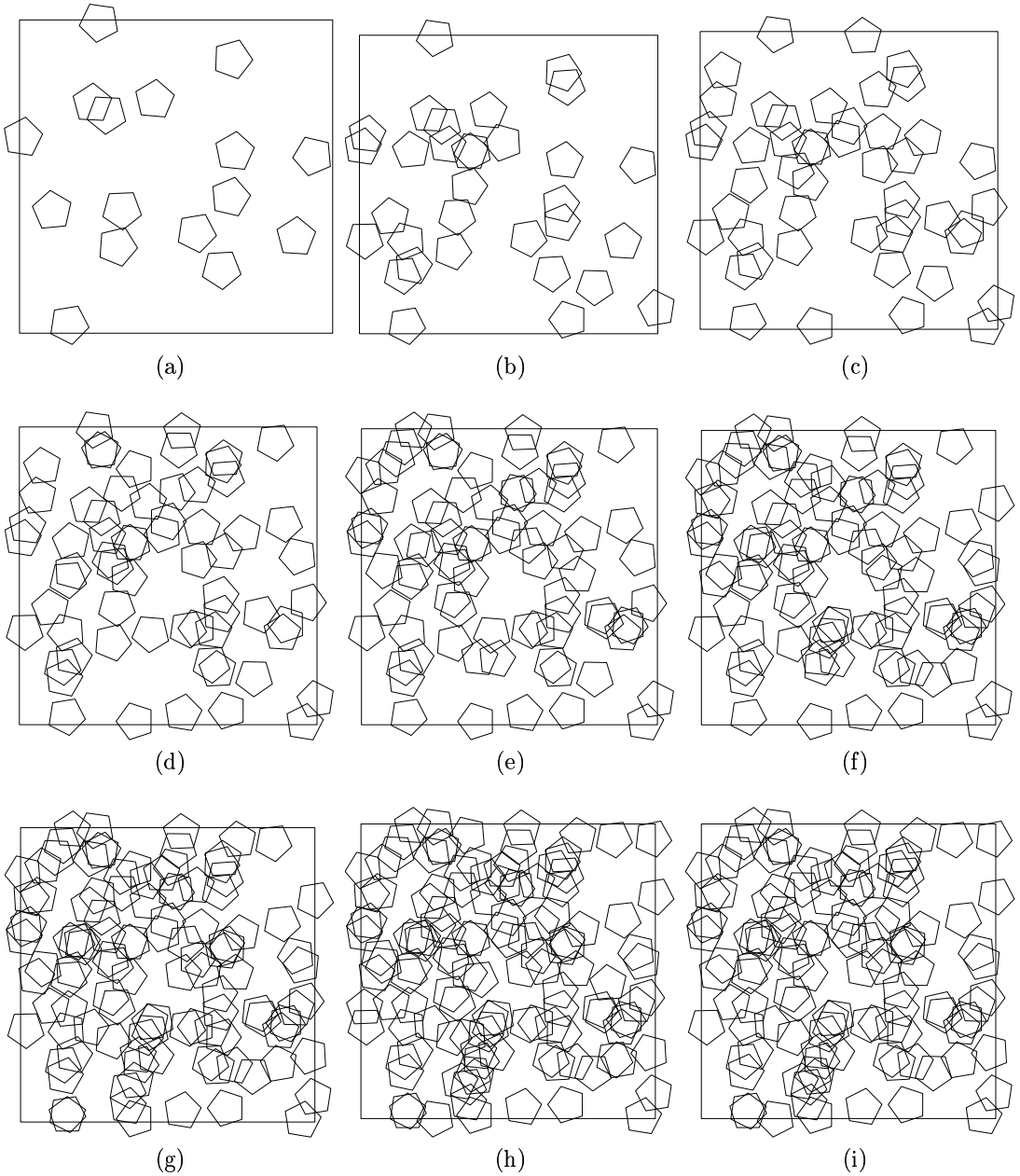

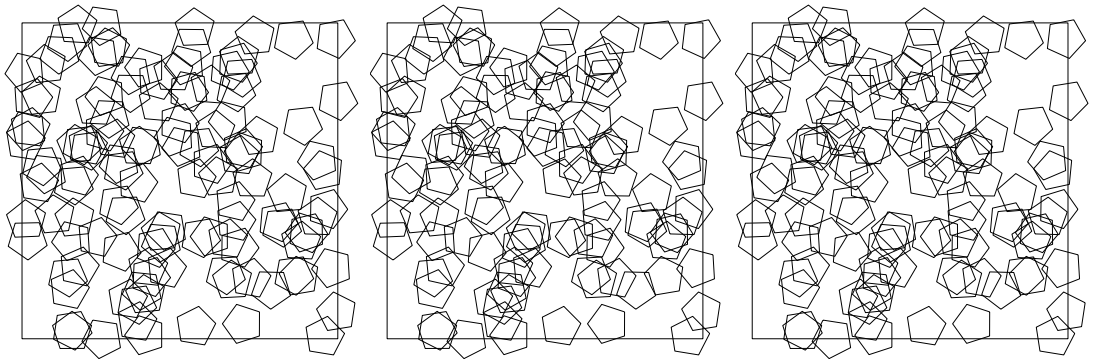

(j) (k) (l)

**Figure 4.10** *Finding the threshold area ratio of pantagons. The number of pentagons from* (a) *to* (h) *increases in step of* $2^4 = 16$. *In* (i), (j), (k) *and* (l) *a binary search proceeds which divides the length of the last interval from 16 to 8, 4, 2 and 1 in sequence. This simulation gives* $\alpha_5 = 1.23$.

The program `ppgk.m` in § A.33 uses $k = 4$ as explained above. Generalising this into a general $k$ gives Algorithm 4.7. Here $v_{ij}$ is the $j^{\text{th}}$ vertex of the $i^{\text{th}}$ $n$-gon. At the completion of the program, if it does complete, we have the aggregate containing $m_{1/2}$ polygons, and our $b^{\text{th}}$ percolation test before last has been on this aggregate.

**Algorithm 4.7** *Threshold area ratio.*

$s \leftarrow 2^k$;
$\beta \leftarrow 2\pi/n$;
$r \leftarrow [1/(n \sin(\beta/2)\cos(\beta/2))]^{1/2}$;
**while** percolation check fails **do**
  $\{(x, y)\} \leftarrow$ **find** $s$ more centre coordinates;
  $\{\theta\} \leftarrow$ **find** $s$ more orientational angles;
  **for** all these new centres and angles **do**
    $v_{ij} \leftarrow (x + r\cos(\theta_i + j\beta), y + r\sin(\theta_i + j\beta))$;
    **check** percolation all the $m$ centres and angles;
  **endfor**
**endwhile**
$(m_0, m_1] \leftarrow$ the last step above;
$b \leftarrow 0$;
**repeat** $k$ times
  $m_{1/2} \leftarrow (n_0 + n_1)/2$;
  **check** percolation all the first $m_{1/2}$ angles and centres;
  **if** percolated **then**
    $m_1 \leftarrow m_{1/2}$;
    $b \leftarrow 0$;
  **else**
    $m_0 \leftarrow m_{1/2}$;
    $b \leftarrow b + 1$;
  **endif**
**endrepeat** □

Figure 4.11 shows the percolation of $n$-gons with various values of $n$, the results of applying Algorithm 4.7 above. Polygons up to the twelve-sided dodecagon are shown here. After this there are of course the triskaidecagon, tetrakaidecagon, ..., enneakaidecagon, icosagon, icosikaihenagon, icosikaidigon, icosikaitrigon, ..., icosiaienneagon, triacontagon, triacontakaihenagon, ..., triacontakaienneagon, tetracontagon, ..., pentacontagon, ..., hexacontagon, ..., heptacontagon, ..., octacontagon, ..., enneacontagon, ..., hectagon, *etc.* But all of these closely approaches the circle.

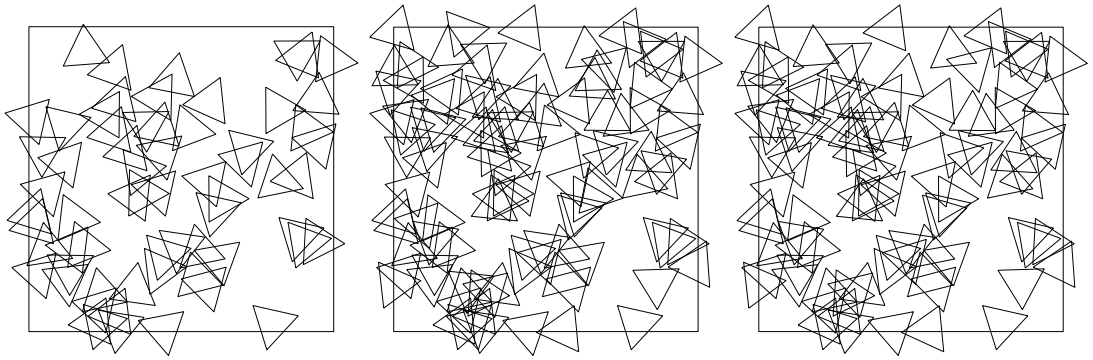

$(t_i)$ $(t_j)$ $(t_k)$

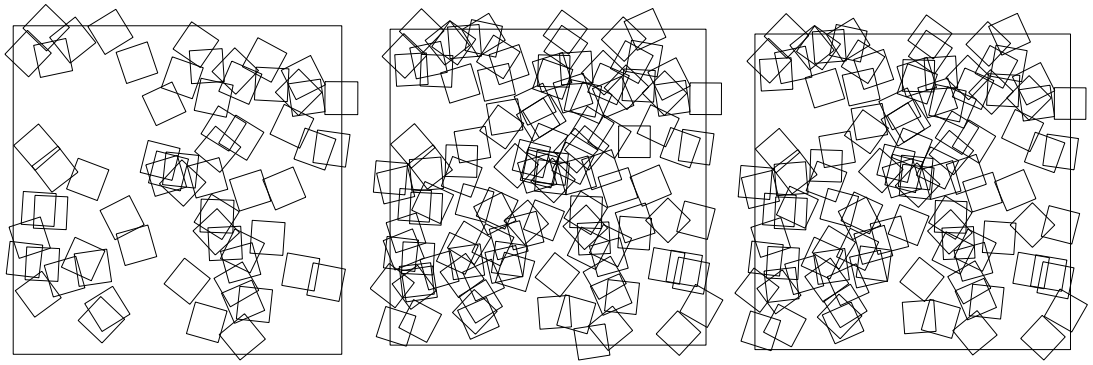

$(q_i)$ $(q_j)$ $(q_k)$

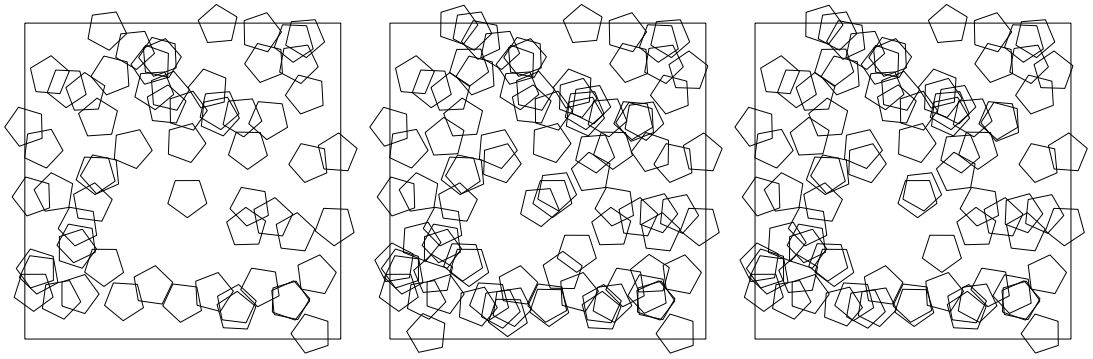

$(p_i)$ $(p_j)$ $(p_k)$

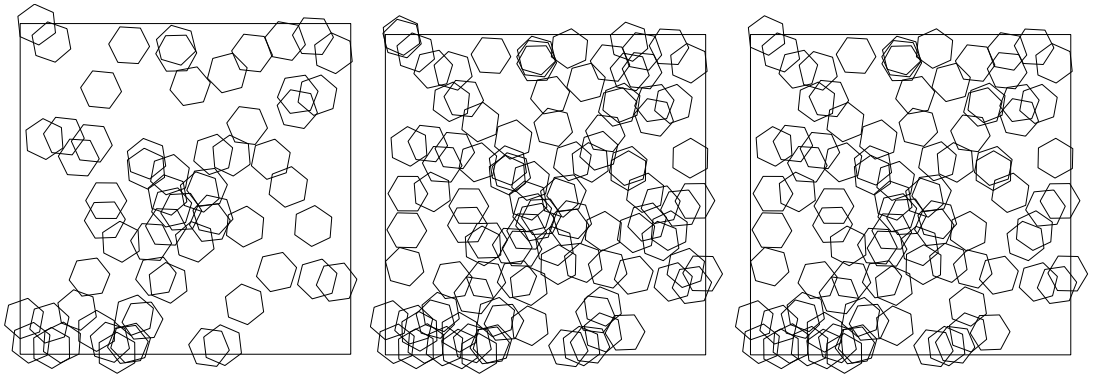

$(h_i)$ $(h_j)$ $(h_k)$

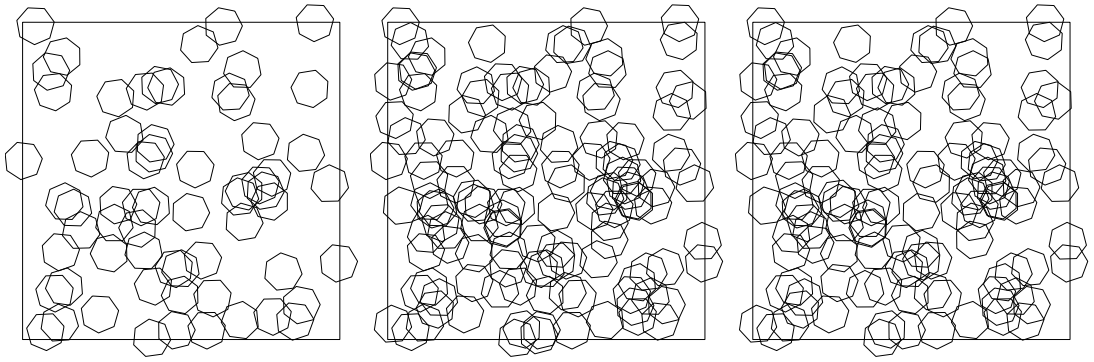

$(k_i)$ $(k_j)$ $(k_k)$

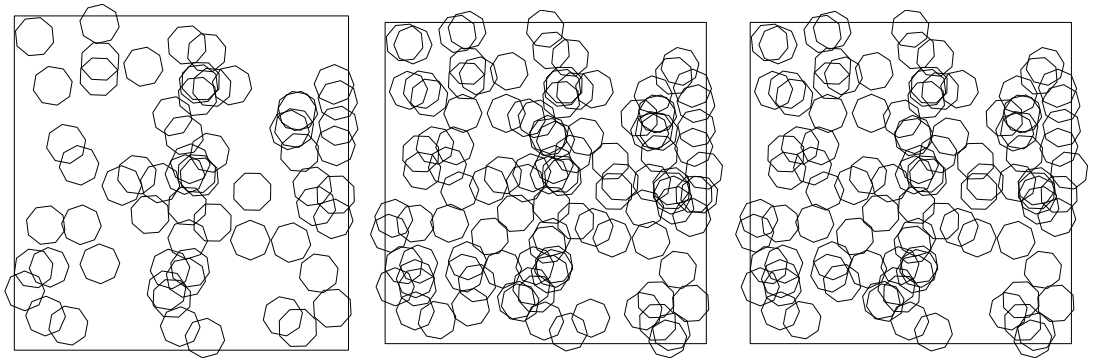

$(o_i)$ $(o_j)$ $(o_k)$

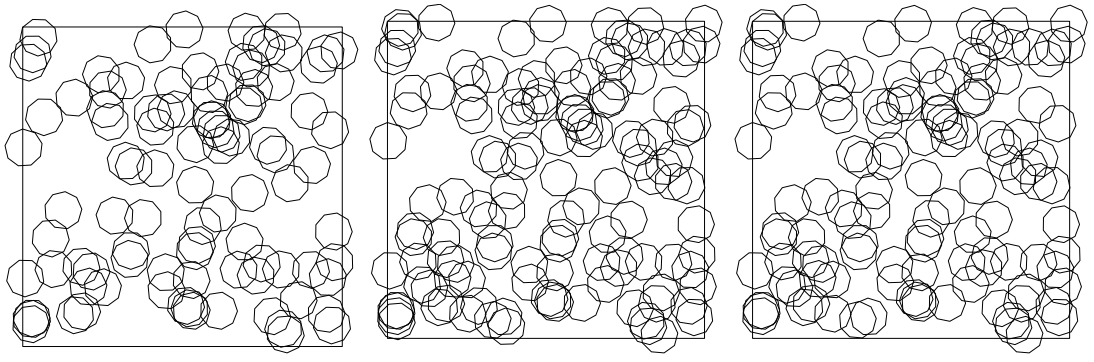

$(e_i)$ $(e_j)$ $(e_k)$

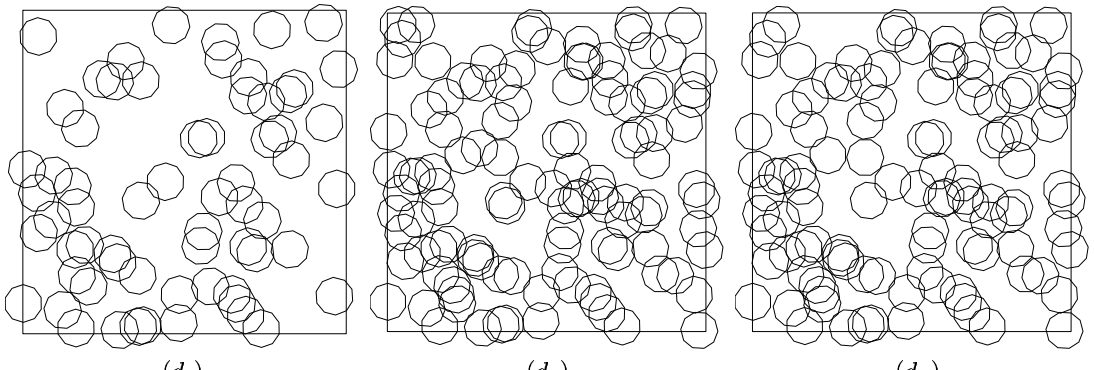

$(d_i)$ $(d_j)$ $(d_k)$

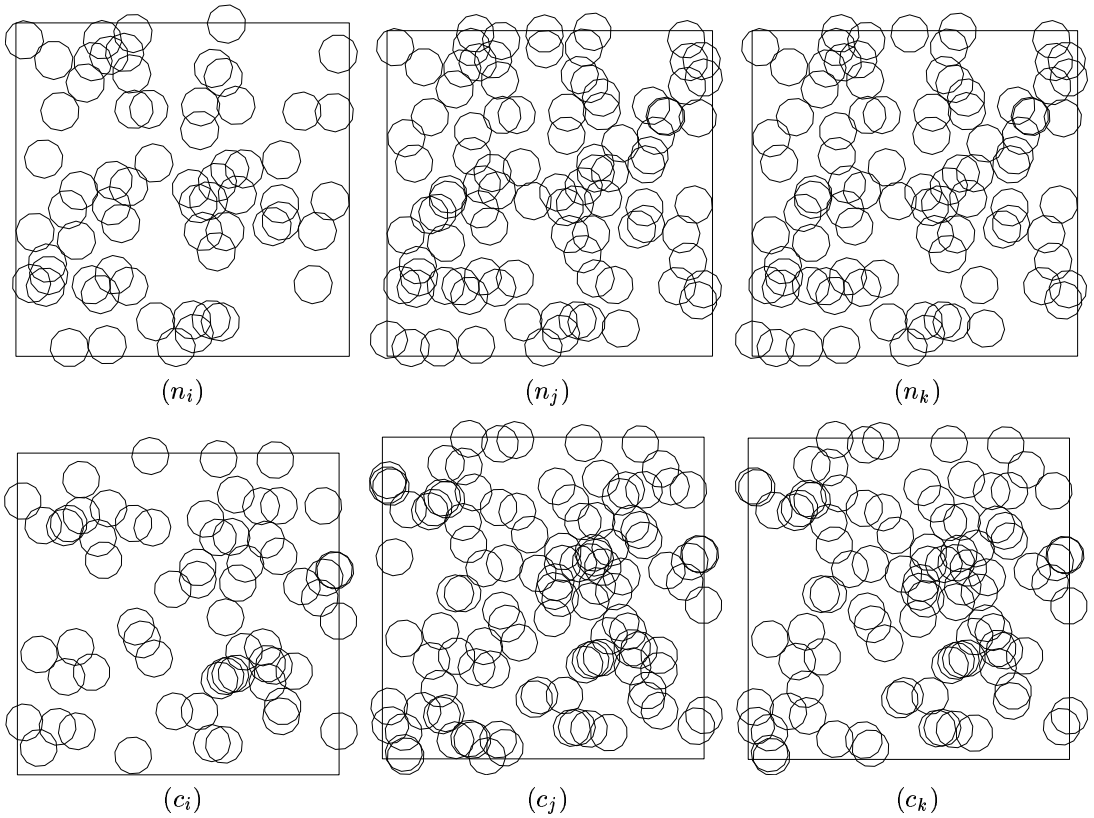


**Figure 4.11** *Percolation of n-gons. Triangle, square, pentagon, hexagon, heptagon, octagon, enneagon, decagon, hendecagon and dodecagon are represented respectively by t, q, p, h, k, o, e, d, n and c. The subscripts i, j and k are respectively the fourth step of the program, the over-percolated case and the critically percolated case.* $\alpha_3 = 1.03$, $\alpha_4 = 1.17$, $\alpha_5 = 0.89$, $\alpha_6 = 0.99$, $\alpha_7 = 1.23$, $\alpha_8 = 1.03$, $\alpha_9 = 1.23$, $\alpha_{10} = 1.07$, $\alpha_{11} = 0.91$ *and* $\alpha_{12} = 0.95$.

## § 4.9 2-homohedral tilings

There are altogether 39 types of 2-homohedral tilings, ie. those which have vertices of the same valence. Of these, there are 26 types of valence 3, 10 of valence 4, and 3 of valence 5 (*cf* Grünbaum *et al*, 1987). The code and the data used in the simulations are in § A.6. In the program, the variable $o$ contains the vertex numbers which must be ordered by scanning the basic tile from left to right and gradually from bottom up. Unless the variable follows this ordering strange results will occur. The variables $m$ and $n$ are respectively the $x$- and $y$-coordinates of the vertices.

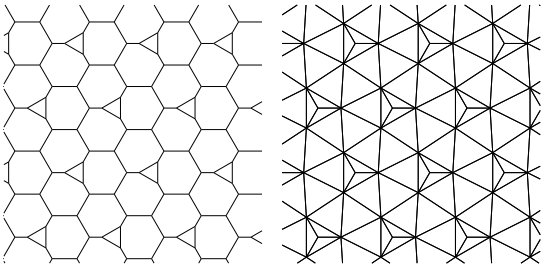

**(1)** $3_3[3^3]7_1[3^7]$

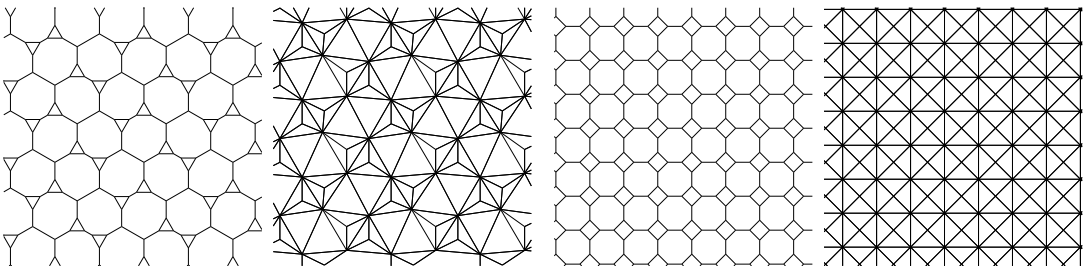

**(2)** $3_3[3^3]9_3[3^9]_{\mathrm{II}}$

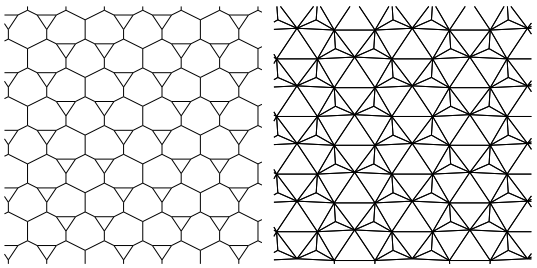

**(3)** $4_4[3^4]8_4[3^8]$

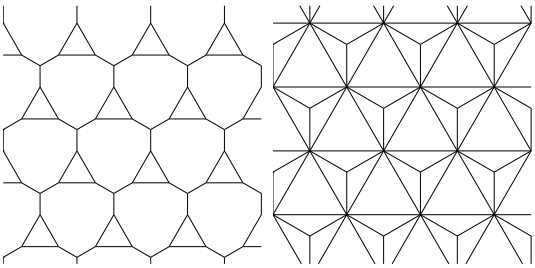

**(4)** $3_3[3^3]8_2[3^8]$

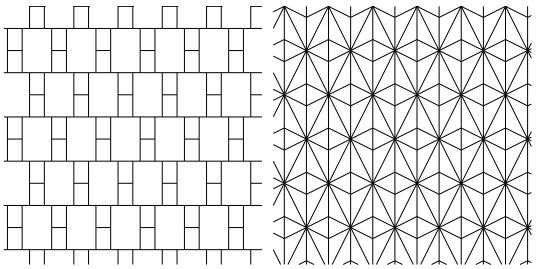

**(5)** $3_3[3^3]9_3[3^9]_{\mathrm{III}}$

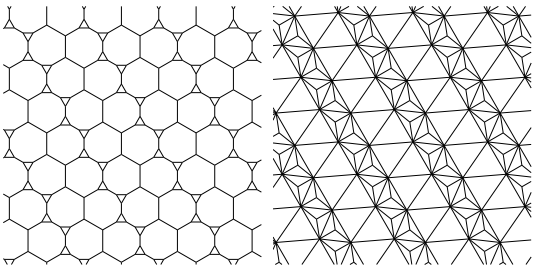

**(6)** $4_3[3^4]10_6[3^{10}]_{\mathrm{I}}$

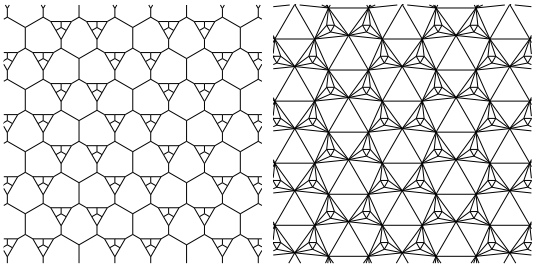

**(7)** $3_3[3^3]9_3[3^9]_{\mathrm{I}}$

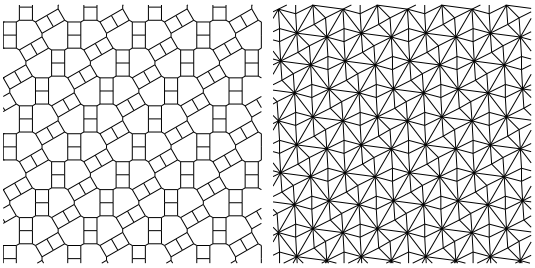

**(8)** $4_2[3^4]10_4[3^{10}]$

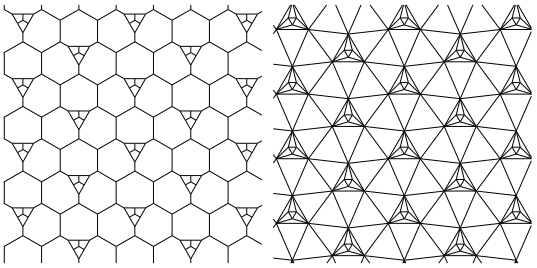

**(9)** $4_3[3^4]10_6[3^{10}]_{\mathrm{II}}$

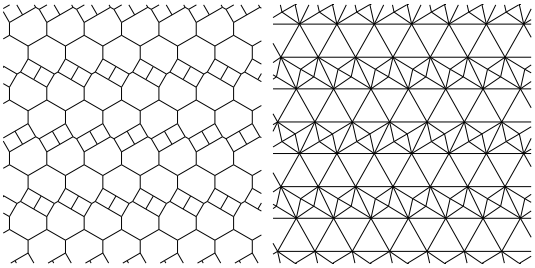

**(10)** $4_2[3^4]8_2[3^8]$

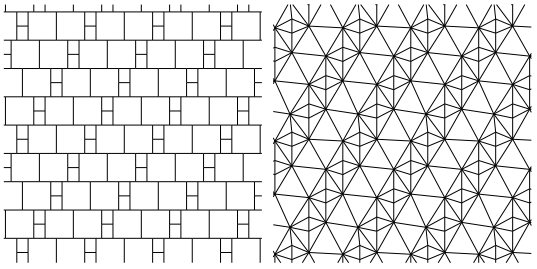

**(11)** $4_3[3^4]8_3[3^8]_{\mathrm{I}}$

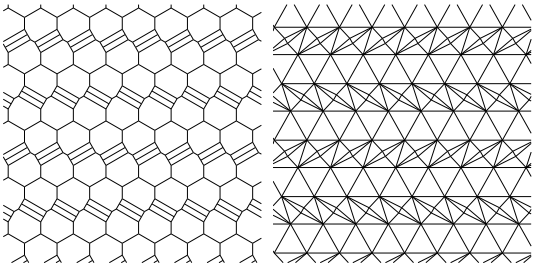

**(12)** $4_3[3^4]8_3[3^8]_{\mathrm{II}}$



**(13)** $4_3[3^4]8_3[3^8]_{\mathrm{III}}$

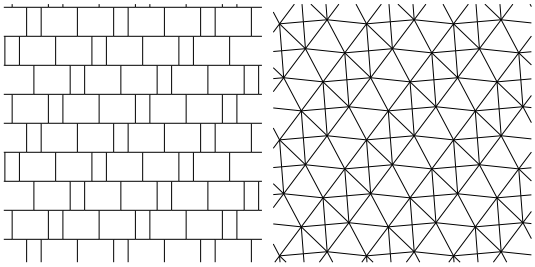

**(14)** $4_4[3^4]7_2[3^7]_{II}$

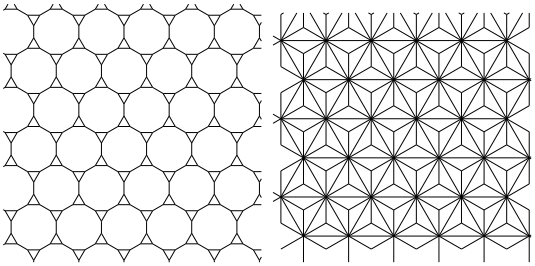

**(15)** $3_3[3^3]12_6[3^{12}]$

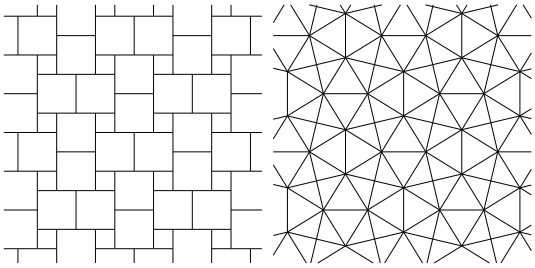

**(16)** $4_4[3^4]7_2[3^7]_{I}$

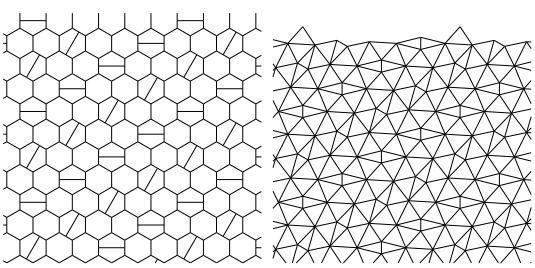

**(17)** $5_4[3^5]7_4[3^7]_{I}$

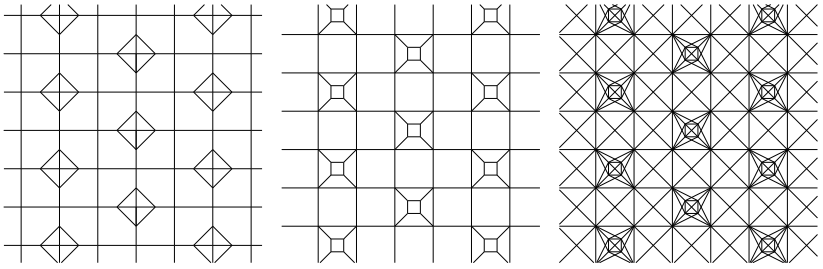

**(18)** $3_1[4^3]5_1[4^5]_{I}$

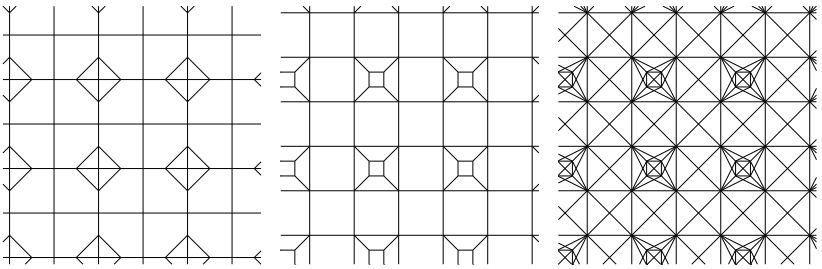

**(19)** $3_1[4^3]5_1[4^5]_{II}$

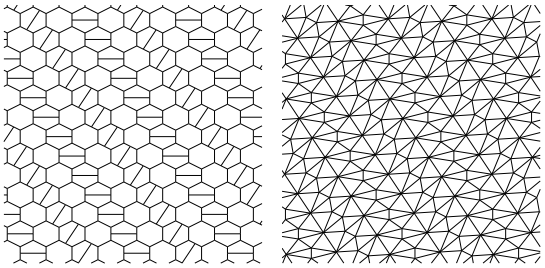

**(20)** $5_3[3^5]8_6[3^8]_{II}$

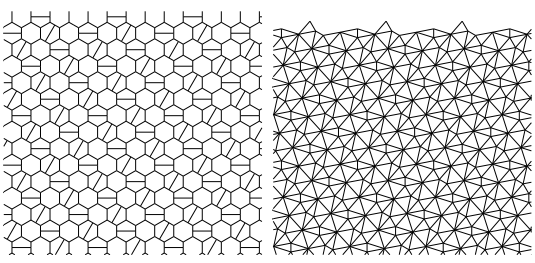

**(21)** $5_3[3^5]8_6[3^8]_{III}$

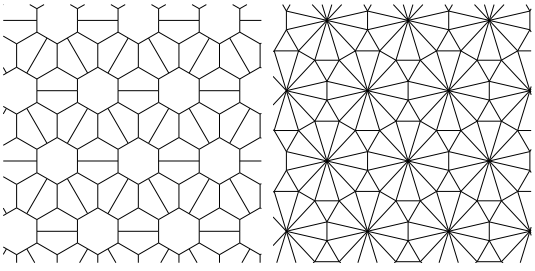

**(22)** $5_2[3^5]12_{12}[3^{12}]$

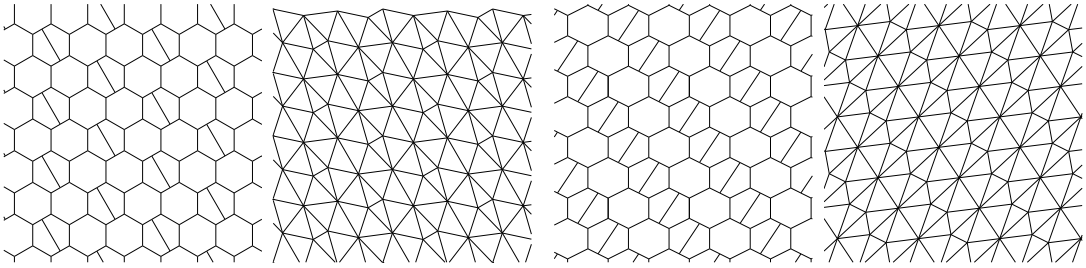

**(23)** $5_4[3^5]7_4[3^7]_{\mathrm{II}}$ **(24)** $5_3[3^5]8_6[3^8]_{\mathrm{I}}$

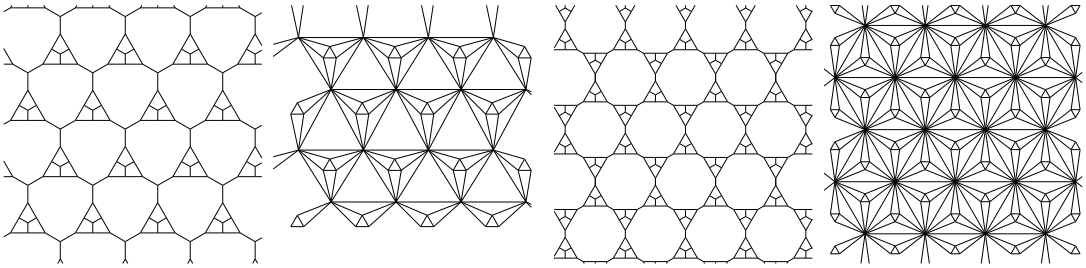

**(25)** $4_2[3^4]12_6[3^{12}]$ **(26)** $4_2[3^4]18_{12}[3^{18}]$

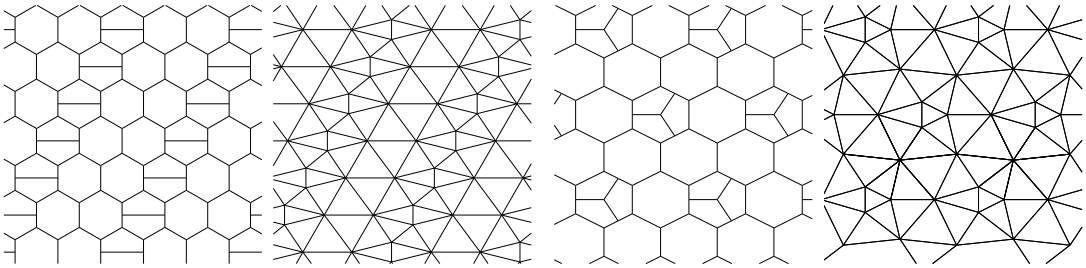

**(27)** $5_3[3^5]7_3[3^7]_{\mathrm{I}}$ **(28)** $5_3[3^5]7_3[3^7]_{\mathrm{II}}$

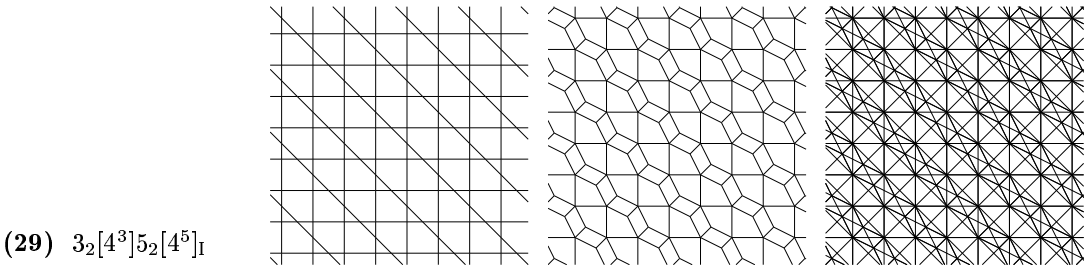

**(29)** $3_2[4^3]5_2[4^5]_{\mathrm{I}}$

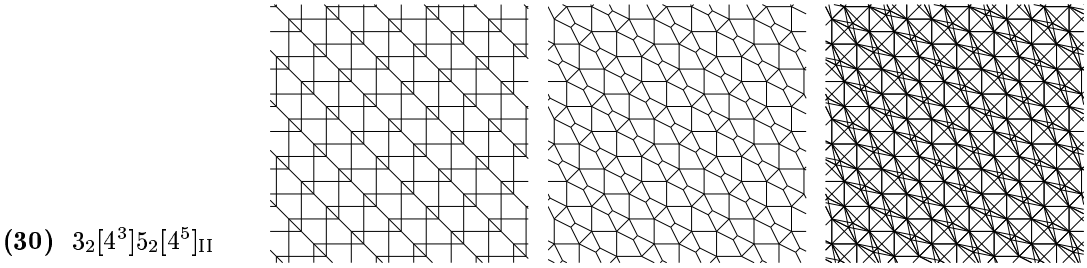

**(30)** $3_2[4^3]5_2[4^5]_{\mathrm{II}}$

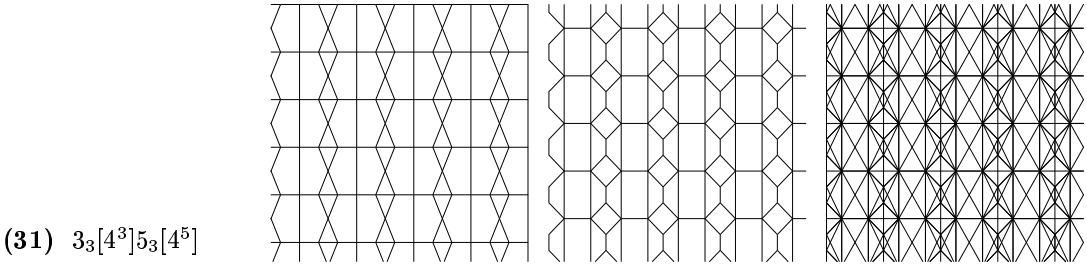

**(31)** $3_3[4^3]5_3[4^5]$

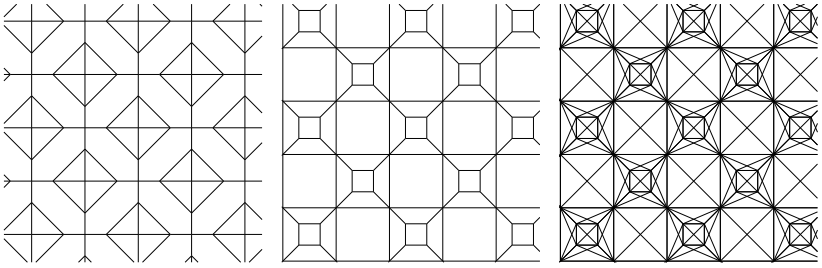

**(32)** $3_1[4^3]6_2[4^6]_{\mathrm{I}}$

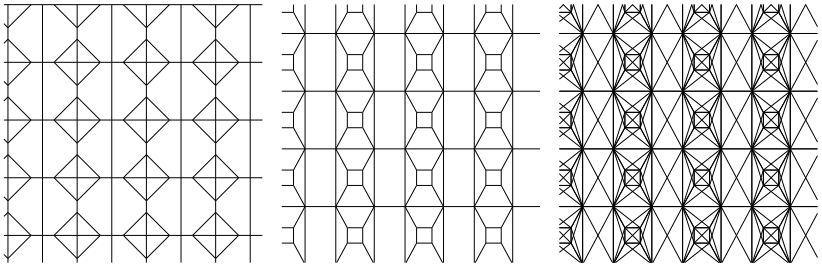

**(33)** $3_1[4^3]6_2[4^6]_{\mathrm{II}}$

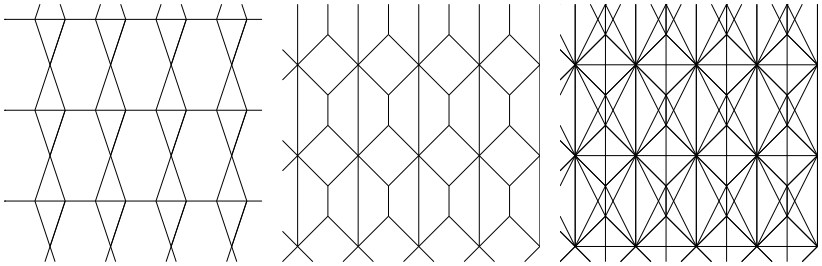

**(34)** $3_2[4^3]6_4[4^6]$

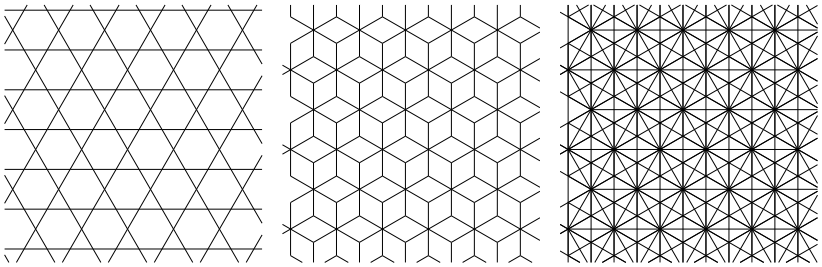

**(35)** $3_3[4^3]6_6[4^6]$

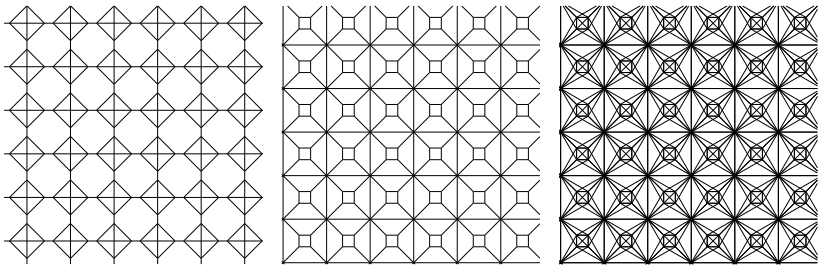

**(36)** $3_1[4^3]8_4[4^8]$

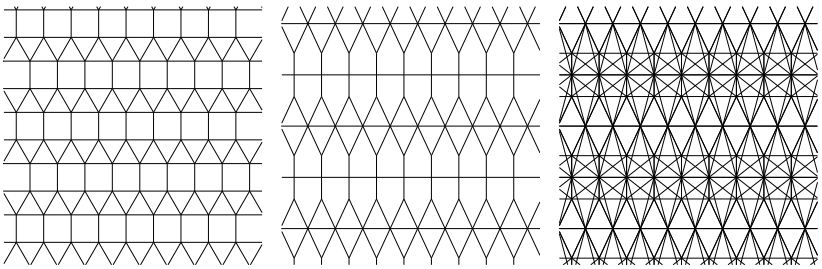

**(37)** $3_1[5^3]4_2[5^4]_{\mathrm{I}}$

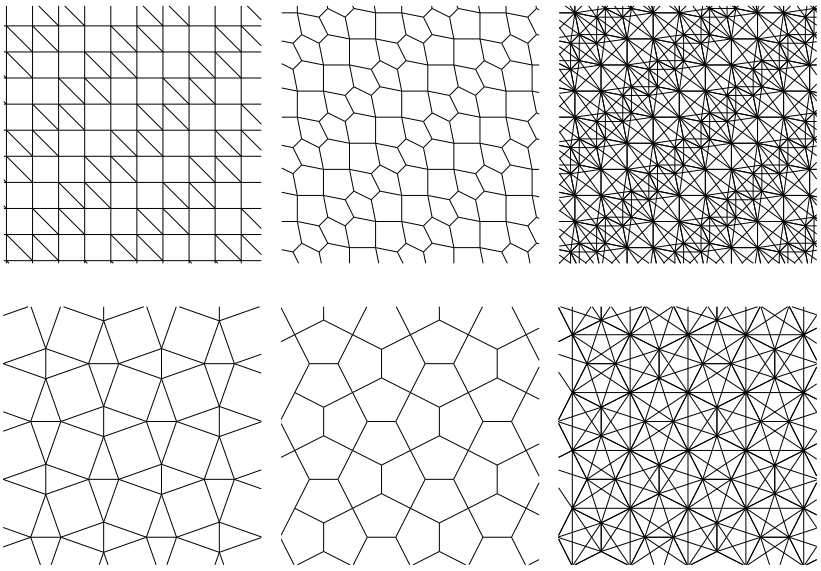

**(38)** $3_1[5^3]4_2[5^4]$

**(39)** $3_2[5^3]4_4[5^4]$

**Figure 4.12** *The thirty-nine 2-homohedral tilings and their covering lattices.*

Once while doing the above simulations I came across an interesting batch of the $4_4[3^4]7_2[3^7]_{\text{II}}$ 2-homohedral tiling where the percolations forward and backward in time gave the same value of $p_c$, that is there is an approximate time symmetry. In other words the $p_c$'s of both the first and the second population are symmetric to each other. Each percolates when its population reaches 756 out of the combined total of 1070, which identically gives $p_c = 0.7065$. Large non-percolating clusters quickly disappears after the onset of percolation as shown in Figure 4.13. In Figure 4.13 (b) the size of the second largest cluster is reduced to one between the population II of 941 and 961, which correspond to the density of 0.8794 and 0.8981 respectively. Interestingly from the population of 961 until 1070 there is only one cluster despite the fact that there are still more than one hundred population I. Here *population II* always refers to any population which percolates or which is being observed with regard to percolation. On the other hand in Figure 4.13 (b) the second biggest cluster is the smallest cluster from population 898 to 1037. Again from the population of 1038 until the maximum 1070 no second clusters appear.

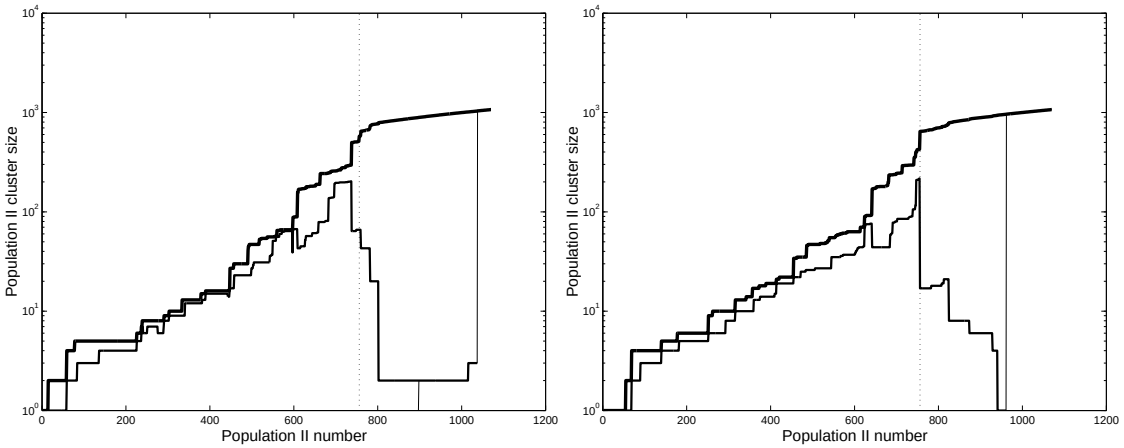


(a) (b)

**Figure 4.13** *The biggest, the second biggest, and the smallest cluster from a batch of the* $4_4[3^4]7_2[3^7]_{\text{II}}$ *2-homohedral tiling where the percolation happens to be symmetry in time, that is (a) and (b) are time symmetric to each other. The vertical dotted line is where the percolation point occurs in each case. The the heaviest to the lightest lines are respectively the progression of the clusters which are biggest, second biggest, and smallest at each population density.*

The percolation considered is that which percolates from the lower bound to the upper bound, both of which are fixed. Because the networks must be constructed such that there would be duplicates of neither vertices nor links, there must be cells some vertices and edges of which belong to one or more of the basic tiles adjacent to them. As a result, those basic tiles on the boundary

sometimes have a few of their cells missing, and depending on whether the basic tile in question is very complex or simple the position of the missing cell may merely lie on its boundary or may lie nearly halfway into its interior as is the case with the $4_3[3^4]8_3[3^8]_{\mathrm{I}}$ and the $4_3[3^4]8_3[3^8]_{\mathrm{III}}$ tilings. The upper and the lower boundaries, which decide the percolation, are chosen as straight lines parallel to the vertical axis and lying in the direction towards the interior of the network and at a fixed distance from the the maximum and the minimum horizontal positions respectively of all the vertices in the network. This fixed distance is defined for each network to be a fixed ratio of its overall width. The value of 0.05 had been used which was later changed to 0.1 due to a problem which occured while simulating the $4_2[3^4]8_2[3^8]$ tessellation, missing cells formed a continuous band disconnecting all the cells on the boundary from the rest of the network, the upper boundary lay within this band when shifted by five percent from the upper limit but not when shifted by ten percent.

The tilings in Figure 4.13 have the basic units shown in Figure 4.14.

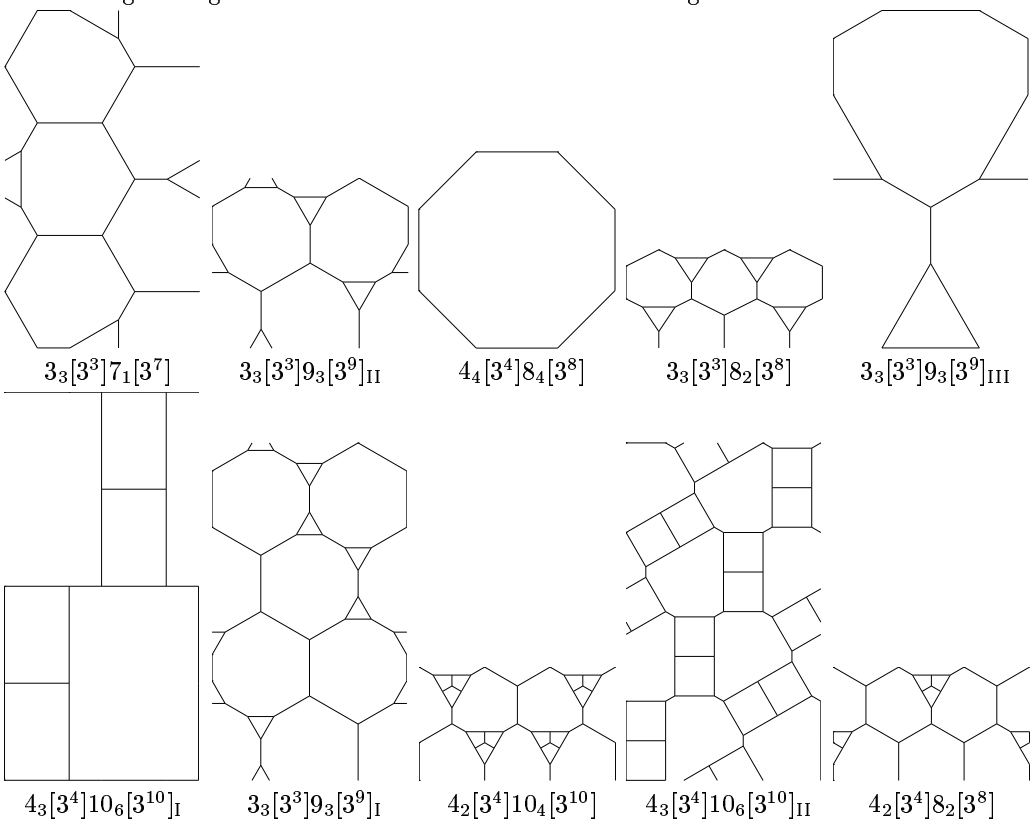

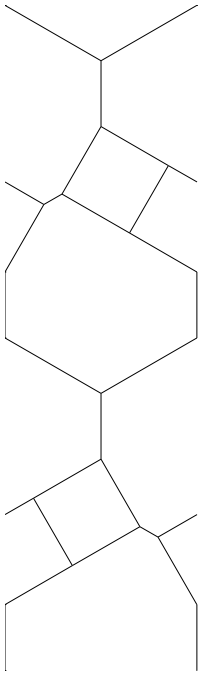

$4_3[3^4]8_3[3^8]_{\mathrm{I}}$

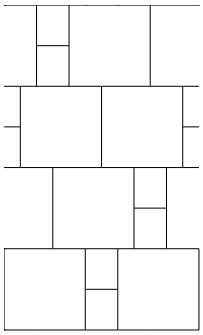

$4_3[3^4]8_3[3^8]_{\mathrm{II}}$

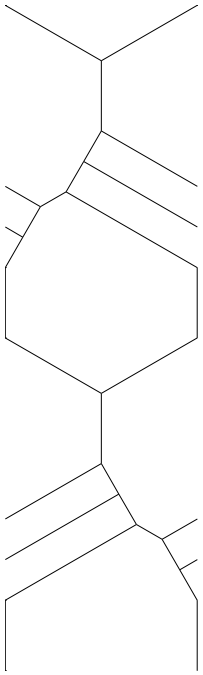

$4_3[3^4]8_3[3^8]_{\mathrm{III}}$

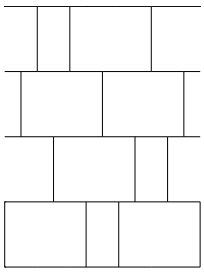

$4_4[3^4]7_2[3^7]_{\mathrm{II}}$

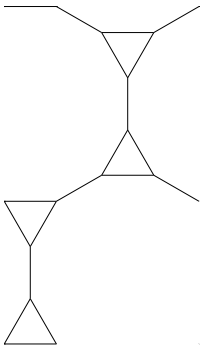

$3_3[3^3]12_6[3^{12}]$

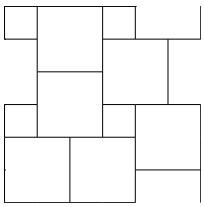

$4_4[3^4]7_2[3^7]_{\mathrm{I}}$

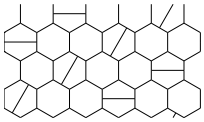

$5_4[3^5]7_4[3^7]_{\mathrm{I}}$

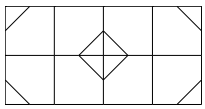

$3_1[4^3]5_1[4^5]_{\mathrm{I}}$

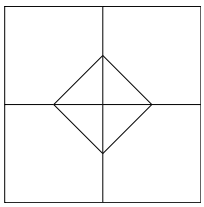

$3_1[4^3]5_1[4^5]_{\mathrm{II}}$

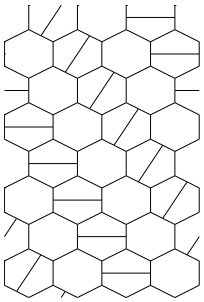

$5_3[3^5]8_6[3^8]_{\mathrm{II}}$

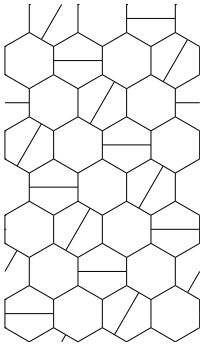

$5_3[3^5]8_6[3^8]_{\mathrm{III}}$

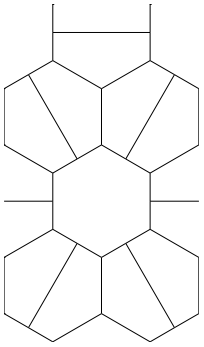

$5_2[3^5]12_{12}[3^{12}]$

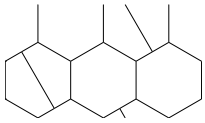

$5_4[3^5]7_4[3^7]_{\mathrm{II}}$

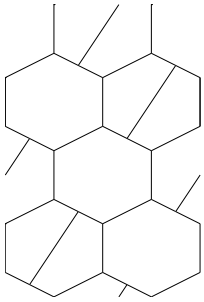

$5_3[3^5]8_6[3^8]_{\mathrm{I}}$

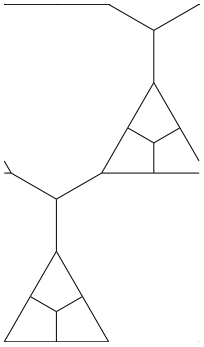

$4_2[3^4]12_6[3^{12}]$

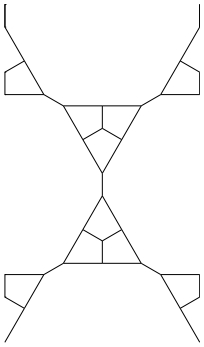

$4_2[3^4]18_{12}[3^{18}]$

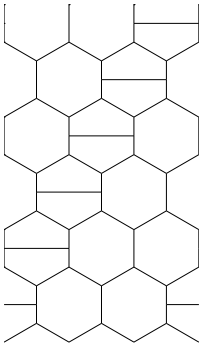

$5_3[3^5]7_3[3^7]_{\mathrm{I}}$

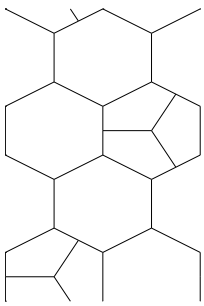

$5_3[3^5]7_3[3^7]_{\mathrm{II}}$

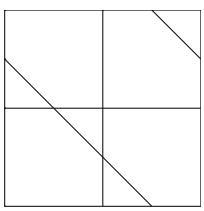

$3_2[4^3]5_2[4^5]_{\mathrm{I}}$

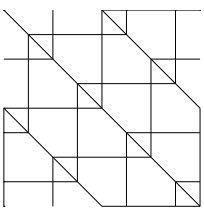

$3_2[4^3]5_2[4^5]_{\mathrm{II}}$

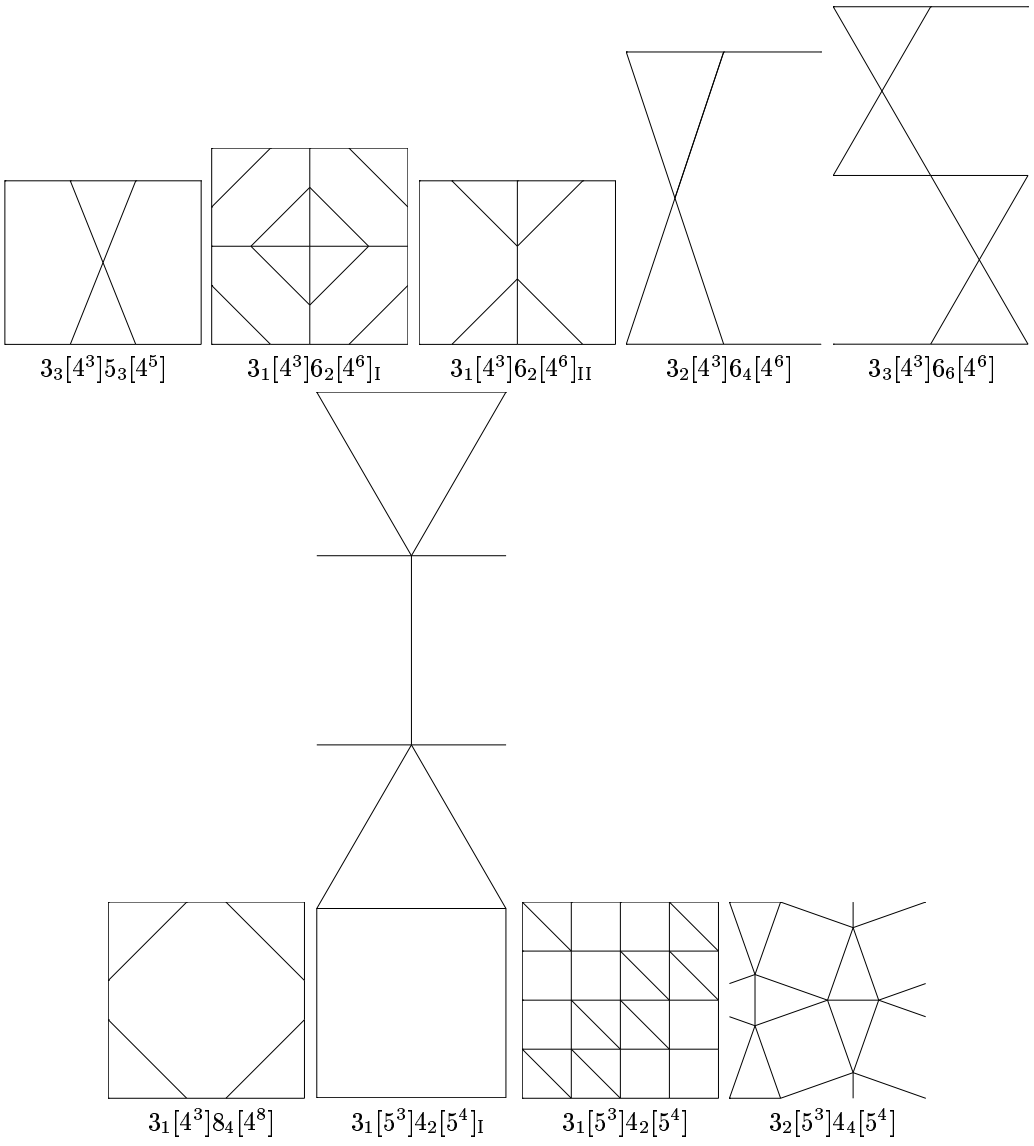


**Figure 4.14** *The unit cells of the* 2*-homohedral tilings.*

In Table 4.7 there are six types of percolation probabilities. Two cells can be neighbours to each other under the criterion of having either one or two vertices in common. This gives rise to two different values of $p_c$'s for cells, and another two for bonds. These can be termed 1-neighbours and 2-neighbours respectively. In Physics and other physical sciences 2-neighbours are more important because the greater the contact area is the stronger the bonding. This is not always the case in other fields, for example in Sociology a smaller point of contact sometimes implies the less duplications of neighbours' neighbours, and thus the larger the resultant networks. Because there is a cost for maintaining the connections, the smaller each contact point is and the larger the network the better, therefore here 1-neighbours seem to be more important.

**1.** $3_3[3^3]7_1[3^7]$

| *Cell* | *Bond* | *cell* | *bond* | *vertex* | *edge* |
|---|---|---|---|---|---|
| $0.4714\pm0.0667$ | $0.3041\pm0.0272$ | | | $0.7212\pm0.0444$ | $0.6771\pm0.0381$ |
| $1.1551\times10^{-6}$ | $-3.3740\times10^{-6}$ | | | $-1.1124\times10^{-4}$ | $-5.2007\times10^{-5}$ |
| $4.0885\times10^{-5}$ | $1.1316\times10^{-6}$ | | | $1.9314\times10^{-5}$ | $9.5566\times10^{-6}$ |
| 5[99], 4[195], | 12[1099] | | | 4[256], 4[470], | 4[349], 4[657], |
| 5.2525 5.4667 | 10.4149 | | | 2.7266 2.7957 | 3.7077 3.7869 |
| 12[391] | | | | 12[894] | 12[1275] |
| 5.6215 | | | | 2.8523 | 3.8494 |

**2.** $3_3[3^3]9_3[3^9]_{\mathrm{II}}$

| *Cell* | *Bond* | *cell* | *bond* | *vertex* | *edge* |
|---|---|---|---|---|---|
| 0.4966±0.0655<br>$-8.2288\times10^{-5}$<br>$3.7765\times10^{-5}$ | 0.2734±0.0206<br>$-5.5513\times10^{-6}$<br>$5.9281\times10^{-7}$ | 0.5042±0.0574<br>$-1.0585\times10^{-4}$<br>$2.1108\times10^{-5}$ | 0.3119±0.0417<br>$4.8211\times10^{-5}$<br>$7.5982\times10^{-6}$ | 0.7628±0.0228<br>$1.0042\times10^{-6}$<br>$7.3299\times10^{-7}$ | 0.7094±0.0435<br>$-2.7590\times10^{-5}$<br>$7.7345\times10^{-6}$ |
| 4[176], 2[139],<br>5.2727 5.1942<br>2[305], 6[412]<br>5.4492 5.5243 | 6[831], 6[1138]<br>12.0144 12.1564 | 2[305], 6[412]<br>5.0557 5.1165 | 2[771], 6[1054]<br>11.0298 11.1556 | 4[415], 2[334],<br>2.8193 2.7964<br>2[692], 6[919]<br>2.8584 2.8770 | 4[585], 2[467],<br>3.8120 3.7859<br>2[989], 6[1322]<br>3.8544 3.8744 |

**3.** $4_4[3^4]8_4[3^8]$

| *Cell* | *Bond* | *cell* | *bond* | *vertex* | *edge* |
|---|---|---|---|---|---|
| 0.4695±0.0858<br>$-3.5574\times10^{-5}$<br>$1.4884\times10^{-4}$ | 0.3044±0.0429<br>$2.8967\times10^{-5}$<br>$6.8367\times10^{-6}$ | | | 0.7194±0.0209<br>$-5.8481\times10^{-6}$<br>$6.5739\times10^{-7}$ | 0.6407±0.0296<br>$2.8990\times10^{-6}$<br>$2.0123\times10^{-6}$ |
| 2[181], 4[265],<br>5.5691 5.6453<br>12[313]<br>5.6741 | 4[748], 12[888]<br>10.5294 10.5946 | | | 1[440], 2[624],<br>2.7273 2.7692<br>6[728]<br>2.7857 | 2[600], 2[864],<br>3.7333 3.7778<br>6[1014]<br>3.7949 |

**4.** $3_3[3^3]8_2[3^8]$

| *Cell* | *Bond* | *cell* | *bond* | *vertex* | *edge* |
|---|---|---|---|---|---|
| 0.4903±0.1015<br>$1.2205\times10^{-4}$<br>$2.1262\times10^{-4}$ | 0.2926±0.0281<br>$-1.8541\times10^{-5}$<br>$1.9682\times10^{-6}$ | | | 0.7447±0.0329<br>$2.1925\times10^{-7}$<br>$2.8427\times10^{-6}$ | 0.7019±0.0270<br>$-6.4679\times10^{-6}$<br>$8.9933\times10^{-7}$ |
| 2[166], 4[301],<br>5.1928 5.3953<br>12[476]<br>5.5168 | 4[812], 12[1313]<br>11.0788 11.2749 | | | 2[381], 2[668],<br>2.8346 2.8743<br>6[1035]<br>2.8986 | 2[540], 2[960],<br>3.8444 3.8833<br>6[1500]<br>3.9067 |

**5.** $3_3[3^3]9_3[3^9]_{\mathrm{III}}$

| *Cell* | *Bond* | *cell* | *bond* | *vertex* | *edge* |
|---|---|---|---|---|---|
| 0.4607±0.0586<br>$7.9409\times10^{-5}$<br>$3.3840\times10^{-5}$ | 0.2483±0.0258<br>$4.8742\times10^{-6}$<br>$7.4553\times10^{-7}$ | | | 0.7482±0.0264<br>$2.4849\times10^{-6}$<br>$1.2161\times10^{-6}$ | 0.7049±0.0195<br>$-1.0461\times10^{-5}$<br>$1.0354\times10^{-6}$ |
| 2[83], 4[357],<br>4.6988 5.3613<br>12[438]<br>5.4247 | 4[957], 12[1188]<br>12.0878 12.1785 | | | 2[212], 2[808],<br>2.6792 2.8317<br>6[980]<br>2.8469 | 2[284], 2[1144],<br>3.6620 3.8322<br>6[1395]<br>3.8480 |

**6.** $4_3[3^4]10_6[3^{10}]_{\mathrm{I}}$

| *Cell* | *Bond* | *cell* | *bond* | *vertex* | *edge* |
|---|---|---|---|---|---|
| 0.5286±0.0511<br>$5.4350\times10^{-5}$<br>$1.7402\times10^{-5}$ | 0.2991±0.0319<br>$-8.0790\times10^{-6}$<br>$2.7687\times10^{-6}$ | | | 0.7789±0.0386<br>$8.7871\times10^{-6}$<br>$4.7653\times10^{-6}$ | 0.7173±0.0391<br>$-1.2114\times10^{-4}$<br>$1.8197\times10^{-5}$ |
| 8[188], 4[295],<br>5.3085 5.4441<br>12[426]<br>5.5352 | 8[499], 4[803],<br>11.2826 11.5691<br>12[1179]<br>11.7574 | | | 4[429], 2[656],<br>2.6853 2.7439<br>6[931]<br>2.7841 | 4[576], 2[900],<br>3.8333 3.8667<br>6[1296]<br>3.8889 |

**7.** $3_3[3^3]9_3[3^9]_{\mathrm{I}}$

| *Cell* | *Bond* | *cell* | *bond* | *vertex* | *edge* |
|---|---|---|---|---|---|
| 0.5206±0.0551<br>$-9.0646\times10^{-6}$<br>$1.7837\times10^{-5}$ | 0.2987±0.0308<br>$7.4580\times10^{-6}$<br>$1.7780\times10^{-6}$ | | | 0.7532±0.0296<br>$-8.9673\times10^{-6}$<br>$1.3152\times10^{-6}$ | 0.7063±0.0222<br>$-4.5643\times10^{-6}$<br>$7.3255\times10^{-7}$ |
| 4[259], 4[473],<br>5.3977 5.5518<br>6[751]<br>5.6431 | 4[699], 4[1313],<br>11.9371 12.2224<br>6[2119]<br>12.3870 | | | 2[594], 2[1048],<br>2.8485 2.8855<br>6[1630]<br>2.9080 | 2[846], 2[1512],<br>3.8440 3.8836<br>6[2370]<br>3.9072 |

**8.** $4_2[3^4]10_4[3^{10}]$

| *Cell* | *Bond* | *cell* | *bond* | *vertex* | *edge* |
|---|---|---|---|---|---|
| 0.4726±0.0684<br>$1.0814\times10^{-4}$<br>$8.0038\times10^{-5}$ | 0.2905±0.0633<br>$5.5163\times10^{-4}$<br>$1.3835\times10^{-4}$ | | | 0.7341±0.0316<br>$-8.0603\times10^{-6}$<br>$2.0508\times10^{-6}$ | 0.6957±0.0303<br>$7.5952\times10^{-7}$<br>$1.6121\times10^{-6}$ |
| 4[309], 4[556],<br>5.3722 5.5288<br>12[875]<br>5.6229 | 4[830], 4[1537],<br>11.3181 11.6695<br>12[2460]<br>11.8756 | | | 2[670], 2[1181],<br>2.9015 2.9263<br>6[1836]<br>2.9412 | 2[972], 2[1728],<br>3.9156 3.9363<br>6[2700]<br>3.9489 |

**9.** $4_3[3^4]10_6[3^{10}]_{\mathrm{II}}$

| *Cell* | *Bond* | *cell* | *bond* | *vertex* | *edge* |
|---|---|---|---|---|---|
| 0.4958±0.0796<br>$1.3909\times10^{-4}$<br>$8.0344\times10^{-5}$ | 0.3020±0.0381<br>$3.9193\times10^{-5}$<br>$6.3920\times10^{-6}$ | | | 0.7490±0.0461<br>$1.0834\times10^{-4}$<br>$1.4492\times10^{-5}$ | 0.6751±0.0199<br>$6.2752\times10^{-7}$<br>$3.7299\times10^{-7}$ |
| 4[325], 4[325],<br>5.3292 5.3292<br>12[532]<br>5.4737 | 4[866], 4[866],<br>11.5727 11.5727<br>12[1456]<br>11.8187 | | | 2[748], 2[748],<br>2.8369 2.8369<br>6[1187]<br>2.8711 | 2[1061], 2[1061],<br>3.8624 3.8624<br>6[1704]<br>3.8920 |

**10.** $4_2[3^4]8_2[3^8]$

| *Cell* | *Bond* | *cell* | *bond* | *vertex* | *edge* |
|---|---|---|---|---|---|
| $0.5102 \pm 0.0568$<br>$4.1767 \times 10^{-5}$<br>$3.0853 \times 10^{-5}$ | $0.3183 \pm 0.0405$<br>$-9.0691 \times 10^{-6}$<br>$7.8890 \times 10^{-6}$ | | | $0.7202 \pm 0.0493$<br>$-1.1640 \times 10^{-4}$<br>$2.1475 \times 10^{-5}$ | $0.6953 \pm 0.0307$<br>$1.5917 \times 10^{-5}$<br>$1.8233 \times 10^{-6}$ |
| 4[259], 4[385],<br>5.2741 5.4026<br>12[535]<br>5.4916 | 4[683], 4[1040],<br>10.3309 10.5096<br>12[1469]<br>10.6331 | | | 2[613], 2[884],<br>2.8189 2.8507<br>6[1203]<br>2.8728 | 2[864], 2[1260],<br>3.8356 3.8651<br>6[1728]<br>3.8854 |

**11.** $4_3[3^4]8_3[3^8]_{\mathrm{I}}$

| *Cell* | *Bond* | *cell* | *bond* | *vertex* | *edge* |
|---|---|---|---|---|---|
| $0.4577 \pm 0.0761$<br>$-2.5782 \times 10^{-5}$<br>$8.4655 \times 10^{-5}$ | $0.2910 \pm 0.0421$<br>$-1.6419 \times 10^{-5}$<br>$7.8109 \times 10^{-6}$ | | | $0.6887 \pm 0.0279$<br>$8.0593 \times 10^{-7}$<br>$7.8808 \times 10^{-7}$ | $0.6532 \pm 0.0340$<br>$-2.5506 \times 10^{-5}$<br>$3.2110 \times 10^{-6}$ |
| 4[195], 4[356],<br>5.3231 5.4944<br>12[487]<br>5.5647 | 4[519], 4[978],<br>10.2736 10.5562<br>12[1355]<br>10.6657 | | | 2[454], 2[797],<br>2.8282 2.8708<br>6[1074]<br>2.8864 | 2[642], 2[1144],<br>3.8349 3.8759<br>6[1550]<br>3.8903 |

**12.** $4_3[3^4]8_3[3^8]_{\mathrm{II}}$

| *Cell* | *Bond* | *cell* | *bond* | *vertex* | *edge* |
|---|---|---|---|---|---|
| $0.5030 \pm 0.0603$<br>$2.6397 \times 10^{-5}$<br>$4.0377 \times 10^{-5}$ | $0.3166 \pm 0.0334$<br>$-1.3936 \times 10^{-5}$<br>$2.7675 \times 10^{-6}$ | | | $0.7385 \pm 0.0255$<br>$-2.6605 \times 10^{-6}$<br>$9.6100 \times 10^{-7}$ | $0.6718 \pm 0.0369$<br>$1.8952 \times 10^{-6}$<br>$3.1533 \times 10^{-6}$ |
| 4[219], 4[419],<br>5.3151 5.4988<br>12[683]<br>5.6047 | 4[582], 4[1152],<br>10.2818 10.5799<br>12[1914]<br>10.7461 | | | 2[517], 2[947],<br>2.7505 2.8131<br>6[1505]<br>2.8505 | 2[711], 2[1332],<br>3.8312 3.8769<br>6[2145]<br>3.9030 |

**13.** $4_3[3^4]8_3[3^8]_{\mathrm{III}}$

| *Cell* | *Bond* | *cell* | *bond* | *vertex* | *edge* |
|---|---|---|---|---|---|
| $0.4931 \pm 0.0560$<br>$1.5620 \times 10^{-4}$<br>$3.1433 \times 10^{-5}$ | $0.2927 \pm 0.0320$<br>$3.0191 \times 10^{-5}$<br>$6.4721 \times 10^{-6}$ | | | $0.7294 \pm 0.0348$<br>$4.5084 \times 10^{-6}$<br>$2.5226 \times 10^{-6}$ | $0.6730 \pm 0.0289$<br>$-2.7067 \times 10^{-5}$<br>$3.4615 \times 10^{-6}$ |
| 4[212], 4[410],<br>5.3491 5.5268<br>12[594]<br>5.6061 | 4[567], 4[1133],<br>10.3069 10.6019<br>12[1665]<br>10.7267 | | | 2[503], 2[927],<br>2.8151 2.8652<br>6[1317]<br>2.8853 | 2[708], 2[1328],<br>3.8107 3.8630<br>6[1900]<br>3.8832 |

**14.** $4_4[3^4]7_2[3^7]_{\mathrm{II}}$

| *Cell* | *Bond* | *cell* | *bond* | *vertex* | *edge* |
|---|---|---|---|---|---|
| $0.4761 \pm 0.0432$<br>$-7.3074 \times 10^{-5}$<br>$9.5057 \times 10^{-6}$ | $0.3174 \pm 0.0396$<br>$3.7498 \times 10^{-5}$<br>$6.2114 \times 10^{-6}$ | | | $0.7144 \pm 0.0228$<br>$7.2116 \times 10^{-6}$<br>$6.1119 \times 10^{-7}$ | $0.6440 \pm 0.0371$<br>$2.2191 \times 10^{-5}$<br>$3.8797 \times 10^{-6}$ |
| 8[345], 12[486]<br>5.5710 5.6379 | 8[961], 12[1370]<br>10.0208 10.1241 | | | 4[767], 12[1063]<br>2.7901 2.8222 | 4[1070], 12[1500]<br>3.8579 3.8800 |

**15.** $3_3[3^3]12_6[3^{12}]$

| *Cell* | *Bond* | *cell* | *bond* | *vertex* | *edge* |
|---|---|---|---|---|---|
| $0.5077 \pm 0.0896$<br>$4.5180 \times 10^{-4}$<br>$3.2202 \times 10^{-4}$ | $0.2640 \pm 0.0333$<br>$2.5513 \times 10^{-6}$<br>$3.2552 \times 10^{-6}$ | | | $0.8273 \pm 0.0209$<br>$1.3947 \times 10^{-5}$<br>$1.6592 \times 10^{-6}$ | $0.7269 \pm 0.0313$<br>$-2.2183 \times 10^{-6}$<br>$1.6715 \times 10^{-6}$ |
| 4[154], 4[223],<br>4.5065 4.7444<br>4[374], 12[520]<br>5.0214 5.1654 | 4[347], 4[529],<br>13.9135 14.2949<br>4[939 ], 12[1343]<br>14.7178 14.9248 | | | 2[359], 2[507],<br>2.8078 2.8402<br>2[827], 6[1133]<br>2.8730 2.8914 | 2[504], 2[720],<br>3.8333 3.8611<br>2[1188], 6[1638]<br>3.8889 3.9048 |

**16.** $4_4[3^4]7_2[3^7]_{\mathrm{I}}$

| *Cell* | *Bond* | *cell* | *bond* | *vertex* | *edge* |
|---|---|---|---|---|---|
| $0.4774 \pm 0.0624$<br>$-1.6958 \times 10^{-4}$<br>$4.8309 \times 10^{-5}$ | $0.3140 \pm 0.0390$<br>$3.5112 \times 10^{-5}$<br>$9.6223 \times 10^{-6}$ | | | $0.7305 \pm 0.0263$<br>$7.4362 \times 10^{-6}$<br>$1.0424 \times 10^{-6}$ | $0.6504 \pm 0.0349$<br>$1.7310 \times 10^{-5}$<br>$3.0145 \times 10^{-6}$ |
| 8[403], 12[554]<br>5.4591 5.5379 | 8[1100], 12[1534]<br>10.0236 10.1213 | | | 4[1050], 6[1421]<br>2.4686 2.4828 | 4[1296], 6[1764]<br>3.8704 3.8889 |

**17.** $5_4[3^5]7_4[3^7]_{\mathrm{I}}$

| *Cell* | *Bond* | *cell* | *bond* | *vertex* | *edge* |
|---|---|---|---|---|---|
| $0.5112 \pm 0.0412$<br>$-5.3542 \times 10^{-5}$<br>$8.4833 \times 10^{-6}$ | $0.3406 \pm 0.0207$<br>$2.1641 \times 10^{-6}$<br>$5.0113 \times 10^{-7}$ | | | $0.7029 \pm 0.0507$<br>$-5.7814 \times 10^{-5}$<br>$1.4169 \times 10^{-5}$ | $0.6645 \pm 0.0300$<br>$9.3355 \times 10^{-6}$<br>$1.5205 \times 10^{-6}$ |
| 4[173], 4[450],<br>5.3179 5.5733<br>12[729]<br>5.6653 | 4[460], 4[1254],<br>9.4391 9.7895<br>12[2065]<br>9.9090 | | | 2[411], 2[1003],<br>2.7932 2.8654<br>6[1590]<br>2.8931 | 2[574], 2[1437],<br>3.8188 3.8859<br>6[2300]<br>3.9096 |

**18.** $3_1[4^3]5_1[4^5]_{\mathrm{I}}$

| *Cell* | *Bond* | *cell* | *bond* | *vertex* | *edge* |
|---|---|---|---|---|---|
| $0.4003 \pm 0.0534$ | $0.2368 \pm 0.0198$ | $0.5786 \pm 0.0400$ | $0.4595 \pm 0.0398$ | $0.6184 \pm 0.0356$ | $0.5109 \pm 0.0531$ |
| $-1.4626 \times 10^{-5}$ | $-5.2284 \times 10^{-6}$ | $3.9800 \times 10^{-5}$ | $-2.9462 \times 10^{-5}$ | $-1.2175 \times 10^{-6}$ | $2.0112 \times 10^{-5}$ |
| $1.5617 \times 10^{-5}$ | $3.5502 \times 10^{-7}$ | $5.2273 \times 10^{-6}$ | $5.1123 \times 10^{-6}$ | $2.6728 \times 10^{-6}$ | $1.7919 \times 10^{-5}$ |
| 4[508] , 6[795] | 4[1872], 6[2979] | 4[508], 6[795] | 4[961], 6[1521] | 4[569], 6[871] | 4[1024], 6[1600] |
| 7.37kk01 7.4943 | 14.1731 14.3411 | 3.7835 3.8264 | 6.1748 6.2406 | 3.5993 3.6739 | 5.6738 5.7387 |

**19.** $3_1[4^3]5_1[4^5]_{\mathrm{II}}$

| *Cell* | *Bond* | *cell* | *bond* | *vertex* | *edge* |
|---|---|---|---|---|---|
| $0.4065 \pm 0.0646$ | $0.2309 \pm 0.0241$ | $0.5898 \pm 0.0633$ | $0.4394 \pm 0.0536$ | $0.6423 \pm 0.0381$ | $0.5049 \pm 0.0271$ |
| $-9.8055 \times 10^{-5}$ | $2.2560 \times 10^{-6}$ | $-1.8568 \times 10^{-6}$ | $-1.3300 \times 10^{-4}$ | $-5.1659 \times 10^{-5}$ | $-9.8556 \times 10^{-7}$ |
| $3.7012 \times 10^{-5}$ | $6.6307 \times 10^{-7}$ | $3.3297 \times 10^{-5}$ | $3.6224 \times 10^{-5}$ | $7.7919 \times 10^{-6}$ | $8.8048 \times 10^{-7}$ |
| 4[512], 6[648] | 4[1954], 6[2486] | 4[512], 6[648] | 4[992], 6[1260] | 4[545], 6[685] | 4[1024], 6[1296] |
| 7.6328 7.6728 | 14.2027 14.2912 | 3.8750 3.8889 | 6.2016 6.2349 | 3.7578 3.7839 | 5.8145 5.8349 |

**20.** $5_3[3^5]8_6[3^8]_{\mathrm{II}}$

| *Cell* | *Bond* | *cell* | *bond* | *vertex* | *edge* |
|---|---|---|---|---|---|
| $0.4631 \pm 0.0471$ | $0.3164 \pm 0.0255$ | | | $0.6800 \pm 0.0384$ | $0.6587 \pm 0.0246$ |
| $2.8969 \times 10^{-5}$ | $3.0266 \times 10^{-6}$ | | | $-9.9185 \times 10^{-6}$ | $1.5506 \times 10^{-6}$ |
| $1.3943 \times 10^{-5}$ | $1.2108 \times 10^{-6}$ | | | $4.4523 \times 10^{-6}$ | $6.3039 \times 10^{-7}$ |
| 4[260], 4[675], | 4[706], 4[1906], | | | 2[608], 2[1490], | 2[857], 2[2149], |
| 5.4308 5.6474 | 9.8669 10.1815 | | | 2.8191 2.8846 | 3.8273 3.8920 |
| 12[1095] | 12[3132] | | | 6[2368] | 6[3442] |
| 5.7205 | 10.2854 | | | 2.9071 | 3.9140 |

**21.** $5_3[3^5]8_6[3^8]_{\mathrm{III}}$

| *Cell* | *Bond* | *cell* | *bond* | *vertex* | *edge* |
|---|---|---|---|---|---|
| $0.5052 \pm 0.0474$ | $0.3211 \pm 0.0274$ | | | $0.7145 \pm 0.0299$ | $0.6469 \pm 0.0242$ |
| $-1.6178 \times 10^{-6}$ | $-9.4980 \times 10^{-6}$ | | | $8.1493 \times 10^{-6}$ | $-1.0841 \times 10^{-5}$ |
| $1.0710 \times 10^{-5}$ | $2.4172 \times 10^{-6}$ | | | $1.7096 \times 10^{-6}$ | $7.2095 \times 10^{-7}$ |
| 8[351], 12[814] | 8[971], 12[2316] | | | 4[804], 6[1782] | 4[1144], 6[2580] |
| 5.5328 5.6904 | 10.0062 10.2366 | | | 2.8458 2.8956 | 3.8531 3.9023 |

**22.** $5_2[3^5]12_{12}[3^{12}]$

| *Cell* | *Bond* | *cell* | *bond* | *vertex* | *edge* |
|---|---|---|---|---|---|
| $0.4897 \pm 0.0718$ | $0.3037 \pm 0.0257$ | | | $0.7384 \pm 0.0258$ | $0.6694 \pm 0.0297$ |
| $-1.4823 \times 10^{-4}$ | $-1.3145 \times 10^{-5}$ | | | $3.3765 \times 10^{-6}$ | $1.5898 \times 10^{-5}$ |
| $1.0656 \times 10^{-4}$ | $1.4342 \times 10^{-6}$ | | | $8.4513 \times 10^{-7}$ | $2.4608 \times 10^{-6}$ |
| 4[192], 8[530], | 4[498], 8[1457], | | | 2[442], 4[1156], | 2[627], 4[1675], |
| 5.1875 5.4981 | 10.8072 11.2972 | | | 2.8371 2.8979 | 3.8405 3.9021 |
| 12[803] | 12[2244] | | | 6[1724] | 6[2514] |
| 5.5890 | 11.4332 | | | 2.9165 | 3.9204 |

**23.** $5_4[3^5]7_4[3^7]_{\mathrm{II}}$

| *Cell* | *Bond* | *cell* | *bond* | *vertex* | *edge* |
|---|---|---|---|---|---|
| $0.5001 \pm 0.0342$ | $0.3327 \pm 0.0329$ | | | $0.6973 \pm 0.0235$ | $0.6688 \pm 0.0303$ |
| $1.7585 \times 10^{-5}$ | $4.4678 \times 10^{-5}$ | | | $-7.2307 \times 10^{-6}$ | $2.4051 \times 10^{-5}$ |
| $3.4856 \times 10^{-6}$ | $5.2573 \times 10^{-6}$ | | | $5.9288 \times 10^{-7}$ | $2.0921 \times 10^{-6}$ |
| 8[371], 12[541] | 8[1027], 12[1519] | | | 4[835], 6[1194] | 4[1195], 6[1722] |
| 5.5364 5.6155 | 9.7254 9.8328 | | | 2.8623 2.8844 | 3.8661 3.8885 |

**24.** $5_3[3^5]8_6[3^8]_{\mathrm{I}}$

| *Cell* | *Bond* | *cell* | *bond* | *vertex* | *edge* |
|---|---|---|---|---|---|
| $0.4867 \pm 0.0459$ | $0.3265 \pm 0.0237$ | | | $0.7108 \pm 0.0200$ | $0.6720 \pm 0.0294$ |
| $-1.0891 \times 10^{-4}$ | $-3.7362 \times 10^{-6}$ | | | $2.8929 \times 10^{-6}$ | $6.2044 \times 10^{-6}$ |
| $3.3218 \times 10^{-5}$ | $7.9808 \times 10^{-7}$ | | | $4.2792 \times 10^{-7}$ | $3.1424 \times 10^{-6}$ |
| 6[214], 8[535], | 4[577], 8[1502], | | | 2[506], 4[1192], | 2[731], 4[1762], |
| 5.3925 5.6150 | 9.8024 10.1278 | | | 2.8261 2.8859 | 3.9398 4.0204 |
| 12[790] | 12[2245] | | | 6[1728] | 6[2573] |
| 5.6835 | 10.2254 | | | 2.9051 | 4.0459 |

**25.** $4_2[3^4]12_6[3^{12}]$

| *Cell* | *Bond* | *cell* | *bond* | *vertex* | *edge* |
|---|---|---|---|---|---|
| $0.5117 \pm 0.0960$ | $0.2637 \pm 0.0295$ | | | $0.7861 \pm 0.0215$ | $0.7273 \pm 0.0227$ |
| $1.0580 \times 10^{-4}$ | $-4.6675 \times 10^{-6}$ | | | $7.1685 \times 10^{-6}$ | $1.1750 \times 10^{-6}$ |
| $2.1578 \times 10^{-4}$ | $1.9508 \times 10^{-6}$ | | | $4.3496 \times 10^{-7}$ | $7.1142 \times 10^{-7}$ |
| 4[200], 8[444], | 4[461], 8[1121], | | | 2[474], 4[997], | 2[664], 4[1428], |
| 4.6100 5.0495 | 11.1714 12.1802 | | | 2.8017 2.8646 | 3.8614 3.9048 |
| 12[629] | 12[1633] | | | 6[1388] | 6[2002] |
| 5.1924 | 12.4850 | | | 2.8847 | 3.9191 |

**26.** $4_2[3^4]18_{12}[3^{18}]$

| *Cell* | *Bond* | *cell* | *bond* | *vertex* | *edge* |
|---|---|---|---|---|---|
| $0.5249 \pm 0.1168$ | $0.2493 \pm 0.0632$ | | | $0.8497 \pm 0.0234$ | $0.7743 \pm 0.0483$ |
| $1.1603 \times 10^{-3}$ | $7.1820 \times 10^{-4}$ | | | $5.2173 \times 10^{-6}$ | $8.6384 \times 10^{-5}$ |
| $6.1479 \times 10^{-4}$ | $2.0594 \times 10^{-4}$ | | | $6.1183 \times 10^{-7}$ | $1.2578 \times 10^{-5}$ |
| 8[237], 4[428], | 8[576], 4[1101], | | | 4[529], 2[929], | 4[774], 2[1376], |
| 4.8608 5.1449 | 15.0868 15.8656 | | | 2.8696 2.9020 | 3.9664 4.0087 |
| 12[675] | 12[1794] | | | 6[1441] | 6[2150] |
| 5.3156 | 16.3155 | | | 2.9216 | 4.0344 |

**27.** $5_3[3^5]7_3[3^7]_{\mathrm{I}}$

| *Cell* | *Bond* | *cell* | *bond* | *vertex* | *edge* |
|---|---|---|---|---|---|
| 0.4882±0.0494<br>$-4.4634\times10^{-5}$<br>$1.5462\times10^{-5}$ | 0.3335±0.0310<br>$-1.2425\times10^{-5}$<br>$2.4243\times10^{-6}$ | | | 0.7149±0.0273<br>$1.6306\times10^{-6}$<br>$9.8464\times10^{-7}$ | 0.6495±0.0278<br>$5.9525\times10^{-6}$<br>$1.4733\times10^{-6}$ |
| 4[170], 4[399]<br>5.3529 5.5739 | 4[455], 4[1112]<br>9.4110 9.7392 | | | 2[413], 2[907]<br>2.7797 2.8512 | 2[574], 2[1293]<br>3.8084 3.8716 |

**28.** $5_3[3^5]7_3[3^7]_{\mathrm{II}}$

| *Cell* | *Bond* | *cell* | *bond* | *vertex* | *edge* |
|---|---|---|---|---|---|
| 0.4345±0.0489<br>$8.3482\times10^{-5}$<br>$4.0009\times10^{-5}$ | 0.2930±0.0243<br>$-9.3058\times10^{-6}$<br>$1.1454\times10^{-6}$ | 0.4785±0.0354<br>$4.7566\times10^{-5}$<br>$7.5326\times10^{-6}$ | 0.3239±0.0187<br>$-4.1986\times10^{-6}$<br>$3.8717\times10^{-7}$ | 0.6900±0.0283<br>$-7.8267\times10^{-6}$<br>$1.5860\times10^{-6}$ | 0.6421±0.0289<br>$3.4481\times10^{-6}$<br>$1.8973\times10^{-6}$ |
| 2[167], 2[61],<br>5.8443 5.2787<br>6[535]<br>6.2430 | 2[161] 6[1670]<br>9.8137 11.3257 | 2[167], 2[61],<br>5.7485 5.2131<br>6[535]<br>6.1234 | 2[480], 2[159],<br>10.4458 9.5849<br>6[1638]<br>11.0000 | 2[386], 2[161],<br>2.7720 2.6460<br>6[1124]<br>2.8665 | 2[535], 2[213],<br>3.8019 3.6901<br>6[1611]<br>3.8845 |

**29.** $3_2[4^3]5_2[4^5]_{\mathrm{I}}$

| *Cell* | *Bond* | *cell* | *bond* | *vertex* | *edge* |
|---|---|---|---|---|---|
| 0.4099±0.0264<br>$4.7650\times10^{-6}$<br>$1.0783\times10^{-6}$ | 0.2271±0.0154<br>$2.1524\times10^{-6}$<br>$1.2777\times10^{-7}$ | 0.5687±0.0469<br>$2.6238\times10^{-5}$<br>$8.5056\times10^{-6}$ | 0.5028±0.0283<br>$1.1978\times10^{-5}$<br>$1.1260\times10^{-6}$ | 0.6228±0.0346<br>$-1.1730\times10^{-5}$<br>$5.5785\times10^{-6}$ | 0.5022±0.0343<br>$3.4916\times10^{-5}$<br>$3.2050\times10^{-6}$ |
| 2[277], 2[379],<br>7.3285 7.4248<br>6[497]<br>7.4970 | 2[1407], 6[1863]<br>14.0640 14.1857 | 2[277], 2[379],<br>3.7473 3.7836<br>6[497]<br>3.8109 | 2[519], 2[717],<br>6.0308 6.1004<br>6[947]<br>6.1521 | 2[325], 2[435],<br>3.5446 3.6046<br>6[561]<br>3.6506 | 2[576], 2[784],<br>5.6285 5.6811<br>6[1024]<br>5.7207 |

**30.** $3_2[4^3]5_2[4^5]_{\mathrm{II}}$

| *Cell* | *Bond* | *cell* | *bond* | *vertex* | *edge* |
|---|---|---|---|---|---|
| 0.4322±0.0512<br>$5.8373\times10^{-5}$<br>$1.9444\times10^{-5}$ | 0.2344±0.0171<br>$-1.5204\times10^{-6}$<br>$2.2157\times10^{-7}$ | 0.5638±0.0590<br>$4.8226\times10^{-6}$<br>$1.5253\times10^{-5}$ | 0.4749±0.0440<br>$-5.1510\times10^{-5}$<br>$1.0399\times10^{-5}$ | 0.6260±0.0368<br>$-2.9282\times10^{-5}$<br>$6.7165\times10^{-6}$ | 0.5468±0.0270<br>$8.1058\times10^{-6}$<br>$1.6103\times10^{-6}$ |
| 2[276], 2[496],<br>7.1812 7.3831<br>6[780]<br>7.5051 | 2[1831], 6[2927]<br>14.1038 14.2890 | 2[276], 2[496],<br>3.6739 3.7540<br>6[780]<br>3.8026 | 2[507], 2[931],<br>5.9961 6.1267<br>6[1483]<br>6.2036 | 2[313], 2[545],<br>3.6422 3.7284<br>6[841]<br>3.7812 | 2[570], 2[1016],<br>5.6702 5.7520<br>6[1590]<br>5.8013 |

**31.** $3_3[4^3]5_3[4^5]$

| *Cell* | *Bond* | *cell* | *bond* | *vertex* | *edge* |
|---|---|---|---|---|---|
| 0.5029±0.0759<br>$8.6335\times10^{-6}$<br>$1.4737\times10^{-4}$ | 0.2504±0.0233<br>$-3.9666\times10^{-6}$<br>$8.6134\times10^{-7}$ | 0.6238±0.0601<br>$-1.3226\times10^{-4}$<br>$3.8526\times10^{-5}$ | 0.5029±0.0359<br>$1.1319\times10^{-4}$<br>$1.9717\times10^{-5}$ | 0.6645±0.0414<br>$1.1038\times10^{-4}$<br>$1.6270\times10^{-5}$ | 0.5801±0.0306<br>$-3.3375\times10^{-5}$<br>$3.6510\times10^{-6}$ |
| 4[161], 2[315],<br>6.9565 7.2317<br>6[473]<br>7.3700 | 2[1139], 6[1743]<br>13.8191 14.0425 | 6[161], 2[315],<br>3.5404 3.6698<br>6[473]<br>3.7294 | 4[285], 6[578],<br>5.8175 6.0104<br>6[882]<br>6.1020 | 4[200], 2[369],<br>3.3600 3.5122<br>6[539]<br>3.5918 | 4[336], 2[648],<br>5.4881 5.6204<br>6[968]<br>5.6880 |

**32.** $3_1[4^3]6_2[4^6]_{\mathrm{I}}$

| *Cell* | *Bond* | *cell* | *bond* | *vertex* | *edge* |
|---|---|---|---|---|---|
| 0.4339±0.0259<br>$4.6901\times10^{-7}$<br>$6.9917\times10^{-7}$ | 0.2335±0.0200<br>$-3.2315\times10^{-6}$<br>$3.6617\times10^{-7}$ | 0.5468±0.0321<br>$3.4990\times10^{-5}$<br>$4.5289\times10^{-6}$ | 0.4235±0.0152<br>$2.5190\times10^{-6}$<br>$1.5119\times10^{-7}$ | 0.6418±0.0638<br>$-1.1180\times10^{-4}$<br>$4.6849\times10^{-5}$ | 0.5715±0.0431<br>$4.9165\times10^{-5}$<br>$7.7330\times10^{-6}$ |
| 2[760], 6[1190]<br>7.5263 7.6202 | 2[2860], 6[4534]<br>15.2503 15.4027 | 2[760], 6[1190]<br>3.8342 3.8672 | 2[1457], 6[2301]<br>6.7138 6.7718 | 2[833], 6[1281]<br>3.6879 3.7471 | 2[1536], 6[2400]<br>5.7513 5.8008 |

**33.** $3_1[4^3]6_2[4^6]_{\mathrm{II}}$

| *Cell* | *Bond* | *cell* | *bond* | *vertex* | *edge* |
|---|---|---|---|---|---|
| 0.4740±0.0681<br>$-1.5376\times10^{-5}$<br>$4.0570\times10^{-5}$ | 0.2803±0.0276<br>$-1.1319\times10^{-5}$<br>$1.3703\times10^{-6}$ | 0.6333±0.0534<br>$-1.4476\times10^{-4}$<br>$2.7149\times10^{-5}$ | 0.4785±0.0260<br>$1.8163\times10^{-5}$<br>$1.3662\times10^{-6}$ | 0.6961±0.0552<br>$2.5890\times10^{-5}$<br>$2.2393\times10^{-5}$ | 0.6132±0.0465<br>$6.0868\times10^{-5}$<br>$1.1922\times10^{-5}$ |
| 2[245], 2[477],<br>7.0531 7.3040<br>6[715]<br>7.4294 | 2[1742], 6[2656]<br>14.8576 15.0715 | 2[245], 2[477],<br>3.6408 3.7400<br>6[715]<br>3.7874 | 2[446], 2[892],<br>6.3184 6.5135<br>6[1354]<br>6.6041 | 2[284], 2[532],<br>3.5493 3.6541<br>6[782]<br>3.7136 | 2[504], 2[972],<br>5.6349 5.7243<br>6[1452]<br>5.7741 |

**34.** $3_2[4^3]6_4[4^6]$

| *Cell* | *Bond* | *cell* | *bond* | *vertex* | *edge* |
|---|---|---|---|---|---|
| 0.4540±0.0687<br>$7.8079\times10^{-5}$<br>$4.6624\times10^{-5}$ | 0.2265±0.0369<br>$-1.5535\times10^{-5}$<br>$2.8752\times10^{-6}$ | 0.6160±0.0685<br>$-1.8755\times10^{-4}$<br>$5.5163\times10^{-5}$ | 0.4908±0.0346<br>$-1.2315\times10^{-5}$<br>$2.5752\times10^{-6}$ | 0.6320±0.0532<br>$1.0557\times10^{-4}$<br>$2.0627\times10^{-5}$ | 0.5527±0.0434<br>$1.0264\times10^{-5}$<br>$1.0088\times10^{-5}$ |
| 2[203], 2[440],<br>6.9754 7.2955<br>6[550]<br>7.3673 | 2[1605], 6[2026]<br>14.9533 15.0642 | 2[203], 2[440],<br>3.6059 3.7318<br>6[550]<br>3.7600 | 2[366], 2[821],<br>6.4645 6.6358<br>6[1034]<br>6.6731 | 2[238], 2[491],<br>3.5294 3.6660<br>6[607]<br>3.6969 | 2[420], 2[900],<br>5.8095 5.9689<br>6[1122]<br>6.0036 |

**35.** $3_3[4^3]6_6[4^6]$

| *Cell* | *Bond* | *cell* | *bond* | *vertex* | *edge* |
|---|---|---|---|---|---|
| 0.4042±0.0580 | 0.2281±0.0277 | 0.5958±0.0567 | 0.4698±0.0313 | 0.6353±0.0449 | 0.5210±0.0370 |
| $3.6150\times10^{-5}$ | $2.6810\times10^{-6}$ | $-4.2796\times10^{-5}$ | $3.1642\times10^{-5}$ | $-2.0589\times10^{-5}$ | $7.9238\times10^{-6}$ |
| $1.8890\times10^{-5}$ | $7.5233\times10^{-7}$ | $1.4656\times10^{-5}$ | $4.6775\times10^{-6}$ | $8.7591\times10^{-6}$ | $2.4104\times10^{-6}$ |
| 2[230], 2[490], | 2[1782], 6[2418] | 2[230], 2[490], | 2[406], 2[902], | 2[267], 2[543], | 2[480], 2[1008], |
| 6.9391 7.2735 | 14.8911 15.0488 | 3.5304 3.6816 | 6.5714 6.7095 | 3.5955 3.7127 | 5.6417 5.7500 |
| 6[656] | | 6[656] | 6[1222] | 6[717] | 6[1344] |
| 7.3720 | | 3.7256 | 6.7496 | 3.7490 | 5.7827 |

**36.** $3_1[4^3]8_4[4^8]$

| *Cell* | *Bond* | *cell* | *bond* | *vertex* | *edge* |
|---|---|---|---|---|---|
| 0.4525±0.0780 | 0.2122±0.0230 | 0.5237±0.0627 | 0.3807±0.0401 | 0.7010±0.0470 | 0.6086±0.0679 |
| $7.1913\times10^{-4}$ | $-9.6553\times10^{-6}$ | $-1.0143\times10^{-5}$ | $3.5308\times10^{-6}$ | $-7.5034\times10^{-5}$ | $1.6014\times10^{-4}$ |
| $1.4678\times10^{-4}$ | $8.2295\times10^{-7}$ | $3.2798\times10^{-5}$ | $5.4378\times10^{-6}$ | $1.2495\times10^{-5}$ | $3.8208\times10^{-5}$ |
| 2[238], 2[490], | 2[1794], 6[2632] | 2[238], 2[490], | 2[435], 2[921], | 2[288], 2[561], | 2[490], 2[1000], |
| 7.0336 7.3224 | 16.9197 17.1071 | 3.6555 3.7592 | 7.3931 7.5831 | 3.4028 3.5651 | 5.4898 5.6420 |
| 6[708] | | 6[708] | 6[1345] | 6[793] | 6[1440] |
| 7.4350 | | 3.7994 | 7.6550 | 3.6318 | 5.7014 |

**37.** $3_1[5^3]4_2[5^4]_{\mathrm{I}}$

| *Cell* | *Bond* | *cell* | *bond* | *vertex* | *edge* |
|---|---|---|---|---|---|
| 0.4047±0.0637 | 0.2185±0.0212 | 0.6180±0.0491 | 0.4930±0.0327 | 0.5516±0.0469 | 0.4101±0.0301 |
| $6.1235\times10^{-5}$ | $5.5289\times10^{-6}$ | $6.5660\times10^{-5}$ | $1.4895\times10^{-5}$ | $4.3305\times10^{-5}$ | $1.2816\times10^{-5}$ |
| $3.1306\times10^{-5}$ | $5.4838\times10^{-7}$ | $1.1080\times10^{-5}$ | $2.1733\times10^{-6}$ | $1.3841\times10^{-5}$ | $2.1196\times10^{-6}$ |
| 2[252], 2[570], | 2[2374], 6[3273] | 2[252], 2[570], | 2[468], 2[1086], | 2[281], 2[613], | 2[632], 2[1428], |
| 8 8.3298 | 16.0126 16.1577 | 3.7143 3.8105 | 6.3932 6.5157 | 4.4982 4.6591 | 7.4525 7.6345 |
| 6[777] | | 6[777] | 6[1491] | 6[827] | 6[1946] |
| 8.4247 | | 3.8378 | 6.5500 | 4.7062 | 7.6865 |

**38.** $3_1[5^3]4_2[5^4]$

| *Cell* | *Bond* | *cell* | *bond* | *vertex* | *edge* |
|---|---|---|---|---|---|
| 0.3457±0.0484 | 0.1820±0.0200 | 0.6226±0.0443 | 0.5695±0.0477 | 0.5527±0.0393 | 0.4162±0.0419 |
| $8.5340\times10^{-5}$ | $-5.3816\times10^{-6}$ | $-5.2469\times10^{-5}$ | $-1.2139\times10^{-4}$ | $-2.9005\times10^{-5}$ | $-3.2254\times10^{-5}$ |
| $2.5074\times10^{-5}$ | $6.0154\times10^{-7}$ | $1.2122\times10^{-5}$ | $1.8902\times10^{-5}$ | $1.0732\times10^{-5}$ | $7.5538\times10^{-6}$ |
| 8[213], 2[380], | 6[950], 2[1745], | 8[213], 2[380], | 8[331], 2[601], | 8[169], 2[289], | 8[360], 2[640], |
| 8.9202 9.1842 | 16.8147 17.2218 | 3.1080 3.1632 | 4.4411 4.5324 | 4.2604 4.4291 | 7.3444 7.5062 |
| 6[595] | 6[2780] | 6[595] | 6[951] | 6[441] | 6[1000] |
| 9.3445 | 17.4626 | 3.1966 | 4.5868 | 4.5351 | 7.6040 |

**39.** $3_2[5^3]4_4[5^4]$

| *Cell* | *Bond* | *cell* | *bond* | *vertex* | *edge* |
|---|---|---|---|---|---|
| 0.3672±0.0405 | 0.1766±0.0243 | 0.6265±0.0398 | 0.5822±0.0505 | 0.5413±0.0515 | 0.4101±0.0536 |
| $-6.6453\times10^{-5}$ | $-3.2608\times10^{-6}$ | $7.1192\times10^{-5}$ | $2.3922\times10^{-5}$ | $-9.8715\times10^{-5}$ | $9.3126\times10^{-5}$ |
| $1.1174\times10^{-5}$ | $1.0035\times10^{-6}$ | $7.0957\times10^{-6}$ | $2.8516\times10^{-5}$ | $1.9319\times10^{-5}$ | $3.1517\times10^{-5}$ |
| 4[168], 4[270], | 2[732], 2[1212], | 4[168], 2[270], | 4[255], 2[418], | 4[141], 4[216], | 4[308], 4[485], |
| 8.7143 8.9778 | 16.5929 16.9868 | 3.0357 3.0963 | 4.4078 4.4928 | 4.3688 4.4907 | 7.2662 7.4144 |
| 6[396] | 6[1812] | 6[396] | 6[621] | 6[307] | 6[702] |
| 9.1515 | 17.2395 | 3.1364 | 4.5475 | 4.5733 | 7.5128 |

**Table 4.7** *Percolation statistics of the 2-homohedral tilings. Each item of the statistics are, from top to bottom, mean ± standard deviation, second moment, and third moment. Similarly each of the items in each box contains the number of runs [the number of network components] and the coordination number.*

The advantage of sparse- over dense networks described by Burt (1992) is an idea similar to that of the benefit of decentralisation and local autonomy in politics. According to him, size still matters but the cost of maintaining the size is also important. The idea can be very general; dense networks are virtually worthless monitoring devices, while sparse networks give more information benefits. Taking opportunity costs into account, the rate of return of a dense network is lower than that of a sparse network. The idea can be applied to a strategic network expansion which is crucial for sales persons and jobs hunting alike.

Something similar to this comes up in a variety of fields. In Sociology it is sometimes called the *strength of weak ties*. A tie between two things is weaker the less each of them has in common with the other. It is well known, *i.e.* the origin unknown, that best friends are usually those who have least in common with each other. It would be interesting to trace this idea back to where it first appeared in literature.

The study above shows that the percolation probability is not a function of the coordination number of the network alone. I suspect that it is a function of both this and the coordination number of the dual lattice of the network, that is $p_c = \mathrm{f}(x_c, x_v)$. In other words, $p_c$ may be a function of not only the connectivity but also the tortuosity of the network.

## § 4.10 Cosmology

The universe is made up of superclusters of galaxies, each of which contains local clusters. Each local cluster contains galaxies, each of which contains stars. When stars explode, gas bubbles are formed which expand to meet one another, forming walls of materials in the manner of the Voronoi tessellation in three dimensions. Within the planets around each stars there exist yet other structures which can be similarly represented by the Voronoi tessellation.

Superclusters are like endless cobwebs covering the space. The Andromeda galaxy, the Sculptor group, the Virgo cluster, and the M81 group are examples of the members of the Local Supercluster in which our Milky Way galaxy reside. The Pisces-Perseus supercluster is 250 million, and the Hercules supercluster 500 million light-years away from us.

Assuming the big bang origin of the universe, the defects originated in the phase transition at the Big Bang could play an important role in the formation of galaxies and their clusters and superclusters. Tom Kibble predicted this in 1976 (*cf* Croswell, 1995), and gave three types of possible defects, namely the point-like monopoles, the line-like cosmic strings, and the plane-like domain walls.

Van de Weygaert (1989) studied the statistics of 3-d Voronoi tessellations for the purpose of understanding the structure of the universe. Here *neighbours* are defined by a common polygonal face whereas *full neighbours* have an additional requirement that the line joining nuclei intersects this common face. Taking a linear section through $d$-d, $d \geq 2$, the mean length is

$$\langle \lambda \rangle = \frac{d\Gamma\left(d-\frac{1}{2}\right)\Gamma\left(\frac{d+1}{2}\right)^2}{(d-1)!\rho^{\frac{1}{d}}2\Gamma\left(\frac{d}{2}+1\right)^{2-\left(\frac{1}{d}\right)}\Gamma\left(2-\frac{1}{d}\right)}, \qquad (\mathbf{20})_{\text{iv}}$$

where $\rho$ is the number density, in other words nucleus density.

In three dimensions we need at least two points in order to establish the distance of an object by a geometrical method. Because the cosmic scale is so large compared with the scale of the solar system and Earth, all the observation points we may choose become the same and only one point in practice. Therefore the determination of the distance to extragalactic objects, which is crucial in cosmology, can only be achieved by the various means of observations from a single point in space. This is a limitation that has caused the establishment of distance to be a hot, long-standing controversial issue. As the universe is expanding with the receding velocity of objects increases with their distance away from us, and as this velocity can be accurately determined by the amount of redshift in the light of these objects observed, the study of distance becomes the study of a single, universal constant called the Hubble constant. This is only a constant in theory not in practice. All numerical values of the Hubble constant used in literature are fictitious to some degree. If its exact value is known, then the accurate distance to any cosmic object is simply its radial velocity, *i.e.* its velocity away from us, divided by this Hubble constant. The reciprocal of the Hubble constant is called the Hubble time. The importance of the Hubble constant, together with the difficulty in finding it, make the observational and the theoretical parts of cosmology inseparable from each other. They are also the cause of the proliferation of the modern literature on Astrophysics. One example of studies of the extragalactic distance scale is that reported by de Vancouleurs (1993) which includes among the objects studied the following objects belonging to the Local Group, namely the Large Magellanic Cloud, M31, M33, NGC 3109, as well as the objects beyond the Local Group, namely NGC300, IC4182, NGC2403, NGC5128, M81, M101, M104 (NGC4594), and NGC4571.

## § 4.11 CCTV, forest fire, the navy and porcupines

Voronoi graph can be used to aid the decision on the locations of Closed-Circuit Television (CCTV) cameras. CCTVs have proved to be very effective in reducing the number of crimes in Manchester as well as other places within the UK. In order to be effective, it is important to have no large gaps within a control area. Strategically placed, the cameras will give the best cost-effective solution while covering the largest possible area.

Within crucial areas cameras could be positioned in such a way that their ranges of operation intersect without gaps. The points of intersection represent the vertices of the Voronoi regions centred around two or three neighbouring cameras. The design objective is to produce the maximum covered area using the least number of cameras.

Outwards from each crucial area extends space not being covered by cameras. Similarly around other crucial areas surrounding this area also extend such unobserved space. The next step in the design is perhaps to make sure that people walking from one covered area to another are safe. To

do this one can consider the whole covered areas as centres of yet another set of Voronoi tessellation orders of unit larger in size. The purpose now is to make sure to position cameras at the positions of vertices of the Voronoi regions of this second set of tessellation.

Both the first and the second tessellations will be subjected to geographical constraints. The former would be predominantly influenced by the shape and the position of buildings and surrounding structures, the latter by the paths connecting the covered regions. Here a vertex of these geographically-constrainted Voronoi regions could be a point which is equally far from three covered regions. Another set of positions to be considered for placing CCTVs is one of those points equally far from two covered regions along the shortest path between them.

At a graduate development programme on $16^{th}$ November 2001 I gave a presentation for ten minutes on a title *division of space*. In it I described the current project of mine as concerning porous media and division of space in general. The part presented is from a section for miscellaneous applications. Mathematical models of partitionings, for example the Voronoi tessellation pioneered by G. F. Voronoi and G. L. Dirichlet in the $19^{\text{th}}$ century, help towards understanding physical Euclidean and non-Euclidean world. Procedures based on these models help solve many physical and strategical problems. When I was fourteen years of age I was trained in a course for those who volunteer to fight forest fires in the area around the Sudẹb mountain, close to where I used to live. Although I never used it afterwards, the knowledge obtained from that course has given me the interest in forest fire fighting.

To mention but one of the relevant topics contained in that course, one can imagine a forest fire station as being a nucleus of a Voronoi partition of area under the protection of that stations. Here the distance from a station to any point on the forest ground is not a straight line but the time it takes a fire fighter from that station to reach the point in question. This time is affected by the *tortuosity* of the path, in other words the degree of winding, as well as the difficulty of the climb. There normally is an observation tower at each fire station, so we may safely assume that every nucleus is equipped with one. Then the exact location of a fire observed can be located on the map from the intersection of lines of sight drawn from the neighbouring towers towards the direction of the fire.

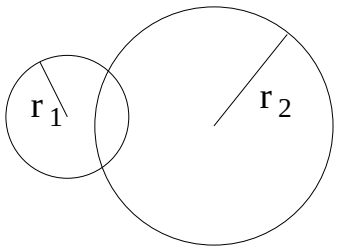


**Figure 4.15.** Range of observatory towers.

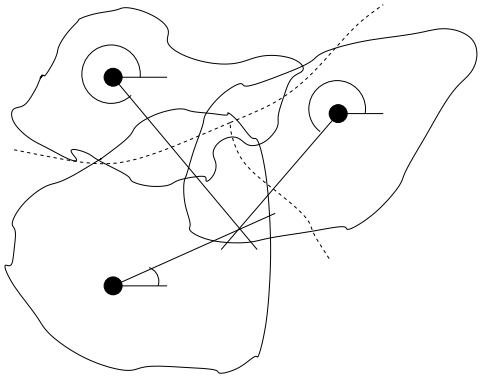

These lines of sight only give the position of the fire on the map. The distance measured along such a line does not necessarily correspond with the Voronoi distance which has a unit of time. The area covered by a tower depends on its height; a higher tower can report a fire occurring at a further distance. The area of covering is circular if the forest is a flat plain. But such a case is rare and in general this area is a distorted circle the degree of distortion of which depends directly on the contour of the land around it. In Figure 4.15 if $h$ is the height of a tower and $r$ its radius, then $r_1 < r_2$ implies $h_2 > h_1$. Suppose the dashed lines are boundaries of Voronoi regions, solid boundaries the observation range of the towers, and straight lines from nuclei the lines of sight. In Figure 4.16 the Voronoi boundaries are not straight lines as a result of tortuosity. Observations from only two towers suffice for finding location of the fire, but an observation from the third tower would reduce the probability of an error.

**Figure 4.16.** Tortuous boundaries.

I also talked about strategic locations. At a job presentation by Tesco we learnt that the company uses the Geographical Information System for placing their new stores in strategical locations.

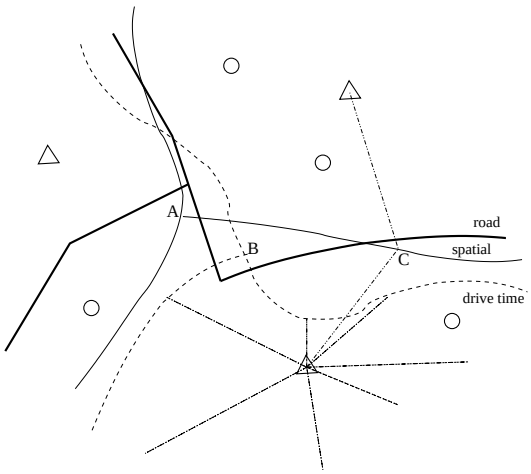


The planning department at Tesco uses the so called the *porcupine diagram* which looks like the rays of light emanating from a star or the quills from a porcupine. The rays radiate from a supermarket and their length represents the drive times required to get to the store from the other end of the line. Factors affecting the locating of new stores include for example drive time, competition, logistic, parking, and traffic. The porcupine diagram superimposed on a map. Triangles are Tesco supermarket stores while circles are those belonging to their competitors. The spatial boundary of the Voronoi diagram is in general different from its drive time boundary, as shown in Figure 4.17 where broken boundary lines represent Voronoi partitions when the distance is the drive time while solid boundary lines that when the distance is the spatial distance.

**Figure 4.17.** Porcupine diagram superimposed on a map.

A similar approach to the above can be applied to help locate the Closed Circuit TeleVision cameras in a strategic location. Suppose that now the triangles in Figure 4.17 are important places, for examle business centres, schools, or universities; let us call these *sensitive areas*. Then security cameras should be placed at both points A and B as well as at the sensitive places. Here the solid

boundary lines meeting at the point A represent the Voronoi boundary for walk time instead of the actual spatial distance. Moreover, a camera should be placed at the point C which is the point where the shortest walkway linking two neighbouring sensitive areas meets with the Voronoi boundary of the walk time, in other words a point which lies midway along the shortest path that joins nextdoor sensitive areas. The reason for this is that these points are likely to be frequented by people going from one sensitive area to another, therefore they are prospectous for robberies. On top of that if a robber wants to flee from one sensitive area to another his sensible choice would pass through C while A with its connecting three different routes would be a clever choice to choose to confound a pursuer, or likewise B if he is driving.

At a police headquarter and at the city council office I wanted to know whether security cameras have been placed at locations analogous to these points A, B, and C, but was told that the information is sensitive. The answer is understandable because at the time M. Bush was trying to get his hand on M. Bin Laden and M. Blair had just declared Britain at war and alert. However this was not good for my theory since we had no way of knowing whether this approach is new, or whether it could be used to improve the security in the city. Hopefully most of these strategic locations A, B and C have already been covered by security cameras even if the decision to do so had been arrived at by some other theories different from the one I suggest. Unlike in the case of sensitive places, the cost of the cameras to be placed at these strategic places may have to be the responsibility of the city council because their importance is not immediately obvious owing to their locations. In contrast, most schools, universities or businesses should be willing to help with the cost of such installation from which they would directly benefit.

On one slide I explain how one can divide transformations into affine and non-affine ones. The affine transformations are governed by the equations $x' = ax + by + p$ and $y' = cx + dy + q$. As a conclusion, mathematical models are beautiful because they give us understanding, and they are useful because they stem ideas and procedures necessary for solving problems. The presentation has gone from forest fire fighting to crime prevention without my knowing it, so the future works are to collect real data and practices, to analyse and compare with the theory and simulations, and then to implement and monitor the operations which I think unlikely to happen because it is impossible for me to become a member of the Greater Manchester police force. Dr. Jim Boran who was present gave *good*'s for project understanding, overview and structure, summary, examples, use of colour, connection with drawings, enthusiasm, pointing at screen, and familiarity with the material. He wrote that the explanations were clear, the content technical but with good personal view, but that I looked at the screen too often and at times was difficult to hear. Bigger labels are suggested.

Naval forts are positioned with an idea similar to forest fire stations. Each fort forms a circle of effective defence around itself. These circles form a chain like beads on a necklace. One example (*cf* Petersburg, 2001) of this are the forts of Kronstadt near Kotlin Island in the Finnish Gulf, 20 kilometres from Saint Petersburg, which have been used as a base for the Baltic Fleet and is now controlled by the Russian Navy. Here seventeen forts had been built between 1704 and 1896 which form a guarding barrier for the city of Saint Petersburg. Examples of these forts are the Totleben Fort, founded 1886–1913, and the Alexander I fort, founded 1836.

In the study of traffic in § ℵ we consider the percolation of roads, which are edges of the structure. We can also use the same structure for the study of fire protection and evacuation in cities, in cases of disaster, but now it is instead the percolation of cells that interests us. Roads form effective fire barriers as well as divide the conflagration into partitions. By carefully managing these, for example putting more efforts on the key or critical partitions, the flames can be contained more quickly and the damage minimised. These zones are also important for evacuation planning, for example that made by the Greater Manchester Police. In Tokyo where there is always a fear of big earthquake, informations are given out in plenty to tell people what to do in case such a disaster as the Great Kanto Earthquakewhich occurred on $1^{st}$ September 1923 should struck. School grounds are usually assigned as evacuation centres. And as the distance one has to walk to get to one of these is crucial for one's safety, the evacuation zones assigned by the city councils there naturally divide the city into domains that approximate the Voronoi tessellation. In 1998 when I was in Tokyo the fear reached its height, since it was generally believed that big earthquakes in Tokyo occur at a period of approximately seventy-five years.

### § 4.12 Fractals

In doing simulations on filtering membranes, one usually assume that the blocking particles are all of the same size. Or one may apply more intuition and experience, and say that particles should

have a normal distribution. Any mineral engineer will be able to tell that it is normally the case that the distribution of aggregates according to their sizes is normally normal. But one must keep in mind that the normal distribution here is by weight not number of particles. Therefore it is unlikely, except in a few special cases, that simulations which assume a normal number distribution of blocking particles will represent the real process.

A pile of aggregates with a normal distribution is likely to have a fractal number distribution (*cf* Liebovitch and Scheurle, 2000). Such fractal distribution is hyperbolic towards the lower size ranges. But the overall distribution is more complicated, that is to say, a mixture of normal- and hyperbolic distribution.

So far we have only considered percolation by competition between two phases. We have looked at networks in a cubic box and have assumed that the network is initially available in its entirety. But what if one has a competition of three phases or more? Or what happens when there are only parts of the network from the start? The picture of this can not be clearer than that of politicians arguing for votes, or the opinion polls of people across the social cross-section. Lustick and Miodownik (2000) consider this problem in the context of politics where the agreement clusters necessarily appear in various colours not merely black and white.

Applying this to percolation and a whole new dimension opens up for investigation. One possible approach is to consider only an arbitrary part of the network within our cubic box. Clearly this is only meaningful if the part being considered is itself a percolating cluster. Carry this one step further and we can have percolation within percolation, when each cluster within the network is itself subject to another percolative process, threatening to destroy it for instance. Such a dynamic scenario is a yet untread water which should open up much ground for investigation.

In the early days of the theory, literature on percolation only concerned itself with fluid wetting or blocking bonds or sites in the kind of situation that is said to be dual to the diffusion problem (Broadbent and Hammersley, 1957; Hammersley, 1957, 1961). The subject generally looked at self-avoiding walks and a measure of connectivity, the connective constant. From then on the appearance of the subject has somewhat changed, and it has become connected to Physics and fractals. The reason why there are very few works on percolation of a random network like the Voronoi tessellation is probably because there seems to be no needs for such study since the applications in Physics have told us that the regular lattices can represent the noncrystalline structure of the metal well. Moreover the only tools we have now, namely the Hamiltonian and power series method, can not be applied in its present form to random tessellations since there are no modulus relationships among the vertices.

## § 5. Porous media

Patrik *et al* (1999) study the propagation in random Delaunay lattice. Particle on arriving at a site in the lattice deflects over the largest possible angle to either the right or the left, depending on the right- or the left scattering nature of the site. After the particle has passed through the site the latter goes into the reverse state. When a similar study is done on the triangular lattice, the entire trajectory quickly becomes confined to a particular strip which is bounded by two adjacent parallel lines of the lattice. They explain the propagation as being due to a blocking mechanism which prevents the particle from moving in a direction opposite to the propagation direction for more than a few steps.

The flow of fluid in porous media follows the Darcy's Law which states that the rate of flow through such a medium is proportional to the potential energy gradient within that fluid. The constant of proportionality is the hydraulic conductivity, which is a property of both the porous medium and the fluid moving through it, $v = Q/A = -k\mathrm{d}h/\mathrm{d}l$.

The average velocity over the entire cross section is called the superficial velocity, $v_s = Q/A = \dot{m}/\rho A$. The velocity that is based on the actual open space within the porous media is called the interstitial velocity, $v_n = Q/(\varepsilon A) = \dot{m}/\varepsilon\rho A$, where $\varepsilon$ is the porosity, $\varepsilon = V_v/V_s = (V_t - V_s)/V_t$, $V_v$, $V_s$ and $V_t$ are respectively the void, solid and total volume.

The definition of porous media is different from that of porous materials. A porous medium is a medium through which other substance may pass, whereas a porous material merely means some certain kind of material the internal structure of which is filled with pores. Most of porous materials can be used as porous media. All of them are useful because of their internal structure, and though we do not need to know this to be able to use them, we do have to understand it if we want to use them efficiently, or if we want to improve upon some of their particular properties.

The outer bark of Quercus suber L., for example, has a property that is ideal for its commercial use as cork. Its material property is such that it neither shrink nor expand when stretched or compressed. This makes it an excellent insulator of both heat and sound as well as good for damping vibration (*cf* Ashby, 1990). It has high frictional coefficient, and is both impervious to liquids and chemically stable. These properties make it ideal as wine corks. By understanding its internal structure and mechanism that makes it stay in the same shape when experiencing external forces, scientists have succeeded in making a synthetic material that shrink, instead of expand radially when pressed. When such material is used as cork, it can be easily pushed inside the neck of a bottle. When we release the force it will expand to its full size and fit snuggly where we placed it.

Pores introduced into a fabric can also increase its commercial value by giving it a lighter weight, higher heat retention rate, which makes it ideal for both ski and snow-board wearer and casual wear (JETRO, 2001).

### § 5.1 Zeolites

Zeolite is the name given to a group of minerals with a porous structure. It is used as molecular sieves as well as in many chemical engineering processes. It may be an important ingredient responsible in lubricating the fault lines in earth crusts, thus making earthquakes less severe. Evan *et al* (1995) found foliated cataclasite and ultracataclasite in the San Andreas faults. These are composed of clay and zeolite. In the case of the ultracataclasite, there are fragments of 20–100 $\mu$m diameter feldspar and quartz embedded in a matrix of clay and zeolite which has grains of sizes smaller than 10 $\mu$m.

The chemical composition of zeolites is that of sand, *i.e.* aluminosilicate. Their general formula is (Dana and Dana, 1997)

$$(\mathrm{Na, Ca, Ba})_{(1\text{–}2)}\,(\mathrm{Al, Si})_5\mathrm{O}_{10}\cdot \mathrm{nH_2O},$$

or, as given by Gottardi and Galli (1985),

$$(\mathrm{Li, Na, K})(\mathrm{Mg, Ca, Sr, Ba})_{\mathrm{d}}[\mathrm{Al}_{(\mathrm{a+2d})}\mathrm{Si}_{\mathrm{n}-(\mathrm{a+2d})}\mathrm{O}_{2\mathrm{n}}]\cdot \mathrm{mH_2O}.$$

Normally $m \leq n$. They differ from sand in that they have large internal cavities. These cavities increase their internal surface area as a result of which they can be used as catalyst or molecular sieves with both shape- and size-selectivity. One example is the use of zeolite as sieve to separate iso octane, which has high antiknock property, and iso pentane from octane and pentane. Zeolites can not withstand high temperature because they rapidly lose water. Even though this process is reversible, their molecules collapse at temperature higher than 600°C. Around 41 types of zeolite occur in nature. Linde Division of the Union Carbide Corporation produced the first synthetic zeolites in 1950s.

The name 'zeolite' was coined by A. F. Cronstedt in 1756 from the Greek *zein*, to boil, and *lithos*, stone. The structural units of zeolite comprises of the primary building units of silicates in the form of $XO_4$ tetrahedra, where $X$ is mainly Si. Other basic units are the chain of fibrous zeolites, the singly connected 4-ring chain, the doubly connected 4-ring chain, the 6-ring either single or double, the hexagonal sheet with handles and the heulandite unit.

## § 5.2 Crystalisation

In the diffusion theory of crystal growth, the overall rate of crystallisation is determined by the rates of two processes occurring one after the other, that is diffusion of solute from the bulk solution to the interface between solution and the crystal, followed by integration of solute atoms into the crystal lattice. The rate of diffusion of the former is $R_g = k'_d(c - c_i)$, while the rate of surface reaction or integration is $R_g = k_r(c_i - c')^n$, where $c_i$ is the interfacial concentration. The value of the diffusion mass transfer coefficients $k'_d$ when estimated from the growth is considerably different from the same value that is obtained from the dissolution experiment. But if we assumed that they are equal, then $R_g = k_r(\Delta c - R_g/k_d)^n$, which, when $n = 1$ gives $R_g = K\Delta c^n$ where $1/K = 1/k_d + 1/k_r$, and when $n = 2$, $R_g = k_d\left[(1 + k_d/(2k_r\Delta c)) - [(1 - k_d/(2k_r\Delta c)^2) - 1]^{1/2}\right]\Delta c.$, but there is no general solution for all $n$'s (*cf* Garside and Mullin, 1968).

Particles in a crystalliser are kept in suspension by a stirrer or a pump. Lim *et al* (1999) study the effect of the attrition when crystals encounter with high speed impellers inside these apparatuses. When the impact energy exceeds the crystal strength, crystals fracture which gives rise to a particle size distribution as a result. Impact can occur at faces, edges or corners of crystals, but in the attrition model only the contact of a crystal corner with another flat, much harder object, for instance the steel impeller, was considered. Furthermore, crystals are assumed to have the shape of a cube or other polyhedra, but in the model the crystal faces forming the contacting corner are replaced by a cone having an included angle of 120°. In the vicinity of impellers the flow is turbulent and crystals travel in a random manner. Repeated attritions reduce the crystal size, assuming no competing effect of crystallisation. They assume a normal volume shape factor distribution and proceed to simulate according to a procedure recaptured here as Algorithm 5.1. The input to the algorithm is the impact energy $W_p$; the outputs are $w_f(J)$ and $c(J)$. The hardness of a solid is its resistance to local plastic deformation. The contact pressure of a plastically deformed cone is assumed to be the same as the Vickers hardness $H_v$. An isotropic material has two independent elastic constants, namely the shear modulus $\mu$ and the Poisson's ratio $\nu$. All the other constants can be determined from these two quantities. Here $\alpha$ is the volume shape factor, $\Gamma$ the fracture resistance, $K_r$ the efficiency of stress field created by the impact between the crystal and the impeller, $\kappa$ stress field parameter, $\kappa = 5$, $\mu_v$ quasi-isotropic shear modulus, $N$ the total number of fragments, $W_p$ impact energy, $H$ dynamic hardness, $L_{\min}$ and $L_{\max}$ respectively the minimum and maximum size of a fragment, $a$ characteristic size of the plastic zone, $r$ the distance from the peak of the cone, $r_{\max}$ the maximum distance from the peak of the cone to the newly created surface and $J$ the particle size classes. The values of $H_v$, $\mu_v$ and $W_c$ used were that of magnesium sulphate heptahydrate and potash alum; $r_1$ and $r_2$ are random numbers.

**Algorithm 5.1** *Fracture by attrition, Lim et al (1999).*

**for** $i = 1$ to $50$ **do**
  $\alpha \leftarrow r_1$;
  $\Gamma/K_r \leftarrow \kappa W_c^{1/3} H^{5/3}/(5.2\mu)$
  $N \leftarrow 7 \times 10^{-4} W_p H^5 K_r^3/(\alpha\mu^3\Gamma^3)$;
  **for** $j = 1$ to $N$ **do**
    $L_{\min} \leftarrow 32\mu\Gamma/(3K_r H^2)$;
    $L_{\max} \leftarrow r_{\max}/2$;
    **calculate** $r_{\max}$;
    $r \leftarrow \exp\left[(13\log a - \log r_2)/13\right]$;
    $L \leftarrow 3\mu\Gamma r^4/(W_p^{4/3} H^{2/3} K r)$;
    **find** $J$ corresponding to $L$;
    $w \leftarrow w + L^3$;
    $w(J) \leftarrow w(J) + L^3$;
    $c(J) \leftarrow c(J) + 1$;
  **endfor**

**endfor**
$w_f(J) \leftarrow w(J)/w$; □

## § 5.3 Fluid flow within networks

Flow of viscous fluids through networks of geometrical objects is an important topic in various disciplines of engineering. Happel (1959) studies two cases of the flow of viscous fluid relative to arrays of cylinders, one parallel while the other perpendicular to the cylinders. This is found in practice as the flow through a bundle of heat exchanger tubes.

The flow pattern within a void of a porous media follows the equations of flows with vorticity, in 2-d,

$$\frac{\partial^2\psi}{\partial r^2} + \frac{1}{r}\frac{\partial\psi}{\partial r} + \frac{1}{r^2}\frac{\partial^2\psi}{\partial\theta^2} = \zeta,$$

and in the axisymmetric case,

$$\frac{\partial}{r\partial r}\frac{\partial\psi}{\sin\theta\partial r} + \frac{\partial}{r^3\partial\theta}\frac{\partial\psi}{\sin\theta\partial\theta} = \zeta \qquad (cf\ Rowe, 1965.)$$

Or equivalently to both equations,

$$\zeta = \frac{1}{r}\left(\frac{\partial(rv_\theta)}{\partial r} - \frac{\partial v_r}{\partial\theta}\right)$$

when $v_\theta = \partial\psi/\partial r$ and $v_r = -\partial\psi/(r\partial\theta)$ in 2-d, and $v_\theta = \partial\psi/(r\sin\theta\partial r)$ and $v_r = -\partial\psi/(r^2\sin\theta\partial\theta)$ in the axisymmetric case. The vorticity, $\zeta$, can be used as boundary conditions, for instance $\zeta|_{r=0} = -\partial v_r/a\partial\theta$ or $\zeta|_{r=a} = \partial v_r/a\partial\theta$. Or it can be used within the hole, for example $\zeta = k\sin\theta$ which gives the solution $\psi = (c_1 r^{-1} + c_3 r + c_4 r^2)\sin\theta$, or $\psi = (c_3 r + c_4 r^2)\sin\theta\sin\theta$ if $c_1 = 0$. This solution is a part of the general polynomial for the stream function,

$$\psi = (\cdots c_0 r^{-2} + c_1 r^{-1} + c_2 + c_3 r + c_4 r^2 + \cdots)\sin\theta.$$

## § 5.4 Material science

A chiral is a group of points, or geometrical figure, whose mirror image can not be brought to coincide with itself. Achiral is the antonym of chiral. A chiral object is an object which fails to be achiral. Chirallity is a purely geometrical property since since all the operations involved, namely the plane symmetry of the reflection, the rotation, and the translation, are all isometries. Chiral is used in the studies of molecules and knots.

The Poisson's ratio, $\nu$, is the ratio between the transverse contraction strain and the longitudinal extension strain, that is $\nu = -\varepsilon_t/\varepsilon_l$. The theoretical value of the Poisson's ratio can range from -1 to 0.5, but for normal materials it is generally positive. At $\nu = 0.5$ the bulk modulus is much greater than the shear modulus and the material is incompressible, while at $\nu = -1$ the opposite is true and the material is very tough and highly compressible. The bulk modulus $B$, and the shear modulus $G$ are related to each other by the equation $B = 2G(1+\nu)/(1-2\nu)$. For rubber this value is 0.5, for aluminium 0.33, while for cork it is approximately zero. Materials with a negative Poisson's ratio have been found whose structure is re-entrant (Lakes, 1987). Applications of such materials include robust shock absorbing material, fasteners, and stoppers of the wine bottles.

Chemical reactions can be thought of as phase changes in percolation. For example the extraction curves for Sb shown in Tiyapan (2003, KNT8(iii), § E.1). These curves represent an $s$-shape starting from one phase, represented by 0% Sb, to another at the maximum per cent extraction where it saturates. All the per cent extraction graphs shown in Tiyapan (2003, KNT8(iii), § E.1) show them with high slope at $t = 0$. This is only for the convenience of drawing, since it is difficult to draw curves with an $s$ shape smoothly on the computer. Also, the data obtained from the experiments do not extend to the time immediately following $t = 0$. Extracting the solution using pipette takes some time to do, and therefore it has not been possible to prove experimentally whether the extraction yields start off with zero slope at $t = 0$ or not, even though one might conjecture that this is likely to be the case if one considers the extraction yield in the leach solution as a developing phase in the continuum of the solution.

Particle sizes come in a variety of definitions. Svarovsky (1977) divides them into three groups, namely definitions by equivalent sphere diameters, by equivalent circle diameters and by statistical diameters. These are listed together in Table 5.1.

| *diameter* | *criterion* |
|---|---|
| volume diameter | equivalent volume of sphere |
| surface diameter | equivalent surface of sphere |
| surface volume diameter | surface to volume of sphere |
| drag diameter | resistance to motion of sphere in the same fluid at the same velocity |
| free-falling diameter | free-falling speed of sphere, same fluid and particle density |
| Stoke's diameter | free-falling speed of sphere if Stoke's Law is used ($Re < 0.2$) |
| sieve diameter | diameter of sphere passing through the same square aperture |
| projected area diameter | projected area of a circle, the particle resting in a stable position |
| projected area diameter | projected area of a circle if the particle is randomly oriented |
| perimeter diameter | perimeter of the outline of a circle |
| Feret's diameter | diatance between two tangents on opposite sides of the particle |
| Martin's diameter | length of the line which bisects the image of the particle |
| shear diameter | particle width obtained using an image shearing eyepiece |
| maximum chord diameter | maximum length of a line limited by the contour of the particle |

**Table 5.1** *Particle size definitions.*

Particle size distribution comes in four types, distribution by number $f_n(x)$, by length $f_l(x)$, by surface $f_s(x)$ and by mass or volume $f_m(x)$. Conversions among them are done by $f_l(x) = k_1 x f_n(x)$, $f_s(x) = k_2 x^2 f_n(x)$ or $f_m(x) = k_3 x^3 f_n(x)$. Conversion is only possible if we know the shape factor's dependence on particle size, because $k_i$ often contain a shape factor. The distribution frequency is by definition $\int_0^\infty f(x)\mathrm{d}x = 1$.

$$(m, \mathrm{d}f(x)/\mathrm{d}x, Q) \xrightarrow{\text{feed}} \text{separator} \xrightarrow{\text{overflow}} (m_f, \mathrm{d}f_f/\mathrm{d}x, O)$$
$$\text{separator} \downarrow \text{underflow}$$
$$(m_c, \mathrm{d}f_c/\mathrm{d}x, U)$$

**Figure 5.1** *Schematic diagram of a separator.*

Small particles tend to flocculate with one another. This makes it impossible to do experiments with very fine powder. Therefore any experiment which claims too fine a size as a control parameter, for instance in the micro metre range, must bear in mind that particles of such small size ranges tend to cluster into hard agglomerates bound by strong chemical bonds, for example from a previous chemical or thermal treatment, or into soft agglomerates by van der Waals attraction or by capillary forces. In ceramic making, this results in nonuniform packing during forming which leads to large voids or flaws after thermal processing. As one expert put it, you can not have powders in the size range of microns because they will disappear instantly into the air. One way to deal with them is to mix them into slurry.

Powder is also subject to impurities from the earliest stage of its life, that is during the comminution, which can be done by various methods, for example mortar and pestle, ball milling, jaw crushers or crushing rollers. The impurity comes from abrasion of the grinding media, which can be effectively avoided in the case of the jet mill, where particles are driven by air streams in opposing directions to collide with one another among themselves. Powder can be characterised by its size distribution, surface area, shape, composition and crystal structure.

Particle size distribution can be determined by means of Stoke's law, screening and microscopy. Stoke's law states that the steady state velocity of a spherical particle travelling through a fluid is $v_r = 2(\rho_p - \rho_f)ar^2/9\eta$, where $a$ can be due to gravity, in which case $a = 9.8$ m$^2$/s, or alternately due to centrifugal force, $a = \omega^2 x$. The time required for a spherical particle of of radius $r$ to travel a depth $x$ is $t_r = x/v_r$. No particles of radius larger than $r$ will be found at depths less than $x$ at time $t_r$. The fraction extracted mass at short time intervals in an experiment using a graduated cylinder is constant, $\pi R^2 \int_{-k}^0 f_o \mathrm{d}x = m$.

The equivalent spherical radius is the radius of a solid sphere that has the same steady state velocity in the slurry as the particle. The volume distribution function is $f_v(r) = \mathrm{d}V/(V_\mathrm{T}\mathrm{d}r)$. The number of particles in the powder having radius $r$ is $N(r) = 3V_\mathrm{T} f_v(r)/4\pi r^3$, the mode of the distribution is the peak and the mean radius is $\int_0^\infty rN(r)\mathrm{d}r / \int_0^\infty N(r)\mathrm{d}r$.

When finding particle size distribution using screening methods, sieves are arranged in a stack with their apertures decreasing from top to bottom. Mass fractions retained on each of the screens is $f_i = m_i/m_\mathrm{T}$, which can then be converted to $N(r)$.

Microscopy methods use a variety of microscopes, for instance optical, SEM or TEM, depending on the magnification required. Measuring the dimensions and determining the shapes of the particles

can be done manually with a ruler, or by using an image analyser.

Powder surface area is determined by gas adsorption methods. The specific surface area, *i.e.* surface area per unit mass, can be found by $s = N\sigma V_m/V_o$, where $N$ is Avogadro's number, $\sigma_0$ the effective cross sectional area of the adsorbate molecule, $V_m$ the volume per gram of a monolayer at STP and $V_0$ the STP number, $2.24 \times 10^4$ cm$^3$/mole.

Monolayer adsorption is used when molecules strongly interact with a surface to in a uniform monolayer. The Langmuir equation is $\theta = kP/(1 + kP)$, where $\theta = V/V_m$ is the fraction of surface covered and $K$ a constant. Then $P/V = 1/(KV_m) + P/V_m$ and the Langmuir isoterms are plots between $V$ and $P/P_0$, $P_0$ being the saturated vapour pressure. For multilayer adsorption, $x/\left[V(1-x)\right] = 1/(cV_m) + x(c-1)/cV_m$, where $x = P/P_0$.

Permeametry measures the flow of gas under a pressure head through a packed bed of particles. The Darcy's law of laminar flow through porous medium is $u = (1/A)(\mathrm{d}V/\mathrm{d}t) = K\Delta P/\ell$. The Poiseuille equation for a fluid flowing through a tube of radius $r$ is $Q = r^4\Delta P/(8\eta\ell)$, where $\eta$ is the viscosity. It is also written as $h/L = 32\eta v/(gd^2)$, where $h/L$ is the headloss per unit length, $\eta$ the kinematic viscosity (m$^2$s$^{-1}$), $\eta = \mu/\rho_w$, $\rho_w$ mass density of the water (kg$\cdot$m$^{-3}$), $\mu$ absolute viscosity of water (kg(ms)$^{-1}$) and $d$ the diameter of the particles. The hydraulic radius is the ratio between the wetted area and wetted perimeter, $r = (\pi d^2/4)/(\pi d) = d/4$. Therefore, $h/L = 2\eta v/(gr^2)$. The number of particles is $n = V_\mathrm{T}/V_i$, and the total wetted surface area of solids is $A_\mathrm{T} = nA_i$. Therefore $A_\mathrm{T} = (1-\varepsilon)(\pi d^2)/(\pi d^3/6) = 6(1-\varepsilon)/d$. Then, replacing the factor 6 with the shape factor $s$, $r = \varepsilon d/[s(1-\varepsilon)]$. Because $v_pA_p = v_fA_f/R$, where $p$ and $f$ means pore and filter surface respectively, $R$ is a constant which accounts for friction loss, and also $J = 1/R$, therefore we have $h/L = 2\eta v_p/(gr^2) = J\eta(1-\varepsilon)^2 v_f s^2/(g\varepsilon^3 d^2)$.

Kozeny used the ratio $V/A = d/4$ for a cylinder and the porosity $p = V_v/(V_v + V_s)$ and gavethe equivalent cylindrical diameter for a packed bed as $d_e = 4pV_s/\left[A(1-p)\right]$. Then the average velocity through the channels is $u_p = \mathrm{d}v_p/\mathrm{d}t = \left[(V_s^2\Delta P)/(2A^2\eta l)\right](p/(1-p))^2$, where $l$ is the channel length. The Carman-Kozeny equation accounts for the tortuosity of the channels in the bed, $s^2 = 2.5p^3\Delta P/(2\rho\eta l v(1-p)^2)$, where $V_s = m/p$, the specific area $s = A/m$ and $\rho$ the solid density of the powder. The determination of the phases and composition of a powder is done by x-ray powder diffraction, thermogravimetric analysis and differential thermal analysis.

Wet methods are preferred when preparing material before firing in order to control agglomeration during forming, for otherwise when the particles are agglomerated the narrowest particle size distribution becomes of little or no help. In wet forming, solid particles are suspended within a liquid the chemistry of which can be adjusted to make them mutually repulsive or mutually attractive, for respectively deflocculation and flocculation. Stabilising makes particles mutually repulsive either by adsorbing polymer chains on to the particles in steric stabilisation or by putting charged ions or polar molecules on the particle surface in electrostatic stabilisation. In steric stabilisation, one end of the long polymer chains, which is hydro- or lyophobic, is adsorbed on the particle while the remaining end, which is hydro- or lyophilic, extends in to the liquid.

Electrostatic stabilisation results in diffusive double layer built around particles. Zeta potential measures the repulsive potential between particles travelling in a medium. It defines the electrical potential in the double layer at the surface of shear slippage when the particle is forced to travel through the fluid when an electric field is applied. The composition and thickness of the double layer can be changed by adjusting the pH of the suspension. The point where the pH gives a zero zeta potential is called the isoelectric point. It is a point where spontaneous agglomeration occurs. The electrophoretic mobility $\nu_e = u(E)/E = \zeta\epsilon_r\epsilon_0/(f_h\eta)$, where $u$ is a steady state velocity, $f_h$ a constant determined by the dispersing medium and the particle size and $1 \leq f_h \leq 3/2$.

## § 5.5 Forces between particles

Essential to the simulation of stochastic models of particles is the consideration of forces acting on each particle (*cf* Schumacher, 1996). Since in theory the forces acting between two particles extend their effects to infinity, one has to make approximations. The degree of justification to these approximations depends on how the force in question vary with distance.

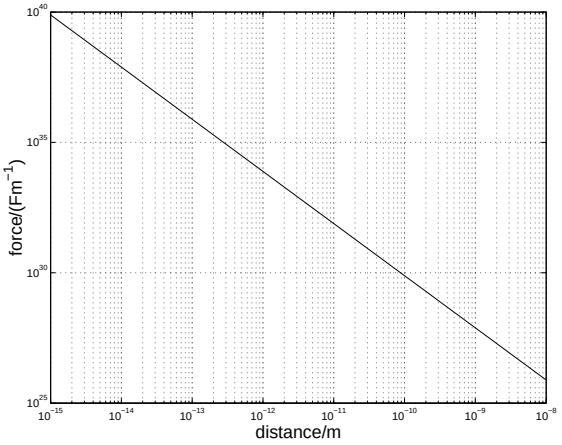


In the case of the Coulomb force where the potential energy is $u(r) = q_1 q_2/(4\pi\epsilon_0\epsilon_r r)$ and the force $f(r) = -\mathrm{d}u(r)/\mathrm{d}r$ is

$$f(r) = q_1 q_2/(4\pi\epsilon_0\epsilon_r r^2),$$

the justification is high as is seen in Figure 5.2 where the force-distance is a decreasing straight line on the log-log graph, $q_1$ and $q_2$ are protons, and $r$ the distance in metre.

**Figure 5.2** Coulomb force *vs* distance in log-log scale..

The effects of the Coulomb force are prominent when sizes of the particles are small. In quantum mechanics where the scale is atomic, for instance, the problem becomes one in which there are a large number of particles interacting with one another, *i.e.* an $n$-particle problem. In theory the Hamiltonian operator can be applied and then the problem solved numerically. But in general this is not possible due to the too many particles involved in the calculation. Theoretical solution is possible by the various methods of approximation, for example the Hartree method (*cf* Brown, 1972) where the best wave function is found in terms of the one electron function, *i.e.* orbitals, $\Phi$, or a Hatree-Fock approximation which reduces the number of equations to $n/2$.

## § 5.6 Arbitrarily shaped particles

An arbitrarily shaped particle in a divided space will necessarily have a harder time travelling around compared with a sphere even if, or rather especially when the space is a mathematical one. Small particles are roughly spherical, or so the lore of science says, but when one's technology has led one down to the realm of dimensions in the order of those small particles, for instance the nano technology, then shape does matter a great deal and the universal spherical assumption can no longer suffice.

This is only one of the reasons which justify the investigation into the cases where the ratio of surface area to volume is not a minimum. When physics and motion are involved, this kind of study can incorporate both the continuous trajectory calculation as well as the discrete raster grids of the digital visualisation technology. The best way to hold such data is as matrix maps or masks.

The best and quickest way to define the boundary of an irregularly shaped object while allowing ease of investigation of its interaction with the surrounding is as raster outlines. To do this, I first investigated such outlines computed from the equation of straight line segments which make up the boundary of the object. Hereafter object boundaries are defined without loss of generality as straight line segments that link all the vertices together with no gaps. The first investigation is unsuccessful as it violates this definition by leaving many gaps, as can be seen in Figure 5.3 (a). The second algorithm calculates the grids from the coordinate axis along the direction of which the slope of the edge is minimum. But this too still leaves gaps along the boundaries.

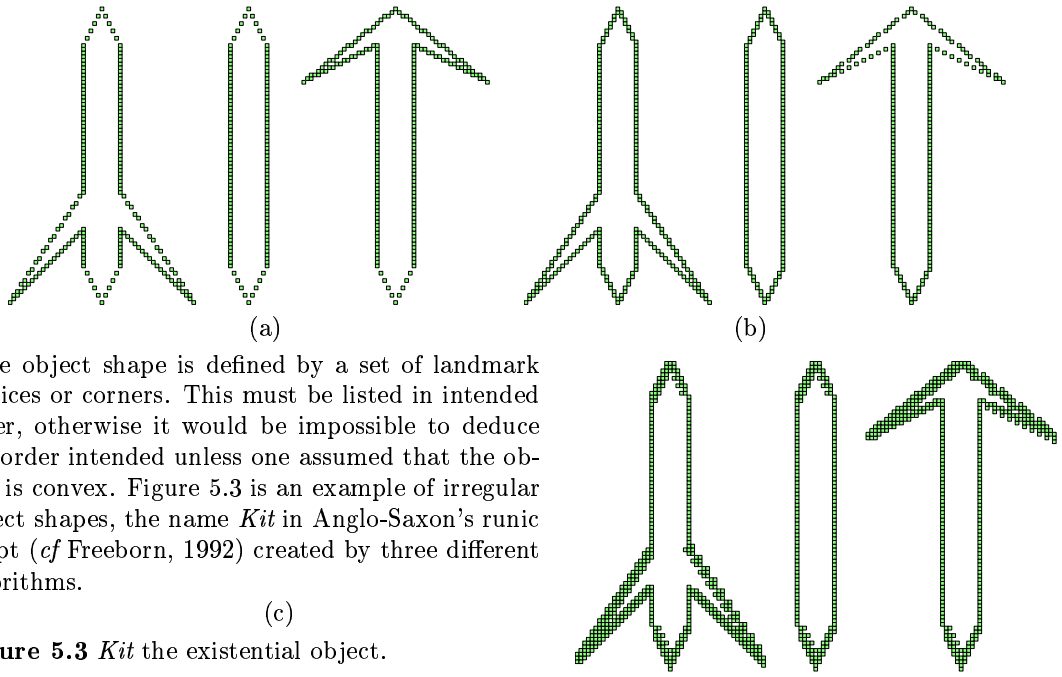

(a) (b)

The object shape is defined by a set of landmark vertices or corners. This must be listed in intended order, otherwise it would be impossible to deduce the order intended unless one assumed that the object is convex. Figure 5.3 is an example of irregular object shapes, the name *Kit* in Anglo-Saxon's runic script (*cf* Freeborn, 1992) created by three different algorithms.

(c)

**Figure 5.3** *Kit* the existential object.

There are three different programs in § A.24. Only the third one, `tioa3.m` gives a satisfactory result which leave no holes in the surface of the objects. In the second program, `tioa2.m`, `v` is a data set which contains the number of vertices, the vertices, slope, map matrix and the object's dimension. In `tiao3.m`, `v` is somewhat different. It contains the number of vertices, the vertices in real dimension, the grid dimension of the box containing the object, the vertices in grid dimension and the matrix map or image of the object. In order to exploit possible parallelisation, the last program ignores the warnings when there is a division by zero as this means that all the grid positions of the whole line can be operated upon together as a vector quantity.

The third program operates as Algorithm 5.2 does. It utilises the same idea as that used by a child or an artist alike when they draw or paint. Drawing and painting are both one-dimensional process which seeks to produce two-dimensional results. Each pencil- or brush stroke travels along a path the direction of which has one dimension. Unless he uses a very thick brush, there will always be a possibility of gaps forming between stroke lines, which can be annoying because however small they may be one needs to use a great deal of paint in order just to cover them up. This problem can be overcome by painting along two directions, for instance perpendicular to each other especially when the person concerned is a child. At a first glance, or to a novice, this may seem a wasteful practice, especially with dear types of ink. But a little practice and experience will show that this proves in most cases to be more economic than painting along only one direction. And since it can be readily seen that painting in two directions perhaps already uses twice the amount of ink required to cover the paper, it follows that doing so in one direction only would use a great deal more ink than this.

**Algorithm 5.2** *Particles or objects with arbitrary shape.*

$(i, j) \leftarrow$ find grid coordinates for $(x, y)$;
**find** all vectors linking vertices;
$\{p_i\}$ **discretise** these vectors into sets of points;
**for** all intervals between consecutive $p_i$'s **do**
  **draw** along $y$-direction to fill gaps;
  **draw** along $x$-direction to fill gaps;
**endfor**

□

The problem of texture quantification is in the difficulty in expressing such quantity by a single parameter. Properties such as coarseness, smoothness, heterogeneity and regularity are finger prints of particles, and are the result of physical and chemical processes. By using fractal geometry, it is possible to describe quantities like texture. A fractal is a set whose metric properties can only be

consistently illustrated with a dimension $D > T$, where $T$ is the standard topological dimension. We can express this dimension as $D = T + (1 - H)$, where $H$ is the codimension. Curves can have their roughness described. By giving a fractal number between one and two the space filling ability of the curves is established (*cf* Van Put *et al*, 1994). The first method defines the fractal dimension of a function in terms of the Fourier power spectrum $P(\omega) \approx \omega^{-(2H+1)}$; $H$ and $D$ are determined by doing a linear regression on the log-log plot of the observed power spectrum as a function of frequency. Another method defines fractal dimension in terms of how the variance of interpixel differences changes with distance; $D$ is estimated from a log-log plot, a variogram, of the variance of increments versus increments $\sigma^2(x) \approx x^{2H}$.

Techniques used for measuring sizes of particles include sieving, microscopic analysis, electronic particle counters, laser diffraction analysis, permeability-, sedimentation and elutriation methods. Usually arbitrarily shaped particles are characterised by a variety of methods. For a single particle this usually means transforming its property to the corresponding value of a sphere. A particle may be represented by a sphere which has the same volume, surface area, surface area per unit volume, or the area projected perpendicular to the flow direction. It may be compared with a sphere which has the same settling velocity in the same fluid, or a sphere which will just pass through a square aperture of the same size. Or its area projected on to the ground, when it is resting in the position of maximum stability, may be compared with that of a sphere in the same situation. To be consistent in one's choice is more important than which choice one chooses from. The sphericity of a particle is defined as $\Psi = A_V^s / A_p$, where $A_V^s$ is the surface area of sphere which has the same volume as the particle and $A_p$ surface area of the particle itself (*cf* Coulson *et al*, 1991).

## § 5.7 Non Poisson number distributions of particles

Let us look at an aggregate of spherical particles whose average diameter is $200 \pm 50$ $\mu$m, density $\rho = 3.7$, and the total weight one gramme. Assuming the gravitational constant to be 9.81 $\mathrm{kg} \cdot \mathrm{ms}^{-2}$.

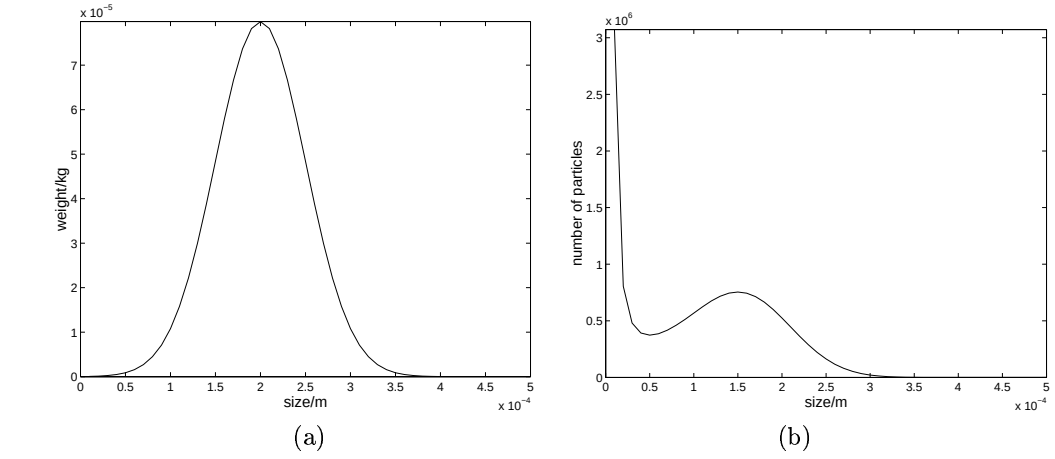


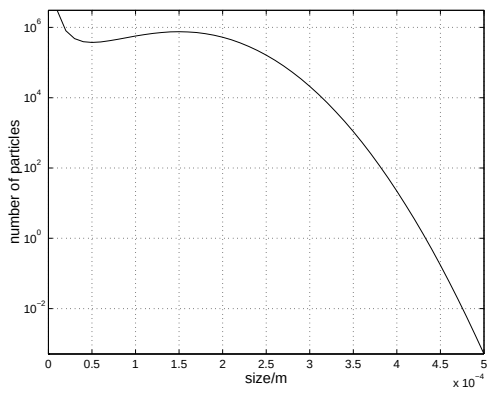


The overall weight is $W = n \cdot w$, where $w = \rho V g$ is the weight of each particle. The particles being spherical their individual volume is thus $V = (4/3)\pi r^3$ and their distributions by weight and by number are shown in Figure 5.4. Figure 5.4 shows (a) distributions by weight, (b) distribution by number in normal scale and (c) with log scale in the $y$-axis.

**Figure 5.4** Distributions by weight and by number.

In particle size classification the separation size, $D_{50}$, is the size where there is an equal chance of particles being reported to the fine or coarse fraction. The grade efficiency curve is normally plotted

between the weight fraction to coarse product and the normalised particle size $\mathrm{D}/\mathrm{D}_{50}$. The choice of classification equipments depends on many factors, for instance the size of the particles in question and their electrical or magnetical property. For fine particles, Treasure (1965) discusses several types of classifier, namely the solid-bowl centrifuge, the Hosokawa micro-separator and the Head, Wrightson air classifier all three of which have $\mathrm{D}_{50} \propto \sqrt{q}/\omega$, the hydrocyclone where $\mathrm{D}_{50} \propto 1/q^{0.5}$ and $q \propto p^{0.5}$, and the Alpine Mikroplex classifier where $\mathrm{D}_{50} \propto u/(w\sqrt{V})$ where $u$ and $w$ are respectively the radial and tangential velocities and $V$ is the volume air flow rate, and $\mathrm{D}_{50} \propto 1/w$ in practice.

The distribution of bubble size in gas fluidised beds had been represented by various kinds of distribution, for example the log normal, Gamma and $\chi^2$ distributions. Rowe and Yacono (1975) preferred the gamma distribution of the volume, that is $\Gamma(V|m,n) = [1/(n^m\Gamma(m))]\, V^{m-1} \exp(V/n)$, in its normalised form $\Gamma(v) = \left[m^m \exp(-mV)V^{m-1}\right]/\Gamma(m)$.

Sieve testing is affected to blinding materials, that is parts of materials under test which lodge themselves in the apertures of the sieve. To account for this Rose and English (1973) give a general rule of thumb which says that a particle for which $\theta < \tan^{-1}\gamma$ will blind the sieve. Here $\theta$ is the angle that the line of reactive force exerted by the material on the particle, which is normal to the contact surface, makes with the horizontal plane. Then they give the empirical value of $\gamma$ to be approximately 20°, which results in $\theta < 0.3358$ radians as being the criterion for blinding to occur. For a spherical particle this gives the ratio $x/r = \cos\theta > 0.9441$, where $r$ is the particle's radius and $x$ half the minimum distance between two normal reactions which act on the particle. Therefore the radius of particles which blind the sieve must be such that $r < 1.0592x$, which corresponds to the aperture of 1.0592 times greater than the aperture if we assume that the aperture is $2x$ through out, or equivalently that the opening has its corresponding faces vertical.

It would be of a theoretical interest to prove this equation $\theta < \tan^{-1}\gamma$ given by them. Also, the angle of friction, $\gamma$, is not a constant but varies for different pairs of materials in contact with each other, as well as changes the value when we change the medium surrounding them to a different type, or even when the moisture content changes for that matter. All of this goes to say that the value $1.1d_{\min}$ extensively used in chemical engineering literature is probably nothing more than an engineering rule of thumb based on two conjectures, one in the limiting value of $\theta$, the other in the value of $\gamma$. But it gives a simple and convenient criterion for use when doing computer simulations, which are nothing but means to visualise the *conceptualised* physics anyway. Other values of $\theta_{\max}$ should give the same qualitative result. We may, for instance, choose the coefficient of our $d_{\max}$ to be 1.02, corresponding to $\theta > 1/\cos 10°$, instead of 1.06 which corresponds to the $\theta > 1/\cos 20°$ used above.

Since no explanation of the formula regarding $\theta$ given by Rose and English has been given elsewhere, I arrive at my own derivation as follows. First, let us recall from our sixth form physics how friction can be described by either the coefficient of friction or the angle of friction, both of which are merely different sides of the same coin. The angle of friction is also known as the angle of frictional resistance, the internal angle of friction and the angle of shearing resistance. For clean sand it is approximately the angle of repose. It reduces with moisture content and is zero for saturated clay. For solid it is approximately the angle of inclination of the surface of one material at the point when a block of another material, placed on top of the former, starts to slide. This is precisely the method by which the coefficient of friction is determined. There are two different coefficients of friction for each pair of material, namely the static- and the kinetic coefficients of friction, the former having a slightly higher value than the latter, and both are defined as being the ratio between the limiting friction and the normal reaction, $\mu = f_k/F_N$. This gives rise to the formula for the friction being $f_k = \mu F_N$, which is equal to $mg\sin\theta$ at the point when the object of the second material slips, $\theta$ being the inclination of the plane made by the first material. Therefore we have $\mu = \tan\theta$, where $\mu$ is the coefficient-, and $\theta$ the angle of friction.

Coming back to our formula in question, $\theta < \tan^{-1}\gamma$. Figure 5.5 shows a spherical object sitting on top of an aperture in a sieve. From Figure 5.5, $\alpha + \theta = \pi/2$. Without loss of generality, assume $\gamma < \pi/4$. Let $\mu = \tan\alpha_c$ be the coefficient of friction at some critical value $\alpha_c$. Furthermore assume that $\alpha_c$ is small, so that we can approximate $\mu$ by the angle of friction $\gamma$. Then we have $\alpha_c = \tan^{-1}\mu = \tan^{-1}\gamma$. It follows that the particle will block the pore whenever $\alpha < \alpha_c$, whereas it will pass through the latter when $\alpha = \pi/4$.

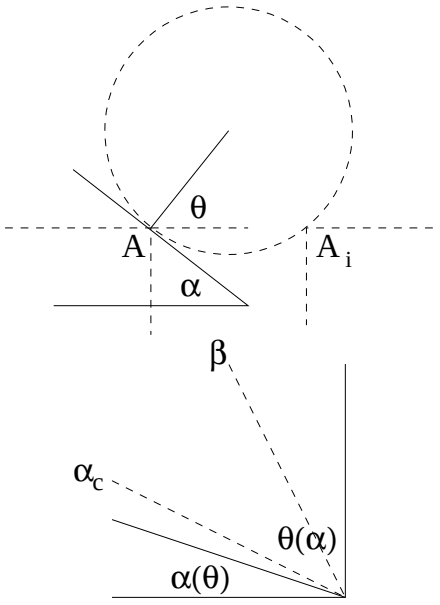


Because we know from experiments that some of the particles does lodge against, and blind the pore, there must exist some $\alpha_c < \beta < \pi/4$ such that this occurs. For the reason that the number of particles that blind is empirically small we know that $\beta$ is small. Since we already have the relationship among $\alpha$, $\theta$ and $\pi/4$, namely $\alpha+\theta = \pi/4$, and since $\alpha_c$ is also small from our assumption, then in order not to unnecessarily introduce another parameter into what necessarily already contains some error due to all the approximations so far made, we let $\beta = \alpha_c$. Now we may say that the particles will blind if and only if $90° - \alpha_c = 90° - \beta < \alpha < 90°$. For other remaining values of $\alpha$, *viz.* both $\alpha_c \leq \alpha \leq 90°$ and $\alpha < \alpha_c$, in other words $0 \leq \alpha \leq 90° - \alpha_c$, then, particles must block. But $\theta = 90° - \alpha$, therefore the particles pass through when $\theta = 0$, blind when $0 < \theta < \alpha_c$ and block when $\alpha_c \leq \theta \leq 90°$. So the blinding particles have $\theta < \alpha_c = \tan^{-1}\gamma$ and the approximation is explained though not *q.e.d.*'ed.

**Figure 5.5** Spherical object on a sieve.

Let $A_a$ be the available area free from blinding material at some instant, $A$ the physical area of the sieve cloth, $G$ the area of cloth blinded by a unit mass of blinding material, and $w_0$ and $w$ the mass of blinding material on the sieve respectively at $t = 0$ and at some $t > 0$. Then $A_a = A - G(w_0 - w)$ and $\mathrm{d}w/\mathrm{d}t = -k_1 w A_a$, where $k_1$ is the diffusion coefficient, and then $\mathrm{d}w/[w(b+w)] = -a\mathrm{d}t$, where $a = -k_1 G$ and $b = (A/G) - w_0$. Assume $b \neq 0$. At $t = 0$, $w = w_0$. It follows that

$$w = \frac{bw_0 \exp(-abt)}{b + w_0(1 - \exp(-abt))}. \qquad (21)_{\mathrm{v}}$$

Furthermore, let $W$ be the total weight of material on the sieve, $W_\infty$ the residue on the sieve for a theoretically infinite time of sieving, and $K$ a constant. Then, $\mathrm{d}W/\mathrm{d}t = -K(W - W_\infty)A_a$, and it follows that $\mathrm{d}W/(W - W_\infty) = -KG(b+w)\mathrm{d}t = -KGb\mathrm{d}t - KGb\exp(-abt)\mathrm{d}t/(q - \exp(-abt))$, where $Q = (b/w_0) + 1$. Again assume $b \neq 0$, and $W = W_0$ at $t = 0$. Then,

$$\ln[(W_0 - W_\infty)(W - W_0)] = K\left\{Gbt + \left(\frac{G}{a}\right)\ln\frac{((b/w_0)+1) - \exp(-abt)}{(b/w_0)}\right\}, \qquad (22)_{\mathrm{v}}$$

and then $W = W_\infty + (W_0 - W_\infty)\delta$, where $\lambda = b/w_0 = (A/Gw_0) - 1$ and

$$\delta = \left[\frac{\exp(a\lambda w_0 t)(\lambda+1)}{\lambda} - \frac{1}{\lambda}\right]^{-KG/a}. \qquad (23)_{\mathrm{v}}$$

When the total amount of blinding material is sufficient to bind the sieve completely, $A/Gw_0 < 1$ and so $-1 \leq \lambda < 0$, when it is exactly enough to completely glind the sieve, $\lambda = 0$, otherwise $A/Gw_0 > 1$ and $0 < \lambda < \infty$, $Gw_0$ being the area of sieve cloth which will be blinded by all the blinding material present. At $t \to \infty$, $\delta = 0$ when $0\lambda < \infty$ and $\delta = (-\lambda)^{KG/a}$, a positive fraction, when $-1 \leq \lambda \leq 0$.

## § 6. Filtering membranes

Tanemura *et al* (1983) give a good algorithm which is both powerful and simple for constructing the three-dimensional Voronoi tessellation. The circumcentre of a DT being a vertex of the VT and the circumsphere of a DT being empty, this second condition of which is known as the *contiguity condition*, they arrive at an algorithm which works for both nondegenerate and degenerate cases. Algorithm 6.1 summarises their algorithm. Associated with the atom $i$, let $V_i$ be the polyhedron, $v_i$ vertex atoms of $V_i$, and $S_i$ set of atoms surrounding $i$, $S_i \supset v_i$. Here $H_i(\alpha\beta|\gamma)$ is the half-space determined by $\{i, i_\alpha, i_\beta\}$ and does not contain $i_\gamma$, $S_i(\alpha\beta|\gamma) \subset S_i \subset H_i$.

**Algorithm 6.1** *Voronoi construction in three dimensions, Tanemura et al (1983)*

**find** $i_1$, nearest, and thus contiguous, to $i$;
$C_i \leftarrow i_1$;
**find** $j = i_2$ s.t. $\{i, i_1, i_2\}$ has the minimum circumradius among all $\{i, i_1, j\}$, $j \in S_i$, $j \neq i_1, i_2$;
$C_i \leftarrow i_2 \cup C_i$;
**find** $j = i_3$ s.t. $\{i, i_1, i_2, i_3\}$ has the minimum circumradius among all $\{i, i_1, i_2, j\}$, $j \in S_i$, $j \neq i_1, i_2$;
$V_i \leftarrow \{i, i_1, i_2, i_3\}$;
$C_i \leftarrow i_3 \cup C_i$;
**clear** $\{m_\alpha\}$ **and** $\{l_{\alpha\beta}\}$;
$\alpha \leftarrow 1$;
**for** all $i_\alpha \in C_i$ **do**
  **if** $m_\alpha = 1$ **then**
    $\alpha \leftarrow \alpha + 1$;
  **else**
    **find** $\{i, i_\alpha, i_\beta, i_\gamma\} \in T_i$, which has $\{i, i_\alpha\}$ in common and where $l_{\alpha\beta} = 1$;
    $S_i(\alpha\beta|\gamma) \leftarrow S_i \cap H_i(\alpha\beta|\gamma)$;
    **describe** a circumsphere to each quartette $\{i, i_\alpha, i_\beta, j\}$, where $j \in S_i(\alpha\beta|\gamma)$ and $m_j \neq 1$;
    **find** $j_{\min}$ for which the centre of the circumsphere of $\{i, i_\alpha, i_\beta, j_{\min}\}$ has the minimum signed $z$-coordinate value among all circumspheres obtained, $z$-axis being normal to $\{i, i_\alpha, i\beta\}$ and lies towards the side of $H_i(\alpha\beta|\gamma)$;
    $T_i \leftarrow \{i, i_\alpha, i\beta, i_\delta\} \cup T_i$;
    **if** $i_\delta \notin C_i$ **do**
      $C_i \leftarrow i_\delta \cup C$; $l_{\alpha\beta}++$; $l_{\alpha\delta}++$; $l_{\beta\delta}++$; $l_{\beta\alpha}++$; $l_{\delta\alpha}++$; $l_{\delta\beta}++$;
    **endif**
    **if** all $\{l_\alpha\}$ are equal to 2, $m_\alpha \leftarrow 1$;
    **if** all $\{l_\beta\}$ and/or $\{l_\delta\}$ are equal to 2, $m_\beta \leftarrow 1$ and/or $m_\delta \leftarrow 1$;
  **endif**
**endfor**
**find** geometrical quantities of $\Pi_i$; □

Algorithm 6.1 is justified by proofs of theorems which confirm that atoms nearest to each other are contiguous to each other, a triangle with the minimum circumradius is a face of a DT, which means that all its three atoms are also mutually contiguous, likewise a tetrahedron with the minimum circumradius is a DT, all its four atoms are mutually contiguous, two DT's sharing a plane have their fourth vertices at a signed minimum distance on either side of the plane they share. Some interesting geometrical lemmas help towards the proof of these theorems.

Jackson (1994) studies porous media and represent them using Voronoi models. His interests are in the synthetic membranes, which can be symmetric or asymmetric, homogeneous or heterogeneous structure, neutral or charged, and passive or active transport. The resistance to mass transfer is mainly in the top layer if it exists. This is a dense layer 0.1–0.5 $\mu$m thick which lies on top of a porous sublayer 50–150 $\mu$m thick. Regular tessellations in two dimensions come in 11 distinct tilings called Archimedean tilings. Tessellations by random lines in 2-d have the equation of the lines $x\cos\theta + y\sin\theta - h = 0$, where $0 \leq \theta \leq \pi$ and $-\infty < h < \infty$, which is analogous to tessellations of random planes in 3-d with the equation of a plane $x\sin\theta\cos\phi + y\sin\theta\sin\phi + z\cos\theta = 0$, where $0 \leq \phi \leq \pi$. The definition he gives of the *Voronoi polygon* is $\bigcap_{i\neq j}^{N} H(x_i, x_j)$, where the half-plane $H(x_i, x_j)$ is $\{x \in E^2 | d(x, x_i) \leq d(x, x_j); i \neq j\}$. The bisector is $B(x_i, x_j) = \{x \in E^2 | d(x, x_i) = d(x, x_j)\}$. There are $n_c + n_b - 2$ triangles in the corresponding Delaunay triangulation if in the Voronoi tessellation

there are $n_c$ interior- and $n_b$ boundary polygons. Scanning electron microscopy is explained and several SEM pictures of cellulose nitrate are given. AVS is used to do the pore perimeter calculation by connecting the modules `read any image` with `image measure` and *image viewer*, the latter two of which are in turn connected together. To calculate the pore area connect `read any image` with `sketch`, `histogram`, and `image viewer`. Then connect `sketch` with `histogram`, `sketch` with `image viewer`, and `histogram` with `print field`. A 3-d process is a homogeneous Poisson point process if the number of points in any region of volume $V$ has a Poisson distribution with parameter $\lambda V$ and the random variables corresponding to the number of points in disjoint regions are independent among one another. Among the characteristics calculated are, in our terminology, the perimeter of polyhedron $P_c = \sum_{i=1}^{n_c^e} e_c^i$, the surface area $A_c = \sum_{i=1}^{n_c^f} \sum_{j=1}^{n_c^{t,i}} A_t^{c,i,j}$, and the volume is $V_c = \sum_{i=1}^{n_c^f} \sum_{j=1}^{n_t^{c,i}} V_t^{c,i,j}$. His numerical results given (see also, Jackson *et al*, 1999) are $n_f^e = 5.203390$, $n_c^e = 39.191489$, $n_c^v = 26.127660$, $n_c^f = 15.063830$, $P_c = 17.358196b$, $A_c = 5.910997b^2$, $b^3$ being the mean cell volume; the coordination number is of course 4. The distribution of $n_c^v$ shows the distinct Voronoi characteristic of containing exclusively of even numbers, whereas that of $n_c^e$ the equally distinct characteristic of being exclusively in multiples of three. This has been explained as odd number implying an impossible fractional number of edges, there being 3/2 edges as there are vertices. For the cross section data he found $n_c^e = 5.831$ and $P_c = 3.563s$, $s^2$ being the mean polygon area. In membranes, if the diameter of a particle is less than that of a pore then the particle will entrain the pore unless it should encounter other fouling particles, but if the particle is bigger than the pore then it will be retained. He assumes fouling particles to be spherical. Ascribed to each face is the diameter or size of its largest inscribed circle. Algorithm 6.2 is used for this purpose; $d$ is the largest inscribed circle diameter sought for.

**Algorithm 6.2** *Find the largest inscribed circle*

$d \leftarrow 0$
**for** *all combinations of three edges of the face*
  **find** the corresponding *triangle*
  **find** the *largest inscribed circle* of this triangle
  **if** the *centroid* lies within the face **then**
    **if** the *perimeter* lies within the face **then**
      **if** the *diameter* $> d$ **then**
        $d \leftarrow$ the *diameter*
      **endif**
    **endif**
  **endif**
**endfor** □

In carrying out his simulation, the mean particle diameter $\bar{d}_p$ is calculated from the mean pore diameter $\bar{d}_v$ by $\bar{d}_p = k\bar{d}_v$ where $k$ is a constant. The corresponding standard deviation of particle sizes is $\sigma_p = \sigma_v(\bar{d}_p/\bar{d}_v)$. The distribution of particle diameters is dependent on both $k$ and another dimensionless parameter $m = (\sigma_p/\bar{d}_p)/(\sigma_v/\bar{d}_v)$. Then the central limit theorem gives the frequency distribution and thus the diameter of the $i^{\text{th}}$ particle as $d_i = \bar{d}_p + \sigma_p \left( \left( \sum_{j=1}^{q} r_j - q/2 \right) / \sqrt{q/12} \right)$, where $0 \leq r_j \leq 1$ are random variables and $q \geq 12$. Interaction between particles and membranes starts from Algorithm 6.3 which has been adapted from Jackson (*ibid.*).

**Algorithm 6.3** *Interaction between particles and surface pores.*

**while** another *particle* exists **do**
  $i \leftarrow i + 1$;
  $p_i \leftarrow$ *particle* ;
  **find** particle entry *coordinates*;
  $c_i \leftarrow$ of the nearest *Voronoi cell*;
  $f_i \leftarrow$ the nearest *face* **of** $c_i$;
  **if** the face is *fouled* **then**
    **for** all the *neighbouring faces* $f_j$
      **if** $f_j$ is *not fouled* **then**
        $\{f\} \leftarrow f_j$;
      **endif**
    **endfor**

**else**
  $\{f\} \leftarrow f_i$;
**endif**
**if** $\{f\}$ is not empty **then**
  $j \leftarrow 0$
  **while** particle *travels* and $j < |\{f\}|$ **do**
    $j \leftarrow j + 1$;
    **if** $d_p > d_i$ **then**
      **if** the centre of $p_i$ lies outside the largest circumscribed circle of $f_i$ **then**
        $f_i \leftarrow$ the neigbouring face $f_i$ of the adjacent cell;
      **endif**
      **if** $d_p > 1.1 d_i$
        particle *cakes* or *blocks* surface;
      **else**
        particle *blinds* surface face;
      **endif**
    **else**
      particle *enters* membrane;
    **endif**
  **endwhile**
**else**
  particle *cakes* or *blocks* surface;
**endif**
**endwhile** □

Backflushing the membrane may clean blocking- but not blinding particles. Once inside the membrane, each particle independently and randomly walks until it can get out of the membrane or can go no further and thereby necessarily fouls a cell. The interpretation shown here as Algorithm 6.4 is an adaptation of that given by Jackson (1994).

**Algorithm 6.4** *Interaction between each internal particle and the pores.*

**for** each *internal particle* $p_i$
  $\{c\}$ *pores* to enter;
  $j \leftarrow 1$
  **while** $j \leq |\{c\}|$ and $p_i$ has *not entered a polyhedron* **do**
    **find** pore to enter;
    **if** the polyhedron is *fouled* **then**
      particle enters the polyhedron;
      **if** *there is no space* in the polyhedron **then**
        particle *blocks* or *blinds* pore;
      **endif**
    **endif**
    $i \leftarrow i + 1$
  **endwhile**
**endfor** □

On the cake, the particles drop, roll, or nest among one another. The cake formation is described as Algorithm 6.5 which closely follows the description which he gave.

**Algorithm 6.5** *Particle cake formation, cf Jackson (1994)*

**while** next particle exists **do**
  $p_i \leftarrow$ **next particle**;
  **if** route not directly leads to surface face **then**
    $p_i$ and $p_1$ collide;
    **find** rolling path;
    **if** $p_i$ does not roll off **then**
      $p_i$ and $p_2$ collide;
      **if** $p_i$ does not roll off **then**
        $p_i$ and $p_3$ collide;
        $p_i$ comes to rest;

**endif**
**endif**
**endif**
**endwhile** □

Fifty particles is the empirical rule of thumb for the number of neighbouring particles to consider at the surface and cake level. Good care has been taken by his program to ensure that no two particles within this set overlap. All of his particles are gentle for they bounce not but often roll, for these no hard billiard balls but mathematical particles with assumptions. In this way a spherical particle would first vertically drops, then touches another particle and starts rolling off the latter along its surface. Once the two particles are abreast with each other they part. A dropping particle can either roll off one- or simultaneously two particles at a time. Rolling simultaneously off three particles is not physically possible. For if we picture $i$ meets 1, rolls off 1, meets 2, starts to roll simultaneously off 1 and 2, and then meet 3. At this point it can either choose to give up 1 to roll simultaneously off only 2 and 3 or, it nests on the cradle of 1, 2 and 3, and thereby stops. There are three phases or layers associated with this membrane packing model. These are the cake-, surface- and internal layers. For the internal layer the thickness is limited by the membrane thickness, for the surface layer by the maximum diameter of the dropping particles, and for the cake layer by their amount and sizes. The flux decline across the membrane model is calculated by Algorithm 6.6. Here $C_n$ is the particle concentration, $P_0$ initial pressure, $P_L$ final pressure, $J_m$ initial volumetric flux rate, that is to say, clean solvent flux for membrane, $d$ diameter of the circular membrane, $n$ the number of particles to be dropped on to the membrane in this simulation, $L$ the depth of the packing retion, $\bar{d}_p$ the mean spherical particle diameter, $\mu$ the solvent viscosity, $\epsilon_v$ the free volume, that is to say, the ratio between the volume of voids and volume of bed, $v$ initial velocity of the fluid, $P_s$ pressure between the cake and the surface fouling layer, $R_1$ the pressure-flux relationship for the particles in contact with the membrane, $R$ the pressure-flux relationship of the membrane,

**Algorithm 6.6** *Flux decline across the membrane model.*

**define** $\Delta t$, $C_n$, $P_0$;
$v \leftarrow (4/\pi)J_m/d^2$;
$t \leftarrow 0$;
**while** simulation should last **do**
  $t \leftarrow t + \Delta t$;
  $n \leftarrow \mathrm{f}(\Delta t, t, J_m)$;
  **find** the *packing density, dimensions* and *number of particles* of the cake;
  **find** the *packing density, dimensions* and *number of blocking-* and *blinding particles* of the surface fouling layer;
  **find** the *packing density, dimensions* and *number of blocking-* and *blinding particles* of the internal fouling layer;
  $P_c \leftarrow$ the *pressure drop across the cake* calculated from $v = \frac{(P_0 - P_L)}{L} \frac{\bar{d}_p^2}{150\mu} \frac{\epsilon_v^3}{(1-\epsilon_v)^2}$
  $P_s \leftarrow P_0 - P_c$
  $P_l \leftarrow$ the *pressure drop* for the *surface layer*;
  $P_i \leftarrow$ the *pressure drop* for the *internal fouling particles*;
  $R_1 \leftarrow \frac{P_l + P_i}{J_m}$;
  $R_2 \leftarrow R_1 + R$;
  $J_m \leftarrow P_s/R_2$;
**endwhile** □

*Flux* is the rate of flow by weight. The number of particles per second is obtained by multiplying† the concentration by the volumetric rate. And if we divide this by the area of the membrane we get the number of particles per second per unit area. The random walk of particles during removal by backflushing is shown here as Algorithm 6.7.

**Algorithm 6.7** *The random walk of particles during removal by backflushing*

**remove** cake and all surface blocking particles;
**while** *next particle exists* and *backflushing* **do**
  *backflushing* $\leftarrow$ false;
  **if** not blocking **then**

† It is possibly a typing error in Jackson (1994) when he says *dividing* instead of *multiplying* here.

```
        remain blinding;
        if there are more particles in cell then
          blocking ← true;
        else
          no more particle;
          backflushing ← true;
        endif
      else
        blocking ← true;
      endif
      if blocking then
        do
          if cell inlet pore unfouled or fouled and the particle passes through adjacent pore then
            move into the next adjacent cell;
          else
            remain blocking;
            backflushing ← true;
          endif
        while the particle is still within the membrane enddo
        particle has left membrane;
        backflushing ← true;
      endif
    endwhile
```

□

Filters are sometimes made of non-woven materials, in which case they are modelled as tessellation by random straight lines. Wilkinson *et al* (1986) studies this type of filter by modelling it as intersecting random rods. The position and orientation of a rod is defined by one point, an angle $0 \leq \theta_i$ 180° and the diameter of the fibre $d_i$. The free area is $\varepsilon_A = (A - \sum A_s)/A$, where the total fibre cross sectional area is $\sum A_s = \sum_m l_i d_i - \sum_m \sum_n \delta_{ij} d_i d_j \operatorname{cosec} \theta_{ij}$, where $l_i$ is the length of the fibre, $\delta_{ij}$ is 1 if lines $i$ and $j$ intersects and 0 otherwise, $\theta_{ij}$ the angle of intersection of the fibres. Their model worked well for small fibre diameters compared to those of the particles.

Algorithm 6.8 rewrites their method in an algorithmic form. Here $0 < r_j < 1$ is a random number with uniform distribution, $d_c$ the critical diameter, that of a circle which just fits the inside an irregular polygon.

**Algorithm 6.8** *Non-woven fibre simulation, cf Wilkinson et al, 1986.*

```
for all particles i do
  d_i ← d̄ + σ(Σ_n r_k − n/2)/√(R/12);
  choose the particle position 0 ≤ x_i ≤ X and 0 ≤ y_i ≤ Y;
  for each layer of the filter j do
    d_j^c ← the largest circle which fits inside the polygon;
    if d_k > d_j^c then
      the particle is retained at this position;
    endif
  endfor
endfor
```

□

The fibre here is in the form of fibre matt, which stacks one upon another in layers. The equation for the volume ratio suspension to inlet of a fibre matt, $V_n/V_0 = \exp(-\xi n)$ where $\xi$ is the mean capture efficiency of the filter, is similar to that of the concentration ratio in deep bed filtration, $C/C_0 = \exp(-Kx)$. The mean capture efficiency is related to the layer efficiencies by $\xi = 1 - [(1-\xi_1)(1-\xi_2)\cdots(1-\xi_n)]^{1/n}$, and is dependent on $\bar{d}$, $\sigma$, $\varepsilon_A$, $\bar{d}_f$, $\sigma_f$, where the subscript $f$ means *filament*.

Jafferali (1995) studies Voronoi tessellation and applies it to microfiltration. The program which he used to create the Voronoi structure has the algorithm of Algorithm 6.9.

**Algorithm 6.9** *Construction of 3-d Voronoi network (cf Jafferali, 1995)*

```
find set S which contains m nuclei nearest to the nucleus point p;
find the nucleus q which is nearest to p;
```

**find** a nucleus $r \in S, r \neq q$, such that the triangle $pqr$ has the minimum circumradius, that is one facet of the Delaunay triangulation;
**do**
**find** $s \in S, s \neq r \neq q$ such that the circumradius of the tetrahedron $pqrs$ is minimised, that is a Delaunay tetrahedron
**find** $m, n, o \in S$ such that $m \neq n \neq o \neq q \neq r \neq s$ and the tetrahedra $pqrm$j, $pqsn$ and $prso$ all have minimum circumradii, these are also Delaunay tetrahedra
**until** each triplet $pp_ip_j$ is in two Delaunay tetrahedra, that is every face of every Delaunay tetrahedron containing $p$ as a vertex is closed **enddo**

To find the centre of the circumscribed circle of the triangle $ABC$, let $\Pi_A$, $\Pi_B$ and $\Pi_C$ be the planes perpendicular respectively to the sides opposite to $A$, $B$ and $C$. Respectively let $n_A$, $n_B$ and $n_C$ be the vectors normal to $\Pi_A$, $\Pi_B$ and $\Pi_C$, and $a$, $b$ and $c$ the position vectors of $A$, $B$ and $C$. Then $\Pi_A$, $\Pi_B$ and $\Pi_C$ will intersect at a point the position vector of whom is $r$ which is obtained by solving the three simultaneous equations $(r - n_i) \cdot a = 0$ where $i = A$, $B$, $C$, $n_B = n_C \times n_A$, $n_A = b - c$, $n_C = b - a$, $d = 0.5(a + b)$, $e = 0.5(b + c)$. It follows that $r_x = [m_1 - (r_x a_y + r_z a_z)]/a_x$, $r_y = m_6 + m_7 r_z$ and $r_z = (m_4 - m_6)/(m_7 - m_5)$ where $m_1 = r \cdot a = a \cdot n_B$, $m_2 = r \cdot d = d \cdot n_C$, $m_3 = r \cdot e = e \cdot n_A, m_4 = (m_2 a_x - m_1 d_x)/(d_y a_x - a_y d_x)$, $m_5 = (a_z d_x - d_z a_x)/(d_y a_x - a_y d_x)$, $m_6 = (m_3 a_x - m_1 e_x)/(e_y a_x - a_y e_x)$, and $m_7 = (a_z e_x - e_z a_x)/(e_y a_x - a_y e_x)$.. The centre $p$ of the circumscribed sphere is obtained by solving the four simultaneous equations the first one of which is $(p_x - A_x)^2 + (p_y - A_y)^2 + (p_z - A_z)^2 = r^2$ while the other three have $B$, $C$ and $D$ in place of $A$. Solving these we get $p_x = (m_2 - m_4)/(m_3 - m_1)$, $p_y = m_1 x + m_2$, $p_z = [2p_x(c_x - d_x) + 2p_y(c_y - d_y) + e_2 - e_1]/[2(d_z - c_z)]$ where $m_1 = [(a_x - b_x)(d_z - c_z) + (d_x - c_x)(b_z - a_z)]/[(c_y - d_y)(b_z - a_z) + (b_y - a_y)(d_z - c_z)]$, $m_2 = [(e_4 - e_3)(b_z - a_z) - (e_1 - e_2)(d_z - c_z)]/[2(c_y - d_y)(b_z - a_z) + 2(b_y - a_y)(d_z - c_z)]$, $m_3 = [(a_x - d_x)(b_z - c_z) + (b_x - c_x)(d_z - a_z)]/[(c_y - b_y)(d_z - a_z) + 2(d_y - a_y)(b_z - c_z)]$, $m_4 = [(e_2 - e_3)(d_z - a_z) - (e_1 - e_4)(b_z - c_z)]/[2(c_y - b_y)(d_z - a_z) + 2(d_y - a_y)(b_z - c_z)]$, $e_1 = a_x^2 + a_y^2 + a_z^2$, $e_2 = b_x^2 + b_y^2 + b_z^2$, $e_3 = c_x^2 + c_y^2 + c_z^2$, and $e_4 = d_x^2 + d_y^2 + d_z^2$. Statistics obtained from his simulation include $n_c$, $n_c^f$, $n_c^v$, $n_c^e$, perimeter of polyhedron, area of face, and volume of polyhedron. The number of faces and the number of edges are found during face construction the method of which is Algorithm 6.10.

**Algorithm 6.10** *Find faces of a polyhedron, cf Jafferali (1995).*

**find** the set of all the $n$ vertices of the polyhedron, $\{v\}$;
**for** all combinations of three vertices $v_i$, $v_j$ and $v_k$ of $\{v\}$ **do**
**find** the plane $\Pi$ which contains $v_i$, $v_j$ and $v_k$;
**if** all the remaining vertices lie on one side of $\Pi$ **then**
$v_i$, $v_j$, $v_k$ together with all the other vertices which lie on $\Pi$ form a face;
**endif**
**enddo** □

To find out whether all the vertices lie on one side relative to a plane, find whether the sign of the distance from each of these points to the plane changes. This distance is $d = \overrightarrow{pa} \cdot n = (a - p) \cdot n$ where $n$ is the unit normal vector, $n = \overrightarrow{pa} \times \overrightarrow{bc}/|\overrightarrow{ba} \times \overrightarrow{bc}| = [(a - b) \times (c - b)]/|(a - b) \times (c - b)|$, and $a$, $b$ and $c$ form a plane while $p$ is the point in question. To arrange the vertices of a face in cyclic order, first pick one point among them and then find the angle made by the lines from it to every two combination of the remaining vertices, by $\theta = \cos^{-1}[(\overrightarrow{v_p v_i} \cdot \overrightarrow{v_p v_j})/|\overrightarrow{v_p v_i}| \cdot |\overrightarrow{v_p v_j}|]$. Two such lines which maximises the angle are both edges, and the angle from either one of them to each of the remaining vertices increases as we tread the edges from one vertex to another in succession.

Nuclei points of the modified point process where $d \geq d_{\min}$ are generated by Algorithm 6.11.

**Algorithm 6.11** *Nuclei points of the modified point process, Jafferali (1995).*

$n$; $d_{\min}$;
**find** $p_1$;
$i \leftarrow 1$;
**while** $i < n$ **do**
$i \leftarrow i = 1$;
**find** $p_i$;
**for** $j = 2$ to $(i - 1)$ **do**
**find** $d(p_i, p_j)$;
**if** $d(p_i, p_j) < d_{\min}$ **then**

$i \leftarrow i - 1$;
**endif**
**endfor**
**endwhile** □

The statistics that he found for these modified Voronoi structures are shown here again in Table 6.1.

| $d_{\min}$ | $n_c$ | $\min(n_f)$ | $\max(n_f)$ | $\min(n_v)$ | $\max(n_v)$ |
|---|---|---|---|---|---|
| 0.0 | 226 | 8 | 23 | 12 | 42 |
| 0.2 | 218 | 8 | 24 | 12 | 44 |
| 0.4 | 215 | 8 | 23 | 12 | 44 |
| 0.6 | 226 | 8 | 24 | 12 | 44 |
| 0.8 | 229 | 9 | 21 | 14 | 38 |
| 1.0 | 214 | 10 | 20 | 16 | 36 |
| 1.2 | 204 | 10 | 20 | 16 | 36 |

**Table 6.1** *Statistics of the modified Voronoi cells, cf Jafferali (1995).*

His asymmetric Voronoi tessellations have cell volume increasing with the $z$-coordinate position of the cell. The procedure for finding the $d_{\min}$ between two cells in such structure is described as Algorithm 6.12. Here the volume ratio is $\delta = V_0/V_1$, and thus $\delta = y_0/y + 1$, $d_{\min} = mz_i + c$ where $m = (y - y_1)/(z - z_1)$.

**Algorithm 6.12** *Asymmetric Voronoi tessellation, cf Jafferali (1995).*

$\delta$;
$y_1 \leftarrow 1$;
$y_0 \leftarrow \delta$;
$c \leftarrow \delta^{1/3}$;
$m \leftarrow (1 - c)$;
$d_{\min} \leftarrow k[(1 - c)z + c]$; □

The statistics that he found are given for reference as Tables 6.2 and 6.3. Real numbers have been rounded to leave at most four decimal points to make it easier to read (*cf* Jafferali, 1995).

| | **point distribution** | | |
|---|---|---|---|
| | *Poisson* | *modified* | *asymmetric* |
| $n_c$ | 1276 | 1171 | 1069 |
| $\sum_i n_i^v$ | 33340 | 29946 | 27749 |
| $n_c^v$ | $26.1285 \pm 6.4207$ | $25.5730 \pm 3.5573$ | $25.9579 \pm 3.5301$ |
| $\sum_i n_i^e$ | 50072 | 44945 | 41643 |
| $n_c^e$ | $39.2414 \pm 9.6235$ | $38.3817 \pm 5.3317$ | $38.9551 \pm 5.2740$ |
| $\sum_i n_i^f$ | 19284 | 17341 | 16032 |
| $n_c^f$ | $15.1129 \pm 3.2114$ | $14.8087 \pm 1.7821$ | $14.9972 \pm 1.7514$ |
| $\sum_i V_i$ | $0.6073b^3$ | $0.6582b^3$ | $0.5912b^3$ |
| $V_c$ | $4.76 \times 10^{-4}b^3 \pm 2 \times 10^{-4}$ | $5.62 \times 10^{-4}b^3 \pm 6.8 \times 10^{-4}$ | $5.53 \times 10^{-4}b^3 \pm 6.0 \times 10^{-4}$ |
| $\sum_i p_i$ | $641.3870b$ | $664.1398b$ | $554.01b$ |
| $p_c$ | $1.0053b \pm 0.2290$ | $1.1343b \pm 0.1058$ | $1.0365b \pm 0.3255$ |
| $\sum_i A_i$ | $40.9930b^2$ | $44.2189b^2$ | $36.4954b^2$ |
| $A_c$ | $0.0321b^2$ | $0.0378b^2$ | $0.0341b^2$ |

**Table 6.2** *Comparative Voronoi statistics, Jafferali (1995).*

| | **distribution** | | | | | |
|---|---|---|---|---|---|---|
| | *Poisson* | | *modified* | | *asymmetrical* | |
| | min | max | min | max | min | max |
| $V$ | $8.8 \times 10^{-5}b^3$ | $1.4 \times 10^{-3}b^3$ | $3.9 \times 10^{-4}b^3$ | $8.4 \times 10^{-4}b^3$ | $9.9 \times 10^{-5}b^3$ | $3.7 \times 10^{-3}b^3$ |
| $n_c^f$ | 7 | 28 | 10 | 21 | 10 | 21 |
| $n_c^e$ | 15 | 78 | 24 | 57 | 24 | 57 |
| $n_c^v$ | 10 | 48 | 12 | 34 | 12 | 34 |

**Table 6.3** *More comparative Voronoi statistics, Jafferali (1995).*

The Voronoi domain created has ragged boundaries due to polyhedra protruding. The method used in his thesis is to slice the domain by a horizontal plane and then redefine those vertices and edges on that plane and at the same time reject everything above it. This is more similar to a

carpenter filing away at a block of wood than a stone mason choosing his stones. The volume of voids was updated by using AVS which does this by counting the number of pixels contained within a given area. Statistics of an asymmetric Voronoi structure were given. His study concerns with the simulation of dead end filtration and cake formation. The particle size distribution is quantified in terms of the ratio of the mean particle diameter to the mean inlet pore diameter, $\alpha$, and that of the standard deviation of the particle diameters to the mean particle diameter, $\beta$. The first parameter indicates the relative size between the particles and pores while the second one that amongst particles. Thus $\alpha > 1$ would mean that the particles are bigger than the inlet pores, while $\beta = 0$ that particles are mono dispersed. The interaction between the particles and cake is essentially the same as that used earlier by Jackson (1994). The evaluation of pore properties described is equivalent to Algorithm 6.13.

**Algorithm 6.13** *Pore property evaluation, cf Jafferali (1995).*

**identify** edge pores;
**identify** inlet- and outlet pores;
**for** all pores **do**
  **find** the largest inscribed sphere;
  **for** all faces of the pore **do**
    **find** the largest inscribed circle;
  **endfor**
**endfor** □

Identifying edge pores amounts to first finding neighbouring polyhedra, and then finding for all faces whether each of them belongs to one and only one polyhedron. Finding neighbouring polyhedra amounts to finding for all polyhedra pairs whether each of them possess no less than three common vertices.

Particles pass through a face into a pore if they could, but since they are spherical whereas the pores and faces are polyhedral and polygonal, the largest inscibed circle of the facet is computed. If the particles are irregularly shaped, they may fit through a polygon when challenging from a certain direction but not another. However, the assumption of spherically shaped particles provides most authors on the subject with an approximation both satisfactory and convenient, because then there is no need whatever to rotate them. Jafferali (1995) applies an algorithm equivalent to our Algorithm 6.14 to find the inscribed circle for all faces. Essentially this involves computing an inscribed circle of a triangle arisen from every one of the possible combinations of three sides of the face. Then the largest one of such circles which lies inside the face is the inscribed circle of the face. Here $a$, $b$ and $c$ are the positional vector of $A$, $B$ and $C$ respectively; $n$ is a unit vector from $A$ to $B$, $q$ normal to the plane $ABC$, and $m$ perpendicular to both; $s_i$ are the sides opposite $(x_i, y_i)$. From 3-d each face is transformed into 2-d in such a manner that $A = (x_1, y_1) = (0, 0)$, $B = (x_2, y_2) = (0, y_2)$ and $C = (x_3, y_3)$. From $c - a = x_3 m + y_3 n$, $x_3$ and $y_3$ are obtained; $z$ – for *Zentrum* – is the centre $(x_z, y_z)$ of the face in 3-d or its equivalent transformed centre $(\tilde{x}_z, \tilde{x}_z)$; $\xi$ is the nucleus of our polyhedron while $\xi_i$ its neighbouring nuclei. Then the $k^{\text{th}}$ combination gives the largest inscribed circle the radius of which is $r_k$.

**Algorithm 6.14** *Inscribed circle of faces, cf Jafferali (1995).*

**for** each face **do**
  **for** all the ${}^{p}\mathrm{C}_3$ combinations $j$ of sides of the face **do**
    $R \leftarrow 0$;
    **find** $A$, $B$ and $C$, the vertices of the circle formed by them;
    $n \leftarrow (b - a)/|b - a|$;
    $m \leftarrow$ **solve** $m \cdot n = 0$, $m \cdot N = 0$, $|m| = 1$ **and** $|n| = 1$;
    $q \leftarrow (b - a) \times (c - a)$;
    $\{x_1, y_1, x_2\} \leftarrow 0$;
    $y_2 \leftarrow |b - a|$;
    $y_3 \leftarrow [(x_3 n_y + y_3 n_y) m_x - (x_3 m_x + n_x y_3) m_y] / (n_y m_x - n_x m_y)$;
    $x_3 \leftarrow [(x_3 m_x + n_x y_3) - y_3 n_x] / m_x$;
    $p \leftarrow \sum_{i=1}^{3} s_i$;
    $S \leftarrow p/2$;
    $r_j \leftarrow \left[ S \prod_{i=1}^{3} (S - s_i) \right]^{1/2} / S$;
    $\tilde{x}_z \leftarrow (s_1 x_3)/p = (s_1 x_3 + s_2 x_1 + s_3 x_2)/p$;

$\tilde{x}_z \leftarrow (s_1 y_3 + s_3 y_2)/p = (s_1 y_3 + s_2 y_1 + s_3 y_2)/p$;
$x_z \leftarrow \tilde{x}_z m_x + \tilde{x}_z n_x$;
$y_z \leftarrow \tilde{x}_z m_y + \tilde{x}_z n_y$;
$z_z \leftarrow \mathrm{ABC}(x_z, y_z)$;
$d \leftarrow |z - \xi|$;
$\zeta \leftarrow 1$;
**for** all $\xi_i$ **do**
$d_i \leftarrow |z - \xi_i|$;
**if** $d_i < d$ **then**
$\zeta \leftarrow 0$;
**endif**
**endfor**
**if** $\zeta = 1$ **then**
**if** $r > R$ **then**
$R \leftarrow r_j$;
$k \leftarrow j$;
**endif**
**endif**
**endfor**
**endfor** □

Algorithm 6.15 finds the inscribed sphere of each polyhedron. A tetrahedron is formed from each combination of four planes of polygonal faces. The largest of all the inscribed spheres of these tetrahedra is the inscribed sphere of the polyhedron. The intersection of bisecting planes $\cap_{ij=i1}^{ik} \Pi_{ij}$ is the facet in $(3 - k \bmod(3))$ dimensions which is equidistant from $\Pi_i$ and $\Pi_j$, $j = 1$ to $k$. Finding $\Pi = ax + by + cz + d = 0$ amounts to solving $A \cdot (B \times C)$ for $a$, $b$, $c$ and $d$. Finding intersection of planes amounts to solving their equations simultaneously. Here $\Pi_i$ is the plane containing the $i^{\text{th}}$ face, $\Pi_{ij}$ the plane bisecting $\Pi_i$ and $\Pi_j$.

**Algorithm 6.15** *Inscribed sphere of a polyhedron, cf Jafferali (1995).*

**for** each polyhedron **do**
$R \leftarrow 0$;
**for** all the ${}^{n_f}\mathrm{C}_4$ combinations $j$ of the polyhedron **do**
**for** $i = 1$ to 4 **do**
$A \leftarrow v_i^2 - v_i^1$;
$B \leftarrow v_i^3 - v_i^1$;
$C \leftarrow v_i^4 - v_i^1$;
$\Pi_i(a_i, b_i, c_i, d_i) \leftarrow$ **solve** $A \cdot (B \times C) = 0$;
**endfor**
**find** $\Pi_{1i}$; $i = 2, 3, 4$;
$p_i \leftarrow \cap_{i=2}^{4} \Pi_{1i}$;
$r_j \leftarrow \mathrm{d}(p_i, \Pi_1)$;
**if** $r_j > R$ **then**
$R \leftarrow r_j$;
$k \leftarrow j$;
**endif**
**endfor**
**endfor** □

Particles move down vertically in discrete time steps towards the membrane. Upon reaching the latter, the $i^{\text{th}}$ particle is greeted by an entrance the aperture of which is circular with radius $r_c$. If $r_i < r_c$ it penetrates into the pore, if $r_c \leq r_i \leq 1.1 r_c$ it blinds and if $1.1 r_c < r_i$ blocks the entrance. Blinded particles are not removed by reversing the flow. They become a part of the membrane. Reaching the membrane is by no mean their destiny, and the particles only begin their long and tortuous pelerinage hereafter by embarking on a random walk in the direction towards the centre of the earth. Each particle enters a pore via the face furthest away from the latter, and it leaves via the face closest to it. The position of a facet is that of its inscribed circle. If the lowest facet is not viable, the particle first repositions itself precisely at the centre of the inscribed sphere, and then either moves out from some facet lower than itself or, when all possibilities of travelling having been exhausted, become a residence of that pore. The repositioning part above may seem

like a gross approximation, but there is no reasons why this should not make a sound assumption if we consider the fact that a real particle is never spherical in the first place. But if the particle blinds or blocks a facet, then the calculation used by Jafferali (*ibid.*) becomes more accurate. That is $\alpha = \xi + \lambda(z - \xi)$, where $\lambda = |d|/(|d| + |a|)$, $|a| = (r_\alpha^2 + r_z^2)^{1/2}$ and $d = |\xi - z| - |a|$. To summarise, a particle is in a perpetual search for a lowest facet, which of course is closest to the centre of the earth. This kind of study is important because it lets us know which part of the membrane is prone fouling by the particles.

Non-woven fibres are simply stacked layers of material. Extra holes produced by needles which are used to increase their strength are difficult to model and are normally assumed away before the simulation (*cf* Chan, 1990). Layers are considered as flat when the fibres which make them are considered to be flexible. Capturing of particles must take into account the separation between the layers as well as the usual aperture perpendicular to the flow direction. This is an example of man-made stacked 2-d layers. Examples in nature are numerous, including the honeycomb and cell growth in tissues.

In his simulation, Chan (1990) represents random lines with $(y - y_i) = \tan\theta_i(x - x_i)$, where $0 \leq \theta_i \leq \pi$, a method of interior randomness. Other possible methods include the $\mu$ randomness where the line is represented by $x \sin\alpha_i + y \sin\alpha_i = d_i$, where $d_i$ is the distance of the line from a pole point $p_i$ which is usually taken as the centre of the area, and surface randomness where the position on the boundary of the area is chosen.

Flow channels within a medium follows Poiseuille's equation for flow within capillaries, $Q = \Delta P \pi r^4 / 8\mu\Delta x$, where $\Delta x$ is the length of the capillary. Darcy's law relates the flow of a fluid through a porous medium to the overall pressure drop, $\Delta P = \mu L u_0 / K$, where $u_0$ is the superficial fluid velocity, $L$ the depth of the medium and $K$ the permeability coefficient. The permeability coefficient for packed media, $K = \varepsilon^3 / \left[K' S^2 (1 - \varepsilon)^2\right]$, where $\varepsilon$ is the voidage of the medium, $S$ the specific surface and $K'$ the Kozeny constant. Particles can blind during both the filtration and the backflushing stages. The backflushing efficiency is the ratio between the volume of the particle flushed away and the total volume of particles captured in the media before backflushing.

## § 6.1 Separation processes

The largest aperture in the screen is the determining factor by which the selection is made, in other words it defines the size of the cut. This is a more logical argument than the one by which it is the mean aperture that defines the cut size (*cf* Rose and English, 1973). This largest aperture determines the smallest size of the particles retained on the screen. But in practice much smaller particles than these will remain on the screen for various reasons the most important one of which is blindings caused by particles with sizes $d_{\min} < d < 1.1 d_{\min}$. The factor 1.1 was first used by Rose and English (*ibid.*), and arises from the angle of friction $\gamma$ being approximately 20°.

On a sieve at each instant, the area that is free from blinding material is $A = A_s - G(m_0 - m)$ where $A_s$ is the sieve area, $G$ the area blinded by a unit mass of blinding material, $m$ and $m_0$ the mass of respectively the blinding- and initial blinding material on the sieve. Also, $\mathrm{d}m/\mathrm{d}t = -kmA = -km\left[A_s - G(m_0 - m)\right] = -\alpha m(\beta + m)$, where $\alpha = kG$ and $\beta = [(A/G) - m_0]$.

In surface straining filtration the particles are larger than the pore size, in depth straining filtration both the pore and the particle sizes are commensurate to each other, and in adsorptive filtration the particle size is smaller than the pore diameter. Adsorptive filters can be made to have higher filtration efficiency, higher capacity and higher flow rate than depth straining filters (Raistrick, 1986).

Examples of solid-liquid separations normally found in Chemical Engineering are filtration, sedimentation, flocculation, centrifugation, electro-osmotic and electro phoretic dewatering and hydrocyclonic separation. Poole and Doyle (1965) listed some of the aspects in filtration which they thought need further investigation: the effect of rapid pressure increases on the approach to equilibrium porosity in cakes, for instance in rotary filtrations; the relation between drag forces on particles and particle arrangements and shapes; migration of fines within cakes and media; the effect of changing flow paths during washing on porosity.

## § 6.2 Dead-end filtration

Because membranes are porous media, the flux across them follows Darcy's Law, $j = \Delta p/(\mu R)$, where $j = \mathrm{d}V/(A\mathrm{d}t)$, $R$ is the hydraulic resistance, $R = R_m + R_c$ where $R_m$ and $R_c$ are membrane

and cake resistances respectively. Assume $R_m = 0$, then $R = R_c = \alpha m/A$, where $\alpha$ is the specific resistance of the cake, $m$ the mass of the filter cake and $A$ the septum area.

## § 6.3 The centre of gravity

The formula for the centre of gravity of objects in general is $c_g = \int xw(x)\mathrm{d}x / \int w(x)\mathrm{d}x$. For a real object the theoretical procedure is complicated, since there is always the possibility that the density is not uniform, but the practical procedure is simple and straight forward, that is by simply hanging the object by strings in various positions and then find the intersection between the lines of string, provided of course that this is possible with the object.

The centre of gravity is important whenever there is a gravitational interaction with an object. Both the translational and rotational motions of objects through space are relative to this point. The c.g. of a triangle is positioned at one third its height whereas that of a half circular disk is $4r/3\pi$ from the straight boundary line. A c.g. always lies on the lines of symmetry when these exist. Other names for c.g. include geocentre, centroid and barycentre.

The centroid of a triangle lies at the intersection of its median. That of a tetrahedron lies at the intersection of all the lines joining the vertices with the centroids of their respective opposite faces. Its coordinates are the mean coordinates of the four vertices.

To find the centroid of a polygon, first tessellate it into triangles and find the centroid of each one of them. Then we have another system of point masses located at the centroids of these triangles, with the mass proportional to their respective areas.

The centroid of a rod is at its mid point, and the weight of a rod is proportional to its length. This can be helpful when we want to find the centroid of a network of rods or tubes.

The centroid of a quadrilateral is the intersection between its two bimedians. This is also the mid point of the lines joining the mid points of the two diagonals.

The medians of a triangle which has its vertices at $(a_1, b_1)$, $(a_2, b_2)$ and $(a_3, b_3)$ are the lines connecting these three vertices to the mid points opposite to them, the first one to $(c_1, d_1)$ where $c_1 = (a_2 + a_3)/2$ and $d_1 = (b_2 + b_3)/2$, and similarly for the other two. Their intersection is obtained by solving their equations, $(d_1 - b_1)/(c_1 - a_1) = (y - b_1)/(x - a_1)$, and so on. This gives the solution as being the average value of the vertices, $[(\sum_3 a_i)/3, (\sum_3 b_i)/3]$.

Having mentioned the centroid, it is natural to add the other two points related to it. On the Euler line also lie the orthocentre, where altitudes intersect, and the circumcentre, where perpendicular bisectors intersect.

Let $a_{ij}$ be $(a_j - a_i)$. Then for the orthocentre we need to solve any two of the three equations of the altitudes. For example, $-a_{23}/b_{23} = (y - b_1)/(x - a_1)$ and $(y - b_2)/(x - a_2) = -a_{13}/b_{13}$ can be simultaneously solved to give $x = [a_1(a_2b_{12} + a_3b_{31}) - (a_2a_3 + b_{21}b_{31})b_{32}] / (a_3b_{21} + a_1b_{32} + a_2b_{13})$ and $y = -[a_{32}(a_1a_2 - a_2a_3 + b_2b_{31}) + a_{31}(a_1a_{23} + b_1b_{23})] / (a_3b_{21} + a_1b_{32} + a_2b_{13})$.

Similarly the circumcentre can be solved from two equations, for instance $(y - b_1)/(x - a_1) = m_1$ and $(y - b_2)/(x - a_2) = m_2$ where $m_1 = -a_{23}/b_{23}$ and $m_2 = -a_{13}/b_{13}$, to give $x = b_{32}(a_2a_3 + b_2b_3)/(a_3b_2 - a_2b_3)$ and $y = a_{32}(a_2a_3 + b_2b_3)/(a_2b_3 - a_3b_2)$.

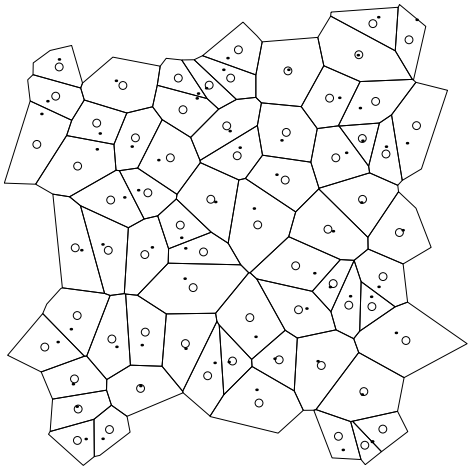

Figure 6.1 shows a 2-d Voronoi tessellation with its nuclei and centroids. Ironically, the centroid represents the position of a cell better than its nuclei, because it positions itself in the most balanced situation relative to the cell, whereas the nuclei does so with regard to its neighbours. The centroids are noticeably more evenly distributed than our Poisson nuclei.

**Figure 6.1** Centroid of the Voronoi tessellation.

Because the centre of gravity is a property which has more to do with the individual cells than with their neighbours, there may be real situations in nature where the c.g. of individual cells in a

network has a role to play. For example, it is usually assumed in a mathematical Voronoi tessellation that all the nuclei stay fixed and do not move. But in a real situation this would imply that there are some nuclei which lie very close to the walls. As no such nuclei would be stable, they more likely move away, and in that case the most reasonable prediction is that they move towards the centre of gravity of the cell.

Because they are stochastic in nature, computational VT could in theory take up any shape however awkward. Jafferali (1995), for instance, imposes constraints on the algorithm which creates VT's, namely in the course of the generation no new nuclei can assume a position too close to those of the existing ones. Thus there is an excluded volume within the network which develops throughout the generation process, and the Poisson point process does not over the whole space. Again, this excluded volume is relative to the neighbours of the cells rather than to themselves.

I suggest that an evolution centred around the centroids of a network can replace such constrint regarding the minimum allowable distance between two nuclei. And that this would be a more natural for a network to do because the nature of the procedure which makes it look inwards to itself, as opposed to being totally governed by its environment. An attractive feature of the movement of the nuclei towards c.g.'s is that the cells in effect takes into account not only themselves but also their surrounding, because, if nothing else, it was the latter who shaped their appearance in the first place. Therefore the nuclei would start to grow from a purely random position according to a Poisson point process. Then it would move towards the centroid of the cell, and as it does so the definition of its boundaries is also changed. The centroid is a stable position, as can be seen in Figure 6.2. Similar to the processes of covering, $\mathrm{C}^{\cdot}(\mathcal{V})$ introduced in § 6.3 on page 172, and dual Voronoi, $\mathcal{V}^n(\cdot)$ in § 6.3 on page 172, this centroid process can be recursive, that is $\mathcal{G}^n(\cdot)$. However, unlike the other two mentioned, this process very quickly becomes stable; Figure 6.2 (b) is much different from (a), whereas it is very similar to (c). The difference is in the size distribution as well as in the location of nuclei. The nonuniformity in the shape of a half-circle which can be seen in Figure 6.2 (a) is propagated to both Figure's 6.2 (b) and (c), but it has become much fainter than in the original.

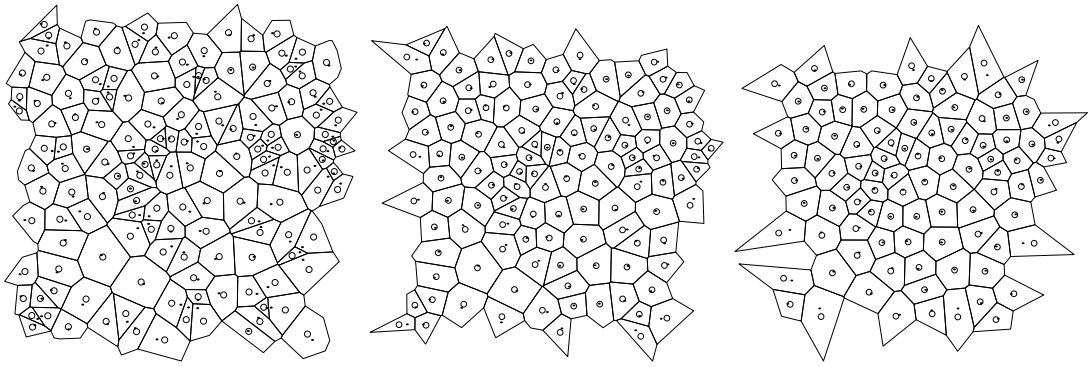

(a) (b) (c)

**Figure 6.2** *Nuclei evolution towards a centroid; (a) a Voronoi tesssellation based on the Poisson point process, $\mathcal{V}$, (b) the VT around its c.g.'s, that is $\mathcal{G}(\mathcal{V})$, and (c) the same process applied again to give the second order $\mathcal{G}^2(\mathcal{V})$.*

The program in § A.22 finds the centroid of a Voronoi network and $\mathcal{G}^n(\cdot)$.

There are three main steps in finding the centroid of a polygon. For each triangle of the triangulation of the polygon, first find the coordinates of its centroid, then its area. And then the centroid of the polygon is the weight average of the centroids of all the triangles. The first step involves finding the equation of two medians, which can be done by finding the mid point of an edge and then the slope to it from the opposite vertex. The second step can be carried out using the Heron's formula which finds the area by means of edge lengths.

Without loss of generality, let the polygon has $n$ vertices at $(a_i, b_i)$, where $i$ increases from 1 to $n$ in the clockwise direction. Assuming that all triangles which triangulate our polygon share one vertex at $(a_1, b_1)$, so that they all are $\triangle_{ijk}$, where $i = 1$, $k = j + 1$ and the three vertices are in the clockwise direction $(a_i, b_i)$, $(a_j, b_j)$ and $(a_k, b_k)$. There are three medians in each triangle, corresponding to the three vertices, but we only need two in order to solve for the centroid. Any two of them will give the same result, but in order to fix the algorithm let us choose those medians going out from the vertices $i$ and $j$. Then, since there is no loop in the procedure, we can save the space by describing it here in linear steps as $c_i \leftarrow (a_j + a_k)/2$, $d_i \leftarrow (b_j + b_k)/2$, $m_i \leftarrow (d_i - b_i)/(c_i - a_i)$,

and the first median has the equation $(y_1 - b_i)/(x_1 - a_i) = m_i$. Likewise the second equation can be obtained as $(y_1 - b_j)/(x_1 - a_j) = m_j$. Here the subscript of the centroid coordinates tells us in which triangle it belongs. As the result of the above, we obtain for the $k^{\text{th}}$ triangle $x_k = (a_i + a_j + a_k)/3$ and $y_k = (b_i + b_j + b_k)/3$.

The second step is to find the area. For this, we first find the edge lengths $s_{k1} \leftarrow (a_{ij}^2 + b_{ij}^2)^{1/2}$, $s_{k2} \leftarrow (a_{jk}^2 + b_{jk}^2)^{1/2}$ and $s_{k3} \leftarrow (a_{ki}^2 + b_{ki}^2)^{1/2}$, then the half-perimeter $s_k \leftarrow (s_{k1} + s_{k2} + s_{k3})/2$, and then the area $A_k \leftarrow (s_k(s_k - s_{k1})(s_k - s_{k2})(s_k - s_{k3}))^{1/2}$.

The third step solves for the polygonal centroid $(x, y)$ as $x \leftarrow (\sum_k x_k A_k)/\sum_k A_k$ and $y \leftarrow (\sum_k y_k A_k)/\sum_k A_k$. Notice that the first step is parallel to the second- but not the third one. Moreover, finding $c$'s and $d$'s are parallel, as well as finding the various $s_{ki}$'s. So we could vectorise these using parallel processing. But on Matlab all the matrix operations are already vectorised, so we only need to put all the components to be run in parallel in a single matrix and then do all the operations at once as a single operation on the matrix, provided that this is possible.

The general algebraic solution to the above algorithmic procedure is obtainable by solving all the equations involved. This gives for any polygon the following theorem.

**Theorem 6.1.**

$$x = \frac{\sum_\kappa (a_i + a_j + a_k)(a_i b_{jk} + a_j b_{ki} + a_k b_{ij})}{3\sum_\kappa (a_i b_{jk} + a_j b_{ki} + a_k b_{ij})} \qquad (24)_{\text{vi}}$$

*and*

$$y = \frac{\sum_\kappa (b_i + b_j + b_k)(a_i b_{jk} + a_j b_{ki} + a_k b_{ij})}{3\sum_\kappa (a_i b_{jk} + a_j b_{ki} + a_k b_{ij})}. \qquad (25)_{\text{vi}}$$

**Proof.** Assuming that we accept the centroid of a triangle to be at the mean coordinates among its vertices, and the centroid of massive point bodies is their average coordinates weighted by their mass, then when $k = 1$ it is obvious by looking at the Equation's 6.24 and 6.25 that this theorem is true. Let us suppose that both these equations are valid for $j$ triangles. We can present both of them in the form $n/d$ where, necessarily, $n = \sum_\kappa x_i A_i$ and $d = \sum_\kappa A_i$. If we now add another triangle to this cluster, the new triangle will also be represented as a massive point and it will add the terms $xA$ to the numerator and $A$ to the denominator, making $n/d = (n + xA)/(d + A) = (\sum_{(J+1)} x_i A_i)/\sum_{(j+1)} A_i$. Now, $x$ for a triangle $\triangle_{ijk}$ is $(a_i + a_j + a_k)/3$, and $A$ calculated from Heron's formula above is $(a_i b_{jk} + a_j b_{ki} + a_k b_{ij})^{1/2}/2$, which yields Equation 6.24 and 6.25 for $\kappa + 1$. This proves both equations, and thus Theorem 6.1, by induction. □

These general formulae, Equation's 6.24 and 6.25, cover the triangle itself, when we consider the latter as a polygon, and the solution when $k = 1$ in this case reduces to $(x, y)$ being simply the average coordinates of the three vertices, which is the same as that we have earlier mentioned.

Earlier we have seen the evolution of the nuclei towards centroids in two dimensions. Let us look at the same thing in three dimensions. For this purpose, the program of § A.21, which is used in § 6.5 and explained by Algorithm 6.18 in page 177, is still inadequate, as its list of faces contains considerable amount of duplicates. This would have increased the resources required to do further work here. Therefore the program has been adjusted to that in § A.23 for the described in the following.

Similar to the idea shown in Figure 6.2, we draw in Figure 6.3 the VT's in three dimensions whose nuclei evolve towards the respective c.g.'s.

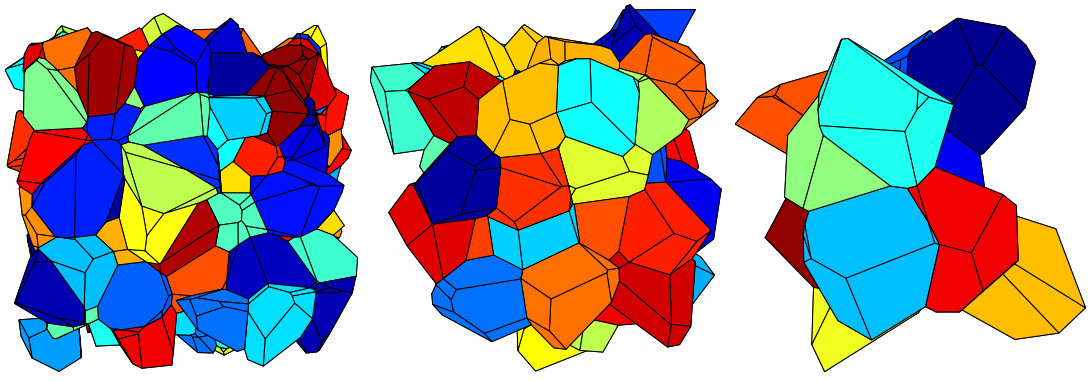

(a) (b) (c)

**Figure 6.3** *Evolution of nuclei towards centroids in three dimensions, namely* (a) $\mathcal{V}^3$, (b) $\mathcal{G}(\mathcal{V}^3)$ *and* (c) $\mathcal{G}^2(\mathcal{V}^3)$.

This shifting in the nuclei positions preserves the mean of the size while cutting down its variance. The pictures in Figure 6.3 show how a 3-d VT transforms into its first- and then second order adjustment. If we plot the cell size distribution, we will come up with a picture similar to Figure 6.4. The appearance of the distribution where sizes are discretised into bins like this depends on the number of bins chosen.

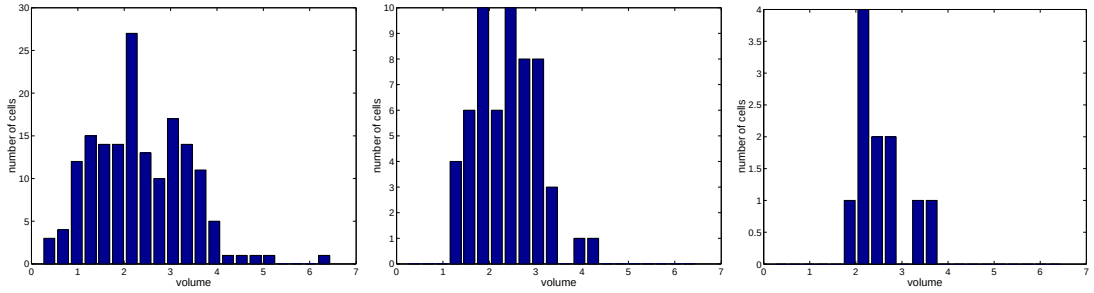


(a) (b) (c)

**Figure 6.4** *Change in size distribution as a result of a nuclei adjustment process,* (a) *the size distribution of a* $\mathcal{V}^3$, (b) $\mathcal{G}(\mathcal{V}^3)$ *and* (c) $\mathcal{G}^2(\mathcal{V}^3)$. *From a view point at 96° azimuth and 0° elevation.*

Figure 6.4 serves as a graphical presentation, but the statistics are the following. For our $\mathcal{V}^3$, $\mathcal{G}(\mathcal{V}^3)$ and $\mathcal{G}^2(\mathcal{V}^3)$ respectively the cell sizes are $0.9345 \pm 0.4025$, $0.9495 \pm 0.2652$ and $1.0315 \pm 0.2086$; the third central moment 0.0332, 0.0059 and 0.0061; the fourth central moment 0.0936, 0.0137 and 0.0036. These means are only meaningful when considered relatively with each other, since it depends on how one chooses the normalising basis. Here the basis chosen is the volume for the original Poisson point process, which is 1, divided by the original number of generators, which is 400. When we built this $\mathcal{V}^3$, 236 cells had been disposed of as they were thought to be those along the boundaries; when $\mathcal{G}(\mathcal{V}^3)$ a further 107 and finally when we built the $\mathcal{G}^2(\mathcal{V}^3)$ 46 more. This leaves us with 164, 57 and 11 cells remaining respectively in our $\mathcal{V}^3$, $\mathcal{G}(\mathcal{V}^3)$ and $\mathcal{G}^2(\mathcal{V}^3)$, all of which are shown in that order as Figure 6.4 (a), (b) and (c). Of course a great part of these are hidden behind others, so you can not possibly see them all there.

The sizes in Figure 6.4 are based on a volume magnification factor of 1,000, which is corresponds to the increase in size by a factor of three, but those in Figure 6.4 are based on a magnification 400, which corresponds to a factor of $(400)^{1/3}$ increase in the size.

As the new program has considerably changed from the old one, it is listed again in § A.23 which has evolved from that which is listed in § A.22 on page 266. Wherever the sign © appears in this monograph it means *copyleft* not copyright.

## § 6.4 Molecular dynamics

The Lennard-Jones function can be written $u(r) = -A/r^6 + B/r^{12}$, where $A$ and $B$ determine respectively the attractive and repulsive parts. Let the range parameter $\sigma = (B/A)^{1/6}$ and the energy parameter $\varepsilon = A^2/4B$, and the equation becomes $u(r) = 4\varepsilon\left[(\sigma/r)^{12} - (\sigma/r)^6\right]$. In other words, $\sigma$ is the diameter of one of the atoms and $\varepsilon$ is the well depth, *i.e.* energy constant. The force here is not $F = -\mathrm{d}u/\mathrm{d}t = (24\varepsilon/r^2)\left[2(\sigma/r)^{12} - (\sigma/r)^6\right]$, but $F = -\mathrm{d}u/\mathrm{d}r$.

Another approach in molecular dynamics simulation is to use numerical methods on the Newton's equation of motion. The most widely used is perhaps the Verlet algorithm, shown here as Algorithm 6.16. The initial values are $r_0$ and $r_1$.

**Algorithm 6.16** *Verlet algorithm, cf L. Verlet (1967)*

**for** $i = 1$ to $n$ **do**
  **find** $f_i$;
  $r_{i+1} \leftarrow 2r_i - r_{i-1} + f_i\Delta t^2/m + \mathrm{O}(\Delta t^4)$ **and**
  $v_i \leftarrow (r_{i+1} - r_{i-1})/(2\Delta t) + \mathrm{O}(\Delta t^2)$.
**endfor** □

There are variants and modifications of Algorithm 6.16, for example the Leapfrog Verlet algorithm which has three steps instead of two, that is $v_{n+1/2} = v_{n-1/2} + f_n/m\Delta t + O(\Delta t^3)$, $r_{n+1} = r_n + v_{n+1/2}\Delta t + O(\Delta t^4)$ and $v_n = (v_{n+1/2} + v_{n-1/2})/2 + O(\Delta t^2)$; or the velocity Verlet algorithm where $r_{n+1} = r_n + v_n\Delta t + f_n\Delta t^2/(2m) + O(\Delta t^3)$ and $v_{n+1} = v_n + \Delta t(f_{n+1} + f_n)/(2m) + O(\Delta t^3)$,

or in the form normally used in practice in which $v_{n+1/2} = v_n + f_n\Delta t/(2m)$, $r_{n+1} = r_n + v_{n+1/2}\Delta t$ and $v_{n+1} = v_n + f_{n+1}\Delta t/(2m)$.

The van der Waals force is an attractive force acting between molecules. In the case of gases, each molecule consumes some space, so the dynamic volume is less than overall volume by an amount $bn$ when $b$ is a constant and $n$ the number of molecules. Here $b$ is $N_A v$, where $v$ is the volume slightly larger than the volume of each molecule of gas and $N_A$ the Avogadro number, $N_A = 6.022 \times 10^{-23}$ mol$^{-1}$. The pressure of gas we see is the pressure of gas detected, which is less than the real pressure by $F/A$, where $F = \sum F_i$ and $F_i = \sum f_j$. Here $i$ runs from 1 to $n$ and $j$ from 1 to $(n-1)$ in the same set of molecules. The reduction of the total force comes from all molecules, but this reduction from each molecule is in turn affected by those molecules around it. Therefore $i \neq j$ and $j$ runs from 1 to $(n-1)$ as mentioned above. Suppose that each molecule attracts another molecule by a force $a$. Then, in a given volume $V$, $F = \sum F_i = \sum_i \sum_j f_{ij} = \sum_i (n-1)a/V = n(n-1)a^2/V^2$. For very large $n$ we can say that $(n-1) \approx n$, and therefore $(P + an^2/V^2)(V - bn) = nRT$.

The nature of this mutual attraction between molecules, which reduces the pressure in gas, comes to light in the case of solids. The distribution of charges around a neutral atom in solid fluctuates in the time scale $\tau < 10^{-16}$ s. This charge imbalance makes each atom behave as an electric dipole. This electric dipole has an electric field around it, which affects other atoms nearby and binds the two together.

The electric dipole moment is $p = qa$, where $a$ is a vector from the negative to the positive charge. The electric field around a charge $q_1$ has a magnitude $E = q/(4\pi\varepsilon_0 r^2)$. It acts on a nearby charge $q_2$ with a force of magnitude $F = u = q_2 E = q_1 q_2/(4\pi\varepsilon_0 r^2)$, where $u$ is the potential energy of the two charges. This force itself is the Coulomb force, and the electric potential around $q_1$ is $u/q_2$, that is $V = q_1/(4\pi\varepsilon_0 r)$.

For an electric dipole, $V = (1/(4\pi\varepsilon_0))(q/r_1 - q/r_2) = q(r_2 - r_1)/(4\pi\varepsilon_0 r_1 r_2)$. Since $a \ll r$, $a$ being of the order of the atomic size, $r_1 r_2 \approx r^2$. Let $\theta$ be the angle between $a$ and $r$. Then, also since $a \ll r$, we have $r_2 - r_1 \approx a\cos\theta$. Therefore we now have $V \approx qa\cos\theta/(4\pi\varepsilon_0 r^2) = p\cos\theta/4\pi\varepsilon_0 r^2$ and consequently $E_r = -\partial V/\partial r = 2p\cos\theta/(4\pi\varepsilon_0 r^3)$ and $E_\theta = -\partial V/(r\partial\theta) = p\sin\theta/(4\pi\varepsilon_0 r^3)$.

We neglect $E_\theta$ for long-range interaction, and simplify $E_r$ to $E_r = a/r^3$. We shall hereafter use the terms *dipole* and *atom* interchangeably. If this electric field is produced by atom $p_1$, it could induce in another atom $p_2 = \alpha E_r$, where $\alpha$ is the molecular polarisability of the second atom. This second atom will have an energy of interaction with the first one, $u = -p_2 E_r = -\alpha E_r^2 = -\alpha a^2/r^6$. This force is attractive.

The repulsive force is more complicated, and is generally thought to arise from the Pauli exclusion principle and the coulombic repulsion of the electrons in the outer orbit. It is generally assumed to be either $u \approx A/r^{12}$ or $u \approx a\exp(-r/\rho)$, where $\rho$ is a range parameter (*cf* de Podesta, 1996).

The Lennard-Jones potential is often written as $u = -4\varepsilon\left[(\sigma/r)^6 - (\sigma/r)^{12}\right]$, where $\sigma$ is a range parameter that indicates the approximate size of an atom and $\varepsilon$ an energy parameter that indicates the strength of the interaction between atoms. In other words, it is the minimum value of $u$.

The Lennard-Jones potential between two atoms has the minimum value $u = \varepsilon$ at $r = 1.1225\sigma$. Figure 6.5 is a plot $y = -4(1/x^6 - 1/x^{12})$, where $y = u/\varepsilon$ and $x = r/\sigma$. The force which the potential curve of Figure 6.5 acts on another particle is shown in Figure 6.6. The force produced by a dipole is calculated from $F = -\mathrm{d}u/\mathrm{d}r = 24(\varepsilon/\sigma)[(\sigma/r)^7 - 2(\sigma/r)^{13}]$. But in our units $y = u/\varepsilon$ and $x = r/\sigma$ above the equation becomes $y = 24(1/x^7 - 2/x^{13})$, which is plotted in Figure 6.6.

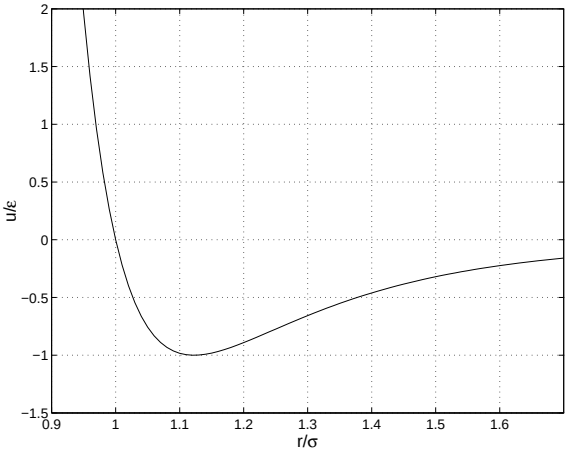


**Figure 6.5** Lennard-Jones potential.

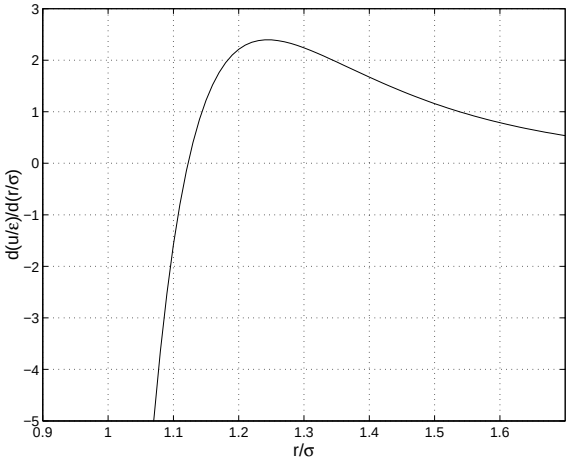


Figure 6.6 shows that the force is zero at the distance $x = 1.1225\sigma$ away from the particle. Closer than this point the repulsive force increases rapidly towards infinity. Further away from this point, however, the attractive force increases to a maximum and then gradually dies down. This maximum force occurs when $\mathrm{d}x/\mathrm{d}y = 0$, that is at $x = 1.2445\sigma$.

**Figure 6.6** Force corresponding to the Lennard-Jones potential.

In gases, the molecules travel past one another so fast that they hardly notice the wells of negative energy surrounding other molecules, let alone stop and rest there. But even here the attractive force produced by these wells is probably what give rise to the term $an^2/V^2$ in the van der Waals equation. Solid molecules, in contrast, hardly have kinetic energy and therefore prefer to sit in such wells of their neighbours, which is the reason why solids hold and neither flow as liquid does nor disperse like gas.

The most cohesive structures of solids are crystals, where the Lennard-Jones potential culminates in a minimum cohesive energy of the lattice. This cohesive energy is $U = N_A u_i/2$. Here $u_i$ is the summation over all pair potential energies of Lennard-Jones type, $u_i = \sum_{i \neq j}^{N_A} u(r_{ij})$. Let $r_{ij} = \alpha_{ij} r_0$, where $r_0$ is the nearest neighbour distance. Then $U = -2\varepsilon N_A [(\sigma/r_0)A_6 - (\sigma/r_0)A_{12}]$, with the lattice sums being $A_6 = \sum(1/\alpha_{ij}^6)$ and $A_{12} = \sum(1/\alpha_{ij}^{12})$. These lattice sums are calculated from the network structure in terms of infinite series that converge very quickly.

To find the optimum value of $\sigma/r_0$ we shall let $b = \sigma/r_0$ and write differentiate $\mathrm{d}U/\mathrm{d}b = -2\varepsilon N_A(6b^5 A_6 - 12b^{11}A_{12}) = 0$. As a result, $r_0 = \sigma(2A_{12}/A_6)^{1/6}$, the cohesive energy per mole $U = -(A_6^2/2A_{12})N_A\varepsilon$ and the cohesive energy per molecule $u = U/N_A = -(A_6^2/2A_{12})\varepsilon$.

## § 6.5 Problem definition and algorithms

Walls in a 3-d Voronoi tessellation are isomorphic to bonds that link between its cells. Therefore we can redefine the problem of a particle passing through the hole in a wall, into the cell chamber and out through a hole in another wall, and so on, as that of the passage of a mathematical particle through a tube that links between two cells, into a cell and out through one of the other tubes. In reality the solid parts which make up the partitions have thickness, therefore the holes through the walls will have a nonzero thickness and the volume of the cell chamber is smaller than that of the otherwise mathematical Voronoi cell.

Each vertex of a Voronoi polygon has three walls of the latter attached to it. The centre of gravity† of these three faces is calculated and linked together. This truncates the coigns and produces for each polygon its dual self. The next step is to link together the midpoints of all those edges of the polygon that have a vertex in common. The edges of this last polygon bound and define the void volume of the cell chamber.

Next, the cross section of the hole within each wall is taken to be the area on the original wall which is bound on all sides by the second order covering lattice of that wall.

The filtering membrane in this case is assumed to be isomorphic and homogeneous. The size of the particles is taken to be reasonably smaller than the void in general, so that the attraction between particles and the adsorption to the wall play a more prominent role than the physical blockages by individual particles. The particles are all assumed to be of the same size.

Algorithm 6.17 is an algorithm to do filtration that is being developed. Here $N$ contains the neighbourhood information

**Algorithm 6.17** *Filtration in Voronoi tessellation*

**find** $(v_a, c_a) \leftarrow$ Voronoi tessellation;

† aka centre of mass, centroid.

**find** $d_l \leftarrow$ Delaunay triangulation;
**find** $N_c \leftarrow$ cell neighbours;
$c \leftarrow c_a$ which lie completely within $[0,1]^3$;
$v \leftarrow v_a$ which belong to some $c$;

□

My work on filtering membranes results in another Voronoi algorithm and program which is different from the programs listed in §'s A.3 and A.4. Because it is also written anew from scratch, this new algorithm has nothing to do with the previous two as regarding the data structure and the logic of its method. It is given in § A.21.

The current convention for variables is this. A single alphabet or entity means a list, for example `c` is the cell list and `va` is the list of all vertices original created. Another example is $b$, a structure for bonds which contains the list of the cells of bonds, the number of vertices of the face represented by each bond, the list and the map of these vertices, the ordered list of the vertices of each face and another list similar to this but cyclic, and the number of cells connected to each bond. Similar to the structure of `b` is that of `bdr`, or $b_d$ in Algorithm 6.18, which is a list of the bonds along the border, each of which is connected to only one cell.

Two entities $xy$ makes $x$ of $y$, for instance `vc` is vertices of cells, which is a structure that contains the number of vertices of each cell and the list and the map of all these vertices. I try to preserve the space by creating a short but easy to understand naming convention. Also, the lines are put together, which means that the number of lines of the codes is more than what appears here, some of the lines having six logical lines or more to them. But the structure of the program still remains intact, therefore it should be possible without much difficulty to compare the program in § A.21 with Algorithm 6.18 which explains it.

Three entities $xy^2$ or $y_x^2$ are $y \times y$ matrix of $x$, where the latter relates two entities of the former, for example `bcc` is the bonds mapped on to a cell matrix. In the algorithm, $v_n$ and $c_n$ are respectively the `vin` and `cin` in the program, the `vn` and `cn` there being verbosely described in the algorithm as the *number of* $v$ and $c$.

**Algorithm 6.18** *Voronoi data structure for the study of membrane filters.*

$(v_a, v_c^a) \leftarrow$ **find** a 3-d Voronoi tessellation;
$v_n \leftarrow$ index of $0 < v_a < 1$;
$c_n \leftarrow$ index of $c$ all the $v$'s of which are in $v_n$;
$v \leftarrow v_a \in v_n$;
$v_c \leftarrow v_c^a \in c_n$;
$t_a \leftarrow$ **find** a 3-d Delaunay tessellation;
**for** all $t_i \in t_a$ which are connected to two cells **do**
  $t \leftarrow t_i$;
**else**
  $b_d \leftarrow t_i$;
**end**
$b \leftarrow c_b^2 \leftarrow t$;
$b \leftarrow b_d$;
**find** Delaunay triangulation in $(3-1)$ dimensions for all faces;
**order** the vertices of each face;

□

## § 6.6 Simplified algorithm for filtration

The first algorithm we shall now develop is a reasonably simplified one. But it turns out to my surprise that this simple algorithm links us to the continuum percolation of hard spheres or even of particles with irregular shapes. This is because of the assumptions that we shall make.

One such assumption is that the variance of the filter cell size distribution is small. For this, Jafferali (1995) would probably have applied his favourite constraint code on a Voronoi tessellation. The approach which I developed uses the operator $\mathcal{G}(\cdot)$ on a $\mathcal{V}$ (*cf* § A.23). It is more logical and therefore is what we shall use for now.

The second assumption is that the particle size is reasonably smaller than the size of the smallest void of the original system. This is the assumption which seems to link us to the percolation of spheres in continuum, the space considered being that of each void.

Also, we assume that the particles are attracted towards one another and towards the walls by various interactions which may include the van der Waals force and the force from electrostatic interactions.

Let $\theta$ be the angle that the line from the c.g. of a each cell to the mid point of a face makes with the horizontal plane. Then another possible assumption is that all particles prefer a trajectory which goes through a face which has the maximum $\theta$.

The third assumption is that the volume of each membrane pore is 80 per cent the volume of the corresponding Voronoi pore. The fourth assumption, blockages due to the clustering caused by the attrition forces between particles can occur within pores. This excludes cake formation and blockage at entrances to, or exits from the pore.

The last assumption above is similar to assuming that clustering due to attrition can occur in stagnation regions. Since the flow of the suspension reaching the membrane is strong, *i.e.* the pressure high, there can be no clustering there. The flow from one pore into another is also faster than the flow within one. This is amount to assuming that the effective diameter of the hole within each face of a pore is considerably smaller than its diameter.

Upon reaching the membrane, each particle in the troop seeks out the bond closest to it, and begins its journey through the membrane. Within the membrane, it always follow the bond which has the greatest gradient available. Therefore the top bonds should map to the bottom ones one to one. But because the possible blockages during the course of operation, this may not be so and the mapping is instead one to many.

First we consider the case in two dimension, so volumes becomes areas and the volumetric flow rate the distance travelled. In our discrete time, if $v$ is the flow velocity, $n$ the number of particles, $\rho_v$ the total volume ratio of the particles and $r$ their radius, then we have $n\pi r^2 = v\Delta t$. Assuming that $v = 1$ ms$^{-1}$ and $r = 100$ $\mu$m, then $n = 10^3\rho_v/\pi$ or approximately $318\rho_v$ particles for each time step.

Next we will study the suspension in a square box in order to find out $\rho_v$. Because we shall assume that the particles flowing through the pores percolate as though there is no flow, we will consider here the suspension that is simply contained within our box without moving about. I feel that the assumption that particles could percolate that way in pores is justified since the flow is in steady state, protected from the turbulence outside by all the solid structures making up the walls of the membrane.

The percolation program first generates random positions of the particles, then moves apart those which are too close together so that in the end they only touch each other. Particles which are separated by a distance less than $1.4r$ move towards each other until they touch. Lastly, touching particles never separate.

We know that the total volume ratio of the particles has the upper limit of 0.9069, because that is the density of the closest packing of circles on a plane.

Packing circles on the plane becomes densest when the circles are arranged as a hexagonal lattice with the packing density of $\pi/2\sqrt{3}$. Packing of spheres is similarly at its highest density if the arrangement is that of the face-centred cubic lattice with the packing density $\pi/3\sqrt{2}$.

## § 6.7 Filtering problem when physical blockage is prominent

Assuming particles to be spherical, the size of particles to be constant, and that this size is compatible with the size of the holes in the walls and the voids so that physical blocking is responsible for most of the blockages in the membrane. As in § 6.7, the hole in each wall is taken to be the polygon which results from recursively finding a covering polygon for the face twice.

Redefine the problem of particles' passage through walls and voids as that of particles travelling along edges of the dual lattice of the Voronoi structure, *i.e.* the Delaunay triangulation. Each of these edges corresponds to a face in the original physical lattice. To each edge is thus ascribed the details of the cross section of the hole through that face, namely the shape and the dimension, as well as the gradient it makes with the horizontal plane. Upon reaching a vertex, the particle ball will choose the next path, *i.e.* bond in the dual lattice, which has the maximum gradient to pass through. However, if this bond is too small or if it is blocked, the particle with choose from among the remaining paths the one which has the maximum gradient, and so forth. If the size of the particle is approximately that of the hole it tries to pass through, within two per cent of the latter, say, then the particle will blind the passage at that point. The difference between blinding and blocking is in the degree of tightness that the particle sits in the hole, which reflects in the degree of difficulty to

remove it by backflushing. This degree is not constant but a function of the relative size between the two parties involved, *i.e.* the particle and the hole.

## § 6.8 Percolative filtering with very small particles

At this point a new filtering algorithm is considered and investigated. We introduce an assumption that the particles are all of the same size which is very small compared with the size of the pores. So there is neither cake formation nor blinding by a single particle. Assume that the solid particles suspended in a fluid medium, being dragged downwards under their own weight.

Assume that the van der Waals force plays a significant part and, similarly to § 6.8 on page 179, that these interactions between particles are governed by the Lennard-Jones equation. Assuming that each particle is spherical and acts as a dipole with the electric dipole $p = 10e$, where $e$ is the electric charge on a proton, $e = 1.602 \times 10^{-19}$ C. Then (*cf* de Podesta, 1996)

$$E_r = \frac{p}{4\pi\varepsilon_0 r^3}, \tag{26}_{\text{vi}}$$

and the energy of interaction between two particles becomes

$$u = -\alpha E_r^2 = \frac{\alpha p^2}{(4\pi)^2\varepsilon_0^2 r^6}, \tag{27}_{\text{vi}}$$

where $\alpha$ is the molecular polarisability of one particle under the influence of the other. If we assume that the repulsive force acts in such a way that the repulsive energy is $u = c/r^{12}$, where $c$ is a constant, the Lennard-Jones potential becomes Equation 6.28.

$$u = -\frac{\alpha p^2}{(4\pi)^2\varepsilon_0^2 r^6} + \frac{c}{r^{12}}. \tag{28}_{\text{vi}}$$

Comparing Equation 6.28 to the form

$$u_r = -\frac{A}{r^6} + \frac{B}{r^{12}}, \tag{29}_{\text{vi}}$$

we have $A = \alpha p^2/((4\pi)^2\varepsilon_0^2)$ and $B = c$. Or if we compare it to the form

$$u_r = -4\varepsilon\left[(\frac{\sigma}{r})^6 - (\frac{\sigma}{r})^{12}\right], \tag{30}_{\text{vi}}$$

then we have $\sigma = (B/A)^{1/6} = (16c\pi^2\varepsilon_0^2/(\alpha p^2))^{1/6}$ and $\varepsilon = (A^2/4B) = \alpha^2 p^4/(4c(4\pi)^4\varepsilon_0^4)$. Notice that here $\sigma$ and $\varepsilon$ are simply parameters, not the Stephan-Boltmann constant and the dielectric constant, $\sigma$ is a range parameter and approximates the size of an atom while $\varepsilon$ is an energy parameter which shows the strength of the interaction between particles. At $r = \sigma$ the value of $u_r$ is zero, whereas $u_r$ has the minimum value of $-\varepsilon$.

The force between two particles is Equation 6.31.

$$F = -\frac{\mathrm{d}u}{\mathrm{d}r} = -\frac{6\alpha p^2}{(4\pi)^2\varepsilon_0^2 r^7} + \frac{12c}{r^{13}}. \tag{31}_{\text{vi}}$$

At the equilibrium separation, $r_0$, $F = 0$ and therefore Equation 6.31 yields the minimum distance in Equation 6.32,

$$r_0 = \left(\frac{32c\pi^2\varepsilon_0^2}{\alpha p^2}\right)^{\frac{1}{6}}. \tag{32}_{\text{vi}}$$

The equation for the minimum energy is obtained by substituting $r_0$ from Equation 6.32 into Equation 6.28, which gives

$$u = -\frac{\alpha p^2}{(4\pi)^2\varepsilon_0^2 r^6} + \frac{c}{r^{12}} \tag{33}_{\text{vi}}$$

$$= \frac{1}{r_0^6}\left(-\frac{\alpha p^2}{(4\pi)^2\varepsilon_0^2} + \frac{c}{r_0^6}\right) \tag{34}_{\text{vi}}$$

$$= \frac{1}{r_0^6}\left(-\frac{\alpha p^2}{(4\pi)^2\varepsilon_0^2} + \frac{c\alpha p^2}{32c\pi^2\varepsilon_0^2}\right) \tag{35}_{\text{vi}}$$

$$= -\frac{\alpha p^2}{32\pi^2\varepsilon_0^2 r_0^6}. \tag{36}_{\text{vi}}$$

Returning to Equation 6.31, the attractive force has the maximum value at the point where $\mathrm{d}F/\mathrm{d}r = 0$. Differentiating $F$ in Equation 6.31 with respect to $r$, we arrive at Equation 6.37.

$$\frac{\mathrm{d}F}{\mathrm{d}r} = \frac{42\alpha p^2}{(4\pi)^2\varepsilon_0^2 r^8} - \frac{156c}{r^{14}} \qquad (\mathbf{37})_{\mathrm{vi}}$$

From this the distance where this maximum force occurs is given by Equation 6.38,

$$r_m^6 = \frac{156c(4\pi)^2\varepsilon_0^2}{42\alpha p^2} = \frac{416c\pi^2\varepsilon_0^2}{7\alpha p^2}. \qquad (\mathbf{38})_{\mathrm{vi}}$$

Then by putting Equation 6.38 into Equation 6.31 we have this maximum force in Equation 6.42.

$$F_m = -\frac{6\alpha p^2}{(4\pi)^2\varepsilon_0^2 r^7} + \frac{12c}{r^{13}} \qquad (\mathbf{39})_{\mathrm{vi}}$$

$$= \frac{1}{r^7}\left(\frac{-6\alpha p^2}{(4\pi)^2\varepsilon_0^2} + \frac{12c(42)\alpha p^2}{156c(4\pi)^2\varepsilon_0^2}\right) \qquad (\mathbf{40})_{\mathrm{vi}}$$

$$= -\frac{9\alpha p^2}{52 r^7\pi^2\varepsilon_0^2}. \qquad (\mathbf{41})_{\mathrm{vi}}$$

$(\mathbf{42})_{\mathrm{vi}}$

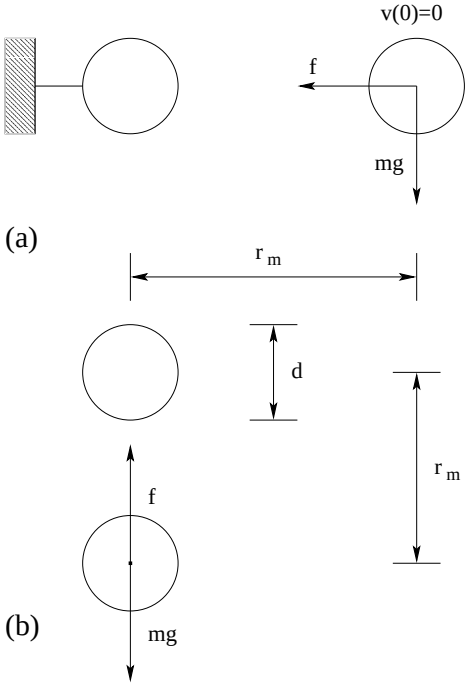


Let each of the spherical particles has a radius $r = 1$ $\mu$m and the density $\rho = 3{,}000$ kg $\cdot$ m$^{-3}$ (compare the density of silicon, which is 2,329 kg $\cdot$ m$^{-3}$). Then the mass of the particle is $m = \rho V = 3000 \times (4/3)\pi \times (10^{-6})^3 = 1.26 \times 10^{-14}$ kg and the weight is $mg = 1.26 \times 10^{-14} \times 9.8 = 1.23 \times 10^{-13}$ N. We may now find the attractive distance, the maximum distance whereby two particles will come together under the van der Waals force. Figure 6.7 shows the capturing of one particle by another when one particle is fixed in space and another particle has zero velocity but is free to move. Recall that the capture occurs when the accelaration due to the weight of the particle $g$ equals the acceleration $a$ due to $f$.

**Figure 6.7** Force balance with one particle fixed.

If we suppose that our particle have the same polarisability as that of a benzene in its gaseous state, $C_6H_6$, *i.e.* $\alpha = 11.61 \times 10^{-40}$, then in this case $\alpha = 11.61 \times 10^{-40}$ F$^{-1}$m$^4$ (*cf* de Podesta, 1996) and Equation 6.42 gives us the separating distance between the two particles which gives the maximum attractive van der Waals force, which is 444 $\mu$m. Giving our particle other values of $\alpha$, with the value of $\alpha$ for methanol gas $CH_3OH$, *i.e.* $\alpha = 3.860 \times 10^{-40}$ F$^{-1}$m$^4$, we have this distance $r = 379$ $\mu$m, and with $\alpha = 1.647 \times 10^{-40}$ F$^{-1}$m$^4$, that of water vapour, the distance becomes $r = 336$ $\mu$m.

These values are rather large compared with the radius of the particles, therefore we shall opt instead to a bigger size of particles, when $r = 5$ $\mu$m. With the radius of five microns, the particle has a mass of $1.571 \times 10^{-12}$ kg and its weight becomes $1.64 \times 10^{-11}$ N. Then if we adopt the value of $\alpha$ for water vapour, $\alpha = 1.647 \times 10^{-40}$ F$^{-1}$m$^4$, then from Equation 6.42 the distance where the force is maximum becomes $r = 167$ $\mu$m.

But this is not everything. So far we have only considered what two particles will do when one of them is fixed and the other one has no initial velocity. There are two other things that can

happen, the particles may both be moving down beside each other under gravity and the path of the particle which is effected by their mutual attraction. Even when two particles do not come together, their path can be deviated by the van der Waals force. But here for simplicity we shall neglect this and assume that particles either come and stay together or they experience no mutual force whatever. Only if they come together will their final path and velocity be affected, and these depend on their combined momentum.

When particles move relative to each other, their captive velocity depends on their relative velocity. They tend to join each other more easily if their paths are along side each other and goes in the same direction. In the extreme case where both particles move in the same direction with zero relative velocity, they would come together across a vast gap in between indeed, had there been no frictional force due to viscosity that acts to drag them.

In the present study, the friction due to the fluid in the medium is neglected, together with the relative velocity between the particles, for the purpose of deciding whether particles will come together. It is expected that on average particles coming to within the capturing radius of each other will come together. This radius is larger than the radius of maximum force in Equation 6.42 above. In other words, we expect our particles to behave like solid spheres with a well defined boundary for their sphere of influence and a much simplified capturing mechanism.

We shall define this radius of captivity, $r_c$, to be one third that of the radius of maximum force $r_m$. From Figure 6.5 this is the point where $r_c = 1.5\sigma$, and because $r_m$ is here 1.2445 we have $r_c/r_m \approx 1.2$. For Figure 6.5, this is the same as saying that $r_c/r_0 = 1.34$.

One additional point is that, in real situation when particles form a cluster their collective value of the molecular polarisability will change, and this value will not be the same for the cluster as it is for the individual particles. But here we assume that they are the same, which means that the capturing radius of a cluster will be the same as that of the particles which form it.

It may worth mentioning here that the molecular polarisability is related to an optical property, *viz.* the refractive index $n_r$, by the relationship $\alpha = \varepsilon_0(n_r^2 - 1)/n$, where $n$ is the number density of molecules. For gases $n = P/(k_B T)$, whereas for liquids $n = N_A \rho/m$, $m$ being the mass.

Next we shall concern ourselves with clusters of particles thus formed. All clusters will be assumed to be a closest-conglomerate of particles which form them, with the densest packing density possible in three dimensions, that is $\pi/3\sqrt{2}$ of the face-centred cubic lattice. Numerically this is 0.7405.

Notice that the packing density in two dimensions can be higher than this. Packing circles on a plane is the densest of all with its packing density of $\pi/2\sqrt{3}$.

Shown in Figure 6.8 are the hexagonal lattice packing in two dimensions and the cubic close pack. In the cubic close packing spheres in every third layer lie vertically straight on top of one another. Each face of its cubic section looks like the second picture in Figure 6.8. Similar to the cubic close packing is the hexagonal close packing spheres in every alternate layer of which lie over one another. Both the cubic- and the hexagonal close packing have the same packing density which, in the case of the former, is calculated, from the second picture, as $\rho = \sum v_s / \sum v_c$, where $v_s$ are the total volume of sphere segments in the unit cell which has the volume $v_c$. Here $v_c = (2\sqrt{2}r)^3$ and $\sum v_s = (8(1/8) + 6(1/2))4\pi r^3/3$. In 2 dimensions, the densest packing is calculated from the first picture.

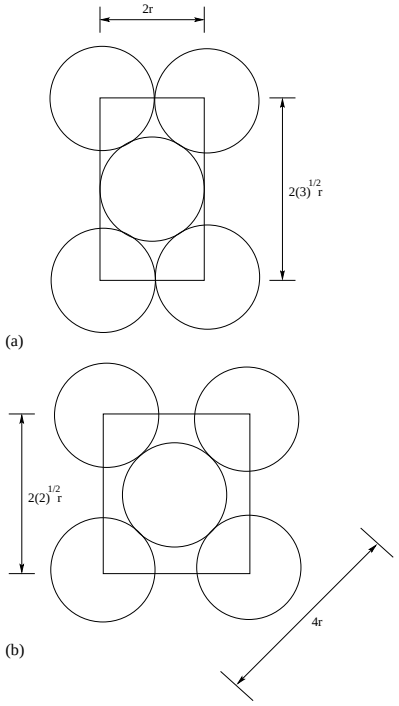


**Figure 6.8** The packing density calculation of the closest-packed densities.

The density of the packing is $\sum a_c/a_r$, where $a_c$ are the areas of the circles and $a_r$ is the area of a rectangle. These two areas are namely $a_c = 2(\pi r^2)$ and $a_r = 2r(2\sqrt{3}r)$, which give the density $\rho = \pi/2\sqrt{3}$.

If the particle size is very small there will be an effect from quantum mechanics. The de Broglie wavelength, $\lambda = h/p$, exists for all particles large and small. Here $p = mv$, $m = \rho V$ and $V = \pi d^3/6$ for a spherical particle. Figure 6.9 shows a graph between diameter and wavelength of particles.

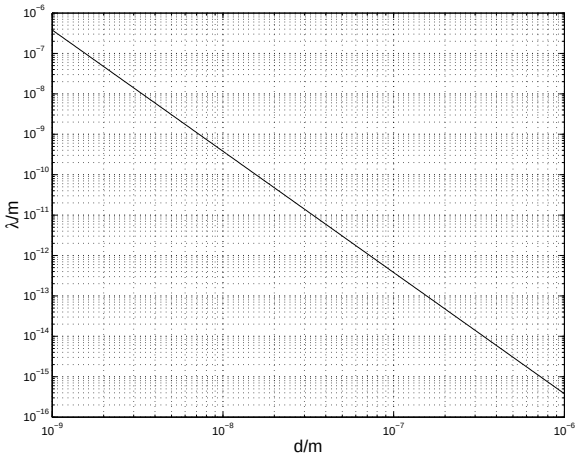


We can see that the quantum-mechanical effect when the pore size is in the order of micrometre will become prominent if the size of particles challenging it is in the order of nanometre. When this is the case there will be not only the interference effect of the particle-wave passing through slids but also the effect of confined particles which produces standing waves of these wave-particles in each pore. These standing waves of the particle-wave have $\lambda_n = 2D/n$.

**Figure 6.9** Quantum-mechanical effect in filtration.

## § 6.9 Percolation within percolation

Particles suspended in a fluid generally have their diameter $d_p$ much smaller than the pore diameter $d_v$ of a filtering membrane. Yet these small particles can cause blockages of the membranes due to attrition among themselves. Since in this case $d_p \ll d_v$, blockages due to blocking or blinding of the individual particles (*cf* Jackson, 1994; Jafferali, 1995) become out of question.

Having investigated both the percolations of networks and continuum, I suggest that the blockage of these smaller particles in membranes is due to a double percolation phenomena, one the percolation of the suspension continuum, the other the percolation of the centroidal Voronoi network. As a reminder of a centroidal Voronoi network, it is a Voronoi tessellation on generator points which are the centroids of a Voronoi network which either is generated from Poisson point generators or is another centroidal Voronoi network.

Because percolation is a study of the behaviour of two phases, and because in general $p_c \neq 1/2$, there are no less than three regions of behaviours to consider in each percolational investigation instead of two (*cf* Tiyapan, 1997, KNT5(ix); also in Tiyapan, 2003, KNT8(iii)). When $p_c < 0.5$, these three regions are $p < p_c$, $p_c \leq p \leq (1 - p_c)$ and $p > (1 - p_c)$. When $p_c > 0.5$, they are $p < (1 - p_c)$, $(1 - p_c) \leq p \leq p_c$ and $p > p_c$. The case where $p_c = 0.5$ is assumed to be very rare in nature, and so can be neglected in the present study.

When a suspension becomes so high that the average interparticle distance has become such that the attrition due to van der Waals force is prominent, the suspension will solidify into a moisted bed of particles. According to the percolation theory, we may define the point where this spontaneous solidification occurs to be that point where there is a single cluster, under a mutual van der Waals force, which traverses the whole continuum in a certain well-conditioned direction, that is to say, a direction which may represent the diameter of the network. Furthermore, let us call a critical concentration $\rho_c$ the minimum concentration at which this infinite cluster appears.

Then we have for our suspension a continuum percolation with three regions of behaviour similar to those we have found in the case of network percolation. Furthermore we map the space of $\rho_c$ on to that of $0 \leq p_c \leq 1$, where $p_c = 0$ means there are no particles suspended in the fluid, in other word $\rho = 0$, and $p_c = 1$ is where the suspended particles form a bed in the closest packed structure, that is $\rho = \rho_{\max}$. We also assume, without the loss of generality, that $p_c > 0.5$. Then we have the following as the three regions, $p < (1 - p_c)$, $(1 - p_c) \leq p \leq p_c$ and $p > p_c$.

We are interested in neither the cases $p < (1 - p_c)$ nor $p > p_c$, since the former implies too dilute a concentration for the attrition due to the van der Waals force to cause an infinite cluster,

while the latter means that the suspension is so concentrated that they solidify instantaneously, simultaneously in all pores.

When $(1 - p_c) \leq p \leq p_c$, all pores has an equal probability of being solidified, and so the per cent total solidified cells now depends on the topology of the network, in this case Voronoi, and the probability where the critical phase change occurs becomes the critical probability of the network.

In the case of dead-end filtration the flow is in one direction, therefore the critical flux reduction which is the result of percolation of the network occurs at the point where the cross section of the network, not the network itself, percolates. This is because such percolation in the cross section in the plane perpendicular to the flow direction will cause a bottle neck in the flow and therefore determines the flux. This phenomenon is summarised in Figure 6.10.

Next we must define the critical probability of the overall system. Since the system involves two kinds of probability, that is continuum and network, and assuming $p_{c_0}$ and $p_{c_2}$ are two independent probabilities, then we have the overall probability is

$$p_c = p_0 p_{c_2}, \qquad (\mathbf{43})_{\text{vi}}$$

where $(1 - p_{c_0}) \leq p_0 \leq p_{c_0}$.

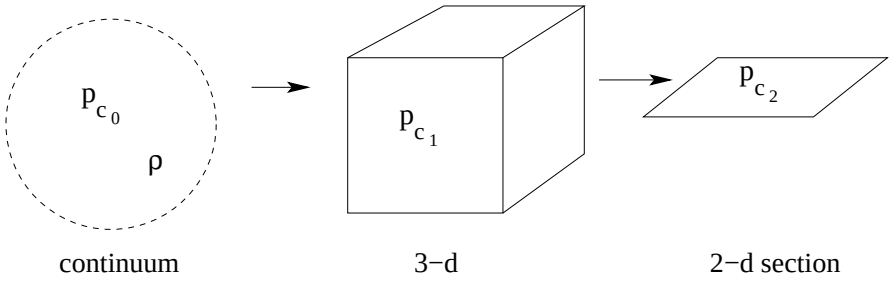


**Figure 6.10** *Percolation within percolation;* $0 \leq \rho_0 \leq \rho_{\max}$, $0 \leq p_0 \leq 1$, $p_c = p_{c_2} \cdot p_0$.

If our membrane is homogeneous, the reduction in the area perpendicular to the flow becomes $\Delta A = A_v p_{c_2}$, where $V_v/V_t = A_v/A_t$, $V_v$ and $V_t$ are respectively the void volume and the total volume of the membrane, and similarly for the areas $A_v$ and $A_t$.

## § 6.10 The first part, suspended particles

Because of the complex nature of the problem, there is no single algorithm but rather there is an algorithm for each job. The first task is to study the percolation of the spherical particles under the van der Waals force.

Continuing from the development in § 6.10, particles are spherical in shape with $r_p = 5$ $\mu$m and the capturing radius is $r_c = 167 \times 1.2 \approx 200$ $\mu$m. First we shall study particles within a cubic box of side length 2 mm. Particles start as a suspension with no obvious velocity. They stick together and to the walls.

When particles come together, they form a porous globule, having the densest packing density of the hexagonal or cubic close packing. When this happens, we discard the individual particles and consider instead the globular cluster which they formed. The cluster is porous, so its new radius is $r = (\pi/3\sqrt{2})(3\sum v_i/4\pi)^{1/3} = (\pi/3\sqrt{2})(3nv/4\pi)^{1/3} = \pi^{2/3}(nv)^{1/3}/(3^{2/3}2^{7/6})$.

But we do not know the rules by which these particles stick themselves together, whether they form a closest-packed globule or some other shapes. It is quite certain that whatever shape they are after, they may not retain it for long because there is a limited space within each pore that will put constraints on the way they grow. We shall call the growth of clusters into globules mentioned above *globular formation.*

Other clustering mechanisms possibly include what we shall call the *tetrahedra formation.* By this I mean that each one of our spherical particles attaches itself to three other particles, forming a tetrahedron whose side lengths are two times their radius. The next free particle may fit into any of the available attachment sites, *i.e.* the free triangular faces of an existing cluster. We may suppose that it always choose the closest one among such sites if this is available; if not, then the next closest one and so on.

These are only two among all the possibilities, namely the globular and tetrahedra formations. There could well be others, as well as a mixture of them. On the other hand, each material of which the particles are made may decide the particular cluster shape it prefers. Detailed analyses in thermodynamics and quantum mechanics are needed if we were to understand this cluster formation in continua under spatial constraints. Neither of these is within the scope and time constraint of the present work, though both of them merit a detailed investigation which I plan to carry out in the future.

Another problem arises when we come to consider percolation of our membrane. We may, for instance, say that it percolates when its structure in three dimensions percolates, or we may say that it percolates if there exists a cross section perpendicular to the flow which percolates in two dimensions. Since percolation of a cross section implies percolation of the structure but not vice versa, these two definitions of percolation due to suspension in membranes are not the same.

Choosing the percolation of sections as a criterion implies that we consider the superficial velocity of the flow whereas choosing the percolation in three dimensions as the criterion means that we focus on its interstitial velocity instead.

The algorithms for the study of percolation by tiny particles due to attrition in membranes which proposed here are Algorithm's 6.19 and 6.20. Algorithm 6.19 prepares the structure while 6.20 does the percolation simulation. Here both VT and $\mathcal{V}$ means the Voronoi tessellation. The appeal factor is the probability that a particle will choose to leave a cell via a certain bond. It is weight by the gradient of each bond, and is calculated over all bonds going in the downward direction from the cell. Transfer grids are square grids which help map the continuous plane at the top layer to bonds connected to it, that is to say, it maps a continuous Euclidean plane into discrete grids and from there on to bonds. In other words, $E^2 \rightarrow D^2 \rightarrow \{b\}$.

**Algorithm 6.19** *Percolation by tiny particles due to attrition in membranes.*

**generate** a Voronoi tessellation in three dimensions;
**transform** the VT into a centroid VT;
**find** the cross section of its top layer;
$C \leftarrow C^2(\mathcal{V})$;
**find** transfer grids of $C$;
**for** every cell in VT **do**
  **find** the maximum chamber capacity of its cell;
  **find** appeal factors for all its bonds;
**endfor** □

Let the gradient of each bond be represented by an angle $\alpha$ that it makes with the horizontal plane. Then the gradient can be calculated from the coordinates of the two end points of each bond, providing that $z_2 > z_1$, from $\alpha = \tan^{-1}(z_{12}/((\Delta x)^2 + (\Delta y)^2)^{1/2})$, where the slope is downwards from $p_2$ to $p_1$, and as usual $z_{12} = z_2 - z_1$. Algorithm 6.20 describes the membrane percolation simulation proposed.

**Algorithm 6.20** *Percolation by tiny particles due to attrition in membranes, percolation simulation.*

**for** each time step **do**
  **for** all arriving particles **do**
    **find** their random arrival position;
    **round** these positions to the precision of the grids;
    **map** positions on to bond numbers, using the grids;
  **endfor**

```
    for all particles do
      update distance travelled;
      update chamber crowding;
      find percolation of blocked chambers;
      if chambers percolate then
        terminate the simulation;
      endif
    endfor
  endfor
```

□

Here we concentrate on the interstitial flow velocity, therefore the percolation is supposed to occur when the chambers percolate in three dimensions. Coincidentally, this also makes the calculation easier. If we were to choose the percolation of sections as the deciding factor for percolation of the membrane, for instance, we would have needed to consider approximately $2n$ sections in total, where $n$ is the number of chambers. With an equal probability for success for all the homogeneous sections, this would still leave us on average $n$ sections to consider before we know that a sample percolates, if it does, though we would still need to test all the $2n$ sections in cases where it does not. This number $2n$ arises from the fact that to completely cover all combinations of grouping cells into sections we need to consider for each cell two sections for each existing cell, one touching its top while the other touches its bottom.

Sphere packing is a rich field of its own, within which the packing density is generally referred to as $\eta$, an efficiency, instead of the usual density symbol $\rho$. The rigid packings of spheres vary in density from the lowest in loose packing where $\eta \approx 0.06$ to the highest, which is shared by the cubic and the hexagonal closest packings, $\eta \approx 0.74$. A rigid packing is a packing in which all spheres touch at least four others, and the points by which each sphere touches its neighbours can neither be all in the same hemisphere nor all on an equator, *i.e.* a greatest circular section. So we can now limit the value of $\rho$ that we shall use to be in accord with $0.06 < \eta < 0.74$. In this early stage we shall not use a Monte Carlo study to find the probable $\rho$, *i.e.* $\eta$, but will approximate it to be some value within the range mentioned. Since the most familiar sphere packing in human history must be that by which oranges are stacked at markets, especially open markets like the one at Bolton, which gives the efficiency of packing $\eta \approx 0.74$, we shall assume that this is the way the clusters arrange themselves.

Notice also that piling oranges in a neat tetrahedral shape on a table and a packing them into a rectangular box both produce the same crystal structure, that is the face-centred lattice, the difference being only in their habits.

For all intents and purposes the percolation probability of spheres under the influence of the van der Waals force must be the same as $p_c$ of a face-centred lattice. This is because the biggest cluster of both cases will have the same structure and their orientation will determine the orientation of the structure. We can do away with the orientation of other minor clusters precisely because they are much smaller, which justifies our grossing over their individual shapes and only concern ourselves about their statistics, that is to say, their number. I think that stacking oranges into a box is cubic close packing while a pile of oranges is hexagonal close packing, but this needs to be checked.

To find $p_c$ of the close-packed cluster of spheres, one needs a program similar to the one mentioned in § 6.10, but which would do the job for three dimensions instead of two. For this purpose, the program for 2-d tilings mentioned in § 6.10 has been developed further to deal with regular lattices in three dimensions. At first I thought that there should be some other way to do this instead of having to develop another program for a general lattice in three dimensions, since this is already the last week of the project and time is running out. But in the end I found it better to spend some time to systematically develop a program for general cases than to opt for some adhoc approaches. As a result, a program that creates regular lattices in three dimensions for the purpose of percolation study has been written and is listed in § A.30.

As the 2-d program in § A.6 does for all 2-d regular lattices, this new program can deal with all possible lattices in three dimensions. The difficulty is, however, in the meticulous nature of identifying all the vertices and links in each unit cell. In this respect, the cubic close packing is much simpler to do than the hexagonal close packing. Therefore we shall only do the first one while leaving out the second, which ideally could be used for the purpose of comparison.

Figure 6.11 shows the lattice generated by the program and one which is used for finding the percolation threshold.

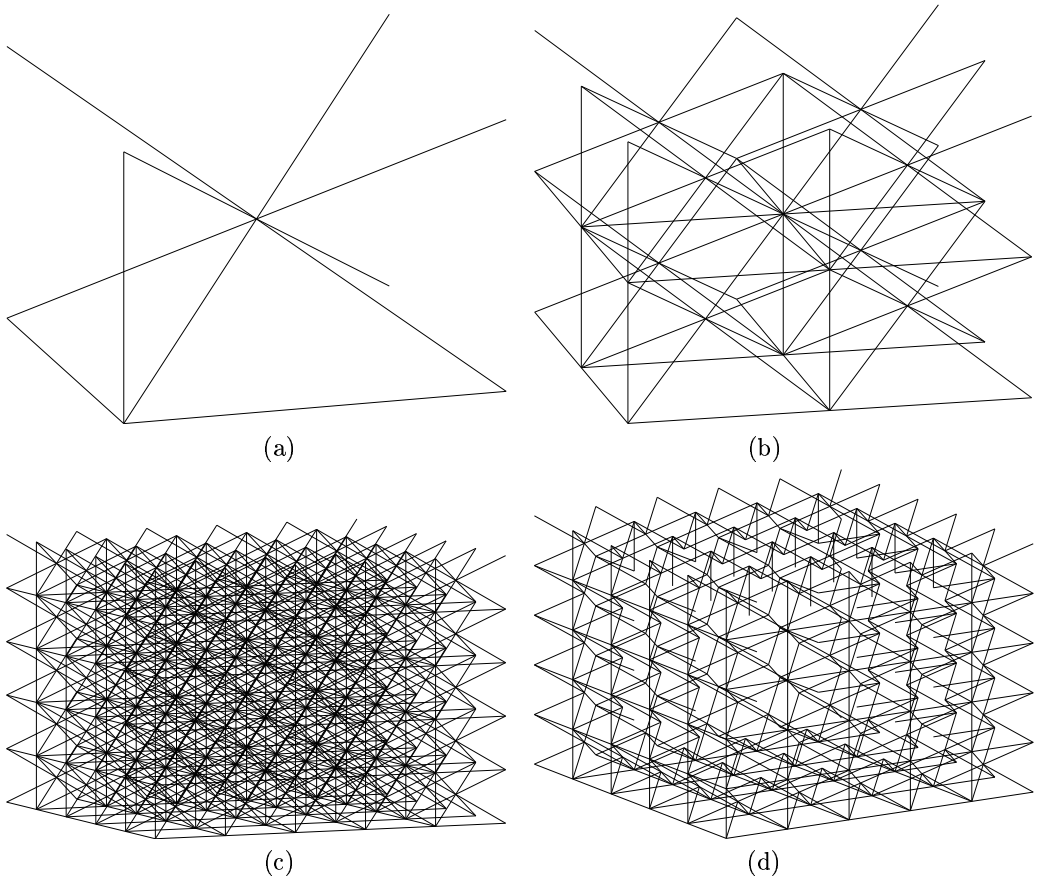


**Figure 6.11** *Percolation of the cubic close-packed lattice;* (a) *a unit cell,* (b) *eight unit cells, one from each of the eight groups,* (c) *network of size* $5 \times 5 \times 5$ *unit cells, which is used in a simulation, and* (d) *the same network with only boundary edges drawn to make it easier to look at.*

At present the program only finds $p_v$, $p_e$, $x_v$ and $x_e$, not $p_c$, $p_b$, $x_c$ and $x_b$. There may be altogether three types of cell and bond pairs, in comparison with two in the 2-d case, depending on whether the number of shared vertices required be 3, 2, or 1. For our purpose in the study of filtration, we only need to know $p_v$, which, when generated from a $5 \times 5 \times 5$ network as shown in Figure 6.11 (c), turns out to be 0.25. All the results from simulations are $p_v = 0.2501 \pm 0.0400$, $x_v = 8.0645$, $p_e = 0.1320 \pm 0.0209$, $x_e = 17.1709$, while $n_v = 341$ and $n_e = 1{,}375$.

This means that when the space will be blocked, *i.e.* percolates, when it is filled up to one quarter of its volume by suspended particles in the form of clusters of the highest packing density. Because the cubic close-packed spheres fill 0.74 of the space, this ratio translates into the real volume ratio of $0.74 \times 0.25 = 0.185$, that is 18.5 per cent by volume. If the fluid in our system is water, then $\rho = 1{,}000$ kg $\cdot$ m$^{-3}$ and the percentage by volume above is equivalent to a density of of the suspended particles of 555 kg $\cdot$ m$^{-3}$. Notice also in our simulation that the cluster shapes need not be convex.

In the light of the symmetry between particles and space, in other words between particles and anti-particles, which give rise to a symmetry and the three types operational regions that I originally proposed in a study of traffic congestion (*cf* § 7), the operational space of our filter may fall into three distinct regions when it is subjected to very small particles suspended in a fluid.

If we specify by $\rho_v$ the ratio of the volume occupied by all the clusters to the total volume, and $\rho$ the density in weight per volume, and if the three regions of operation are labelled I, II and III, then in the case of I, $0 \leq \rho_v < 0.25$, while for II, $0.25 \leq \rho_v < 0.75$ and for III, $0.75 \leq \rho_v \leq 1$. In other words, for I, II and III, we have respectively $0 \leq \rho < 555$, $555 \leq \rho < 1{,}665$ and $1{,}665 \leq \rho \leq 2{,}220$, where the unit of $\rho$ is kilogram per cubic metre. Generalising this, the regions I, II and III correspond respectively to $0 \leq \rho < \rho_{c_1} = \rho_1$, $\rho_1 \leq \rho < \rho_{c_2} = \rho_2$ and $\rho_2 \leq \rho < \rho_c$, where $\rho_c$ is determined by a physical constraint, namely the packing efficiency mentioned.

Qualitatively speaking, these three regions may correspond to the operational-, blocked and non-operational regions. If our system also contains other particles which are larger than the pores,

then in Region I filters will operate normally until the effects of blocking or blinding by the large particles become prominent, as has been studied in literature (*cf* Jackson, 1994; Jafferali, 1995). In this case fouling of the filter is caused exclusively by the blocking or blinding of these larger particles, which result in the formation of cake, and unless $\rho = 0$ there will be some blockages of internal pores due to the blockage caused by small suspended particles forming cluster. This latter type of blockage, which is of our concern, is to be expected due to various reasons. Cluster formation may be caused by nonhomogeneity in the concentration of the suspension which raises the concentration in some region such that it exceeds $\rho_1$.

Additional reduction in the flux is to be expected from two reasons. Firstly blocking clusters may block some of the pores. And secondly, the suspended particles together with free clusters, *i.e.* those which are smaller than they could block pores, displace the volume of the liquid surrounding them and thereby reduce the flux. The first one of these will produce an effect similar to blinding described in literature (*cf* Jackson, 1994; Jafferali, 1995, *ibid.*), where no backflushing may recover the filters to their virginal state. On the other hand, the majority of those particles and clusters in the second scenario is expected to be easily removed when backflushed. Among these latter there could yet be some which adhere themselves to the walls, whose fixation defies backflushing. But these last ones are expected to be small in number, and thus can be neglected, because we shall assume that the combination of $\rho$ and channelling results in the possibility that pores are blocked being very close to either zero or one.

The channelling effect, or the occurrence of rivulets by some other authors, is the formation of preferred paths through a porous media through which liquid and the solids it contains pass. It is not yet clear what these rivulets would do to our system. If all the channels channel equally both the liquid and the solids, then the blockage along these path may be expected to rise above the average value of the whole structure if only because this becomes more probable statistically. But if there exist some channels which prefer channelling liquid to particles or vice versa, then the effect they produce will vary and become complicated. For example, channels which like to channel particles are more likely to find themselves blocked in the end by those particles which pass through them. On the other hand those channels which channel liquid better than solids will be less prone to blocking on average, but will leave other pores around them with the excess particles, and these latter will necessarily become blocked more often than usual. But, for our purpose here, we shall assume that it is solid particles that are being channelled. This should raise the possibility of blocking in some of the pores by certain amount. Channelling in general needs further investigation which will not be covered here.

Before going on to the next step of our study we should briefly look at the core idea that makes the program in § A.30. There are eight types of unit blocks here, compared with the four types in the case of the program in § 6.10. These correspond to the area drawn and labelled in Figure 6.12.

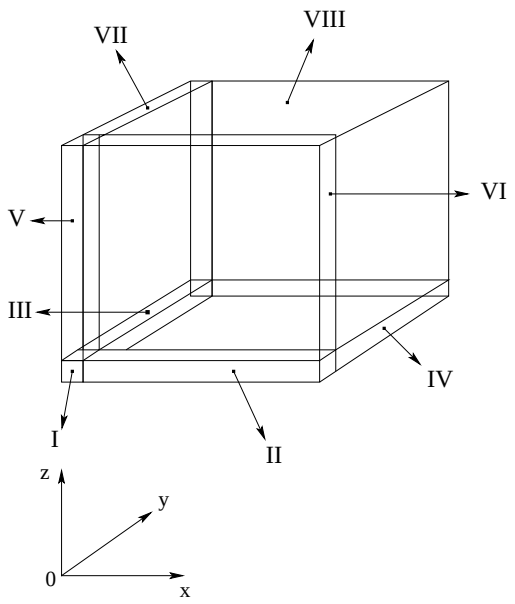


Figure 6.12 shows the eight areas defined by the eight types of unit blocks they contain. Area's from I to IV correspond to those previously defined for the 2-d program. Although unit blocks in the various areas works differently, that is to say, they adopts different set of vertices from different sources, and create different edges, all of them follow the same four rules. These four rules in the mnemonic not cryptic forms which I use are, *take vertices from behind*, *make front vertices*, *draw edges behind* and *draw no front edges*. With these rules in mind, both programs should become self-illuminating to such extent that no further explanation is needed. This set of rules does two things, namely organise vertices and then link them with bonds. The unit vectors in the three directions being orthogonal means that we will have a nice and square end product suitable for a percolation study.

**Figure 6.12** The eight areas defined by the eight types of unit blocks.

In fact it is wrong to say that all four rules work differently for each unit group. Only the two on vertices, *viz.* the first two, are different. The rest, *viz.* the last two which concern edges, are the same for all basic units. These are the only two crucial tasks with the discovery of which the writing of both program becomes worthwhile.

The input data needs only contain details regarding units in Area II, III and V. Area I, being at the origin, is trivial, or should one rather say unique. Area IV can be derived from Area's II and III. Like wise VI is derived from II and V, and VII from III and V. Finally Area VIII turns out to be nothing but II, III and V combined.

So far we have only mentioned the situation where $0 \leq \rho < \rho_1$. In the second case, where $\rho_1 \leq \rho < \rho_2$, many more pores are blocked from small particles than in the first case. The concentration is already beyond the first critical point. But while the second critical point is still not reached, there would still be an infinite cluster of space – in this case the liquid – surrounding the particles. In other words the space still percolates. The presence of this infinite cluster, or continuum of the medium, means that the filter can still be in operation until it should be blocked or blinded by larger particles which individually can physically block the pores as found in existing literature earlier mentioned.

The third and last case, where $\rho_2 \leq \rho \leq \rho_c$, represents the extreme which can be easily comprehended. Here the solid particles occupy more space than the liquid does, as a result of which the combination is no longer a suspension but a slurry. Clay material produced by this slurry would block most of the pores within the structure and make filtration impossible. Backflushing will not be effective on filters which have undergone such fate.

## § 6.11 The second part, flow through the cells

Next we will investigate briefly the effect that channelling may have on the value of $p_c$. There are three cases considered here. The program for this purpose is listed in § A.31. The program creates a centroidal Voronoi tessellation in three dimensions. The first set of simulations works on a normal case of cell percolation, similar to that in § 6.11 but here the system is a centroidal Voronoi, which implies a constraint on cell sizes and distribution. The function `perd` in it is obtained by inputting the `Blocked` variable instead of generating it internally.

This section is written along with my developing the programs, so the contents should be easier to follow than in other sections. This is not to say that in those other sections I had not kept records of things discovered. Every Ph.D. student starts off doing his project knowing that he should write along as he goes, and plans to nothing but that. But the truth is that even though we always write,

but the way we write develops with our experience. Also, with the the increase in the understanding of our problem, we no doubt would be able to write a better description of what we do and how we do it. This is unavoidable, and it is probably the reason why we should keep on working.

So much for an aside. From one hundred generators originally, Voronoi operator is applied twice. After the rims has been trimmed there are 280 centroidal Voronoi cells remaining, and this is the value of $n_c$. For $x_c$ the value is 10.7929, while $p_c$ from $2 \times 5$ simulations is $0.2314 \pm 0.0602$.

Next investigate the effect of channelling by assuming that the steepest gradient of all the bonds arriving at a cell decides how quick it percolates. Here cells are sorted according to their steepest gradient of incoming bonds. Working on the same network as previously, if the percolating order is such that the steeper the quicker, then $p_c = 0.2107$. But if on the other hand steeper incoming bond means slower percolation, then $p_c = 0.1429$. The critical probability is constant in this case since the order of percolation is predetermined by the orientation of bonds with respect to cells.

If instead of looking at only a single bond we take the signed summation of bonds entering and leaving a cell, then $p_c = 0.1321$ when the criterion is $\min(\sum b_i - \sum b_o)$, and $p_c = 0.1393$ when it is $\max(\sum b_i - \sum b_o)$, where $b_i$ and $b_o$ are respectively the incoming and outgoing bonds.

Our studies up to now tell us that if the suspension is homogeneous and there is a rivuleting effect, then the location of the blockages made by clusters of suspended particles among all pores of the structure is predetermined. This is in contrast with the blinding and blocking of large particles, where such location is random. In fact, even for these latter large particles, the location can only be random when the particles have a variety of sizes. It can never be wholly random, however, if this is not the case, since in the former case the randomness is introduced by the distribution of sizes which is random, but in the latter the blinding or blocking will be determined by the size of pore openings which is fixed by the geometry of each network. The randomness then can only be in the order not location of blockings.

The next study is a combination between continuum and network percolations. Here suspended particles are grouped into quanta, each channelling through a path or rivulet of interstitial distance with some interstitial velocity.

At the top, the layer of the structure where the incoming particles arrive, is a cross section all the cells of which are gridded to provide means to determine the path at the beginning of each quantum. The partitions in this layer is conveniently found by cutting some faces of the convex hull of each cell in the top layer by the plane $z = 0.9z_{\max}$, where $z_{\max}$ is the maximum $z$-coordinate of all the cells under consideration.

Given coordinates of two points, $(x_1, y_1, z_1)$ and $(x_2, y_2, z_2)$, and a plane equation $z - a = 0$, we may think of the plane equation as being one coordinate given, $z = a$, and find the coordinates of intersection between a line passing through the two points and the plane from the parametric equations for the line. Parametric equations are in fact interpolation done on each of the coordinates. In this case, which is useful when finding the intersection between an edge of a triangle and a plane perpendicular to some coordinate axis, the parametric equations are $x = x_1 + x_{12}t$, $y = y_1 + y_{12}t$ and $z = z_1 + z_{12}t$. From the plane equation $z = a$, therefore $t = (a - z_1)/z_{12} = (a - z_1)/(z_2 - z_1)$.

The program being written finds the intersection of cells with the horizontal plane by finding the intersection of the faces of its convex hull with the same. Since every face of the convex hull is a triangle, the program essentially finds intersection between edges of these triangles and the horizontal plane. The result obtained from an intermediate state during the course of development of the program is shown in Figure 6.13. The partitions look incomplete because the picture is taken as a test while developing the program as mentioned. A picture with the same degree of incompleteness as this one is not to be obtainable from the completed program.

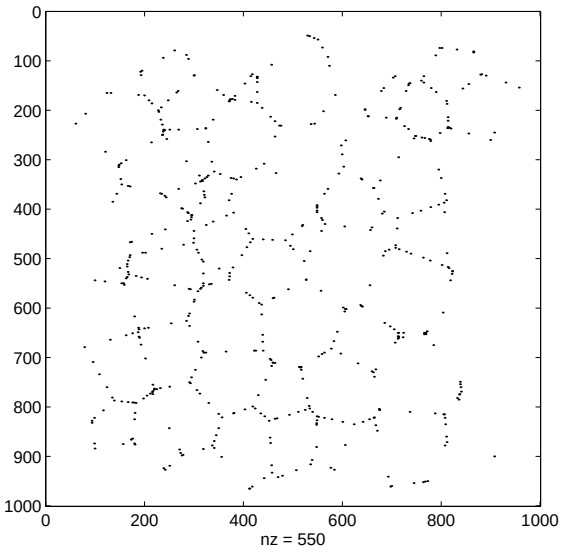


**Figure 6.13** Intersection of convex hull faces and the horizontal plane.

For each face of the convex hull that intersects the plane, there will be two points of intersection arising from the two edges of the triangle intersecting it. Let $(x_1, y_1)$ and $(x_2, y_2)$ represent these two points. Then we may scan up in the $y$ direction finding $x = x_1 + (y - y_1)x_{12}/y_{12}$ for each $y$ along the way, and then scan in the $x$ direction, this time finding instead $y = y_1 + (x - x_1)y_{12}/x_{12}$. Afterwards we could fill in the space by scanning along the $x$ direction for all $y$ positions.

Figure 6.14 shows the progress of my programming the codes, step by step, trying to close all the partitions such that no gaps remain. Two problems have been discovered, namely those of rounding and precision. Before the correction the resul looks like Figure 6.14 (a) and (b), and after rounding problem corrected Figure 6.14 (c).

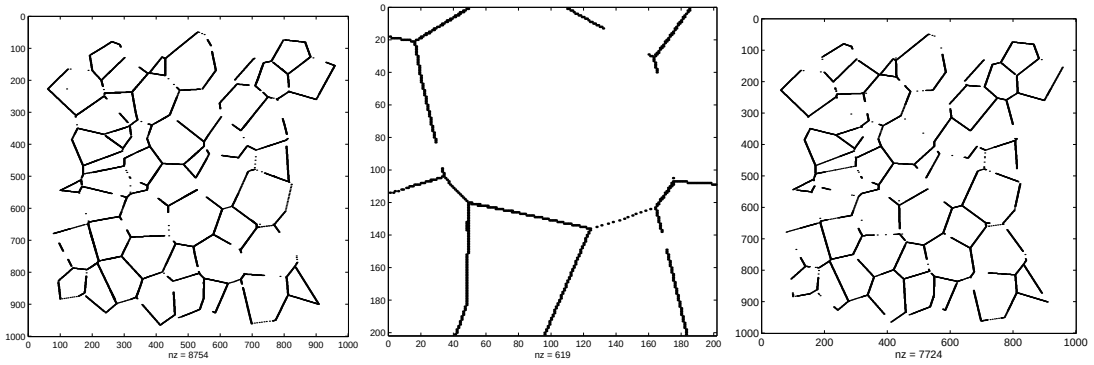


(a) (b) (c)

**Figure 6.14** *Correcting the effect of rounding, in other word discretisation.* (a) *The gaps resulted from rounding or discretisation,* (b) *a closed-up view of (a) and* (c) *partial remedy where roundings have been solved but with the degree of precision not yet raised.*

After having corrected the problem regarding precision, by increasing the number of steps when calculating $x$ or $y$, the result still misses several walls, the cause of which is still unknown at present. This is shown in Figure 6.15.

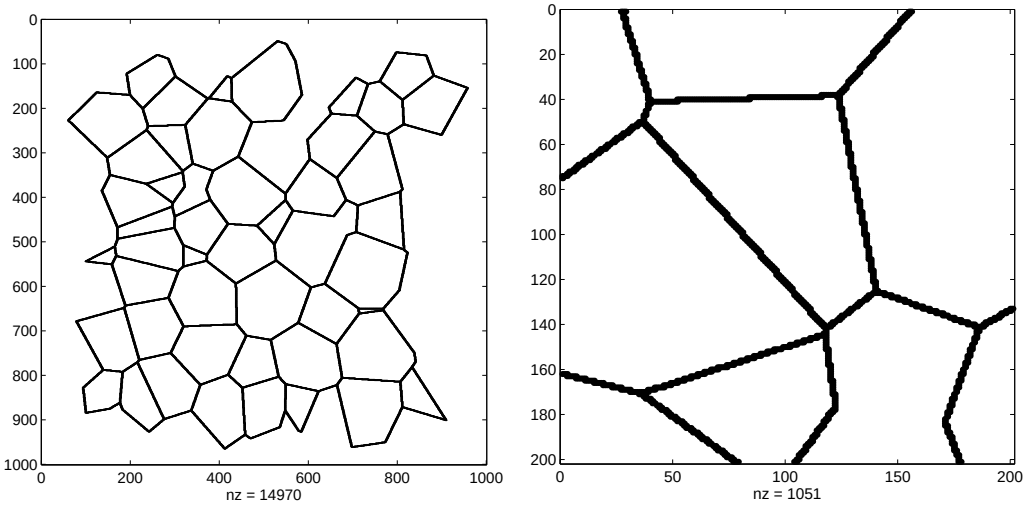


(a) (b)

**Figure 6.15** *After having increased the precision to ten times the previous value,* (a) *and a closed-up view,* (b).

It seemed at first that there might be some triangular faces missing from the surface of the convex hull, which would have accounted for the missing boundary in the section. But after having tested the minimum number that an edge of each hull appears as the edges of all its triangular faces, and see that it's value is correctly two, this becomes out of question.

The figures, *viz.* Figure 6.13, 6.15 and 6.15, are produced from the `spy` command in Matlab, as a result of which the $x$-axis runs downwards while the $y$-axis runs to the right. This command looks at a matrix from above as we look at a map. In the present case our matrix is a full-, not sparse matrix. The number written at the bottom is the number of all its nonzero components, which is

less than the number of times that we calculate them since we need to calculate some of the points more than once in order to increase the precision to eliminate gaps in other places.

The command `spy` is used more often with sparse matrices since these are often too large to list, and listing their members in pairs makes it difficult to visualise. As an example, Figure 6.16 (a) is what we get when we `spy` our neighbour matrix `necc`, while in Figure 6.16 (b) are all the neighbours that the $100^{\text{th}}$ cell has. Cells which have few neighbours generally live along the border. For example the $110^{\text{th}}$ cell has only three neighbours, and it is located not far from the lower $x$ limit.

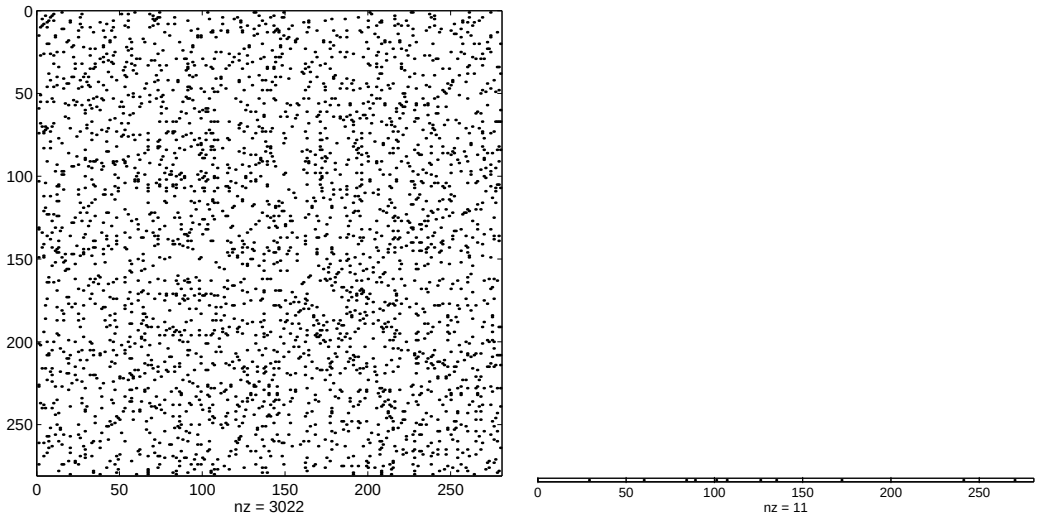


**Figure 6.16** *The result when we* `spy` *our neighbour matrix. Here* (a) *shows the neighbours of every cells while* (b) *only shows those of the* $100^{\text{th}}$ *cell.*

At this stage the neighbour matrix of the program is double-checked, and find that it includes poorly defined neighbours, that is those which only have one vertex in common. Therefore the program is first altered to make it only look for neighbours who share at least two vertices. But this has shown no noticeable changes in the results that we have so far.

The next step is to colour the cells. Like a child painting a picture, there are so many ways one can paint or label the tiles of a tessellation. For example one could draw a vertical line first and then branch out either horizontally or diagonally. On the other hand, one could also draw the diagonals first Yet another way is to expand radially, spiraling outwards. With parallel computing we could also divide the area into domains, paint each domain, and then merge the resulted areas together.

But here we opt for painting the cells by scanning horizontally, moving upwards in layers. Once past a wall, the program moves on until the next wall is reached while gathering all the grids that are between the two walls into one group. It then colour the whole group by a colour picked up from one layer below it. If no colours exist, then it creates a new colour which in turn gradually propagates upwards this way until the upper wall is reached.

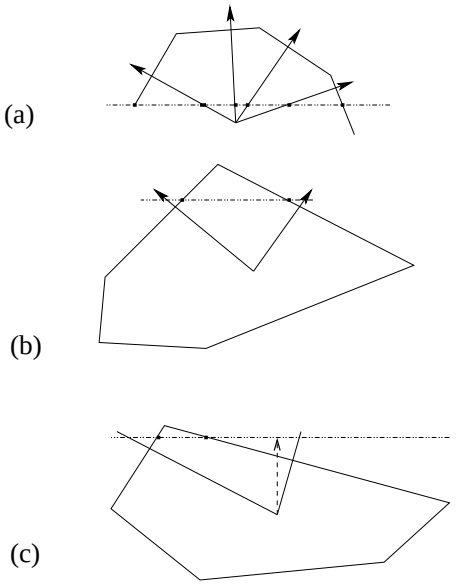


The intersection of bonds will not always coincide with the intersection of the cell, neither is the projection of a cell perpendicular to the plane the sectional plane of the cell. This is because of the three possible situations shown in Figure 6.17. In Figure 6.17 (a) the cell section contains several points, while both (b) and (c) contain none.

**Figure 6.17** Sections of bonds and cells.

And here sadly the time runs out, so I will suffice myself to describing what I see should be done next. Up to now we have a three-dimensional network and its top section. We also have the list of all its bonds, which contains the connections and the draining angles sorted in a descending order.

Next we should find a mapping from each cell section to the corresponding nuclei. Then the times it takes to traverse each bond must be calculated. This time for each bond is then divided by half, one belonging to each of the two cells connected by the bond.

When it comes to bombarding the filter with our small particles, we can not keep track of millions of particles and therefore we should quantise them into units. These units or quanta can then be treated as individual particles. When a quantum enters a cell, it is assigned $t$, the time to reach the nucleus. Later time sees this $t$ decreases in steps until it finally reaches its destination, the nucleus. Once there, it is assigned the next bond to go along, taking into account what bonds are available at the time and their comparative probabilities, which in turn depend on their gradient as mentioned. When this is decided, it is given $t_1$, the time it would take to reach the border that lies at mid point of the bond.

This goes on forever, apart from that at each time step we look to see whether the blockages in our filter has percolated. After updating the list of blocked cells, if we find that percolation has occurred then the simulation would end. Percolation occurs in each cell whenever its concentration has reached a certain value. This value we have found in § 6.11 to be 18.5 per cent by volume.

To calculate the flux decrease we find instead the decrease in the superficial area. This is calculated from the total volume of the void subtracted by the volume of all cells that had percolated, and then subtracted by the total volume of solid particles which are suspended inside the network. The area of the cross section is then the volume which remains divided by the thickness of the filter.

It is not a little to have to leave things unfinished after having started it off. But as one New Zealander poet says, 'Alone we are born and die alone, yet see the red-gold cirrus over the snow mountains shines. Upon the up-land road ride easy, stranger. Surrender to the sky your heart of anger.' And with this we go on to the next chapter.

## § 7. Percolation in traffic modelling

It does not take much imagination for an average person to see that traffic congestion is a percolative process. As I have lived and studied in Bangkok where, at that time, the traffic jams were renowned. Now I relate traffic jam to percolation of the network of streets. I remember once in 1990 it took me more than five hours on a bus to travel the distance of ten kilometers along the Sukhumvit Road in Bangkok. The newspaper of the following day reported that that traffic jam had been on the BBC news broadcasted all over the world.

Soon after having decided to investigate the application of percolation to traffic, I gave a poster presentation at the Fourth Annual Conference of Thai Researchers in Japan in 1997, the proceedings of the event of which also contain a number of abstracts from some of the researches that I was currently working on (Tiyapan, 1997, KNT5(i) to KNT5(iv)). The poster presentation was considerably a success.

The paper listed in § E.20 of Tiyapan (2003, KNT8(iii)) is a reproduction of what I had submitted to the Journal of Statistical Physics in 1997. I tried but could not receive any reply for the paper I submitted. Afraid that the ideas in it could have been plagiarised, I decided to put it in the book above quoted.

In 2002 I did some more works on it. I have developed the theory further and done a number of simulations. I plan to carry on doing research along this line in the future, together with another area where percolation is used to explained economics transition (Tiyapan, 1997, KNT5(viii)).

In his paper submitted to the Journal of Statistical Physics Tiyapan (1997) introduces a new idea of considering the development of clusters in both phases at the same time. Applied to the context of traffic network, these phases are namely cars and spaces. Furthermore, because both phases reside in one and the same network, there is a symmetry which divides the probability space into three regions, symmetric with respect to $p = 0.5$. This helps divide the traffic condition into three regions as existing literature in traffic study at the time described, namely free flowing, congested and stand still. In particular, this idea explains the difference between the congested and the stand still states. There has been no reply from the journal.

In the 2002 simulation the networks are drawn which have their vertices as points where two or more roads meet one another. The proposed study is to compare the robustness of two traffical networks by comparing their percolation thresholds. When a new motorway is planned, for example a ring road around a city, the two networks, one with the ring road and the other one without, can be simulated to find their percolation thresholds and then these values compared.

Traffic status or condition when the percolation probability $p_c$ of cars is more than 0.5. The traffic condition is generally described as free-flowing, congested, or stand-still. For cases where $p_c > 0.5$ as the one shown in Figure 7.1 the stand-still traffic corresponds to the situation where only cars have percolated but not the space, that is the places on the road available and accessible to the cars.

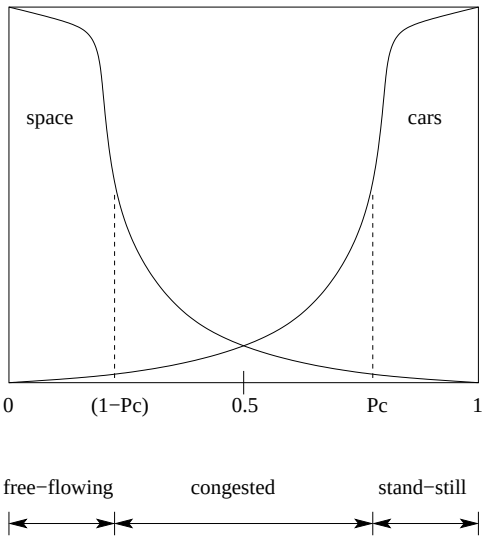


**Figure 7.1** Traffic status, $p_c > 0.5$.

A free-flowing traffic is where only the space but not the cars has percolated, and a congested traffic is that when neither of the two has. Traffic status or condition when $p_c$ is less than 0.5.

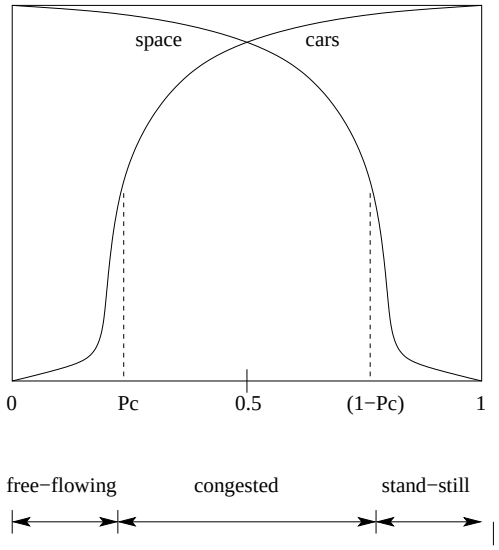


On the other hand, in the case where $p_c < 0.5$ shown in Figure 7.2 the critical probability of cars is now on the left hand side of the middle line instead of on the right hand side thereof in the previous case where $p_c > 0.5$. Definitions of the free-flowing and the stand-still statuses remain the same, but the congested traffic is now the traffic where both cars and space have percolated. An interesting question is whether or not there is a difference between the congested area in Figure 7.1 and the one in Figure 7.2. A *modelling algorithm* which studies the percolation of a traffical networks starts by finding all the vertices and edges forming a network from the road data. Then a blocking algorithm operates by randomly shutting off one edge after another until the network percolates when the critical probability of the network may be calculated.

**Figure 7.2** Traffic status, $p_c < 0.5$.

A *control algorithm* for the real time traffic control, however, is as shown in Figure 7.4.

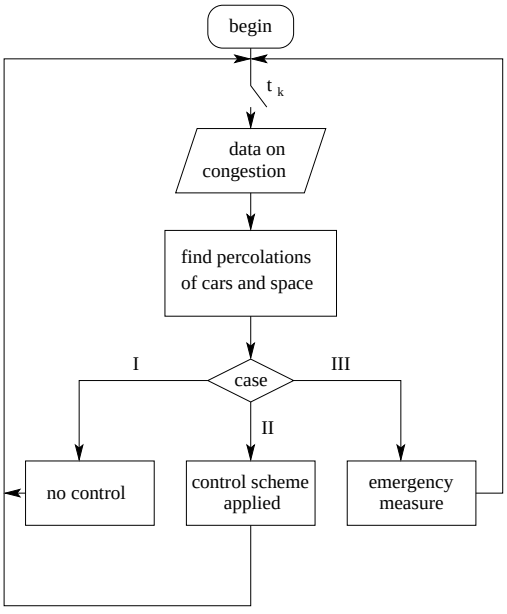


Let $C$ means *cars have percolated* and $S$ means *space has percolated*, then in Figure 7.4 the cases I, II, and III are respectively $\neg C \wedge S$, $(\neg C \wedge \neg S) \vee (C \wedge S)$, and $(C \wedge \neg S)$. Case I is the normal congestion, nothing to worry about. Examples of the control schemes used in Case II are overriding of the traffic lights by the manual control of traffic polices at certain strategic points, temporary one-way systems, bird-eye view observation and feedback from helicopters, traffic control centre, distributed control centres together with traffic radio channel broadcast. And lastly the most important and critical Case III the emergency plan of which may include directing all cars away from congested clusters or if necessary out from the city, and directing all incoming traffic such that no more cars may enter the city until the emergency status ends.

**Figure 7.4** Proposed traffic control in real time..

A congested cluster can be broken up by forming a one way flow channel cutting through it which leads cars away from the cluster. How far the channel needs to go before letting the cars

on it circle and seep back into town depends on how badly congested the traffic is. Although it is a normal practice to lead cars along a long detour because this brings in more road surface and thus enlarges the network, identifying the percolating cluster and cutting it into two or more parts by guarded flow channels is much less common or even unheard of. The latter seems to be more important and will lead to a better and more effective control, namely the control of the percolating, in other words the biggest, cluster.

The percolation probability is important for the networks of traffic both inside cities and among them. It shows the degree of connectivity of the area being considered. Urban road networks have a general character which differ from one country to another, the simplest construction of which seems to be that of the square lattice. One can find this theme of the square lattice and its variations, similar to the dislocations and defects found in minerals, in America. Examples are Denver, Aspen, Durango, Pueblo, Salida and La Junta in Colorado; Boise, Pocatello and Twin Falls in Idaho; Butte, Bozeman, Coeur d'Alene, Kalispell in Montana; and Cheyenne, Laramie and Sheridan in Wyoming (*cf* Florence *et al*). The Great Junction in Colorado and the Great Falls in Montana are very close to being perfect square lattices. As more examples of these (*cf* Collins USA, 1999), in Arizona there are Phoenix, Yuma, Tucson; in California Bakersfield, Central San Francisco, Central Sandiego, Fresno, (Central) Los Angeles and vicinity, Modesto, Sacramento; in Colorado Fort Collins, Denver and vicinity, Greeley; in Florida Central Miami; in Georgia Central Atlanta; in Illinois Champaign and Urbana, (Central) Chicago and vicinity,, Quad Cities, Rockford; in Indiana Fort Wayne and Indianapolis; in Kansas Topeka and Wichita; in Louisiana Central New Orleans; in Maryland Central Baltimore; in Minnesota Central Minneapolis and Central St. Paul; in Missouri Central Kansas City; in Nebraska Lincoln; in Nevada Las Vegas; in New York Manhattan; in Oklahoma Lawton, Norman, Oklahoma City and Tulsa; in Pennsylvania Central Philadelphia; in South Dakota Sioux Falls; in Amarillo, Central Houston and Lubbock; in Utah Central Salt Lake City; in Washington Central Washington D. C. and Central Seattle; and in Wisconsin there is Central Milwaukee. One example in Canada is Toronto. The square lattices of these cities are sometimes cut through by motorways or interstate highways as is the case in Amarillo, Texas. Or they can be surrounded by a ring road or a county highway as is what happens with Lubock, also in Texas.

When the percolation probability is greater than 0.5, we have the interval $p_c \pm (p_c - 0.5)$ where neither the blocked nor the free roads percolate. If this interval is narrow, that is if $p_c - 0.5$ is small, then within this interval the condition of the traffic is very sensitive, and even a seemingly small change may lead to a standstill or instead to a free-flowing traffic. This is easily visualised, since in such situation there would be small islands of free-flowing roads within a large congested cluster, and vice versa small clusters of congested roads within an otherwise noncongested area. Despite their sizes, such small islands of anomaly in either of the phases are particularly important. Moreover, their importance increases the closer $p_c$ is to 0.5. The same characteristic happens in politics where, in the case of coalition governments, a minority party which has relatively few representatives can become critically important and influential to the major party when the latter needs them in order to be able to govern (Ireland, 2002).

Plan to build a ring road around a city usually includes flyovers, overbridges, and tunnels in order to avoid having intersections. The design philosophy used in Europe is to have heavier traffic goes under a lighter one, which results in either the ring road going into a tunnel or having overbridges or viaducts over it. The philosophy used in Thailand which used to be for the heavier traffic go over the lighter traffic, which puts a more severe limit on the weight of trucks and is therefore not economic in the long run, but this has started to changed, if only to follow the practice of the west. Ring roads do not necessarily resemble a circle, as in the case of the circular speedway proposed around Saint Petersburg (Petersburg, 2001), which is in the shape of a cashew nut. It will link the arterial roads of the city to Helsinki, Kiev, Moscow, Murmansk, and Tallinn into a network. The route proposed is 155 kilometres in length, has 31 bridges, 16 overbridges, 55 viaducts, and will support the volume of traffic of 21 million tonnes. The implementation and contract work is looked after by a joint-stock company KAD Sankt-Peterburga, under the order of St. Petersburg and Leningradskaya Oblast.

One classical example of a ring road is the M25 motorway which forms a circumscribed ring around London. Another more recent example is the M60 orbital motorway around Manchester. In the case of M60, various sections of existing motorways have been put together and renumbered. The northwest quarter used to be M62, the southwest one M63, and parts of the remaining used to be M66. The motorway forms a complete ring around Manchester since 2000 with the opening of the final northeastern part which stretches from Denton to Prestwich. There is another smaller

ring, an inner ring, which is formed by the A6010 and A576. Orbital motorways around cities have now become indispensable and are the hallmark of a city.

## § 7.1 Percolation of road networks

I began my study of the traffic networks in 1997 while in Japan. In the same year I submitted two papers,

Tiyapan in 1997 (KNT5(ix)) has a novel idea of linking percolation to the management of street congestion. In his work submitted that year to the Journal of Statistical Physics, also in § E.19 and § E.20 of Tiyapan (2003, KNT8(iii)), electronically though the paper became lost and was never published, he explains how three phases could result from structures containing only two phases. Recently there have been some papers published in 2001 in the Journal of Statistical Physics which used this very idea that Tiyapan introduced in 1997. But what has passed is past and past cure, we need to think about it no further now. Everything comes from and goes to God, let that suffice! I have developed a program and a procedure for finding the percolation thresholds of road networks. These programs are listed in § A.27. They are different from the usual percolation programs used for other kinds of networks including Voronoi. Because of the existence of flyovers and elevated express ways, we can not use the duality operator to transform a network of vertices and edges into one of cells and bonds. Having said that, the said transformation could become useful in the future in some other applications, in some other areas or even within the study of traffic network itself. But at present I have only one application in mind for the dual networks of roads, and that is related to fire prevention where such an application is by no mean obvious. Therefore, here the boundary is defined again to obtain the cells which represents the zones.

The codes also contain data of several towns and cities, namely Amsterdam, Brussel, Freiburg and Manchester. There are three main datasets. The first one contains a list of the coordinates of all the vertices. The second one is a list of edges, together with the numbers of the cells that each of them connects. The third one contains the coordinates of turns in each of the roads listed in the second dataset. This is in order for the graph to look like the actual roads it represents, instead of containing only straight lines, as would have been the case were the windings of the roads not to be taken into account. Also, these coordinates will make it possible to calculate the true length of each road. Even though we have no use for these lengths at the present stage, future developments may need them.

The procedures developed for gathering the data and processing them can be carried out by a single researcher, and require no sophisticated tools. Were these tools become available in the future, the former could be adjusted to accommodate them.

To my surprise, so much so that I at first thought that there was something wrong with the program, the mean coordination number of the road networks of Manchester turns out to be exactly 3. The second simulation gives $x_v = 3.0513$, which is still very close to three.

(a) (b)

**Figure 7.5** *For Manchester in this picture,* $n_v = 220$, $n_e = 330$, $n_c = 25$, $n_b = 50$, $x_v = 3.0000$, $x_e = 4.7273$, $x_c = 4.0000$ *and* $x_b = 6.5200$.

Figure 7.6 shows the largest clusters plotted against $p$, the probability that each vertex, edge, cell or bond respectively for (a), (b), (c) or (d). Here $p_v^s$ is the percolation probability of the space in the network of vertices, and similarly for $p_e^s$, $p_c^s$ and $p_b^s$. Each plot represents one of the runs of simulation which, for networks of these sizes and variances, literally distributes the critical probabilities all over the place. But the plots of the largest cluster sizes always look very symmetrical. This seems to suggest that these sizes may represent the point of percolation better than the percolation probability.

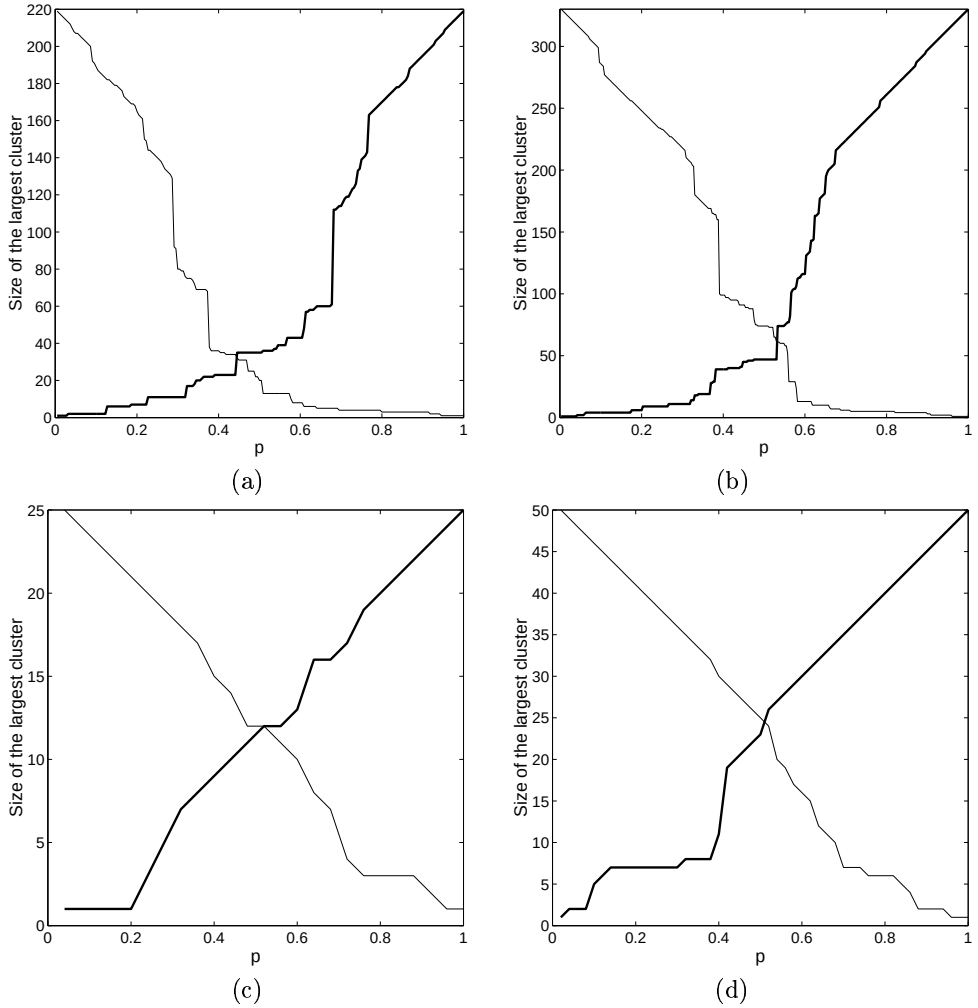


**Figure 7.6** *Manchester. Plots of the largest clusters of,* (a) *vertices,* (b) *edges,* (c) *cells and* (d). *Here* $(p_v, p_v^s) = (0.5455, 0.7182)$, $(p_e, p_e^s) = (0.6152, 0.4939)$, $(p_c, p_c^s) = (0.6400, 0.6000)$ *and* $(p_b, p_b^s) = (0.1200, 0.5000)$ *respectively for the cases of* (a), (b), (c) *and* (d).

The mean percolation probabilities from $(2 \times 10)$ similar simulations as the two shown in each of the four cases of Figure 7.6 are $\bar{p}_v = 0.6723 \pm 0.0762$, $\bar{p}_e = \mathrm{Er}[0.6083, 0.0838]$, $\bar{p}_c = \mathrm{Er}[0.6240, 0.0921]$ and $\bar{p}_b = \mathrm{Er}[0.3720, 0.1149]$.

Next consider Amsterdam in The Netherlands. The map for our purpose is shown in Figure 7.7. Areas shown in Figure 7.7 (b) are usually bound by main roads or the rims of the picture. There is no definite relations between vertices and edges on one hand, and cells and bonds on the other.

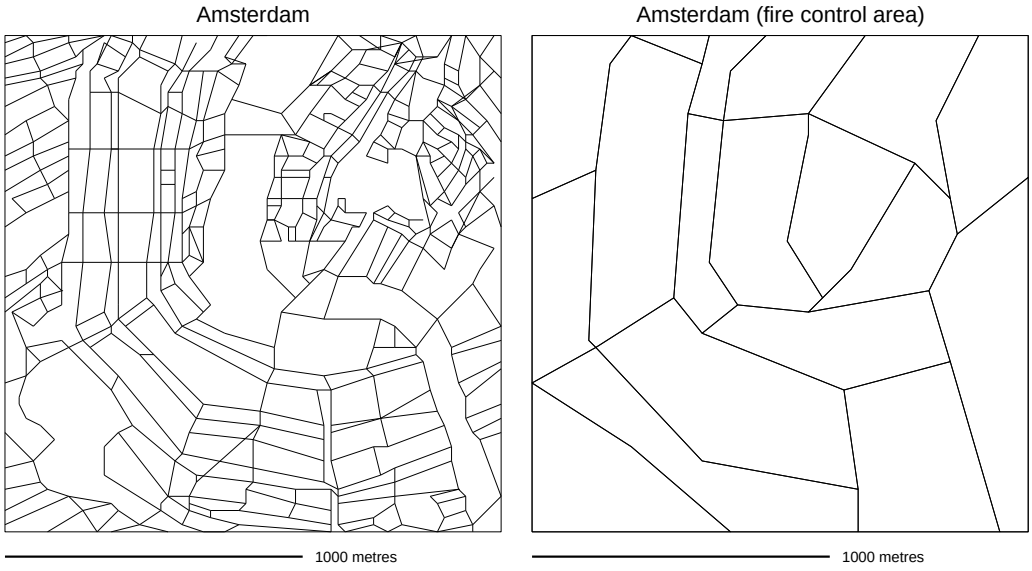


**Figure 7.7** *Amsterdam in this picture has $n_v = 487$, $n_e = 745$, $n_c = 18$, $n_b = 35$, $x_v = 3.0513$, $x_e = 4.7007$, $x_c = 3.8889$ and $x_b = 6.8000$.*

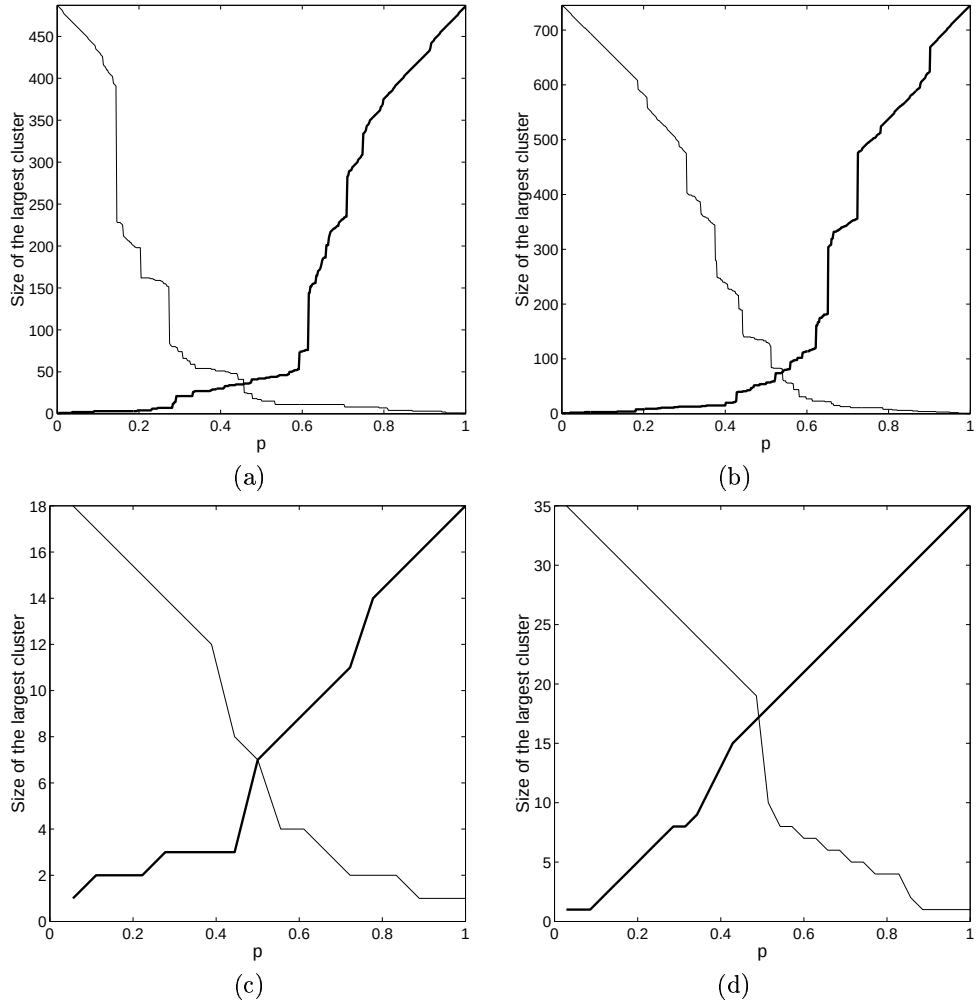


**Figure 7.8** *Amsterdam. Plots of the largest clusters of,* (a) *vertices,* (b) *edges,* (c) *cells and* (d). *Here $(p_v, p_v^s) = (0.7187, 0.7146)$, $(p_e, p_e^s) = (0.6309, 0.5597)$, $(p_c, p_c^s) = (0.7778, 0.4444)$ and $(p_b, p_b^s) = (0.4286, 0.2571)$ respectively for the cases of* (a), (b), (c) *and* (d).

From $(2 \times 10)$ simulations we obtain $\bar{p}_v = 0.7374 \pm 0.0500$ and $\bar{p}_e = 0.6328 \pm 0.0595$, whereas

from $(2 \times 11)$ simulations $\bar{p}_c = 0.5960 \pm 0.1395$ and $\bar{p}_b$ $0.3922 \pm 0.1395$.

Then consider the road networks of Brussel in Belgium, as shown in Figure 7.9, to gether with the fire control area, and the largest cluster sizes in Figure 7.10. Fire control strategy is only one possible application to which the percolation of areas. Many other applications which are similar in nature, for instance emergency evacuation zones, earthquake evacuation zones, zones prepared as measure against a terrorist gas attack, *etc.* There are also other applications, for example strategic areas in market planning and the study of mineral deposits.

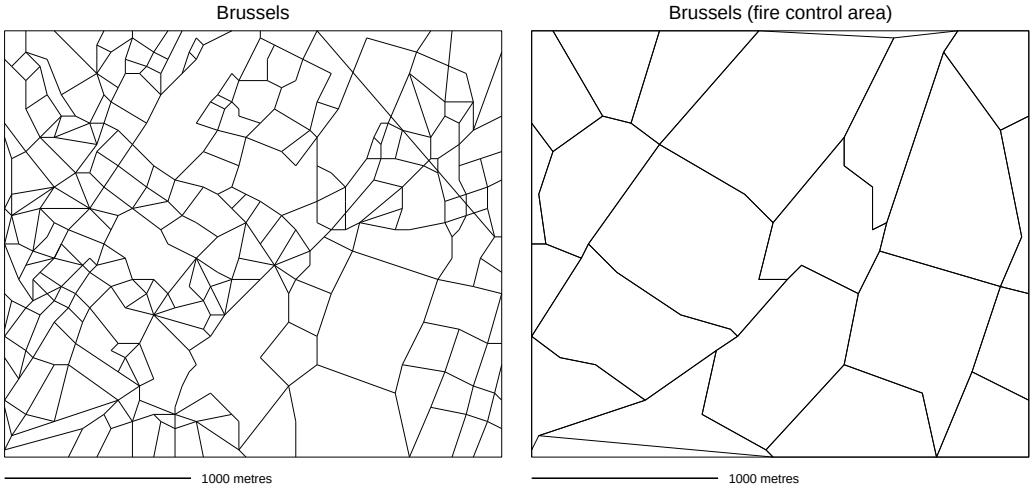


**Figure 7.9** *Brussel has $n_v = 287$, $n_e = 454$, $n_c = 21$, $n_b = 42$, $x_v = 3.1568$, $x_e = 3.1568$, $x_c = 4.0000$ and $x_b = 7.0476$.*

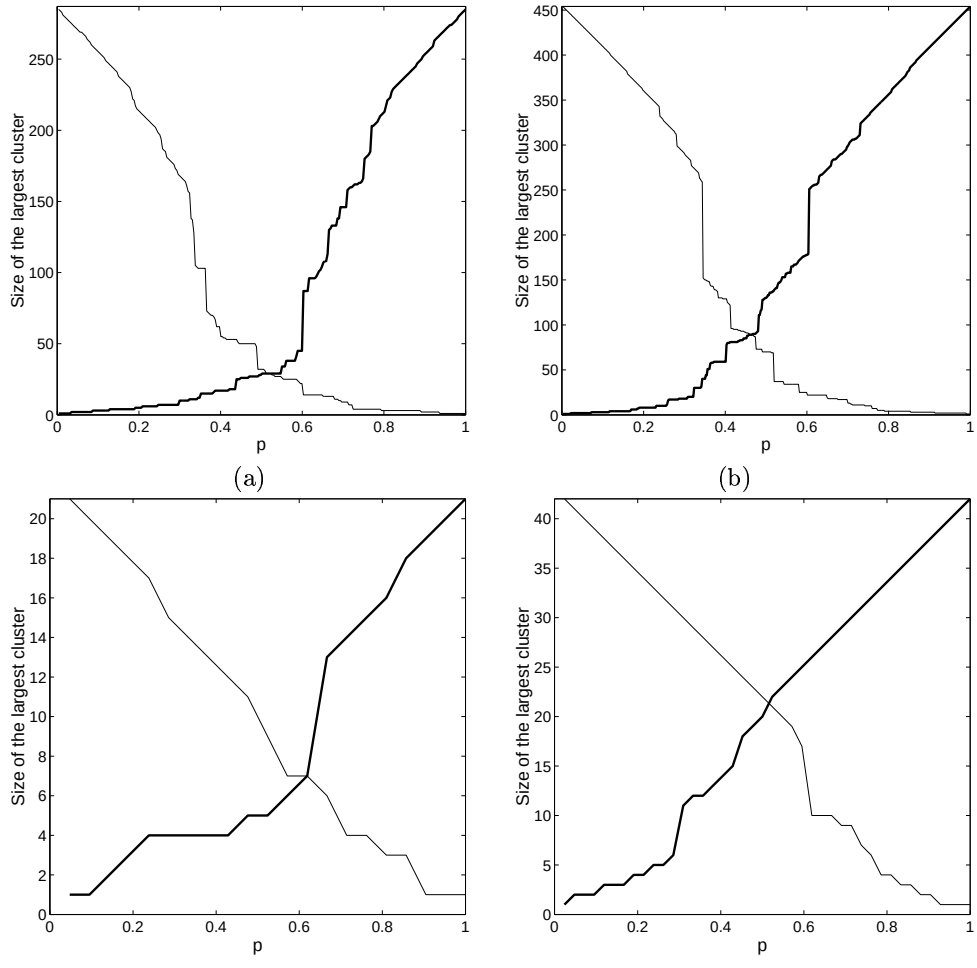

(c) (d)

**Figure 7.10** *Brussel. The largest clusters when percolate by means of* (a) *vertices,* (b) *edges,* (c) *cells and* (d). *Here* $(p_v, p_v^s) = (0.6167, 0.6411)$, $(p_e, p_e^s) = (0.6057, 0.6586)$, $(p_c, p_c^s) = (0.6667, 0.5714)$ *and* $(p_b, p_b^s) = (0.3095, 0.4286)$ *respectively for the cases of* (a), (b), (c) *and* (d).

From $(2 \times 10)$ simulations on Brussel we obtain $\bar{p}_v = 0.6580 \pm 0.0771$, $\bar{p}_e = 0.6205 \pm 0.0540$, $\bar{p}_c = 0.6286 \pm 0.1043$ and $\bar{p}_b = 0.3786 \pm 0.0924$.

And then consider a small town Freiburg in Germany, where the many roads that are reserved for pedestrians only seem at a first glance to have altered much of the structure. But simulations have shown that the percolation probabilities remain comparable with networks of other towns. The area- and bond coordination numbers obtained for Freiburg are rather low compared with other towns. This could mean that the emergency properties of the town is different from those of others. Its lower connectivity could mean that it is more robust than others against an attack or in the face of catastrophe. But it could also make it more difficult to evacuate from an area. More precise relationship between the valence and the interpretation in terms of physical networks can only be possible by more extensive investigations in the future.

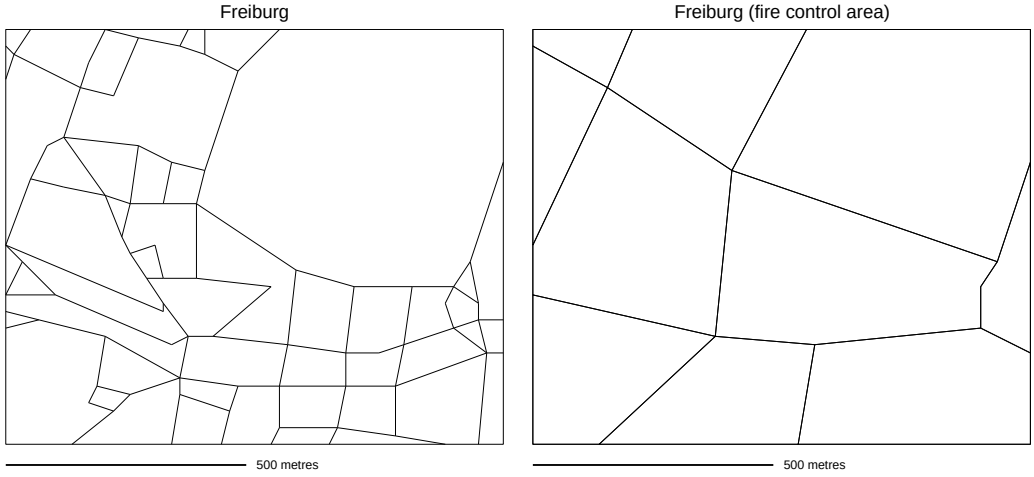


(a) (b)

**Figure 7.11** *Freiburg has* $n_v = 75$, $n_e = 102$, $n_c = 10$, $n_b = 15$, $x_v = 2.7200$, $x_e = 4.4510$, $x_c = 3.0000$ *and* $x_b = 4.5333$.

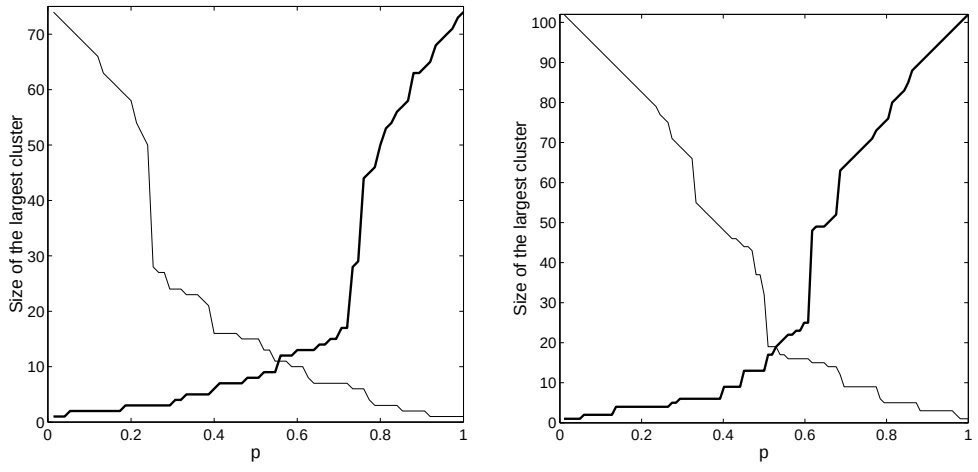


(a) (b)

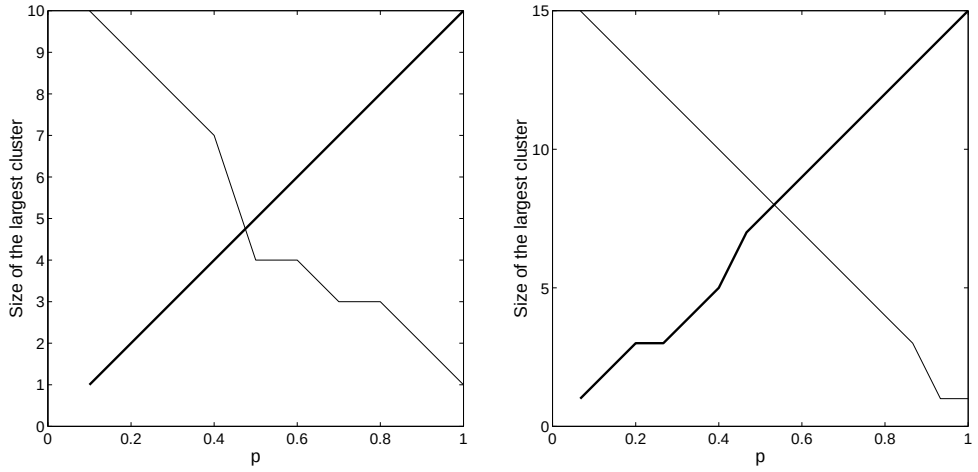


(c) (d)

**Figure 7.12** *Freiburg. The largest clusters when percolate by means of* (a) *vertices,* (b) *edges,* (c) *cells and* (d). *Here* $(p_v, p_v^s) = (0.7333,\ 0.7733)$, $(p_e, p_e^s) = (0.6863,\ 0.6275)$, $(p_c, p_c^s) = (0.4000,\ 0.5000)$ *and* $(p_b, p_b^s) = (0.4000,\ 0.3333)$ *respectively for the cases of* (a), (b), (c) *and* (d).

Again, from $(2 \times 10)$ simulations we obtain for our Freiburg $\bar{p}_v = 0.7400 \pm 0.1214$, $\bar{p}_e = 0.6490 \pm 0.0787$, $\bar{p}_c = 0.5450 \pm 0.1276$ and $\bar{p}_b\ 0.3767 \pm 0.1190$.

## § 7.2 Graphs theory and its applications

Gay and Preece (1975) study graphs on square lattices, represent them as matrices and then apply this to the study of networks of fluid distribution through pipes where there are branch flows and nodal pressures. Such a graph has $n$ nodes, $m = b - n + 1$ meshes, where $b$ is the number of branches, and any one of its trees contains $(n-1)$ branches. The direction of a mesh is the direction of the link connected to it. Define the branch-mesh incidence matrix $C = [C_T; C_L] = [C_T; U]$ and the node-datum incidence matrix $B = [B_T; B_L] = [B_T; 0]$, where $c_{ij}$ is 0, 1, or -1 when the branch $i$ respectively is not in the mesh $j$, has the same-, or opposite direction; similarly, $b_{ij}$ is 0, 1, or -1 when the branch $i$ is not included in the node to datum path $j$, is going away from, or towards the datum node. Then $V = E + e$, $J = I + i$, $V = ZJ$, $J = YV$, where $E$ is the vector of branch pressure sources, *i.e.* pumps, $e$ the vector of branch pressure rise, $I$ the vector of branch flows due to the external inputs and outputs, $i$ the vector of branch flows due to other causes. Then the mesh method has the solution $i' = (C_T^T Z_T C_T + Z_L)^{-1}(E_L' - C_T^T Z_T B_T I')$ and $E_L' = C_T^T E_T + E_L$, where $\gamma = [B, C]$, $V' = \gamma^T V$, $J = \gamma J'$, $J' = [I'; i']$ and $V' = [V_T'; V_L']$. The node method, on the other hand, gives $e' = (A^T Y A)^{-1}(I' - A^T Y E)$.

Operation research uses graphs to help in its search for optimum solutions. For example the Evolutionary Operation (EVOP) and its variant Rotating Square Evolutionary Operation (REVOP) use covering graphs on a body-centred lattice in two- or three dimensions (Lowe, 1964) – corresponding to the cases of considering two- or three factors respectively – in finding its solution. Simplex EVOP is another variation, where 2- and 3-factor regular simplexes are used, which has the advantage that it uses the least amount of experimental points. An $n$-factor regular simplex has $(n+1)$ points, in particular a 2-factor simplex is the equilateral triangle and a 3-factor simplex is the regular tetrahedron. All of these methods are possible at number of factors higher than three, but the procedure becomes more complicated and can not be shown graphically.

A graph is connected if it cannot be divided into two subgraphs without common vertices and edges. A linear combination of oriented edges, $\sum a_i e_i$ where $e_i = \pm 1$, is a simple cycle if $a_i$ is 1, $-1$ or 0. It is a cycle if $a_i$ are integers satisfying some linear relations, and a chain if they are arbitrary integers.

If vectors from the origin to vertices $A_i$ follow the relation $A = \sum m_i A_i$, then $m_i$ are the barycentric coordinates of $A$. Here $m_i \geq 0$, $\sum m_i = 1$ and $A$ is the centre of gravity of the point masses $A_i$. A convex linear hull of $A_i$ is then the space covered by changing $m_i$ to give all possible $A$'s. It is also known as a rectilinear-, Euclidean- or $n$-dimensional simplex. Simplices can simply be represented by the of their vertices. An $n$-dimensional simplex $s_i^n$ has $n+1$ $(n-1)$-dimensional faces the $i^{\text{th}}$ one of which is where $m_i = 0$. A $k$-dimensional face of $s^n$ is the set of those points of $s^n$

for which $n-k$ barycentric coordinates are zero, while the rest change such that the corresponding $m_i$ are non-negative and their sum is equal to unity. The number of $k$-d faces in $s^n$ is ${}_{k+1}\mathrm{C}_{n+1}$.

The boundary of $s^n$ is the union of all its $(n-1)$-d faces. The centre of a simplex is a point where $m_i = m$.

## § 8. Conclusion

To summarise, we have begun our study from the Voronoi network, and then went on to study continua and then tried to combine them together. I have suggested the idea that a percolation in continua can be represented by a percolation in a lattices the type of which depends on the attrition mechanism of the particles in that continuum, in other words the way they pack together. Even though percolation already models a great many natural phenomena, I think it will prove to underly the fundamental structure of a great many more, even of the Big Bang. Therefore I truly believe that a better percolation theory may be what is behind the working of the universe.

I have written programs, and have listed here a full half of them which is already quite a lot in any programmer's standard. This is because I try to write everything myself, and not to copy even when it comes to taking codes from programs that I have written myself in the past. I try to do it this way whenever possible, and as a result the various programs should have at least a few things out of common with each other.

The results shown in Table 4.7 on page *tuntp* show that the percolation probability depends not only on the valence but also on the way in which the verticesdistribute themselves with relative to one another. From Figure 4.12 we can see that the comparative study of tilings is best done by looking at both the tiling itself and its covering lattice. The tilings $5_3[3^5]8_6[3^8]_{\rm I}$ and $5_3[3^5]7_3[3^7]_{\rm I}$ (number 24 and 27) look similar to each other and all the values of their $p_c$ are similar to the corresponding values of $p_c$'s of the other; likewise the tilings $5_4[3^5]7_4[3^7]_{\rm I}$ and $5_3[3^5]8_6[3^8]_{\rm III}$ (17 and 21). The coverings of the tilings $3_3[3^3]9_3[3^9]_{\rm II}$ and $3_3[3^3]9_3[3^9]_{\rm I}$ (2 and 7) look different from each other even though they themselves are similar in appearance, and this is reflected in the values of the cell- and bond-probabilities. Both the tilings $4_3[3^4]10_6[3^{10}]_{\rm I}$ and $4_3[3^4]10_6[3^{10}]_{\rm II}$ (6 and 9) as well as their coverings look different from each other, and it is not surprising to see that all their $p_c$ values are quite different.

### § 8.1 Suggestions for future work

Jackson (1994) and Jafferali (1995) study filtration as stochastic process within porous media which they model as a Voronoi Tessellation. Here all the blockages are assumed to be of physical mechanism in nature. Schumacher (1996) asserts how in those cases where particles much smaller than the pores' size come together to form clusters and thereby block the pores, there is involved an effect of Van der Waals electrostatic interaction between particles. Tiyapan (2003) formulates these into a problem of a continuum percolation within a network percolation.

All particles large and small are subjected to the quantum-mechanical effect and exhibit at the same time both particle and wave characteristics. The smaller a particle is, however, the more prominent its wave nature stands out. For particles of the size range in nanometres the wave length involved, depending on their velocity and density, may be in the region of micrometres. If they pass through pores of diameters in the order of $10^{-6}$ metres their path will deflect from a straight line by the interference effect similar to that experienced by electron passing through slids in a screen. The blockage, therefore, will not be wholly random but depend to a certain degree on their quantum-mechanical properties. Moreover, once inside a pore these particles will undergo the effect of particles in confinement where, depending on their size relative to the size of the pores, their wavefunction may form some standing wave pattern. Then their probable location within the pore, and thus their future trajectory to other pores, will depend on the quantum-mechanical consideration. The de Broglie wave length is $\lambda = h/p$ where $h$ is the Planck's constant and $p$ the particle's momentum. The standing wave equation is $n(\lambda/2) = D$ where $n$ is a positive integer greater than zero and D the diameter of the pore, which gives the wavelength of the standing waves $\lambda = 2D/n$ and the corresponding total energy of the particle $E = h^2n^2/(8mD^2)$. The probability of finding the particle at the area of space $\delta V$ within the pore is $P = |\psi_{\delta V}|^2\delta V$ (*cf* Walters, 1982) if the pore is totally enclosed. Here $\psi$ is the standing probability wave of the particle. One needs to know this $\psi$ for Voronoi and and irregularly-shaped pores This is what I intend to investigate further in the future. And it is also what I suggest people working in this area bear in mind.

## § 9. Bibliography


George O. Abell. The distribution of rich clusters of galaxies. *The Astrophysical Journal. Supplement Series.* **3**, Supplement Number 31, 211–288. May, 1958.

D. A. Aboav and T. G. Langdon. The shape of grains in a polycrystal. *Metallography.* **2**, 171–178. 1969.

D. A. Aboav. The arrangement of grains in a polycrystal. *Metallography.* **3**, 383–390. 1970.

– The stability of grains in a polycrystal. *Metallography.* **4**, 425–441. 1971.

– The arrangement of cells in a net. *Metallography.* **13**, 43–58. 1980.

– The arrangement of cells in a net. II. *Metallography.* **16**, 265–273. 1983.

Joan Adler and Amnon Aharony. Diffusion percolation. I. Infinite time limit and bootstrap percolation. *Journal of Physics A. Mathematical and General.* **21**, 1387–1404. 1988.

P. K Ahnelt., E. Fernandez, O. Martinez, J. A. Bolea, A. Kubber-Heiss. Irregular S-cone mosaics in felid retinas. Spatial interaction with axonless horizontal cells, revealed by cross correlation. *Journal of the Optical Society of America. A, Optics, Image Science, and Vision.* **17**, 3, Mar. 2000, p. 580–8.

John Algeo. *Problems in the origins and development of the English language.* 3rd ed. Harcourt Brace Jovanovich. 1966 (1982).

J. Ammermuller, W. Mockel, P. Rujan. A geometrical description of horizontal cell networks in the turtle retina. *Brain Research.* **616**, 1–2, $9^{th}$ Jul. 1993, p. 351–6.

Alizabeth Andrews. *Healthy practice for musicians.* Rhinegold. London. 1997.

M. F. Ashby. Cork. in *Encyclopedia of Material Science and Engineering.* 854–858. Pergamon. 1990.

Francis Bacon. *Novum Organum.* (The new organon. or true directions concerning the interpretation of nature.) 1620. Translation. James Spedding, et al. Taggard and Thompson. 1863.

C. Bradford Barber, David P. Dopkin and Hannu Huhdanpaa. The Quickhull algorithm for convex hulls. *ACM Transactions on Mathematical Software.* vol. 22, no. 4, 469–483. December, 1996.

J. M. Benoit, B. Corraze, S. Lefrant, W. J. Blau, P. Bernier and O. Chauvet. Transport properties of PMMA-carbon nanotubes composites. *Synthetic Metals.* **121**, 1–3, 1215–1216. March 2001.

Claude Berge. *The theory of graphs and its applications.* 1958. Translation. Alison Doig. Methuen. Wiley. 1962(1964).

G. Birkhoff and S. M. Lane. *A survey of modern algebra.* A K Peters. 1997.

Reginald Horace Blyth. *Oriental Humour.* Hokuseido. Tokyo. 1959.

A. Bravais. *A. Bravais' Abhandlungen über symmetrische polyeder.* (1849). Ostwald's Klassiker der Exakten Wissenschaften. no. 17, 46–49. Wilhelm Engelmann. Leipzig. 1890.

S. R. Broadbent and J. M. Hammersley. Percolation processes I, Crystals and mazes. *Proceedings of the Cambridge Philosophical Society.* 54, 629–641. 1957.

K. Broderix, H. Lowe, P. Muller and A. Zippelius. Critical dynamics of gelation. *Physical Review E.* **6301**, 1, 1510–1526. January 2001.

G. E. Brown. *Many-body problems.* North-Holland. 1972.

Ronald S. Burt. *Structural holes. The social structures of competition.* Harvard University Press. 1992.

Robert Wolfgang Cahn. *Encyclopedia of Material Science and Engineering.* Pergamon. 1990.

A. G. W. Cameron. Abundance of the elements in the solar system. *Space Science Reviews.* 15, 121–147. 1973.

J. Chalupa, P. L. Leath and G. R. Reich. Bootstrap percolation on a Bethe lattice. *Journal of Physics C, Solid State Physics.* **12**, L31–L35. 1979.

Chamber's Encyclopedia. New revised ed. International Learning Systems. London. 1970.

X. Cheng, A. M. Sastry and B. E. Layton. Transport in stochastic fibrous networks. *Journal of Engineering Materials and Technology, Transactions of the ASME.* **123**, 1, 12–19. January 2001.

Sen Chung Chan. *Studies of separation of dilute dispensions.* Ph.D. thesis. UMIST, Manchester, U.K. 1990.

K. Clarkson and P. Shor. Applications of random sampling in computational geometry, II. *Discrete Computational Geometry.* **4**, 387–421. 1989.

W. D. Clayton. Studies in the *Gramineae.* XXI. *Coelorhachis* and *Rhytachne.* A study in numerical taxonomy. *Kew Bulletin.* **24**, 309–314. 1970.

W. D. Clayton. Studies in the *Gramineae.* XXVI. Numerical taxonomy of the *Arundinelleae. Kew Bulletin.* **26**, 111–123. 1972.

Collins USA *Collins Road Atlas USA. Canada and Mexico.* Rand McNally. 1999.

J. H. Conway and N. J. A. Sloane. *Sphere packings, lattices and groups.* Springer-Verlag, N.Y.. 1988.

Alan Cooper, Russel Stannard and Barrie W. Jones. *The formation and evolution of the stars.* The Open University. 1985.

J. M. Coulson, J. F. Richardson, J. R. Backhurst and J. H. Harker. *Chemical Engineering. V. 2.* 4th ed. Particle technology and separation processes. Pergamon. 1991.

K. G. Cox, N. B. Price and B. Harte. *An introduction to the practical study of crystals, minerals, and rocks.* revised 1st ed. McGrawHill. 1974.

Ken Croswell. *The alchemy of heaven.* Oxford. 1995.

H. M. Cundy and A. P. Rollett. *Mathematical models.* $3^{rd}$ edition, 1989. Tarquin.

C. A. Curcio, K. R. Sloan. Packing geometry of human cone photoreceptors, variation with eccentricity and evidence for local anisotropy. *Visual Neuroscience.* Vol. 9, No. 2, Aug. 1992, p. 169–80.

James Dwight Dana and Edward Salisbury Dana. *Dana's new mineralogy.* 8th ed. Wiley. 1997.

Paul Davies. Liquid space. *New Scientist.* 30–34. $3^{rd}$ November 2001 .

P. Dean. A new Monte Carlo method for percolation problems on a lattice. *Proceedings of the Cambridge Philosophical Society.* **59**, 397–410. 1963.

P. G. de Gennes, P. Lafore and J. P. Millot. Amas accidentels dans les solutions solides désordonnées. *Journal of Physics and Chemistry of Solids.* **11**, 105–110. 1959.

Michael de Podesta. *Understanding the properties of matter.* 2nd ed. Taylor & Francis. 1996 (2002).

Renati Des-cartes *Principia philosophiæ.* 1644. Ludovicum Elzevirium. *cf* René Descartes. Œuvres philosophiques. Vol.III. 1973. Garnier Frères. Ferdinard Alquié ed.

G. de Vancouleurs. The extragalactic distance scale VIII. A comparison of distance scales. *The Astrophysical Journal.* **415**, 10–32. $20^{th}$ September 1993 .

Charles Dickens. *A child's history of England.* 1851(1868).

G. Lejeune Dirichlet. Über die Reduction der positiven quadratischen Formen mit drei unbestimmten ganzen Zahlen. *Crelle.* Journal für die reine und angewandte Mathematik. Bd. 40, 209–227. 1850. *cf* Tiyapan (2001)

Ian L. Dryden and Kanti V. Mardia. *Statistical shape analysis.* John Wiley & Sons. 2002.

R. Eisenthal and M. J. Danson. *Enzyme Assays.* 2nd ed. Oxford. 1992 (2002).

J. W. Essam. Percolation theory. *Reports on Progress in Physics.* vol. 43, 835–912, 1980.

Arthur Eugene Fitzgerald, Charles Kingsley Jr. and Alexander Kusko. *Electric Machinery.* McGraw-Hill Kogakusha. 3rd Ed. 1971.

James P. Evans and Frederick M. Chester. Fluid-rock interaction in faults of the San Andreas system. In ferences from San Gabriel fault rock geochemistry and micro structures. *Journal of Geophysical Research.* **100**, B7, 13007–13020. 10 July 1995.

Rachel Farmer. *Beginner's Russian. An easy introduction.* Teach Yourself Books. 1996.

H. L. Frisch, E. Sonnenblick, V. A. Vyssotsky, and J. M. Hammersley. Critical percolation probabilities (site problem). *Physical Review.* vol. 124, no. 4, 1021–1022. $15^{th}$ November 1961 .

L. Flandin, Y. Brechet and J. Y. Cavaille. Electrically conductive polymer nanocomposites as deformation sensors. *Composites Science and Technology.* **61**, 6, 895–901. 2001.

Mason Florence, Marisa Gierlich and Andrew Dean Nystrom. *Rocky Mountains. Colorado, Wyoming, Montana and Idaho.* Lonely Planet. 3rd ed. 2001.

E. M. Forster. *Howards End.* 1910.

Dennis Freeborn. *From Old English to standard English. A course book in language variation across time.* Macmillan. 1992.

J. Garside and J. W. Mullin. The crystallization of aluminium potassium sulphate, a study in the assessment of crystallizer design data. Part III. Growth and dissolution rates. *Transactions of the Institution of Chemical Engineers.* vol. 46, no. 1, T11–T18. 1968.

B. Gay and P. E. Preece. Matrix methods for the solution of fluid network problems, Part I–mesh methods. *Transactions of the Institution of Chemical Engineers.* vol. 53, no. 1, 12–15. January 1975.

J. W. Giles, C. Hanson and J. G. Marsland. Drop size distributions in agitated liquid-liquid systems with simultaneous interface mass transfer and chemical reaction. in *Proceedings of the International Solvent Extraction Conference, ISEC 71.* vol. 1, 94–111. 1971.

A. S. Glassner. Ed. *Graphics gems.* Academic Press. 1990.

Nigel Gotteri and Joanna Michalak-Gray. *Polish.* Teach Yourself Books. 1997.

P. J. Green and R. Sibson. Computing Dirichlet tessellations in the plane. *The Computer Journal.* vol. 21, February to November, 168–173, 1978.

G. Grimmett. *Percolation.* Second edition. Springer. 1999.

Patrick Grosfils, Jean Pierre Boon, E. G. D. Cohen and L. A. Bunimovich. Propagation and organization in lattice random media. *Journal of Statistical Physics.* vol. 97, nos. 3/4, 575–608, 1999.

Branko Grünbaulm. *Convex polytopes.* Inter Science, Wiley. Pure and applied mathematics series, vol. XVI. 1967,

Branko Grünbaum and G. C. Shepherd. *Tilings and patterns.* W. H. Freeman. N.Y. 1987.

J. M. Hammersley and W. Morton. Poor man's Monte Carlo. *Journal of the Royal Statistical Society (B).* 16, 23–38. 1954.

J. M. Hammersley. Percolation processes. II. the connective constant. *Proceedings of the Cambridge Philosophical Society.* **53**, 642–645. 1957.

J. M. Hammersley. Comparison of atom and bond percolation processes. *Journal of Mathematical Physics.* vol. 2, no. 5, 728–733. September-October, 1961.

Allen Hammond. *Which World? scenarios for the* $21^{st}$ *century.* Earthscan. 1998.

C. Hammond. *The basics of crystallography and diffraction.* Oxford. 2001.

Thomas L. Hankins. Triplets and triads. Sir William Rowan Hamilton on the metaphysics of mathematics. *Isis.* **68**, 242, 175–193. 1977.

John Happel. Viscous flow relative to arrays of cylinders. *American Institute of Chemical Engineers Journal.* vol. 5, no. 2, 174–177. June, 1959.

G. H. Hardy and E. M. Wright. *An introduction to the theory of numbers.* 1938. Oxford. or $5^{th}$ ed. 1979.

H. W. Harrison and P. M. Trotman. *Foundations, basements and external works. Performance, diagnosis, maintenance, repair and the avoidance of defects.* BRE. 2002.

P. M. Heertjes. Filtration. *The Transactions of the Institution of Chemical Engineers.* vol. 42, no. 7, T266–T274, 1964.

H. S. Hele-Shaw. The flow of water. *Nature.* Vol. 58, p. 34–36. May 12, 1898.

– The motion of a perfect liquid. *Nature.* Vol. 60, p. 446–451. September 7, 1899.

M. Hindermann-Bischoff and F. Ehrburger-Dolle. Electrical conductivity of carbon black-polyethylene composites- Experimental evidence of the change of cluster connectivity in the PTC effect. *Carbon.* **39**, 3, 375–382. 2001.

Franz E. Hohn. *Elementary matrix algebra.* $3^{rd}$ ed. Macmillan. 1958 (1973).

D. Houi and R. Lenormand. Experimental and theoretical study of particle accumulation at the surface of a filter. in *The Proceedings of* $4^{th}$ *World Filtration Contress.* no. 1, 1.1–1.6. 1986.

Fred Hoyle. *Ten faces of the universe.* Heinemann. London. 1977.

Fred Hoyle and Chandra Wickramasinghe. *Life cloud* the origin of life in the universe.

J. M. Dent & Sons. 1978.: Fred Hoyle and Nalin Chandra Wickramasinghe. *Diseases from space.* J. M. Dent & Sons. 1979.

Q. Huang, Z. W. Li, J. Li and C. K. Ong. The magnetic, electrical transport and magnetoresistance properties of epitaxial $La_{0.7}Sr_{0.3}Mn_{1-x}Fe_xO_3$ (x=0–0.20) thin films prepared by pulsed laser deposition. *Journal of Physics-Condensed Matter.* **13**, 18, 4033–4047. May 2001.

A. G. Hunt. Applications of percolation theory to porous media with distributed local conductances. *Advances in Water Resources.* **24**, 3–4, 279–307. 2001.

C. Isenberg. *The science of soap films and soap bubbles.* Tieto. 1978.

A. F. Ismail, R. Norida and A. R. Sunarti. Latest development on the membrane formation for gas separation. *Songklanakarin Journal of Science and Technology.* **24** (suppl.), 1025–1043. 2002.

K. J. Ives. Deep bed filtration. in *Solid–Liquid Separation.* $2^{nd}$. Butterworths Monographs in Chemistry and Chemical Engineering. Ladislav Svarovsky. ed. 284–301. 1977.

N. M. Jackson. *A mathematical model to simulate the structure and performance of porous media.* Thesis. UMIST, Manchester, 1994.

N. M. Jackson, R. Jafferali, D. J. Bell and G. A. Davies. A study of the structure of micro and ultra filtration membranes. The Voronoi tessellation as a stochastic model to simulate the structure. *Journal of Membrane Science.* **162**, 23–43. 1999.

Riaz Jafferali. *A stochastic model to simulate the structure and performance of microfiltration media and the growth of animal cell cultures.* Thesis. UMIST, Manchester, 1995.

Harold James. *The German slump. Politics and economics 1924–1936.* Clarendon. Oxford. 1986(1987).

Vera Javarek and Miroslava Sudjić *Serbo-Croat.* $2^{nd}$ ed. Teach Yourself Books. 1963(1972).

G. R. Jerauld, J. C. Hatfield, L. E. Scriven and H. T. Davis. Percolation and conduction on Voronoi and triangular networks. A case study in topological disorder. *Journal of Physics C. Solid State Physics.* **17**, 1519–1529. 1984.

M. M. Jevtic, Z. Stanimirovic and I. Stanimirovic. Evaluation of thick-film resistor structural parameters based on noise index measurements. *Microelectronics Reliability.* **41**, 1, 59–66. January 2001.

A. J. Jones. *Crystalization process sytems.* Butterworth Heinemann. 2002.

JTRO. Nylon 66 Spun Fiber Fabric. *New Technology. Japan.* vol. 29, no. 6, p. 32. Japan External Trade Organisation. September, 2001.

Immanuel Kant. Beantwortung der Frage. Was ist Aufklärung. *Berlinische Monatsschrift.* **4**. December. 1784. 481–494.

F. August Kekulé Sur la constitution des substances aromatiques. *Bulletin de la societé chimique de Paris.* **3**, 98–111. 1865.

Alan R. Kerstein. Equivalence of the void percolation problem for overlapping spheres and a network problem. *Journal of Physics A. Mathematical and General.* **16**, 3071–3075. 1983.

Daniel Keyes. *The minds of Billy Milligan.* Bantam. 1999.

C. Klein and C. S. Hurlbut, Jr. *Manual of mineralogy.* $21^{st}$ Edition. Wiley. 1993.

D. E. Knuth. *The TEX.* Addison Wesley. 1970.

Donald E. Knuth. *The art of computer programming. V. I Fundamental algorithms.* 3rd ed. Addison-Wesley. 1997

Donald E. Knuth. *The art of computer programming. V. II.* 3rd ed. Addison-Wesley. 1998.

J. W. de Kock and M. R. Judd. The flow pattern within a void in a porous mass. *The Transactions of the Institution of Chemical Engineers.* vol. 43, no. 3, T78–T84. 1965.

J. M. Kosterlitz and D. J. Thouless. Ordering, metastability and phase transitions in two-dimensional systems. *Journal of Physics C. Solid State Physics.* vol. 6, 1181–1203.

John Krige. *Science, revolution and discontinuity.* The Harvester Press. 1980.

Roderic Lakes. Foam structures with a negative Poisson's ratio. *Science.* **235**, 1038–1040. 1987.

Leslie Lamport. *LaTEX document preparation system.* 2nd ed. 1985 (1994).

Russel D. Larsen. Kekulé's benzolfest speech. A fertile resource for the sociology of science. in *The Kekulé riddle. A challenge for chemists and psychologists.* 178–193. Cache River. 1993.

A. Levy, S. Reich and P. Meakin. The shape of clusters on rectangular 2D lattices in a simple "phase separation" computer experiment. *Physics Letters.* vol. 87A, no. 5, 248–252. $11^{th}$ January 1982 .

Larry S. Liebovitch and Daniela Scheurle. Two lessons from fractals to chaos. *Complexity.* vol. 5, no. 4, 34–43. March-April, 2000.

K. C. Lim, M. A. Hashim and B. Sen Gupta. The effect of volume shape factor on the crystal size distribution of fragments due to attrition. *Crystal Research Technology.* vol. 34, no. 4, 491–502. 1999.

J. Litwiniszyn. Colmatage considered as a certain stochastic process. *Bulletin de L'Academie Polonaise des Sciences.* vol. XI, no. 3, 117–121. 1963.

J. Litwiniszyn. On some mathematical models of the suspension flow in porous medium. *Chemical Engineering Science.* vol. 22, 1315–1324. 1967.

C. W. Lowe. Some techniques of evolutionary operation. *Transactions of the Institution of Chemical Engineers.* vol. 42, no. 9, T334–T344. 1964.

Ian S. Lustick and Dan Miodownik. Deliberative democracy and public discourse. The agent-based argument repertoire model. *Complexity.* vol. 5, no. 4, 13–30. March-April, 2000.

T. Magay and L. Országh. *A concise Hungarian–English dictionary.* Oxford University Press. Akademiai Kiadó 1981 (1990).

K. R. Mecke and A. Seyfried. Strong dependence of percolation thresholds on polydispersity. *Europhysics Letters.* **58** (1), 28–34, $1^{st}$ April 2002 .

Hans Meinhardt. *The algorithmic beauty of sea shells.* Springer-Verlag. 1995 (1998).

R. K. Merton. *On the shoulders of giants.* A Shandean Postscript, Harvest/Harcourt. 1965.

Stephen A. Miler and Amos Nur. Permeability as a toggle switch in fluid-controlled crustal processes. *Earth and Planetary Science Letters.* **183**, 133–146. 2000.

R. E. Miles. A random division of space. *Special Supplement to Advances in Applied Probability.* 243–266. 1972.

Gian Maria Milesi-Ferretti and Assaf Razin. Current account reversals and currency crises. Empirical regularities. in *Currency Crisis.* Paul Krugman. ed. University of Chicago Press. 2000.

I. Mironi-Harpaz and M. Narki. Electrical behavior and structure of polypropylene/ultrahigh molecular weight polyethylene/carbon black immiscible blends. *Journal of Applied Polymer Science.* **81**, 1, 104–115. July 2001.

U. Mizutani. *Introduction to the electron theory of metals.* Cambridge. 2001.

K. K. Mohanty, J. M. Ottino and H. T. Davis. Reaction and transport in disordered composite media. Introduction of percolation concepts. *Chemical Engineering Science.* vol. 37, no. 6, 905–924. 1982.

J. Møller. Random tessellations in $\Re^d$. *Advances in Applied Probability.* vol. 21, p. 37–73, 1989.

M. Mulder. *Basic principles of membrane technology.* Kluwer. 1992.

T. Mulder and R. Gimbel. On the development of high performance filtration materials for deep bed filters. in *The proceedings for the* $5^{\text{th}}$ *World Filtration Congress.* vol. 3, 45–57. Nice, 1990.

M. Narkis, G. Lidor, A. Vaxman and L. Zuri. Innovative ESD thermoplastic composites structured through melt flow processing. *IEEE Transactions on Electronics Packaging Manufacturing.* **23**, 4, 239–245. October 2000.

Andrew Nathaniel Nelson. *Japanese–English Character Dictionary.* Charles E. Tuttle. 1962.

D. Neilson, J. S. Thakur and E. Tosatti. Characterising the metal-insulator transition in two dimensions. *Australian Journal of Physics.* **53**, 4, 531–535. 2000.

Johann Nittmann, Gérard Daccord and H. Eugene Stanley. Fractal growth of viscous fingers, quantitative characterization of a fluid instability phenomenon. *Nature* Vol. 314, 14 March 1985, p. 141–144

A. Okabe, B. Boots and K. Sugihara. *Spatial tessellations concepts and applications of Voronoi diagrams.* Wiley. 1992.

R. K. Pathria. *Statistical Mechanics.* $2^{\text{nd}}$ ed. Butterworth-Heinemann. 1996 (1997).

C. Pennetta, L. Reggiani, G. Trefan, F. Fantini, A. Scorzoni and I. de Munari. A percolative approach to electromigration in metallic lines. *Journal of Physics D, Applied Physics.* **34**, 9, 1421–1429. May, 2001.

C. Pennetta, G. Trefan and L. Reggiani. Scaling law of resistance fluctuations in stationary random. *Physical Review Letters.* **85**, 24, 5238–5241. December, 2000.

Roger Penrose. *The emperor's new mind. Concerning computers, minds, and the law of physics.* 1989.

R. Penrose. Tilings and quasi-crystals. a non-local growth problem? in *Introduction to the mathematics of quasicrystals.* Marko V. Jarić Ed. 53–79. Aperiodicity and order. Vol. 2. Academic Press. 1989.

Petersburg *Investment projects of St. Petersburg* Information and Consulting Centre. International Finance and Enterprise Week. Manchester International Conference Centre. $31^{\text{st}}$ October–$2^{nd}$ November 2001 .

V. Y. Petrovsky and Z. S. Rak. Densification, microstructure and properties of electroconductive Si3N4-TaN composites. Part II *Electrical and mechanical properties.* Journal of the European Ceramic Society.

**21**, 2, 237–244. February 2001.: F. C. Phillips. *An introduction to crystallography.* Longmans. $3^{\text{rd}}$ ed. 1949 (1963).

H. W. Piekaar and L. A. Clarenburg. Aerosol filters – the tortuosity factor in fibrous filters. *Chemical Engineering Science* vol. 22, 1817–1827. 1967.

Plato. [Aristocles] *Phaedo.* [Phaidon] 360 BC.

Michael de Podesta. *Understanding the properties of matter.* Taylor & Francis. $2^{\text{nd}}$ ed. 2002.

J. B. Poole and D. Doyle. Research in solid-liquid separation. *The Chemical Engineer.* no. 190, CE169–CE172. July–August, 1965.

K. E. Porter. Liquid flow in packed columns. Part I. The rivulet model. *The Transactions of the Institution of Chemical Engineers.* vol. 46, no. 3, T69–T73. 1968.

J. G. Powles and N. Quirke. Fractal geometry and Brownian motion. A new parameter to describe molecular motion. *Physical Review Letters.* Vol. 52, No. 18, 1571–1574. 30 April 1984.

Burkhard A. Prause. *Magnetic resonance imaging of structure and coarsening in three-dimensional foams.* Ph.D. Dissertation, the University of Notre Dame. 2000.

Franco P. Preparata and Michael Ian Shamos. *Computational Geometry. An introduction.* Springer-Verlag. 1985.

Przemyslaw Prusinkiewicz and Aristid Lindenmayer. *The algorithmic beauty of plants.* Springer-Verlag. 1990.

L. R. Pujara and Naresh Shanbhag. Some stability theorems for polygons of polynomials. *IEEE Transactions on Automatic Control.* Vol. 37. No. 11. Nov. 1992. 1845–1849

L. Rai. Pujara. On the pseudoboundary of unstable polytopes of polynomials. *IEEE Transactions on Automatic Control.* **41**, 8. 1188–1190. August 1996.

Annick van Put, Akos Vertes, Darek Wegrzynek, Boris Treiger and René van Grieken. Quantitative characterization of individual particle surfaces by fractal analysis of scanning electron microscope images. *Fresenius Journal Analytical Chemistry.* **350**, 440–447, 1994.

J. H. Raistrick. The nature of adsortive filtration. in *Proceedings of the* 4th *World Filtration Congress.* R. Vanbrabant, J. Hermia and R. A. Weiler, Eds. Part I. p. 1.65–1.72. 1986.

N. Rivier. Recent results on the ideal structure of glasses. *Journal de Physique.* Colloque C9, Supplément au no. 12, **43**, C9-91–C9-95. December, 1982.

Steven Rodelet and Jeffrey Sacs. The onset of the East Asian Financial Crisis. in *Currency Crisis.* Paul Krugman. ed. University of Chicago Press. 2000.

Min Zhi Rong, Ming Qiu Zhang, Yong Xiang Zheng, Han Min Zeng and K. Friedrich. Improvement of tensile properties of nano-$SiO_2$/PP composites in relation to percolation mechanism. *Polymer.* **42**, 4, 3301–3304. March 2001.

H. E. Rose and J. E. English. The influence of blinding material on the results of test sieving. *Transactions of the Institution of Chemical Engineers.* vol. 51, 14–21. 1973.

P. N. Rowe and R. Collins. The flow pattern within a void in a porous mass, *The Transactions of The Institution of Chemical Engineers.* vol. 43, no. 7, T217–T220. 1965.

P. N. Rowe and C. Yacono. The distribution of bubble size in gas fluidised beds. *Transactions of the Institution of Chemical Engineers.* vol. 53, no. 1, 59–60. January, 1975.

G. S. Rushbrooke and D. J. Morgan. On the magnetically dilute Heisenberg and Ising ferromagnetics. *Molecular Physics.* vol. 4, 1–15, 1961.

Joan Russell. *Swahili.* Teach Yourself Books. 1996.

Oliver Sacks. *Awakenings.* Piccador. Pan Books. 1973(1982).

– *seeing voices. A journey into the world of the deaf.* Piccador. Pan Books. 1989(1990).

Muhammad Sahimi. *Applications of percolation theory.* Taylor & Francis. 1994.

George Salmon. *A treatise on the analytic geometry of three dimensions.* revised by Reginald a. P. Rogers. 5th ed. Longman, Green and Co. 1912.

Vinod K. S. Shante and Scott Kirkpatrick. An introduction to percolation theory. *Advances in Physics.* **20**, 325–357. 1971.

Arnold Schoenberg. *Harmonielehre.* 1978. English translation. Theory of Harmony. Farber. 1983.

Ralf Schumacher. *A stochastic model to simulate the structure and performance of cellular polymeric membranes in dead end filtration.* Diplomarbeit. [Ph.D. thesis] Institute für chemische Verfahrenstechnik der Technischen Universität Clausthal and UMIST. 1996.

B. Sharp, D. Morton and A. E. Clark. Effectiveness of metal surface treatments in controlling microleakage of the acrylic resin-metal framework interface. *Journal of Prosthetic Dentistry.* **84**, 6, 617–622. 2000.

Madan G. Singh. Ed. *Systems & Control Encyclopedia.* Pergamon. 1987.

John Maynard Smith and Eörs Szathmáry. *The major transitions in evolution.* W. H. Freeman. 1995.

Herbert Warington Smyth. *Five years in Siam, from 1891–1896.* J. Murray. London. 1898. in two volumes.

Rupert Snell. *Beginner's Hindi script.* Teach Yourself Books. 2000.

Murray R. Spiegel. *Probability and Statistics.* Schaum's outline. McGraw-Hill. 1975.

David J. Srolovitz. Computer simulation of microstructural evolution. in *Encyclopedia of Material Science and Engineering.* 845–854. Pergamon. 1990.

Dietrich Stauffer and Amnon Aharony. *Introduction to percolation theory.* 1985. 2nd ed. Taylor & Francis. 1992. and 2nd revised ed. 1994 (1998)

O. Stenull, H. K. Janssen, K. Oerding. Effects of surfaces on resistor percolation. *Physical Review E.* **6305**, 5, 6128–6141. May 2001.

R. L. Stevenson. *Dr. Jenkyll and Mr. Hyde.* 1886.

Robert Louis Stevenson. *The amateur emigrant.* 1895.

William C. Stokoe Jr., Dorothy C. Casterline and Carl G. Croneberg. *A Dictionary of American Sign Language on Linguistic Principles.* Gallaudet College Press. 1965

L. Svarovsky. Characterization of particles suspended in liquids. in *Solid-liquid separation.* 2nd ed. L. Svarovsky, Ed. Butterworths. p. 8–32. 1977.

Masaharu Tanemura, Tohru Ogawa and Naofumi Ogita. A new algorithm for three-dimensional Voronoi tessellation. *Journal of Computational Physics.* **51**, 191–207. 1983.

Aspasia Theodosiou. personal communication. 2002.

J. R. R. Tolkien. *Lord of the Rings.* 1955.

C. R. G. Treasure. Fine particle-size classification. *Transactions of the Institution of Chemical Engineers.* vol. 43, no. 6, T199–T205. 1965.

U. of Man. *Mathematics, the University of Manchester, 2000 and 2001 entry.* booklet. the University of Manchester. 2000.

Rüdiger Vaas. Ed. Urknall für Einsteiger. *Bild der Wissenschaft.* May 2002.

G. F. Voronoï New application of continuous parameters to the theory of quadratic form. First memoir. On some properties of the perfect positive quadratic forms. *Journal für die reine und angewandte Mathematik.* **133**, 97–178, 1908. *cf* Tiyapan (2001).

G. F. Voronoï New application of continuous parameters to the theory of quadratic form. Second memoir. Research on the primitive parallelohedron. *Journal für die reine und angewandte Mathematik.* **134**, 1908. *cf* Tiyapan (2001).

G. F. Voronoï New application of continuous parameters to the theory of quadratic form. Second memoir. Studies on the primitive parallelohedra. *Journal für die reine und angewandte Mathematik.* **136**, 67–181, 1909. *cf* . Tiyapan (2001).

Tuan Duc Vuong and John Moore. *Colloquial Vietnamese. A complete language course.* Routledge. 1994.

N. Walsh. *Making TEX work.* O'Reilly. 1994.

John Walters. *Quantum mechanics, theory and applications.* Science second level course, S271 Discovering Physics. The Open University. 1982.

David Ward. Language cull could leave people speechless. *The Guardian.* Saturday $25^{th}$ May 2002 . National news, 13.

D. Weaire. Some remarks on the arrangement of grains in a polycrystal. *Metallography.* **7**, 157–160.

S. H. Wen and D. D. L. Chung. Cement as a thermoelectric material. *Journal of Materials Research.* **15**, 12, 2844–2848. 2000.

Magnus Joseph Wenninger. *Polyhedron models.* Cambridge University Press. 1971.

R. van de Weygaert and V. Icke. Fragmenting the universe II. Voronoi vertices as Abell clusters. *Astronomy and Astrophysics.* **213** 1–9. 1989.

R. van de Weygaert. Fragmenting the universe III. The construction and statistics of 3-d Voronoi tessellation. *Astronomy and Astrophysics.* **283**, 361–406. 1994.

Elaine Wilcock. *A study of mesh mist eliminators.* PhD thesis. UMIST. 1994.

David Wilkinson and Jorge F. Willemsen. Invasion percolation. a new form of percolation theory. *Journal of Physics A. Mathematical and General.* **16**, 3365–3376. 1983.

E. T. Wilkinson, A. R. N. Fairclough and G. A. Davies. The filtration of dilute suspensions using nonwoven cloths and membranes. in *Proceedings of the* $4^{\text{th}}$ *World Filtration Congress.* R. Vanbrabant, J. Hermia and R. A. Weiler, Eds. Part I. p. 1.7–1.18. 1986.

Trevor Williams and Rolf Bjerknes. Stochastic model for abnormal clone spread through epithelial basal layer. *Nature.* vol. 236, 19–21. $3^{rd}$ March 1972 .

John H. Wotiz. *The Kekulé riddle. A challenge for chemists and psychologists.* Cache River. 1993.

P. J. Wray, O. Richmond and H. L. Morrison. Use of the Dirichlet tessellation for characterizing and modeling nonregular dispersions of second-phase particles. *Metallography.* **16**, 39–58. 1983.

X. J. Zhan, J. B. Troy. Modeling cat retinal beta-cell arrays. *Visual Neuroscience.* Vol. 17, No. 1, Jan.–Feb. 2000, p. 23–39.

H. J. Zhang, J. W. Wang, J. Li, S. K. Cao and A. Shan. Toughened polypropylene with balanced rigidity, III, compositions and mechanical properties. *Journal of Applied Polymer Science.* **79**, 8, 1345–1350. February 2001.

## § 9.1 Publication and writings, Kittisak Nui Tiyapan

1991 Antimonytrioxide extraction from stibnum ore by hydrometallurgical method. Senior project. [Final year project]. Mining Engineering, Chulalongkorn University, Thailand. 1991. KNT1(i).

1994 Cyberspace. *Articles Online.* ATSIST. $12^{th}$ December 1994 . also at www.nectec.or.th/bureaux/atsist KNT2(i).

1995 The End of Stars. *Articles Online.* ATSIST. $20^{th}$ February 1995 . also at www.nectec.or.th/bureaux/atsist KNT3(i).

1995 Self-tuning Extremum Control. *Design Exercise Report.* under the supervision of Dr. M. B. Zarrop. M.Sc. Course in Control and Information Technology 1994/1995. Control System Centre, UMIST. KNT3(ii).

1995 Computation of Fluid Flow. *M.Sc. dissertation.* under the supervision of Professor G. A. Davies and Professor D. J. Bell. September. UMIST. KNT3(iii).

1995 The story of Andromedra. *Sakkayaphab.* November. **3**, 2, 24–25. ATPIJ, Japan. Thai translation by *Sroemśakdži Ụatrongcitta.* KNT3(iv).

1996 Let's start at the very beginning. *Sakkayaphab.* January. **3**, 4, 23–25. ATPIJ, Japan. Thai translation by *Sroemśakdži Ụatrongcitta.* KNT4(i).

1996 To be unkempt. *Sakkayaphab.* April. **3**, 7. ATPIJ, Japan. Thai translation by *Suvanjay Bongṣasukicvaḍhâṅa.* KNT4(ii).

1996 I see a white car before me. *Sakkayaphab.* June. **3**, 9, 12–13. ATPIJ, Japan. Thai translation by *Taśāṇiya Meḍhabisiṭh.* KNT4(iii).
1996 Critical probability and other properties of 2-d tessellation *Mathematical Theory of Networks and Systems–96.* $24^{th}$ –$28^{th}$ June ($27^{th}$ June , Session on Analysis of Queuing Networks). The Ritz-Carlton, St. Louis, Missouri. KNT4(iv).
1996 Some properties of stochastic optimal control. submitted in July 1996 to the $7^{\text{th}}$ International Symposium on Dynamic Games and Applications (16–18 December 1996). Japan. KNT4(v).
1996 On an algorithm for object-location problem. [Object location using Extremum Control] *1996 Advanced Theory and Application of Control Systems.* $6^{th}$ –$8^{th}$ October . Izu Recreation Centre, Atagawa Heights, Atagawa, Japan. Fu-I1–Fu-I5. KNT4(vi).
1996 On pragmatists and idealists. submitted to the Sakkayaphab journal. $21^{st}$ October 1996 . KNT4(vii).
1996 [Nhạun khạung Mạuṙris] (The Morris Worm). *Sakkayaphab.* December. **4**, 3, 20–22. ATPIJ, Japan. KNT4(viii).
1997 Fractals in traffic control. *The Fourth Annual Conference of Thai Researchers in Japan.* abstract. $23^{rd}$ February . Nippon Seinenkan Hotel, Tokyo. TSAJ and ATPIJ. p. 18 KNT5(i).
1997 Distributed parameter systems. *The Fourth Annual Conference of Thai Researchers in Japan.* abstract. $23^{rd}$ February . Nippon Seinenkan Hotel, Tokyo. TSAJ and ATPIJ. p. 19 KNT5(ii).
1997 Vision robots. *The Fourth Annual Conference of Thai Researchers in Japan.* abstract. $23^{rd}$ February . Nippon Seinenkan Hotel, Tokyo. TSAJ and ATPIJ. p. 20 KNT5(iii).
1997 Singular perturbation. *The Fourth Annual Conference of Thai Researchers in Japan.* abstract. $23^{rd}$ February . Nippon Seinenkan Hotel, Tokyo. TSAJ and ATPIJ. p. 21 KNT5(iv).
1997 Simulation techniques using RLS algorithm for object-locaition problem. *Proceedings of the World Congress on Systems Simulation.* $1^{\text{st}}$–$3^{rd}$ September . Pan Pacific Hotel, Singapore. 518–522. KNT5(v).
1997 Report for German Literature course. TIT. presented to Professor Ishikawa. $9^{th}$ September 1997 . KNT5(vi).
1997 Modelling the economics. *1997 Advanced Theory and Application of Control Systems.* $10^{th}$ –$12^{th}$ October . National Olympic Memorial Youth Centre, Yoyogi, Shibuya-ku, Tokyo. Fu-A1–Fu-A2. KNT5(vii).
1997 Modelling economics as a flow of money within networks. submitted to the American Journal of Physics. $4^{th}$ November 1997 . KNT5(viii).
1997 Modelling of traffic congestion. submitted to the Journal of Statistical Physics. $4^{th}$ November 1997 . KNT5(ix).
1998 Simulation techniques using RLS algorithm for object-location problem. Paper presented to the Furuta Laboratory on an in-house seminar. TIT, Tokyo. 4-5pm. $3^{rd}$ January 1998 KNT6(i).
1998 Critical probability in traffic modelling and control. Paper presented to the Furuta Laboratory on an in-house seminar. TIT, Tokyo. $2^{nd}$ April 1998 . KNT6(ii).
1998 Technical report number 1. presented to Professor Katsuhisa Furuta, TIT, Japan. $16^{th}$ July . KNT6(iii).
1998 Technical report number 6. On controlling the synchronous machines. presented to Professor Katsuhisa Furuta, TIT. Japan. $23^{rd}$ August . KNT6(iv).
1998 Variable structure control for a singularly perturbed system. *1998 Advanced Theory and Application of Control Systems.* $26^{\text{th}}$–$28^{th}$ September . Hotel Ohashi, Lake Kawaguchi, Yamanashi, Japan. Fu-C1–Fu-C8. KNT6(v).
1998 Technical report number 2 (in System and Control). presented to Professor Katsuhisa Furuta, TIT. Japan. $1^{st}$ November 1998 . KNT6(vi).
2000 *Interesting English. [Bhạṣạ Angkṛiṣ an nạ̀ soncaị]* Kittix Books. Chulalongkorn University Printing House. Bangkok. KNT7(i).
2000 *Free translation of English. [Plạe kleḱ Angkṛiṣ]* Kittix. CU. Bangkok. KNT7(ii).
2001 *The study of Voronoi tessellation.* unpublished. $22^{nd}$ May 2001 KNT8(i).
2001 *Voronoi Translated, Introduction to Voronoi tessellation and essays by G. L. Dirichlet and G. F. Voronoi.* Kittix Library Networks. CU. Bangkok. KNT8(ii).
2003 *Percolation within percolation and Voronoi Tessellation.* KLN. CU. BKK. KNT8(iii).
2003 *Thai grammar, poetry and dictionary.* KLN. CU. BKK. KNT8(iv).
2003 *A Lanna in town.* KLN. CU. BKK. KNT8(v).
2003 *A Kiwi Lanna.* KLN. CU. BKK. KNT8(vi).
2003 *A British Lanna.* KLN. CU. BKK. KNT8(vii).
2003 *Edokko no Lanna.* KLN. CU. BKK. KNT8(viii).
2003 *The Siamese Lanna.* KLN. CU. BKK. KNT8(ix).